National Library of Canada
Canadian Theses Service
Ottawa, Canada
K1A 0N4

Bibliothèque nationale du Canada
Service des thèses canadiennes

NOTICE

The quality of this microform is heavily dependent upon the quality of the original thesis submitted for microfilming. Every effort has been made to ensure the highest quality of reproduction possible.

If pages are missing, contact the university which granted the degree.

Some pages may have indistinct print especially if the original pages were typed with a poor typewriter ribbon or if the university sent us an inferior photocopy.

Previously copyrighted materials (journal articles, published tests, etc.) are not filmed.

Reproduction in full or in part of this microform is governed by the Canadian Copyright Act, R.S.C. 1970, c. C-30.

AVIS

La qualité de cette microforme dépend grandement de la qualité de la thèse soumise au microfilmage. Nous avons tout fait pour assurer une qualité supérieure de reproduction.

S'il manque des pages, veuillez communiquer avec l'université qui a conféré le grade.

La qualité d'impression de certaines pages peut laisser à désirer, surtout si les pages originales ont été dactylographiées à l'aide d'un ruban usé ou si l'université nous a fait parvenir une photocopie de qualité inférieure.

Les documents qui font déjà l'objet d'un droit d'auteur (articles de revue, tests publiés, etc.) ne sont pas microfilmés.

La reproduction, même partielle, de cette microforme est soumise à la Loi canadienne sur le droit d'auteur, SRC 1970, c. C-30.

NL-339 (r. 88/04)

Canada

THE UNIVERSITY OF ALBERTA

MOBILITY CONTROL IN WATERFLOODING OIL RESERVOIRS WITH A BOTTOM-WATER ZONE

by

© M.Rafiqul Islam

A THESIS
SUBMITTED TO THE FACULTY OF GRADUATE STUDIES AND RESEARCH
IN PARTIAL FULFILMENT OF THE REQUIREMENTS FOR THE DEGREE
OF Doctor of Philosophy
IN
PETROLEUM ENGINEERING

DEPARTMENT OF MINING, METALLURGICAL AND PETROLEUM ENGINEERING

EDMONTON, ALBERTA
Fall, 1987

Permission has been granted to the National Library of Canada to microfilm this thesis and to lend or sell copies of the film.

The author (copyright owner) has reserved other publication rights, and neither the thesis nor extensive extracts from it may be printed or otherwise reproduced without his/her written permission.

L'autorisation a été accordée à la Bibliothèque nationale du Canada de microfilmer cette thèse et de prêter ou de vendre des exemplaires du film.

L'auteur (titulaire du droit d'auteur) se réserve les autres droits de publication; ni la thèse ni de longs extraits de celle-ci ne doivent être imprimés ou autrement reproduits sans son autorisation écrite.

ISBN 0-315-40859-6

THE UNIVERSITY OF ALBERTA

RELEASE FORM

NAME OF AUTHOR M.Rafiqul Islam

TITLE OF THESIS **MOBILITY CONTROL IN WATERFLOODING OIL RESERVOIRS WITH A BOTTOM-WATER ZONE**

DEGREE FOR WHICH THESIS WAS PRESENTED Doctor of Philosophy

YEAR THIS DEGREE GRANTED 1987

Permission is hereby granted to THE UNIVERSITY OF ALBERTA LIBRARY to reproduce single copies of this thesis and to lend or sell such copies for private, scholarly or scientific research purposes only.

The author reserves other publication rights, and neither the thesis nor extensive extracts from it may be printed or otherwise reproduced without the author's written permission.

(SIGNED) ...Rafiq..Islam..

PERMANENT ADDRESS:

C/O Mr. Sulaiman

T.B. Road, Laxmipur

Rajshahi, Bangladesh

DATED October 14, 19 87

THE UNIVERSITY OF ALBERTA

FACULTY OF GRADUATE STUDIES AND RESEARCH

The undersigned certify that they have read, and recommend to the Faculty of Graduate Studies and Research, for acceptance, a thesis entitled **MOBILITY CONTROL IN WATERFLOODING OIL RESERVOIRS WITH A BOTTOM-WATER ZONE** submitted by M.Rafiqul Islam in partial fulfilment of the requirements for the degree of Doctor of Philosophy in PETROLEUM ENGINEERING.

....

Supervisor

....

....

....

....

....

External Examiner

Date Oct 9, 87

Dedication

TO

MY PARENTS,

AND ALL MY TEACHERS

ABSTRACT

This research addresses the problem of waterflooding a medium gravity oil-bearing formation with a water leg, and offers recommendations for process selection. The presence of a bottom-water zone results in poor areal and vertical sweep efficiencies. However, waterflooding still remains the most widely used oil recovery technique for such reservoirs. Waterflood performance can be improved if an effective method of partially plugging the water zone can be developed; e.g. by a slug of mobility control agent. This possibility was investigated extensively in this study using a large flow model, for a series of mobility control agents. Numerical simulations of the experiments were also carried out. Scaling criteria were derived for several types of displacements.

Polymer, emulsion, biopolymer gel, air, foam and carbon dioxide-activated silica gel, in various slug sizes, were used as mobility control agents in over 80 runs for waterflooding an oil-saturated (1 to 200 mPa.s) sand pack with a bottom-water layer. The variables examined were: permeability contrast, relative water-oil layer thickness, oil viscosity, slug size, concentration of the mobility control agent, and injection point. Also, a series of runs were conducted with artificial barriers of different lengths. It is shown that for polymer and emulsion, injection of the mobility control agent as a slug is more efficient than alternating slugs of water and mobility control agent. An optimum slug size is proposed for various mobility control agents. It is shown that for polymer, emulsion, foam and silica gel the worse the conventional waterflood performance is, the more efficient the mobility control agents are likely to be.

For polymer and emulsion floods, two different numerical models were developed within the framework of three-phase, three-dimensional flow, and used to simulate experimental data, with excellent agreement.

A set of scaling criteria for polymer, emulsion and foam flooding experiments was derived for the first time using inspectional and dimensional analyses. Emphasis was on complex interactions and mass transfer between phases, interfacial tension, fractional flow, dispersion, adsorption, mechanical entrapment, slug size, polymer transport, and foam and emulsion formation and stability. A variety of scaling options were investigated and their relative merits pointed out.

Acknowledgement

I would like to express my sincere regards and thanks to Dr. S.M. Farouq Ali for his kind supervision, guidance and encouragement throughout the period of this study. I am also grateful to Dr. Ted Cyr of the Alberta Research Council for his valuable suggestions and encouragement during the early part of this study.

It is also important to thank Mrs. Sara Thomas for her help in designing some of the experimental runs. Thanks are also due to Mr. Robert Smith for his help in designing the experimental equipment and to Miss Raymonde Gratton for her kind help in production of the thesis.

I would like to thank the Alberta Oil Sands Technology and Research Authority (AOSTRA) for providing the financial assistance necessary for conducting this study.

Table of Contents

Chapter Page

1. INTRODUCTION 1

2. LITERATURE REVIEW 4

   2.1 STRATIFIED RESERVOIR MODELS 4

   2.2 MOBILITY CONTROL IN WATERFLOODING 7

      2.2.1 Mobility Control with Polymer Slugs 8

      2.2.2 Mobility Control with Emulsion Slugs ...22

         2.2.2.1 Blocking Mechanism with Emulsion 24

      2.2.3 Mobiloty Control with Foam 27

         2.2.3.1 Laboratory Studies 39

         2.2.3.2 Field Examples 41

   2.3 NUMERICAL SIMULATION 48

      2.3.1 Numerical Simulation of Polymer Flood ..48

      2.3.2 Numerical Simulation of Emulsion Flood .49

   2.4 SCALING OF POLYMER, EMULSION AND FOAM 50

      2.4.1 Flow Mechanism of Polymer in Porous Media 50

      2.4.2 Flow Mechanism of Emulsion in Porous Media 54

      2.4.3 Flow Mechanism of Foam in Porous Media .55

3. STATEMENT OF THE PROBLEM 58

4. EXPERIMENTAL APPARATUS AND PROCEDURE 60

   4.1 EXPERIMENTAL APPARATUS 60

   4.2 CHEMICALS 63

   4.3 PACKING AND PREPARATION OF RUNS 66

5. PRESENTATION OF EXPERIMENTAL DATA 69

   5.1 Base Waterfloods Without Bottom Water 69

5.2 Bottom Water: Water and Polymer Injection Runs 76

5.2.1 Effect of Water-to-Oil Zone Thickness and Permeability Ratio 76

5.2.2 Effect of Viscosity Ratio 96

5.2.3 Polymer Flood and Waterflood in a Homogeneous Pack 103

5.2.4 Effect of Polymer Injection Point 107

5.2.5 Effect of Polymer Slug Size and Viscosity 109

5.3 Mobility Control Mechanism with Polymer 126

5.4 Artificial Impermeable Barrier 129

5.4.1 Effect of Water-to-Oil Zone Thickness Ratio 129

5.4.2 Effect of Barrier Length 132

5.5 Emulsion Injection 135

5.5.1 Effect of Oil Content on Emulsion Blockage in the Presence of a Bottom-Water Zone 135

5.5.2 Emulsion Injection in a Homogeneous Pack 143

5.5.3 Effect of Oil-Water Thickness and Permeability Ratio 145

5.5.4 Effect of Viscosity Ratio on Emulsion Flood 164

5.5.5 Effect of Emulsion Slug Sizes 171

5.5.6 Mobility Control Mechanism with Emulsion Flood 180

5.6 Air Injection 182

5.6.1 Effect of Water-to-Oil Zone Thickness and Permeability Ratio 183

5.7 Biopolymer Gel Injection 199

5.8 Foam Injection Runs 205

5.8.1 Effect of Viscosity Ratio 211

5.8.2 Effect of Water-to-Oil Zone Thickness and Permeability Ratios 214

5.8.3 Effect of Waterflood on Foam Injection 227

5.9 Silica Gel Injection 230

5.9.1 Role of Carbon Dioxide in Mobility Control with Silica Gel 234

5.9.2 Effect of Water-to-Oil Zone Thickness and Permeability Ratio 236

6. EXPERIMENTAL RESULTS AND DISCUSSION 250

6.1 Waterflood 250

6.1.1 Waterflood in a Homogeneous Pack 250

6.1.2 Waterflooding in the Presence of a Bottom-Water Zone 253

6.1.2.1 Effect of Water-to-Oil Zone Thickness and Permeability Ratio 254

6.1.2.2 Effect of Viscosity Ratio 263

6.2 Waterflood with Polymer Slugs 265

6.2.1 Polymer Flood in a Homogeneous Pack ...266

6.2.2 Delay in Response 267

6.2.2.1 Mobility Control Mechanism with Polymer Flood...........271

6.2.3 Effect of Polymer Injection Point 280

6.2.3.1 Effect of Polymer Slug Size ..284

6.2.3.2 Effect of Polymer Viscosity ..289

6.2.3.3 Effect of Viscosity Ratio 292

6.2.3.4 Effect of Impermeable Barrier 295

6.2.3.5 Effect of Water-to-Oil Zone Thickness and Permeability Ratio 295

6.3 Effect of Impermeable Barrier 305

6.4 Waterflood with Emulsion Slugs 306

  6.4.1 Emulsion Stability 306

  6.4.2 Effect of Oil Content on Emulsion Blockage 308

  6.4.3 Emulsion Flood in Homogeneous Oil Reservoirs 312

  6.4.4 Emulsion Flood in the Presence of a Bottom-Water Zone 312

    6.4.4.1 Effect of Water-to-Oil Zone Thickness and Permeability Ratio 313

    6.4.4.2 Effect of Viscosity Ratio 326

    6.4.4.3 Effect of Emulsion Slug Size .329

  6.4.5 Mobility Control Mechanism with Emulsions 333

6.5 Waterflood with Air Injection 337

6.6 Injection of Biopolymer Gel 346

6.7 Foam Injection 347

  6.7.1 Flow of Foam in a Homogeneous Porous Medium 347

    6.7.1.1 Effect of Surfactant Concentration 347

    6.7.1.2 Effect of Injection Pressure .351

  6.7.2 Foam Flow in the Presence of a Bottom Water Layer 353

    6.7.2.1 Effect of Surfactant Concentration 353

    6.7.2.2 Effect of Viscosity Ratio 355

    6.7.2.3 Effect of Bottom-water Zone Permeability 357

    6.7.2.4 Effect of Water-to-Oil Zone Thickness Ratio 361

6.7.3 Effect of Waterflood on Foam 366

6.7.3.1 Mobility Control Mechanism with Foam 367

6.8 Carbon Dioxide-Activated Silica Gel Injection 369

6.8.1 Effect of CO_2 Injection 369

6.8.2 Effect of Water-to-Oil Zone Thickness and Permeability Ratio 370

6.9 Comparison of Different Mobility Control Agents 379

7. NUMERICAL SIMULATION 392

7.1 MODEL ASSUMPTIONS AND FORMULATION 392

7.1.1 Assumptions 393

7.1.1.1 Polymer Flow 393

7.1.1.2 Emulsion Flow 394

7.1.2 Formulation 394

7.1.3 Mechanisms and Evaluation of Properties 397

7.1.3.1 Fluid and Rock Properties 398

7.1.3.2 Relative Permeabilities 398

7.1.4 Computational Algorithm 401

7.1.5 Sensitivity Studies and Model Accuracy 406

7.2 Grid Sensitivity 407

7.3 History Matching 408

7.4 DISCUSSION OF RESULTS 409

7.4.1 Waterflood 410

7.4.2 Waterflood in a Homogeneous Core 411

7.4.3 Waterflood in the Presence of a Bottom-Water Zone 415

7.4.4 Polymer Flood and Waterflood 419

7.4.5 Polymer Flood in a Homogeneous Core with Irreducible Water Saturation 422

7.4.6 Polymer Flood in the Presence of a Bottom-Water Zone 425

7.4.6.1 Effect of Oil-Water Viscosity Ratio 433

7.4.6.2 Effect of Polymer Slug Size for $h_b/h_o=1$ 435

7.4.6.3 Effect of Polymer Slug Size for $h_b/h_o=0.2$ 436

7.4.6.4 Effect of Oil-Water Zone Permeability Ratio 438

7.4.7 Emulsion Flood 440

7.4.8 Continuous Emulsion Injection in a Homogeneous Porous Medium 443

7.4.9 Emulsion Flood in the Presence of a Bottom-Water Zone 446

7.4.9.1 Effect of Emulsion Slug Size for $k_o/k_b=2.67$ and $h_b/h_o=0.33$ 456

7.4.9.2 Effect of Oil-Water Zone Permeability Ratio 457

8. SCALING CRITERIA FOR POLYMER, EMULSION AND FOAM INJECTION 460

8.1 DEVELOPMENT OF THE SCALING CRITERIA 461

8.1.1 Polymer Flood 461

8.1.1.1 Boundary and Initial Conditions 462

8.1.1.2 Constitutive Relationships and Constraints 463

8.1.2 Emulsion Flood 464

8.1.3 Emulsion Flood: Two-Phase Flow 465

8.1.3.1 Boundary and Initial Conditions 466

8.1.3.2 Constitutive Relationships and Constraints 467

8.1.4 Emulsion Flood: Emulsion Miscible in Aqueous Phase Only 468

8.1.4.1 Boundary and Initial Conditions 468

8.1.4.2 Constitutive Relationships and Constraints 469

8.1.5 Emulsion Flood: Three-Phase Flow 470

8.1.5.1 Boundary and Initial Conditions 471

8.1.5.2 Constitutive Relationships and Constraints 472

8.1.6 Foam Injection 473

8.1.7 Foam Injection: Four-Phase Flow 473

8.1.7.1 Boundary and Initial Conditions 475

8.1.7.2 Constitutive Relationships and Constraints 477

8.1.8 Foam Injection: Three-Phase Flow 478

8.1.8.1 Boundary and Initial Conditions 480

8.1.8.2 Constitutive Relationships and Constraints 481

8.2 DIMENSIONLESS PROPERTIES AND CONDITIONS 482

8.2.1 Polymer Flood 482

8.2.2 Emulsion Flood: Two-Phase Flow 483

8.2.3 Emulsion Flood: Emulsion Miscible in Aqueous Phase Only 483

8.2.4 Emulsion Flood: Three-Phase Flow 483

8.2.5 Foam Injection: Four-Phase Flow 484

8.2.6 Foam Injectiion: Three-Phase Flow 485

8.3 DIFFERENT APPROACHES TO SATISFY THE SCALING CRITERIA 485

8.3.1 Polymer Flood 486

8.3.1.1 Approach #1 - Same Fluids, Different Porous Media, Different Pressure Drop, Geometric Similarity 486

8.3.1.2 Approach #2 - Same Fluids, Same Porous Medium, Same Pressure Drop, Geometric Similarity 487

8.3.1.3 Approach #3 - Same Fluids, Same Porous Medium, Same Pressure Drop, Geometric Scaling Relaxed 488

8.3.1.4 Approach #4 - Same Fluids, Same Porous Medium, Same Pressure Drop, Geometric Scaling Relaxed, Dispersion at High Flow Rate 490

8.3.1.5 Approach #5 - Same Fluids, Different Porous Media, Different Pressure Drop, Geometric Scaling Relaxed, Dispersion at High Flow Rate .491

8.3.2 Emulsion Flood: Two-Phase Flow 492

8.3.2.1 Approach #1 - Same Fluids, Different Porous Media, Different Pressure Drop, Geometric Similarity 492

8.3.2.2 Approach #2 - Same Fluids, Same Porous Medium, Same Pressure Drop, Geometric Similarity 493

8.3.2.3 Approach #3 - Same Fluids, Same Porous Medium, Same Pressure Drop, Geometric Scaling Relaxed 495

8.3.2.4 Approach #4 - Same Fluids, Same Porous Medium, Same Pressure Drop, Geometric Scaling Relaxed, Dispersion at High Flow Rate 496

8.3.2.5 Approach #5 - Same Fluids, Different Porous Media, Different Pressure Drop, Geometric Scaling Relaxed, Dispersion at High Flow Rate .497

8.3.3 Emulsion Flood: Emulsion Miscible in Aqueous Phase Only 498

8.3.3.1 Approach #1 - Same Fluids, Different Porous Media, Different Pressure Drop, Geometric Similarity 498

8.3.3.2 Approach #2 - Same Fluids, Same Porous Medium, Same Pressure Drop, Geometric Similarity 499

8.3.3.3 Approach #3 - Same Fluids, Same Porous Medium, Same Pressure Drop, Geometric Scaling Relaxed 500

8.3.3.4 Approach #4 - Same Fluids, Same Porous Medium, Same Pressure Drop, Geometric Scaling Relaxed, Dispersion at High Flow Rate 501

8.3.3.5 Approach #5 - Same Fluids, Different Porous Media, Different Pressure Drop, Geometric Scaling Relaxed, Dispersion at High Flow Rate .502

8.3.4 Emulsion Flood: Three-Phase Flow 503

8.3.4.1 Approach #1 - Same Fluids, Different Porous Media, Different Pressure Drop, Geometric Similarity 503

8.3.4.2 Approach #2 - Same Fluids, Same Porous Medium, Same Pressure Drop, Geometric Similarity 504

8.3.4.3 Approach #3 - Same Fluids, Same Porous Medium, Same Pressure Drop, Geometric Scaling Relaxed 504

8.3.4.4 Approach #4 - Same Fluids, Same Porous Medium, Same Pressure Drop, Geometric Scaling Relaxed, Dispersion at High Flow Rate 505

8.3.4.5 Approach #5 - Same Fluids, Different Porous Media, Different Pressure Drop, Geometric Scaling Relaxed, Dispersion at High Flow Rate .507

8.3.5 Foam Injection - Four-Phase Flow 508

8.3.5.1 Approach #1 - Same Fluids, Different Porous Media, Different Pressure Drop, Geometric Similarity 508

8.3.5.2 Approach #2 - Same Fluids, Same Porous Medium, Same Pressure Drop, Geometric Similarity 509

8.3.5.3 Approach #3 - Same Fluids, Same Porous Medium, Same Pressure Drop, Geometric Scaling Relaxed 510

8.3.5.4 Approach #4 - Same Fluids, Same Porous Medium, Same Pressure Drop, Geometric Scaling Relaxed, Dispersion at High Flow Rate 512

8.3.5.5 Approach #5 - Same Fluids, Different Porous Media, Different Pressure Drop, Geometric Scaling Relaxed, Dispersion at High Flow Rate .513

8.3.6 Foam Injection: Three-Phase Flow 514

8.3.6.1 Approach #1 - Same Fluids, Different Porous Media, Different Pressure Drop, Geometric Similarity 514

8.3.6.2 Approach #2 - Same Fluids, Same Porous Medium, Same Pressure Drop, Geometric Similarity 515

8.3.6.3 Approach #3 - Same Fluids, Same Porous Medium, Same Pressure Drop, Geometric Scaling Relaxed 516

8.3.6.4 Approach #4 - Same Fluids, Same Porous Medium, Same Pressure Drop, Geometric Scaling Relaxed, Dispersion at High Flow Rate 517

8.3.6.5 Approach #5 - Same Fluids, Different Porous Media, Different Pressure Drop, Geometric Scaling Relaxed, Dispersion at High Flow Rate .519

8.4 **Dimensional Analysis** 520

8.5 COMPARISON OF DIFFERENT SCALING APPROACHES ...522

8.5.1 Polymer Flood 522

8.5.2 Emulsion Flood 524

8.5.3 Foam Injection 525

9. SUMMARY AND CONCLUSIONS 527

10. REFERENCES 531

11. APPENDIX - A 543

11.1 DERIVATION OF THE FLOW EQUATION 543

11.1.1 Mass Balance 543

11.2 Finite Difference Equations 554

11.3 Solution Methods 557

11.4 Well Representation 558

11.4.1 Oil Production Rate Specified 558

11.4.2 Injection Rate Specified 559

11.4.3 Implicit Pressure Constraint Representation 560

12. APPENDIX-B 562

12.1 Governing Equations in Terms of Their Dimensionless Variables 562

12.1.1 Polymer Flood 562

12.1.2 Emulsion Flood 567

12.1.2.1 Emulsion Flood: Two-Phase Flow 567

12.1.2.2 Emulsion Flood: Emulsion Miscible in Aqueous Phase Only 572

12.1.2.3 Emulsion Flood: Three-Phase Flow 574

12.1.3 Foam Injection 575

12.1.3.1 Foam Injection: Four-Phase Flow 575

12.1.3.2 Foam Injection: Three-Phase Flow 585

LIST OF TABLES

TABLE		PAGE
4.1	Properties of Oils Used in Different Runs	65
5.1	Characteristics and Results of Different Experimental Runs	71
5.2	Results of Polymer Injection Runs	111
5.3	Results of Emulsion Injection Runs	139
5.4	Results of Foam Injection Runs	206
5.6	Results of Silica Gel Injection Runs	231
6.1	Breakthrough Recovery and Instability Numbers for Waterflood Runs	252
6.2	Results of Waterflood Runs	254
7.1	Grid Size Sensitivity for Waterflood, Polymer flood and Emulsion flood simulation Runs	408
7.2	Characteristics of Experimental Runs Chosen for Numerical Simulation	410
8.1	List of variables considered for dimensional analysis	521

LIST OF FIGURES

FIGURE		PAGE
1	Experimental Set-up	63
2	Characteristics of Experimental Runs Conducted	70
3a	Recovery Performance for Run 1	74
3b	Recovery Performance for Run 2	76
4	Recovery Performance for Run 3	78
5	Recovery Performance for Run 4	81
6	Recovery Performance for Run 5	83
7	Recovery Performance for Run 6	86
8	Recovery Performance for Run 7	88
9	Recovery Performance for Run 8	90
10	Recovery Performance for Run 9	93
11	Recovery Performance for Run 10	95
12	Recovery Performance for Run 11	98
13	Recovery Performance for Run 12	100
14	Recovery Performance for Run 13	102
15	Recovery Performance for Run 14	105
16	Recovery Performance for Run 15	107
17	Recovery Performance for Run 16	109
18	Recovery Performance for Run 17	112
19	Recovery Performance for Run 18	115
20	Recovery Performance for Run 19	116
21	Recovery Performance for Run 20	118
22	Recovery Performance for Run 21	120
23	Recovery Performance for Run 22	122

24 Recovery Performance for Run 23 125
25 Recovery Performance for Run 24 128
26 Recovery Performance for Run 25 130
27 Recovery Performance for Run 26 132
28 Recovery Performance for Run 27 133
29 Recovery Performance for Run 28 134
30 Recovery Performance for Run 29 137
31 Recovery Performance for Run 30 141
32 Recovery Performance for Run 31 145
33 Recovery Performance for Run 32 147
34 Recovery Performance for Run 33 151
35 Recovery Performance for Run 34 153
36 Recovery Performance for Run 35 157
37 Recovery Performance for Run 36 159
38 Recovery Performance for Run 37 162
39 Recovery Performance for Run 38 164
40 Recovery Performance for Run 39 165
41 Recovery Performance for Run 40 168
42 Recovery Performance for Run 41 170
43 Recovery Performance for Run 42 172
42 Recovery Performance for Run 43 175
45 Recovery Performance for Run 44 177
46 Recovery Performance for Run 45 179
47 Recovery Performance for Run 46 181
48 Recovery Performance for Run 47 185
49 Recovery Performance for Run 48 187

50	Recovery Performance for Run 49	190
51	Recovery Performance for Run 50	191
52	Recovery Performance for Run 51	194
53	Recovery Performance for Run 52	197
54	Recovery Performance for Run 53	199
55	Recovery Performance for Run 54	201
56	Recovery Performance for Run 55	204
57	Recovery Performance for Run 65	208
58	Recovery Performance for Run 66	209
59	Recovery Performance for Run 67	210
60	Recovery Performance for Run 68	212
61	Recovery Performance for Run 69	214
62	Recovery Performance for Run 70	216
63	Recovery Performance for Run 71	219
64	Recovery Performance for Run 72	220
65	Recovery Performance for Run 73	222
66	Recovery Performance for Run 74	224
67	Recovery Performance for Run 75	226
68	Recovery Performance for Run 76	229
69	Recovery Performance for Run 77	233
70	Recovery Performance for Run 78	235
71	Recovery Performance for Run 79	228
72	Recovery Performance for Run 80	240
73	Recovery Performance for Run 81	242
74	Recovery Performance for Run 82	244
75	Recovery Performance for Run 83	246

76 Recovery Performance for Run 84 247

77 Recovery Performance for Run 85 249

78 Comparison of Waterflood Recovery for Different h_b/h_o and $k_o/k_b=1$ 255

79 Comparison of Waterflood Recovery for Different h_b/h_o and $k_o/k_b=0.06$ 257

80 Comparison of Waterflood Recovery for Different h_b/h_o and $k_o/k_b=2.67$ 258

81 Waterflood Performance as a Function of k_o/k_b and h_b/k_o 260

82 Comparison of Waterflood Performance as a Function of h_b/h_o and $k_o/k_b=1$ 262

83 Waterflood Recovery for Different h_b/h_o and k_o/k_b 263

84 Effect of Oil-Water Viscosity Ratio on Waterflood Recovery 264

85 Delay in Recovery Response (% PV) as a Function of h_b/h_o and k_o/k_b 268

86 Delay in Recovery Response (% PV_b) as a Function of h_b/h_o and k_o/k_b 270

87 Comparison of Oil Recovery by Polymer and Glycerine Injection 273

88 Relative Contribution of Different Mechanisms Involved in Polymer Flooding 274

89 Polymer Breakthrough as a Function of Slug Volume 276

90 Viscosity (in mPa.s) of the Effluent Aqueous Phase After Polymer Breakthrough 279

91 Comparison of Oil Recoveries for Different Polymer Injection Points 282

92 Effect of Polymer Slug Size on Ultimate Oil Recovery 285

93 Effect of Polymer Slug Size on Oil Recovery 288

94 Effect of Polymer Viscosity on Ultimate Oil Recovery 290

95 Effect of Oil-Water Viscosity Ratio on Oil Recovery 293

96 Comparison of Oil Recoveries for Different h_b/h_o and k_o/k_b=1.0 (Polymer Flood) 296

97 Comparison of Oil Recoveries for h_b/h_o and k_o/k_b=0.06 (Polymer Flood) 297

98 Comparison of Oil Recoveries for h_b/h_o and k_o/k_b=2.67 (Polymer Flood) 298

99 Polymer Flood Performance as a Function of k_o/k_b and h_b/h_o 300

100 Polymer Flood Performance as a Function of k_o/k_b and h_b/h_o 301

101 Comparison of Polymer Flood with Waterflood 303

102 Improvement Over a Waterflood for Different Polymer Flood Runs 304

103 Effect of Surfactant Concentration on Emulsion pH Stability 307

104 Effect of Oil Content on Emulsion Blockage 311

105 Comparison of Oil Recoveries for Different h_b/h_o and k_o/k_b=1.0 (Emulsion Flood) 315

106 Comparison of Oil Recoveries for h_b/h_o and k_o/k_b=0.06 (Emulsion Flood) 316

107 Comparison of Oil Recoveries for h_b/h_o and k_o/k_b=2.67 (Emulsion Flood) 317

108 Delay in Recovery Response for Emulsion Flood Runs 318

109 Emulsion Flood Performance as a Function of k_o/k_b and h_b/h_o 320

110 Emulsion Flood Performance as a Function of k_o/k_b and h_b/h_o 322

111 Comparison of Emulsion Flood with Waterflood 324

112 Improvement Over a Waterflood for Different Emulsion Flood Runs 326

113 Effect of Oil-Water Viscosity Ratio on Emulsion Flood Runs 328

114 Effect of Emulsion Slug Size on Emulsion Flood Performance 330

115 Effect of Emulsion Slug Size on Ultimate Oil Recovery 332

116 Relative Contribution of Different Mechanisms in Emulsion Flooding 334

117 Emulsion Breakthrough as a Function of k_o/k_b and h_b/h_o 336

118 Comparison of Oil Recoveries for Different h_b/h_o and $k_o/k_b=1.0$ (Air Injection) 339

119 Comparison of Oil Recoveries for h_b/h_o and $k_o/k_b=2.67$ (Air Injection) 340

120 Air Injection Performance as a Function of k_o/k_b and h_b/h_o 341

121 Air Injection Performance as a Function of k_o/k_b and h_b/h_o 343

122 Comparison of Air Injection with Waterflood 344

123 Improvement Over a Waterflood for Different Air Injection Runs 345

124 Effect of Surfactant Concentration on Foam Injection Performance $h_b/h_o=0$) 348

125 Contribution of Air and Foam in Oil Recovery for $h_b/h_o=0$ 351

126 Effect of Injection Pressure on Foam Injection Performance for $h_b/h_o=0$ 352

127 Effect of Surfactant Concentration on Foam Injection Performance for $h_b/h_o=0.33$ 354

128 Effect of Oil-Water Viscosity Ratio on Oil Recovery (Foam Injection) 356

129 Foam Injection Performance as a Function of k_o/k_b and h_b/h_o 358

130 Foam Injection Performance as a Function of k_o/k_b and h_b/h_o 362

131 Comparison of Foam Injection with Waterflood 363

132 Improvement Over a Waterflood for Different Foam Injection Runs 365

133 Relative Contribution of Different Chemicals in Foam Injection 368

134 Comparison of Oil Recoveries for Different h_b/h_o and $k_o/k_b=1.0$ (Silica gel) 371

135 Comparison of Oil Recoveries for h_b/h_o and $k_o/k_b=0.06$ (Silica gel) 372

136 Comparison of Oil Recoveries for h_b/h_o and $k_o/k_b=2.67$ (Silica gel) 373

137 Silica Gel Inj. Performance as a Function of k_o/k_b and h_b/h_o 374

138 Silica Gel Inj. Performance as a Function of k_o/k_b and h_b/h_o 376

139 Comparison of Silica Gel Inj. with Waterflood 378

140 Improvement Over a Waterflood for Different Silica Gel Inj. Runs 379

141 Comparison of Oil Recoveries with Different Recovery Procedures for k_o/k_b of 1.0 380

142 Comparison of Oil Recoveries with Different Recovery Procedures for k_o/k_b of 2.67 381

143 Comparison of Oil Recoveries with Different Recovery Procedures for k_o/k_b of 0.06 382

144 Effect of Oil-Water Viscosity Ratio on Oil Recoveries with Different Procedures 385

145 Comparison of Different Mobility Control Agents for k_o/k_b of 1.0 388

146 Comparison of Different Mobility Control Agents for k_o/k_b of 2.67 389

147 Comparison of Different Mobility Control Agents for k_o/k_b of 0.06 390

148 Flow Chart of Computational Algorithm 405

148 Continued 406

149 Oil/Water Capillary Pressure Curve Used for Simulation 412

150 Comparison of Oil/Water Relative Permeability Curves (JBN and Trial-and Error) 413

151 Comparison of Experimental and Numerical Results with Waterflood for $h_b/h_o=0$ (Run 14) 414

152 Comparison of Experimental and Numerical Results with Waterflood for Run 4 416

153 Comparison of Experimental and Numerical Results with Waterflood for $h_b/h_o=1.0$, $k_o/k_b=2.67$ (Run 7) 418

154 Comparison of Experimental and Numerical Results with Waterflood for $h_b/h_o=0.33$, $k_o/k_b=2.67$ (Run 6) 419

155 Relative Permeability to Different Phases After and Before Polymer Flooding 423

156 Comparison of Experimental and Numerical Results for Run 15 ($h_b/h_o=0.$) 424

157 Comparison of Experimental and Numerical Results for Run 19 427

158	Comparison of Experimental and Numerical Results for Run 18	428
159	Comparison of Experimental and Numerical Results for Run 16	430
160	Comparison of Experimental and Numerical Results for Run 17	431
161	Comparison of Experimental and Numerical Results for Run 22	433
162	Comparison of Polymer Floods for Different Oil-Water Viscosity Ratio (h_b/h_o=0.33, k_o/k_b=1.0)	435
163	Effect of Slug Size on Polymer Flood Recovery for h_b/h_o=1.0 and k_o/k_b=1.0	436
164	Effect of Slug Size on Polymer Flood Recovery for h_b/h_o=0.2 and k_o/k_b=1.0	438
165	Effect of k_o/k_b on Polymer Flood Recovery for h_b/h_o=0.33	439
166	Relative Permeability to Each Phase in Oil/Water/Emulsion System	443
167	Correlation of Permeability Reduction with Emulsion	445
168	Comparison of Experimental and Numerical Results for Run 31 (h_b/h_o=0)	446
169	Comparison of Experimental and Numerical Results for Run 30	448
170	Comparison of Experimental and Numerical Results for Run 42	449
171	Comparison of Experimental and Numerical Results for Run 45	451
172	Comparison of Experimental and Numerical Results for Run 34	453
173	Comparison of Experimental and Numerical Results for Run 36	454
174	Comparison of Experimental and Numerical Results for Run 32	455

175 Comparison of Oil Recoveries for Different Slug Sizes (h_b/h_o=0.33, k_o/k_b=2.67) 457

176 Comparison of Oil Recoveries for Different k_o/k_b for h_b/h_o=0.33 459

A-1 Control Volume for the Mass Balance 544

NOMENCLATURE

A_{inj}	Area open for flow in an injection or producer well
A_p	$B \cdot C_{rp}^*$
B	K_1/K_2
bt	Breakthrough
C_{ij}	Concentration of component j in phase i
C_{rp}	Amount of polymer adsorbed per unit mass of rock
C_{rp}^*	Maximum adsorptive capacity of rock
D^*	Molecular diffusion coefficient
D_T	Transverse hydrodynamic dispersion coefficient
D_L	Longitudinal hydrodynamic dispersion coefficient
D_i	Convective dispersion tensor for i phase
D_{ij}^*	Molecular diffusion tensor for component j in phase i
D_{ij}	Hydrodynamic dispersion tensor for component j in phase i
d	Diameter of the polymer coil
d_g	Grain diameter
d_p	Mean particle diameter in the porous medium
F	Formation electric resistivity factor
g	Acceleration due to gravity
GLR	Gas-liquid ratio
GOR	Gas-oil ratio
h_o	Height of the oil zone

h_b	Height of the bottom-water zone
h_w	Depth of the injection well
H	Height or thickness of the reservoir or model
I_{sr}	Instability number for a rectangular system
IOIP	Initial oil in place
k_o	Absolute permeability to the oil zone
k_b	Absolute permeability to the bottom water zone
k_{or}	Effective permeability to oil at irreducible water saturation
k_{ro}	Relative permeability to oil
k_{rp}	Relative permeability to polymer
k_{rw}	Relative permeability to water
k_{wr}	Effecttive permeability to water at irreducible oil saturation
K	Absolute permeability
K_i	Effective permeability to phase i
K_1	Kinetic rate constant for adsorption m^3/kg-day
K_2	Kinetic rate constant for adsorption kg/kg-day
L	Length of the reservoir of model
P_{cij}	Capillary pressure for phases i and j
PV	Pore volume
PV_b	Pore volume of the bottom-water zone
R_{ij}	Solubility of phase j in phase i
S	Slug size in PV
S_i	Saturation of i phase
S_{wi}	Irreducible water saturation
t	Time

v,V	Superficial velocity
W	Width of the reservoir or model
W_{ij}	Injection rate of component j in i phase
WOR:	Water-oil ratio
x_i	Cartesian coodinates
y	Cartesian Coordinate
z	Elevation of reservoir above a datum
ϕ	Porosity of reservoir
ρ_i	Density of i phase
μ_i	Viscosity of i phase
σ_e	Effective pseudointerfacial tension
χ	Inhomogeneity factor

Subscripts

a	aqueous phase
D	dimensionless quantity
f	foam phase
g	gas phase
inj	located at the injection well
i	initial
l	oleic phase
m	emulsion phase or component
N	nitrogen component
n	normal to the boundary
o	component oil
p	polymer

prod	located at the producer well
R	reference quantity
r	reservoir rock
s	surfactant
w	component water

1. INTRODUCTION

Many reservoirs in Alberta and Saskatchewan contain some type of high water saturation zone underlying the oil reservoir. Such reservoirs show rather poor performance under a conventional waterflood. However, the medium to light gravity of the reservoir oil and the plant facilities often dictate that waterflooding is the most suitable technique for these reservoirs. Therefore, there is a need to develop techniques that will improve the performance of a waterflood in such reservoirs. This problem has received attention for more than two decades and several techniques have been proposed in the literature to control the mobility of the injected water or gas. But, none of the previous studies reports a systematic study of all these mobility control agents tested in a reservoir model. Besides, few techniques have been tested specifically for bottom water. With these ideas in view, the first objective of this research is to screen a variety of techniques to waterflood an oil reservoir with a bottom-water zone using polymer, emulsion, biopolymer, air, silica gel, and foam as mobility control agents in various slug sizes and to study the effect of permeability contrast, relative oil-water layer thickness, oil viscosity, injection rate, slug size and use of an artificial barrier.

A mechanistic understanding of oil displacement by a waterflood in the presence of a mobility control agent is the basis for predicting field performance. The petroleum engineering industry relies heavily on fully compositional models to acquire this mechanistic understanding. These models should be capable of predicting performance of laboratory-scale displacements. The results of such predictions will identify important variables that control oil recovery and that must be incorporated in field simulators. Further, confidence in field models will be enhanced greatly by the demonstrated ability to predict laboratory floods. However, in the case of a waterflood with additives, the inclusion of various complex phenomena specific to the mobility control agent used is required. Such a treatment needs a great deal of phase and fluid-property data, and even after a tedious treatment one has to depend on empiricism for simulating additional effects like mechanical entrapment, instability in displacement, non-Newtonian flow, etc. Besides, no attempt to numerically simulate emulsion flood in the presence of oil and water has been reported. Therefore, there is a need to develop a new model for some of these additives using a simplified approach in the face of limited mechanistic information. Such an approach is the second objective of this research. New mathematical reservoir models were developed for polymer and emulsion floods.

It is well known that in order to scale up laboratory experiment results for field applications the laboratory model has to be mechanistically scaled. Even though the scaling criteria of a waterflood are well-established, most of these scaling criteria are not applicable if one considers the use of additives as mentioned above. Scaling criteria for these cases are not available. In the past, most of the laboratory experiments with polymer, emulsion and foam have been performed in unscaled or partially scaled models. This is due to the lack of scaling criteria for processes employing emulsion, polymer or foam. Therefore, starting from governing flow equations, new scaling criteria are derived for polymer, emulsion and foam flood experiments, and situations where, by relaxing the requirement of geometric similarity, the same fluid and the same porous media can be used, are discussed.

2. LITERATURE REVIEW

There have been numerous laboratory model studies investigating the effect of various parameters on oil recovery from stratified reservoirs. It is well known that such reservoirs show rather poor performance under conventional waterflooding. Moreover, the presence of bottom water, as reported to be present in many cases, often aggravates the situation due to high producing water-oil ratios. As a consequence, starting from the early sixties, many techniques have been proposed to improve waterflood performance in stratified reservoirs with bottom water.

2.1 STRATIFIED RESERVOIR MODELS

Henley et al.(1961) investigated the effects of well spacing, fluid mobilities, rate of production, capillary and gravity forces, well penetration and well completion techniques on the oil recovery performance in a scaled model of a bottom water drive. They conducted displacement tests for different effective interwell distance to the oil-zone thickness ratios and showed that this ratio plays an important role in determining oil recovery for certain producing water-oil ratios. They observed that extremely high-capacity, large radius fractures at the top of the productive zone result in greatly improved sweep efficiencies. However, fractures that are practically obtainable did not have any appreciable impact on recovery.

In another test, they placed an impermeable pancake barrier at the bottom of the well. This increased to some extent the oil recovery efficiency both at water breakthrough and at high water-oil ratios. They observed a very poor breakthrough recovery for a 12:1 ratio of inter-well distance to reservoir thickness.

Barnes(1962) studied waterflood efficiency in reservoir models with a bottom-water layer. He used a scaled model to observe the improvement in waterflooding efficiency with a miscible viscous water slug (viscosity of water being increased by adding some miscible additives). In order to create a bottom-water layer, he injected water through an inlet end close to the bottom of the oil-saturated core at a very slow displacement rate. He observed that for conventional waterflooding a considerable amount of displaced fluid was left unswept at the end of the run. He showed that the injection of a viscous water slug decreased the underrunning of the displacing fluid. The best performance was observed when viscous water was injected continuously. He also observed that an increase in injection rate, regardless of the type of displacing fluids used, increased volumetric sweep.

Fitch and Griffith(1964) conducted an experimental and mathematical investigation of some factors controlling miscible flood performance. They observed that alternate gas-water injection behind a miscible front significantly improved miscible flood performance, both within a single layer and in multi-layer reservoirs. In an effort to explore possible methods of improving flooding efficiency, they concluded that an economically optimal solvent volume would probably be the one that will not support miscibility throughout the reservoir. They also observed that preinjection of a small volume of water ahead of the solvent can improve the distribution of solvent in a stratified system.

Khan and Caudle(1969) investigated oil production performance of thin-oil-column type reservoirs producing by natural water drive. They used a scaled model to show that greater recovery of oil resulted for lower production rates, mobility ratio across the moving boundary, water-sand thickness, and mobility ratio across the fixed boundary or residual oil saturation in the water-invaded region of oil sand.

In an effort to study water coning, Khan(1970) used a scaled layered model. He modeled the oil zone using graded sand consolidated with epoxy resin, and the water zone with unconsolidated sands of different mesh sizes. The consolidated sand was prepared by pouring loose sand into the aquifer space. Therefore, the producing well was placed on the underside, and simulated fluid densities were also reversed to obtain the proper gravitational gradient. The model had provision for changing the thickness of aquifer space. He observed that the mobility ratio had a great influence on the water cut and the degree of water coning for a given production rate.

Mungan(1979) used a cylindrical layered model to study the effect of coning. The fluids were injected from the bottom. He observed a substantial decrease in oil recovery due to the existence of coning for an oil viscosity as low as 13 mPa.s. In his experiment, the tighter layers appeared to have higher water saturations at the time ~~of~~ breakthrough. He attributed this to a higher imbibition rate in the tighter region. He also used 0.10 PV of 1000 ppm of polymer solution. Even though cumulative oil produced was higher in the case of polymer, breakthrough occurred earlier and the water-oil ratio remained higher. He explained this phenomenon in terms of viscous fingering and recommended that a larger polymer bank be used for the case of active bottom-water drive reservoirs. He also observed that high viscosity and high production rate led to lower oil recovery and a higher water-oil ratio.

2.2 MOBILITY CONTROL IN WATERFLOODING

In order to improve the performance of a waterflood in a heterogeneous reservoir there have been numerous proposals of different techniques. These include: use of chemicals, such as polymers, use of an emulsion in the high permeability layer, use of various gelling agents with an activator following, etc. These techniques will be discussed in the following sections.

2.2.1 Mobility Control with Polymer Slugs

One of the oldest techniques for mobility control is the use of a polymer slug that is followed by a waterflood. In the rest of this chapter a review of polymer solution injection techniques will be presented.

Pye(1964) showed that a polyacrylamide solution could radically increase waterflood oil recovery. He recognized the resistance property of the polymer and quantified it as "resistance factor". This "resistance factor" was defined as:

$$R = \left(\frac{k_b}{\mu_w}\right)/\left(\frac{K_p}{\mu_p}\right) \qquad (2.1)$$

where k_b and K_p are effective permeabilities of water and polymer, respectively, and μ_p is the apparent viscosity of the polymer solution in the core. Here it is assumed that the absolute permeability remains invariant even with polymer flow. He also observed that the maximal departure of the apparent polymer viscosity occurred at low concentrations and at higher concentration the effect was approximately proportional to the solution viscosity. He suggested that a high core flooding rate should be avoided in order to keep the resistance factor constant.

Sandiford(1964) concluded that a polymer flood increased oil recovery by improving sweep efficiency as well as microscopic displacement efficiency. He observed a 15-20 percent (of the IOIP) increase for polymer floods over ordinary waterfloods at a water-oil ratio of 10. One of his interesting observations was that a polymer flood led to a significant increase in oil recovery for linear sandpacks that contained layers of different permeabilities. He cited several field examples where the injection of polyacrylamide solution improved oil recovery.

Burcik(1965) reported a substantial decrease in permeability after a polymer flood. He concluded that this decrease was due to strong adsorption of the polymer as well as mechanical entrapment.

Mungan et al.(1966) studied the nature of polymer floods in porous media by consecutive flow tests with brine, filtered polymer solution and brine at the same flow rate. Therefore, any change in pressure would indicate a change in mobility. In order to determine adsorption, they employed both static and dynamic methods. Polymer concentration was determined from the viscosity. They observed that the shear dependence and apparent viscosity increased with concentration and polymer molecular weight. Also, the viscosity and shear dependence decreased upon addition of salt because of the neutralization of electrical charge within the molecules by the oppositely charged ions of the salt. They observed higher permeability reduction for smaller pore openings and higher polymer molecular weight. This permeability reduction was attributed to adsorption and mechanical entrapment. They also used watered-out and previously unflooded Berea core containing 12 mPa.s refined oil for conducting polymer floods. They observed that the additional oil was recovered sooner if polymer injection was initiated early in the flood.

Pasini(1966) reported oil recovery tests using polymer solutions. He observed an increase in the recovery of low-viscosity oils from low-permeability sands.

In an effort to understand polymer solution flow in porous media, Gogarty(1967) performed displacement tests in cores of zero oil saturation. He reported a considerable decrease in permeability when a polymer solution was used to displace water in a core. The permeability could be restored to 80 percent of the original value by flushing the core with water. He postulated that the permeability reduction was due to plugging of smaller pores and polymer retention due to adsorption. He observed that the degree of permeability reduction was higher when low permeability cores or high viscosity polymer solution was used.

Dauben and Menzie(1967) used polyethylene oxides and reported a "dilatant" rather than pseudo-plastic flow behaviour. Unlike previous researchers, they observed unexpectedly high flow resistance that was a function of flow rate, pore-size, polymer molecular weight and concentration. They showed that the apparent viscosity of a polymer solution approached the solution viscosity at very low flow rates and increased as the flow rate increased (similar to a dilatant fluid). From this, they concluded that polymer flooding did not affect the absolute permeability as opposed to what was observed by Gogarty(1967). They attributed the high flow resistance of polyethylene oxide solutions to the effects created by viscoelastic effects. They also found that the apparent viscosity of polymer solutions increased with an increase of polymer molecular weight and decrease in pore-size.

Sherborne et al.(1967) recognized, as did Pye(1964) and Sandiford(1964), that the polymer solution is a more effective flooding agent than other viscous fluids (such as sugar solution) due to "abnormal flow resistance", not predictable from viscosity considerations alone. They observed that the presence of interstitial water helped the displacement efficiency by a waterflood as it established the water flow channels rather uniformly. However, opposite behaviour was observed when a polymer flood was used.

At high rates of flow, another effect was observed first by Burcik(1967) and then by Burcik and Ferrer(1968). It was found that dilute solutions of partially hydrolyzed polyacrylamides are pseudo-dilatant. In other words, the solution viscosity increases with increasing rate of flow when flow occurs through porous media containing adsorbed polymer. This effect, therefore, helps in causing more even flood-out from a group of parallel beds with different permeabilities. A possible explanation of this pseudo-dilatancy was given by saying that the polymer molecules retained in the flow channels tend to uncoil under the imposed velocity gradients. They argued that polymer molecules, having a diameter twenty times less than that of a typical pore channel, would be able to lower the water permeability and also cause pseudo-dilatant flow because of the microgels associated with polymer solutions. They showed that when millipore filters are used to partially remove the microgels, the resulting polymer solution would show a much lower resistance factor than the original solution.

Harrington and Zimm(1968) attributed persistent reduction of the permeability of a porous medium to chemical adsorption. They observed that no such reduction took place in straight capillaries. This would, thus, indicate that the structure as well as the pore size of the medium is important.

Mungan(1969) conducted displacement tests in Berea sandstone cores as well as in Hele-Shaw models. He observed very little improvement in microscopic efficiency by polymer flooding. By comparing with sucrose, he showed that a considerable amount of polymer is adsorbed by the solid surface of the porous media. This adsorption would not only cause loss of polymer but would also decrease recovery efficiency by a polymer flood. He also compared the slug process with the so-called "programmed slug process". In the latter procedure, after injecting a constant concentration polymer slug for a given time, he injected polymer solution with continually decreasing concentration. Even though the total volume of polymer was the same, a five percent increase in oil recovery was observed by this technique.

Smith(1970) investigated the effect of polymer molecular weight, rock and fluid properties, flow rate and temperature on polymer solution properties. He reported that the polymer flow led to a permanent reduction in the permeability to brine, even after flushing the core with tens and hundreds of pore volumes. However, this reduction was less for the lower molecular weight polymer and low flow rate of polymer flooding. He observed the dilatant nature (increased apparent viscosity with increasing flow rate) of polymer solutions when the flow rate was greater than 3.05 m/D. He contended that the pseudoplastic nature of the polymer would appear at lower flow rates and higher concentrations. He reconfirmed the previous observation that the lower the initial permeability, the greater the permeability loss.

Harvey and Menzie(1970) described a technique for analysis of rate-dependent effects in the polymer solution flow through unconsolidated porous media. Similarly to previous researchers, they observed that high flow rate increases the resistance to flow which might be due to the fact that polymer molecules are uncoiled by high flow rate and thereby impede the movement of the fluid, or due to simple viscoelastic effects as previously observed by Dauben(1967).

Desremaux et al.(1971) observed for single-phase flow that the curve representing mobility reduction for stabilized flows versus rate showed a minimum for a rate of approximately one metre per day. They observed that while polymer flooding porous media, if the velocity is increased the concentration increased gradually. Also, when the flooding was stopped for a while and restarted it resulted in higher concentration than that of the polymer solution injected. This concentration then decreases slowly until a concentration equal to that of the injected fluid was obtained. Based on these tests, they came to the conclusion that the mobility reduction is not only a function of the flow rate, but depends also on the interaction between polymer and the rock; and as this interaction is rather slow the rheology of the polymer solution at a certain moment depends on the flow history. They also concluded that the mobility reduction by injection of polymer solution was a function of flow rate and no simplistic relation may be obtained between the flow rate and the mobility reduction. As observed by some of the previous authors, they confirmed that for low flow rates, the mobility reduction decreased with increasing flow rate, whereas for high flow rates the reverse phenomenon took place.

Jennings et al.(1971) carried out a detailed study of the correlation of rheological properties of polymers with their behaviour under reservoir flow conditions. They obtained a correlation between the effects produced by certain polymer solutions at low rates and at very high flow rates in porous media. They argued that the similarity between high flow rate behaviour of the polymer solutions in orifices, screens, and sandstone should imply that this effect is due to solution properties rather than polymer retention as postulated by Burcik(1967) and Burcik and Ferrer(1968). They observed that the permeability alteration effect appeared to be rate-dependent below that flow rate at which viscoelastic effects become evident, and a single value for permeability reduction can be used. (This was done by Gogarty(1967)). Contrary to Smith(1970), they found that permeability changes took place once the core was polymer flooded. They also observed that the effectiveness of the polymer decreased as the size of the pore or the permeability increased. They concluded, as did Mungan et al.(1966), Smith(1970), and Mungan(1969), that decreasing adsorption of polymers would increase the effectiveness of a polymer flood.

Dawson and Lantz (1972) observed earlier breakthrough of polymers in the flow of polyacrylamide solutions through Berea sandstone cores. They explained this behaviour by inaccessible pore volume. They indicated that solutions of partially hydrolyzed polyacrylamide did not flow through all of the pore volume in a porous medium and introduced the concept of the inaccessible pore volume, defined as the pore space occupied by water that contains no polymer, but is in equilibrium with the polymer solution. Inaccessible pore volume may consist of pores that are too small to permit entry of polymer molecules and pores plugged by polymer molecules, as well as the hydrodynamic volume occupied by polymer adsorbed on the surface of the porous medium or retained in the pore space. They, thereby, suggested that the effective polymer porosity be used instead of total porosity as a multiplier of the time derivative of fluid concentration. They argued that the inaccessible pore volume would have a favourable impact in field displacements as polymer response would be felt by the production wells sooner than expected.

Maerker(1973) observed an intense flow rate dependence on adsorption of polymer in flow experiments on a Berea core (121 md) for 500 ppm polysaccharide in 2 percent NaCl solution. He showed that an increase in flow rate would result in increased adsorption of polymer molecules. He explained the effect of velocity in terms of molecular relaxation. It was observed that there was a sharp increase in effluent concentration when the flow was resumed after 16 hours. He also studied the shear degradation of hydrolyzed polyacrylamide by measuring the shear viscosities before and after flow through sandstone plugs. He observed that the degree of degradation was higher with larger dimensionless flow distance, i.e., the length of the core divided by the average sand grain diameter. Besides, higher degradation took place for lower permeabilities.

Knight (1973) observed the degradation of partially hydrolized acrylamide in the presence of oxygen. He concluded that dissolved oxygen in solution promoted degradation of polymer molecules.

Szabo(1975a,b) performed displacement tests in order to obtain an optimal polymer concentration while polymer flooding a porous medium. He also investigated the effect of salinity and observed polymer flood performance in stratified reservoir models. He measured the polymer concentration by the use of radioactive tracers. He observed that both increasing polymer concentration and decreasing salinity gave better recovery only for low volumes of injected fluid. Also, the effect of viscosity was strongly reduced for higher polymer viscosity (high viscosity due to either higher concentration or lower salinity). He also observed the effect of initial water saturation. He concluded that the amount of oil recovered was less in the case of polymer injection at a later stage than if polymer injection took place at irreducible connate water saturation. When he used a stratified reservoir model, he observed significantly higher recovery than what one would expect from theoretical considerations. In this sense, crossflow between different layers enhanced the mechanism of maintaining a high polymer concentration in the high permeability zone. He showed experimentally that mechanical entrapment plays a more important role in low-permeability than in medium- and high-permeability formation.

Sparlin(1976) used a vertical rectangular model to study the effect of polyacrylamide at the interface of an oil-water contact. The model consisted of an epoxy-coated Berea core held vertically with a one-inch-deep perforation drilled in the midpoint of one side and headers at the top, bottom and side. An irreducible water saturation was established at the top by injecting diesel oil from the top and letting it come out from the perforation. After establishing an irreducible water saturation in the top half, the whole core was treated with six pore volumes of polymer solution dissolved in two percent KCl, and then was overflushed with one pore volume of two percent KCl solution and shut-in overnight. He observed that after this treatment the oil permeability of the top half did not have any significant change whereas there was a significant decrease in water permeability in the water-saturated zone. He observed this same phenomenon in unconsolidated sandpacks and calcium carbonate cores as well. He also observed that higher concentrations had greater effect on reducing water permeability. He attributed this effect to a greater thickness of the film adsorbed on the sand grains, since polymer viscosity should not play any role after the pack is washed several times.

Thomas(1976) performed experiments in glass capillary arrays and observed an adsorbed layer of polymer on the capillary wall. He found that the thickness of the adsorbed surface was independent of pore size for pores with diameters larger than three to four times the average molecular diameter of the polymer solution. He therefore concluded that, for consolidated cores, permeability reduction would be the combined result of an adsorbed polymer layer on the pore walls and mechanical entrapment in small pores and constrictions. One of his important observations was that the thickness of the adsorbed polymer surface did not change significantly with flow rate.

Dabbous(1977) studied flow of polymer at waterflood residual oil saturations in advance of a miscible fluid slug and the interactions between the preinjected polymer and a subsequent micellar flood system. He observed a considerably higher resistance and residual resistance factor at residual oil saturation than those measured for the same rock at 100 percent water saturation. This was explained to be due to the fact that the effective pore aperture available for polymer flow was smaller in the presence of an oil saturation than in 100 percent water saturation.

Dominguez and Willhite(1977) used compacted Teflon powder as a porous medium in order to study the effect of mechanical entrapment in polymer flooding. They observed that polymer retention was affected by flow rate, increasing with flow rate. However, a decreased flow rate led to the expulsion of a part of the retained polymer. They reported that the rate of mechanical entrapment was a function of polymer concentration. Even though the mechanical entrapment in the Teflon core led to polymer retention of a quantity comparable to that of porous media, the resistance factors in the Teflon cores were lower than those reported for natural cores by a factor of two to three. They deduced the following analogy for inaccessible pore volume:

$$\frac{d}{d_g} \Big| \frac{d_{pore}}{d_g} = \frac{d}{d_{pore}} > 0.678 \tag{2.2}$$

where, d_g is the grain diameter. Here, d_{pore} is related with the size of the constriction area. According to the above analogy, one can expect that polymer with a diameter d (if it is assumed to be a rigid spherical ball) will not be able to pass through the constriction area. But in a limiting case, the polymer may be able to pass because the molecule is in the form of a flexible coil, not a rigid spherical ball.

Duda et al.(1981) studied the coupling of adsorption, mechanical entrapment, shear rate, and inaccessible pore volume effects on the effective and residual permeabilities. They showed that the residual permeability was only a weak function of the flow rate of the polymer solution. They confirmed, as did some of the previous researchers (Dominguez and Willhite,1977; Smith, 1970) that the amount of polymer retained in the porous medium was a strong function of polymer flow rate. They showed that mechanical entrapment was the major reason for permeability reduction with polyacrylamide, whereas an adsorbed layer of polymer molecules was the major reason for permeability reduction with polysaccharides. One of their interesting observations was that at low values of initial permeability, the percent reduction of the residual permeability increased with increasing initial permeability. This indicates that an adsorbed layer of polymer molecules is more effective for hindering flow in larger pores. Also, they showed that the percent reduction attained a maximal value when the initial permeability was 250 md. This anomalous increase in permeability reduction was explained in terms of inaccessible pore volume that increased with decreasing permeability.

2.2.2 Mobility Control with Emulsion Slugs

McAuliffe (1973a) used oil-in-water emulsions as selective plugging agents to improve oil recovery in waterfloods. He argued that as oil-in-water emulsion was injected, a greater amount of emulsion entered the more permeable zones. As this occurred, flow became more restricted, so water began to flow into less permeable zones, resulting in greater sweep efficiency. In order to observe the effect of emulsion flow, he used emulsion diluted to 0.5 percent oil. He observed that average diameter of the oil droplets dictated if the emulsion flow would substantially decrease the water permeability of a core. However, with adequate diameter, the permeability was reduced greatly (one to 10 percent of the original permeability), even though complete plugging never occurred. Moreover, he observed that when a waterflood was carried out after an emulsion flood, the permeability was restored by an insignificant amount even with a large pore volume of water injected. When emulsion was injected in parallel system of different permeabilities, permeability reduction took place in the highest permeability zone first and so on until all three (high, medium, and low) zones attained the same permeability. In these tests, it was observed that the droplet sizes in the emerging emulsion were smaller than the initial ones for medium or low permeability zones whereas it approached that of initial ones for the high permeability zone. Finally, he observed an improvement in displacement efficiency by emulsion flood over a waterflood. McAuliffe (1973b) reported a field test that was conducted to see if oil-in-water emulsions, prepared from petroleum crude oils, would reduce water channeling from injection to production wells. In order to avoid breaking of the caustic prepared emulsion, a fresh-water emulsion was placed between the emulsion and the reservoir brine. An amount of emulsion equivalent of three percent pore volume of the affected area was injected. A 14 percent oil-in-water emulsion was chosen for injection. The emulsion slug was later pushed by a cushion of fresh water of four percent pore volume and finally saline water was injected. In a two-year period after emulsion treatment of three water-injection wells, fluid production from offset wells showed increased oil recovery and lower water-oil ratios, with a considerable increase in volumetric sweep efficiency.

Johnson (1976) reviewed the status of caustic and emulsion methods. He discussed the usefulness of emulsions (in situ or external) for recovering viscous oils or oils in heterogeneous reservoirs where sweep efficiency is poor. He mentioned the following mechanisms through which caustic waterflooding improved waterflooding oil recovery:

a) emulsification and entrainment of oil at S_{or}.

b) wettability reversal (from oil-wet to water-wet)

c) wettability reversal (from water-wet to oil-wet)

d) emulsification and entrapment of oil at S_{or}

Broz et al.(1985) reported laboratory results in the development of a new emulsion blocking technique for the correction and control of steam override and channeling. They showed that emulsions formed in situ do not perform as well as those produced externally. However, even though the emulsion originally formed with 50 percent oil-in-water was diluted to 0.5 percent oil-in-water, the permeability reducing efficiency was remarkable. Permeability reduction occurred whether oil was present or not. They observed, as did AcAuliffe (1973a), that a waterflood following an emulsion flood does not "wash away" the emulsion and the permeability remains at a low value. However, they did not report any emulsion flood performance at an oil saturation higher than the residual value.

2.2.2.1 Blocking Mechanism with Emulsion

McAuliffe(1973a) argued that the emulsion droplets have to be large enough to create blockage by lodging within the pore throat. Therefore, for an emulsion to be effective, the oil droplets in the emulsion should be slightly larger than the pore throat constriction in the porous medium. As a basis for this argument, they presented the observation of

Uzoigwe and Marsden (1970) who found that no flow restriction took place with oil-in-water emulsion through glass beads where the oil droplet size was probably smaller than the average pore throat size.

Jennings et al.(1974) showed that if interfacial tension were low enough, residual oil in a preferentially water-wet core could be emulsified in situ and, thereby, move downstream with the flowing caustic and could be entrapped again by pore throats too small for the oil emulsion droplets to penetrate. This mechanism of emulsification and entrapment results in reduced water mobility that improves both vertical and areal sweep efficiency. Cooke et al.(1974) attributed the permeability reduction by the formation of water-in-oil emulsions to the high viscosity of those emulsions or to the formation of an oil film (lamella) across the pore throat. They argued that the oil lamellae formed in the pore spaces effectively close many of the flow paths that were formerly available for the flow of water. The resistance to flow of the lamellae and the bridging of pores by lamellae cause the large increase in pressure gradient that is observed immediately behind the displacement front. The low mobility of fluid in the region where lamellae exist and the small amount of oil within the lamellae cause the sharp gradient in oil saturation that is observed at the displacement front.

Soo and Radke (1984) suggested another mechanism for permeability reduction by an emulsion. They argued that when emulsions are injected into a porous medium, droplets not only block pores of throat sizes smaller than their own, but they are captured on pore walls and in crevices. The drops remain in place by hydrodynamic pressure forces with a velocity increase simply wedging the drops tighter into the crevice. Droplets caught in recirculation eddies and dead spaces called cavern sites were not affected by velocity effects. Neither crevice nor cavern sites were affected unless significant redistribution of flow, pressure impulses, or vibrations were imposed. Therefore, a reduction in permeability from emulsion plugging may not necessitate that the median droplet size equal or exceed the median pore throat diameter. Consequently, an ensemble of smaller droplets crowding in a single pore throat would have the same effect in blocking the pore throat as would one large droplet. In this context, they pointed out the importance of pH and ionic strength of the aqueous phase on the capture of droplets on the rock surface. Studies of the effects of drop size showed that as the drop size of the emulsion increased the drop retention increased. However, for equivalent capture volumes of emulsions, the smaller droplets were more effective at restricting the flow in the transient state prior to steady-state flow. Eventually, as steady-state was approached, the larger droplets led to a larger reduction in absolute permeability than the smaller droplet flow alone due to the combined superiority in drop retention and flow restriction.

2.2.3 Mobiloty Control with Foam

Fried(1961) was the earliest researcher who studied the usefulness of foam in enhancing the displacement efficiency in oil recovery. He reported that foam causes a rapid reduction in gas phase relative permeability, leading to delayed gas breakthrough. He contended that the presence of surfactant alone did not improve the oil recovery and that the improvement with foam was mainly due to reduction in gas permeability. He observed that the presence of surfactant increased the residual gas saturation. His observation would suggest that the relative permeability to gas is not a single-valued function of saturation and the curve shifts to the left as the interfacial forces resisting flow increase. He showed that the flow resistance of the foam increases with increasing surfactant concentration. Therefore, the effective permeability to gas is also a multivalued function of surfactant concentration. This leads to the belief that the effective permeabilty to gas would depend on surface tension and surface viscosity. He recognized the fact that a weak foam cannot block gas flow. In the case of weak foam, he observed that foam flowed with continuous breaking and reformation of lamela.

In 1963, Bernard observed in a laboratory study that the gas drive efficiency improved in the presence of foam. His experiments showed that while foam was very effective as a displacing agent in sandpacks containing water only, it did not show a high efficiency in sandpacks containing oil only. For sandpacks containing both water and oil, foam performance fell between the two extremes. The initial work with foam indicated that it could improve the conformance of gas-drive oil recovery processes because it selectively reduced the gas permeability of the reservoir rock (Bernard and Holm, 1964). Kolb (1964) suggested that a large portion of gas is trapped in the porous medium and only a small fraction flows as a free gas. He concluded that the flow of free gas can be described by Darcy's law. In 1965, Bernard et al. (1964) showed that foam-flooding recovered more oil from a linear stratified sand system than a conventional waterflood. The effect of foam was to create a higher trapped-gas saturation which indirectly yielded a lower relative permeability to water. The trapped gas saturation was found to be lower for a system containing both water and oil than for an all-water system. Bernard et al.(1965) stated that gas flowed as a discontinuous phase and water flowed as a free phase. They concluded that at a given fluid saturation the relative permeability to water is the same whether or not foam is present in the system. One of their important findings was that foam did not break down during the passage of surfactant-free water even after injecting 0.10 to 0.25 PV of water.

Marsden and Khan (1966) suggested that foam components flow simultaneously through the channels of the porous medium. Also, their results showed a decrease in foam mobility with increasing quality. However, this rate of decrease in mobility is lower as the absolute permeability of the porous medium decreases. They also reported an increase in apparent viscosity of foam with increasing surfactant concentration. Holm (1968) disagreed with this observation. He conducted flow experiments and visual studies to investigate the mechanism of gas and liquid flow through porous media in the presence of foam. He reported that it was unlikely that foam would move through the media as a body. Instead, the liquid and gas forming the foam separated as the foam films broke and then re-formed in the porous medium. When enough foam was present, the flow of gas through the foam stopped and the flow of liquid was reduced. Consequently, he suggested that it would not be practical to drive foam through a reservoir; however, foam can be expected to improve the sweep of fluid injection processes in heterogeneous reservoirs by reducing or blocking flow in more permeable zones. He observed that the mobility of the foam increased with increasing quality. He reported that gas could not flow as a continuous phase. This observation differs from that of Marsden and Khan

(1966). He attributed this difference to the different experimental techniques used. He argued that, since Marsden and Khan used a very small pressure drop across the core, very little expansion of the foam bubbles took place leading to enhanced stability for some small bubbles that created less resistance to flow. Since low quality foam contains more of these smaller bubbles, wetter foam gave higher mobility (due to low apparent viscosity).

Bond and Bernard (1966) described foam flow as a flow of a portion of the liquid and gas in a foam body and suggested that only excess surfactant solution would flow as a free phase. They concluded that liquid flow through a porous medium followed fixed channels, whether or not foam was present, and that these channels depended solely on the liquid saturation. This conclusion was based on Chatenever's idea of channel flow (Chatenever, 1952).

Holm (1970) reported successful field application of foam in selectively plugging a high-permeability channel. It was observed that the plugging action was the greatest if gas, instead of water, was injected after the foam. Even though Bernard _et al_.(1965) reported that the permeability of a porous system to water following a foam bank was reduced in many cases to between 10 to 50 percent of its initial value, Holm (1970) contended that water following a foam bank tended to dilute the foamer solution and wash it away. He also reported that, when the permeability of a channel was high, the blocking action by foam was the most effective.

Raza (1970) made a detailed study of variables that affect the generation, propagation, quality, and nature of foam produced inside of a porous medium. Unlike some of the previous researchers (Bernard et al., 1965; Holm, 1968) he observed that foam can be propagated in a reservoir rock at pressure levels ranging from 100 kPa to 6700 kPa, and under pressure differentials ranging from one to 1100 kPa/m. However, the quality of the foam depended on the type of foaming agent, surfactant concentration, the physical properties of the porous medium, the pressure level, and the composition and saturation of fluids present. He recognized that the flow behaviour of foam in a porous medium could not be correctly described in terms of high apparent viscosity of foam alone. One of the interesting properties that he pointed out was that the foam in a porous medium restricted the flow of all the fluids. However, he argued that the flow of gas was the most restricted, and the restriction could last for an indefinitely long period of time whereas the restriction in the flow of water lessened as the foam decayed. On the other hand the flow of hydrocarbons was only temporarily restricted. He observed that the injectivity of gas decreased continuously with the growth of the foam bank and asymptotically approached a low value.

Minssieux (1974) observed, for a fixed ΔP across the core bed, a continually decreasing foam rate until gas flow stopped completely. He concluded that a minimum ΔP was necessary to overcome the elastic limit of films impeded by pore constrictions. He recognized, as did Raza (1970), that foam stability decreased upon contact with oil for any type of surfactant used. He confirmed the observation of Holm (1968) that foam was constantly regenerated by breaking and reforming gas bubbles rather than being a single phase. He also found that gas moved faster than water without forming a continuous phase inside the medium. Due to this partial foam dissociation of gas and liquid during the flow of foam through porous media the apparent viscosity of the foam produced decreased as the quality increased. This observation was opposite to what was observed outside porous media. This continually decreasing foam quality at the outlet end makes it difficult to obtain a set of steady-state relative permeability curves. Also, he observed that foam flow could not be treated as an equivalent of gas flow since, in relation to oil, the foam appeared as the wetting phase. Consequently, he suggested the same relative permeability could be assumed for both water and foam. He reported that the highest drive efficiency occurred with the lowest quality foams. For porous media, this corresponded to the lowest mobility ratio. In his experiments, he showed, for homogeneous porous media, that the oil recovery was much improved compared with a gas drive but remained slight compared with a waterflood. He attributed the loss of viscosity on contact with oil, and the contamination of the films of surfactant molecules adsorbed at the interfaces (by reducing their elasticity) to such a poor performance. He proposed the use of a thickening agent to the surfactant in order to prevent the foam degradation in the presence of oil.

Heller et al.(1982) conducted high temperature and pressure displacement tests with CO_2 foam. They observed that the mobility of foam was not constant with flow rate, but increased at higher velocity. They also observed that the foam mobility decreased with increasing surfactant concentration whereas only a small decrease of mobility took place with increasing quality.

Owette et al.(1983) used visual models of a porous medium. They used models saturated with surfactant solutions. They observed that when gas alone was injected only a few interfaces were formed behind the gas liquid front. However, when foam was injected the bubbles were larger. They also observed that the larger channels could not be blocked by the foam and most of the gas flow took place through those larger channels. They also studied the stability of foam as a function of surfactant concentration. They observed that at one percent surfactant in water very little breakage of foam occurred, whereas considerable breakage occurred at 0.1 percent surfactant concentration. This observation was previously made by Raza (1970).

Wang(1984) studied the displacement mechanism with CO_2 foam. The results indicated that an increase in pressure promotes foam stability whereas an increase in temperature does the contrary. He concluded that CO_2-foam generated either in situ or externally was susceptible to quick disintegration upon contact with crude oil. Consequently, he suggested that any improvement in oil recovery was obtained as a result of foam blockage of the permeable streaks or channels in the injection formation. He also observed that excessively high surfactant concentrations led to a foam barrier, thus decreasing sweep efficiency.

Maini and Ma (1984) investigated the relationship between foam stability measured in static tests and in a porous medium. For EOR-200 (Alcohol ether sulfonate), the slowest rate of foam decay was observed at 0.25 percent concentration. The foam decayed considerably faster when the concentration was increased or decreased. However, the halftime for liquid drainage continued to increase with increasing concentration for a concentration up to 0.5 percent. They explained the existence of an optimal concentration by considering the influence of an adsorbed surfactant monolayer on surface tension. For the same surfactant used, they obtained an optimal concentration of 25 g/l for which a maximal mobility reduction was obtained.

Borchardt et al.(1985) compared the performance of more than 40 surfactants and concluded that the surfactant which performed best during foaming experiments conducted at one atmosphere in the presence of oil performed best at high pressure as well.

Best et al.(1985) conjectured that the gas flowed as a discrete phase in the presence of a surfactant solution. They observed that a portion of water moved through the same pore network as the gas, and also through the finer pores, in the absence of gas. They contended that the portion of water flowing through the gas-free pores depended on pore-size distribution, volumetric flow rate, etc. They attributed the reduction in relative permeability to gas to the capillary resistance to the liquid interfaces that constituted the foam. Therefore, they argued that the magnitude of the reduction in relative permeability to gas would depend on the number of those interfaces per unit length of pore, the bubble size relative to the pore size and their stability. They also concluded that the relative permeability to water was affected only for very stable interfacial films, where pendular flow of water made a significant contribution to overall water flow.

Khatib et al.(1986) introduced the notion of 'limiting capillary pressure' in porous media. This was the capillary pressure in a porous medium that represented a characteristic value approached by the capillary pressure after an initial increase when the fractional flow of gas in a foam was raised at a fixed gas velocity. They observed that if the gas fractional flow was increased once the limiting capillary pressure has been attained, coalescence coarsened foam texture whereas the liquid saturation remained constant and the relative gas saturation became proportional to the ratio of gas to liquid fractional flow. They contended that the limiting capillary pressure depended on surfactant type, gas velocity, and absolute permeability. They reported a significant dependence of relative gas mobilities on both the gas flow rate and gas fractional flow. It was observed that at low gas fractional flow, the relative gas mobility was nearly constant, leading to the belief that the foam texture remained constant in this region. On the other hand, for higher gas fractional flow the relative gas mobility increased rapidly. They argued that this increase corresponded to a limiting value of capillary pressure and that coalescence caused the foam texture to coarsen. This observation was analogous to what was observed in smooth capillaries (Hirasaki and Lawson,1985). For a given surfactant concentration the limiting capillary pressure decreased as the absolute premeability increased. This was interpreted as increased permeability having a destabilizing effect on the flowing foam. They reported an interesting relationship between gas mobility and permeability. The gas mobility decreased rapidly as permeability increased up to 12 μm^2. This was followed by a region for which the gas mobility remained insensitive to absolute permeability. For higher permeability the gas mobility increased rapidly.

Maini(1986) studied the effect of residual oil on the mobility control performance of foams. He recognized the existence of a compatible set of surfactant and oil in order to have an effective mobility control with foam. He also concluded that, in order to mobilize residual oil (after steam flood), the foam did not necessarily have to be effective in reducing mobility.

Nicolov _et al._(1986) studied foam stability in the presence of crude oil and pure hydrocarbons. They suggested that foam destabilization in the presence of oil was a more complex mechanism than oil droplets spreading upon foam film surfaces and involved the migration of emulsified oil droplets from the foam film lamellae into the Plateau borders where phenomena like the Marangoni effect in the pseudoemuslion film, the pseudoemulsion film tension, the droplet size and number of droplets would contribute to destabilizing or stabilizing the foam structure. They conducted both constant pressure and constant volumetric flow rate displacement tests and obtained similar ultimate oil recoveries. A maximal pressure drop (for constant flow rate case) was observed just prior to the gas breakthrough.

Huh and Handy(1986) reported relative permeabilities of foaming agent solution-nitrogen gas as measured by both steady- and unsteady-state methods. They compared these permeabilities to those obtained in the absence of foaming agent. They observed that the permeability reduction factor for the gas phase was mainly a function of lamellae stability. They observed a significant difference between steady- and unsteady-state relative permeabilities. They observed that, for unsteady-state flow the change in relative permeability to gas was insignificant and exhibited no blocking effect. However, for steady-state flow the simultaneous flow of liquid and gas could be stabilized only above a minimal gas saturation of about 35-40 percent. They attributed this behaviour to the formation of a large number of foam lamellae by the continuous supply of foaming solution. They also concluded that a higher gas fraction corresponded to a greater blocking effect.

Fiedmann and Jensen(1986) showed that the foam texture became finer as the flow rate was increased in a porous medium in the absence of oil. In the presence of oil, they observed that there existed a maximal oil saturation above which a foam could not form.

Isaacs et al.(1986) reported laboratory study results of foam flow in porous media at elevated temperature. They recognized the existence of an optimal surfactant concentration beyond which no additional mobility reduction could be achieved. However, this optimal surfactant concentration was found to be higher in the presence of oil. They observed that the highest oil recovery was obtained when surfactant slugs were injected with non-condensible gas.

2.2.3.1 Laboratory Studies

Al-Khafaji et al.(1982) examined the static properties of surfactants at high temperatures and pressures. Their experiments were conducted to investigate the effect of temperature on surfactant degradation and partitioning into the oil phase. Two surfactants were employed: Suntech IV and Corco 180A. It was found that at a temperature of 205°C and a pressure of 2.8 MPa, Suntech IV exhibited high thermal stability, while Corco 180A showed thermal degradation. The stability of Suntech IV remained unaltered when 1 percent wt NaCl was added to the surfactant. Chemical degradation occurred, however, when 1 percent wt $CaCl_2$ was added to the solution. Partitioning experiments were conducted at different Suntech IV concentrations. It was noted that partitioning into the oil phase increased rapidly with increasing surfactant concentration at low concentrations, and increased slowly at high concentrations.

Experiments were carried out by Duerksen(1984) to investigate the foamability and thermal stability of various surfactants at steamflood conditions. The results showed that sulfonate surfactants were thermally stable at high temperatures, but had a reduced stability in the presence of NaCl. Surfactant foamability increased from 0.01 to 0.05, but did not further increase at higher liquid volume fraction values. Brine was found to reduce the foamability of alpha olefin sulfonate surfactants. In addition, foamability was noted to decrease with decreasing nitrogen concentration in the foam, and increasing temperature.

A study aimed at determining whether a relationship exists between foam stability index in static tests, and mobility reduction in displacement tests, was carried out by Maini and Ma(1985). From static tests, they noted that foam stability generally decreased with increasing temperature. For each surfactant, an optimal concentration was observed, above and below which foam stability decreased. Tests in porous media showed that the highest mobility reduction obtained for each surfactant occurred at the same optimal concentration observed in the static tests. The mobility reduction factor increased with increasing foam stability.

Maini(1985) investigated the thermal stability of various types of sulfonate surfactants at 200 and 300°C. Most of the surfactants tested were found to be thermally stable at 200°C. At 300°C, a rapid surfactant degradation was observed for all surfactants, with the exception of alkyl benzene sulfonates. Maini concluded that alkyl benzene sulfonates were the most thermally stable, followed by alpha olefin sulfonates. Petroleum and alcohol ether sulfonates were found to be the least stable. Dynamic tests showed that the mobility reduction factors varied widely among these surfactants. For each surfactant, the value of mobility reduction was dependent on surfactant concentration and gas/liquid ratio of the foam. The highest mobility reduction obtained varied with the type of, and concentration of, the surfactant tested.

Novosad et al.(1985) examined the adsorption characteristics of two foam-forming surfactants: an alpha olefin sulfonate (Enordet AOS 1618), and an alkyl toluene sulfonate (Suntech IV). The alkyl toluene sulfonate was found to adsorb more than the alpha olefin sulfonate. Surfactant adsorption decreased with increasing temperature, and increased when clay was added to the sandpack. While the presence of brine increased the adsorption of Suntech IV, no significant change in Enordet adsorption was noted in the presence of brine.

2.2.3.2 Field Examples

One of the earliest field results was reported by Holm (1968). He discussed field results of foam injection tests in the Siggins Field of Illinois. In this field test, severe channeling of air was stopped by injecting 0.06 pore volume of a one-percent solution of foaming agent and following it by air injection alone. A reduction in the total liquid production rate took place during the foam treatment. However, a larger reduction took place in water production. As a consequence, the average WOR dropped from 15 to 12 during the foam injection period. For the rest of the field the WOR increased up to 28 during the same period.

The use of foam to improve steam drive operations was tested in the North Kern Front Field, California (Eson et al.,1981; 1982; 1983a;1983b). The reservoir was characterized by very wide variations in vertical permeability, a steep structural updip, and an edgewater drive, which led to steam channeling and premature steam breakthrough. Foam was injected in selected parts of the field using three types of surfactants: two inverted nine-spot patterns were treated with COR-180 steam foam, two with a COR-GEL steam foam-polymer combination, and one inverted five-spot pattern was treated with Suntech IV steam foam. The steam foam was designed to break down after three to five days, and the steam foam-polymer combination was employed because the gel coating the foam delayed the foam activation in the reservoir. Eson et al.(1983a;1983b) reported that the vertical sweep efficiency and the oil production rates in the areas tested were improved due to foam treatment. No emulsion problems were experienced at the producing wells during the COR-180 and COR-GEL treatments; however, emulsions were detected when Suntech IV was employed. An estimate of the cost per incremental barrel of oil produced after foam treatment showed that COR-180 was the least expensive, while Suntech IV was the most expensive. Eson et al.(1983a) observed that even though steam foam was effective with COR-180 and COR-GEL, in order to obtain a stable foam utilizing Suntech-IV a non-condensible gas had to be used.

Eson and Cooke(1985) reported additional field results on the Midway-Sunset Field. This field was treated with surfactant along with steam and non-condensible gas for five years. Air was injected along with 10 percent-concentration surfactant slugs. Even though nitrogen was used during initial tests, it was replaced by air for economic reasons. The field results showed that air could be utilized as a non-condensible gas along with surfactants in order to create a foam despite the oxidizing effects of the air on the surfactants.

The test data of the North Kern Field was reevaluated by a different group of investigators (ERW,1987), who concluded that steam foam did not improve oil recovery in that field. In the site investigated the steam foam injection started in 1980 at six inverted nine-spot patterns. The wells in this location had received five to 10 cyclic steam injections before initiating the foam treatment. COR-180 was injected in a 60 percent concentration as a weekly slug. After injecting such slugs of 100 gallons each for a year, it was observed that the pattern receiving foam treatment had dropped in oil production while the control pattern (receiving only steam injection) remained flat or dropped more slowly in the same period. One of the reasons for such a failure is the fact that steam injection by itself was not the major mechanism displacing oil from the reservoir. It was also concluded that water influx into the reservoir was a key production mechanism. This leads to the speculation that water invasion causes foam performance to deteriorate.

Following extensive laboratory studies, a pilot test of foam injection was conducted in Midway Sunset, California, and was reported to be successful (Doscher and Hammershaimb,1981,1982) This field contains an 11° API crude and a variable oil saturation. The test was carried out in a five-spot pattern which had previously produced by steam drive and cyclic steam stimulation. Prior to foam treatment, oil production rates from the pattern were very low (less than 20bbl/day), and water cuts were very high (95 percent). Foam was formed in situ by the injection of a surfactant solution into the flowing steam, followed by air injection. Analysis of the test performance showed that the water cut decreased significantly, and oil production improved due to foam injection. It was suggested that the main drive mechanism in this field was the increase in steam viscosity, which allowed a more efficient displacement of the heated oil to be attained.

Greaser and Shore(1981) reported successful field application of in situ foaming in a steam drive process in the Kern River Area. Getty Oil used COR-180, a steam-diverter foam on nine injectors to determine its effect on steam flood oil recovery. Radioactive tracer surveys showed that in most of the injection wells the steam injection profile was improved. Also, average daily oil production increased significantly during the foam test period.

Foam injection was tested in Shell's Mecca lease (Dilgren et al.,1982) of the Kern River Field, to evaluate the ability of foam to decrease steam mobility and improve sweep efficiency. The test was initiated in a single five-spot pattern, and was later expanded to four-spot patterns. The steam foam was reported to yield increased bottomhole injection pressures and improved oil recoveries.

Brigham et al.(1984) reported results that showed a considerable improvement in oil recovery by steam drive with the addition of surfactant and nitrogen to the steam. For this field test Suntech-IV was used as the foaming agent. A control pattern with conventional steam drive without surfactant was used. Surfactant-water slugs were followed by nitrogen and then by steam. They reported a pronounced upward trend in oil production within weeks of the commencement of each of the slugs. An increase of 50 BOPD prior to slug injection was observed. It culminated in a peak of about 150 BOPD. The peak in oil production appeared to be related to the duration of the slug. The shorter- and higher-rate slugs were followed more rapidly by the peak in production. They concluded that in order to have an effective foam injection the following conditions should be fulfilled:

- the foam must be stable at relatively high temperatures
- the foam must preferentially penetrate the steam-swept zones and reduce their permeability
- the 'blocking action' should persist for an extended period of time under reservoir conditions.

Lee and Kamilos(1985) reported the use of a newly developed diverter Chevron SD 1000 in a pilot project in the Kern River Field. This was used as a steam drive additive along with nitrogen using two-day slugs once a week for a total of 15 slugs. The surfactant concentration was 0.5 percent by weight. A positive response was observed within four weeks of the commencement of the slug injection. They reported successful application both for a nine-pattern (incremental oil recovered= 88,800 bbl/month) and a six-pattern (incremental oil recovered= 39,000 bbl/month) pilots.

Keizer et al.(1986) reported the results of a pilot test, operated by Maraven, in the Tia Juana Field in an attempt to improve the injection profile in steam-soak wells. The results show successful application of steam foam for

- reducing the effective steam permeability
- plugging the most depleted layer
- diverting the injected steam to non-producing sands
- enhancing oil production

For all the wells under test the WOR dropped from an initial value of 90 percent to 20 percent over about eight months. For this test, C_{18} alkyleryl sulphonate was used as the surfactant.

Falls et al.(1986) reported field data acquired during Shell Oil Company's steam foam drive pilots in the Kern River Field in California. They concluded that a steam foam was more effective when non-condensible gas was present. As a possible explanation, they mentioned that the foam lifetime was longest when transport of non-condensible gas limited mass transfer between steam bubbles.

Mohammadi and McCollun(1986) reported results of a steam-foam pilot project in Guadalupe Field in California. The case studied in this test had severe steam-channeling conditions prevailing before the chemical treatment. During the initial injectivity test, a 0.75 wt percent surfactant was added to the steam. Also, nitrogen was added to the steam at a rate of 25 scf/bbl of steam. Overall incremental oil production from this pilot was 29,400 bbl over a period of three weeks.

2.3 NUMERICAL SIMULATION

2.3.1 Numerical Simulation of Polymer Flood

Several authors have investigated simulation of the various complex compositional effects that occur during the displacement of oil with surfactants and polymers (Pope et al., 1979; Flemming et al, 1981; Al-Seehati, 1979). Many supporting laboratory studies have been published, which have contributed to the understanding of polymer behaviour (e.g. adsorption) but very few attempts have been made to model mathematically the experimental polymer floods.

Usually, the simulation of polymer flow took account of polymer dispersion and polymer adsorption by the solid rock surface. Even after introducing polymer dispersion and adsorption, a 'resistance factor' is introduced to allow for the reduction in absolute permeability caused by the injected polymer solution. This leads to redundancy if polymer adsorption is considered to be the main cause of any reduction in absolute permeability. Another shortcoming of this approach is that the polymer is considered only as a component of the aqueous phase and two-phase relative permeabilities are used. Besides, only the absolute permeability is considered to be affected by polymer injection leading to an improper simulation of the relative permeabilities to water. On the whole, the present approach of simulation of polymer flood cannot properly simulate the mobility control property of polymer which is most efficient in the presence of mobile water. Also, a polymer solution is not readily miscible with water and assumption of two-phase flow would lead to a considerable error, especially at the initial stage of polymer injection. This error is magnified when the polymer slug volume is small as compared to slug volume.

2.3.2 Numerical Simulation of Emulsion Flood

Numerical simulation of emulsion flow in an oil reservoir needs a proper description of the flow behaviour of emulsions. This needs the knowledge of transport properties of these fluids and the physical laws controlling their flow. Recently, Abou-Kassem and Farouq Ali (1986) have reviewed the rheology of emulsions, their formation in porous media, and subsequent flow, from a mathematical standpoint. In another study, they (Abou-Kassem and Farouq Ali, 1986a) have developed a correlation for flow behaviour of emulsions in porous media. These studies give insight for a one-dimensional, isothermal, single-phase flow of emulsions through porous media. However, todate no literature has been reported to have attempted numerical simulation of the emulsion flow in a multi-phase flow system. Nevertheless, several researchers have pointed out that O/W macroemulsions of low and up to 0.5 quality will exhibit a Newtonian behaviour.

2.4 SCALING OF POLYMER, EMULSION AND FOAM

The use of polymer, emulsion and foam has been a subject of many investigations in the petroleum industry for many years. These materials have been used as mobility control or diverting agents in different enhanced oil recovery techniques, such as gas drive, steam injection, waterflood or micellar flood. Many studies have shown that these materials may improve oil recovery by a substantial amount. However, laboratory studies performed todate have used unscaled or only partially scaled models. Therefore, the quantitative results obtained from polymer, emulsion and foam flooding experiments are not applicable to the field. In order to scale up laboratory experiment results for field application, the model has to be properly scaled. This requires detailed knowledge of polymer, emulsion and foam flow through porous media. The mechanism of improved oil recovery with these materials will be discussed in the following sections.

2.4.1 Flow Mechanism of Polymer in Porous Media

It has been well recognized that a polymer solution is more effective flooding agent than other viscous fluids (Pye, 1964; Sandiford, 1964; Sherborne et al., 1967). The abnormal resistance property of polymer was recognized by Pye and was quantified as the "resistance factor". Ever since this early work, there have been numerous studies on polymer flooding. Even though these researchers contradicted each other on different details of polymer flooding, there seems to be unanimity on attributing polymer adsorption and machanical entrapment as the cause of improved oil recovery with polymer. This unique property of polymer causes a reduction in the effective permeability to water without affecting the effective permeability to oil. The polymer adsorption in porous media was mathematically represented by Bondor et al.(1972). They simulated polymer adsorption by treating it explicitly. Satter et al. (1977) treated polymer adsorption implicitly in their mathematical simulation. This approach was later followed by several other researchers (Al-Seehati, 1979). As far as adsorption is concerned, a mathematical representation seems to be straightforward. However, complications arise due to the fact that adsorption alone cannot account for the selective reduction of the effective permeability to water. Mechanical entrapment, dispersion and diffusion have to be considered with other complicated phenomena, such as viscous fingering (while a waterflood follows an initial polymer flood). Todate, there has been only one approach to represent mathematically mechanical entrapment with polymer; that is, by introducing the notion of "resistance factor". This has been incorporated into reservoir simulators with a certain degree of empiricism. Diffusion and dispersion are also important phenomena due to miscibility of polymer in water. At very low longitudinal interstitial velocities, diffusion dominates whereas at higher velocities dispersion dominates. Pozzi and Blackwell (1963) pointed out that precise scaling of transverse dispersion coupled with the requirement of geometric similarity would require an impractically large laboratory model and a long time for experiments. They determined that under specific conditions, the requirements of geometric similarity and gravitational scaling could be relaxed to allow scaling of miscible displacements. These would be applicable to either of the cases for which transverse mixing takes place by molecular diffusion or convective dispersion. In this regard, Rojas (1985) found, in a scaled study of immiscible carbon dioxide displacement of heavy oil, that breakthrough recoveries depend very little on the transverse dispersion group for $D_T L/W^2 V < 4.10^{-4}$ or, on the longitudinal dispersion group for $D_T L/D_L W < 0.3$.

Several models have been proposed in the past in order to express the dispersion tensor in terms of macroscopic variables representing the microscopic configuration of the field. For the present study, the model proposed by Bear and Bachmat (1982) has been adopted. He showed that for isotropic media, for which an orthogonal co-ordinate system parallel to the flow is selected, the dispersion tensor becomes

$$D = \begin{bmatrix} D_L & 0 & 0 \\ 0 & D_T & 0 \\ 0 & 0 & D_T \end{bmatrix} \qquad (2.3)$$

According to Perkins and Johnston (1962), the dispersion coefficient is the sum of diffusion and dispersion coefficients. He further defined dispersion coefficients in the following form

$$D_L = D^*/F\phi + 0.5vxd_p \qquad (2.4)$$

$$D_T = D^*/F\phi + 0.0157vxd_p \qquad (2.5)$$

This model will be used throughout the present study.

Recent studies (Coskuner and Bentsen, 1987) indicate that viscous fingering plays an important role in the waterflood that follows the polymer flood. However, the mechanism for unstable flows is not well understood and creates difficulty in scaling such a system. Even though an unstable displacement (presence of viscous fingers) can be modelled by using the same flow regime in the model and the prototype in the case of simple miscible displacement, it is not yet known what how to model an unstable displacement in the case of a complex system for which a miscible displacement takes place along with an immiscible displacement.

2.4.2 Flow Mechanism of Emulsion in Porous Media

Emulsions (oil-in-water or water-in-oil) have been proven to be effective in blocking more permeable zones in a hetrogeneous reservoir (McAuliffe, 1973), or in controlling steam override and channeling (Broz _et al_., 1985). It has also been shown that emulsions formed _in situ_ do not perform as well as those produced externally.

While emulsions are well accepted as effective blocking agents, there has been a lot of controversy in describing how emulsions actually create such a blockage. McAuliffe (1973) argued that the emulsion droplets have to be large enough to create blockage by lodging within the pore throats. As a basis for this argument, they presented the observation of Uzoigwe and Marsden (1970) who found that no restriction in flow occurs with oil-in-water emulsion through glass beads for which the oil droplet size was probably smaller than average pore throat size. Jennings _et al._(1974) showed that emulsification could take place _in situ_ if the interfacial tension were low enough. This would mobilize even residual oil but these droplets could be entrapped again by pore throats too small for the oil emulsions to penetrate. They described this emulsification and entrapment as the cause of reduced water mobility that improves both vertical and areal sweep efficiency.

Cooke _et al_.(1974) attributed the permeability reduction by the formation of water-in-oil emulsion to the high viscosity of those emulsions or to the formation of an oil film (lamella) across the pore throat. They argued that the oil lamellae formed in the pore spaces effectively close many of the flow paths that were formerly available for the flow of water.

Soo and Radke (1980) presented another mechanism for reducing permeability by emulsions. They argued that, when emulsions are injected into a porous medium, droplets not only block pores of throat sizes smaller than their own but they are captured on pore walls and in crevices. Therefore, a reduction in permeability from emulsion plugging may not necessitate that the median droplet size equal or exceed the medium pore throat diameter.

These recent findings are not enough to delineate the exact flowing nature of emulsion. However, in order to represent emulsion flow mathematically, the flow models that have been used in the past years must be considered. Abou-Kassem and Farouq Ali (1986) reviewed the emulsion-flow models. They pointed out that for oil-in-water emulsion the flow is essentially Newtonian for low emulsion quality up to 0.5.

2.4.3 Flow Mechanism of Foam in Porous Media

There have been several attempts to use foams as blocking agents. However, most of these tests were applied in enhanced oil recovery by gas or steam injection (Eson _et_ al., 1981). The initial work with foam indicated that it could improve the conformance of gas-drive oil recovery processes because it selectively reduces the gas permeability of reservoir rock (Bernard and Holm, 1964). Also, Bernard et al.(1965) showed that foam flooding recovered more oil mainly because it created a higher trapped-gas saturation which indirectly yielded a lower relative permeability to water.

Huh and Handy (1986) pointed out that foam flow may be described as a three-phase flow process. However, they argued that foam would not travel as an independent phase but its existence would be felt in terms of effective permeability to gas. They pointed out that the steady- and unsteady-state relative permeability will be different for gas in the presence of foam.

Five major mechanisms of flow have been recognized. These are:

1. A large portion of the gas is trapped in the porous medium and a small fraction flows as free gas, following Darcy's law (Kolb, 1964).

2. The foam structure moves as a body; the rate of gas flow is the same as the rate of liquid flow (Fried, 1961).

3. Gas flows as a discontinuous phase by breaking and re-forming films. Liquid flows as a free phase (Bernard et al., 1965).

4. Foam flows as a combination of liquid and gas in a foam body and the liquid flow in a porous medium follows fixed channels, whether or not foam was present; these channels depend solely on the liquid saturation (Bond and Bernard, 1966).

5. Foam flows in a porous medium with constantly changing quality and, in certain regions, there may be four different phases flowing simultaneously. The production of emulsion (depending on the amount of free gas) complicates this mechanism even further.

Raza (1970) related foam quality to the presence of smaller pores in low-permeability porous media. This observation was supported by Mast (1970).

It has been postulated that four different phases flow simultaneously, at least for a certain period, for foam flow in a porous medium in the presence of oil. Still there will remain some ambiguity in terms of considering foam to flow as an entity or in two different phases.

3. STATEMENT OF THE PROBLEM

The principal objective of this work is to examine ways of efficiently waterflooding oil reservoirs (in the 1 to 200 mPa.s range), with a bottom-water zone. In particular, it is intended to

(a) study all or some of the following effects on waterflood with polymer, emulsion, air, foam, biopolymer gel, and silica gel as mobility control agents:

(i) effect of the oil-to-water zone thickness ratio,

(ii) effect of oil-water viscosity ratio,

(iii) effect of the oil-to-water zone permeability ratio,

(iv) effect of slug size of the mobility control agent,

(v) effect of concentration of the mobility control agent;

and

(b) determine the optimal slug size for the best-suited mobility control agents.

The theoretical investigation is to use the above information to

(a) explain the flow mechanisms involved in the respective processes, and obtain a simplified description of the process involved;

(b) develop and use a numerical simulator using the above formulation, and employ the experimental data to validate the numerical simulation; and

(c) derive scaling criteria for experimental design using the most effective mobility control agents.

4. EXPERIMENTAL APPARATUS AND PROCEDURE

4.1 EXPERIMENTAL APPARATUS

For the displacement tests conducted, the experimental apparatus consisted of a pump and a specially designed rectangular core holder.

A constant-rate, computer-controlled, positive displacement syringe pump was used. The pump was connected to two cylinders containing floating pistons. This gave the choice of alternating two different fluids without contaminating one with the other. The pump had a capability of pumping a maximum of 1200 ml/hr with a maximum allowable pressure of 7000 kPa. The pump was monitored and controlled by an IBM PC and the flow rate could be adjusted with a precision of 0.1 ml/hr. The pump displaced the piston of the floating-piston cylinder that was connected to the core holder with a flexible Tygon tubing. At the entrance of the core holder, a pressure transducer (0-172 kPa and 0-345 kPa) was connected so as to record the inlet pressure during the displacement test.

A rectangular core holder was built from a tubular aluminum block. The inside dimensions of the core are 122 cm length, 7.62 cm depth, and 5.08 cm width. The depth was greater as two or more different layers were planned to be used. The width was limited to 5.08 cm in order to avoid having too large a pore volume. On the other hand, this width was judged to be sufficient to avoid wall effects. The length was chosen to be long enough to have a macroscopic capillary number (Islam, 1985) low enough to obtain stabilized displacement (Bentsen, 1978). It should be mentioned here that it is commonly believed that most of the field displacements are stabilized and unstable (Islam and Bentsen, 1986). A flow regime is called stabilized when the macroscopic capillary number, which incorporates the end-point effective permeabilities and the area under the capillary pressure vs. saturation curve, is lower than 0.01. Whether a displacement is stable or unstable depends on the instability number which incorporates the effects of viscosity ratio, interfacial tension, flow rate and geometry of the porous medium. Therefore, a stabilized and unstable displacement would mean a low macroscopic capillary number and a high instability number. It was decided to employ unstable displacements to simulate the reservoir case, at least for the case of waterflooding.

The core holder is capable of resisting a maximal pressure of 2100 kPa. It has one inlet and one outlet at the middle of the inlet and outlet faces, respectively. These enable the packing of the glass beads and measurement of absolute permeability. The injection and production wells are located at 2.54 cm from each end of the core. The wells are 0.635 cm in diameter and are fitted with porous metal caps that prevented any flow of glass beads. The wells are so fitted that their penetration can be adjusted to any depth up to a maximum of 7.62 cm (total depth of the core). While waterflooding the core, only injection/production wells were used. On the other hand, for polymer treatment both inlet/oulet and production/injection wells were used depending on the thickness of the bottom-water layer.

The core holder had a lid along the bottom side. This enabled the packing of several layers in the lateral direction. Figure 1 depicts the schematic of the experimental set-up.

4.2 CHEMICALS

The materials used for the tests conducted are listed below :

a) Porous media: 80-120 mesh glass beads were used in layers where irreducible water saturation was established. 200-240, 80-120 or 20-30 mesh glass beads were used to model the water-saturated zone.

b) Oil phase : Four different oils were used as the displaced phase. These are :

(1) MCT-10: This oil was supplied by Imperial Oil Ltd. It was used for most of the runs.

(2) Kerosene: This oil was used for Runs 11, 39.

(3) Mineralube+kerosene: It was a blend of Mineralube (lubricating oil supplied by Esso Ltd.)

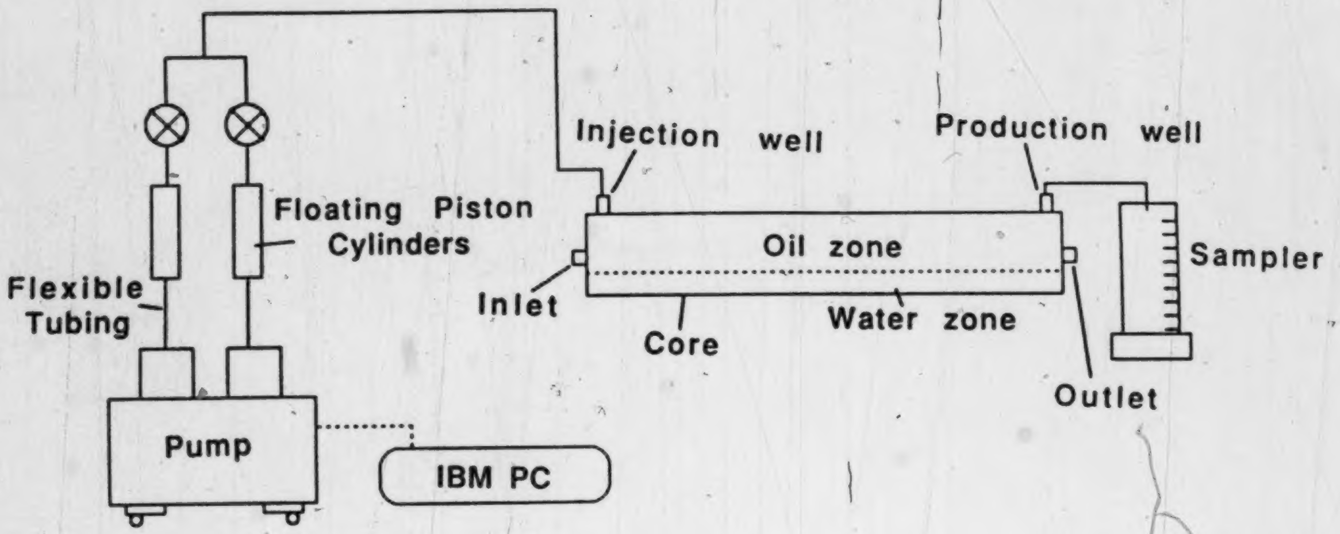
Injection well
Production well
Floating Piston Cylinders
Oil zone
Sampler
Flexible Tubing
Inlet
Core
Water zone
Outlet
Pump
IBM PC

Fig. 1 Schematic of the Experimental Set-up

and kerosene (60 percent Mineralube + 40 percent kerosene). This oil was used for Runs 12, 40, and 68.

(4) Faxam-100: It was supplied by Imperial Oil Ltd. This was used for Runs 13, 41, 69.

The properties of these oils are listed in Table 4.1.

c) Water phase : Distilled water was used in all waterflooding tests.

d) Polymer : A Dow-pusher 700 polyacrylamide solution was used in the polymer displacement tests. For most of the tests conducted, 500 ppm solution was prepared with distilled water. This solution had a viscosity of 64 mPa.s at a shear rate of 6 rpm.

e) Emulsion: Oil-in-water emulsion was prepared by mixing oil (MCT-10) with an aqueous solution of emulsifier. This so-called agent-in-water method is suitable for preparation of the emulsion formed externally (Broz et al., 1985). In order to obtain stable emulsion, 10 percent (of the total emulsion volume) of oil was added to distilled water containing 200 ppm of surfactant. EOR-300, as supplied by Ethyl Corporation, was used as a surfactant. The oil droplets had an average diameter of 1.5 microns. The proportion of oil and surfactant was selected after analyzing emulsion stability and average oil droplet diameter. Emulsion viscosity was found to be 1.8 mPa.s at

TABLE 4.1: Properties of Oils Used in Different Runs

Oil	Viscosity (cp)	Density(g/cc)	water/oil Interfacial Tension (dynes/cm)
MCT-10	50.0	.86	35.
Kerosene + Mineralube	7.5	.81	32.
Faxam-100	200	0.83	36.

six rpm. The stress-strain behaviour of the emulsion deviated slightly from that of a Newtonian fluid. For Runs for which Faxam-100 was used as the oil phase, emulsion was prepared from Faxam-100.

f) Biopolymer: Biopolymer FLOCON 4800 was used with cross linking of Cr^{+3}.

g) Surfactant: The surfactant that was used to generate foam in situ was supplied by Dow Chemicals. It was the best performer among many others tested. It was a 42-percent active, sulphonate base surfactant and was used at four percent concentration for most of the foam-flooding runs.

h) Silica gel: CO_2 was injected in an acidified (with HCl) solution of sodium orthosilicate. Acidified solution was first injected and was followed by CO_2 in order to produce silica gel.

4.3 PACKING AND PREPARATION OF RUNS

Glass beads were packed wet. No settlement was observed by vibrating the core. This is more likely the case as the glass beads are uniform in size, unlike sand. Once the core was packed, air was driven through the packing overnight in order to dry the core. Then a vacuum was pulled on the core and distilled water was allowed to be imbibed into the core. Then the core was connected to the pump and distilled water was pumped through. An accurate material balance, then, gave the pore volume of the core.

The pressure was recorded by a transducer at the core inlet. Once the pressure was stabilized, the pressure was recorded for subsequent calculation of the absolute permeability. At this point, an oil flood was conducted in order to establish the irreducible water saturation. A flow rate higher than that anticipated for the waterflood was used for this oil flood. This was important to avoid any flow of irreducible water during waterflooding. During the oil flood, the core was placed vertically and oil was injected from the top to assure maximal stability of the displacement (most suitable position for piston-like displacement). As the oil flood was conducted at a favourable mobility ratio (< 1) oil breakthrough took place very late and a very small fractional flow of water took place after breakthrough. However, the oil flood was continued until the water cut fell below one percent of the total flow. It took about 1.2 PV to reach this condition. At this point, the irreducible water saturation, S_{wi} was assumed to have been reached. Then the core was opened by taking the lid off. The top part was scraped off until the desired height of the oil zone was reached. Meanwhile, a wet packing of glass beads (of desired mesh-size) was prepared and the absolute permeability was calculated. This water-wet packing layer was then added to the top of the oil-flooded layer of the core. As glass beads are easily compacted (due to uniform size), the added layer was assumed to have the same absolute permeability as the previously packed glass beads. Whenever a barrier was desired, a plastic sheet (of desired length) was simply laid down on top of the oil zone and then the water-saturated layer was added. Once the water-saturated layer was in place, the lid was put back on and the core was rotated 180° axially to bring the oil zone on top and water zone at the bottom. At this point the core was ready for a waterflood, or other displacements.

5. PRESENTATION OF EXPERIMENTAL DATA

Eighty-five displacement tests were performed. Figure 2 depicts the different types of experimental runs conducted. The results of all the runs are summarized in Table 5.1. Initially, base waterflood runs were performed in the absence of any bottom-water zone. Following this, various runs were performed with a bottom-water zone. Each of these runs is described under different sections according to the mobility control agents used.

5.1 Base Waterfloods Without Bottom Water

Runs 1 & 2: Waterfloods at different flow rates

For these runs a single layer was used. This was done to observe the waterflood performance without a bottom-water layer. Two displacement tests were carried out at different waterflood rates. These runs were used to obtain the reservoir performance under base conditions so as to be able to compare the results with those obtained with a bottom-water layer. These runs were performed in a smaller core. This core holder was used because the currently used core holder was not available at the time. For Run 1, a waterflood rate of 400 ml/h was used. Water breakthrough occurred at 26 percent of the pore volume injected. Figure 3 shows the oil recovery, oil cut and WOR curves. For Run 2, an injection rate of 800 ml/h was used. For this run, the water breakthrough took place at an earlier point

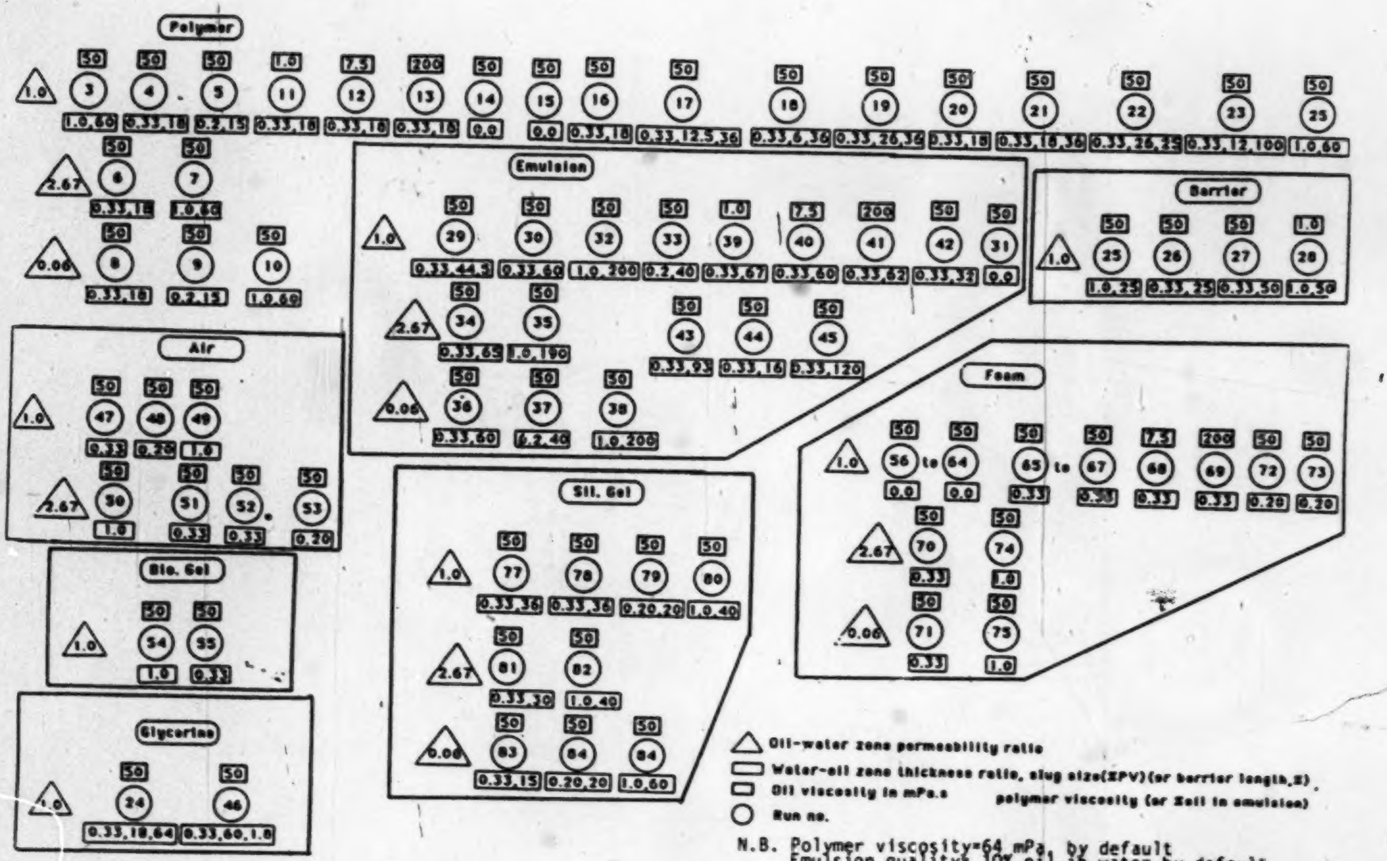
Polymer
Emulsion
Barrier
Air
Bio. Gel
Glycerine
Sil. Gel
Foam
Oil-water zone permeability ratio
Water-oil zone thickness ratio, slug size(%PV)(or barrier length,%)
Oil viscosity in mPa.s
polymer viscosity (or %oil in emulsion)
Run no.

N.B. Polymer viscosity=64 mPa, by default
Emulsion quality= 10% oil-in-water by default

Fig. 2 Characteristics of Different Experimental Runs Conducted

TABLE 5.1: Characterstics of Packing and Results of Different Runs

Run no.	k_o (μm^2)	k_o/k_b	Blocking Agent	μ_o/μ_w	h_b/h_o	Recovery[1]
1	16.2	N.A.	None	50.	0.00	64
2	15.8	N.A.	None	"	0.00	N.Av.
3	16.4	1.00	Polymer	"	1.00	62
4	16.0	1.00	"	"	0.33	70
5	15.8	1.00	"	"	0.20	73
6	16.2	2.67	"	"	0.33	73
7	15.9	2.67	"	"	1.00	68
8	16.0	0.06	"	"	0.33	60
9	16.2	0.06	"	"	0.20	65
10	16.0	0.06	"	"	1.00	45
11	16.2	1.00	"	1.0	0.33	66.5
12	16.4	1.00	"	7.5	0.33	72
13	16.0	1.00	"	200.	0.33	26.5
14	16.2	N.A.	"	50.	0.00	77
15	16.0	N.A.	"	"	0.00	74
16	16.0	1.00	"	"	0.33	65
17	16.0	1.00	"	"	0.33	53
18	16.2	1.00	"	"	0.33	51
19	16.0	1.00	"	"	0.33	57
20	16.0	1.00	"	"	0.33	53
21	15.9	1.00	"	"	0.33	60
22	15.9	1.00	"	"	0.33	50.5
23	16.2	1.00	"	"	0.33	53
24	16.2	1.00	Glycerine (64 mPa.s)	"	0.33	42.5
25	16.0	1.00	Polymer+ Barrier(25%)	"	1.00	67
26	16.1	1.00	Barrier(25%)	"	0.33	49
27	16.2	1.00	Barrier(50%)	"	0.33	54
28	16.0	1.00	Barrier(50%)	"	1.00	33
29	16.3	1.00	Emulsion (5% oil)	"	0.33	32
30	16.1	1.00	Emulsion (10% oil)	"	0.33	54
31	16.0	N.A.	"	"	0.00	79

N.A. Not applicable

[1] %IOIP at WOR=20 or GLR=7000 (after using blocking agents)

[a] Injection pressure=69 kPa

TABLE 5.1 ...Cont'd.

Run no.	k_o (μm^2)	k_o/k_b	Blocking Agent	μ_o/μ_w	h_b/h_o	Recovery[1]
32	16.15	1.00	Emulsion(10% oil)	50.	1.00	49
33	16.0	1.00	"	"	0.20	61
34	16.0	2.67	"	"	0.33	59.5
35	16.0	2.67	"	"	1.00	61
36	15.8	0.06	"	"	0.33	35
37	16.2	0.06	"	"	0.20	43
38	15.8	0.06	"	"	1.00	29
39	16.1	1.00	"	1.00	0.33	66.5
40	16.0	1.00	"	7.5	0.33	76
41	16.0	1.00	"	200.	0.33	33
42	16.0	1.00	"	50.	0.33	49.5
43	16.0	1.00	"	"	0.33	56.5
44	16.0	1.00	"	"	0.33	38
45	16.0	1.00	"	"	0.33	57.5
46	16.0	1.00	Glycerine (1.8mPa.s)	"	0.33	28
47	16.2	1.0	Air	"	0.33	41.5
48	15.7	1.00	"	"	0.20	61
49	16.1	1.00	"	"	1.00	16
50	16.0	2.67	"	"	1.00	37
51	16.0	2.67	"	"	0.33	58
52	16.1	2.67	Air (Inj. thr. prod. well)	"	0.33	59
53	15.8	2.67	Air	"	0.20	64
54	16.0	1.00	Biopolymer Gel	"	1.00	11.5
55	16.0	1.00	"	"	0.33	43
56	16.0	N.A.	Foam	"	0.00	28
57	16.2	N.A.	"	"	0.00	32
58	15.5	N.A.	"	"	0.00	43
59[a]	16.0	N.A.	"	"	0.00	50
60	15.7	N.A.	"	"	0.00	49
61	16.0	N.A.	"	"	0.00	33
62	16.0	N.A.	"	"	0.00	25

N.A. Not applicable
N.Av. Not available
1 %IOIP at WOR=20 or GLR=7000 (after using blocking agents)

TABLE 5.1 ...Cont'd.

Run no.	k_o (μm^2)	k_o/k_b	Blocking Agent	μ_o/μ_w	h_b/h_o	Recovery[1]
63[b]	16.2	N.A.	Foam	50.	0.00	43
64[c]	16.0	N.A.	"	"	0.00	41
65	15.6	1.0	"	"	0.33	46
66	16.2	1.0	"	"	0.33	57
67	16.0	1.0	"	"	0.33	50
68	15.6	1.0	"	7.5	0.33	62
69	15.9	1.0	"	200.	0.33	23
70	16.2	2.67	"	50.	0.33	46
71	16.0	0.06	"	"	0.33	30
72	15.7	1.0	"	"	0.20	64
73	16.0	1.0	"	"	1.0	47
74	16.0	2.67	"	"	1.0	49
75	16.0	0.06	"	"	1.0	15
76[d]	16.2	1.00	"	"	0.33	46
77	15.8	1.00	Silica Gel	"	0.33	57
78	16.0	1.00	"(without CO_2)	"	0.33	52
79	16.0	1.00	Silica Gel	"	0.20	64
80	16.1	1.00	"	"	1.00	48
81	16.0	2.67	"	"	0.33	58
82	15.9	2.67	"	"	1.00	62
83	16.2	0.06	"	"	0.20	48
84	16.0	0.06	"	"	0.33	41
85	15.8	0.06	"	"	1.00	38

N.A. Not applicable
1 %IOIP at WOR=20 or GLR=7000 (after using blocking agents)
b Injection pressure=138 kPa
c Injection pressure=340 kPa
d Alternated with surfactant-free water slugs

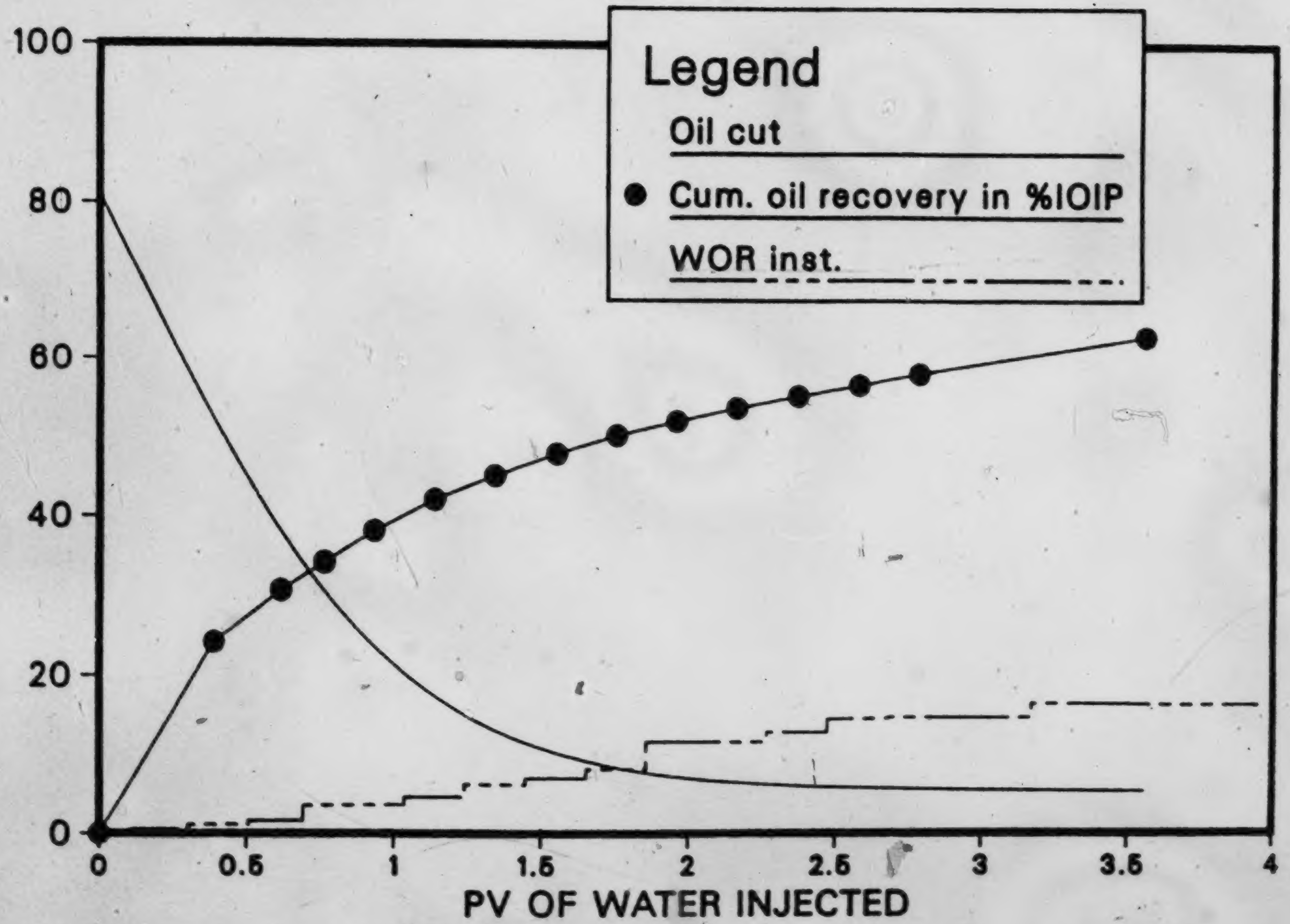

Fig.3a Waterflood Performance for Run 1 ($h_b/h_o=0$)

in time (at 0.24 PV as compared to 0.26 PV in Run 1). This flow rate-dependence of the breakthrough recovery is expected for an unstable displacement (Islam and Bentsen, 1985; Sigmund et al., 1985). Figure 3a depicts the WOR, oil recovery and oil cut for Run 2. To determine the exact flow regime, one has to calculate the instability number for the displacement system (Bentsen, 1985). This number needs knowledge of the capillary pressure data for the fluid/matrix system involved in order to estimate the pseudointerfacial tension of the system. By approximating the pseudointerfacial tension from the oil-water interfacial tension one can estimate the instability number. This number was calculated for each of the waterflood runs in a homogeneous pack.

5.2 Bottom Water: Water and Polymer Injection Runs

5.2.1 Effect of Water-to-Oil Zone Thickness and Permeability Ratio

Run 3: $h_b/h_o=1$, $k_o/k_b=1$

Run 3 was conducted with a bottom-water layer of thickness equal to that of the oil zone. Both the production and injection wells were situated at a penetration depth of 50 percent of the total height of the oil zone. The waterflood started with a flow rate of 800 ml/h. As the oil recovery and the oil cut curves indicate

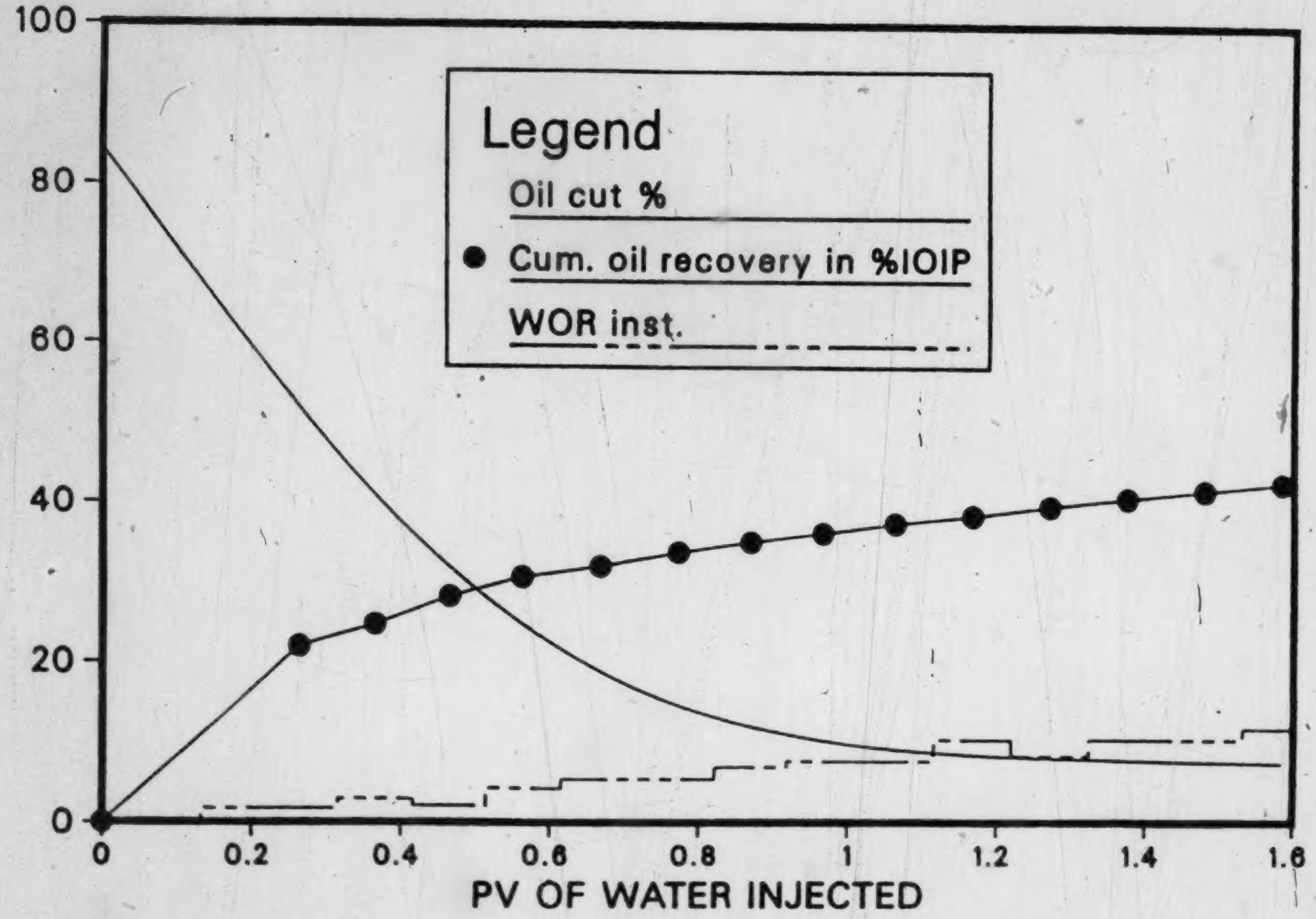

Fig.3b Waterflood Performance for Run 2 (h_b/h_o=0)

in Figure 4, the oil recovery performance was extremely poor. The water breakthrough occurred almost instantaneously. The WOR was very high from the beginning of the displacement and the oil cut fell to a very low value. After injecting more than two pore volumes of water, the volumetric injection rate was lowered to 400 ml/h in order to examine the effect of flow rate on the WOR values. It was observed that the WOR value decreased to almost half of the previous value (from a value of 42 to about 22). However, this value was still very high, and even after injection of two pore volume of water the total oil recovery was only 11 percent of the IOIP. At this time, the waterflood was stopped and injection of a polymer solution slug was planned. A polymer concentration of 500 ppm was used.

As the oil recovery was very poor for the waterflood, it was most likely that the injected water channeled through the bottom water without sweeping the oil zone. The polymer solution was expected to follow the same path and as a result of this polymer flow the effective permeability to water would decrease. This decrease will lead to a mobility reduction of the bottom water. Also, since the bottom-water layer was very close to the injection well, it was decided to inject the polymer solution through the injection well instead of the inlet end. Polymer solution was injected at a flow rate of 400 ml/h. The injection pressure increased

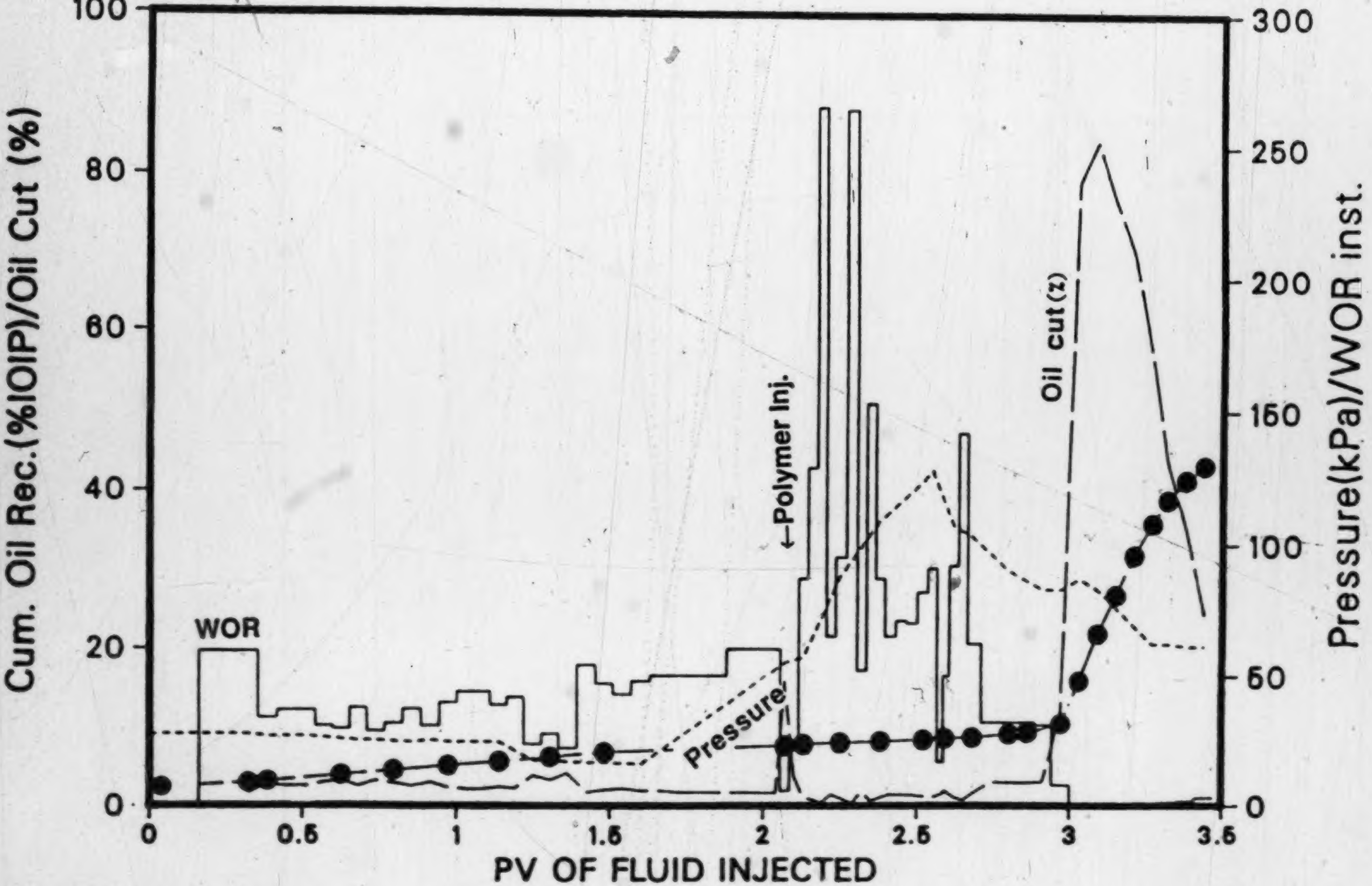

Fig. 4 Waterflood and Polymer Flood Performance for Run 3 (h_b/h_o=1.00, k_o/k_b=1.00)

markedly. This is evident from Figure 4. The polymer solution had a viscosity of 64 mPa.s at 6 rpm. Such an increase was expected. Polymer solution injection continued until a slug of 60 percent of the oil zone pore volume was injected. However, this was only 30 percent of the pore volume of the entire system. As a consequence, during the polymer flood very little improvement in oil recovery was observed. This indicated that the water near the production well was still mobile. This also confirmed that the polymer solution indeed travelled through the bottom-water zone.

Immediately following polymer injection, a waterflood was carried out at a flow rate of 400 ml/h. This was the injection rate that was used during the latter part of the waterflood. As this phase of the waterflood continued, a slow increase in oil cut took place. This slow response continued until 0.25 PV was injected. At this point, a sudden increase in the oil cut was observed. This was accompanied by a drastic decrease in the producing WOR value. This delay in response of the increased oil recovery was because the polymer-rich aqueous phase had to travel a long distance in order to reduce the mobility of the water phase around the production well. As the water mobility was reduced by the polymer solution, the bottom-water layer was practically isolated from the oil zone, and oil recovery increased considerably. The oil cut kept increasing for a certain time. After that, it started decreasing slowly.

Run 4: $h_b/h_o=0.33$, $k_o/k_b=1$.

In order to examine the effect of the ratio of the oil zone and bottom water thickness ratio, Run 4 was conducted. For this run, the oil zone was three times as thick as the bottom-water zone. The wells, this time, were located at a depth of 0.75 inch from the top compared to the thickness of two inches of the oil zone. The water injection was conducted at a flow rate of 400 ml/h. The WOR, pressure, oil recovery and oil cut are depicted in Figure 5. The oil recovery in this run is clearly better than that in Run 3. However, the breakthrough still took place almost immediately after the waterflood started and oil recovery performance was much poorer than that for a homogeneous porous medium. Eighteen percent of the IOIP was produced after injecting a volume of 0.76 PV.

At this point, polymer solution (500ppm) was injected at a flow rate of 400 ml/h. As the bottom-water zone was thinner than that in Run 3 and as the oil recovery curve indicated that at least a part of the injected water was flowing through the oil zone, it was decided to inject the polymer solution through the inlet end (see Figure 1). A polymer slug of 230 ml was injected. This was only 18 percent of the pore volume of the oil zone. But since this volume was equal to about 0.60 PV_b, the polymer slug volume was considered to be sufficient to block the bottom-water zone. As before, there was no immediate perceptible effect,

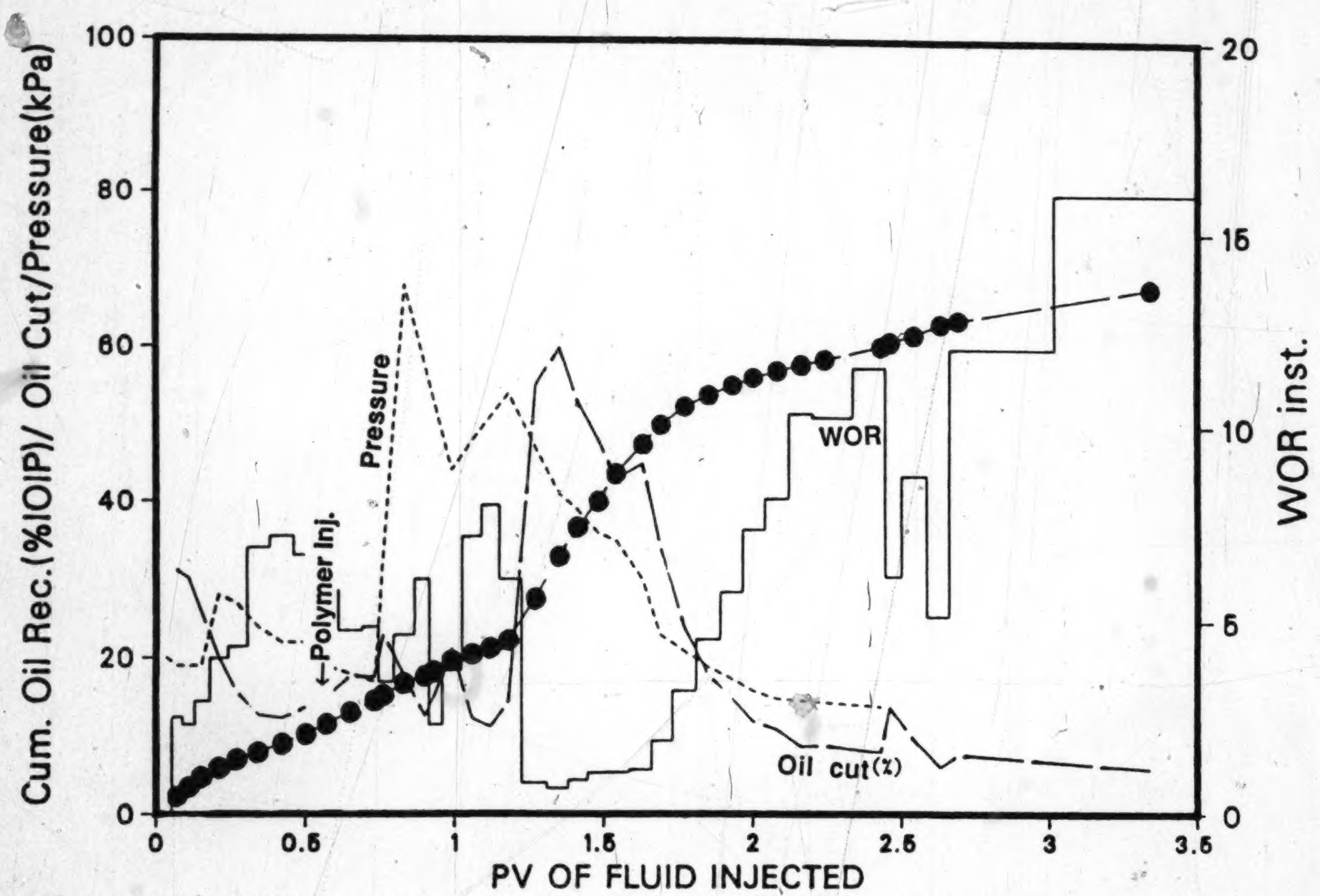

Fig. 5 Waterflood and Polymer Flood Performance for Run 4 (h_b/h_o=0.33, k_o/k_b=1.00)

except that the injection pressure increased. The polymer slug was followed by water injection. As observed in the previous run, a sudden decrease in WOR and an increase in oil cut started after injecting about 0.18 PV of water. As the waterflood continued, the WOR increased gradually. With a water injection of 1.5 PV, a total of 70 percent of the IOIP was recovered. This performance is better than that of a waterflood in a homogeneous layer, showing the effectiveness of the polymer flood in heterogeneous media.

Run 5: h_b/h_o=0.2, k_o/k_b=1

Run 5 was conducted to investigate further the effect of the oil-to-water zone thickness ratio. For this run the oil zone was five times thicker than the bottom-water zone and the absolute permeabilities were the same. The injection and production wells were located 1.6 cm (fractional penetration, h_w/h_o=0.25) into the oil zone. The displacement test started with a waterflood at 400 ml/hr. The WOR, pressure, oil recovery and oil cut are depicted in Figure 6. The oil recovery was much better than that in Run 4 for which a thicker (h_b/h_o=0.33) bottom-water zone was used. The waterflood was continued until one pore volume of water was injected. About 25 percent of the IOIP was recovered during the waterflood when the WOR reached a value of 10.

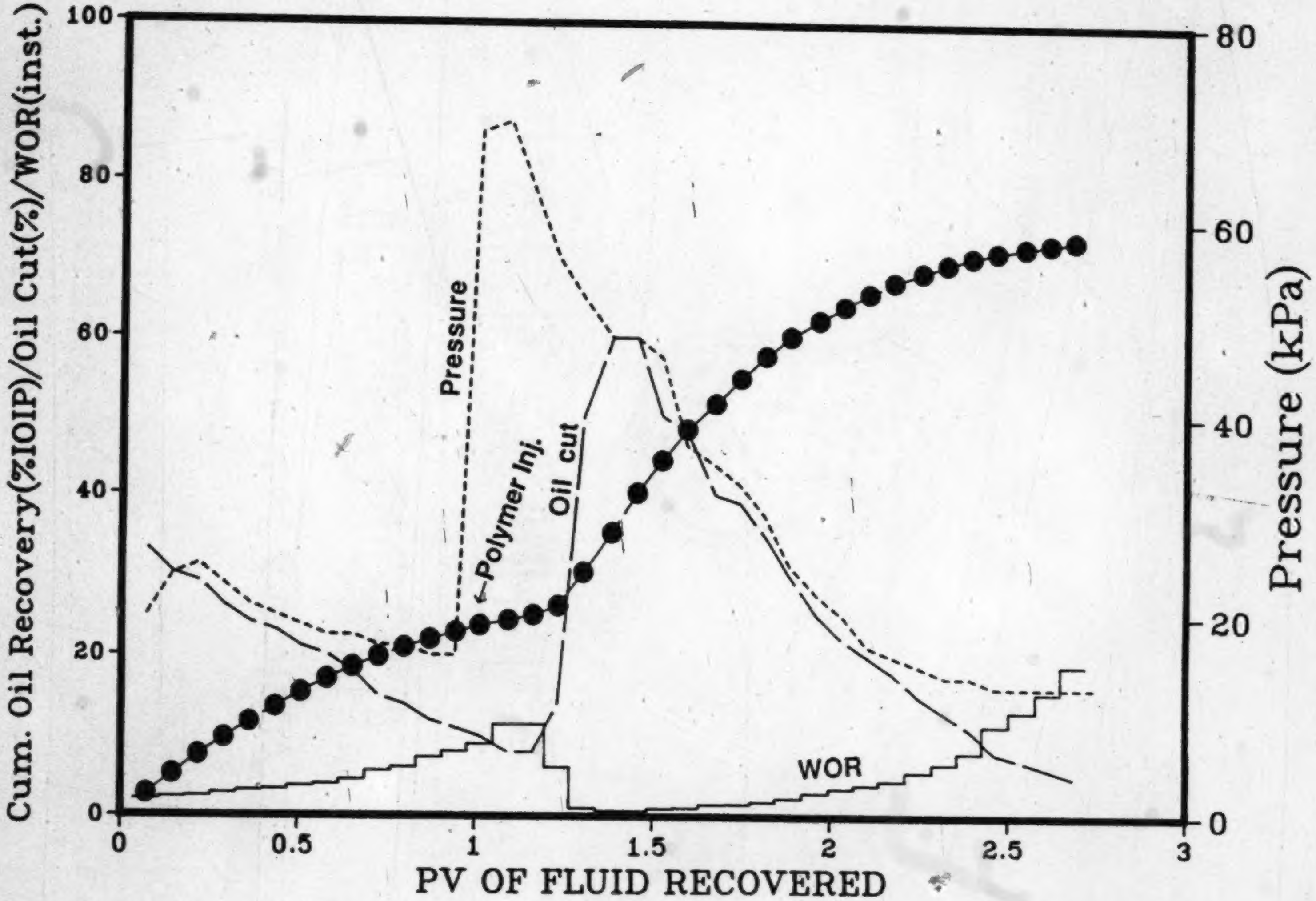

Fig. 6 Waterflood and Polymer Flood Performance for Run 5 (h_b/h_o=0.20, k_o/k_b=1.00)

A polymer slug of 0.15 pore volume was injected at a flow rate of 400 ml/hr following the waterflood. This volume was approximately 60 percent of the pore volume of the bottom-water zone. The polymer flood was again followed by a waterflood. Even though the injection pressure was high during water injection, any perceptible effect in oil cut took place only after injecting 0.30 PV of fluid (after commencing the polymer flood). A similar delay was observed for other polymer injection runs as well. The oil cut continued to increase for another 0.30 PV of water injection. As the oil cut reached a peak of around 80 percent, more than 44 percent of the IOIP was recovered. Following the peak, the oil cut started decreasing rather rapidly. However, a total of 73 percent of the IOIP was recovered when WOR reached a value of 20. Even though this value is close to what was obtained in Run 4 (70 percent of the IOIP), this WOR was reached much earlier.

Run 6: $h_b/h_o=0.33$, $k_o/k_b=2.67$

For this run, h_b/h_o was equal to 0.33, and this time (see Table 5.1) the bottom-water zone had a permeability less than that of the oil zone($k_o/k_b=2.67$). This enabled one to examine the recovery performance with a bottom-water layer having lower permeability. The production/injection wells penentrated one-quarter of the way through the oil zone. The waterflood started with an injection rate of 400 ml/h. This flow rate was chosen to compare the recovery with that in Run 4, that had a similar oil-water zone thickness ratio but had no permeability contrast. Even though breakthrough occurred very early, the oil recovery was much better than that in Run 4, showing thereby that the decrease in permeability of the bottom-water zone is favourable to oil recovery. After a water injection of 0.41 PV, the recovery was 18 percent, compared to over 30 percent recovery in homogeneous media.

At this point, the polymer injection was carried out through the inlet end rather than the injection well. The same injection point was used in Run 6. This selection of the polymer injection point was made based on the common field practice of dual completions for which different mobility control agents may be injected selectively through different layers of the reservoir. The sudden increase in pressure is evident from Figure 7. A polymer slug of 0.18 PV was injected. As usual, there was a delay in response before a sudden increase in oil cut occurred. As the waterflood continued, a total of over 70 percent IOIP was produced after injecting one pore volume of water.

Run 7: $h_b/h_o=1$, $k_o/k_b=2.67$

The oil-water zone thickness ratio was similar to that for Run 3 but the permeability of the water zone was 6 μm^2, that is about 2.67 times smaller than that of the oil zone.

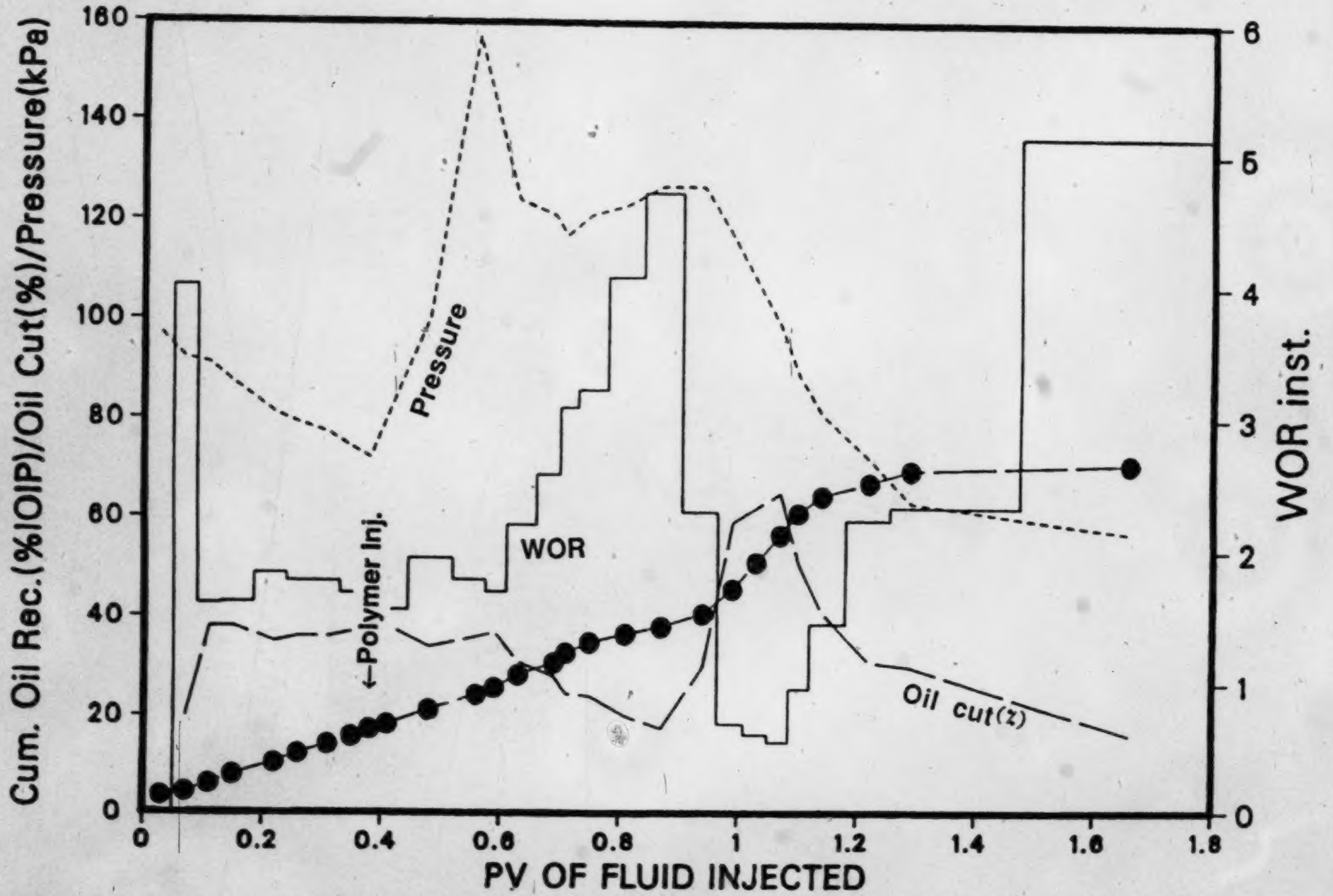

Fig. 7 Waterflood and Polymer Flood Performance for Run 6 (h_b/h_o=0.33, k_o/k_b=2.67)

The waterflood started with a flow rate of 400 ml/h. The water breakthrough occurred almost immediately after the waterflood was started but the oil recovery was much better than that for Run 3 where the bottom-water zone had the same permeability as the oil zone. As a matter of fact, the oil recovery performance by the waterflood was similar to that in Run 4, for which the h_b/h_o value was 0.33 and the k_o/k_b value was 1. Note that Runs 4 and 7 had similar capacities of the bottom-water zone. After injecting 1.1 PV of water, the waterflood was stopped and polymer solution injection started. Figure 8 shows the recovery, WOR, oil cut and pressure performance for this run.

A polymer flood took place at a flow rate of 500 ml/h and the injection well was used for injecting the polymer. A polymer slug of 0.60 PV was injected. As before, the increase in oil cut did not take place during the polymer flood but the injection pressure increased. The polymer flood was followed by water injection at 400 ml/h. The increase in oil cut took place rather gradually. It was followed by a decrease in WOR. As the waterflood continued the total oil recovery reached about 70 percent of the IOIP after injecting a total of 3.3 PV.

Run 8: h_b/h_o=0.33, k_o/k_b=0.06

In order to examine the effect of a high-permeability bottom-water zone (k_o/k_b=0.06) Runs 8 through 10 were

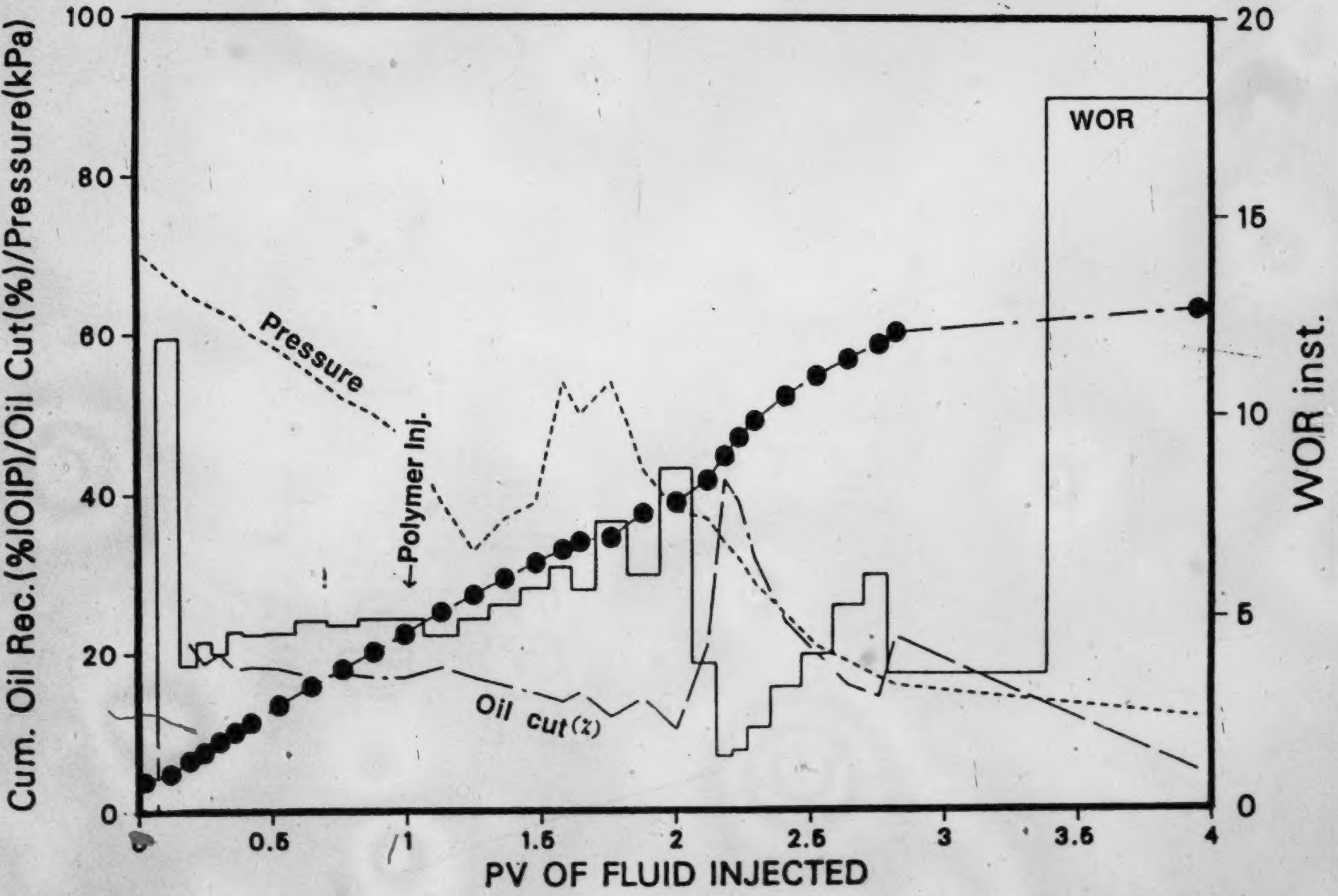

Fig. 8 Waterflood and Polymer Flood Performance for Run 7 (h_b/h_o=1.00, k_o/k_b=2.67)

conducted. For Run 8, the oil zone was three times thicker than the bottom-water zone. The wells were located at a depth of 0.75 cm into the oil zone. The displacement test started with a waterflood at a flow rate of 400 ml/hr. As expected, a high-permeability bottom-water zone led to a high WOR even though the h_b/h_o was relatively low. As the waterflood continued, the WOR increased rapidly. By the time the WOR reached a value of 20, only five percent of the IOIP was recovered. This poor performance shows the ineffectiveness of a waterflood in the presence of a highly permeable bottom-water zone. Figure 9 depicts the WOR, pressure, oil cut and oil recovery for this run. The water injection was continued until 1.2 pore volumes had been injected. It was then followed by a polymer flood. Polymer solution was injected through the inlet end in order to have better access to the bottom-water zone (see Figure 1 for the distinction between inlet end and injection well). After injecting 0.18 PV of polymer solution, the waterflood was resumed. Similarly to previous polymer injection runs, no improvement in oil cut was observed instantly. The oil cut started increasing after an injection of 40 percent pore volume of fluid (polymer solution and water). Following this, the oil cut increased very rapidly for about 0.30 PV. After reaching a peak of around 80 percent, the oil cut started decreasing rapidly but led to a total oil recovery of 60 percent of the IOIP as the WOR reached a value of 20.

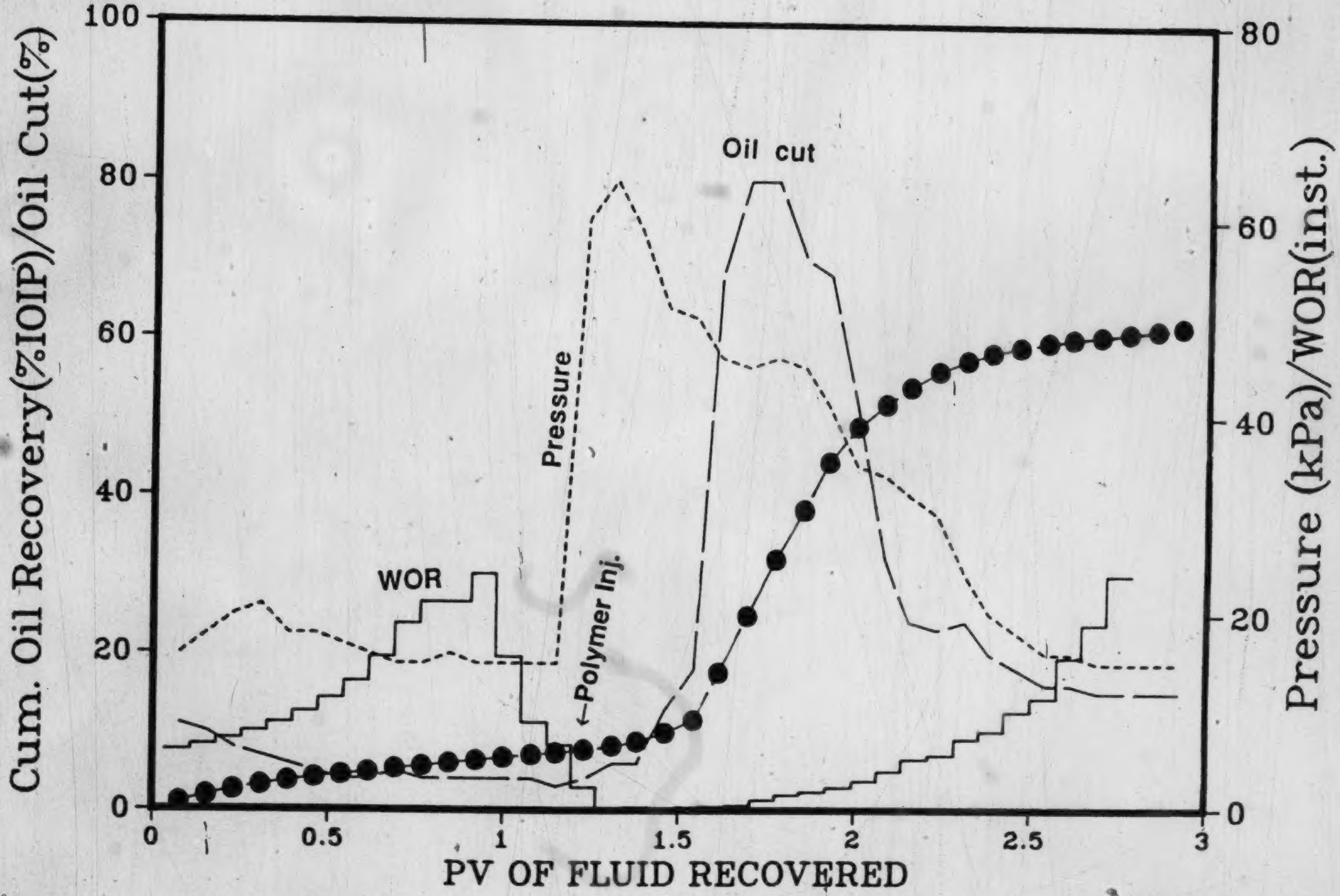

Fig. 9 Waterflood and Polymer Flood Performance for Run 8 ($h_b/h_o=0.33$, $k_o/k_b=0.06$)

This indicated a 12-fold improvement over a conventional waterflood.

Run 9: $h_b/h_o=0.2$, $k_o/k_b=0.06$

In order to investigate the effect of the oil-to-water zone thickness ratio for a k_o/k_b of 0.06, Run 9 was conducted with an oil-to-water zone thickness ratio of five. The wells were located at 1.6 cm (one-quarter of the total thickness of the oil zone) into the oil zone. The displacement test was started with a waterflood at a flow rate of 400 ml/hr. The WOR was only slightly lower than that in Run 8 for which an h_b/h_o of 0.33 was used. Note that much greater improvement was observed for the same decrease in h_b/h_o for $k_o/k_b=1$. It appears that as the k_b/k_o value increases, the effect of permeability contrast is greater than the effect of the oil-to-water zone thickness ratio. When the WOR reached a value of 20, only seven percent of the IOIP of oil was recovered. After injecting one pore volume of water, a polymer flood was started at a flow rate of 400 ml/hr. The polymer injection was carried out through the inlet end. Even though the injection pressure was high, no immediate improvement in oil cut was observed. The polymer flood was ended after injecting 0.15 PV volume of polymer solution. This slug size was the same as that injected in Run 5 ($h_b/h_o=0.2$, $k_o/k_b=1$). It was assumed that only the thickness of the bottom-water zone determines the size of the polymer slug. This assumption implies that a change in slug size is not required for the change in permeability of the bottom-water zone. The polymer flood was then followed by another waterflood. As the waterfood continued, the oil cut started increasing rapidly. This point at which the oil cut started to increase corresponded to a total fluid injection of 0.25 pore volume after the commencement of polymer injection. This delay was smaller than that of Run 5 for which the same thickness but a tighter bottom-water zone was used. Figure 10 depicts the WOR, pressure, oil cut and oil recovery in Run 9. As can be seen from this figure, the oil cut decreased rapidly after reaching a peak of around 80 percent. At the end of the displacement test a total of 65 percent of the IOIP was recovered. This shows more than a 9-fold improvement over a conventional waterflood. Also, the ultimate oil recovery for this run was 7.7 percent higher than that observed in Run 8 for which an h_b/h_o of 0.33 was used.

Run 10: $h_b/h_o=1$, $k_o/k_b=0.06$

In order to investigate further the effects of the oil-to-water zone thickness ratio for k_o/k_b of 0.06, Run 10 was conducted with an h_b/h_o of 1. The wells were located at 50% depth of the oil zone. Initially, a waterflood was started at a flow rate of 400 ml/hr. The waterflood gave an

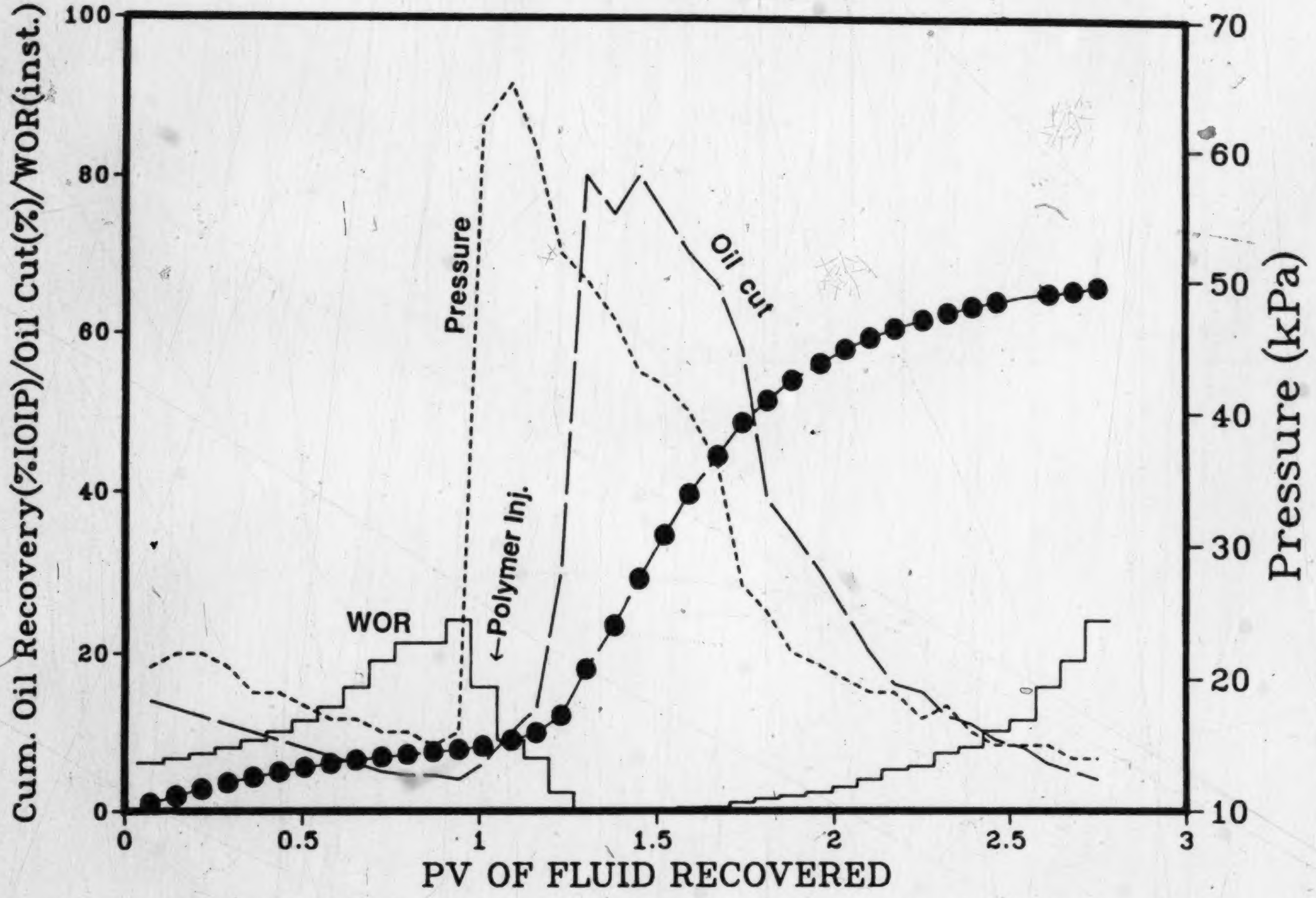

Fig. 10 Waterflood and Polymer Flood Performance for Run 9 (h_b/h_o=0.20, k_o/k_b=0.06)

extemely poor performance for this run. This behaviour was expected as both the thickness and permeability of the bottom-water zone were very unfavourable for this run. Only two percent of the IOIP was recovered as the WOR reached a value of 20. As the waterflood continued, the WOR increased very rapidly. Consequently, water injection was terminated at 0.75 PV of water injection. This was followed by a polymer injection at a flow rate of 400 ml/hr. The oil cut continued to be low even after polymer injection that was being carried out though the injection well. A polymer slug of 0.60 PV was injected. Before polymer slug injection was terminated, the oil cut started increasing and continued to increase as the polymer flood was followed by a waterflood. Soon, the oil cut reached a peak of 60 percent. This value was considerably lower than the peak attained in other polymer injection runs. However, considering the very poor waterflood performance this could be considered as significant improvement over a conventional waterflood. Figure 11 depicts the WOR, pressure, oil cut and oil recovery performance for this run. As can be seen from this figure, a delay of 0.34 pore volume was observed after the commencement of the polymer flood to obtain an increase in oil recovery. This value was much smaller than that observed in Run 3 ($h_b/h_o=1$, $k_o/k_b=1$). Apparently, a higher permeability of the bottom-water zone led to a quicker response to polymer flooding. At the end of the

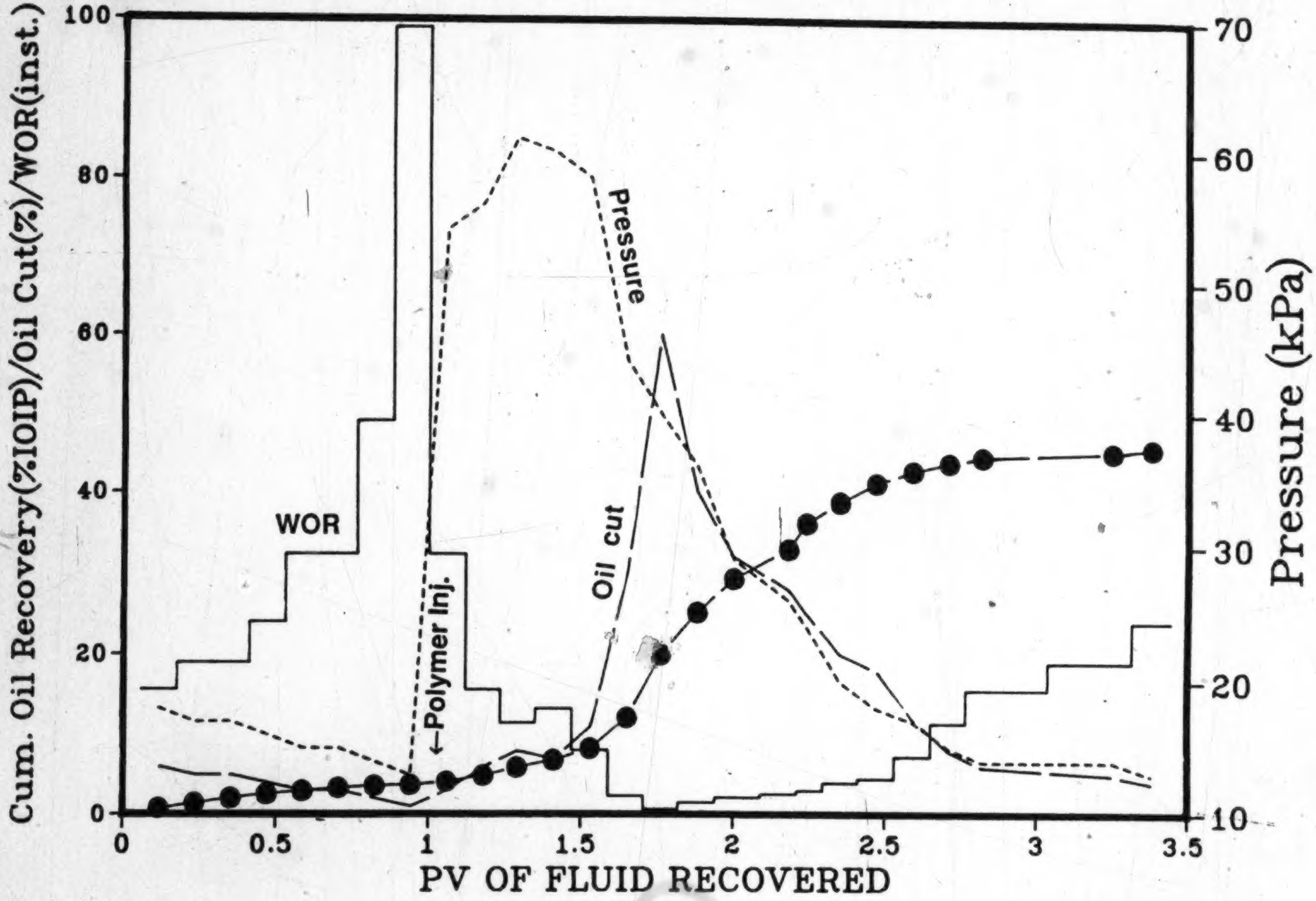

Fig. 11 Waterflood and Polymer Flood Performance for Run 10 (h_b/h_o=1.00, k_o/k_b=0.06)

displacement test 45 percent of the IOIP was produced when the WOR reached a value of 20. Even though this value of the ultimate oil recovery was significantly lower than that for other polymer injection runs, considering the unfavourable bottom-water zone characteristics the polymer flood performance was remarkably good and corresponded to more than a 22-fold improvement over a conventional waterflood.

5.2.2 Effect of Viscosity Ratio

Several runs were conducted to examine the effect of viscosity ratio on polymer injection runs. All these runs were conducted with $h_b/h_o=0.33$ and $k_o/k_b=1$. Similar packing characteristics were necessary to be able to compare the results.

Run 11: Viscosity Ratio=1

In order to examine the effect of low oil viscosity, Run 11 was conducted. The packing characteristics were the same as those of Run 4 (i.e., bottom-water zone one third as thick as the oil zone). Both the injection and production wells penetrated 25 percent inside the oil zone. Kerosene was used as the oil phase for this displacement test. The waterflood was started at 400 ml/h. For this run water breakthrough did not take place until 0.075 PV of water injection. The oil cut was very high (above 75 percent) at the initial stage. This resulted in accelerated oil recovery. As a consequence, 56 percent of the IOIP was recovered after injecting only 0.638 PV of water. This can be seen from Figure 12. This compares to only 15.5 percent of oil recovery in Run 4 after injecting same pore volume of water. At this point, a polymer slug of 0.265 PV (equivalent to 0.79 PV_b) was injected. The polymer injection took place at 400 ml/h. The injection pressure increased considerably but the WOR continued to increase. As the polymer slug was later followed by a waterflood at 400 ml/h, the inlet pressure decreased slightly and stabilized at a value much higher than that attained before polymer injection (see Figure 12). Even though the inlet pressure increased, no increase in oil cut was observed. For a WOR value of 20, a total of 66.5 percent of the IOIP was recovered. A similar oil recovery was obtained in Run 4. However, only 2.4 PV of fluid was injected for this recovery in Run 11, whereas over three pore volumes of fluid were injected in Run 4. Another point of interest is that, in Run 4 only about 18 percent of the IOIP was recovered by initial water injection of 0.76 PV and most of the oil was recovered after polymer injection that was marked by a considerable reduction in WOR. In Run 11, on the contrary, most of the oil was recovered by waterflooding and no decrease in WOR took place after polymer injection. It appears, therefore, that polymer injection following a

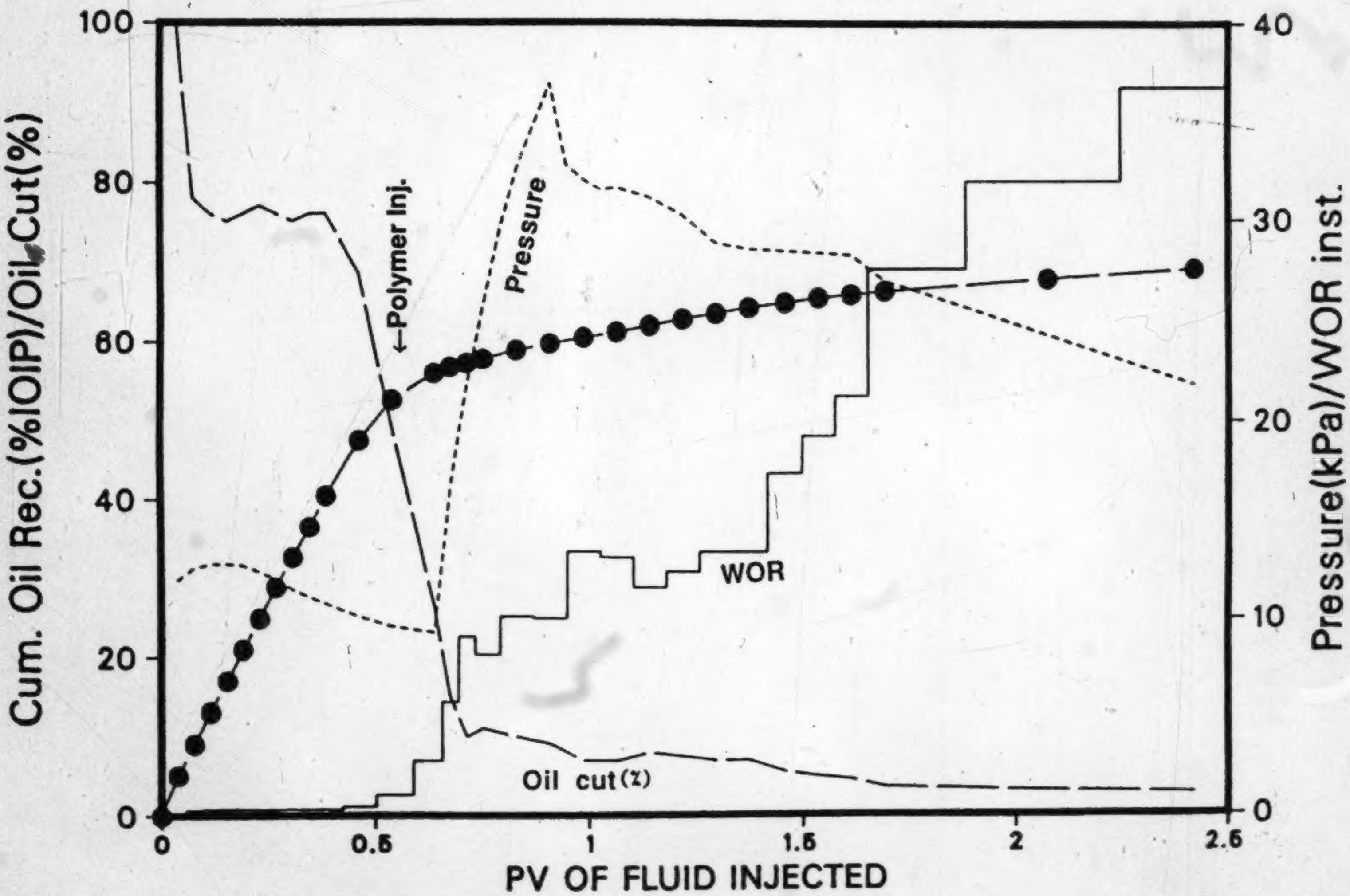

Fig. 12 Waterflood and Polymer Flood Performance for Run 11 (h_b/h_o=0.33, k_o/k_b=1.00)

waterflood is not efficient in the case of a very light oil.

Run 12: Viscosity Ratio=7.5

An oil of 7.5 mPa.s viscosity was selected to examine the effects of oil viscosity on polymer flooding in this range. The packing characteristics are given in Table 5.1. As the thickness of the bottom-water zone was similar to that for Runs 4 and 11, the results can be compared directly. At the beginning of the run, a waterflood was started at 400 ml/h. The water breakthrough occurred at six percent pore volume of water injection. However, as the waterflood continued the oil cut was still high as compared to that of Run 4, but was low as compared to that of Run 11 for which the oil viscosity was only one mPa.s. By the time one pore volume of water was injected, 32.5 percent of the IOIP was recovered. The oil cut, inlet pressure, WOR and cumulative oil production are plotted in Figure 13. This value, once again, is much higher than 18 percent as evidenced in Run 4 (μ_o/μ_w=50) but is lower than 60 percent as evidenced in Run 11 (μ_o/μ_w=1). After injecting little more than one pore volume of water, a polymer slug of 0.2 PV was injected. This slug size was also equivalent to 60 percent of the bottom water zone pore volume, PV_b. During polymer injection, the injection pressure increased but there was no effect on oil cut. After injecting this polymer slug, a waterflood was started at 400 ml/h. The oil

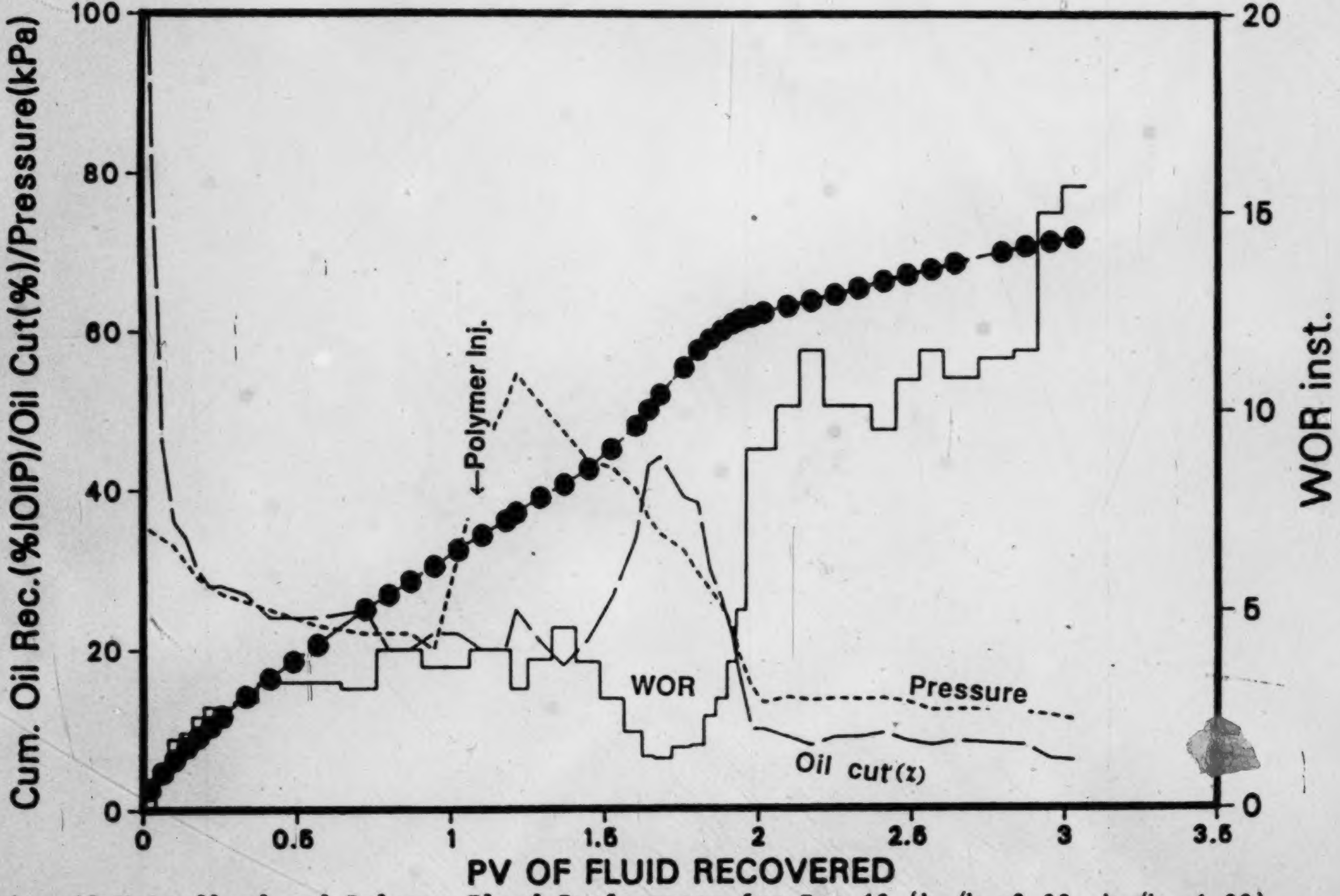

Fig. 13 Waterflood and Polymer Flood Performance for Run 12 (h_b/h_o=0.33, k_o/k_b=1.00)

cut started to increase after 0.3 PV of polymer was injected. This increase in oil cut continued until a peak was obtained. The injection pressure followed a very similar trend as well. The waterflood continued until the WOR reached a value of 20. A total of 72 percent of the IOIP was recovered during this period. As can be seen from Table 5.1, the ultimate recovery in this run was higher than that in Run 4 (μ_o/μ_w=50) or Run 11 (μ_o/μ_w=1.0).

Run 13: Viscosity Ratio=200

In order to examine the effect of higher oil viscosity, Run 13 was conducted. For this run, a 200 mPa.s oil (Faxam-100) was used as the oil phase. Figure 14 shows the recovery performance for this run. This run was started with a waterflood at a flow rate of 400 ml/hr. As can be seen from Figure 14, oil recovery by a water flood was extremely poor. Even though, h_b/h_o was 0.33 for this run, the high viscosity of the oil led to poor oil recovery. The waterflood was followed by a polymer flood. The polymer flood continued until about 0.18 PV of polymer was injected. A similar slug size was used for other polymer injection runs as well (for which a different oil viscosity was used). Similarly to previous polymer injection runs, no immediate improvement in the oil cut was observed. However, after a delay of 0.34 PV, the oil cut increased suddenly and soon reached a peak. Consequently, a considerable amount of oil

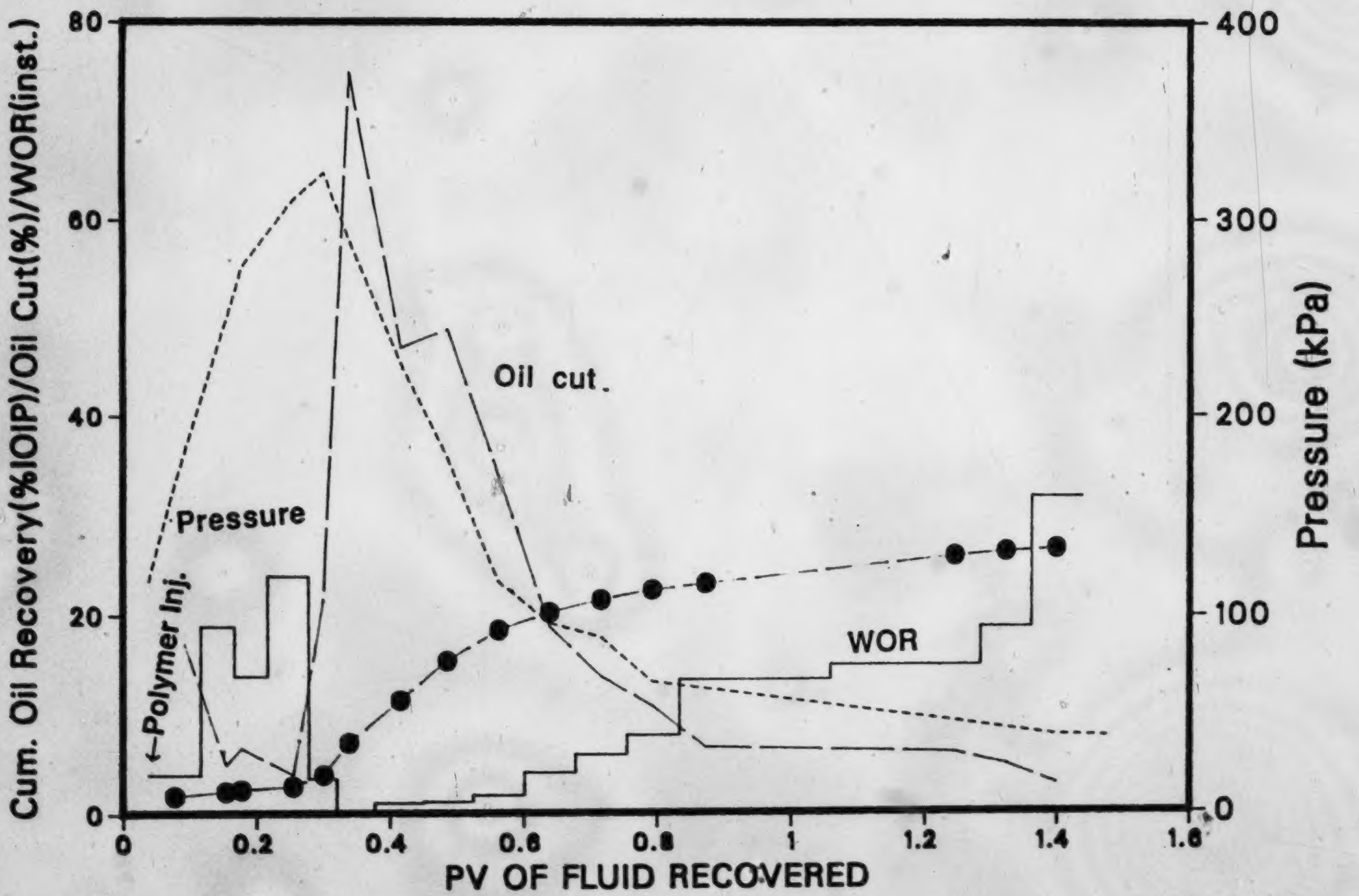

Fig. 14 Waterflood and Polymer Flood Performance for Run 13 (h_b/h_o=0.33, k_o/k_b=1.00)

was produced during this short period. However, as the waterflood continued the oil cut started decreasing rapidly. Finally, a total of 26.5 percent of the IOIP was produced when the WOR reached a value of 20. Although this value is very small compared to that which was obtained for the lower viscosity of oil, this is not unexpected as the oil recovery by a waterflood would have been quite low even in the absence of a bottom-water zone.

5.2.3 Polymer Flood and Waterflood in a Homogeneous Pack

Runs 14 and 15 were conducted to investigate polymer flood and waterflood performance in a homogeneous pack. The injection points in terms of time were varied for these two runs.

Run 14: Homogeneous Pack Waterflood/ Polymer Flood

Run 14 was conducted to observe waterflood and polymer flood performance in homogeneous media. It should be recalled that Runs 1 and 2 were conducted for the same purpose also. But in Run 14, a bigger core was used. This time, a flow rate of 500 ml/h was used. Water breakthrough occurred at 0.27 PV.

The polymer flood started at a PV of 1.2 when over 47 percent of the IOIP was recovered. The beginning of the polymer injection was chosen arbitrarily. A slug size of 0.45 PV was injected at a flow rate of 500 ml/h. The pressure, WOR, oil cut and recovery data are shown in Figure 15. The oil cut remained more or less steady during the polymer flood. However, when the polymer flood was followed by water injection, the oil cut increased quite rapidly at 1.7 PV. This was followed by a decreasing water cut.

Run 15: Continuous Polymer Flood in a Homogeneous Pack

This run was conducted to observe the effect of continuous polymer flooding on a homogeneous core. The core was prepared as in Run 14. However, this time no waterflood was performed at the outset. A 500-ppm polymer solution was injected at a flow rate of 400 ml/h. Recall that in Run 14 a flow rate of 500 ml/h was used. It was postulated that the flow rate would not have an impact on the recovery performance for a change from 500 to 400 ml/h. Consequently, these results could be compared. Even though the actual viscosity of polymer is much higher than that of water, breakthrough occurred quite early (at 15 percent of pore volume). A comparison with Run 14 shows that the polymer flood performance is not any better than that of a waterflood until 0.4 PV of fluid injection. During the initial stages of the displacement test, most of the injected polymer channeled through the bottom-water zone. Consequently, the oil cut at the producing end was not improved immediately even though the polymer solution had a viscosity much higher than that of water. Beyond this

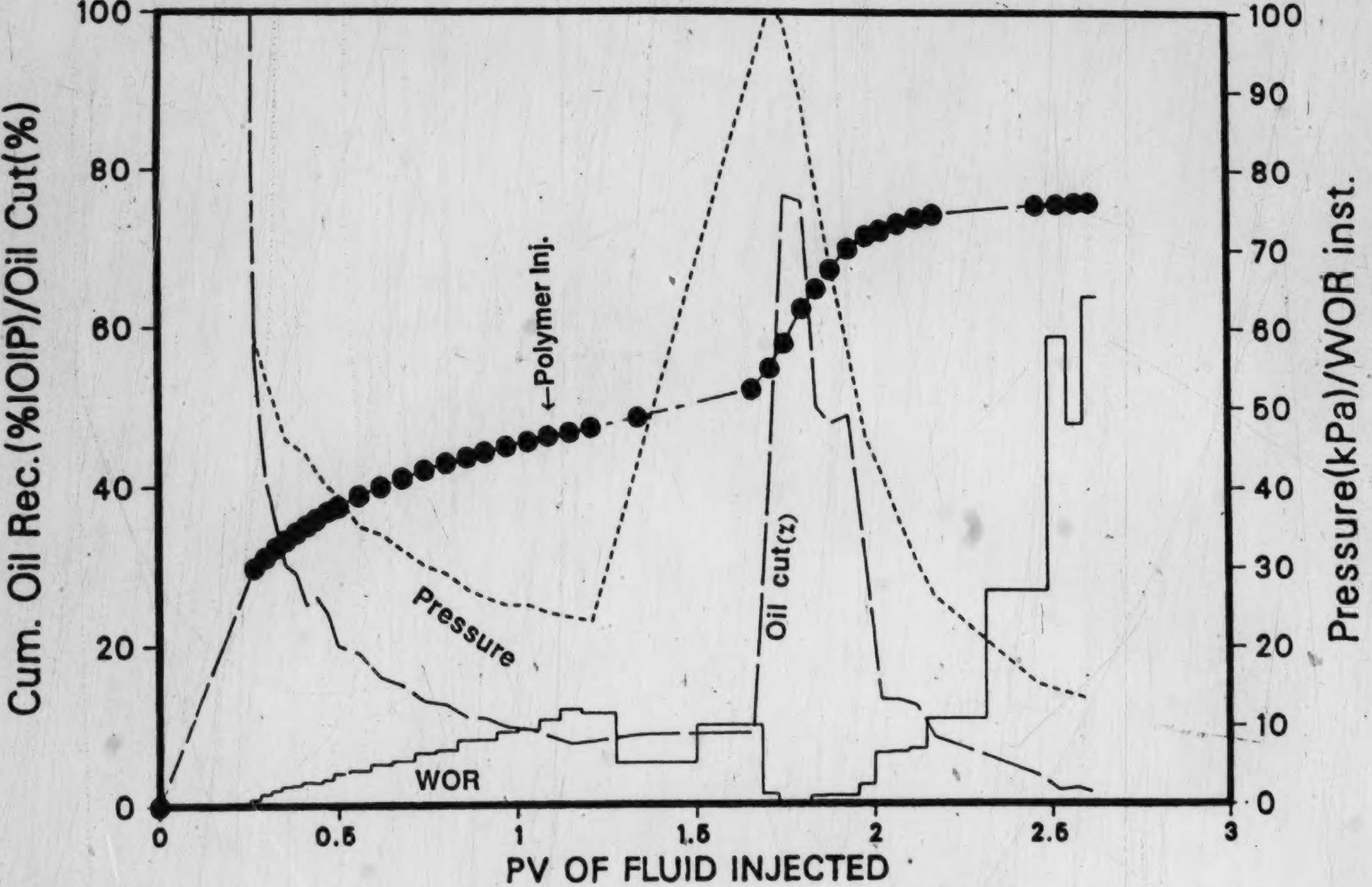

Fig. 15 Waterflood and Polymer Flood Performance for Run 14 (h_b/h_o=0)

point, however, the polymer flood gives distinctly better recovery than that of a waterflood. Figure 16 shows the pressure, WOR, oil cut and recovery curves for this run. After injecting 0.73 PV of polymer, a waterflood was started. The injection of water following an initially injected polymer slug enabled comparison for various polymer injection points over time. The WOR remained low for an additional 0.4 PV of water injection. This low oil cut value indicates that the polymer-rich aqueous phase had to approach the production well before an improvement in oil cut could be observed. As the waterflood continued the water-cut started increasing. However, a total of 74 percent of the IOIP was recovered with a total injection of less than two pore volumes.

5.2.4 Effect of Polymer Injection Point

Run 16: Injection of Polymer followed by waterflooding

This run was conducted in order to examine the effects of varying the polymer injection point over time. The polymer used for this run had a viscosity of 64 mPa.s. A similar viscosity of polymer was also used for Run 4; however, in Run 16 run the polymer solution injection was preceded by a waterflood. For Run 16, the polymer solution was injected at the beginning of the displacement test. As the polymer injection started through the inlet end, the oil

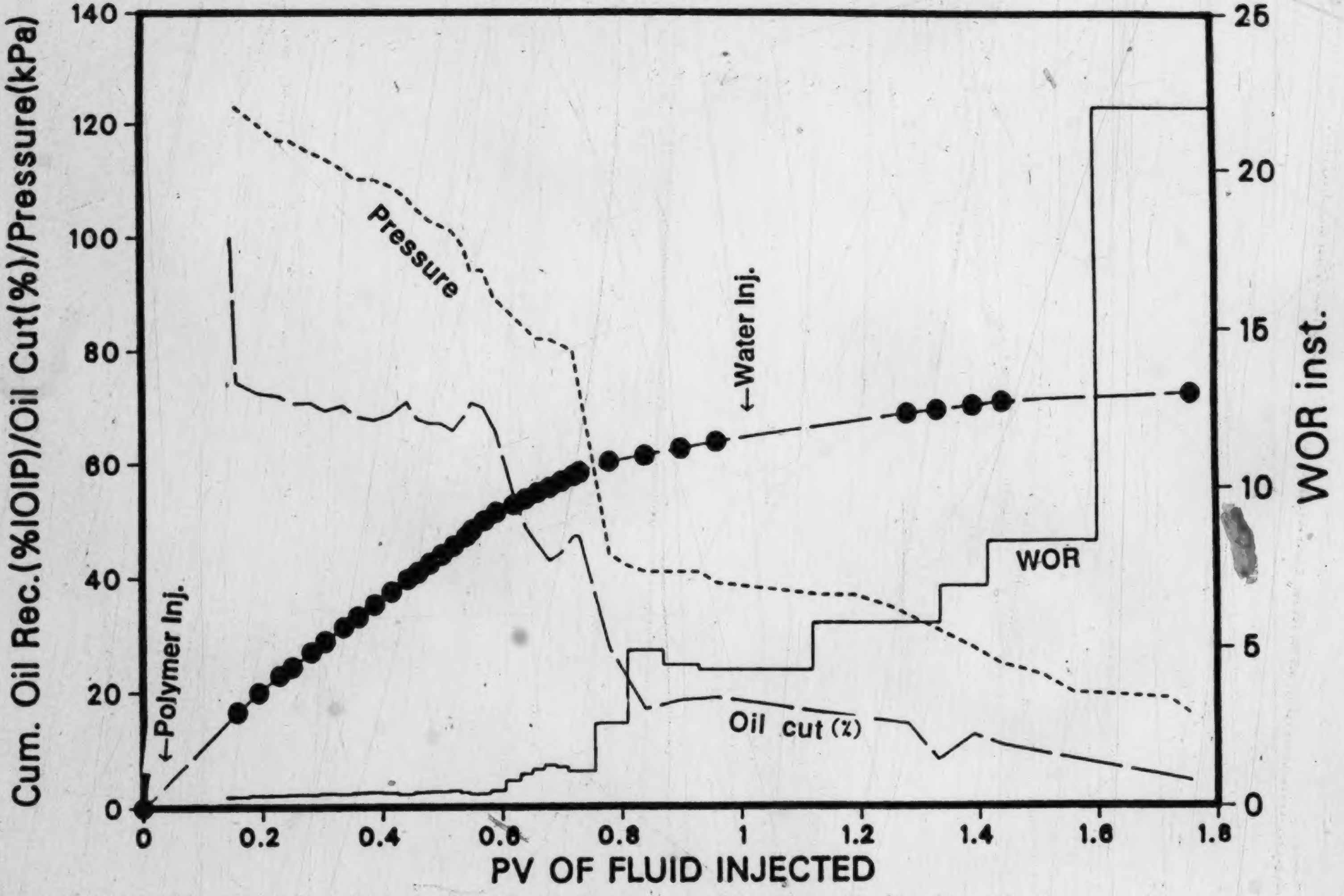

Fig. 16 Waterflood and Polymer Flood Performance for Run 15 ($h_b/h_o=0$)

cut was higher than that observed during previous polymer injection runs. However, the oil cut decreased sharply as polymer injection continued. During this time, the inlet pressure continued to increase. After injecting 0.18 PV of polymer, a waterflood was initiated at 400 ml/h. As the waterflood started, both the oil cut and inlet pressure continued to increase and reached a peak at the same time. This observation is slightly different from that which was observed in previous runs. After reaching the maximum, both the inlet pressure and oil cut (see Figure 17) started decreasing. Polymer breakthrough occurred at 0.63 PV of total fluid injection. At this point, a total of 41 percent of the IOIP was recovered. After polymer breakthrough, a sharp decrease in oil cut was observed. Following this sudden drop, the oil cut decreased slowly as the waterflood continued. When the WOR reached a value of 20, 65 percent of the IOIP was recovered. This value compares with 70 percent of the IOIP as recovered in Run 4 at the same value of the WOR.

5.2.5 Effect of Polymer Slug Size and Viscosity

Several runs were conducted to examine the effects of polymer slug sizes and viscosity. All these runs had h_b/h_o=0.33 and k_o/k_b=1. This enabled one to compare the results directly. Other characteristics of these runs are summarized in Table 5.1. Unlike previous polymer slug

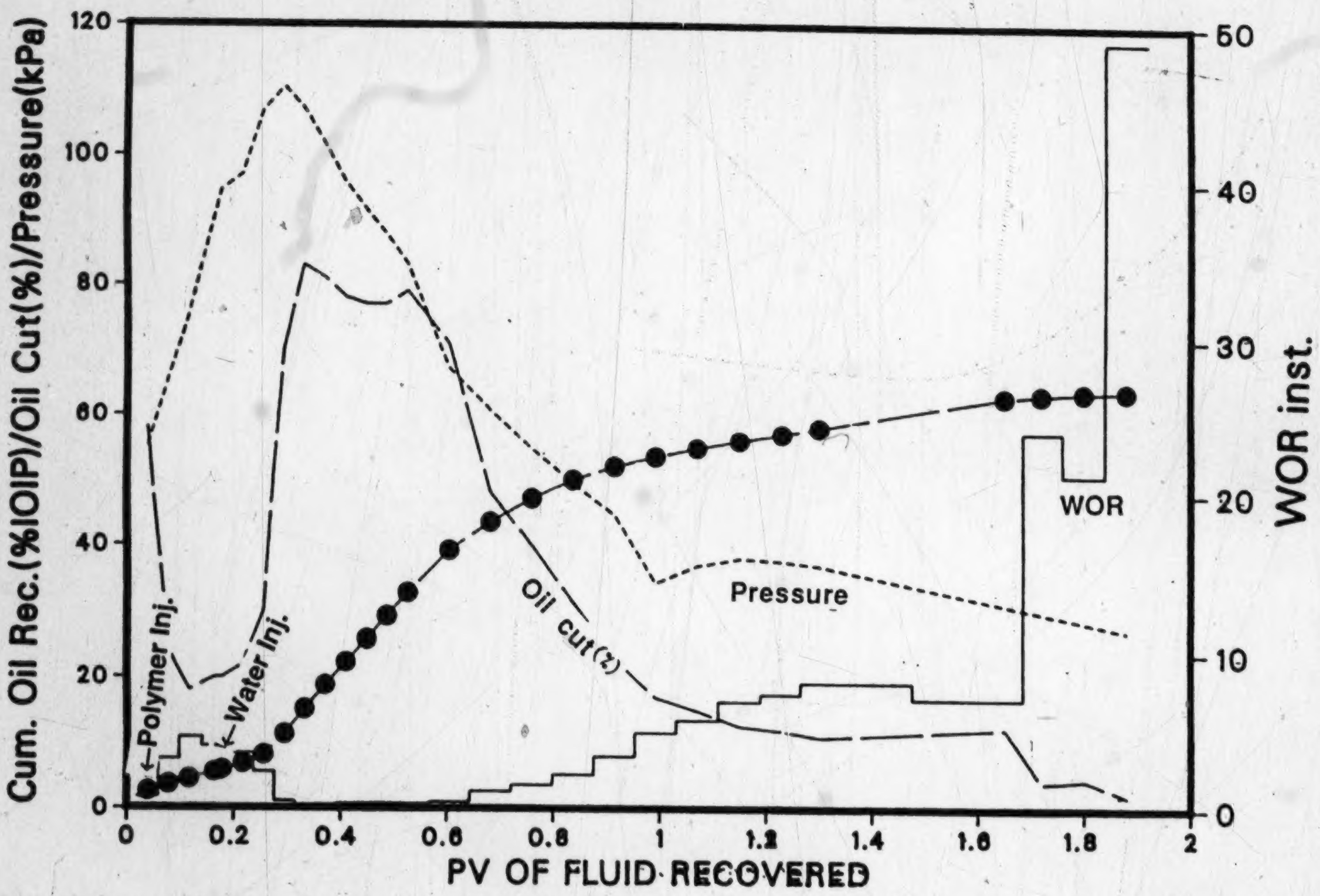

Fig. 17 Waterflood and Polymer Flood Performance for Run 16 ($h_b/h_o=0.33$, $k_o/k_b=1.00$)

injection runs, polymer slug was injected at the beginning for all these runs. This enabled one to see the effect of polymer slug size and viscosity. For these runs, polymer breakthrough time was monitored along with polymer concentration in the effluent fluid. The results are summarized in Table 5.2.

Run 17: Polymer Slug Size= .125 PV, Viscosity=36 mPa.s

Run 17 was conducted to examine the effects of polymer viscosity and slug size. As can be seen from Table 5.2, the polymer solution was injected at the beginning of the displacement test. The inlet end was used to inject the polymer solution into the core. The oil cut decreased and the inlet pressure started increasing as the polymer flood continued. A polymer slug of 0.125 PV was injected before a waterflood was initiated at 400 ml/h. During the waterflood, injection pressure continued to increase, soon reached a peak, and then started to decrease. This can be seen from Figure 18. As the inlet pressure attained a maximum, the oil cut dropped to a minimum. Soon after this minimum, the oil cut started increasing rapidly and reached a maximum from which point it started decreasing slowly. As detected by measuring the polymer concentration in the aqueous phase, polymer breakthrough occurred after a total fluid production of 0.57 PV. At this point, a total of 37 percent of the IOIP was produced (see Table 5.2). As

TABLE 5.2: Results of Polymer Flood Runs

Run no.	Polymer Visco. (mPa.s)	Polymer bt(PV)	Polymer inj. Point (PV)	Polymer Slug Vol. (PV)	Recovery at Polymer bt(%IOIP)	Delay in Response (PV)	IOIP (ml)
3	64.	N. Av.	2.00	0.60	N. Av.	1.00	715
4	"	"	0.76	0.18	"	0.46	1180
5	"	"	1.0	0.15	"	0.30	1210
6	"	"	0.41	0.18	"	0.54	1170
7	"	"	1.1	0.60	"	1.1	775
8	"	"	1.20	0.18	"	0.40	1120
9	"	"	1.0	0.15	"	0.25	1200
10	"	"	1.0	0.60	"	.80	770
11	"	"	0.75	0.18	"	0.34	1100
12	"	"	0.64	0.26	"	No Response	970
13	"	"	1.00	0.20	"	0.50	1110
14	"	"	1.20	0.45	"	0.50	1460
15	"	0.30	0.00	1.00	"	No Response	1525
16	"	0.63	0.	0.18	41	0.30	1110
17	36.	0.57	0.	0.125	37	0.35	1120
18	36.	0.56	0.	0.06	33	0.30	1120
19	36.	0.61	0.	0.26	38.5	0.32	1120
20	64.	0.60	0./.6/ 1.1/1.7	.05/.06/ .06/.06	38.3	0.30	1100
21	36.	0.64	0.	0.50	39.0	0.33	1110
22	25.	0.61	0.	0.26	34	0.40	1125
23	100.	0.54	0.	0.12	34.0	0.31	1115
25	64.	N. Av.	1.00	0.60	N. Av.	0.80	775

N. Av. Not available

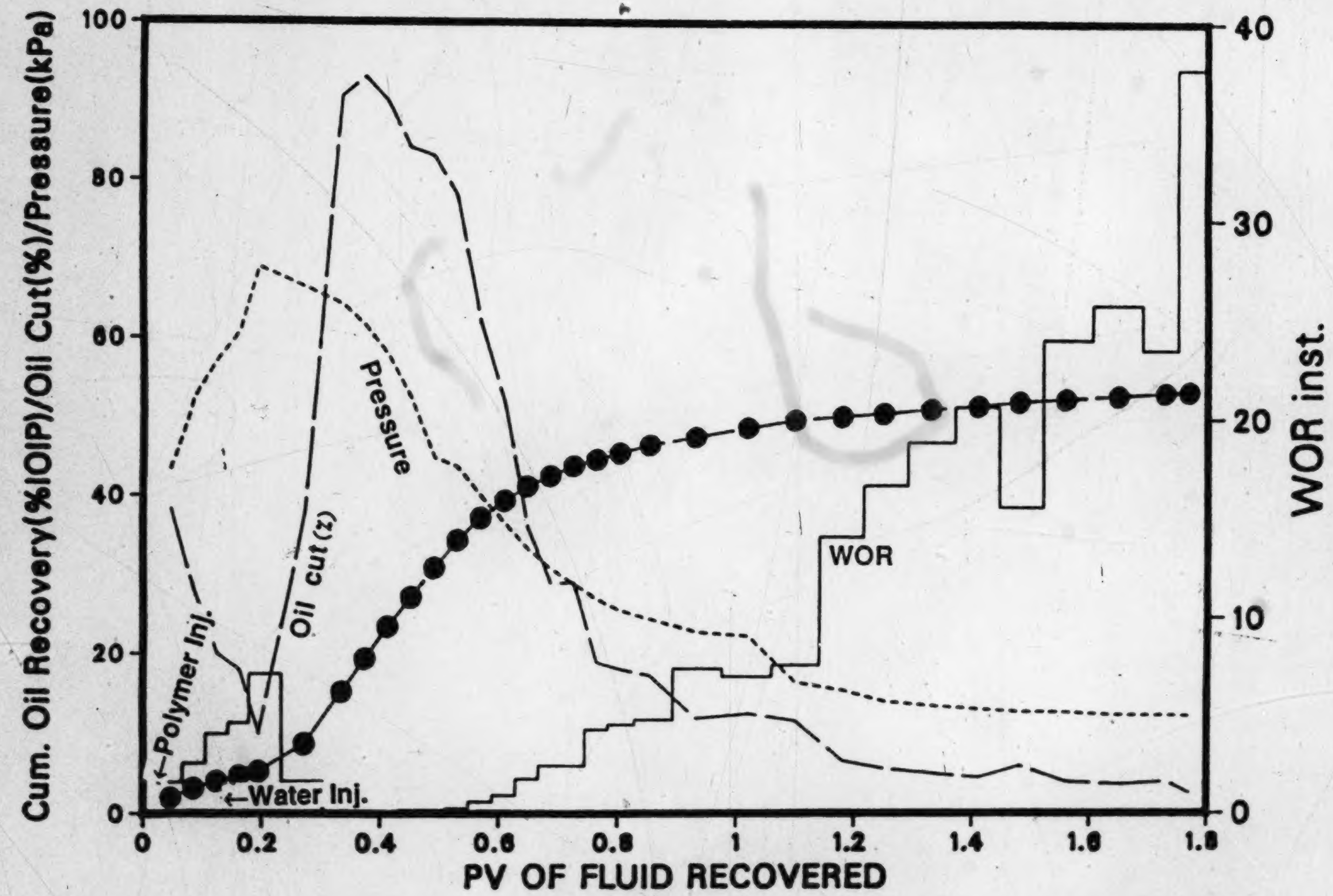

Fig. 18 Waterflood and Polymer Flood Performance for Run 17 (h_b/h_o=0.33, k_o/k_b=1.00)

observed in the previous run, the polymer concentration in the produced aqueous phase was much lower than that of the injected polymer. Soon after polymer breakthrough, a sudden drop in oil cut took place. Then the oil cut started decreasing slowly. The inlet pressure also dropped slowly following a rapid decrease after the maximal peak was attained. As the waterflood continued, the WOR value continued to increase slowly. When the WOR reached a value of 20, a total of 53 percent of the IOIP was produced.

Run 18: Polymer Slug Size= .06 PV, Viscosity= 36 mPa.s

In order to examine further effects of polymer slug size, Run 18 was carried out. A polymer solution of viscosity 36 mPa.s was injected at the beginning of the displacement test. The polymer injection continued until 0.06 PV of polymer solution was injected. The inlet end was used for injecting the polymer solution. As observed in previous polymer injection runs, the inlet presure increased and the oil cut decreased during the initial stage of the displacement test. As the waterflood started after polymer injection, the injection pressure continued to increase and attained a maximum at a point for which the oil cut reached a minimum. As the waterflood continued, the oil cut increased suddenly and soon attained a maximum of 92 percent. Such a high value of oil cut was not observed in any of the previous runs. However, as the waterflood continued, both the oil cut and inlet pressure decreased (see Figure 19). Polymer breakthrough occurred after a total fluid recovery of 0.56 PV. This was followed by a sudden drop in the oil cut. During the later stages of the displacement test, the inlet pressure stabilized at around a value slightly higher than that observed for Run 17. Note that 33 percent of the IOIP was produced at the time of the polymer breakthrough. When the WOR reached a value of 20, a total of 51 percent of the IOIP was recovered (see Table 5.1 for comparison with other runs).

Run 19: Polymer Slug size= 0.26, Viscosity= 36mPa.s

Run 19 was conducted to see the effect of larger polymer slugs. The polymer solution injected had a viscosity of 36 mPa.s, and was injected at the beginning of the displacement test. As polymer injection continued, the injection pressure increased and reached a maximum of 70 kPa. At the same time, the oil cut dropped to a minimum (see Figure 20 for detail). The polymer solution injection continued until 0.26 PV was injected. This was followed by a waterflood at 400 ml/h. The injection pressure started decreasing as soon as the waterflood started. The oil cut started increasing at a time slightly earlier than when the inlet pressure attained a maximum. At the end of the polymer injection, the oil cut was already at a peak of 90 percent. This value of oil cut was maintained during the

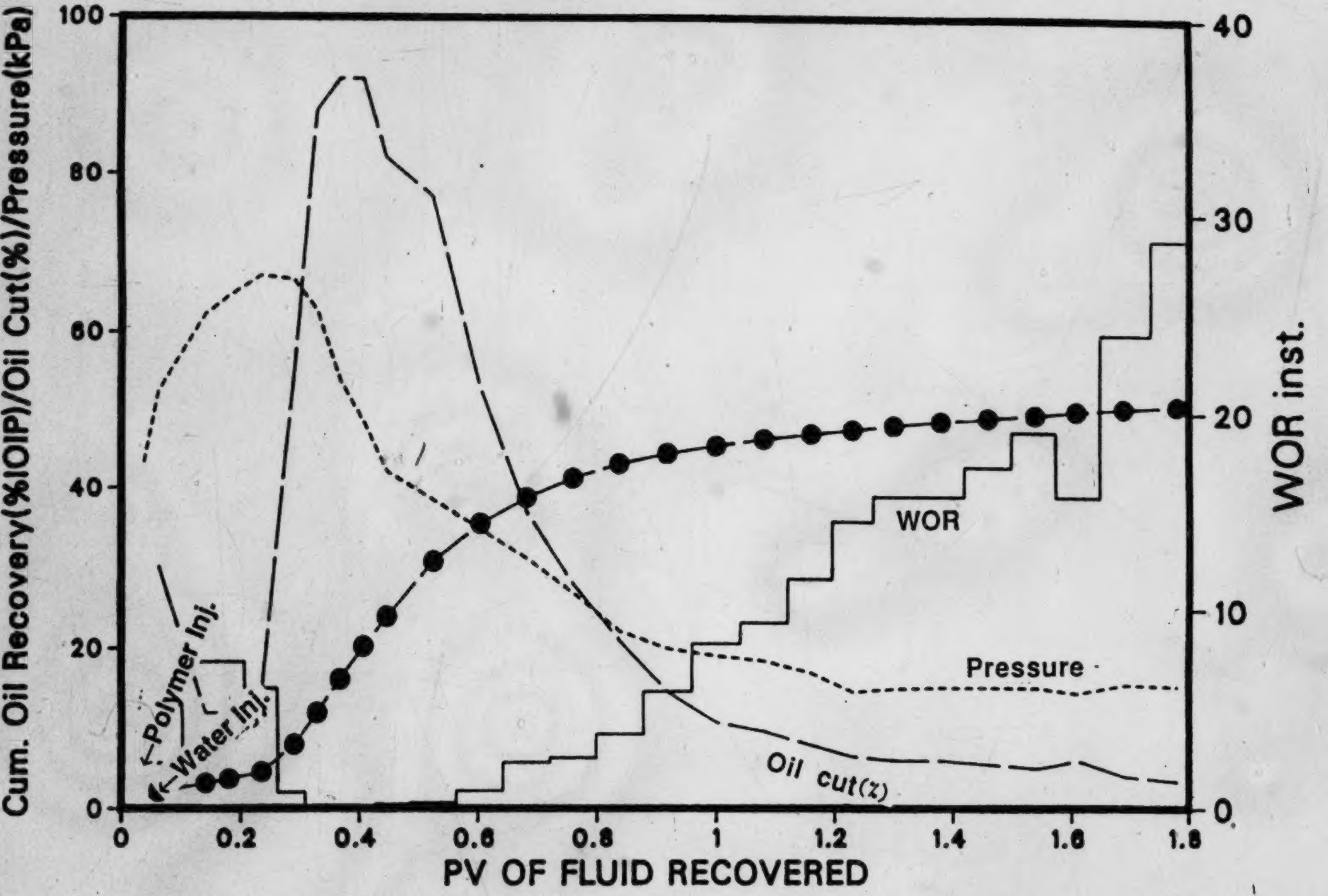

Fig. 19 Waterflood and Polymer Flood Performance for Run 18 (h_b/h_o=0.33, k_o/k_b=1.00)

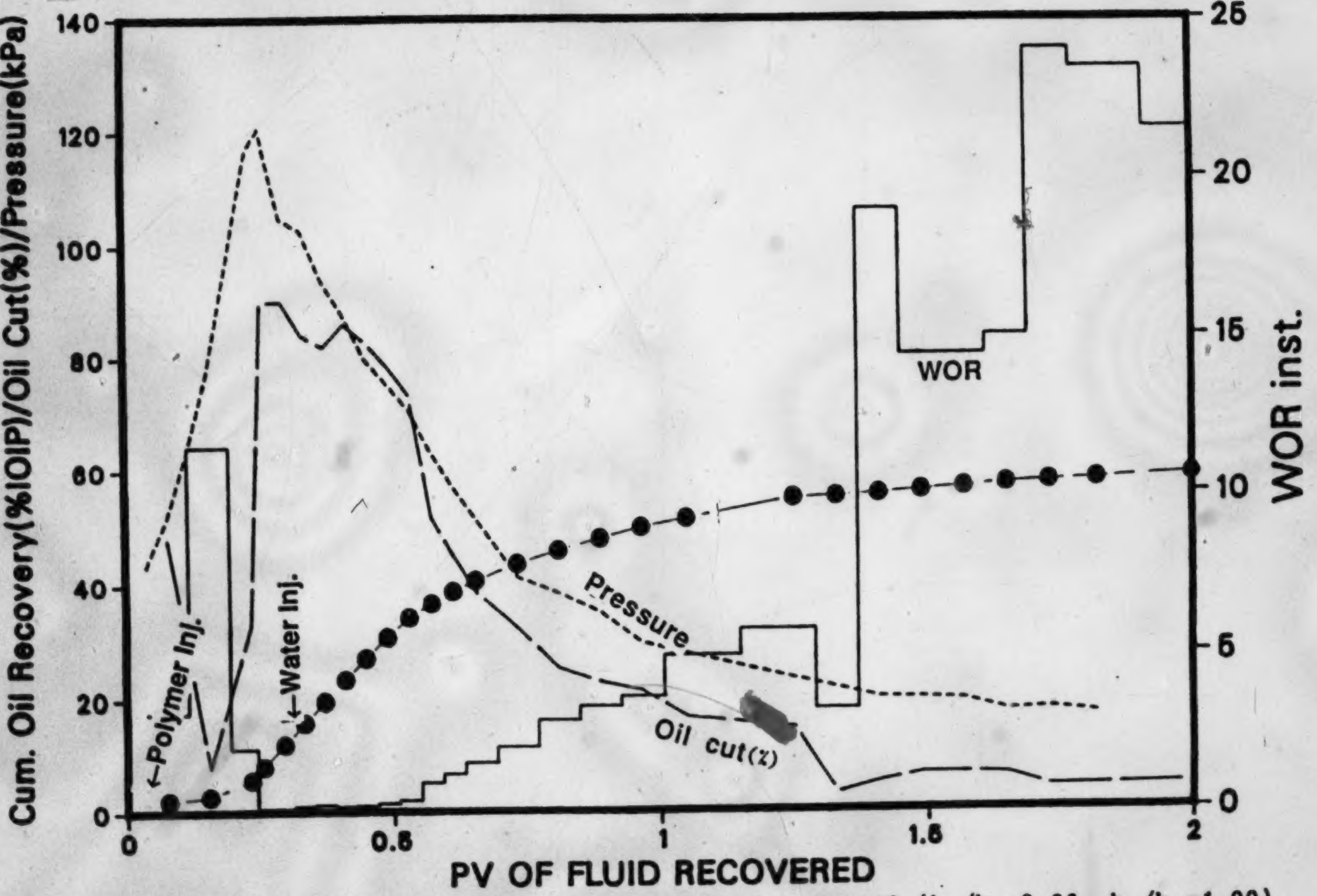

Fig. 20 Waterflood and Polymer Flood Performance for Run 19 (h_b/h_o=0.33, k_o/k_b=1.00)

initial stages of the waterflood. Then the oil cut started decreasing. Polymer breakthrough occurred when 0.61 PV of fluid was injected. At this point, 39 percent of the IOIP was produced (see Table 5.2). Polymer breakthrough was also marked with a sudden decrease in oil cut. Then the oil cut decreased at a slower pace. When the WOR reached a value of 20, a total of 57 percent of the IOIP had been produced.

Run 20: Polymer slugs alternated with water slugs

In order to examine the effect of polymer slugs alternated with water slugs, Run 20 was conducted. Figure 21 depicts the WOR, oil recovery, pressure and oil cut for this run. For this run an initial polymer slug of 0.05 PV was injected. This was followed by a water injection of 0.5 PV. Following this, another polymer slug of 0.06 PV was injected. This process was continued until a total of 23 percent pore volume of polymer was injected. At the end of the displacement test, only 53 percent of the IOIP was recovered at a WOR of 20. This value is quite low as a total of 0.23 PV of polymer slug was injected.

Run 21: Slug size= 0.50 PV, polymer viscosity= 36mPa.s

In order to examine the effect of polymer slug size, Run 21 was conducted with a polymer viscosity of 36 mPa.s and a polymer slug volume of 0.50 pore volume. At the beginning of the displacement test the polymer solution was

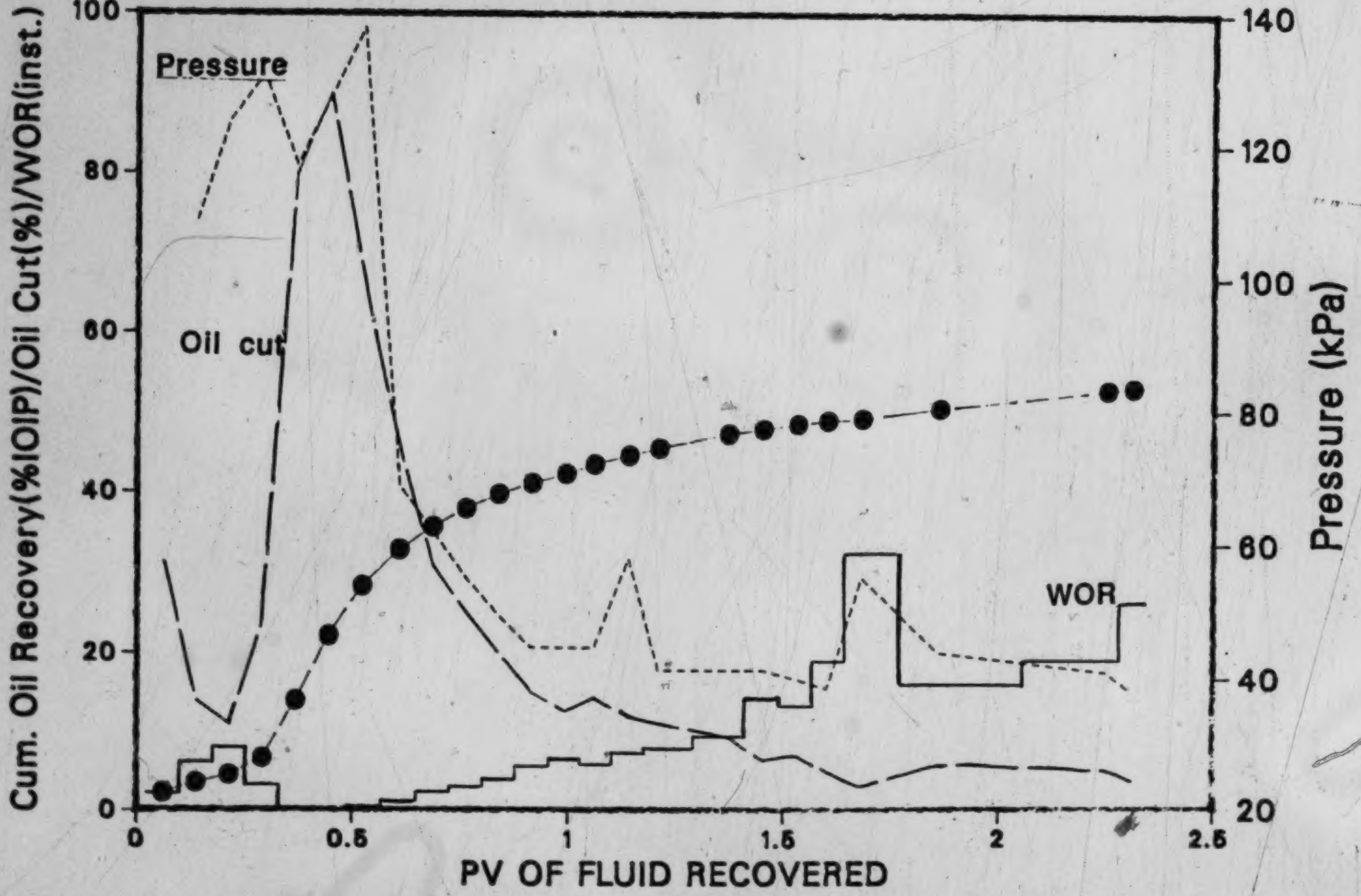

Fig. 21 Waterflood and Polymer Flood Performance for Run 20 (h_b/h_o=0.33, k_o/k_b=1.00)

injected at a flow rate of 400 ml/hr through the inlet end. Figure 22 depicts the oil recovery, pressure, WOR, and oil cut performance for this run. As can be seen from this figure, the oil cut decreased rapidly during the initial stages showing no immediate improvement over a conventional waterflood. However, after an injection of 0.33 PV of polymer solution the oil cut started to show a response and increased sharply, reaching a peak of about 90 percent. The injection pressure followed a similar trend, but with a slight lag. When the polymer slug was followed by a waterflood at 400 ml/hr the oil cut started decreasing while still maintaining a relatively high value. The injection pressure decreased in a similar way. However, the injection pressure stabilized towards the end even though the oil cut continued to decrease.

Polymer breakthrough was detected at a pore volume of 0.64 PV. This value is higher than that observed with smaller slug sizes. At the end of the displacement test a total of 60 percent of the IOIP was recovered when the WOR reached a value of 20. This value is slightly higher than that observed with the smaller slug sizes even though a much larger slug size was used for this run.

Run 22: Slug size= 0.26 PV, Polymer viscosity= 25mPa.s

For Run 22, a polymer solution of viscosity 25 mPa.s was used. At the beginning of the displacement test,

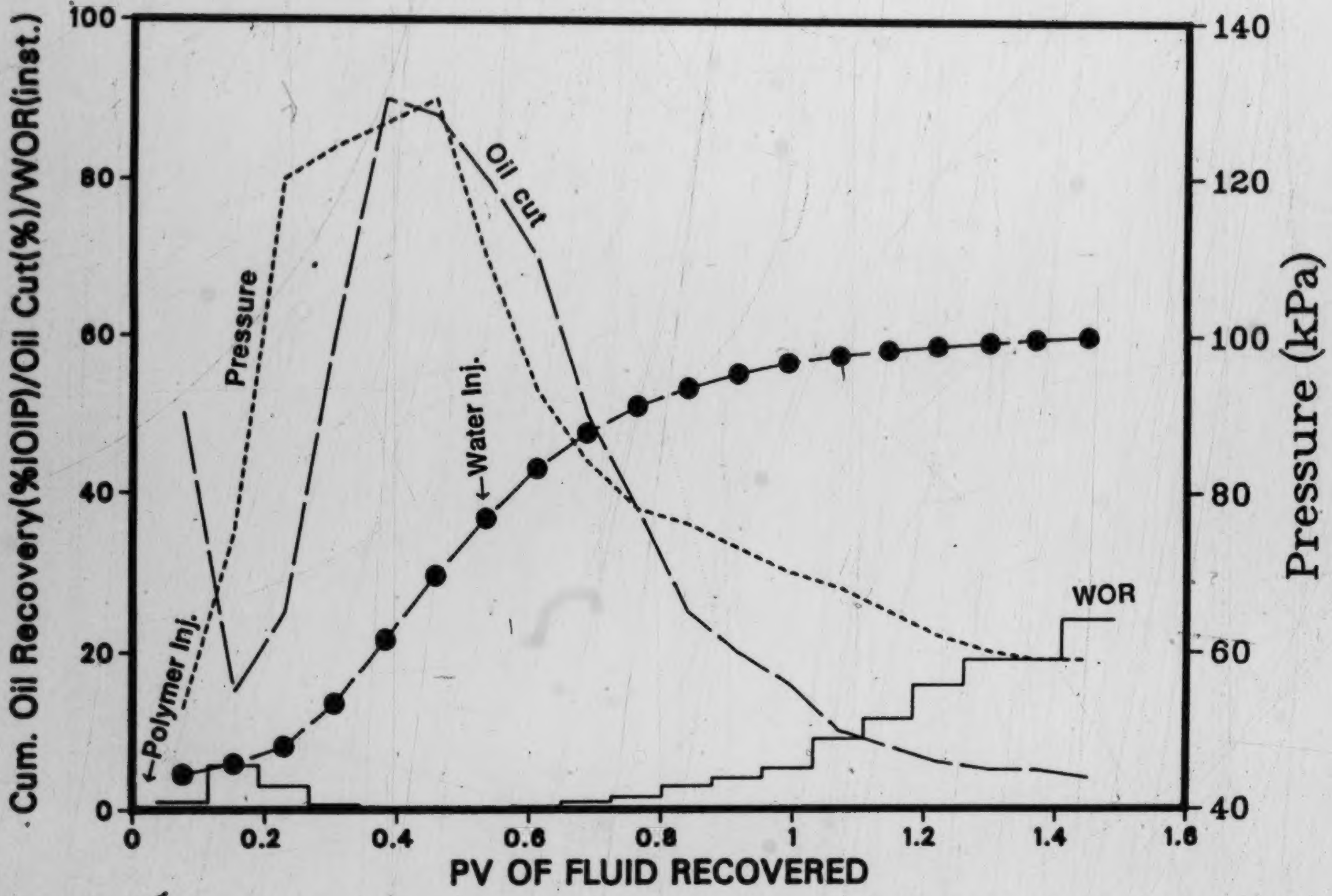

Fig. 22 Waterflood and Polymer Flood Performance for Run 21 (h_b/h_o=0.33, k_o/k_b=1.00)

polymer solution was injected at 400 ml/h. The polymer injection continued until 0.26 PV of polymer solution was injected through the inlet end. As can be seen from Figure 23, the oil cut declined rapidly during polymer slug injection. However, the oil cut still remained somewhat higher than that for a waterflood. During this period, the inlet pressure increased rapidly. After injecting 0.26 PV of polymer solution, a waterflood was started through the injection well at a flow rate of 400 ml/h. This was marked by a sudden decrease in pressure. However, no new trend in oil cut was observed immediately. As the waterflood continued, the inlet pressure started increasing and reached a peak. A the same time, the oil cut dropped to a minimal value. However, soon after this, the oil cut started increasing very rapidly to reach a maximal value of 87 percent. Then it started decreasing, at first slowly and then more rapidly. At this point both the oil cut and inlet pressure followed a very similar trend (see Figure 23). The polymer concentration in the produced aqueous phase was measured periodically. The first trace of polymer was found after a total fluid injection of 0.612 pore volume. When polymer breakthrough occurred, the injection pressure dropped significantly. Following the pressure decline, the oil cut dropped suddenly from above 70 percent to about 40 percent. At the time of breakthrough a total of 34 percent IOIP was produced. It was noticed that the polymer

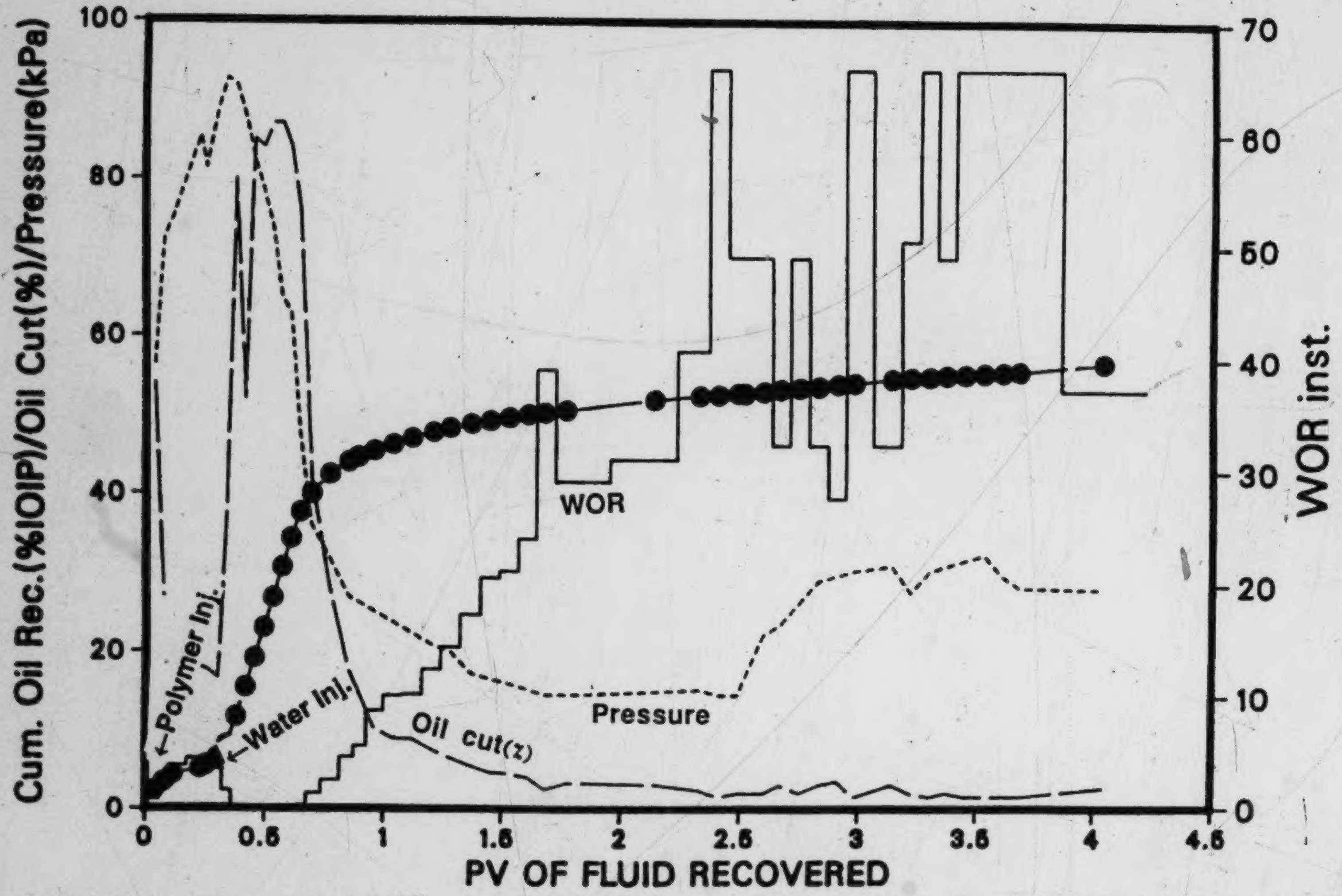

Fig. 23 Waterflood and Polymer Flood Performance for Run 22 (h_b/h_o=0.33, k_o/k_b=1.00)

concentration in the effluent aqueous phase was much smaller than that in the injected polymer. This resulted from adsorption of polymer on the surface of the glass beads. Also, the presence of bottom water (polymer solution was injected very close to the bottom-water zone) and viscous instability due to displacement of polymer by water might be responsible for possible thinning of the polymer solution. As the waterflood continued, the inlet pressure stabilized at a value higher than that obtained by a waterflood (Run 4). This indicated a permanent decrease in effective permeability to water as a result of polymer slug injection. The oil cut decreased slowly as a result of continuing the waterflood. When the WOR reached a value of 20 (see Table 5.1), the total oil recovery was 50.5 percent of the IOIP. This is much lower than the 70 percent of the IOIP recovered in Run 4, in which 0.18 PV of polymer solution was injected following an initial waterflood. In Run 4, the viscosity of the polymer solution was 64 mPa.s.

When the oil cut dropped below three percent, it was decided to use an emulsion slug in order to examine the effect of an emulsion flood on residual oil saturation for the reservoir model under consideration. A slug of 0.5 PV of 10 percent oil-in-water emulsion was injected at 400 ml/h. The injection pressure increased rapidly showing an effective resistance to flow. However, the emulsion had a viscosity of 1.8 mPa.s at 6 rpm and such an increase in inlet pressure was expected. After injecting the emulsion slug a waterflood was resumed. Even though the oil cut increased slightly at the beginning of the emulsion injection, the oil cut dropped to the previous value as the waterflood continued and no significant improvement in oil cut was noticed even after injecting nearly one pore volume of water.

Run 23: Slug size= 0.12, Polymer Viscosity= 100 mPa.s

In order to investigate further the effects of polymer viscosity, Run 23 was conducted with a polymer viscosity of 100 mPa.s. As has been discussed already, an attempt was made to compare runs with different polymer viscosities but with the same amount of polyacrylamide. For this reason, a polymer slug size of 0.12 PV was selected for this run. Figure 24 depicts the WOR, pressure, oil cut and oil recovery performance for this run. As can be seen from this figure, at the initial stage of the displacement test the injection pressure increased with a rapidly decreasing oil cut. Even though a very high polymer viscosity was used for this run the injection pressure was not very high as compared to that observed in other runs with lower-viscosity polymers. Possible thinning of the polymer solution with bottom water may be responsible for this behaviour. As can be seen from Table 5.2 and Figure 24, a delay of 0.31 pore volume occurred before the oil cut showed any perceptible

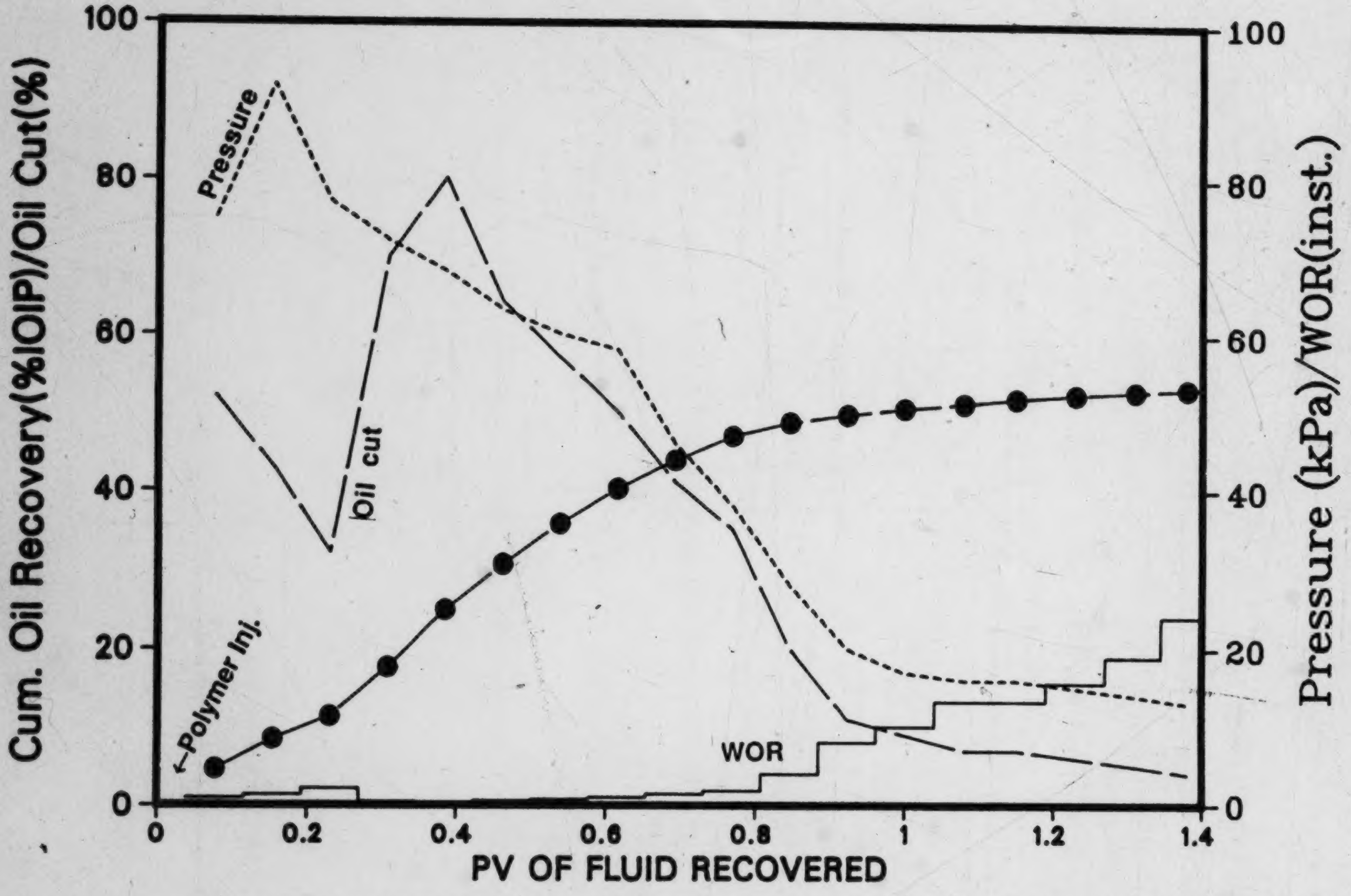

Fig. 24 Waterflood and Polymer Flood Performance for Run 23 (h_b/h_o=0.33, k_o/k_b=1.00)

response to the polymer flood. This delay is much smaller than that observed for other polymer injection runs. However, even with a quicker response due to high polymer viscosity the oil cut did not sustain a high value for a long time. Consequently, the oil recovery was 53 percent of the IOIP when the WOR reached a value of 20. This recovery is considerably lower than the other runs with lower polymer viscosity (but the same amount of polyacrylamide).

5.3 Mobility Control Mechanism with Polymer

Run 24: Effect of Glycerine Injection: $h_b/h_o=0.33$, $k_o/k_b=1$.

In order to examine the mechanisms involved in mobility control with polymer solution Run 24 was conducted using a glycerine slug.

The objective of Run 24 was to determine the quantitative contribution of the different mechanisms involved in the mobility control with polymer solutions. With this objective a glycerine solution with a viscosity of 64 mPa.s was chosen for this run. Glycerine is known not to adsorb on the rock surface, or exhibit mechanical entrapment. Therefore, the improvement with glycerine solution would be due only to its viscosity. A comparison of this run with Run 4, in which the same bottom water size and permeability and flood rates were used, will determine the relative contribution of the above-mentioned mechanisms involved in polymer flooding.

This run was started with an initial waterflood at a flow rate of 400 ml/hr. Figure 25 depicts the WOR, pressure, oil cut and oil recovery performance for this run. As can be seen from this figure the recovery performance during the early stages is very close to that observed in Run 4, showing a good replication of the displacement test. In order to match injection points for polymer and glycerine, glycerine injection was started, also at 400 ml/hr, after injecting 0.76 PV of water. The injection pressure with glycerine was slightly higher than that with polymer. Since polymer injection introduces adsorption and higher diffusion in the aqueous phase, a lower injection pressure was expected for polymer injection. Similar to the observation with polymer, no immediate improvement in oil cut was observed for this run. After injecting 0.18 pore volume of glycerine solution the waterflood was resumed. After a delay of about 0.6 pore volume from the commencement of glycerine injection the oil cut started increasing. However, the peak attained by the oil cut was only 60 percent as compared to more than 70 percent for polymer injection runs. Also, the increased oil cut did not last for long. Consequently, at the end of the displacement test only 42.5 percent of the IOIP was recovered when the WOR reached a value of 20. This was only about 60 percent of what was recovered in Run 4 for which polymer solution,

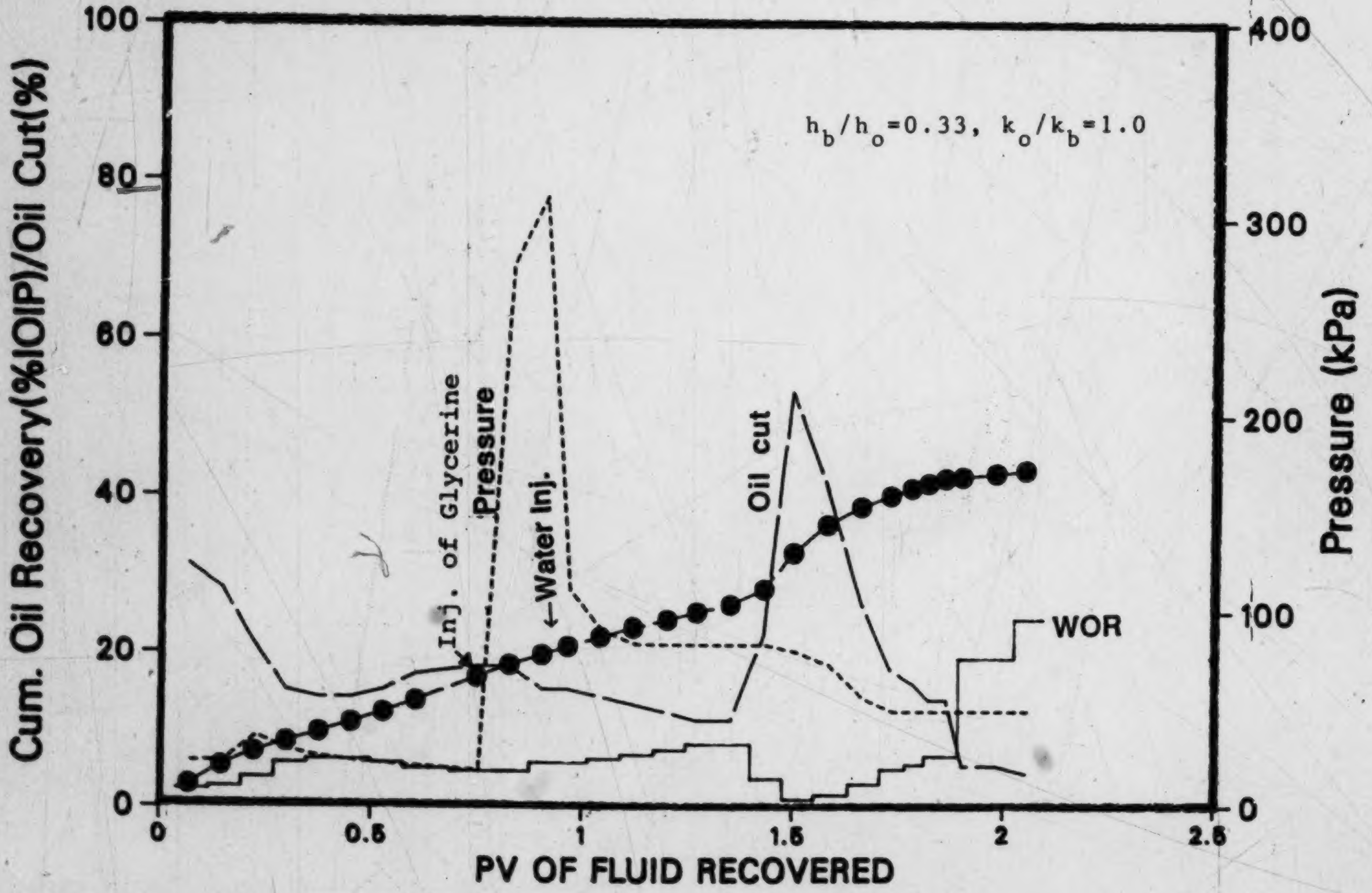

Fig. 25 Waterflood and Glycerine (64mPa.s) Injection Performance for Run 24

rather than glycerine solution, was used.

5.4 Artificial Impermeable Barrier

5.4.1 Effect of Water-to-Oil Zone Thickness Ratio

Run 25: $h_b/h_o=1$, $k_o/k_b=1$, Barrier length= 25% of the total length

In order to examine the effect of an impermeable barrier, Run 25 was conducted. In this run, a plastic sheet was inserted between the oil zone and the bottom-water zone. This barrier extended over 25 percent of the total length of the core. Other than this, the conditions were the same as those in Run 3. A waterflood rate of 800 ml/h was chosen to have waterflood conditions similar to those in Run 3. The performance was slightly better than that in Run 3 yet extremely poor in comparison to other runs.

After injecting about one PV of water the total oil recovery was only seven percent of the IOIP. A polymer slug of 0.60 PV was injected. The response was similar to Run 3. This indicates that the limited permeability barrier did not have a pronounced effect on either the waterflood or the polymer flood performance. The WOR, oil cut, oil recovery and pressure are depicted in Figure 26.

Run 26: $h_b/h_o=0.33$, $k_o/k_b=1$, Barrier length= 25% of the total length

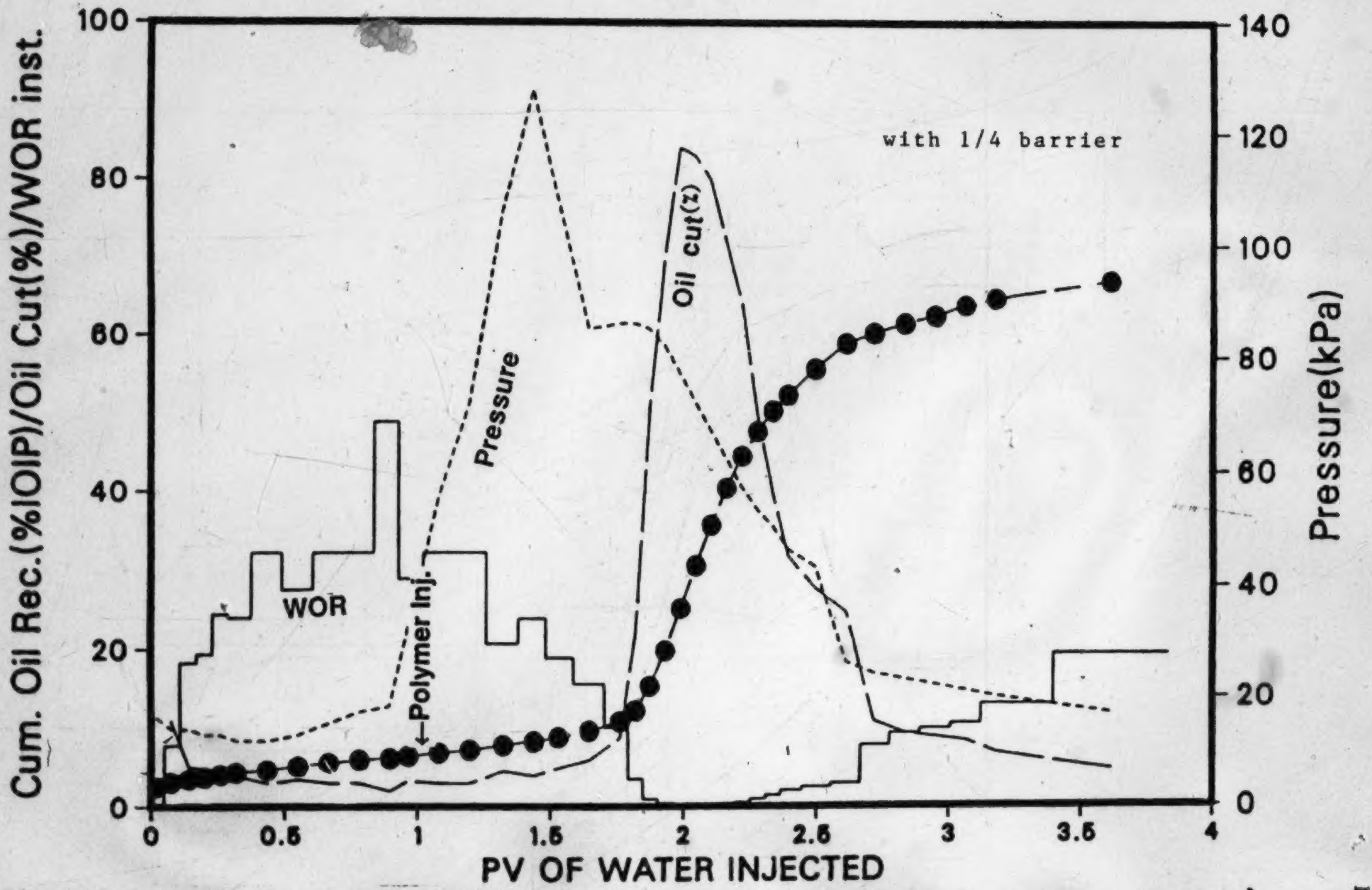

Fig. 26 Waterflood and Polymer Flood Performance for Run 25 (h_b/h_o=1.00, k_o/k_b=1.00)

In order to examine the effect of an impermeable barrier for reservoirs with a thinner bottom-water zone (h_b/h_o=0.33.), Run 26 was conducted. The impermeable barrier extended over 25 percent of the total length of the core. Other packing characteristics are summarized in Table 5.1.

A waterflood was started at a flow rate of 400 ml/h. The same flow rate was used in Run 4 (that had similar thickness and permeability of the bottom-water zone). Figure 27 depicts the recovery performance for this run. The oil recovery in this run is much better than that in Run 4. This difference is due only to the presence of the impermeable layer used in Run 26. A comparison of these runs shows that the impact of an impermeable barrier is much smaller for the thicker bottom water case. From this observation it may be concluded that the barrier length has to increase as the thickness of the bottom-water zone increases. This point is important for determining the volume of the mobility control agent.

5.4.2 Effect of Barrier Length

Runs 27 and 28 were conducted to examine the effect of barrier length for h_b/h_o of 0.33 and 1, respectively. For these runs a barrier length equal to 50 percent of the total length was used. Figures 28 and 29 depict the WOR, pressure, oil cut and oil recovery performance for these

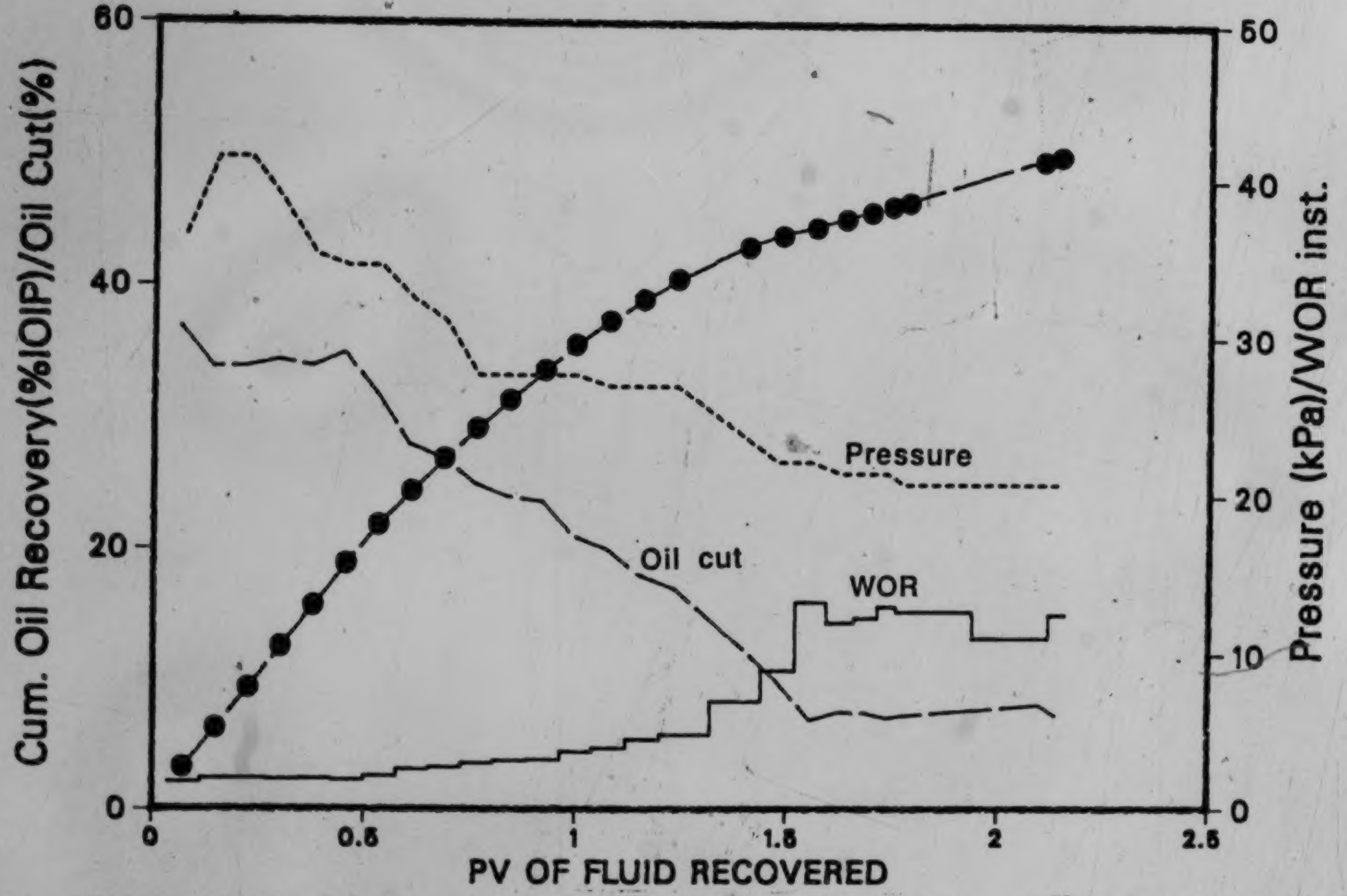

Fig. 27 Waterflood Performance for Run 26 (h_b/h_o=0.33, k_o/k_b=1.00, with 1/4 Barrier)

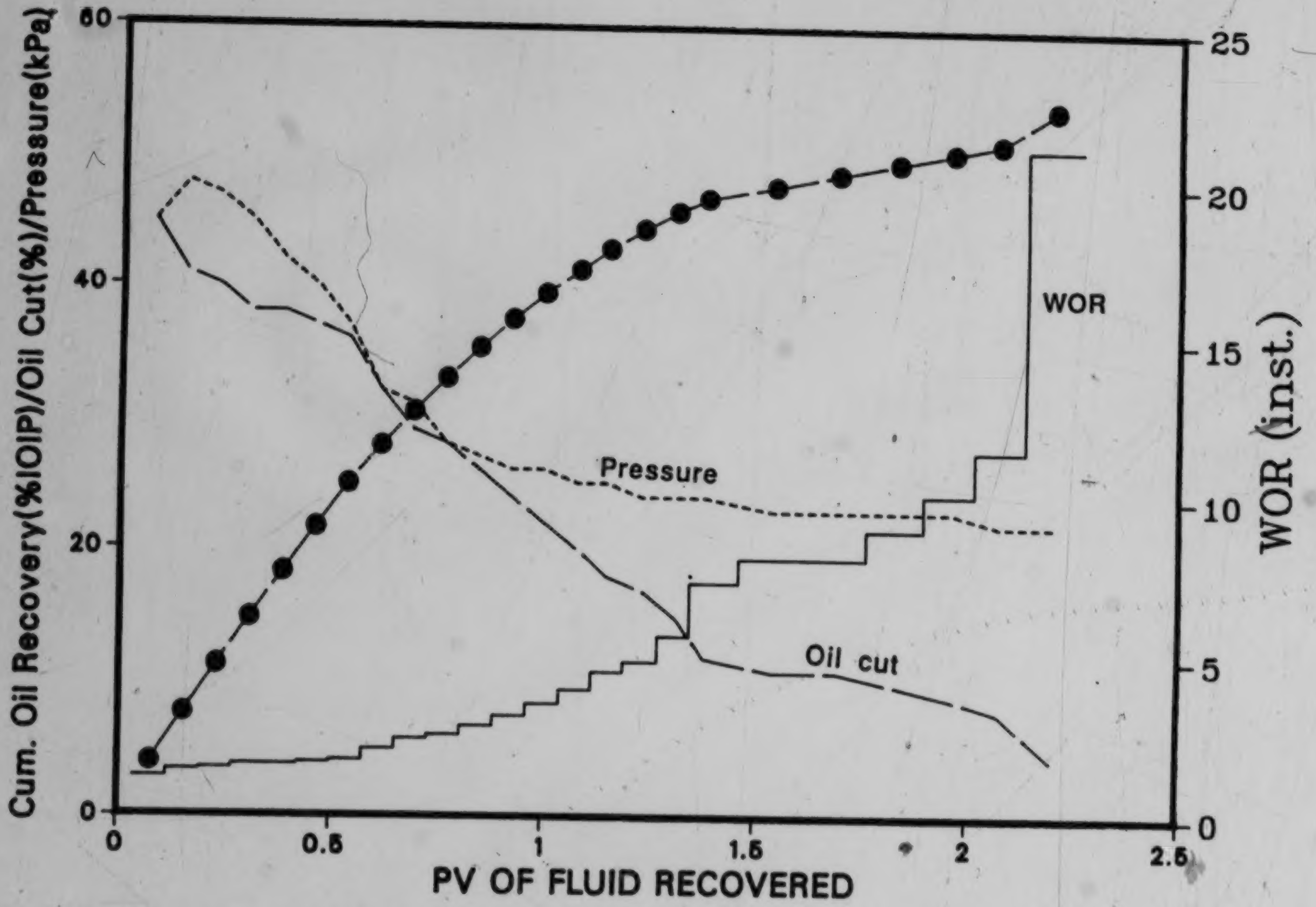

Fig. 28 Waterflood Performance for Run 27 (h_b/h_o=0.33, k_o/k_b=1.00, with 1/2 Barrier)

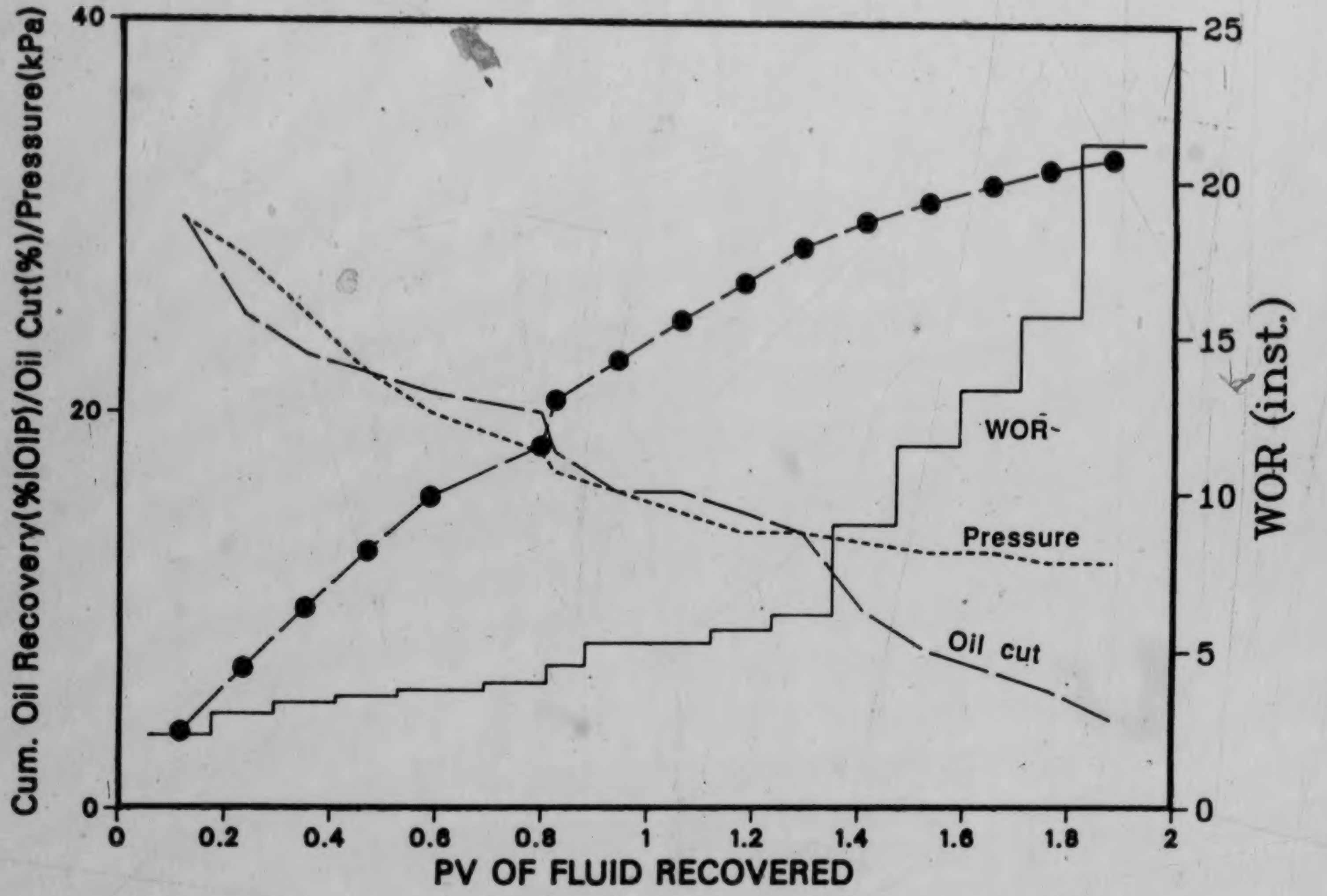

Fig. 29 Waterflood Performance for Run 28 (h_b/h_o=1.00, k_o/k_b=1.00, with 1/2 Barrier)

runs. The results and characterstics of these runs are summarized in Table 5.1. As can be seen from Figure 29, the oil recovery in Run 28 was much higher than that observed in Run 25 for which a waterflood was conducted at the beginning of the displacement test. This indicates that when the bottom-water zone is as thick as the oil zone, a much longer barrier is required to obtain a perceptible improvement for a waterflood. On the other hand for h_b/h_o=0.33, a barrier length as small as 25 percent of the total length improves waterflood performance considerably. As a matter of fact, by increasing the barrier length from 25 percent to 50 percent oil recovery was improved by only 10 percent for h_b/h_o=0.33 whereas for the same increase in barrier length oil recovery was improved by 370 percent for h_b/h_o=1.

5.5 Emulsion Injection

5.5.1 Effect of Oil Content on Emulsion Blockage in the Presence of a Bottom-Water Zone

In order to examine the effect of oil content in the emulsions on blocking performance, Runs 29 and 30 were performed with 5 and 10 percent oil-in-water respectively. This result was used in determining the ideal oil-content for other emulsion injection runs.

Run 29: Five percent oil-in-water Emulsion, h_b/h_o=0.33,

$k_o/k_b=1$

This run was conducted with an oil zone three times as thick as the bottom water zone. The h_w/h_o value for this runs was equal to 0.25. A five percent oil-in-water emulsion was first tried to observe any improvement over a conventional waterflood. The emulsion injection was conducted at flow rate of 200 ml/h. The characteristics and results of this displacement run are given in Table 5.1. Figure 30 depicts the pressure, WOR, oil cut and cumulative oil recovery of the displacement test. The emulsion was initially injected through the inlet end. This same injection point was used for polymer flooding in Run 4. At the beginning of the run, the oil recovery was slightly higher than that obtained with a waterflood. But emulsion breakthrough took place after 16 percent pore volume of emulsion injection. This early emulsion breakthrough meant a very small surface area contacted by the emulsion. After injecting 0.21 PV of emulsion, the emulsion flood was followed by a waterflood at 400 ml/h. Water was injected through the injection well. As the waterflood continued, the oil cut was fairly stable at around 10 percent. After injecting slightly more than one PV of water, another emulsion slug was injected at 400 ml/h through the injection well. This time, 0.23 PV of emulsion was injected before starting another waterflood at 400 ml/h. At the beginning of water injection the oil cut increased slightly for a

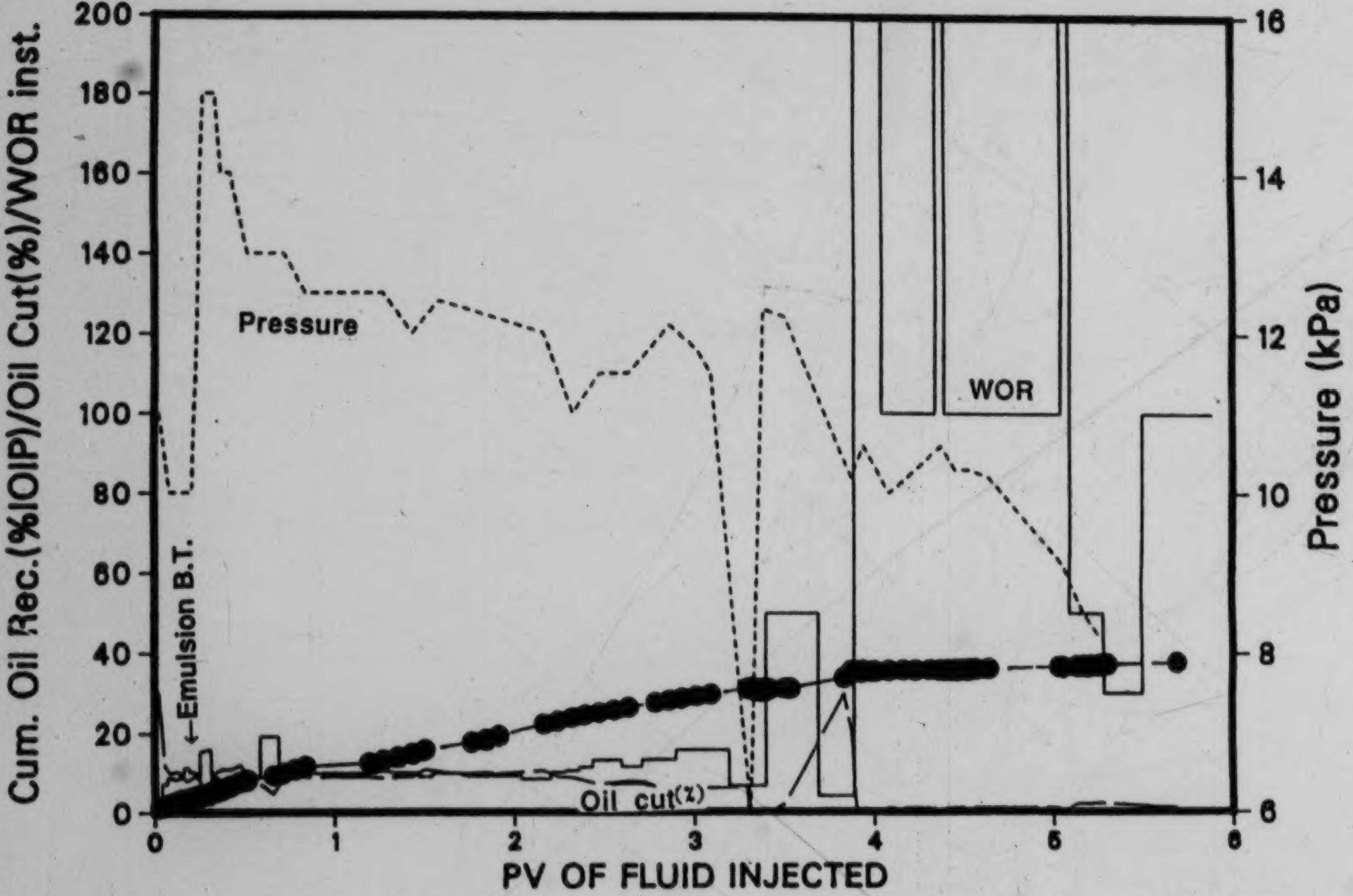

Fig. 30 Emulsion Flood and Waterflood Performance for Run 29 ($h_b/h_o=0.33$, $k_o/k_b=1.00$)

while but started decreasing with the progress of the waterflood. Waterflooding was continued for another 0.8 PV of water injection. At this point, another emulsion slug of 0.30 PV was injected. This time a 10 percent oil-in-water emulsion was injected. During emulsion injection, this emulsion slug was again followed by a waterflood. But the oil cut continued to decline and no peak in the oil recovery curve was observed.

It was hypothesized that the five percent oil-in-water emulsion was not efficient enough in creating blockage in the bottom water layer. Even though the emulsion was stable when tested outside the core, a considerable amount of coalescence took place after the emulsion travelled through the core. This might have been responsible for incomplete blockage. Moreover, the emulsion itself showed considerable inhomogeneity in distribution of oil droplets. This was found by microscopic observation of the emulsion. A more homogeneous and stable emulsion was produced with 10 percent oil by volume of emulsion. Consequently, it was decided to use 10 percent oil-in-water emulsion for future runs. An analysis of the emulsion produced at the production well showed that coalesence took place and the quality of emulsion deteriorated even though the emulsion remained an independent phase.

The results of the emulsion flood tests are summarized in Table 5.3.

TABLE 5.3: Results of Emulsion Flood Runs

Run no.	Emulsion bt(PV)	Recovery at bt (%IOIP)	Emulsion Inj. Point(PV)	Emulsion Slug Vol. (PV)	IOIP (ml)
29	0.16	3.2	0./1.27	0.21/0.23	1160
30	0.47	21.0	0./2.2	0.6/0.72	1144
31	0.36	0.36	0.	Continuous	1520.
32	0.85	7.2	0./4.0	2.0/1.3	740
33	0.44	24.0	0.	0.4	1205
34	0.69	36.7	0./2.5	0.65/0.4	1125
35	0.83	20.4	0./3.6	1.9/1.0	740
36	0.33	16.0	0.	0.5	1120
37	0.38	18.0	0.	0.4	1200
38	0.78	12.0	0.	2.0	762
39	1.09	65.5	0./1.3	0.67/0.7	975
40	0.68	51.5	0.	0.60	1150
41	0.46	4.93	0.	0.62	1095
42	0.45	18.0	0.	0.32	1135
43	0.48	21.4	0.	0.93	1140
44	0.36	8.3	0./1.64	.16/.16	1125
45	0.46	53.0	0.	1.2	1100

Run 30: 10 percent Oil-in-Water Emulsion, $h_b/h_o=0.33$, $k_o/k_b=1$

This run was conducted to examine the efficiency of a 10 percent oil-in-water emulsion in creating blockage for a subsequent waterflood. For Run 29, a five percent oil-in-water emulsion was used and the initial emulsion slug was 0.21 PV. In this run the packing conditions were same as those of Run 29. Initially, an emulsion flood was started at 400 ml/h through the injection well. The inlet pressure, as depicted in Figure 31 along with WOR, cumulative recovery and oil cut, was relatively higher than that in Run 29. The injection rate (400 ml/h as compared to 200 ml/h with Run 29) was higher for this run and a higher inlet pressure was expected. The emulsion flood continued until 0.6 PV of emulsion was injected. This value was equivalent to about two pore volumes of the bottom water zone. It was reported (Broz et al., 1985) that most of the permeability reduction by emulsion flood took place after injecting two pore volumes of emulsion (in the case of 100 percent water saturated core). During the emulsion flood, the oil cut decreased rapidly from 53 percent to 24 percent after an injection of 0.23 PV of emulsion. During this period, however, the inlet pressure increased showing that a considerable emulsion blockage was taking place. As the emulsion flood continued, the oil cut increased rapidly to a maximum of 60 percent. At this point the emulsion

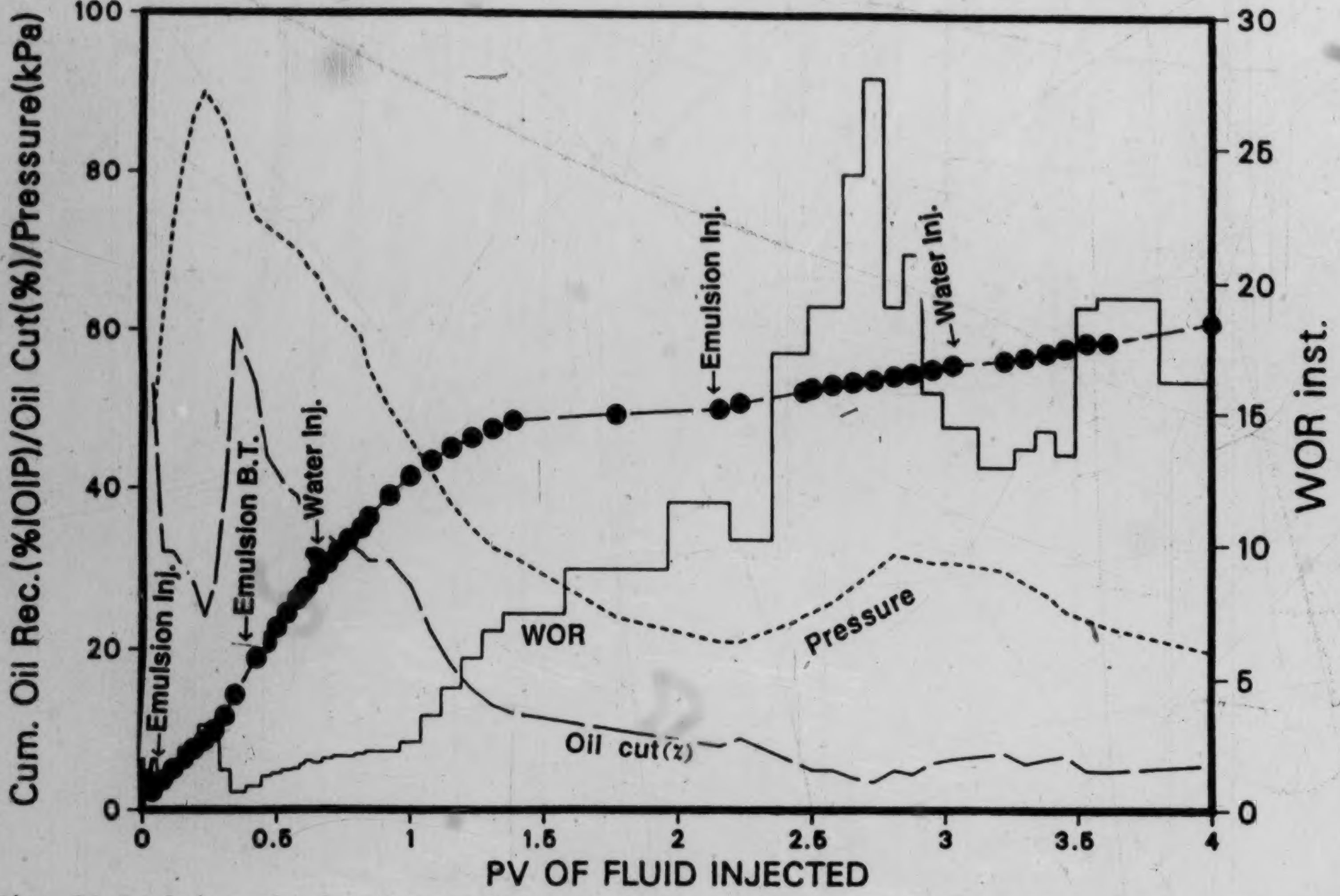

Fig. 31 Emulsion Flood and Waterflood Performance for Run 30 ($h_b/h_o=0.33$, $k_o/k_b=1.00$)

breakthrough took place (0.47 PV). This breakthrough time is longer than that which was observed in Run 29 (at 0.16 PV). Following emulsion breakthrough, the oil cut decreased again and dropped to a value of 37 as 0.60 PV of emulsion was injected. Also the injection pressure started decreasing at the same time. A waterflood was started at a flow rate of 400 ml/h at 0.60 PV of emulsion injection. As the emulsion breakthrough took place, the cumulative producing water-oil ratio of 1.51. This indicated that a sufficient amount of bottom water was replaced by emulsion to create blockage in the subsequent waterflood. As the waterflood continued the oil cut continued to decrease but at a slower rate than that of emulsion injection. Also, the injection pressure was quite high. This high injection pressure was due to an effective emulsion blockage. After an injection of two pore volumes of water, the oil cut dropped below 10 percent. At this point another emulsion slug of 0.7 PV was injected at 400 ml/h. During this emulsion flood the oil cut continued to decrease and as 0.7 PV of emulsion was injected, the oil cut dropped from nine percent to 4.5 percent. As this second emulsion slug was injected, the inlet pressure started increasing until the end of emulsion injection. Interestingly, because the emulsion flood was followed by a waterflood at a flow rate of 400 ml/h, the oil cut increased as the injection pressure decreased steadily. As the waterflood continued, the oil cut decreased very slowly. The waterflood was stopped when the WOR reached a value of 20. At this point, a total of 63.5 percent of the IOIP was produced as compared to 70 percent with polymer slug (as in Run 4) and 64 percent in the homogeneous case with waterflood (see Table 5.1). However, a total of 54 percent of the IOIP was recovered when the WOR reached a value of 20. As the second emulsion slug was injected, the WOR decreased and an excess of 9.5 percent of the IOIP was recovered before the WOR reached a value of 20 again. Recall that at a WOR value of 20, only 31 percent was recovered in Run 29, for which five percent oil in emulsion was used. This improvement seems to be due to more effective blockage by this type of emulsion (10 percent O/W), which was stable even after traveling through the core. Also, during an emulsion flood a considerable amount of emulsion invaded the water zone. This created an effective blockage for the waterflood and water invaded the oil zone, resulting in a steady oil cut and improved cumulative oil recovery.

5.5.2 Emulsion Injection in a Homogeneous Pack

Run 31: Continuous Emulsion Injection (h_b/h_o=0)

In order to investigate the effect of emulsion injection for a homogeneous core, Run 31 was conducted with continuous emulsion injection. A 10 percent oil-in-water emulsion was injected at a flow rate of 400 ml/hr. The pressure, WOR, oil cut and recovery data are depicted in Figure 32. As can be seen from this figure, emulsion injection resulted in a relatively high injection pressure. The injection pressure continued to increase during the initial 0.36 pore volume at which point emulsion breakthrough took place. Following emulsion breakthrough the injection pressure decreased rapidly. However, the injection pressure always remained higher than that observed with a waterflood (initial part of Run 14). This increase in injection pressure is higher than that which one would expect from the viscosity consideration alone. Emulsion injection led to the flow of water that was residual after a waterflood. Also, as the emulsion injection continued the irreducible oil saturation was decreased. Consequently, a total of 79 percent of the IOIP was produced when the WOR reached a value of 20. This compares to only 64 percent of oil recovered with a waterflood.

5.5.3 Effect of Oil-Water Thickness and Permeability Ratio

Several runs were conducted with different oil-to-water zone thicknesses and permeability ratios. The results of these runs are summarized in Tables 5.1 and 5.3. These runs will be presented individually in the following section.

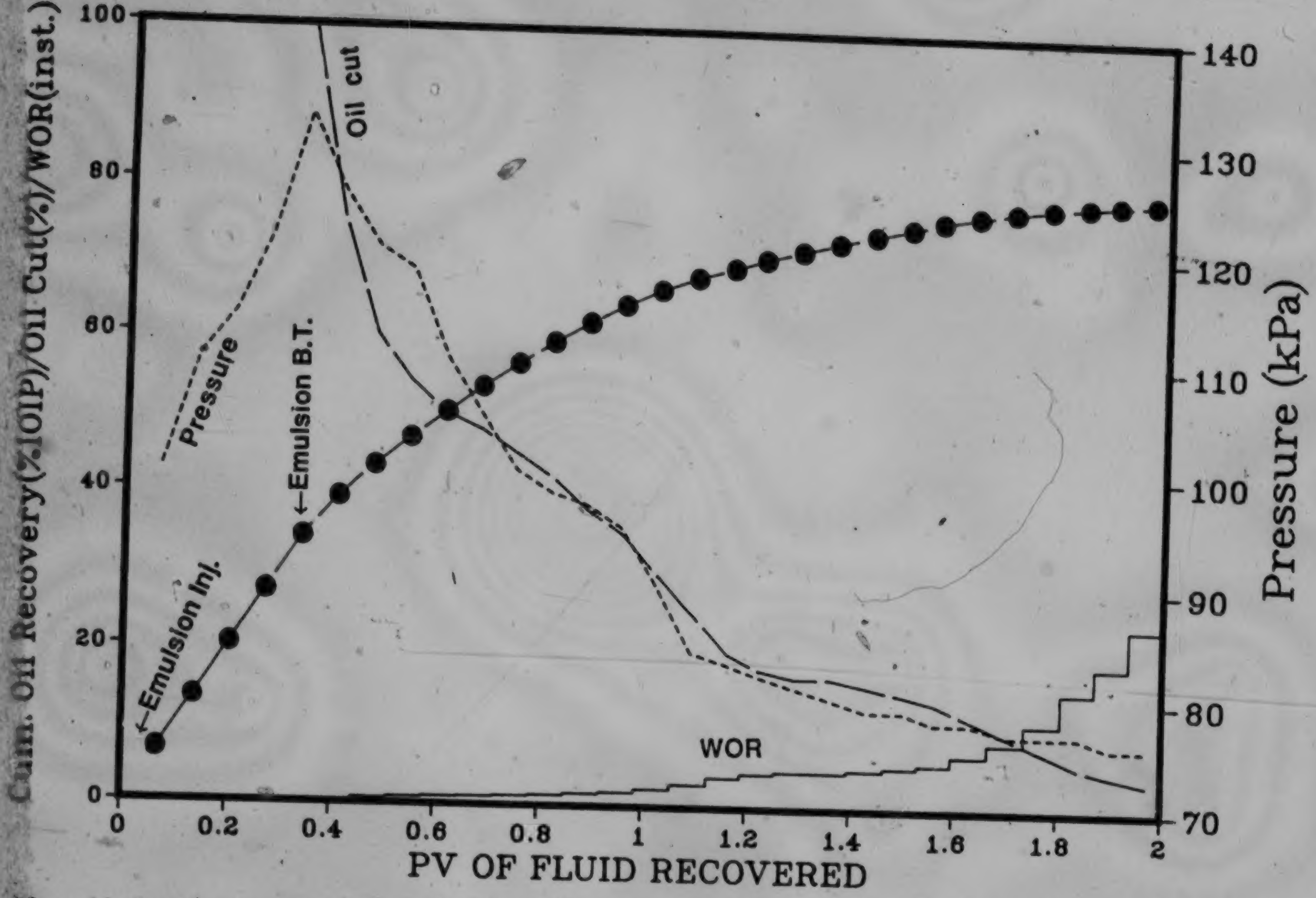

Fig. 32 Continuous Emulsion Flood Performance for Run 31 (h_b/h_o=0)

Run 32: $h_b/h_o=1$, $k_o/k_b=1$

Run 32 was conducted in order to examine the effect of the oil zone and bottom-water zone thickness ratio. In this run, this ratio was 1:1. The h_w/h_o ratio was equal to 0.50 for both the injection and the production well. As it was observed during Run 30 that an emulsion slug of two pore volumes of the bottom-water zone improved oil recovery, the same size of emulsion slug was used for this run as well. The emulsion flood started at a flow rate of 400 ml/h. The emulsion was injected directly through the injection well. Recall that the injection wells were used also during polymer flooding in Run 3 ($h_b/h_o=1$, $k_o/k_b=1$). Initially, the oil cut was low (below 10 percent) but yet higher than that obtained with a waterflood. The oil cut, inlet pressure, WOR and cumulative oil production are depicted in Figure 33. Emulsion breakthrough occurred at 0.85 PV of emulsion injection. This value is greater than that with Run 30 even though the thickness of the bottom-water zone for this run was higher than that in Run 30. However, only 7.2 percent of the IOIP was produced during this period. This may be compared to 21 percent of the IOIP produced at the time of breakthrough in Run 30. Even after the emulsion breakthrough occurred the inlet pressure continued to increase indicating improved blockage as more and more emulsion was injected. At the point of emulsion breakthrough the cumulative water-oil ratio was 13. This

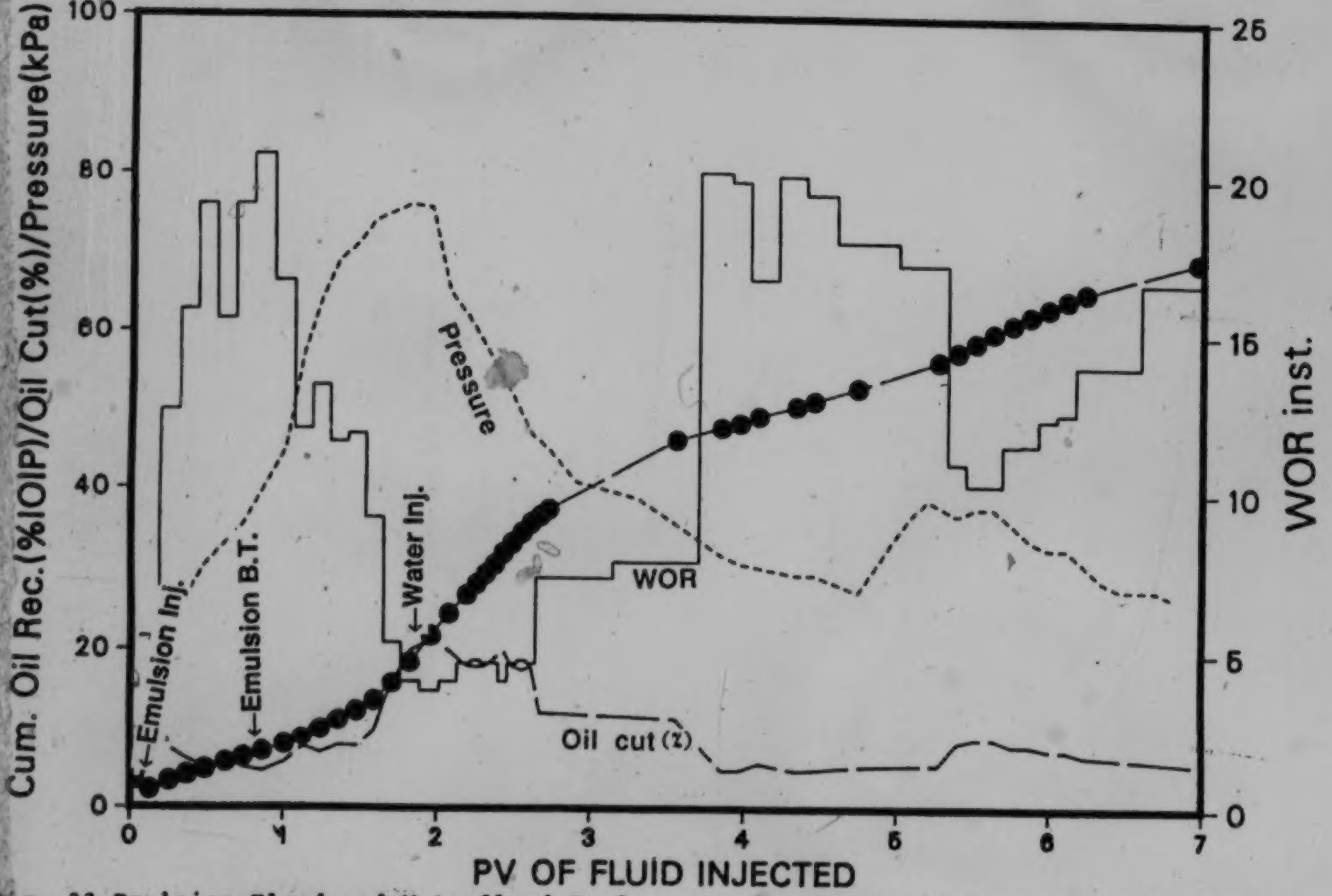

Fig. 33 Emulsion Flood and Waterflood Performance for Run 32 (h_b/h_o=1.00, k_o/k_b=1.00)

indicated that a large portion of the emulsion went into the bottom-water zone, creating effective blockage. This was indicated by improved sweep when the waterflood followed the emulsion flood. The emulsion flood was terminated after two pore volumes of emulsion injection. The oil cut was around 20 percent at this point. The emulsion flood was followed by a waterflood at 400 ml/h. The inlet pressure decreased, first rapidly, then slowly, but the oil cut remained steady until 0.6 PV of water was injected. At this point the oil cut started to decline and dropped to a value lower than five percent as two more pore volumes of water were injected. The inlet pressure indicated a partial restoration of the permeability of the water zone. However, the inlet pressure stabilized at a value much higher than that which was obtained with a waterflood. It is not quite accurate, however, to comment on permeability reduction, because the system under discussion is not a case of single-phase flow; and the channeling of water into the bottom-water zone, which was more affected by the injected emulsion, could not be monitored. After injecting two pore volumes of water, the emulsion flood was started again. In the beginning, no increase in inlet pressure was observed. This indicated that no blockage was building up near the injection well. However, as the emulsion flood front advanced, the inlet pressure increased gradually. This was followed by an increase in oil cut. This time, 1.2 PV of emulsion was injected. After that, the waterflood was started. During the waterflood the inlet pressure dropped slowly to a previously stabilized value and the oil cut increased from 5.5 percent to nine percent. As the waterflood continued, the oil cut decreased slowly. A total of 49 percent of the IOIP was recovered when the WOR reached a value over 20. By comparison, 54 percent of the IOIP was recovered at this WOR value in Run 30 for which the bottom-water layer was thinner. But, to reach this value seven pore volumes, as compared to four pore volumes in Run 30, of fluid was injected in this run. Moreover, the oil cut in Run 32 never approached 60 percent which was the maximal value observed in Run 30. It appears that as the bottom-water layer thickness increased, it became more difficult to obtain a high oil cut. However, with an emulsion flood, a reasonable value (around 20 percent) for oil cut was easily obtained.

Run 33: $h_b/h_o=0.2$, $k_o/k_b=1$

Run 33 was conducted to investigate further the effect of the oil-to-water zone thickness ratio. For this run the oil zone was five times thicker than the bottom-water zone even though the absolute permeabilities were the same. The injection and production wells were located 1.6 cm (one-quarter of the total thickness of the oil zone) into the oil zone. The displacement test started with an emulsion flood at a flow rate of 400 ml/hr. The WOR, pressure, oil recovery and oil cut are depicted in Figure 34. The oil recovery was much better than that in Run 30 for which a thicker (h_b/h_o=0.33) bottom-water zone was used. The emulsion flood was continued until 0.4 PV of emulsion was injected. About 25 percent of the IOIP was recovered during the emulsion flood and the WOR remained lower than 5. The volume of emulsion slug injected was equivalent to two pore volumes of the bottom-water zone. Usually, the slug size was determined as a function of the bottom-water zone pore volume rather than the oil zone pore volume. During emulsion injection the oil cut decreased initially but soon started increasing rapidly to a peak of 60 percent. Following the emulsion slug, a waterflood was started at a flow rate of 400 ml/hr. During the waterflood, emulsion breakthrough occurred at 0.44 pore volume of fluid injection (emulsion and water). The oil cut continued to increase until emulsion breakthrough took place. However, the oil cut decreased rapidly after emulsion breakthrough. As the waterflood continued, a total of 61 percent of the IOIP was recovered when the WOR reached a value of 20.

Run 34: h_b/h_o=0.33, k_o/k_b=2.67

This run was conducted to examine the effect of a tight bottom water zone. The packing characteristics (as shown in Table 5.1) were the same as those of Run 6. The h_w/h_o value

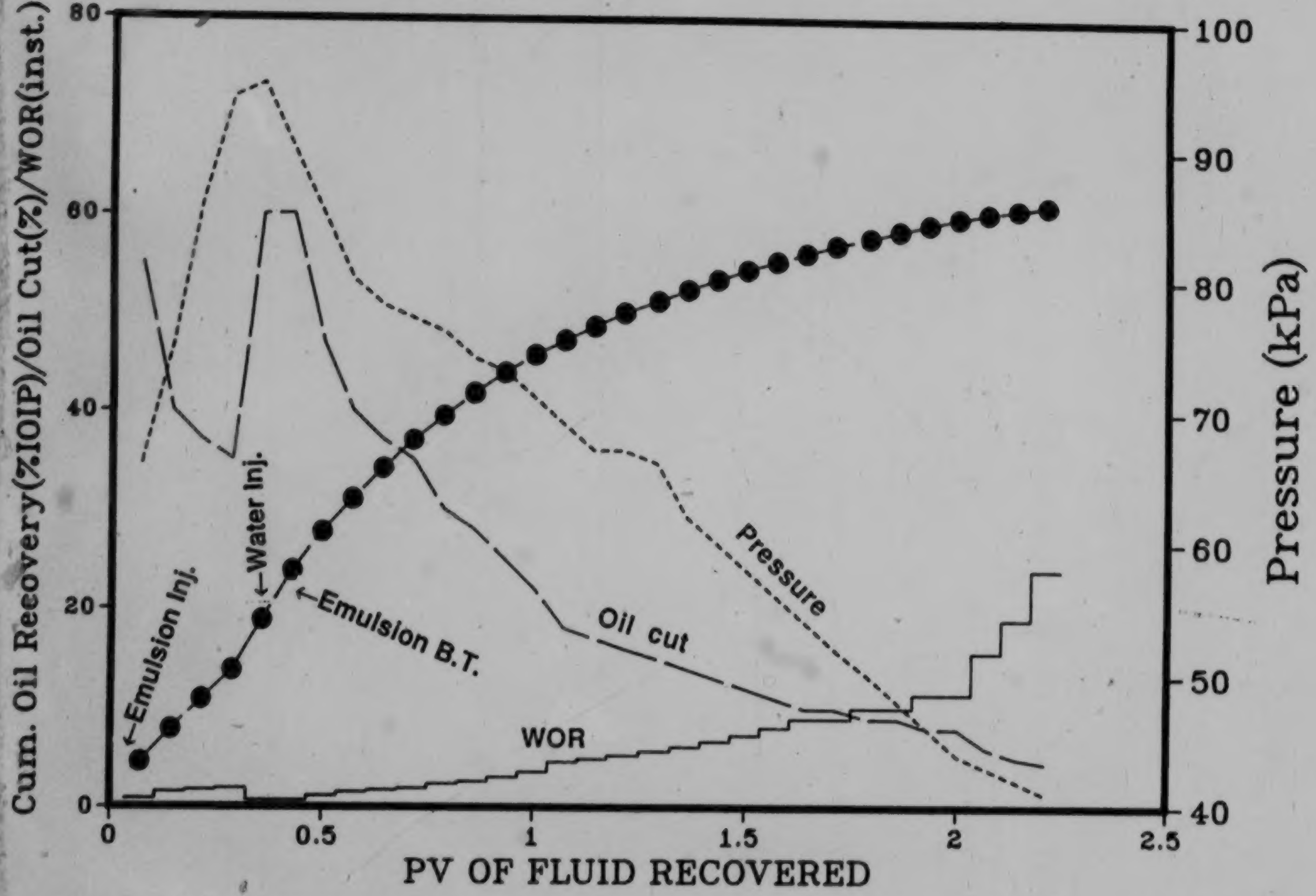

Fig. 34 Emulsion Flood and Waterflood Performance for Run 33 (h_b/h_o=0.20, k_o/k_b=1.00)

was 0.25 for both the injection and the production well.

A 10 percent oil-in-water emulsion was injected at a flow rate of 400 ml/h. The emulsion flood was characterized by a relatively higher inlet pressure as compared to that of Run 30 for which a similar height for the bottom-water zone was used. However, the inlet pressure was initially comparable to that of Run 6 with a waterflood. But as the emulsion flood continued, the inlet pressure increased showing more resistance to flow. A similar performance was observed during emulsion flooding in Runs 30 to 32. The oil recovery was distinctly better than in all the previous cases. The inlet pressure, WOR, oil cut and oil recovery are depicted in Figure 35. Note here that the same emulsion quality (10 percent oil-in-water) was used for this run, whereas the bottom-water layer had smaller pore openings (as can be deduced from the low permeability). During the initial stages of the emulsion flood, the oil cut increased rapidly to reach a value as high as 61 percent. Actually, the maximal oil cut was attained when emulsion breakthrough occurred at 0.069 PV volume injected. This breakthrough was later than that of previous runs (Runs 30 to 32). However, at the point of breakthrough the cumulative water-oil ratio was equal to 1.15. This compared to 13 for Run 32 and 1.51 for Run 30. The breakthrough time was longer than that for the previous runs. This length of time was sufficient to create blockage for the waterflood that followed the

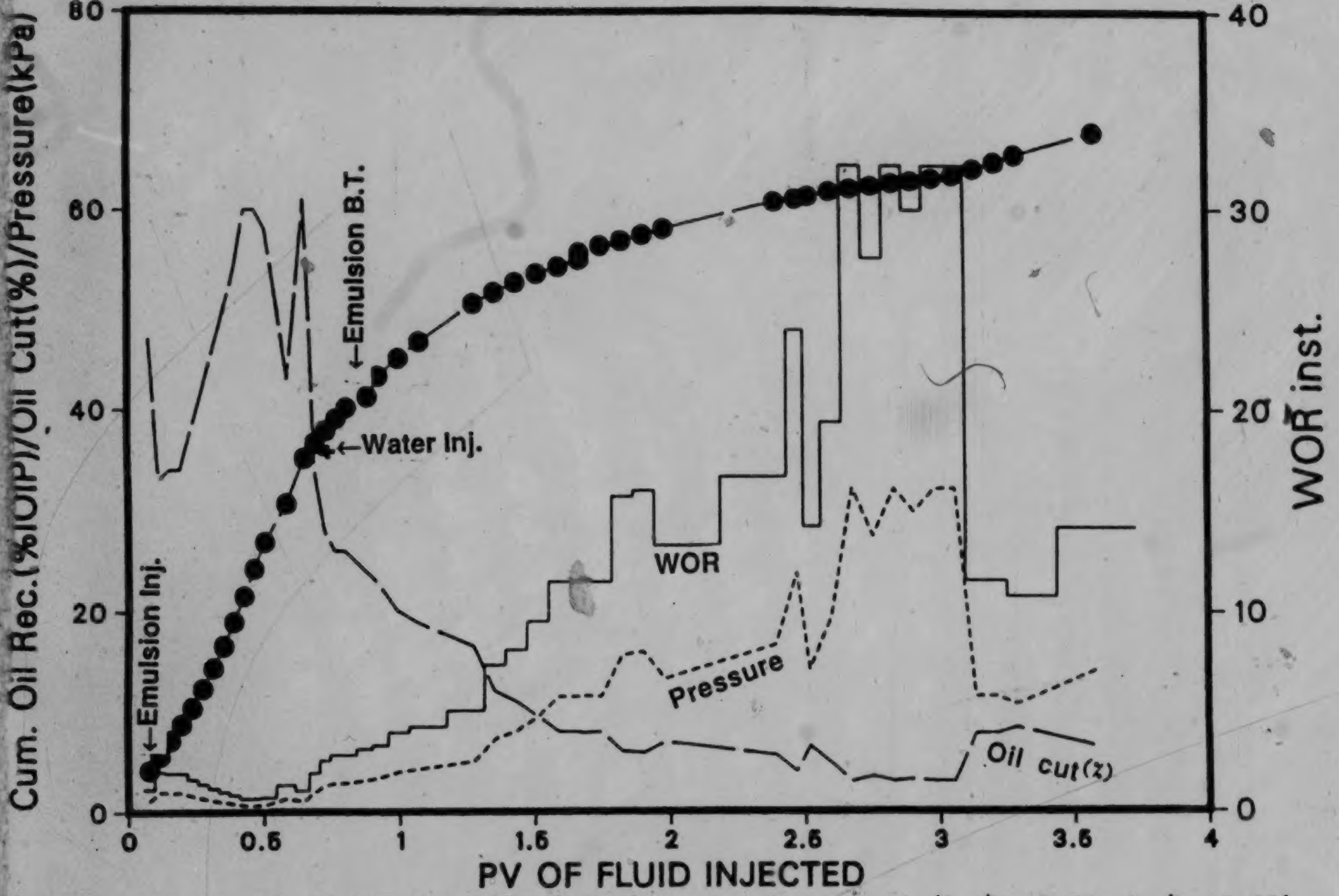

Fig. 35 Emulsion Flood and Waterflood Performance for Run 34 (h_b/h_o=0.33, k_o/k_b=2.67)

emulsion injection and it isolated the bottom-water zone, to create a low permeability interface between the oil and water zone. The hypothesis of partial invasion of the bottom-water zone was further supported by a rapid decline in both oil and water cuts after emulsion breakthrough. The emulsion produced had a quality similar to that injected. This indicated little contamination by connate water and a piston-like displacement by emulsion. However, even though the oil cut decreased after emulsion breakthrough, it remained fairly steady at a somewhat lower value. The emulsion flood was stopped as soon as emulsion breakthrough took place and a waterflood was started at 400 ml/h. The emulsion slug size of 65 percent pore volume was also equivalent to about two pore volumes of the bottom-water zone. As the waterflood continued, the inlet pressure decreased following a trend very similar to that of the oil cut. As in the previous cases, this indicated partial restoration of the permeability of the emulsion-affected zone. However, the inlet pressure that was attained after injecting about two pore volumes of water was still higher than that expected from a conventional waterflood. This value was comparable to the inlet pressure attained at the final stage of Run 30. In the mean time, the oil cut decreased slowly and dropped below five percent. At this point, another emulsion slug was injected at 400 ml/h. During the emulsion flood, the inlet pressure increased but the oil cut continued to decline. This time, the emulsion slug volume was 0.3 PV. The emulsion flood was followed by a waterflood at 400 ml/h. No significant change occurred during the waterflood except that the pressure decreased slightly. But as the waterflood continued, the oil cut increased again indicating improvement in blocking of the bottom-water zone by the leading emulsion slug. After injecting the second emulsion slug, a total of 60 percent of the IOIP was recovered as the WOR reached a value of 20. This was quite significant as only 3.6 PV of fluid was injected up to this point. Note, however, that for a similar bottom-water zone thickness and permeability, but with the use of a polymer slug (Run 6), the WOR was controlled much more effectively. With a similar total oil recovery the WOR was maintained below six percent. This point should be considered if any attempt to compare the two techniques is made. However, it was felt necessary to study the effect of a tight but thicker bottom-water zone and with that view Run 35 was planned.

Run 35: Emulsion Flood: $h_b/h_o=1$, $k_o/k_b=2.67$

In order to examine the effect of the oil-to-water zone thickness ratio for the tight bottom-water zone case, Run 35 was conducted. The oil-to-water zone thickness ratio was 1:1 in this case. The h_w/h_b value was 0.50 for both the production and the injection well. The run started with emulsion injection at 400 ml/h. As observed in the previous runs with emulsion flood, the inlet pressure gradually increased as the emulsion flood continued. The oil cut was higher than that observed with a waterflood (Run 7) and remained steady in the beginning. However, as the emulsion flood continued, the oil cut started increasing. The inlet pressure, WOR, oil cut and cumulative oil recovery are depicted in Figure 36. Emulsion breakthrough occurred at 0.83 PV of emulsion injection. This value is higher than that observed with Run 32. At this point, the cumulative water-oil ratio was 3.70. This indicated that a considerable volume of the bottom-water zone was invaded by emulsion. However, this volume was somewhat less than that for the case with a higher permeability for bottom water zone. The emulsion flood continued until two pore volumes of emulsion were injected. As in previous emulsion flood runs, the peak in oil cut coincided with the emulsion breakthrough. As the emulsion flood continued, the oil cut slowly decreased. The injection pressure, however, continued to increase until the end of emulsion flood. The emulsion flood was followed by a waterflood at 400 ml/h after injecting two pore volumes of emulsion. The waterflood was characterized by a decreasing pressure. The oil cut also declined slowly. As 1.6 PV of water were injected, the oil cut dropped below five percent. But by this time 61 percent of the IOIP was produced. This value

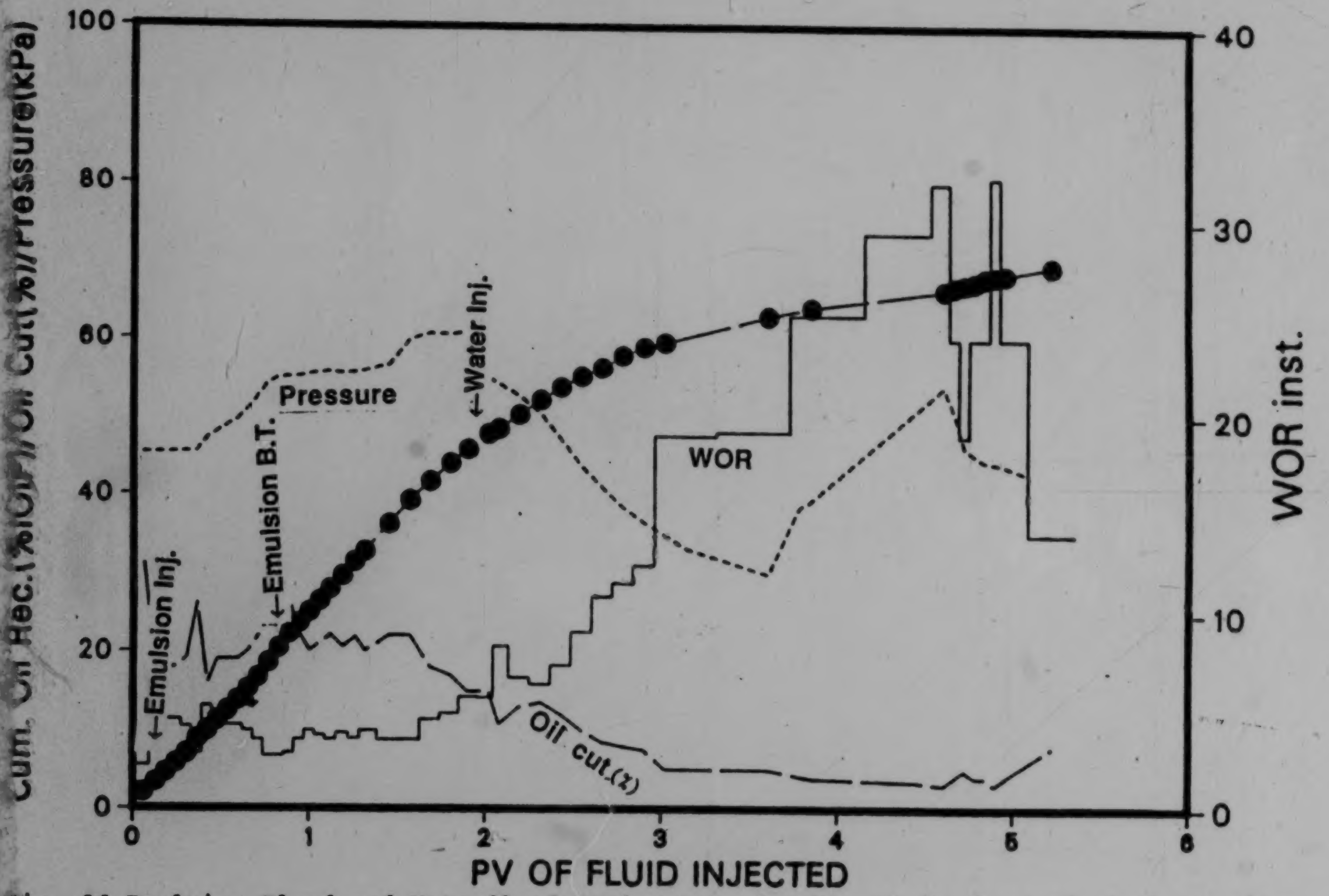

ig. 36 Emulsion Flood and Waterflood Performance for Run 35 (h_b/h_o=1.00, k_o/k_b=2.67)

compares with 49 percent of the IOIP recovered at the same WOR in Run 32. Another emulsion slug was tried but resulted in insignificant recovery.

Run 36: $h_b/h_o=0.33$, $k_o/k_b=0.06$

In order to examine the effect of high-permeability bottom-water zone ($k_o/k_b=0.06$) Runs 36 through 38 were conducted. For Run 36, the oil zone was three times thicker than the bottom-water zone. The wells were located at a depth of 0.75 cm into the oil zone. The displacement test started with an emulsion flood at a flow rate of 400 ml/hr. As expected, a high-permeability bottom-water zone led to a high WOR even though h_b/h_o was relatively low. However, the WOR was still much lower than that observed in a waterflood (early part of Run 8). This improvement shows the effectiveness of an emulsion flood even in the presence of a highly permeable bottom-water zone. Figure 37 depicts WOR, pressure, oil cut and oil recovery for this run. During emulsion injection the oil cut started increasing rapidly and attained a peak of more than 60 percent. Emulsion breakthrough took place at 0.33 PV. This value was lower than that observed in runs with tighter bottom-water zones. At the point of emulsion breakthrough 16 percent of the IOIP was recovered. Emulsion injection was continued until 0.5 pore volume of emulsion injection. It was then followed by a waterflood. During the waterflood the injection pressure

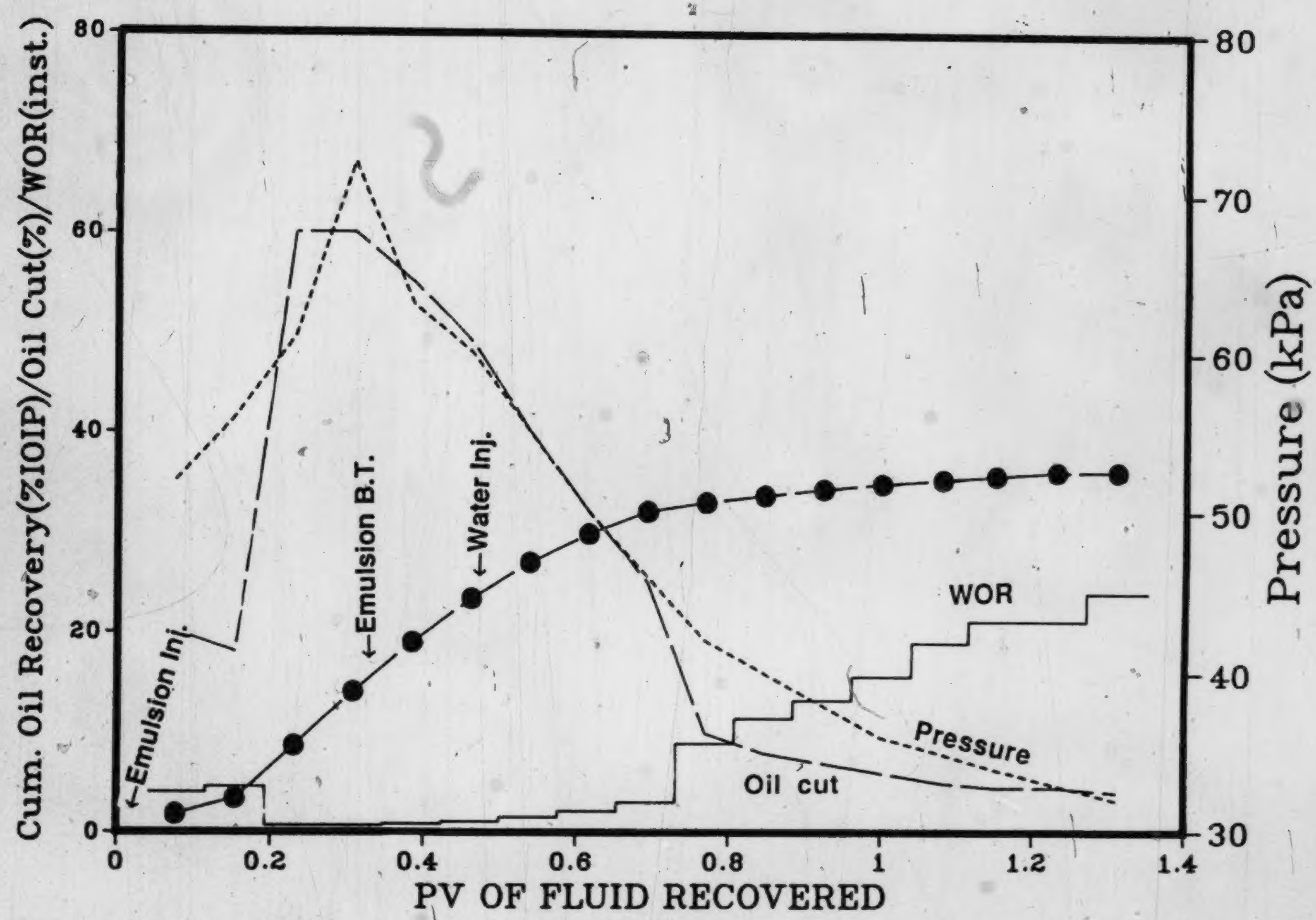

Fig. 37 Emulsion Flood and Waterflood Performance for Run 36 (h_b/h_o=0.33, k_o/k_b=0.06)

as well as the oil cut decreased rapidly. However, even with this decreasing oil cut a total of 35 percent of the IOIP was recovered as the WOR reached a value of 20. This indicated a seven-fold improvement over a conventional waterflood.

Run 37: $h_b/h_o=0.2$, $k_o/k_b=0.06$

In order to investigate the effect of the oil-to-water zone thickness ratio for a k_o/k_b of 0.06, Run 37 was conducted with an oil-to-water zone thickness ratio of five. The wells were located at 1.6 cm (one-quarter of the total thickness of the oil zone) into the oil zone. The displacement test was started with an emulsion flood at a flow rate of 400 ml/hr. The WOR was much lower than that in Run 36 for which an h_b/h_o of 0.33 was used. Recall here that in the case of polymer injection only a slight decrease in WOR took place for a similar decrease in h_b/h_o. It appears that the oil-to-water zone thickness ratio plays an important role in mobility control with emulsions in a highly-permeable bottom-water zone. During emulsion injection the oil cut increased rapidly to reach a peak higher than 60 percent. Also, this value was higher than that observed in Run 36. An emulsion slug of 0.40 PV was injected. This volume corresponded to about two pore volumes of the bottom-water zone. A waterflood was started at a flow rate of 400 ml/hr following the emulsion flood.

Emulsion breakthrough occurred at 0.38 PV. At this point 18 percent of the IOIP was recovered. Figure 38 depicts the WOR, pressure, oil cut and oil recovery performance for this run. At the end of the displacement test a total of 43 percent of the IOIP was recovered. This indicates more than a six-fold improvement over a conventional waterflood.

Run 38: $h_b/h_o=1$, $k_o/k_b=0.06$

In order to investigate further the effects of the oil-to-water zone thickness ratio for a k_o/k_b of 0.06, Run 38 was conducted with an h_b/h_o of 1. The wells were located at 50% depth of the oil zone. Initially, an emulsion flood was started at a flow rate of 400 ml/hr. This run represented the most adverse situation. The emulsion flood performance was much poorer than that of Runs 36 and 38 but yet was much better than a conventional waterflood. During the emulsion flood, the oil cut increased rapidly but could not sustain a high value for long. An emulsion slug of two pore volumes was injected. Emulsion breakthrough took place at 0.68 pore volume and 15 percent of the IOIP was recovered during this period. This value was much lower than that observed with tighter bottom-water zones. Emulsion injection was followed by a waterflood at a flow rate of 400 ml/hr. At the end of the displacement test a total of 29 percent of the IOIP was recovered when the WOR reached a value of 20. This indicated more than a 14-fold improvement

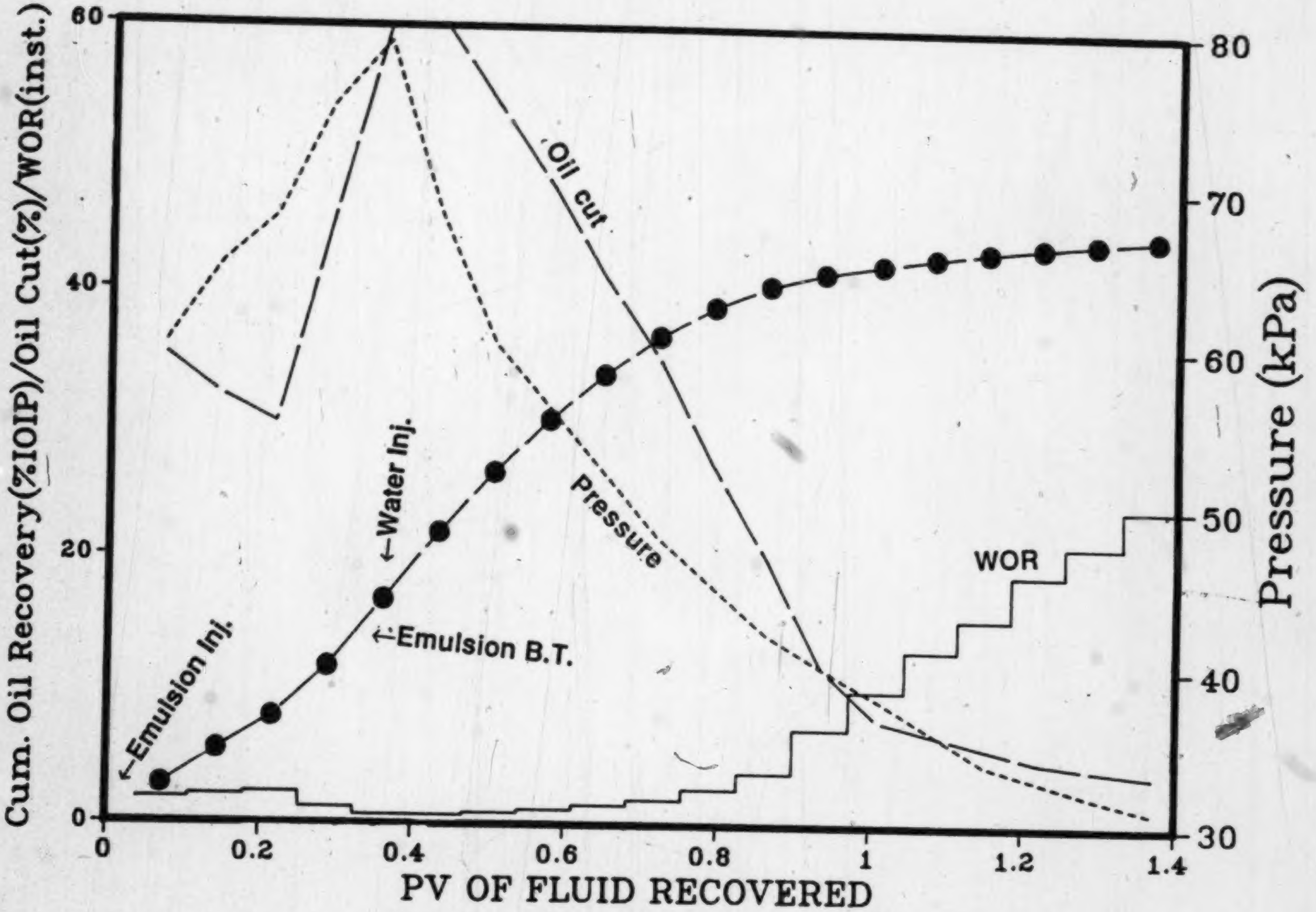

Fig. 38 Emulsion Flood and Waterflood Performance for Run 37 ($h_b/h_o=0.20$, $k_o/k_b=0.06$)

over a conventional waterflood. Figure 39 depicts the pressure, WOR, oil cut and oil recovery performance for this run. The results are also summarized in Tables 5.1 and 5.3.

5.5.4 Effect of Viscosity Ratio on Emulsion Flood

Run 39: Viscosity Ratio=1

In order to examine the effect of viscosity ratio on emulsion flooding, Run 39 was conducted. As can be seen from Table 2.2, the size of the bottom-water zone was the same as that used in Run 30. However, in this run, kerosene was used as the oil phase. The h_w/h_o value was 0.25 for both the injection and the production well. The emulsion flood started at 400 ml/h. Unlike other emulsion flood runs (with 50 mPa.s oil), the pressure initially fluctuated and then decreased continually. This can be seen from Figure 40. This indicated that no resistance or blockage was building up. For all previous runs, the emulsion floods were characerized by a short but sharp increase in pressure at the beginning of the emulsion flood. This trend in inlet pressure showed that emulsion was actually going into the oil zone rather than the bottom-water zone. This idea was further supported by the fact that water breakthrough occurred when 0.079 PV of emulsion has been injected. In Run 30, water breakthrough occurred almost immediately after emulsion injection was started. As the emulsion flood continued, the oil cut remained high throughout. But the

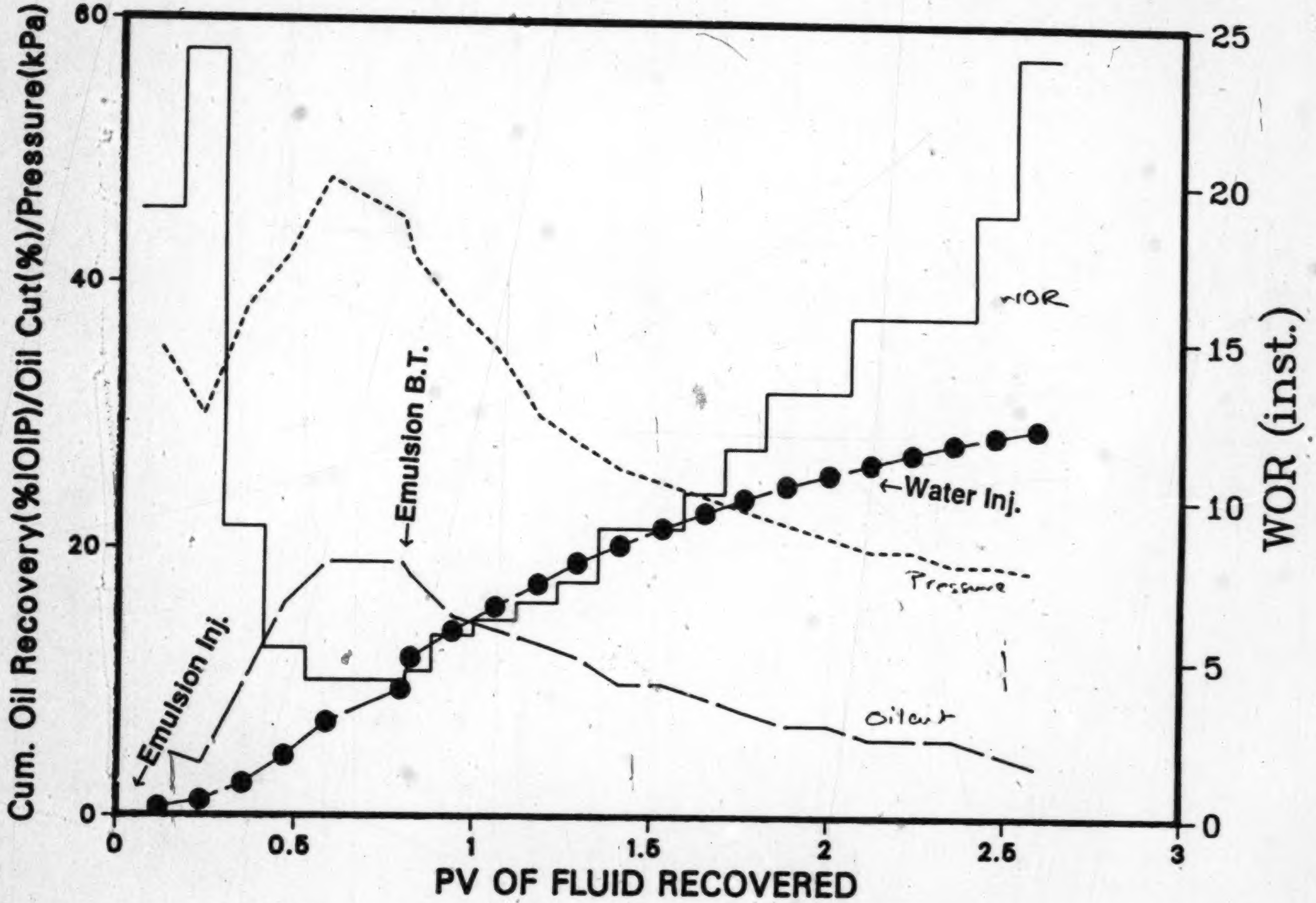

Fig. 39 Emulsion Flood and Waterflood Performance for Run 38 (h_b/h_o=1.00, k_o/k_b=0.06)

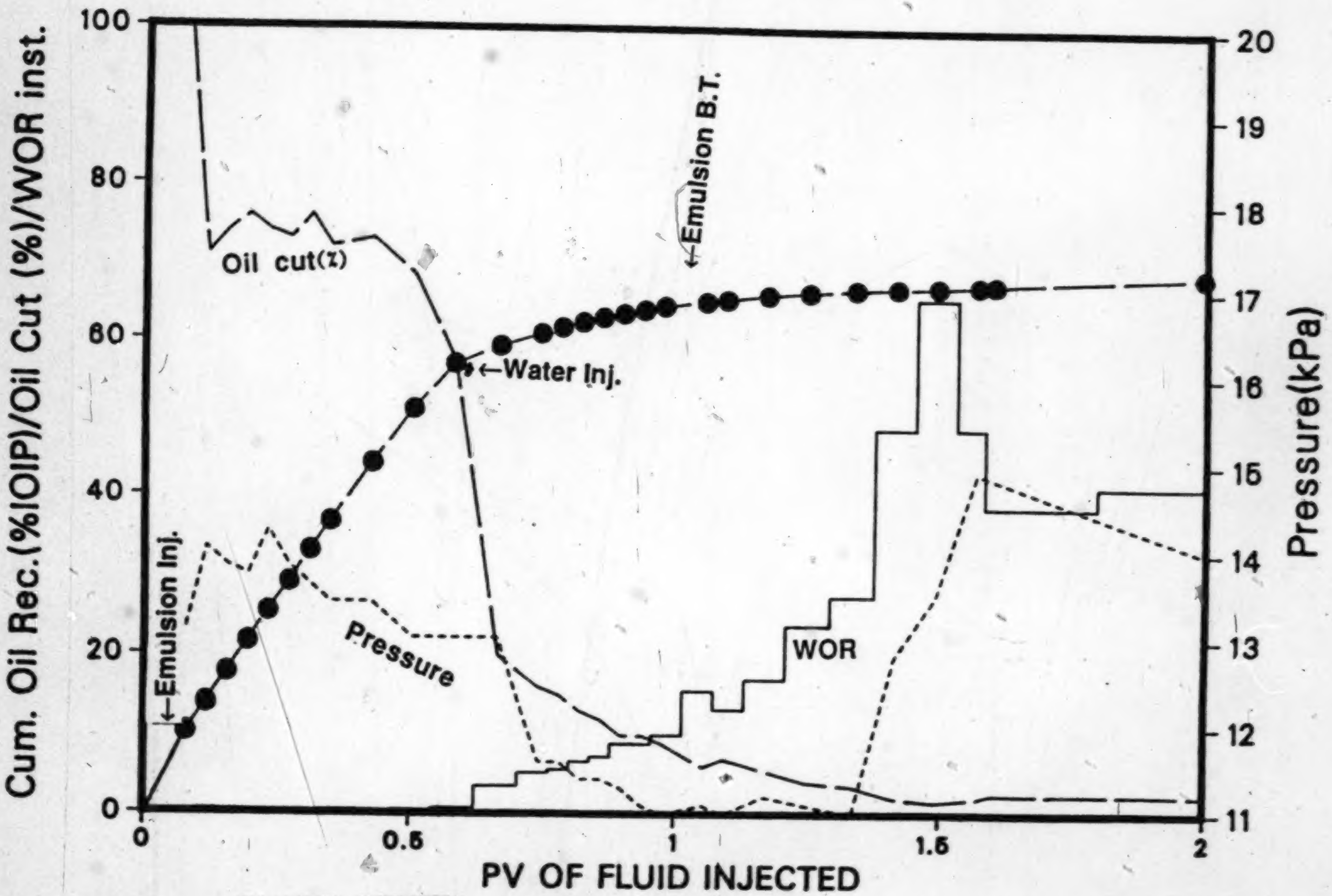

Fig. 40 Emulsion Flood and Waterflood Performance for Run 39 (h_b/h_o=0.33, k_o/k_b=1.00)

recovery was almost as good with a conventional waterflood (Run 11), even though breakthrough occurred later for this run. As a matter of fact the recovery curves for Runs 11 and 39 follow almost the same pattern until 0.48 PV of emulsion was injected. After this period the emulsion flood showed better recovery than the waterflood. Recall that the polymer injection was initiated in Run 11 after 0.64 PV of water injection. As the emulsion flood was terminated and was followed by a waterflood, the oil recovery continued to be better than water and polymer floods (Run 11). As compared to more viscous oil (Run 30), the oil recovery remained much higher throughout the run. However, unlike Run 30, the WOR in Run 39 did not show any fluctuation and increased monotonically (even though slowly). Another point of interest was the delayed emulsion breakthrough in this run. Emulsion breakthrough occurred at 1.09 pore volumes of total fluid injection. At this point the cumulative water-oil ratio was 1.21. This indicates that a considerable amount of emulsion went into the oil zone unlike previous cases with higher oil viscosity. Evidently, because the oil and water had similar viscosities, preferential flow of emulsion into the bottom-water zone did not occur as before.

Run 40: Viscosity Ratio=7.5

The packing characteristics of this run are given in Table 5.1. As similar packings were used in Runs 30 and 39, the results for these runs could be compared directly to obtain an idea of the effect of the oil-water viscosity ratio. An emulsion flood was started at the beginning of the run at a flow rate of 400 ml/h. Water breakthrough occurred when 0.031 PV of water had been injected. This value is slightly higher than that for an emulsion flood with a 50 mPa.s viscosity oil (Run 30). It can be seen by comparing Figure 41 with Figure 12 that the oil cut in Run 41 was considerably higher than that for a waterflood with the same type of oil (Run 12). As was observed in previous cases of emulsion flood, the oil cut decreased during the initial stages and then increased to reach a peak. After injecting 0.6 pore volume of emulsion (which is equivalent to two pore volumes of the bottom water zone), a waterflood was started at 400 ml/h. Soon after the waterflood started, emulsion breakthrough occurred at 0.7 PV of total fluid injection. Even though emulsion breakthrough occurred earlier for this run, the fraction of the total oil recovered at this point was quite comparable to that of Run 39. As evidenced in previous emulsion floods, the oil cut started to decrease after emulsion breakthrough took place. The injection pressure decreased as well. But the pressure decreased slowly and stabilized quickly. This trend of pressure decline showed an efficient blockage by emulsion.

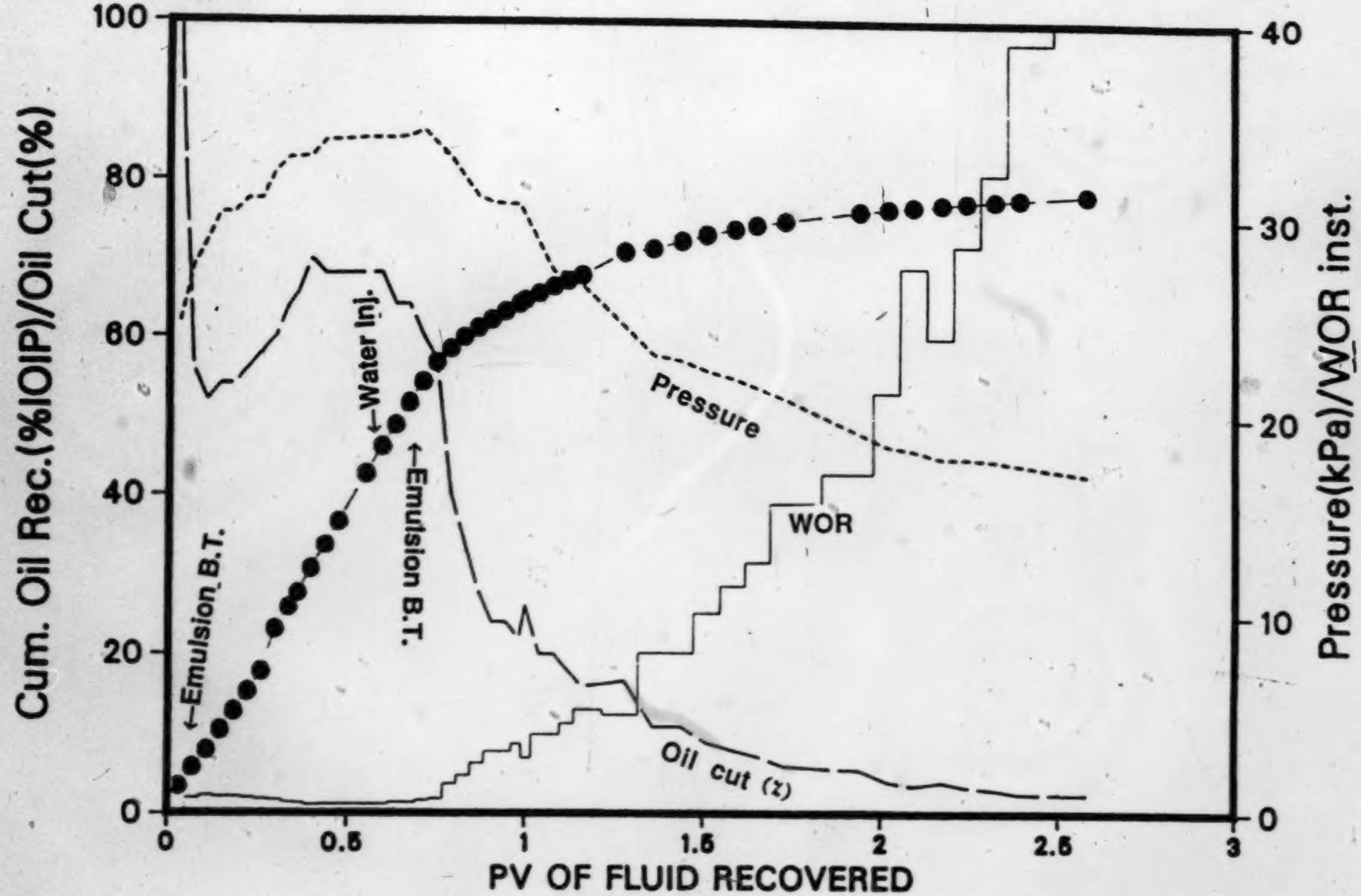

Fig. 41 Emulsion Flood and Waterflood Performance for Run 40 ($h_b/h_o=0.33$, $k_o/k_b=1.00$)

As the waterflood continued, 76 percent of the IOIP was produced by the time the WOR increased to 20. This compares with 54 percent in Run 30, and 66.5 percent in Run 39.

Run 41: Viscosity Ratio=200

In order to examine the effect of a higher oil viscosity on an emulsion flood , Run 41 was conducted using Faxam 100 (viscosity=200 mPa.s) as the oil phase. Run 13 showed that, for this high viscosity of oil, the oil recovery by a waterflood was almost negligible. For Run 41, the emulsion flood started at the beginning of the displacement test. For this particular run, the emulsion was produced from 10 percent Faxam-100 and distilled water (with 300 ppm surfactant). An emulsion slug of approximately two pore volumes of the bottom water zone was injected. During emulsion injection, the oil cut was clearly higher than that obtained for a waterflood. As the emulsion flood continued, the oil cut increased gradually. Figure 42 depicts the WOR, oil cut, oil recovery and pressure data for this run. Emulsion breakthrough occurred when 0.46 PV of emulsion had been injected. This value is fairly close to that observed for Run 30 for which MCT-10 oil (50 mPa.s) was used. When emulsion breakthrough occurred, the oil cut started decreasing. The emulsion slug was followed by a waterflood. The initiation of the waterflood did not lead to any sudden change in oil

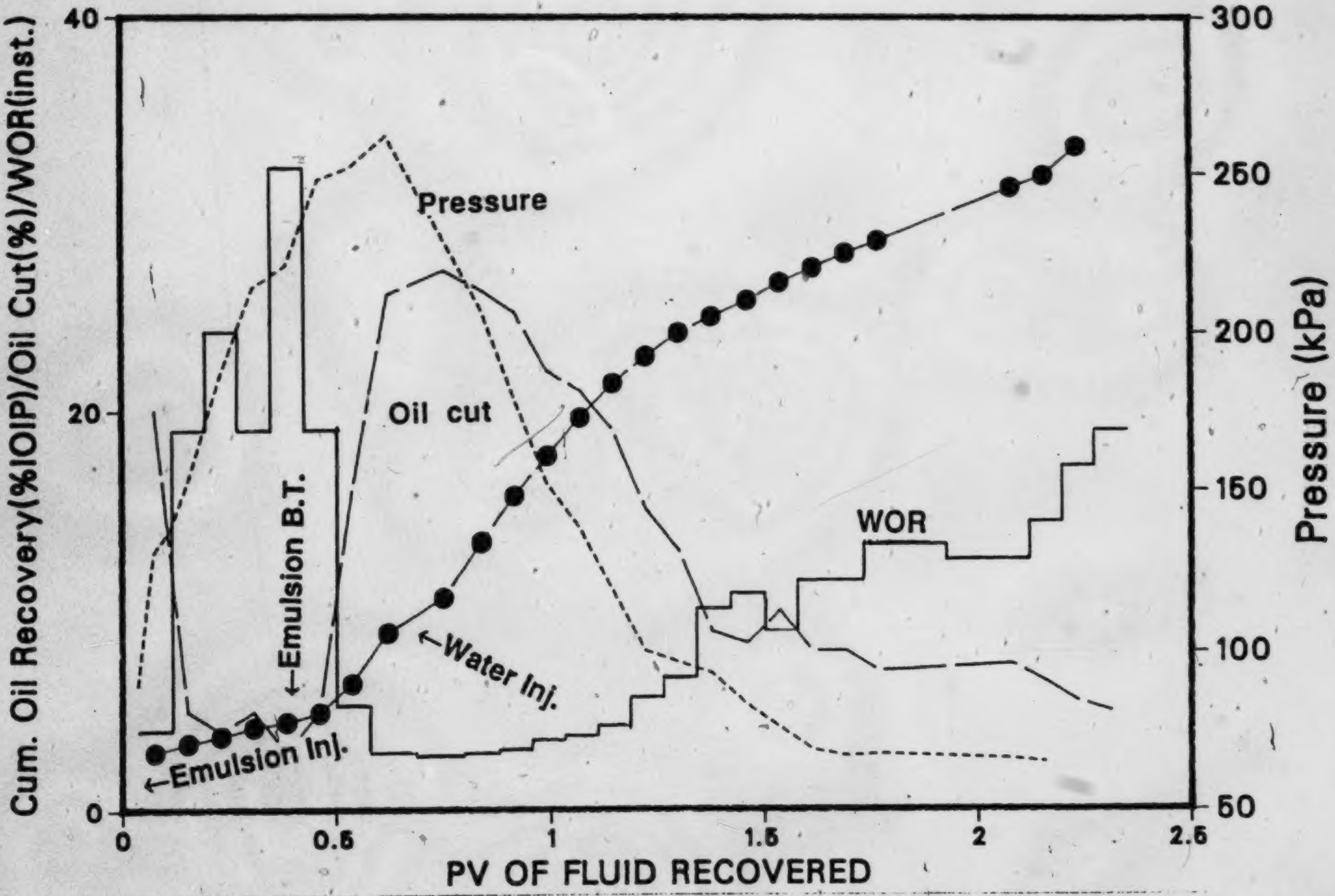

Fig. 42 Emulsion Flood and Waterflood Performance for Run 41 (h_b/h_o=0.33, k_o/k_b=1.00)

recovery. However, the oil cut decreased gradually. At the end of the displacement test, a total of 33 percent of the IOIP was produced. This value, even though low as compared to other runs (with lower viscosity oils) is higher than that with Run 13 for which a polymer slug was used.

5.5.5 Effect of Emulsion Slug Sizes

In order to examine the effect of emulsion slug size Runs 42 through 45 were performed. These runs could be compared with Run 30 as all these runs had an h_b/h_o value of 0.33 and a k_o/k_b value of 1. Besides, a similar emulsion injection strategy was used for all these runs (i.e., emulsion slug was injected initially through the inlet end and was followed by a waterflood through the injection well). For all these runs 400 ml/hr was used as the volumetric injection rates for both the emulsion and water injections.

Run 42: Emulsion Slug Size= 0.32 PV (One PV of the water zone)

In order to examine the effect of smaller emulsion slugs, Run 42 was conducted. Recall that a 0.60 PV of emulsion slug was used in Run 30. The emulsion slug was injected at the beginning of the displacement test. As the emulsion slug injection continued the injection pressure increased rapidly. Figure 43 depicts the injection pressure

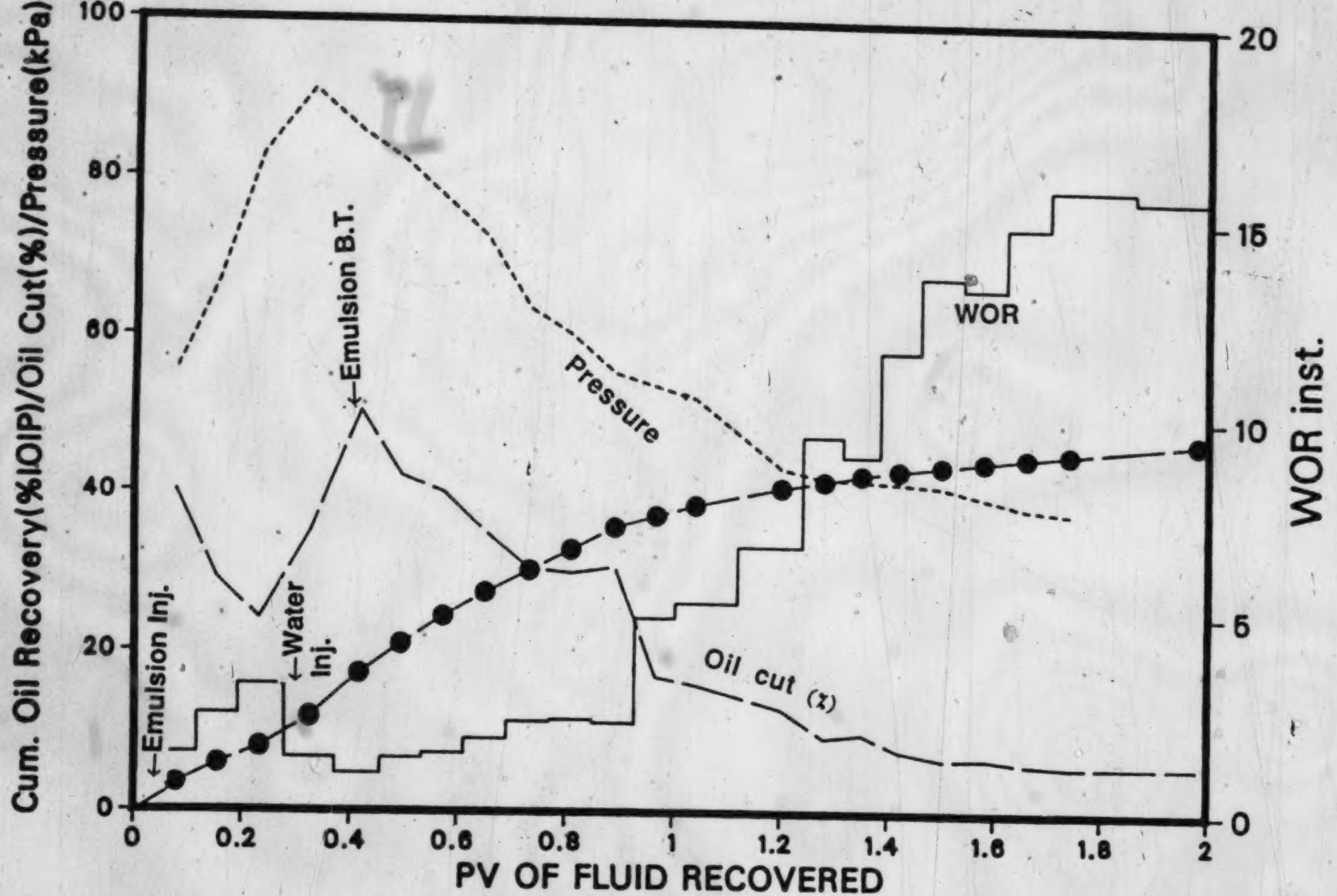

Fig. 43 Emulsion Flood and Waterflood Performance for Run 42 ($h_b/h_o=0.33$, $k_o/k_b=1.00$)

along with the WOR, oil cut, and cumulative oil recovery. As the injection pressure was increasing, the oil cut was decreasing during the early part of the displacement test. Even though the inlet pressure continued to increase until the end of the emulsion injection (0.32 PV), the oil cut started increasing shortly after 0.24 PV of emulsion was injected. A minimal in oil cut was also observed in Run 30 for which a larger emulsion slug was used. As a waterflood at 400 ml/h was started following the emulsion slug injection, the injection pressure started decreasing. This was expected because water has a lower viscosity than emulsion. Emulsion breakthrough took place shortly after water injection was started (at 0.45 PV). At this point, 18 percent of the oil in place was recovered. The cumulative WOR at the point of breakthrough was 1.76. This compares to a cumulative WOR of 1.51 that was obtained in Run 30. After emulsion breakthrough took place, the oil cut started dropping. As the waterflood following the emulsion flood continued the oil cut dropped below 10 percent and at a WOR value of 20, a total of 49.5 percent of the IOIP was recovered. This value is considerably lower than that observed in Run 30 (see Table 3.1 for comparison of ultimate recoveries).

Run 43: Emulsion Slug Size=0.93 PV(three PV of the water zone)

In order to examine the effect of a larger emulsion slug, Run 43 was conducted. The packing characteristics for this run were similar to those in Run 30 (see Table 5.1 for details). When emulsion injection was started, the injection pressure increased at the beginning of the run as the oil cut decreased. A peak in oil cut was observed at around 0.45 PV of emulsion injection. Shortly after this, the emulsion breakthrough took place. Figure 44 depicts the WOR, pressure, oil cut and cumulative oil production for this run. As can be seen from this figure, both the injection pressure and the oil cut started declining following emulsion breakthrough. At the time of breakthrough, 21.5 percent of the IOIP was already recovered. The cumulative WOR at this point was 1.6. This value is slightly higher than 1.51, which was observed in Run 30. This comparison shows that at least up to the breakthrough point, an increase in emulsion slug from 60 percent to 93 percent did not improve the flooding efficiency. Following emulsion breakthrough, the oil cut dropped continually even though the injected fluid was always emulsion unlike previous emulsion runs. The emulsion slug was followed by a waterflood at 400 ml/h. When the waterflood started, the injection pressure did not undergo a drop as did the injection pressure in Run 30. This is probably because of the fact that continous emulsion injection led to a total replacement of the bottom water and

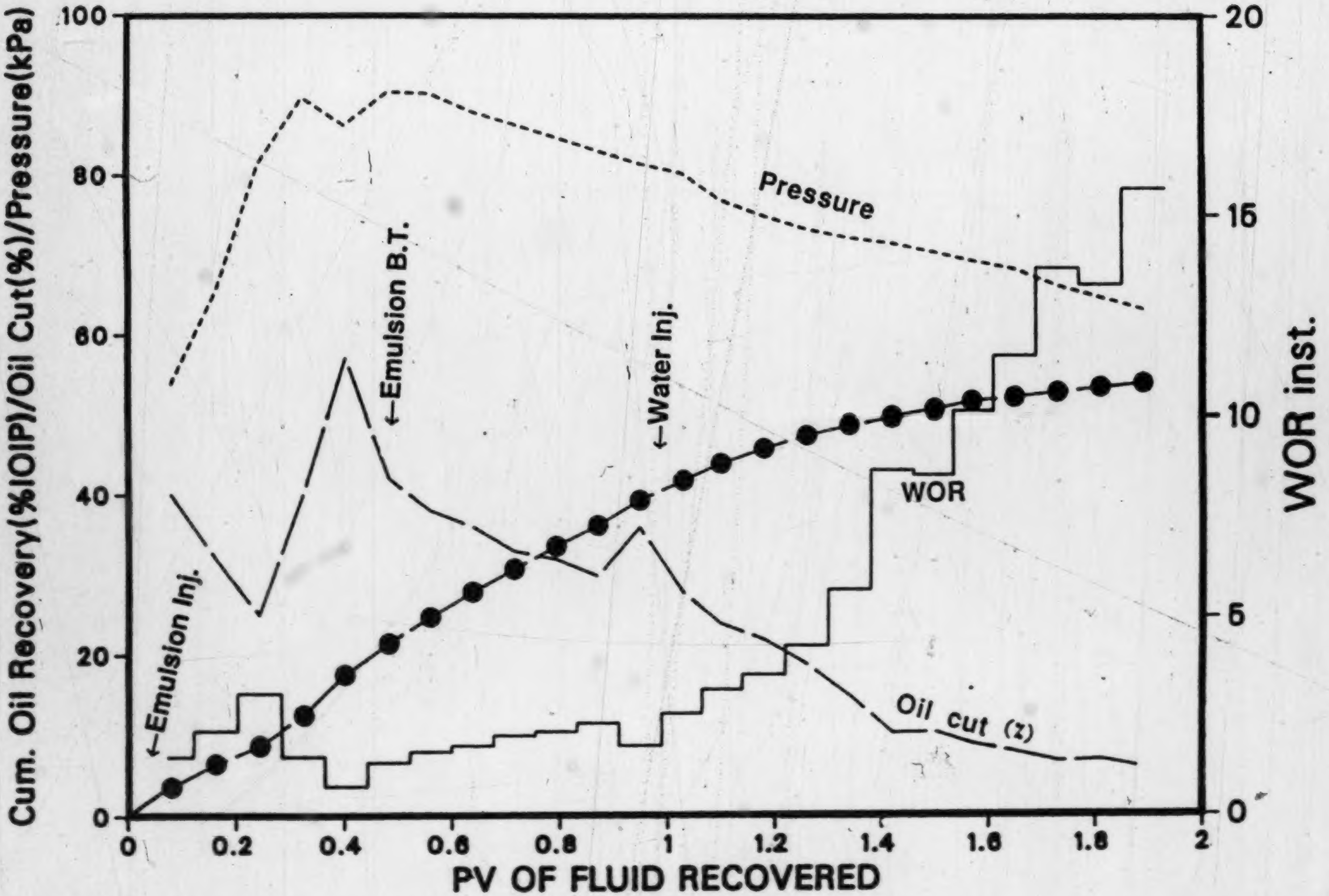

Fig. 44 Emulsion Flood and Waterflood Performance for Run 43 ($h_b/h_o=0.33$, $k_o/k_b=1.00$)

that injected water did not encounter a higher mobility zone (such as the bottom water). Even though the injection pressure was high for a waterflood, the oil cut decreased in the same manner as in previous emulsion flood runs. When the WOR increased to a value of 20, a total of 57.5 percent of the IOIP was recovered. This value is higher than that which was observed with other emulsion runs (with MCT-10 oil).

Run 44: Emulsion Slug Size= 0.16 PV (0.5 PV of the water zone)

In order to examine the effect of very small emulsion slugs, Run 44 was performed. Details of the packing characteristics are listed in Table 5.1. For this run, the displacement test was started with the injection of 0.16 PV of emulsion. As can be seen from Figure 45, the injection pressure increased during emulsion injection but as soon as the waterflood started the injection pressure decreased substantially. This showed that the blocking action by emulsion was not permanent. Also emulsion breakthrough occurred very early (0.36 pore volume) for this run. This is listed in Table 5.1. Such an early breakthrough indicated that the emulsion was diluted by both the connate and injected water. Also, only 8.3 percent of the IOIP was recovered at the time of emulsion breakthrough. As the waterflood continued, the oil cut decreased quickly. This

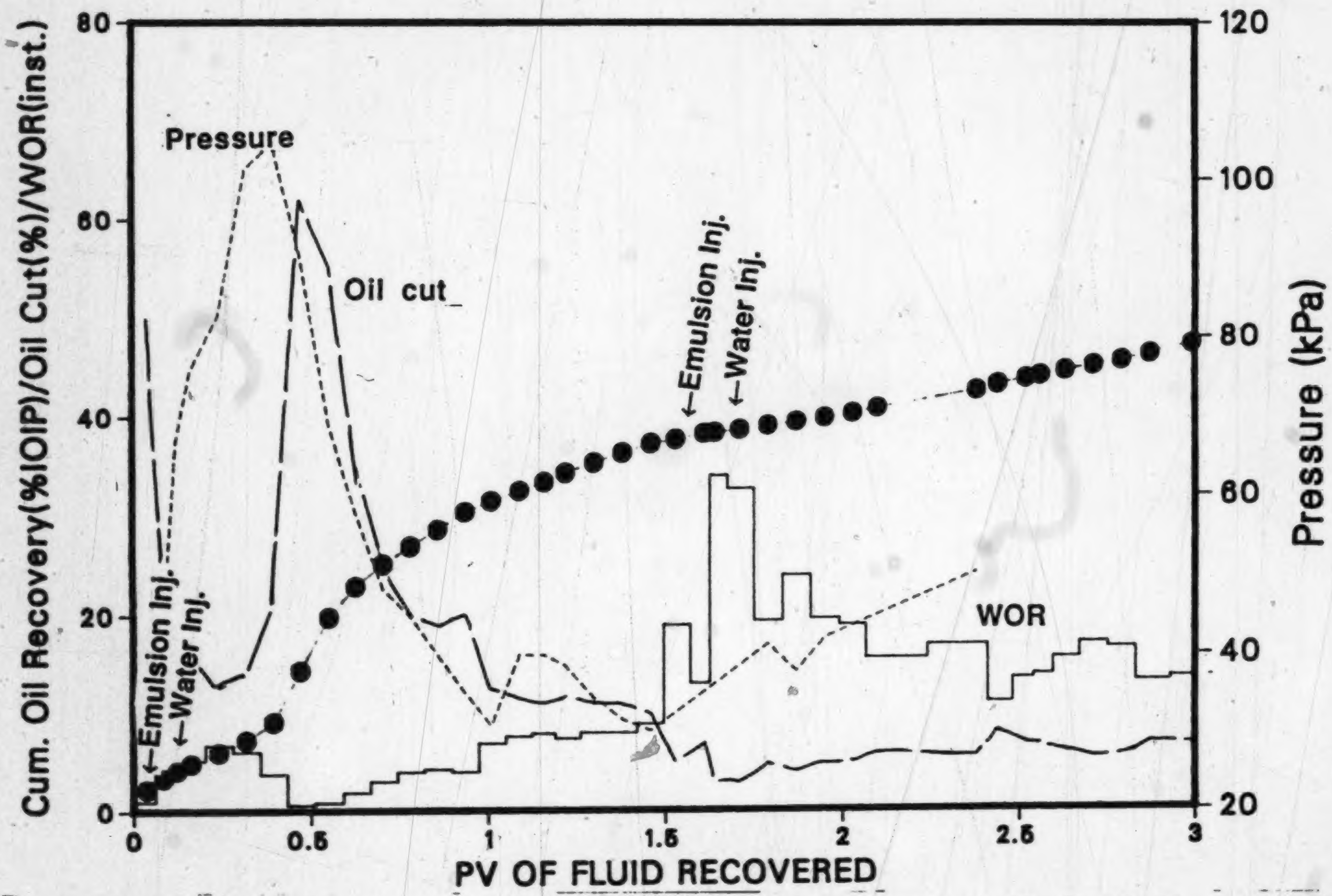

Fig. 45 Emulsion Flood and Waterflood Performance for Run 44 ($h_b/h_o=0.33$, $k_o/k_b=1.00$)

resulted in a very poor ultimate recovery of only 38 percent of the IOIP as the WOR reached a value of 20.

Run 45: Emulsion Slug size= 1.2 PV (Four pore volumes of the bottom-water zone)

In order to examine the effect of a very large emulsion slug size, Run 45 was conducted with an emulsion slug size of 1.2 pore volumes. Similar to previous runs, this run had an h_b/h_o=0.33 and k_o/k_b=1. During the initial stages of the displacement test, the injection pressure increased rapidly even though the oil cut decreased during the initial stages of the displacement test. However, as the emulsion injection continued the oil cut started increasing. Emulsion breakthrough took place at 0.46 pore volume of emulsion injection. A total volume of 1.2 pore volumes of emulsion was injected. Figure 46 depicts the WOR, pressure, oil cut and oil recovery performance for this run. Following the emulsion flood, a waterflood at 400 ml/hr was carried out. After an initial increase, the oil cut started decreasing continually. At the end of the displacement test a total of 57.5 percent of the IOIP was recovered when the WOR reached a value of 20. This value may be compared to that of Run 30, in which 54 percent of the IOIP was recovered with only 0.60 PV of emulsion injection. It appears that emulsion flood recovery attains a plateau and does not improve very much for higher emulsion slug volumes.

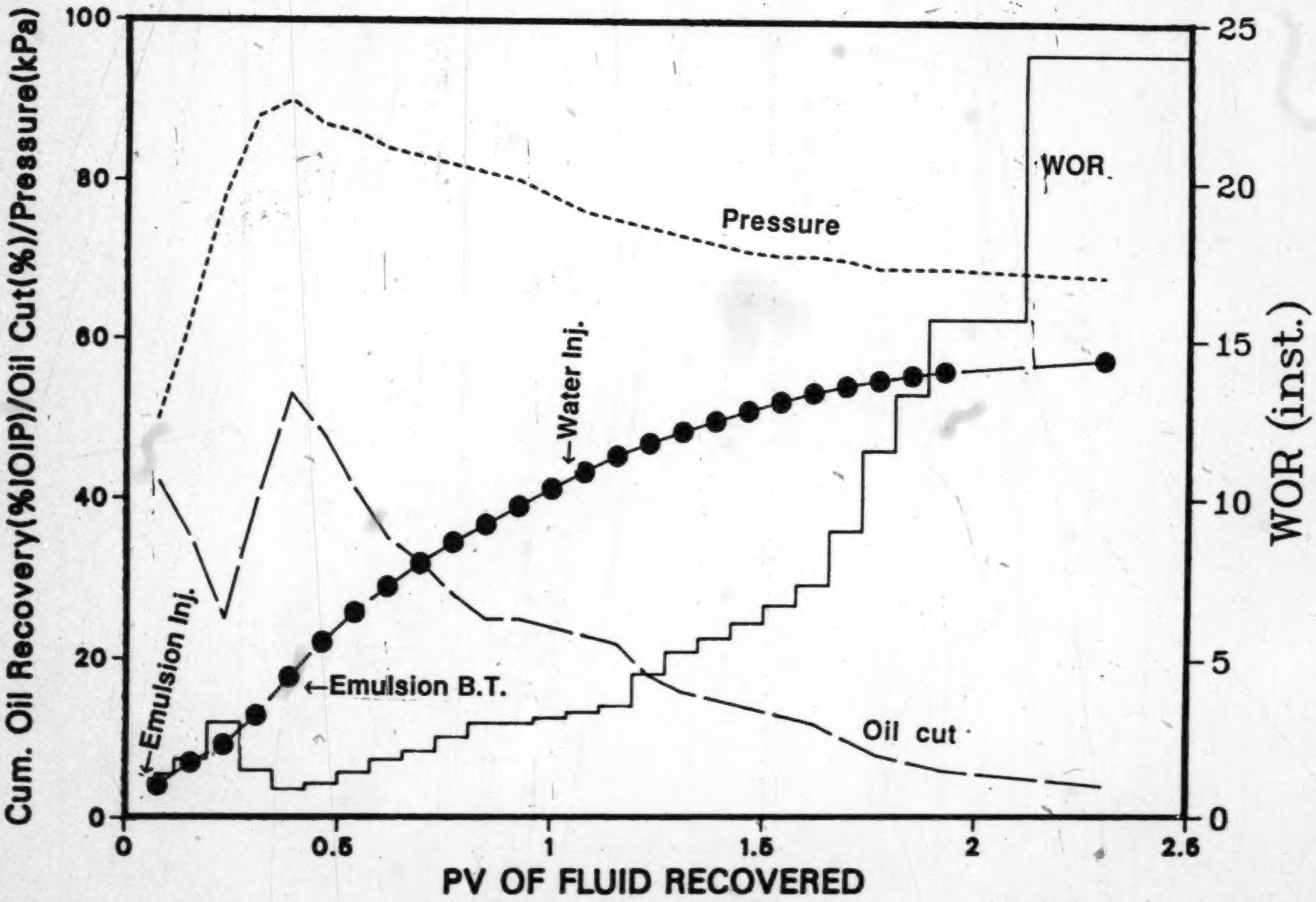

Fig. 46 Emulsion Flood and Waterflood Performance for Run 45 ($h_b/h_o=0.33$, $k_o/k_b=1.00$)

5.5.6 Mobility Control Mechanism with Emulsion Flood

Run 46: Effect of Glycerine Injection: $h_b/h_o=0.33$, $k_o/k_b=1$.

In order to examine the mechanisms involved in mobility control with emulsions, Run 46 was conducted using a glycerine slug. It has been noted that emulsion improves waterflood performance in the presence of a bottom-water zone due to

- its viscosity leading to a favourable mobility ratio
- its ability to create a blockage in the bottom-water zone rendering it less accessible to the water that follows the polymer.

The objective of Run 46 was to determine the quantitative contribution of each of the mechanisms involved in the mobility control with emulsions. With this objective in mind, a glycerine solution having a viscosity of 1.8 mPa.s was chosen for this run. Recall that the 10 percent oil-in-water emulsion had the same viscosity at six rpm. Therefore, a comparison of this run with Run 30, for which the same bottom-water zone thickness and permeability and flood rates were used, will determine the relative contribution of the above-mentioned mechanisms involved in emulsion flooding.

This run was started with injection of glycerine solution at a flow rate of 400 ml/hr. Figure 47 depicts the WOR, pressure, oil cut and oil recovery performance for this

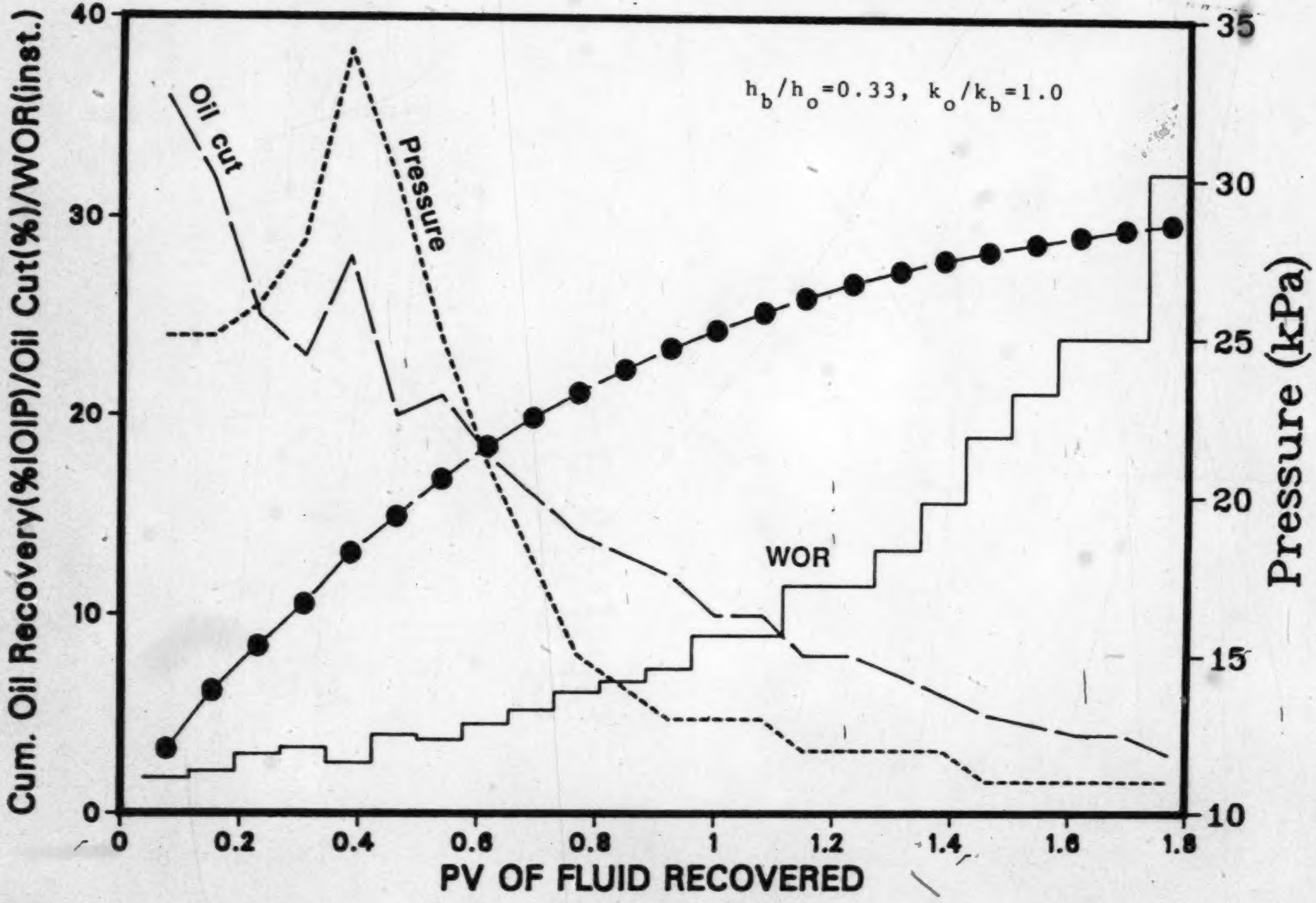

Fig. 47 Glycerine (1.8 mPa.s) Injection and Waterflood Performance for Run 46

run. As can be seen from this figure the recovery performance during the early stages is much poorer than that observed in Run 30. As opposed to the observation in Run 30, the oil cut increased for a very short period of time. Even though the injection pressures were very similar, oil recovery was much lower than that for Run 30. Glycerine solution injection was continued until 0.60 PV was injected and was followed by a waterflood, also at a flow rate of 400 ml/hr. At the end of the displacement test only 28 percent of the IOIP was recovered as compared to 54 percent of the IOIP recovered in Run 30. This run shows clearly that the effectiveness of emulsion in improving oil recovery in the presence of a bottom-water zone is not due to its viscosity alone.

5.6 Air Injection

Six different runs were carried out to examine the effect of air injection under different bottom-water zone thickness and permeability conditions. Also, the effect of air injection through the production well, rather than through the injection well, was investigated with one of the runs.

5.6.1 Effect of Water-to-Oil Zone Thickness and Permeability Ratio

Run 47: $h_b/h_o=0.33$, $k_o/k_b=1$

As can be seen from Table 5.1, the packing characteristics and well locations for this run were similar to those in Run 4. In this run, air was injected through the inlet end (rather than the injection well) in order to have an easier access to the bottom-water zone. A high flow rate was used for the air injection to assure that air is forced into the bottom water zone. However, constant pressure rather than constant flow rate was used for air injection. The volumes of water and oil produced were measured and the volume of air was not measured, as the main objective of this run was to observe qualitatively the effect of the presence of air. After recovering 0.046 PV of water and oil, air injection was followed by a waterflood. It was postulated that the air entered preferentially into the water zone. Due to the presence of air in the bottom-water zone, the effective permeability to water was supposed to decrease. This hypothesis was supported by the fact that the inlet pressure during the waterflood following the air slug increased. As the waterflood continued, the oil cut fluctuated between 12 and 20 percent. Eight percent of the oil in place was recovered after a total fluid recovery of 0.323 pore volume. At this point, another slug of air was injected through the inlet end. During air injection a total liquid volume equal to 0.038 pore volume was recovered. The oil cut, oil recovery, pressure and WOR are depicted in Figure 48. The second air slug was again followed by a waterflood. This time the oil cut increased slightly and assumed a stable value. The inlet pressure continued to increase. After injecting 0.4 PV of water, another air slug was injected. After recovering 50 ml of liquid, another waterflood was initiated. The inlet pressure continued to increase and the oil cut increased as well. Up to this point, the oil recovery was better than that obtained by a waterflood. This, along with the fact that the injection pressure increased every time a waterflood followed air injection, indicated that a resistance to water flow was building up. This resistance forced the injected water to invade the oil zone. However, more systematic study of the slug-size effect should be done before making further comments on the air injection mechanism. A fourth air slug was injected and it was followed by a waterflood. This time, however, the inlet pressure did not increase, nor did the oil cut. It appears that, as the waterflood front travelled farther, the air injected through the injection well did not have much impact on the direction taken by the flood front. At this time, it was decided to inject polymer solution to examine what effect the injection of polymer has on a reservoir containing three phases. A polymer slug of 0.164 PV was injected at 400 ml/h through the injection well. It was assumed that the polymer would eventually reach the

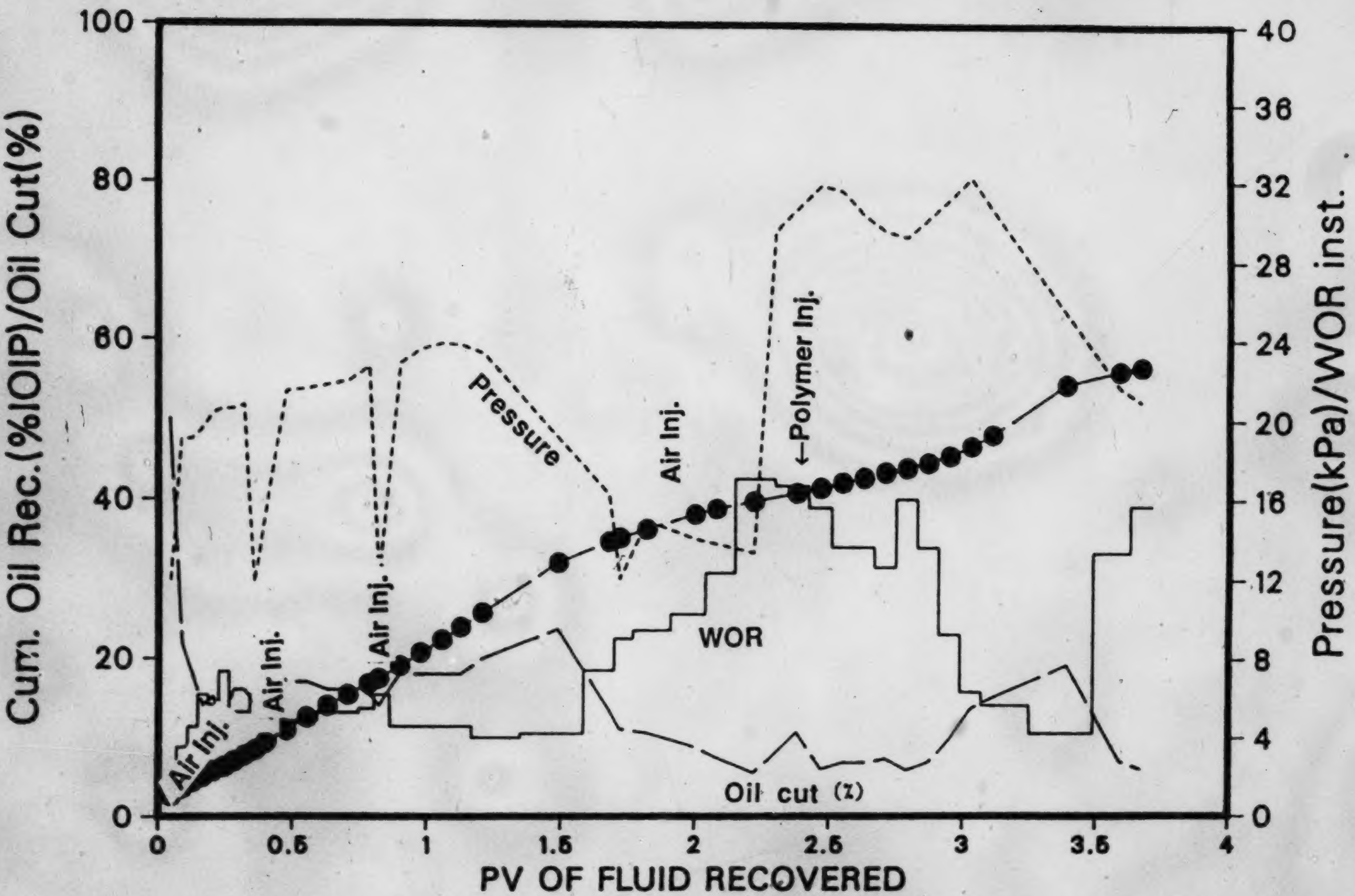

Fig. 48 Air Injection and Waterflood Performance for Run 47 (h_b/h_o=0.33, k_o/k_b=1.00)

bottom-water zone (due to least resistance to flow). When the polymer slug was driven by a waterflood, the inlet pressure remained higher than the previously attained value. During this period the oil cut remained steady, but when about 0.8 PV of water had been injected, the inlet pressure increased and the oil cut increased considerably. This delay in response by the oil cut after polymer slug injection was characteristic of previous polymer flood tests as well. But in this run, the increased oil cut value was not maintained for long before a rapid decrease took place. At the end, as the WOR reached a value of 20, a total of 64 percent of the IOIP was recovered. This recovery is not as high as that in Run 4. This inefficiency may be due to the possibility that polymer could not invade a water zone that contained air along with water. Also, the presence of air might decrease the quality of polymer that shows degradation due to oxidation.

Run 48: h_b/h_o=0.2, k_o/k_b=1

In order to examine the effect of the oil-to-water zone thickness ratio, Run 48 was conducted with an h_b/h_o of 0.2 and a k_o/k_b of 1. In this run, air was initially injected through the inlet end to have better access to the bottom-water zone. Air was injected at a constant pressure. After recovering 0.04 PV of total fluid, a waterflood was carried out through the injection well. Figure 49 depicts

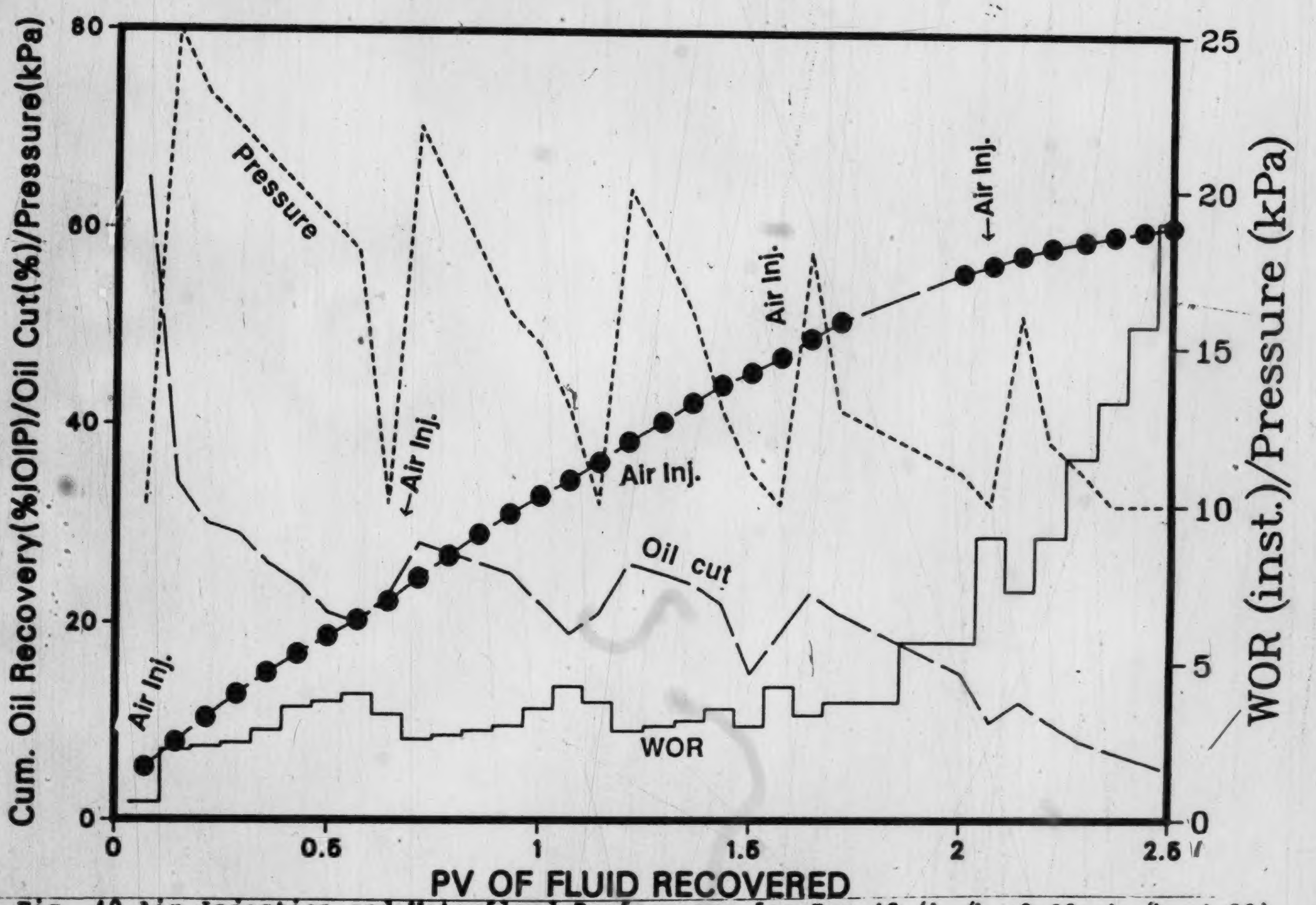

Fig. 49 Air Injection and Waterflood Performance for Run 48 (h_b/h_o=0.20, k_o/k_b=1.00)

the WOR, oil cut, pressure and oil recovery performance for this run. As was the case in the previous run, several other air slugs were alternated with water slugs. The oil recovery for this run was much better than that in Run 47. It appears that air slugs are more effective in the presence of a thinner bottom-water zone. At the end of the displacement test, a total of 61 percent of the IOIP was recovered. This value is close to the oil recovered by a waterflood in a homogeneous core and represents close to a two-fold improvement over a conventional waterflood in a reservoir with the same type of bottom-water zone.

Run 49: $h_b/h_o=1$, $k_o/k_b=1$

A 1:1 ratio for the oil-to-water-zone thickness ratio was used in this run. As can be seen from Table 5.1, the characteristics of this run are similar to those for Run 3. Consequently, one is able to compare the results for these runs to examine the relative [illegible]rit of air injection and a waterflood. It was seen in Run 3 that during water injection water went into the bottom-water zone due to the high mobility in that zone. It was assumed, therefore, that during air injection air would also go into the bottom-water zone to create blockage for the waterflood that was to follow the air slug. The air was initially injected at a constant pressure of 10.3 kPa. The air injection was stopped when 0.116 PV of liquid had been recovered. This was followed by a waterflood at 400 ml/h. During this period the oil cut decreased rapidly but still retained a value much higher than that obtained during a waterflood (Run 3). Another air slug was injected and it was noticed that the oil cut increased during air injection (see Figure 50). However, when the waterflood followed air injection, the oil cut dropped again. A similar performance was evidenced when one more air slug was injected. After a total recovery of 2.1 PV of fluid, 16.6 percent of the IOIP was recovered. This compares to 7.8 percent of the IOIP at a similar point in Run 3. However, this performance is quite poor when compared to that of Run 51 which had a thinner and tighter bottom-water zone, and which recovered 55 percent of the IOIP. It is also poor compared to that of Run 47 which had a thinner bottom-water zone, and which recovered 39 percent of the IOIP after a total recovery of 2.1 PV. On the whole, air injection is most effective in the small and tight bottom-water zone case. However, before making any conclusive remark, one should study further the effects of flow rate and volume of air slugs.

Run 50: $h_b/h_o=1$, $k_o/k_b=2.67$

In order to examine further the effects of the oil-to-water zone thickness ratio for an oil-to-water zone permeability ratio of 2.67, Run 50 was conducted with an h_b/h_o of 1. Figure 51 depicts the WOR, oil cut, pressure

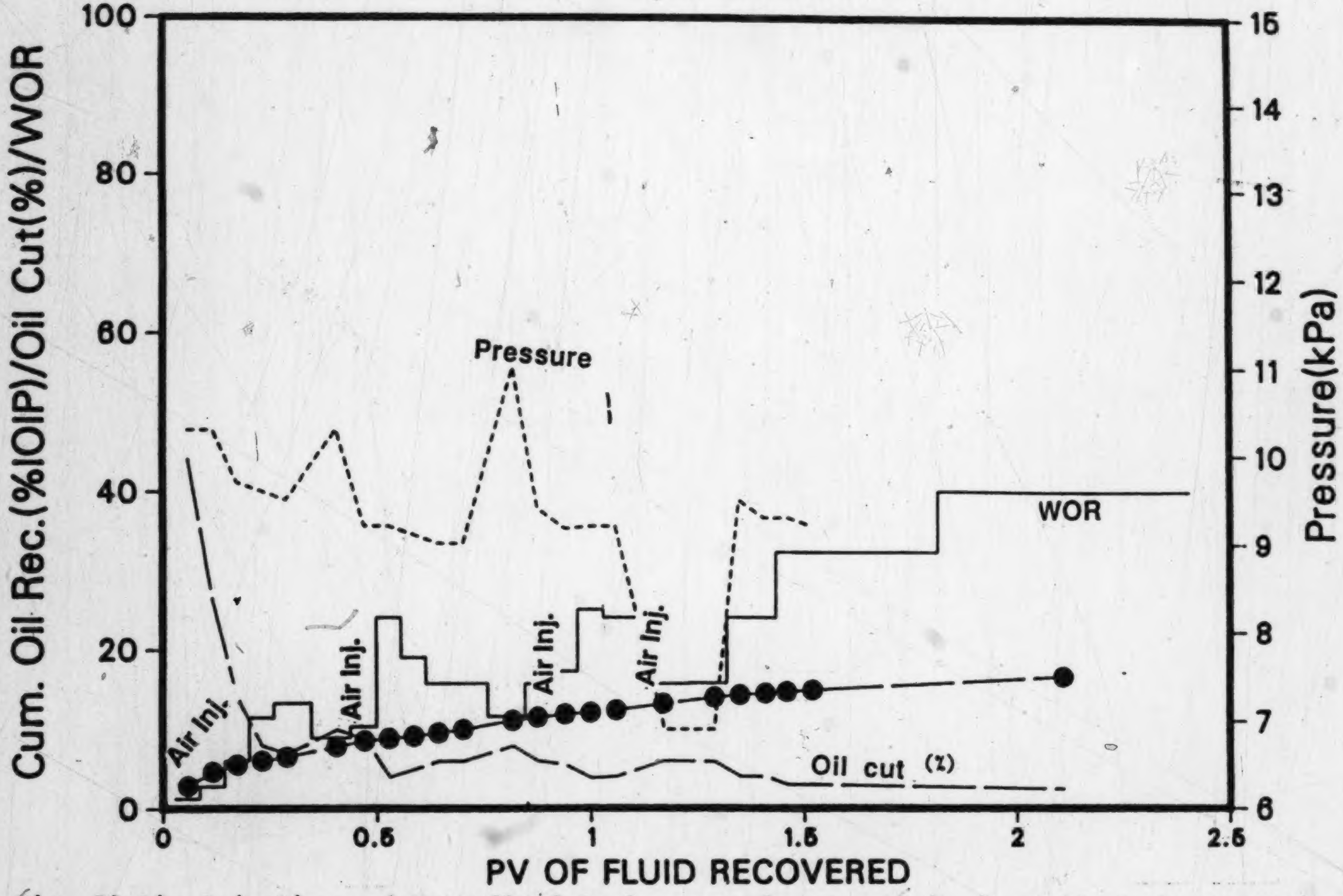

Fig. 50 Air Injection and Waterflood Performance for Run 49 (h_b/h_o=1.00, k_o/k_b=1.00)

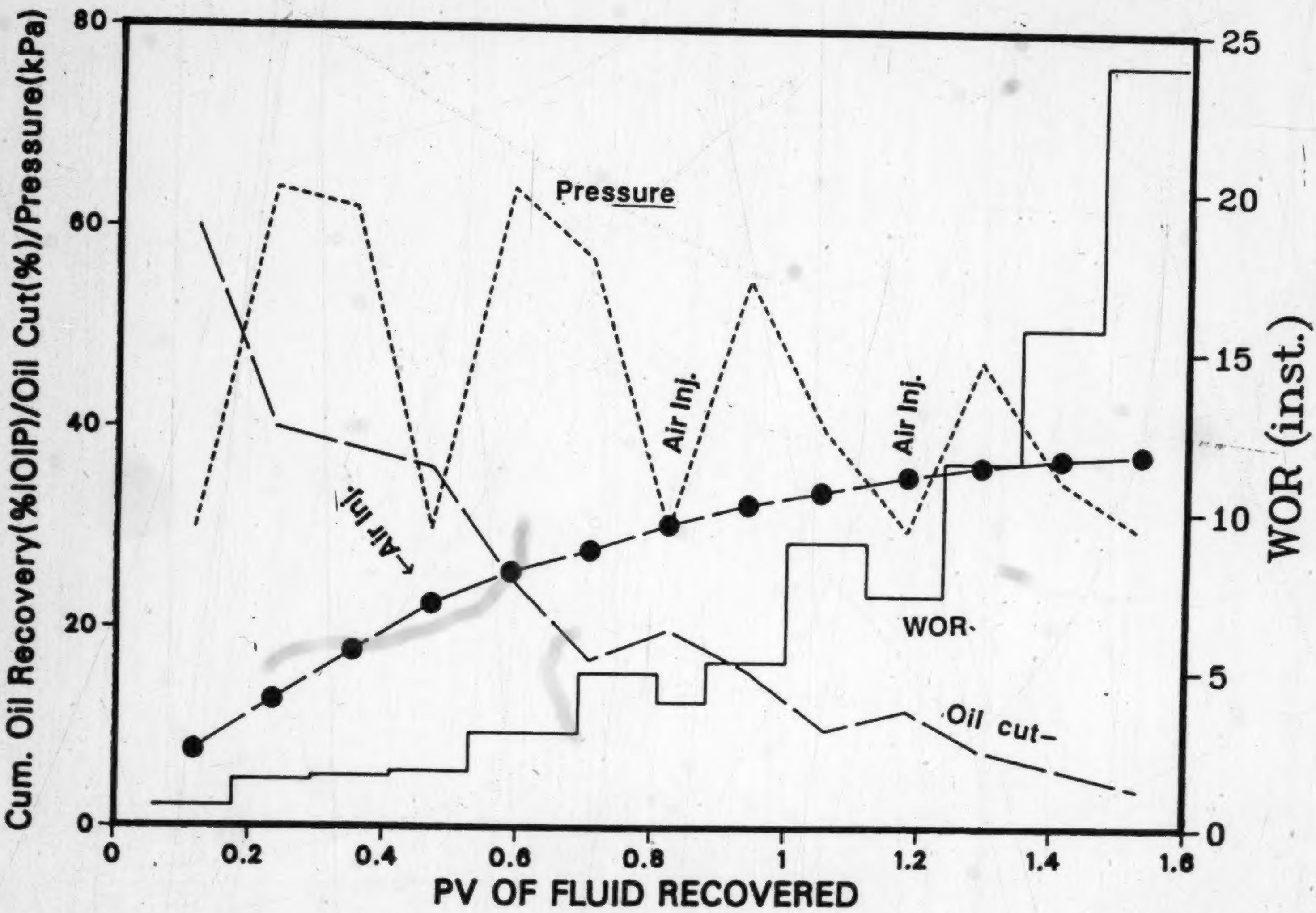

Fig. 5.1 Air Injection and Waterflood Performance for Run 50 (h_b/h_o=1.00, k_o/k_b=2.67)

and oil recovery performance of this run. As was the case with other air injection runs, the displacement test was started with air injection at a constant pressure. After collecting 0.116 pore volume of total liquid, the air slug was followed by a waterflood. As can be seen from Figure 51, the oil recovery for this run was much better than that in Run 49. This shows that air injection is much more effective in the presence of a tight bottom-water zone. At the end of the displacement test, a total of 37 percent of the IOIP was recovered for this run under similar injection conditions those used in Run 49. This shows approximately a 50 percent improvement over a conventional waterflood. This value is still much smaller than that observed for thinner bottom-water zones. It appears that the air injection loses its effectiveness as the bottom-water zone thickness increases.

Run 51: $h_b/h_o=0.33$, $k_o/k_b=2.67$

In order to test the effect of air injection for a tight bottom-water zone, Run 51 was conducted. The oil-to-water zone thickness ratio for this run was 3:1. Other characteristics of this run may be found in Table 5.1. This run had the same characteristics as those of Run 6. Initially air was injected at a constant pressure of 24 kPa. The inlet end was used to inject the air. After recovering 0.039 PV of liquid, air injection was stopped. This was followed by a waterflood at 400 ml/h. Unlike the previous case (Run 47), the injection pressure decreased slowly. But the oil cut was high and the recovery curve was distinctly better than that obtained in Run 6 with a waterflood. Another air slug was injected at 0.32 PV of total liquid recovery. This slug was injected at a constant pressure of 28 kPa and was terminated after producing 53 ml (0.041 PV) of liquid. This was followed by a waterflood at 400 ml/h. Once again, the pressure dropped quickly as the waterflood continued. Even though the oil cut continued to be reasonably high, the decrease in pressure indicated that water was going into the bottom-water zone, at least partly. However, as the pore volume of liquid produced reached 0.6, the oil cut suddenly dropped from around 50 percent to around 25 percent. This can be seen from Figure 52. A total volume of 36 percent of the IOIP was produced by this time. This sudden decrease, most likely, corresponded to breakthrough of the injected water. A similarly sudden decrease in oil cut was evidenced also in Run 6 at around 0.6 PV injected. As it appeared that not much of the air injected actually went into the bottom water zone (as manifested by a low injection pressure in the waterflood phase), it was decided to inject a larger air slug at a much higher pressure. During this air slug injection, 180 ml (0.159 PV) of liquid were produced. During the waterflood following the air injection, the injection pressure was

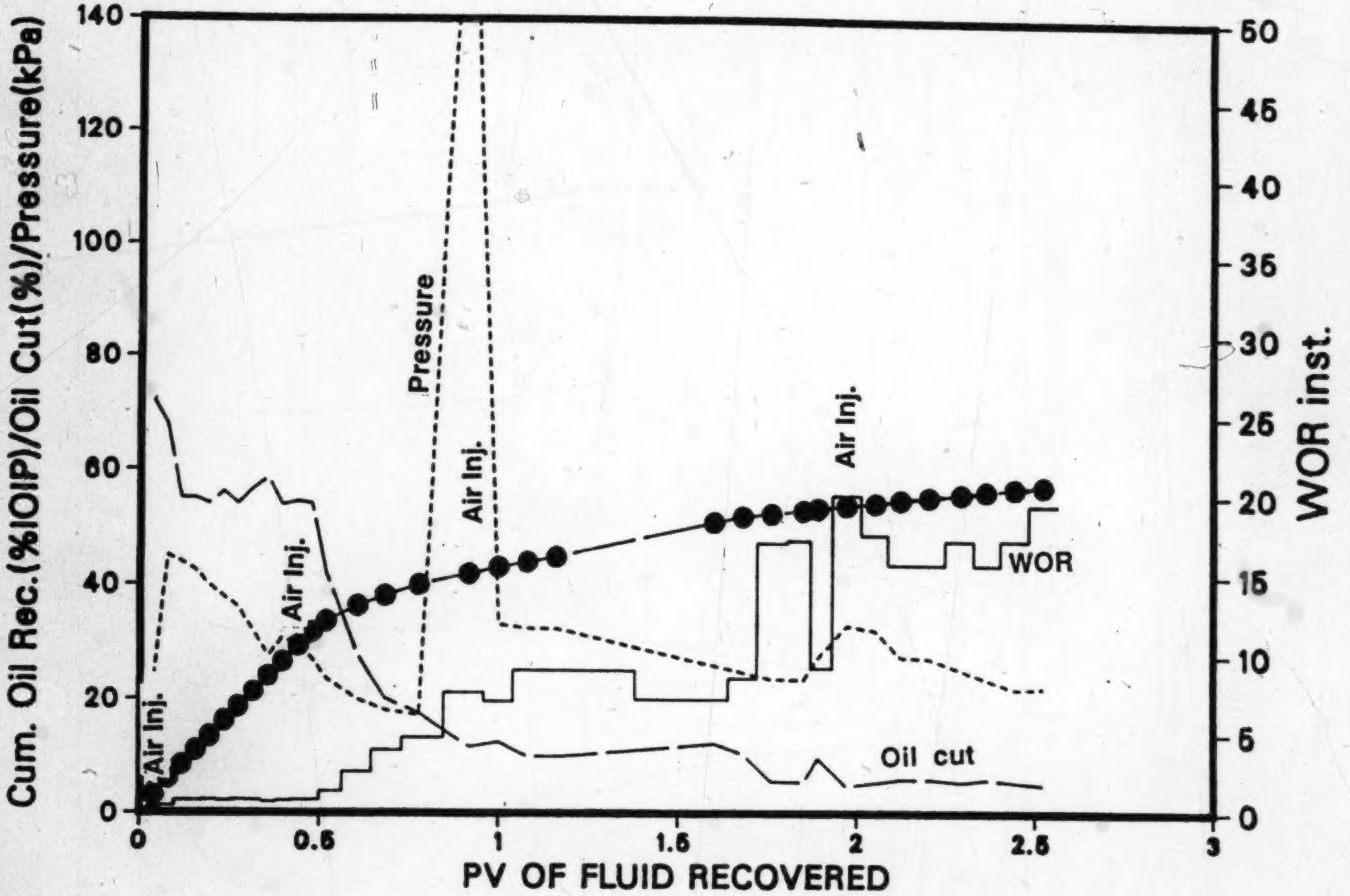

Fig. 52 Air Injection and Waterflood Performance for Run 51 (h_b/h_o=0.33, k_o/k_b=2.67)

quite high but it started to decline as the waterflood continued. The oil recovery remained steady for a while and then dropped to about six percent. At this time, another air slug was injected until 0.04 PV of liquid was recovered. When the air slug was followed by a waterflood, the injection pressure increased but the oil cut slowly decreased. The waterflood was stopped when the WOR reached a value of 20. A total of 58 percent of the IOIP was produced at this point. This value is comparable to that obtained with an emulsion flood but lower than that with polymer flood.

On the whole, the recovery by air injection alternating with waterflood appears to be more effective in the tighter bottom-water case. In this run the oil recovery was better than that obtained by a waterflood throughout the run. Even though the injection pressure did not increase in the same way as it did in Run 47, the high oil cuts suggest that the injected water encountered substantial blockage while moving into the water zone. However, air injection seems to be less effective during the later stages of the run. This might be due to the fact that as the waterflood front moves away from the injection well, it becomes more and more difficult to direct it away from the bottom-water zone.

Run 52: $h_b/h_o = 0.33$, $k_o/k_b = 2.67$ Air injection through production well

In order to examine the effect of the air injection point, Run 52 was performed. All characteristics of this run were similar to those of Run 51 except that air was injected through the production well. During this period, the injection well was used for fluid production. Figure 53 depicts the WOR, pressure, oil cut and cumulative oil recovery performance of this run. For this run each of the air slugs was injected until 0.04 PV of fluid was produced. Even though the recovery performances are very similar in the beginning of the displacement test, as the run continues Run 52 shows consistently better oil recovery than that of Run 51. Such injection through a production well was only performed for a tight and thin bottom-water zone since the efficiency by air injection appeared to be best for this type of bottom-water zone. The ultimate recovery (at WOR=20) for this run was 59 percent IOIP as compared to 58 percent of the IOIP in Run 51.

Run 53: $h_b/h_o=0.2$, $k_o/k_b=2.67$

In order to examine further effects of the oil-to-water zone thickness ratio for a $k_o/k_b=2.67$, Run 53 was conducted with an oil-to-water zone thickness ratio of 5. This run represented the most favourable conditions for air injection as the bottom-water zone was tight as well as thin. In this run, air was initially injected through the inlet end to have better access to the bottom-water zone. Air was

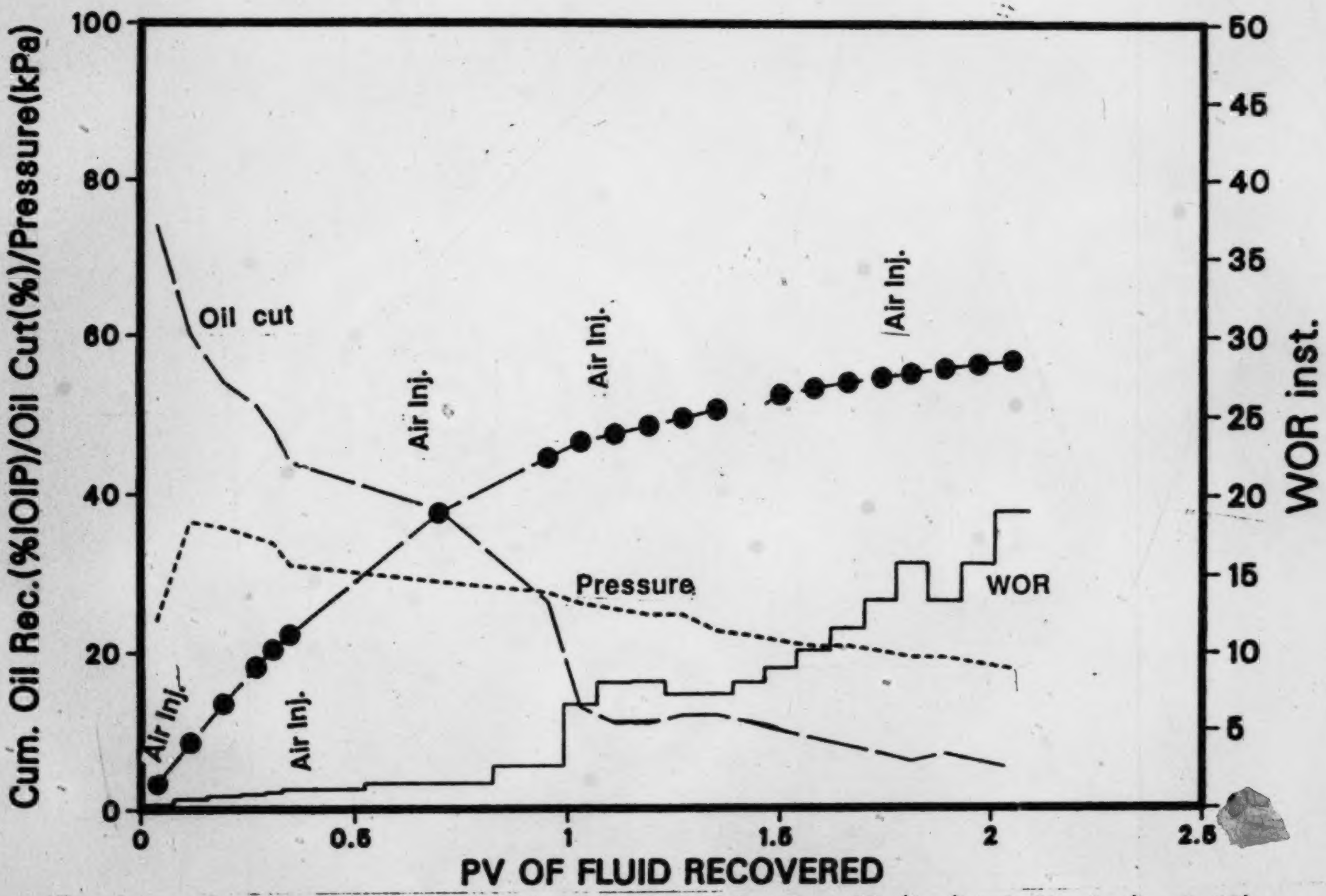

Fig. 53 Air Injection and Waterflood Performance for Run 52 (h_b/h_o=0.33, k_o/k_b=2.67)

injected at a constant pressure. After recovering 0.04 pore volume of fluid, a waterflood was carried out through the injection well. Figure 54 depicts the WOR, oil cut, pressure and oil recovery performance for this run. As was the case with previous air injection runs, several other air slugs were alternated with water slugs. The oil recovery for this run was much better than that of Run 51 or 52. At the end of the displacement test, a total of 64 percent of the IOIP was recovered. This value is higher than the oil recovery by a waterflood in a homogeneous core and represents more than 50 percent improvement over a conventional waterflood in a reservoir with the same type of bottom-water zone.

5.7 Biopolymer Gel Injection

Run 54: Gel (Biopolymer+cross-linking) Injection: $h_b/h_o=1$, $k_o/k_b=1$

A biopolymer with cross-linking forms a stable and shear-resistant gel. It was decided to produce the gel outside the core. It was considered that by producing gel externally the gel formation could be monitored better. For this run, the oil-to-water zone thickness ratio was one, and both zones had the same absolute permeability. These characteristics are summarized in Table 5.1. The results of this run can be compared to those of Run 3 as they had similar packing characteristics. Initially, the gel was

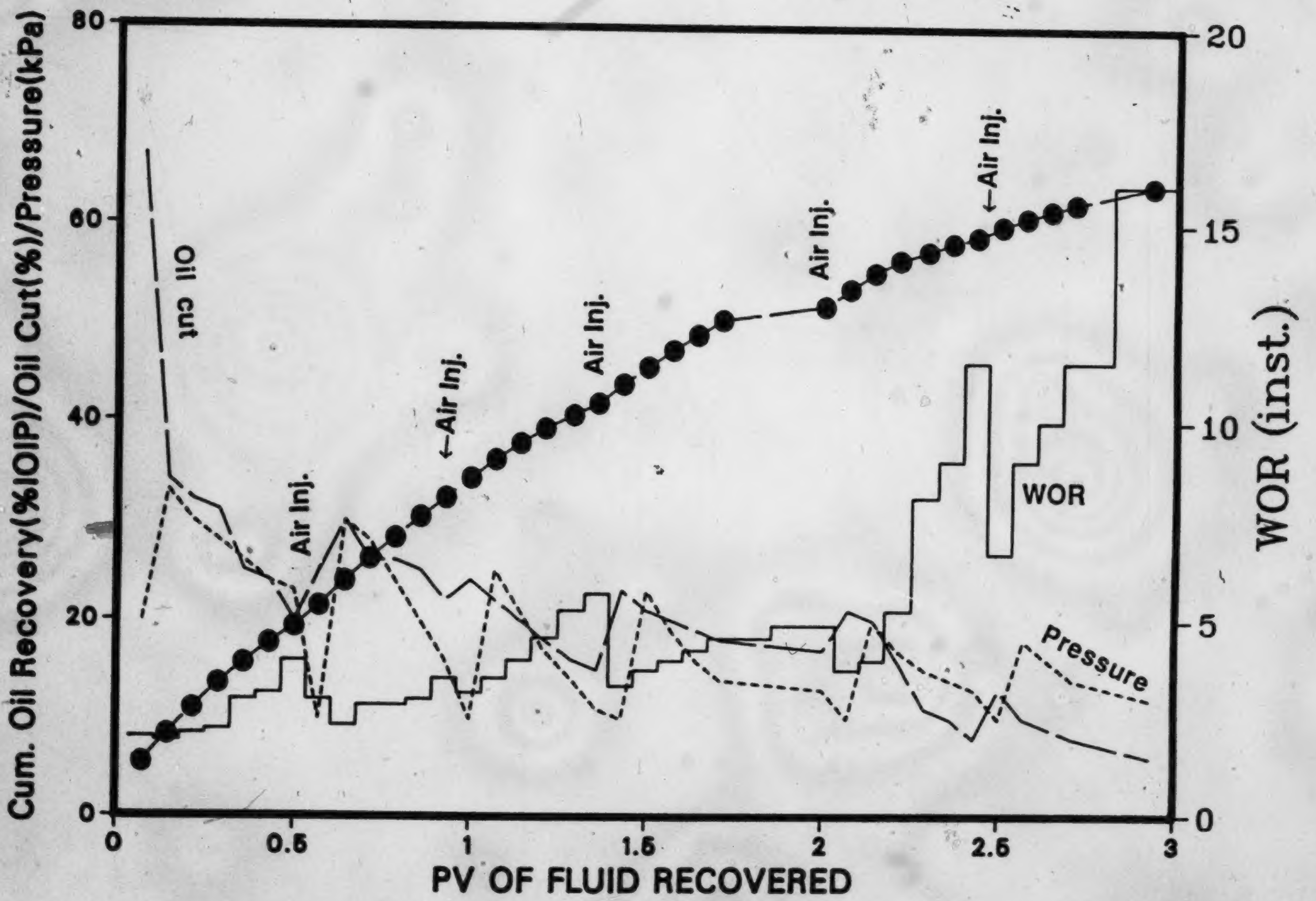

Fig. 54 Air Injection and Waterflood Performance for Run 53 (h_b/h_o=0.20, k_o/k_b=2.67)

prepared from 2000 ppm FLOCON 4800 cross-linked with Cr^{+3} at a proportion of 1:20. The gel was injected at a flow rate of 200 ml/h through the injection well. This flow rate required a very high injection pressure. But the oil cut was also quite high when compared to that for a waterflood (Run 3). After injecting 0.39 PV of gel, a waterflood was started at 400 ml/h. As soon as the waterflood started, the oil cut decreased rapidly and dropped below five percent as 0.425 PV of water was injected. By this time 10.5 percent of the IOIP had been recovered. This compares with 4.8 percent of the IOIP produced at the same WOR with a waterflood (Run 3). At this point of the waterflood, it was decided to inject gel at the outlet end of the core with a view to decreasing the WOR. Consequently, 0.384 PV of gel was injected through the outlet end. During this period, as production was allowed through the injection well, 100 percent water was produced. After injecting gel at the production end, a waterflood was carried out after waiting for two hours. This delay was allowed to permit the gel to restore its original form after suffering shear thinning due to the high injection rate. When the waterflood started at 400 ml/h, the oil cut retained its low value, even though the injection pressure was very high. This can be seen from Figure 55. The oil recovery performance was still much better than that for a waterflood but it was considerably poorer than that for an emulsion or polymer flood. In order

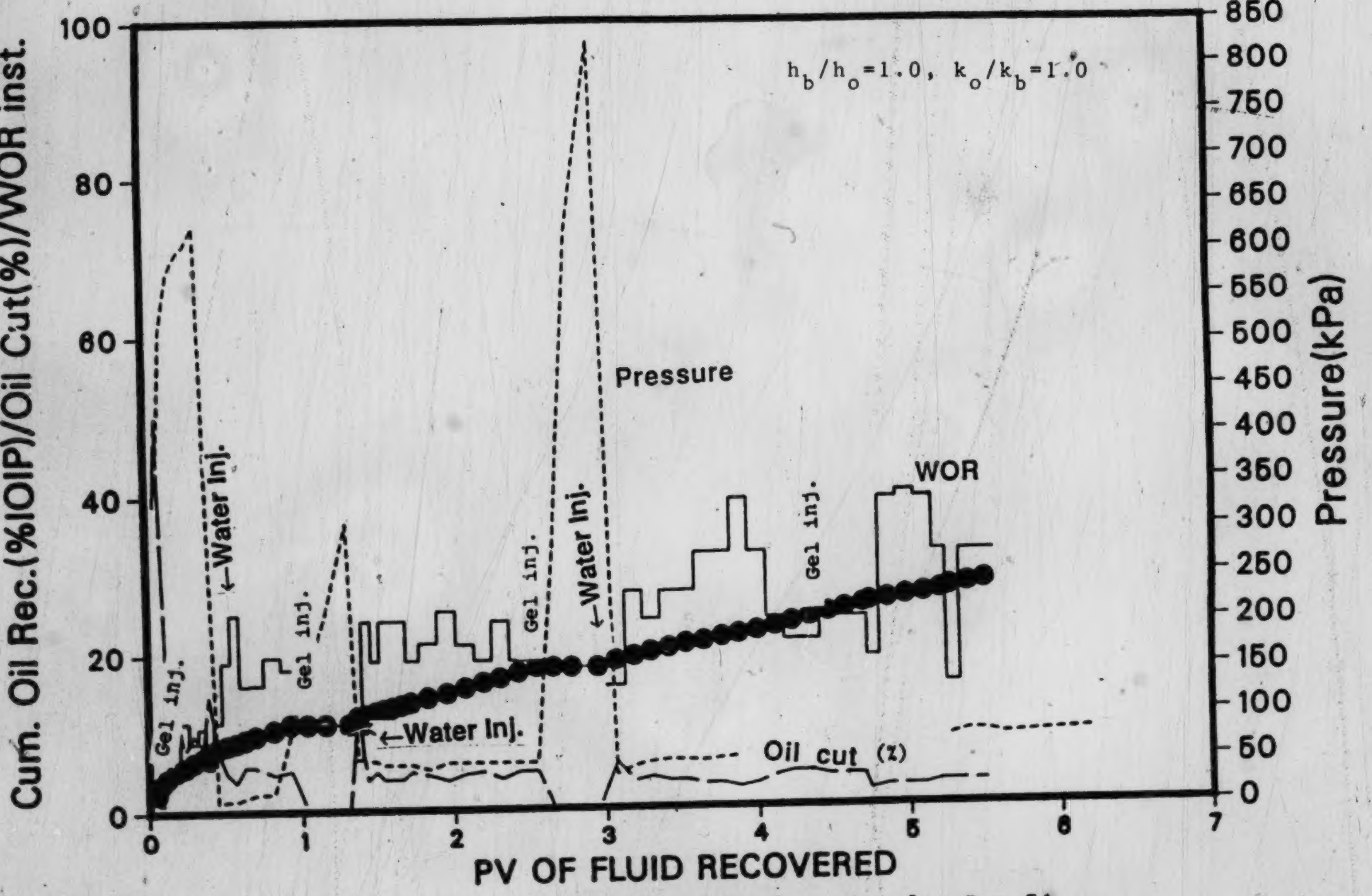

Fig. 55 Biopolymer Gel Injection and Waterflood Performance for Run 54

to improve the oil cut, several more gel slugs were injected separately, or simultaneously with water, but the recovery did not improve. Finally, 4000 ppm FLOCON 4800 gel was injected in liquid form to obtain better injectivity and then it was allowed to gel _in situ_. When the waterflood followed the gel injection, the injection pressure increased considerably but no improvement in oil cut took place.

The gel injection did not perform as expected. It is likely that the gel invaded the water zone but when the waterflood followed, shear thinning of the gel occurred due to the high rate of water injection. Consequently, the blockage created by the gel was nullified. No permanent reduction in effective permeability to water took place (as was observed after a polymer flood in previous runs). Each time a slug of gel was injected, it resulted in increased injection pressure. This would correspond to a decrease in both oil and water production for a constant pressure injection case. At the end of the run, the core pack was opened and it was found that the gel created a solid barrier over a distance only about one fourth of the total length. Recall that it was observed in Run 25 that a perfect barrier of such a length did not have very much impact on oil recovery by a waterflood. Therefore, for subsequent runs it was decided to inject a larger volume of gel.

Run 55: $h_b/h_o=0.33$, $k_o/k_b=1$

In order to examine the effect of a thinner bottom-water zone on gel injection, Run 55 was performed. As the gel formed outside could not go a long way along the length of the core (as seen in Run 54), it was decided to inject the biopolymer along with a cross-linking product before gelation occurred. This required a long gelation time. The biopolymer and cross-linking product were properly mixed and immediately injected through the inlet end at a flow rate of 200 ml/h. As can be seen from Figure 56, the injection pressure was low with the liquid form of the gel. The oil recovery was quite comparable to that for a waterflood (Run 4). An immediate increase in oil cut was not expected, anyway, as it would take some time to block the entire water zone. The gel injection was continued until 0.319 PV of gel (this was equivalent to one pore volume of the bottom-water zone) was injected. During this time 68.5 percent of the total water in place (including bottom-water zone) was produced. It was expected, therefore, that the waterflood following gel injection would have a high oil cut. A waterflood was started after a delay of 12 hours. This time was thought to be sufficient for the gelation to occur. The waterflood was carried out at 200 ml/h. This lower flow rate was used because the injection pressure was very high for higher flow rates. When the waterflood continued, the oil cut was high as compared to the base waterflood but was still much lower than that which

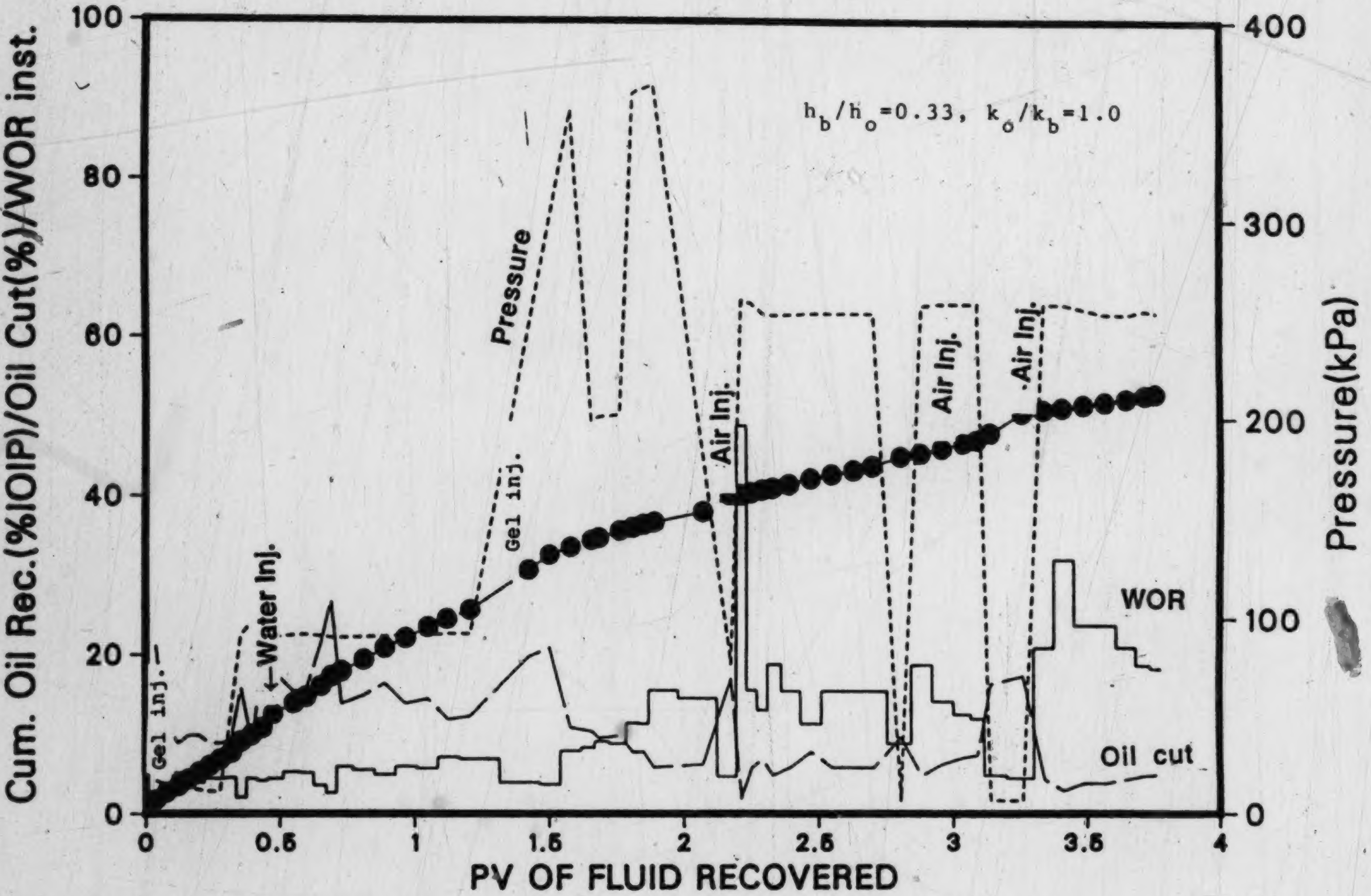

Fig. 56 Biopolymer Gel Injection and Waterflood Performance for Run 55

was observed with polymer or emulsion injection. The oil cut fluctuated from 12 to 27 percent. After injecting about 0.9 PV of water, another slug of gel was injected at 200 ml/h. This slug had a size of 0.22 PV. During the liquid biopolymer injection the oil cut increased from 12 to 20 percent. The waterflood was started after waiting for 12 hours. As before, the oil cut was high at the beginning of the waterflood but dropped quickly as the waterflood continued. After injecting 2.7 PV of total fluid, 43.9 percent of the IOIP was recovered. This value is considerably smaller than that obtained by a polymer or emulsion flood. However, the the oil recovery performance in this run was much better than that in Run 54 in which a thicker bottom-water zone was used. The injection of liquid biopolymer with gelation *in situ* holds some promise, but it must be recalled here that the injection pressure was very high and this might cause serious injectivity problems.

5.8 Foam Injection Runs

Runs 56 through 64 were conducted with a homogeneous core in order to investigate the effect of surfactant concentration and injection pressure for nitrogen. The characteristics of these runs are listed in Tables 5.1 and 5.4. For these runs only foam breakthrough and ultimate oil recovery (at gas-liquid ratio, GLR=7000) was measured. The

TABLE 5.4: Results of Foam Injection Runs

Run no.	Foam bt (PV)	Surf. Conc.	IOIP (ml)
56	0.04	0.01	1512
57	0.07	0.10	1527
58	0.24	1.00	1520
59	0.45	2.00	1510
60	0.44	5.00	1520
61	0.05	10.0	1525
62	0.01	0.00	1515
63	0.40	2.00	1520
64	0.30	2.00	1520
65	0.32	1.00	1125
66	0.40	4.00	1120
67	0.33	10.0	1115
68	0.46	4.00	980
69	0.47	"	1110
70	0.36	"	1115
71	0.35	"	1110
72	0.34	"	1200
73	0.81	"	745
74	0.82	"	745
75	0.24	"	750
76	0.37	10	1120

results are presented in detail in the following chapter and will not be discussed here. Several other runs were conducted in order to examine the efficiency of foam as a blocking agent in the presence of a bottom-water zone. Runs 65 through 67 were conducted with h_b/h_o=0.33 and k_o/k_b=1. However, surfactant concentrations of 1, 4, and 10 percent were used in Runs 65, 66, and 67, respectively. Figures 57 through 59 depict the WOR, pressure, oil cut and oil recovery performance in Runs 65, 66, and 70, respectively. These runs showed the existence of an optimal surfactant concentration. The comparison and discussion of these results are presented in the next chapter. Also, the oil-to-water zone thickness and permeability ratios were varied for different runs. In one run, foam injection was alternated with a waterflood to observe what effect, if any, the waterflood had on foam injection performance.

Run 66: Foam Injection, h_b/h_o=0.33, k_o/k_b=1.0

In order to examine the role of foam as a mobility control agent, Run 66 was conducted with a bottom-water zone of h_b/h_o=0.33 and k_o/k_b=1. For this run, surfactant water was alternated with nitrogen. At the beginning of the displacement test, 0.26 PV of surfactant water (four percent surfactant in water) was injected. During this time the oil cut was similar to that observed with a waterflood. This showed that the use of surfactant water resulted in no

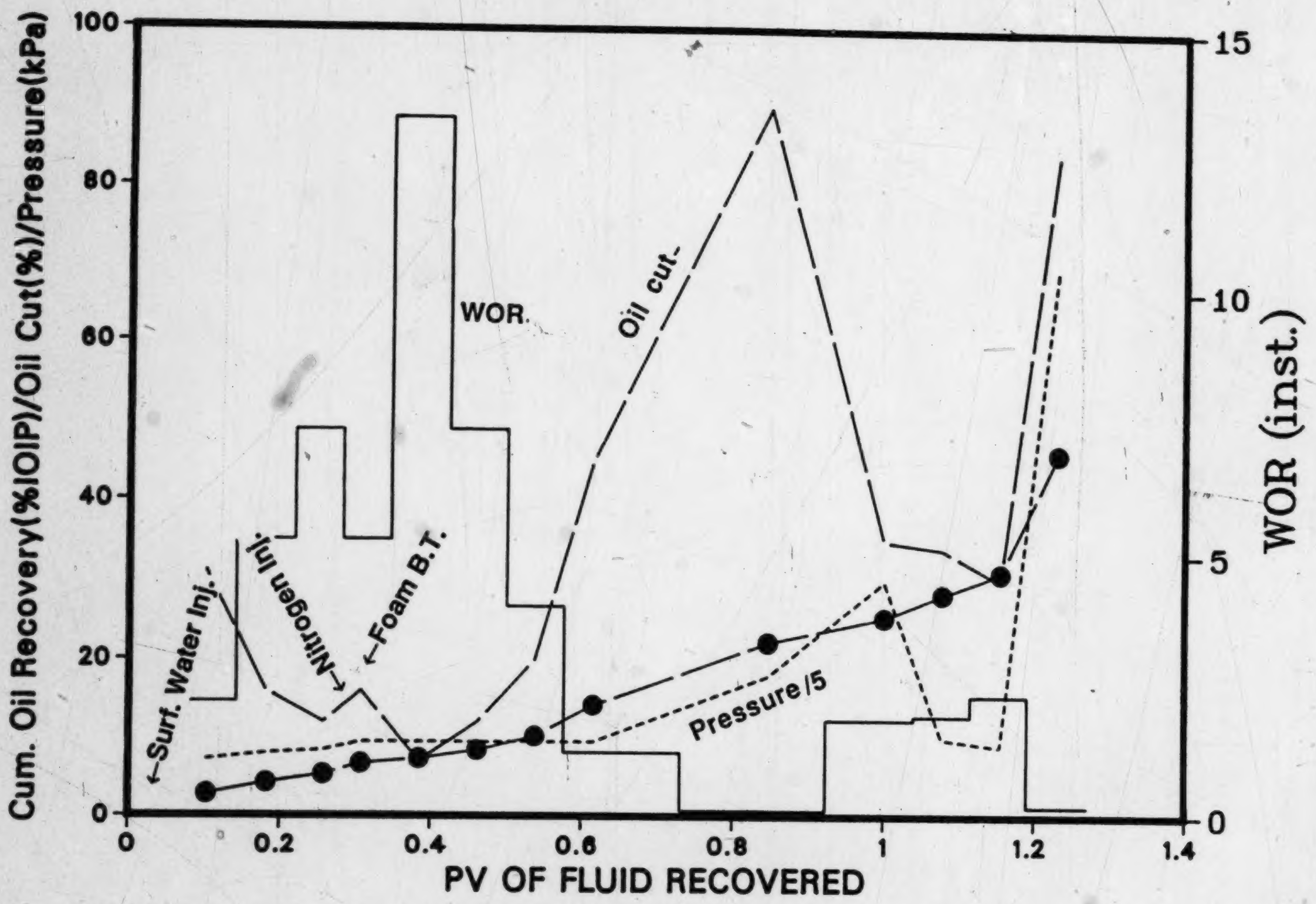

Fig. 57 Foam Injection Performance for Run 65 ($h_b/h_o=0.33$, $k_o/k_b=1.00$)

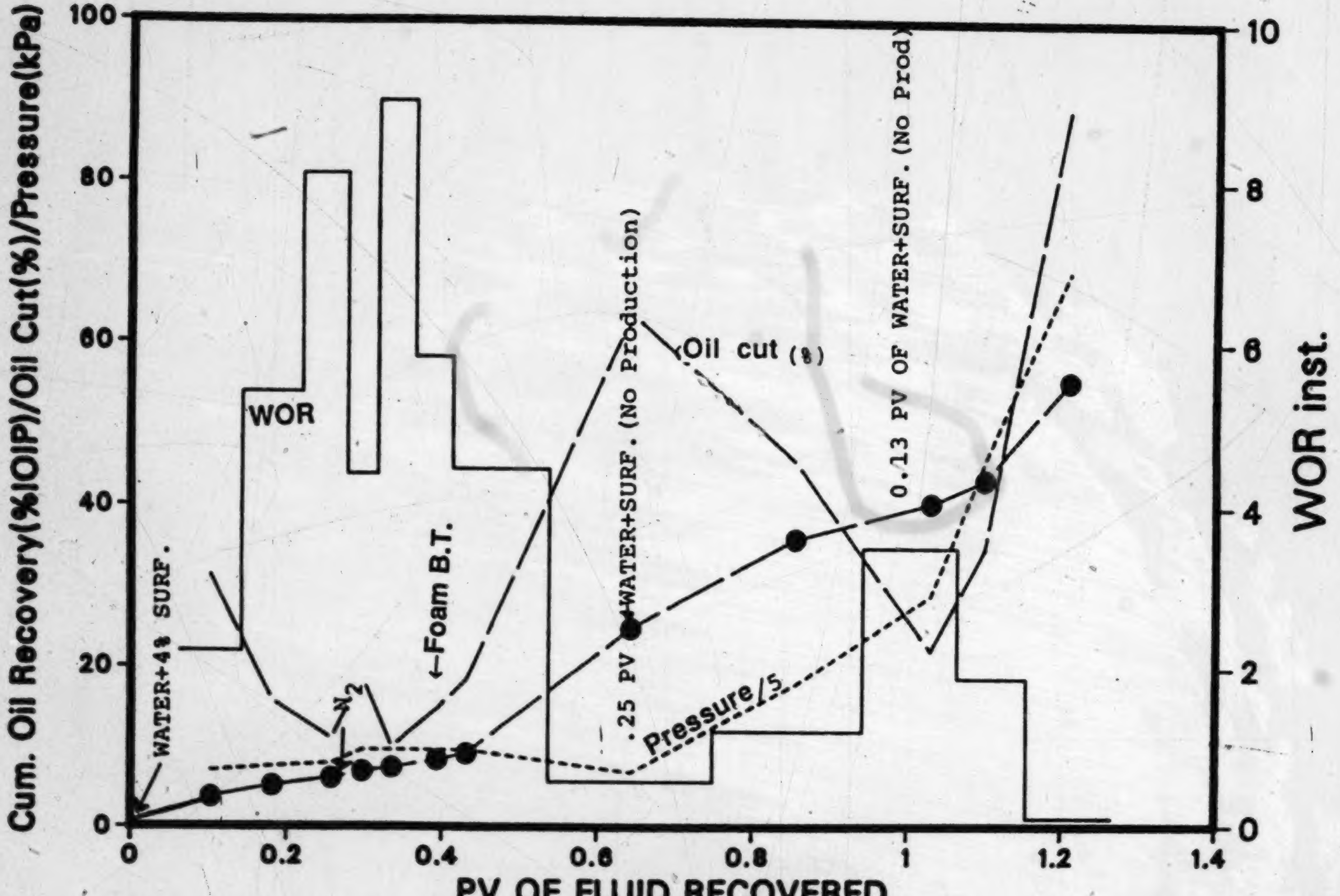

Fig. 58 Foam Injection Performance for Run 66 (h_b/h_o=0.33, k_o/k_b=1.00)

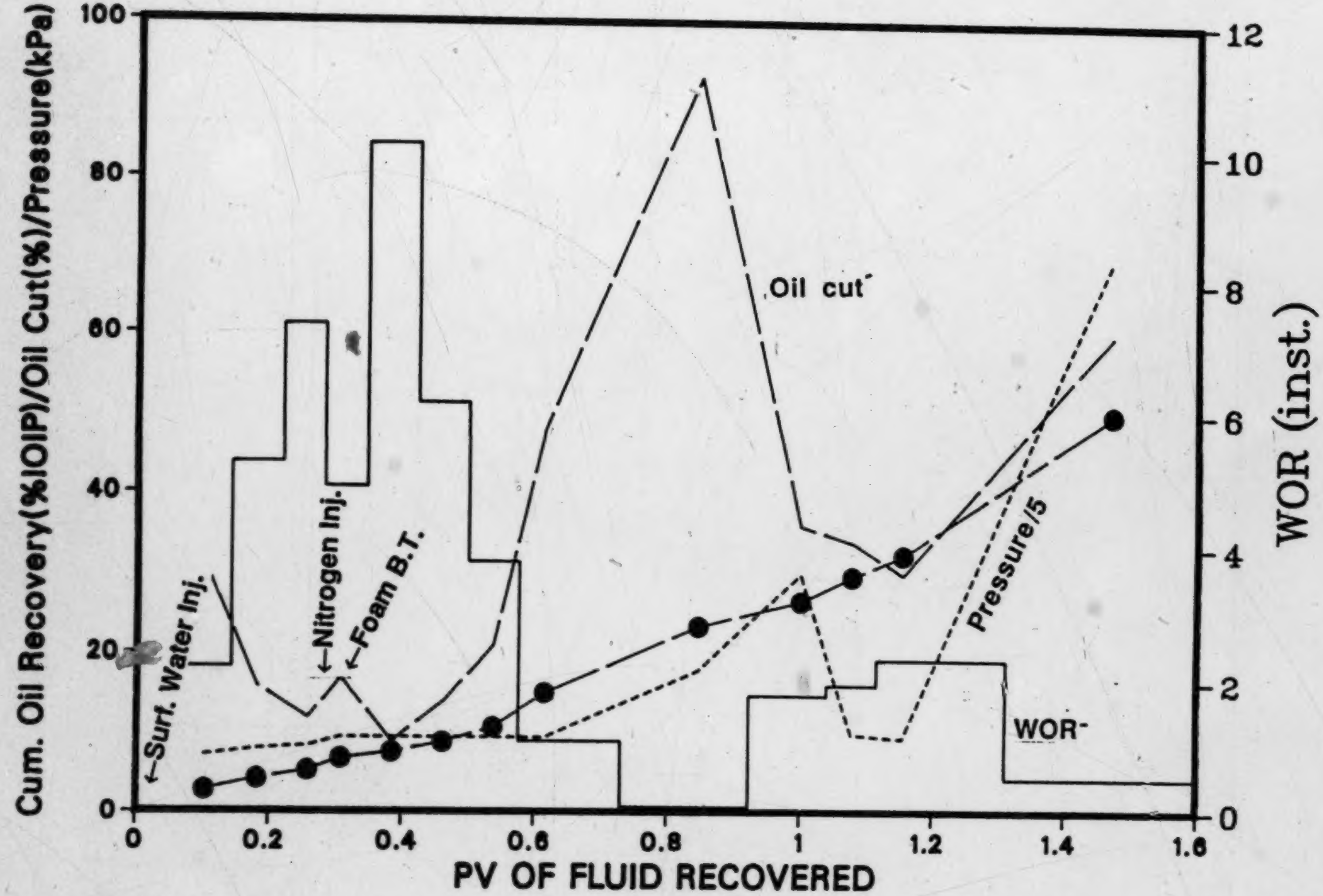

Fig. 59 Foam Injection Performance for Run 67 (h_b/h_o=0.33, k_o/k_b=1.00)

improvement over a waterflood. The surfactant water injection was followed by nitrogen injection. During nitrogen injection, the WOR value decreased as can be seen from Figure 58. Foam was not produced through the production well until 0.4 PV of total fluid was produced. Following foam breakthrough, injected air was also produced along with oil but the WOR decreased substantially. When 0.64 PV of total liquid had been produced, another surfactant slug was introduced. This time the slug size was 0.25 PV. During surfactant-water injection no fluid was produced through the production well. Nitrogen injection was resumed following the surfactant slug injection. The WOR was still low but the gas-liquid ratio started increasing. Before stopping the run due to a very high gas-liquid ratio, another surfactant-water slug was injected. At the end of the run (GLR=7000), 57 percent of the IOIP was recovered.

5.8.1 Effect of Viscosity Ratio

Runs 68 and 69 were conducted with oil-water viscosity ratios of 7.5 and 200 respectively. For both of these runs a surfactant concentration of four percent was used. These runs, therefore, could be compared with Run 66 for which an oil-water viscosity ratio of 50 was used. The recovery performance for Run 68 is depicted in Figure 60. This run is compared with other runs in the following chapter.

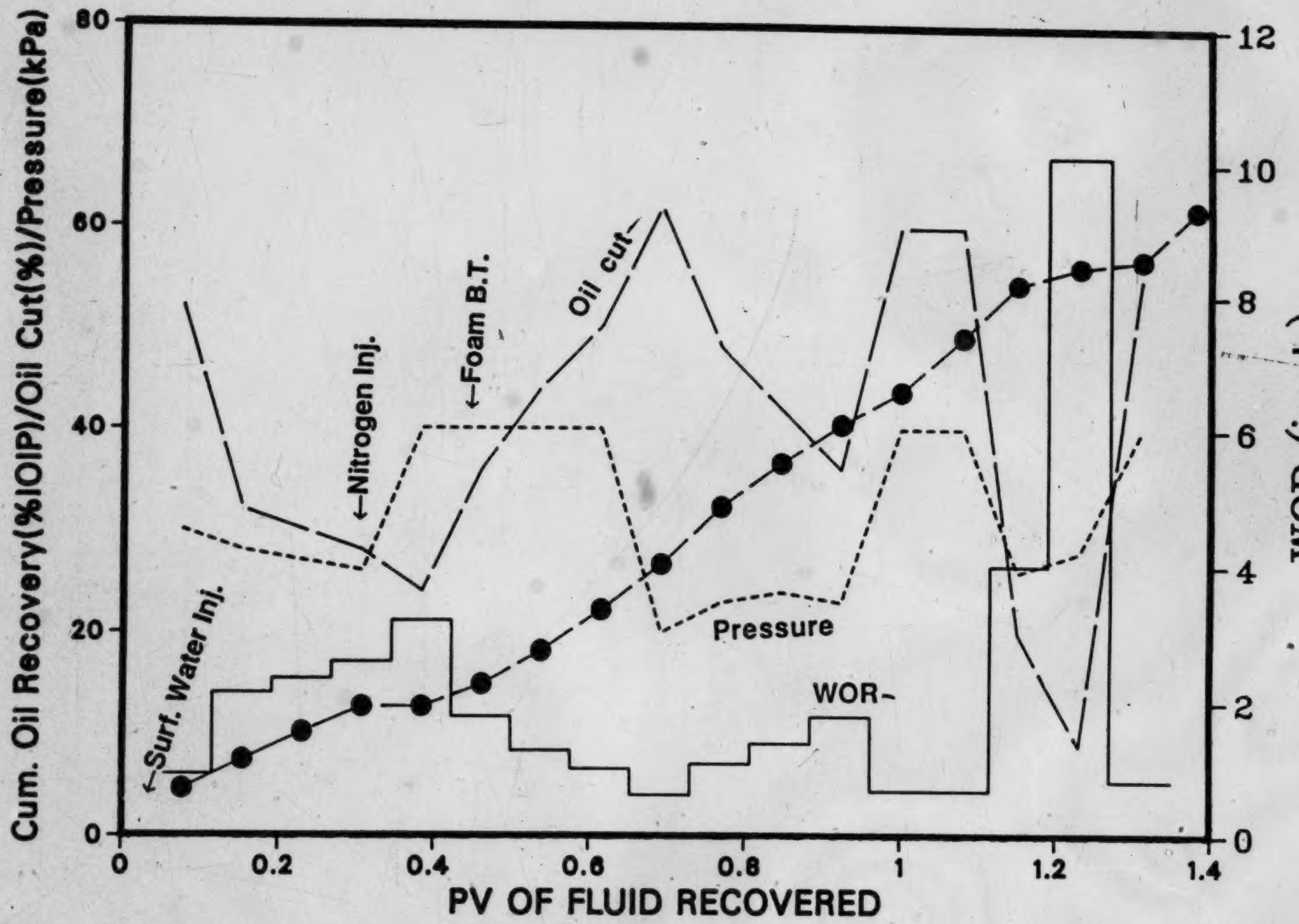

Fig. 60 Foam Injection Performance for Run 68 (h_b/h_o=0.33, k_o/k_b=1.00)

Run 69: Viscosity Ratio=200

In order to examine the effect of high oil viscosity on foam injection, Run 69 was conducted using Faxam-100 (viscosity=200 mPa.s) as the oil phase. As was the case with other foam injection runs, four percent surfactant water was alternated with nitrogen. During surfactant-water injection, oil recovery was slightly better than that observed with a waterflood. For runs with a lower oil viscosity, no such improvement was observed. Figure 61 depicts the recovery performance for this run. As can be seen from this figure, the recovery is poor but yet considerably better than that obtained by a waterflood. When the displacement test was ended (GLR=7000), a total of 23.3 percent of the IOIP was produced. This value, even though low, is comparable to that which was observed with either polymer or emulsion flood, without a bottom-water zone.

5.8.2 Effect of Water-to-Oil Zone Thickness and Permeability Ratios

Run 70: $h_b/h_o=0.33$, $k_o/k_b=2.67$

In order to examine the effect of a tight bottom-water zone on foam injection performance, Run 70 was conducted. The height of the bottom-water zone was three times smaller than that of the oil zone, and the bottom water was tighter than the oil zone. Further details are given in Table 5.1.

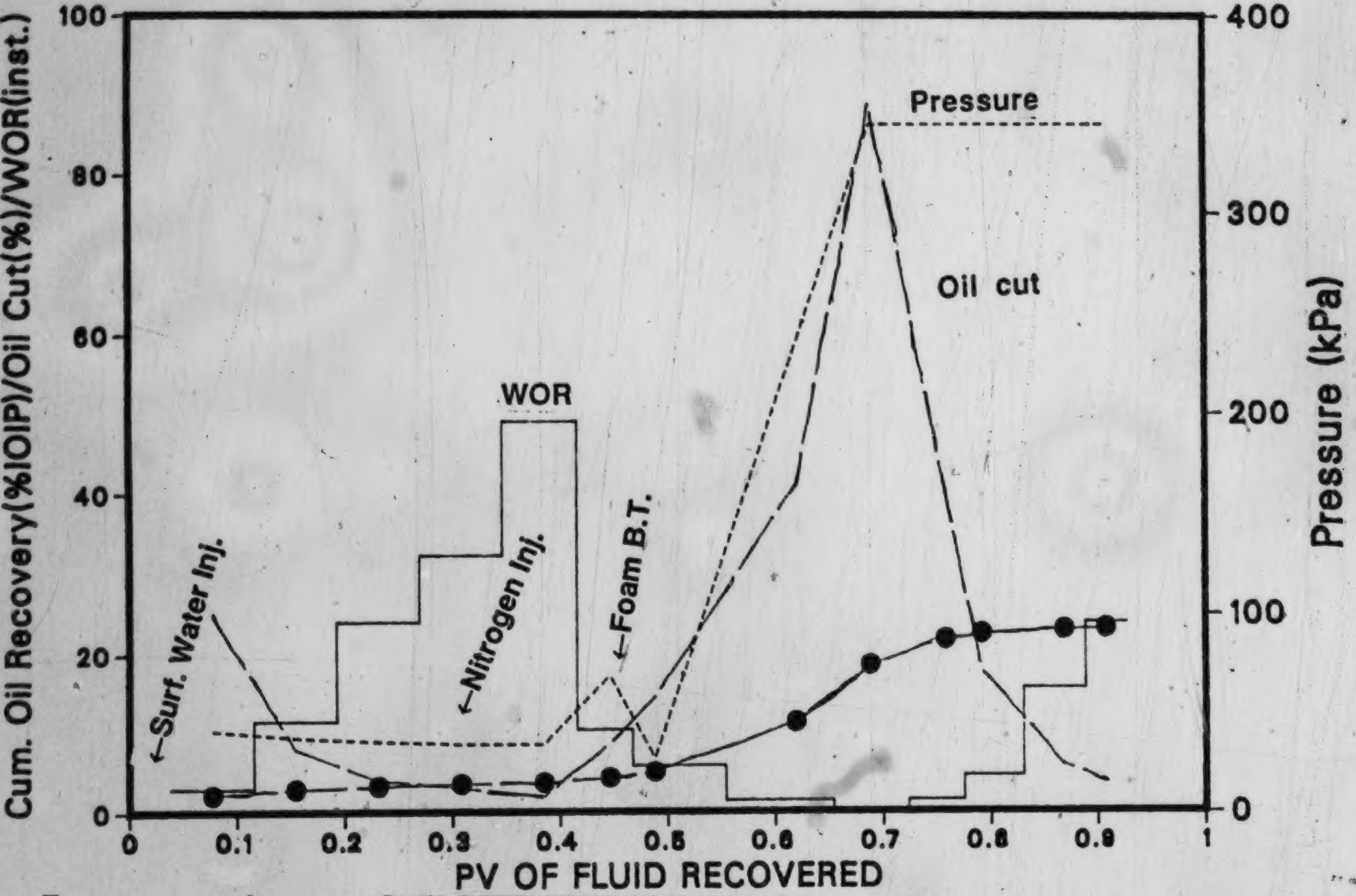

Fig. 61 Foam Injection Performance for Run 69 (h_b/h_o=0.33, k_o/k_b=1.00)

The run started by injecting 0.24 PV of surfactant water (four percent surfactant in water). This surfactant water was followed by nitrogen. Soon after the nitrogen injection started, foam breakthrough took place at 0.36 PV of fluid production. This time, breakthrough was earlier than was the case for Run 66 for which the bottom-water zone had the same height but a higher permeability than that of this run. This early breakthrough might indicate that the foam generated in situ was not displacing much of the bottom water due to excessive resistance from within the bottom-water zone. A similar observation of excessive resistance from a water-saturated rather than an oil-saturated zone was previously observed by Bernard (1963). Another reason might be the low quality of the foam production due to the presence of a low permeability zone (Raza, 1970). Nitrogen injection was continued until 0.67 PV of total liquid was produced. During this period, the WOR was quite low but the gas-liquid ratio was increasing. Figure 62 depicts the WOR, pressure, oil cut and cumulative oil recovery for this run. Another slug of surfactant water (0.23 PV) was injected. No production took place during this injection. As nitrogen injection was resumed following this surfactant slug, foam production took place after a delay of about 20 minutes and the gas-liquid ratio started increasing very rapidly. Consequently, the run was stopped when the gas-liquid ratio increased above 7000. At this

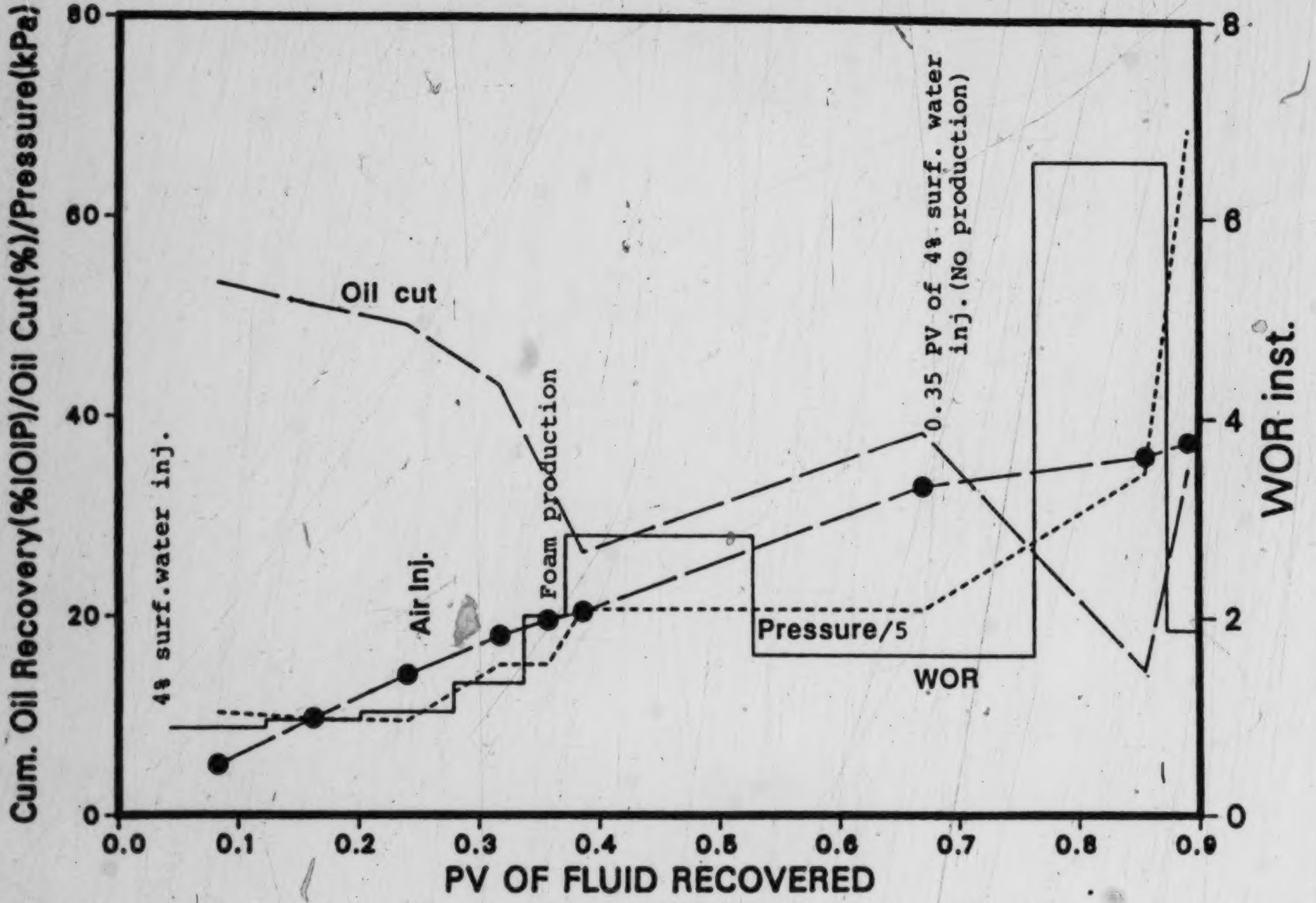

Fig. 62 Foam Injection Performance for Run 70 (h_b/h_o=0.33, k_o/k_b=2.67)

point a total of 40 percent of the IOIP was recovered. As can be seen from Table 3.1, this value is considerably lower than the ultimate recovery observed in previous runs with similar bottom water characteristics. This indicates that foam injection does not perform very well in the presence of a tight bottom-water zone. It was observed by previous researchers (Holm, 1970) that foam generation would not create blockage for very high permeability channels, but it was also observed that (Raza, 1970) tight porous media would degrade the quality of the foam generated *in situ*. It appears from the results of this run that the quality of the foam produced in a tight bottom-water zone (since surfactant water would go to the bottom-water zone due to least resistance) was not high enough to improve recovery by the nitrogen injection that followed the surfactant water.

Run 71: $h_b/h_o=0.33$, $k_o/k_b=0.06$

In order to examine the effect of a high permeability bottom-water zone ($k_o/k_b=0.06$) Run 71 was conducted. For Run 71, the oil zone was three times thicker than the bottom-water zone. The wells were located at a depth of 0.75 cm into the oil zone. The displacement test started with injection of surfactant water (four percent surfactant) at a flow rate of 400 ml/hr. As expected, a high-permeability bottom-water zone led to a high WOR even though the h_b/h_o was relatively low. As the waterflood continued, the WOR increased rapidly. Figure 63 depicts the WOR, pressure, oil cut and oil recovery for this run. The waterflood was then followed by nitrogen injection. During nitrogen injection, the foam breakthrough occurred when 0.16 PV of fluid was recovered. This value was considerably lower than that observed for thinner and tighter bottom-water zones. However, the oil recovery was much improved as compared to that for conventional waterfloods. At the end of the displacement test 30 percent of the IOIP was produced. This indicated a six-fold improvement over a conventional waterflood.

Run 72: $h_b/h_o=0.2$, $k_o/k_b=1$

Run 72 was conducted to investigate further the effect [illegible] the oil-to-water zone thickness and permeability ratio. [illegible] this run the oil zone was five times thicker than the bottom-water zone even though the absolute permeabilities were the same. The injection and production wells were located 1.6 cm (one-quarter of the total thickness of the oil zone) into the oil zone. The displacement test started with surfactant-water injection at a flow rate of 400 ml/hr. The WOR, pressure, oil recovery and oil cut are depicted in Figure 64. The oil recovery was much better than that for Run 66 in which a thicker ($h_b/h_o=0.33$) bottom-water zone was used. The waterflood was followed by nitrogen injection at a constant pressure. Foam breakthrough took place at 0.58

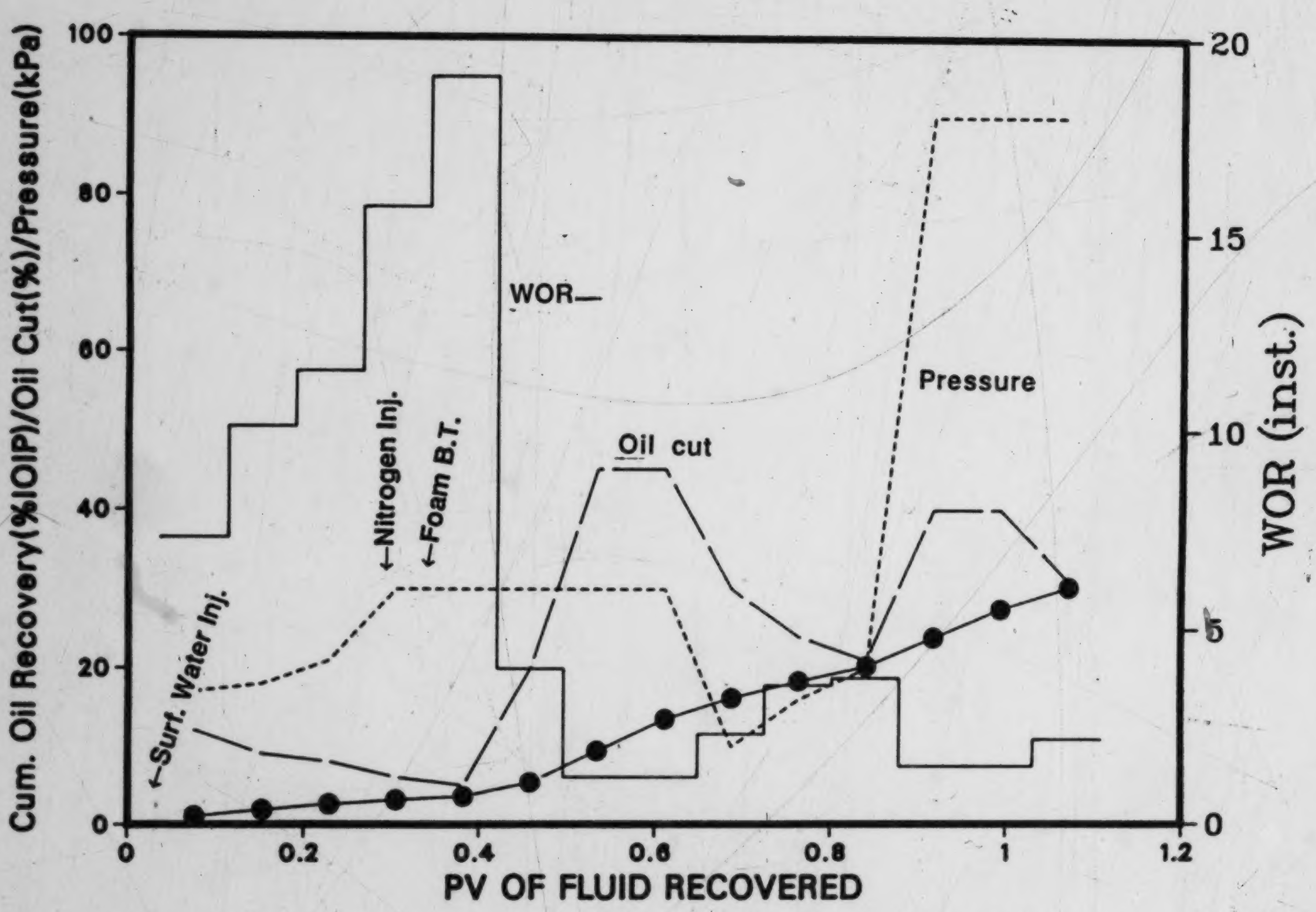

Fig. 63 Foam Injection Performance for Run 71 (h_b/h_o=0.33, k_o/k_b=0.06)

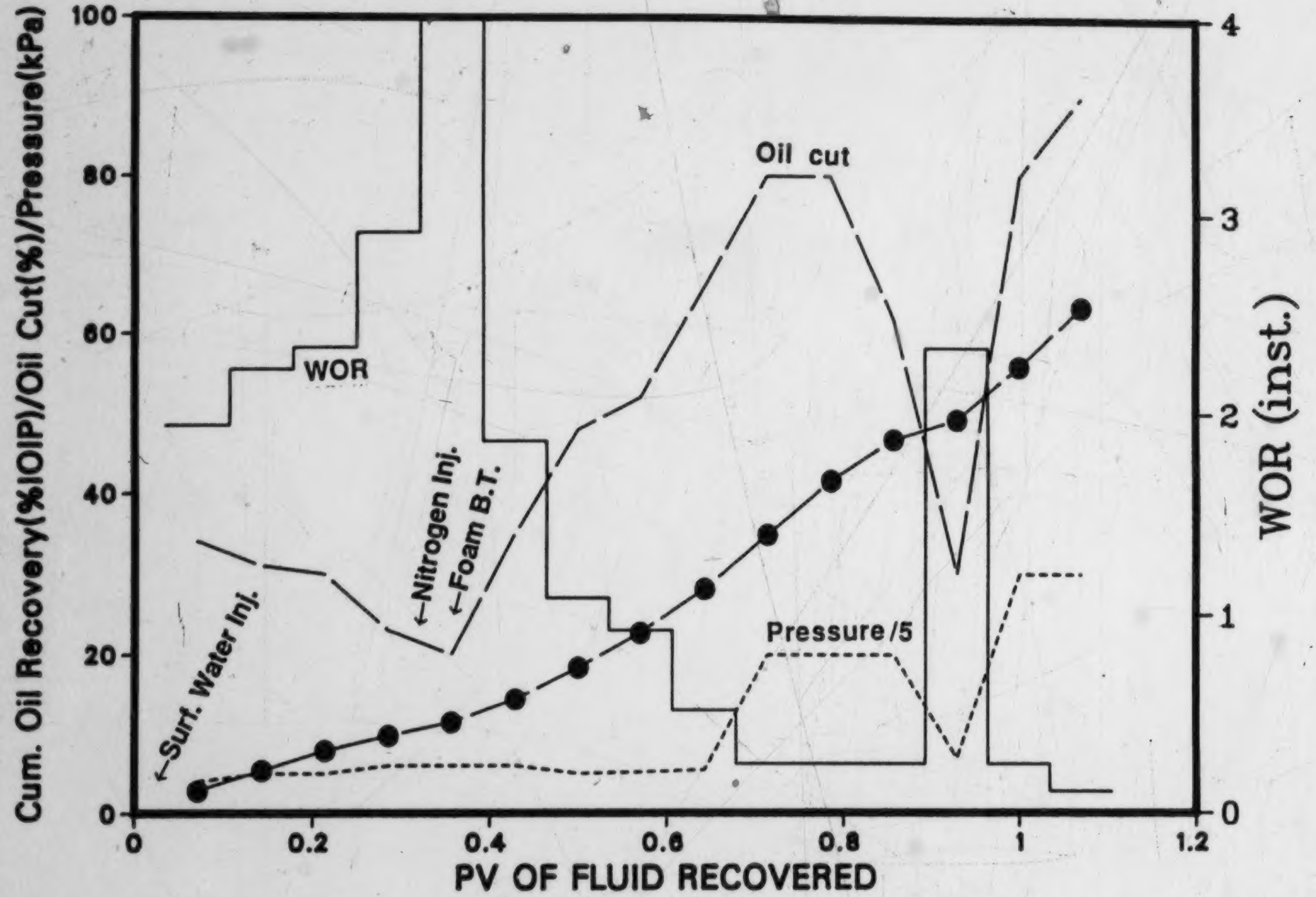

Fig. 64 Foam Injection Performance for Run 72 (h_b/h_o=0.20, k_o/k_b=1.00)

pore volume. This value is considerably higher as compared to previous runs. At the end of the displacement test, a total of 64 percent of the IOIP was recovered. This would indicate more than two-fold improvement over a conventional waterflood.

Run 73: $h_b/h_o=1$, $k_o/k_b=1$

In order to examine the effect of the oil-to-water zone thickness ratio for a k_o/k_b of 1.0, Run 73 was conducted. For this run the bottom water was as thick as the oil zone and had the same permeability. Table 5.1 lists the detailed packing characteristics of this run. Surfactant-water (four percent surfactant in water) was injected at the beginning of the displacement test. During this period the recovery was very poor. A similar performance was observed also with Run 3 for which a waterflood was performed at the initial stage. When 0.358 PV of surfactant water had been injected, nitrogen injection was initiated. During nitrogen injection the oil cut did not change significantly until foam breakthrough took place at 0.81 PV. The time to breakthrough is longer than that observed in Run 66. This shows that the existence of a larger bottom-water zone actually increased the time to foam breakthrough. Following foam breakthrough the WOR decreased substantially but nitrogen started being produced. Nitrogen injection was stopped (see Figure 65) when 1.42 PV of liquid had been

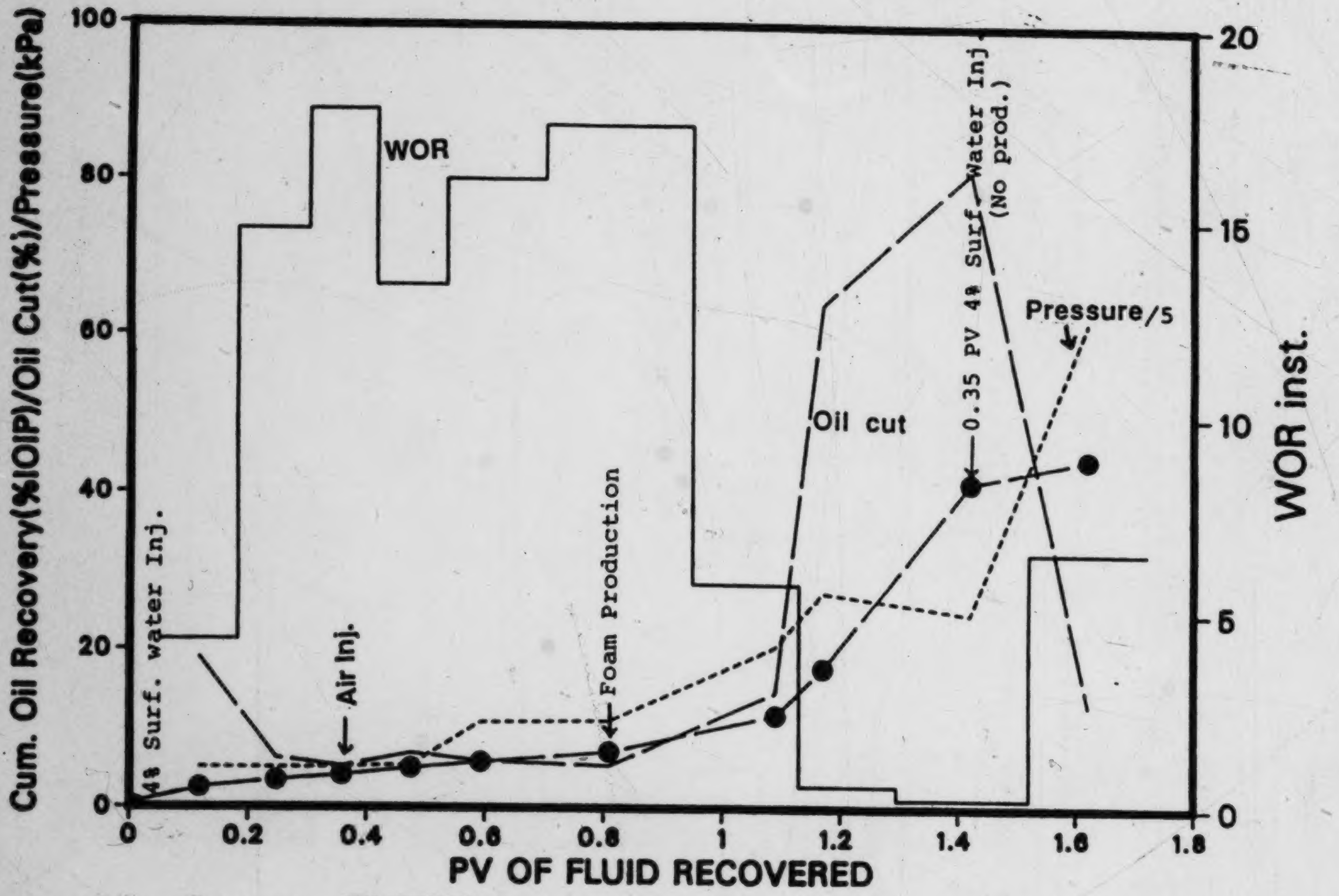

Fig. 65 Foam Injection Performance for Run 73 ($h_b/h_o=1.00$, $k_o/k_b=1.00$)

produced. This was followed by another slug of surfactant water. No production was observed during this period of surfactant-water injection. This time, the surfactant-water slug size was 0.35 PV. Then, nitrogen was injected until the gas-liquid ratio was as high as 7000. At this point 44.5 percent of the IOIP had been recovered. Table 5.1 compares this ultimate recovery with that of other runs. Table 5.4 lists the summary of this run along with other runs with foam injection.

Run 74: $h_b/h_o=1$, $k_o/k_b=2.67$

In order to examine the effect of a tight and thick bottom water zone on the performance by foam injection, Run 74 was conducted. For this run, the bottom-water zone was as thick as the oil zone but had lower permeability. Further details are available in Table 5.1. The run started with the injection of surfactant water (four percent surfactant in water). After injecting 0.471 PV of surfactant water, nitrogen was injected. The WOR value (see Figure 66 for WOR, pressure, oil cut and cumulative oil recovery) remained quite high while the nitrogen injection continued. This particular run was characterized by a delayed foam breakthrough, which took place after a total fluid production of 0.824 PV. This value was very close to that which was observed in Run 73 for which a similar thickness but higher permeability was used for the

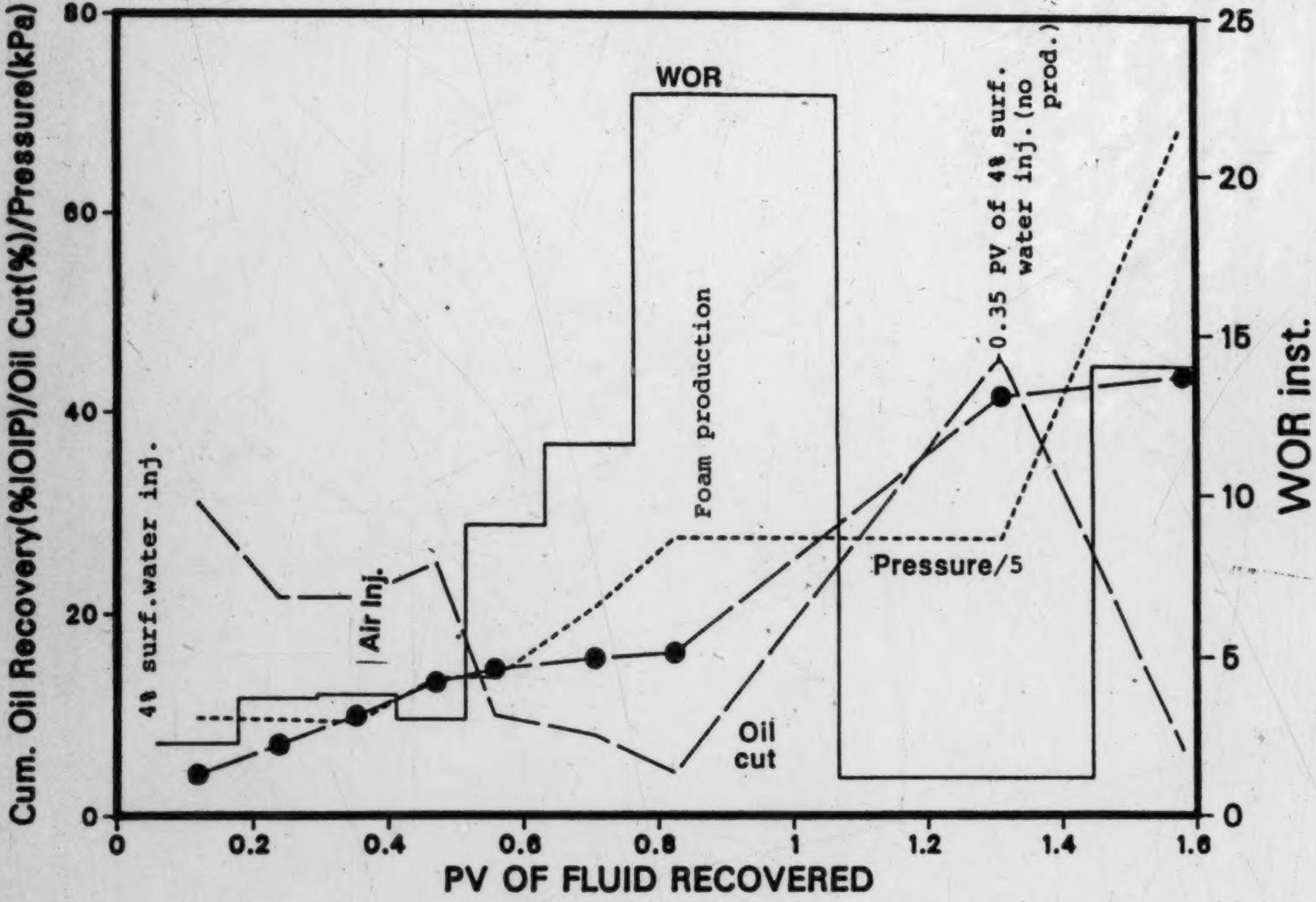

Fig. 66 Foam Injection Performance for Run 74 (h_b/h_o=1.00, k_o/k_b=2.67)

bottom-water zone. As was observed in previous foam injection runs, the WOR decreased substantially following foam breakthrough while the gas-liquid ratio started increasing. Another slug of surfactant water (0.35 PV) was injected. As before, no production occurred during the injection of surfactant water. Nitrogen injection was resumed and when the gas-liquid ratio increased above 7000, the displacement test was stopped. The ultimate recovery for this run was 44 percent of the IOIP. This value is comparable to 47 percent of the IOIP recovered in Run 73 that had similar thickness but higher permeability of the bottom-water zone.

Run 75: $h_b/h_o=1$, $k_o/k_b=0.06$

In order to investigate further effects of the oil-to-water zone thickness ratio for a k_o/k_b of 0.06 Run 75 was conducted with an h_b/h_o of 1. The wells were located at 50% depth of the oil zone. Initially, a surfactant water was injected at a flow rate of 400 ml/hr. The waterflood gave extremely poor performance showing no improvement due to the presence of a surfactant. Figure 67 depicts the WOR, pressure, oil cut and oil recovery performance for this run. However, when nitrogen was injected following the surfactant water injection, the oil cut increased considerably. Foam breakthrough occurred at 0.24 PV of fluid recovery. As nitrogen injection was alternated with more surfactant

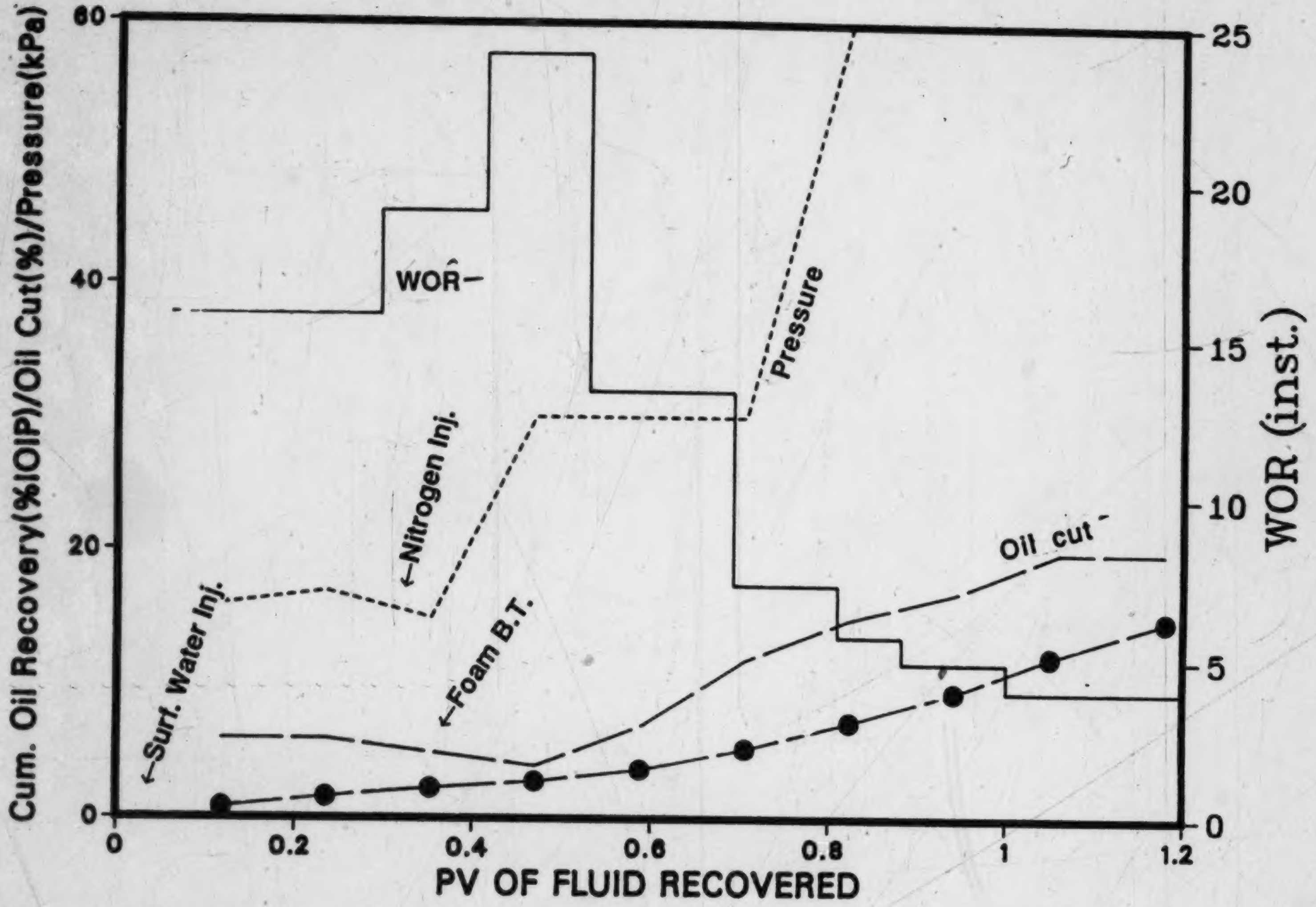

Fig. 67 Foam Injection Performance for Run 75 ($h_b/h_o=1.00$, $k_o/k_b=0.06$)

water, the recovery improved considerably over that for a waterflood but was still much poorer than that obtained with an emulsion or polymer flood. At the end of the displacement test a total of 15 percent of the IOIP was recovered. This value, even though very low, represents a seven-fold improvement over a conventional waterflood.

5.8.3 Effect of Waterflood on Foam Injection

Run 76: Foam Injection - Effect on Waterflood

In order to examine the effect of a surfactant-free waterflood on the blocking action of foam, Run 76 was conducted. The oil zone was three times as thick as the bottom-water zone and both had a similar permeability. Other packing characteristics are detailed in Table 5.1. A 10 percent surfactant concentration was chosen for this run. Therefore, this run can be compared with Run 67. At the beginning of the displacement test, surfactant water was injected for a pore volume of 0.5. During this time 12.6 percent of the IOIP was produced. This value is very close to that which was expected from a waterflood (e.g., the primary stage of Run 4). This showed that surfactant water does not improve performance over a waterflood. Nitrogen was injected following the surfactant-water injection. When nitrogen injection was initiated, foam started coming through the outlet almost immediately. Note that during the injection of surfactant-water, a total of 500 ml of water was produced along with 141 ml of oil. This volume (bottom water volume is 430 ml) indicates that the surfactant water reached the production well by replacing most of the bottom water. Consequently, when nitrogen was injected, it quickly reached the production end to generate foam throughout the bottom-water zone. Nitrogen was injected until approximately 0.1 PV of fluid was produced. This was followed by a waterflood at 400 ml/h. A total of 0.22 PV of water was injected. During the water injection, no production took place until the first 0.14 PV of water was injected. This indicated compression of the foam. Following this, flow through the production well started as the waterflood continued. However, the WOR was very high (over 16) for this period of water injection. Figure 68 depicts the WOR, along with injection pressure, oil cut and cumulative oil recovery. During the waterflood, no foam was produced indicating a possible 'wash away' effect by water. This effect was also reported by Holm (1970). Following this waterflood, nitrogen was again injected until a total of 1.16 PV of liquid was produced. During nitrogen injection, the WOR value remained very high and even though a considerable amount of foam was being produced (possibly due to the fact that surfactant added to the surfactant water solution was large enough to create foam even after dilution with a waterflood). Following this nitrogen slug, 0.5 PV of surfactant water was injected again. This was

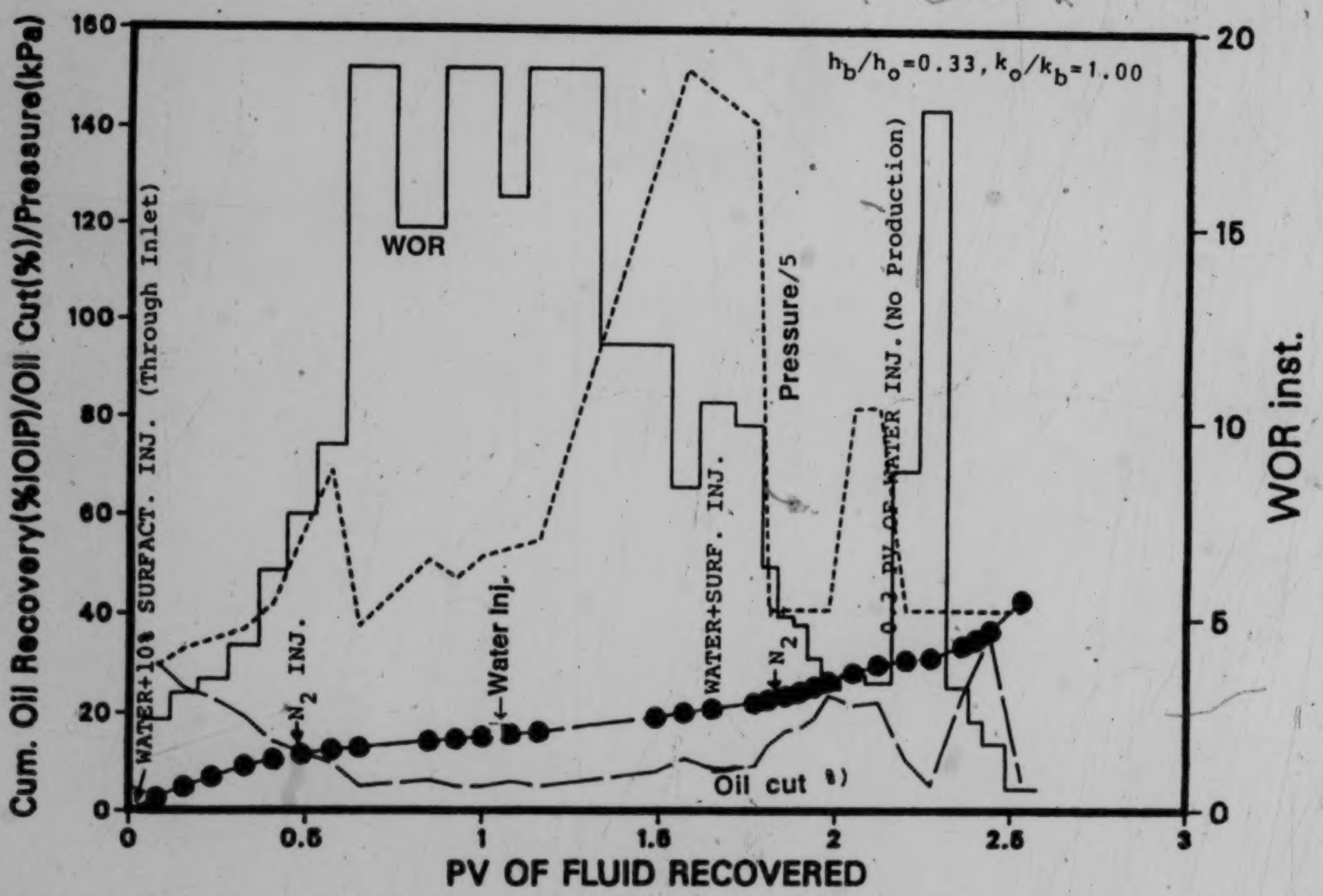

Fig. 68 Foam Injection (Alternated with Waterflood) Performance for Run 76

followed by nitrogen injection. During nitrogen injection the WOR value decreased considerably but the gas-liquid ratio started increasing rapidly. The displacement test was stopped when the gas-liquid ratio increased above 7000. A total of 46 percent of the IOIP was recovered at the end of the displacement test. This value is lower than the 50 percent of the IOIP recovered in Run 67 for which the same surfactant concentration was used but for which surfactant water was alternated with nitrogen only. Water injection after nitrogen injection does not seem to have any positive impact on recovery.

5.9 Silica Gel Injection

Runs 77 through 85 were conducted to examine the effectiveness of silica gel as a blocking agent in the presence of a bottom-water zone. For most of the runs, acidified sodium orthosilicate was injected first and then activated with carbon dioxide. Since carbon dioxide flows into the bottom-water zone preferentially, efficient gelation was expected in the bottom-water zone. After injecting carbon dioxide a delay of few hours was allowed for gelation. A waterflood was then carried out through the injection well. The results of these runs are summarized in Tables 5.1 and 5.5.

TABLE 5.5: Results of Silica Gel Inj. Runs

Run no.	Gel bt (PV)	Recovery at bt (%IOIP)	Sodium orthosilicate Slug Vol. (PV)	IOIP (ml)
77	0.70	42	0.36	1110
78	0.80	42	0.36	1115
79	0.60	41	0.20	1310
80	0.88	37	0.40	750
81	0.70	44	0.30	1120
82	0.90	42	0.40	765
83	0.50	32	0.15	1300
84	0.56	30	0.20	1110
85	0.87	18	0.60	760

Run 77: $h_b/h_o = 0.33$, $k_o/k_b = 1$

Run 77 was conducted in order to examine the impact of carbon dioxide-activated silica gel in the presence of a relatively thin bottom-water zone. Initially, a five-percent sodium orthosilicate solution was acidified with HCl to obtain a pH of 9.3. This pH was found to be optimal for gel formation when activated by carbon dioxide. The orthosilcate solution was injected through the inlet end in order to have better access to the bottom-water zone. Figure 69 depicts the WOR, pressure, oil cut and oil recovery performance for this run. As can be seen from this figure, the recovery was much better than that with a waterflood (as compared to the initial stage of Run 4). A slug of 0.36 pore volume of acidified solution was injected. During this period alone, 23 percent of the IOIP was recovered. Following this slug injection, carbon dioxide was injected at an average flow rate of 1150 ml/hr. Even with this relatively high flow rate the injection pressure was low (15 kPa). During carbon dioxide injection, the oil cut remained high (at around 70 percent). After injecting 2340 ml of carbon dioxide, the displacement test was stopped and a three hour delay was allowed for gelation. After this delay, a waterflood was started through the injection well. A high injection pressure was observed during the water injection. This indicated very good gelation at least near the injection well bore. However, the oil cut started to decrease. After 0.7 PV of total liquid injection, gel

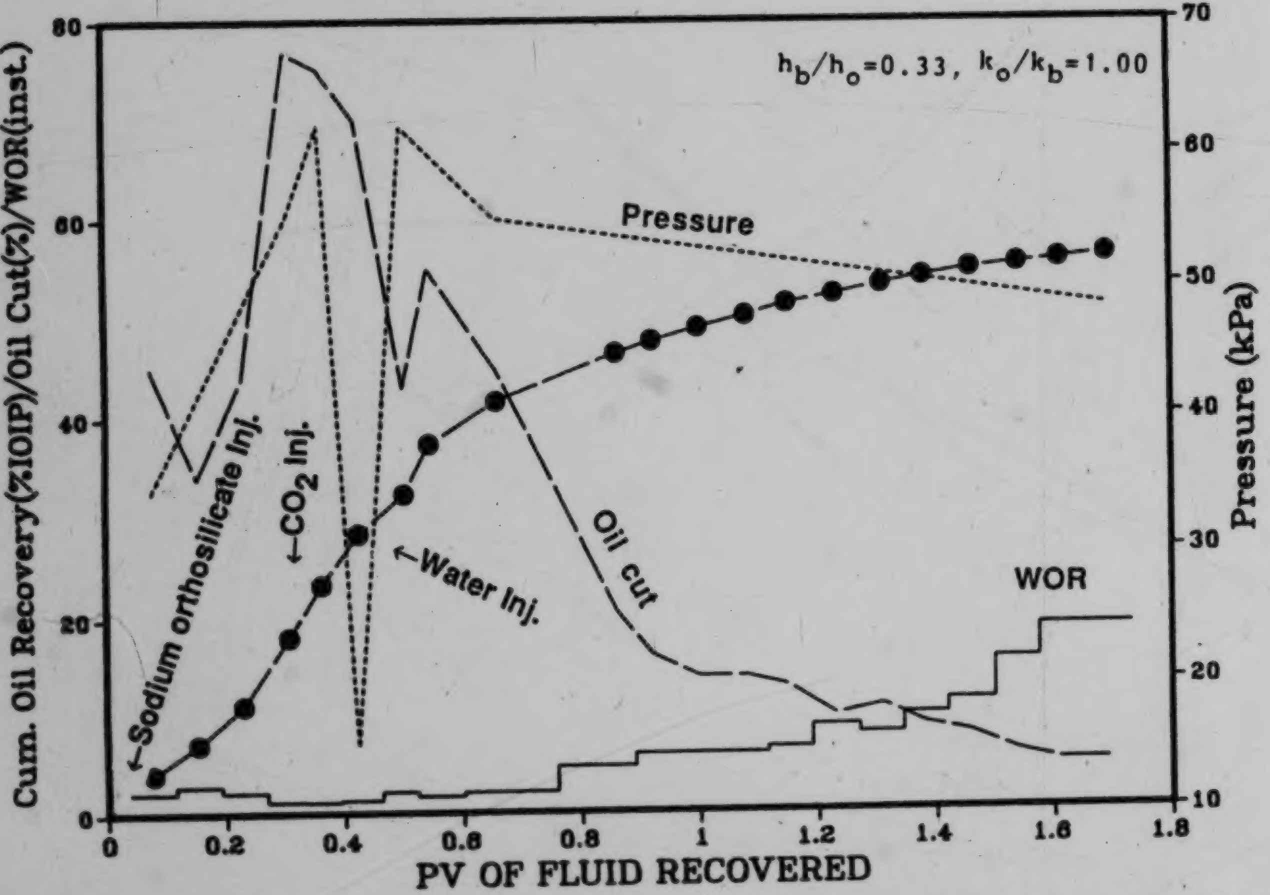

Fig. 69 CO_2 Activated Silica Gel Inj. and Waterflood Performance for Run 77

started to be produced, and the oil cut declined rapidly even though the injection pressure remained at a high value. Even with this decrease in oil cut, at the end of the displacement test a total of 57 percent of the IOIP was produced. This indicates more than a 2.5-fold improvement over a conventional waterflood. Such a high level of improvement was observed only with polymer solution injection.

5.9.1 Role of Carbon Dioxide in Mobility Control with Silica Gel

Carbon dioxide enhances the gelation of acidified sodium orthosilicate solution. However, carbon dioxide is not indispensible for the formation of gel. With proper pH (around 9.2), gelation takes place even without carbon dioxide. To investigate the contribution of carbon dioxide in mobility control with silica gel Run 78 was conducted.

Run 78: Silica gel without CO_2, $h_b/h_o=0.33$, $k_o/k_b=1$

This run was a repeat of Run 77 except that no carbon dioxide was injected in this run. Therefore, a comparison of these two runs allowed determination of the contribution of carbon dioxide. Figure 70 depicts the WOR, pressure, oil cut and oil recovery performance for this run. As can be seen from Figure 70, the oil recovery was very good during sodium orthosilicate injection. However, when this slug was

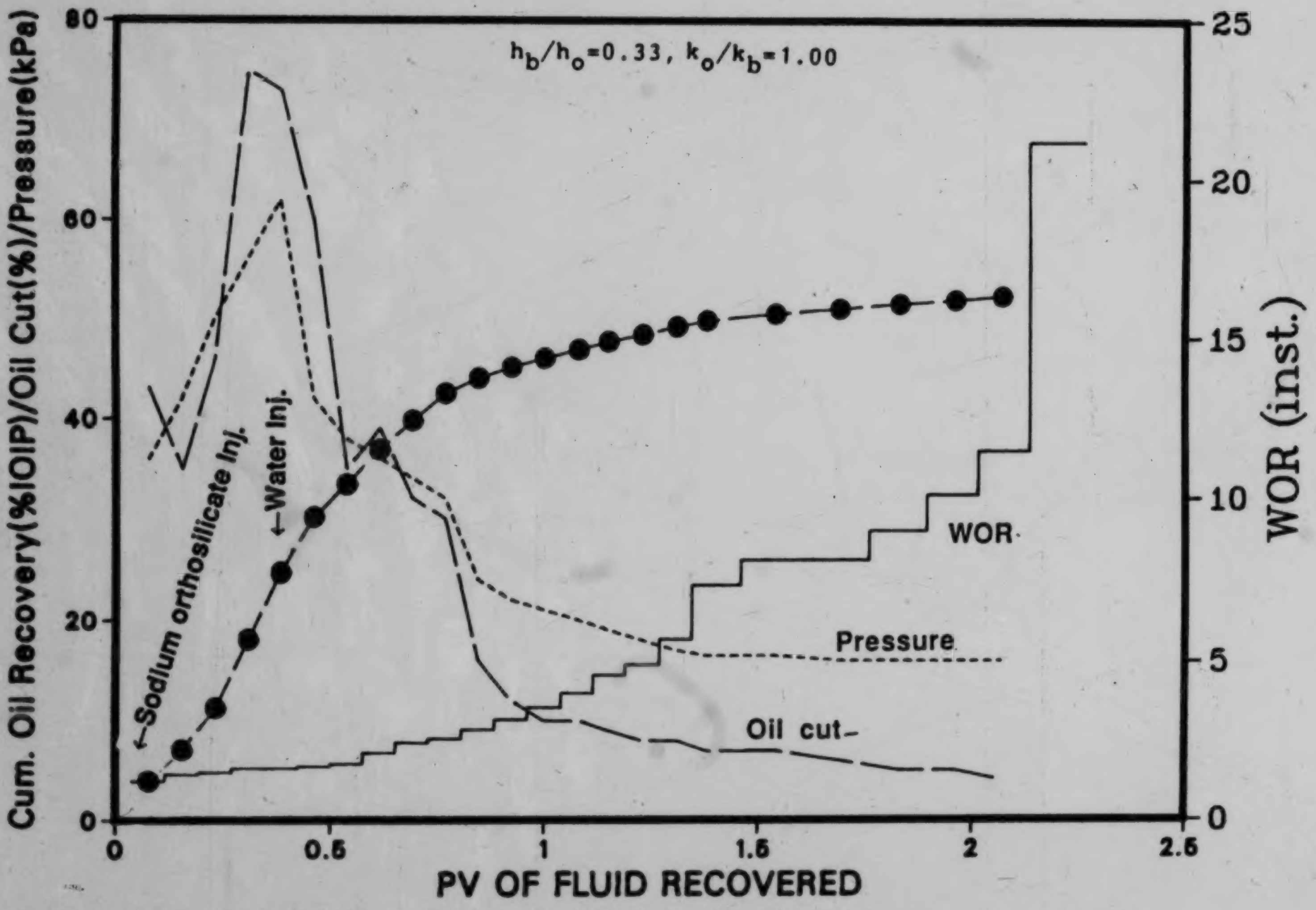

Fig. 70 Silica Gel (without CO_2) Inj. and Waterflood Performance for Run 78

followed by a waterflood the oil recovery decreased rapidly. The gel started being produced at around 0.80 PV of liquid produced. This breakthrough is slightly higher than that of the previous run. The injection of carbon dioxide enhanced the gelation far along the length of the bottom-water zone. After gel breakthrough, the oil cut started decreasing even faster than at the early stage of the waterflood. At the end of the displacement test a total of 52 percent of the IOIP was recovered. Even though this is about 2.5-fold improvement over a conventional waterflood, this value is still 10 percent smaller than that in Run 77. Therefore, one may conclude that the injection of carbon dioxide improved the oil recovery by 10 percent.

5.9.2 Effect of Water-to-Oil Zone Thickness and Permeability Ratio

In order to examine the effect of oil-water zone thickness and permeability ratio, Runs 79 through 85 were conducted with various bottom-water zone thicknesses and permeabilities.

Run 79: $h_b/h_o = 0.20$, $k_o/k_b = 1$

Run 79 was conducted to examine the effect of a relatively thin bottom-water zone. Initially, a slug of acidified sodium orthosilicate solution (0.20 PV) was injected through the inlet end. This was followed by the injection of a slug of carbon dioxide injected at 1000 ml/hr. A total volume of 1300 ml of carbon dioxide was injected. As was the case with Run 77, a delay of a few hours was allowed for gelation. Then a waterflood was carried out through the injection well. Even though the sodium orthosilicate solution and carbon dioxide were injected through the inlet end in order to avoid gelation around the injection well, a high injection pressure was required to maintain a flow rate of 400 ml/hr for the waterflood. For this run, gel breakthrough took place at 0.60 PV of fluid recovered. Even though this breakthrough led to a considerable decrease in the injection pressure, the oil cut curve did not change its slope. Consequently, at the end of the displacement test a total of 64 percent of the IOIP was recovered. This indicates more than a two-fold improvement over a conventional waterflood. This high improvement was observed only with polymer solutions. Figure 71 depicts the WOR, pressure, oil cut and oil recovery for this run.

Run 80: $h_b/h_o= 1.0$, $k_o/k_b=1$

In order to examine the effect of a relatively thicker bottom-water zone, Run 80 was conducted with a bottom-water zone as thick as the oil zone. For this run the acidified sodium orthosilicate solution was injected through the injection well. During this slug injection, the oil cut

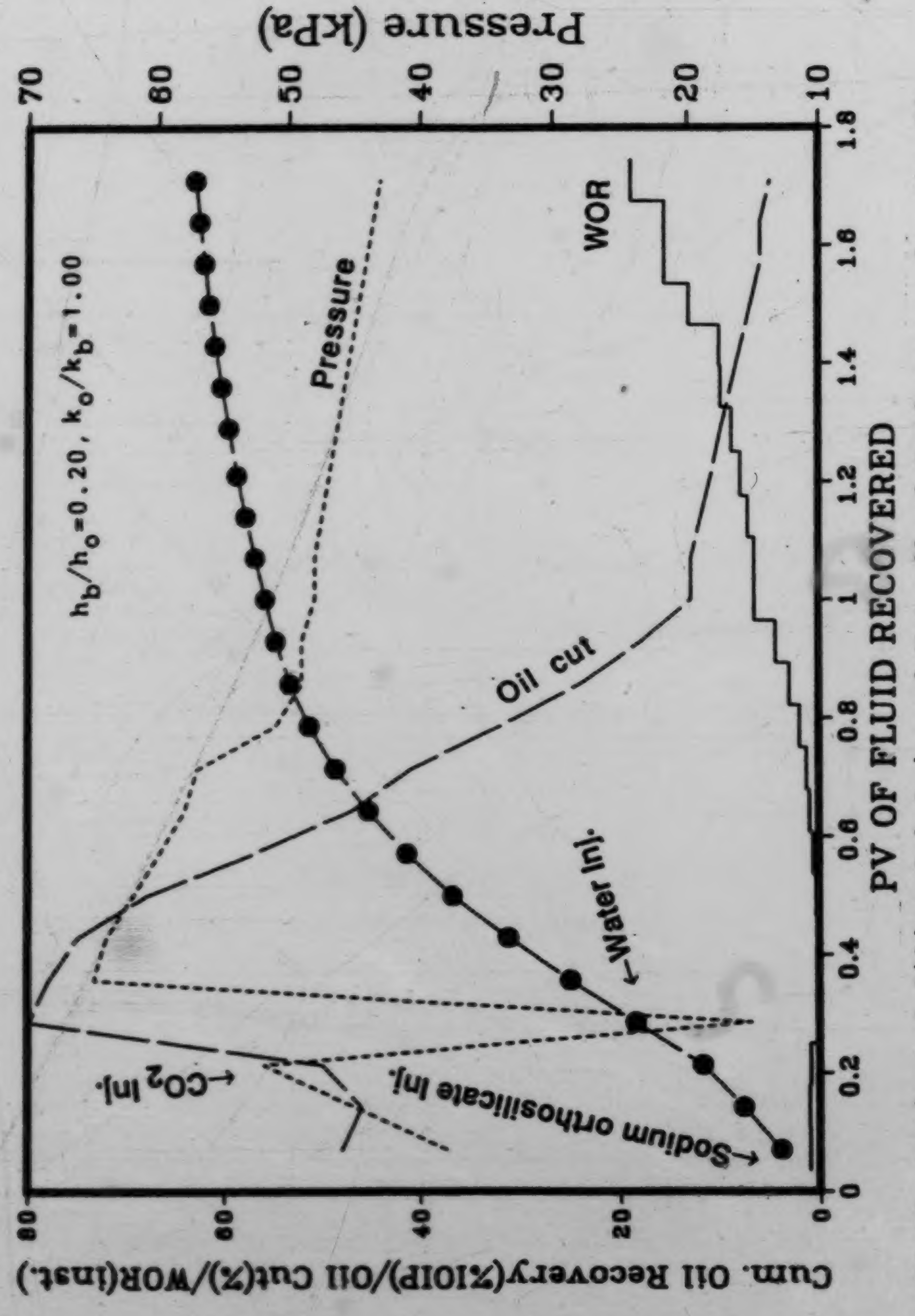

Fig. 71 CO₂ Activated Silica Gel Inj. and Waterflood Performance for Run 79

started with a very high value (80 percent). Such a high oil cut during the initial stages of the displacement was not observed with any other mobility control agent. The initial sodium orthosilicate slug (0.40 PV) was followed by carbon dioxide through the injection well. The injection of carbon dioxide led to an increase in injection pressure when a waterflood was followed. However, the oil cut decreased continually and the injection of carbon dioxide or water did not alter the shape of the oil-cut curve. Figure 72 depicts the WOR, pressure, oil cut and oil recovery performance for this run. At the end of the displacement test a total of 48 percent of the IOIP was recovered as the WOR reached a value of 20. This indicates a 16-fold improvement over a conventional waterflood.

Run 81: $h_b/h_o = 0.33$, $k_o/k_b = 2.67$

Run 81 was conducted with $k_o/k_b = 2.67$ in order to examine the effect of a tight bottom-water zone. Even though the bottom-water zone permeability was less adverse than that in Run 77, the oil recovery during sodium orthosilicate injection remained quite similar for both of these runs. However, the injection pressure was higher for this run. Following the injection of sodium orthosilicate solution carbon dioxide was injected at a flow rate of 1000 ml/hr for a total volume of 2300 ml. This carbon dioxide injection condition was similar to that in Run 77. It was

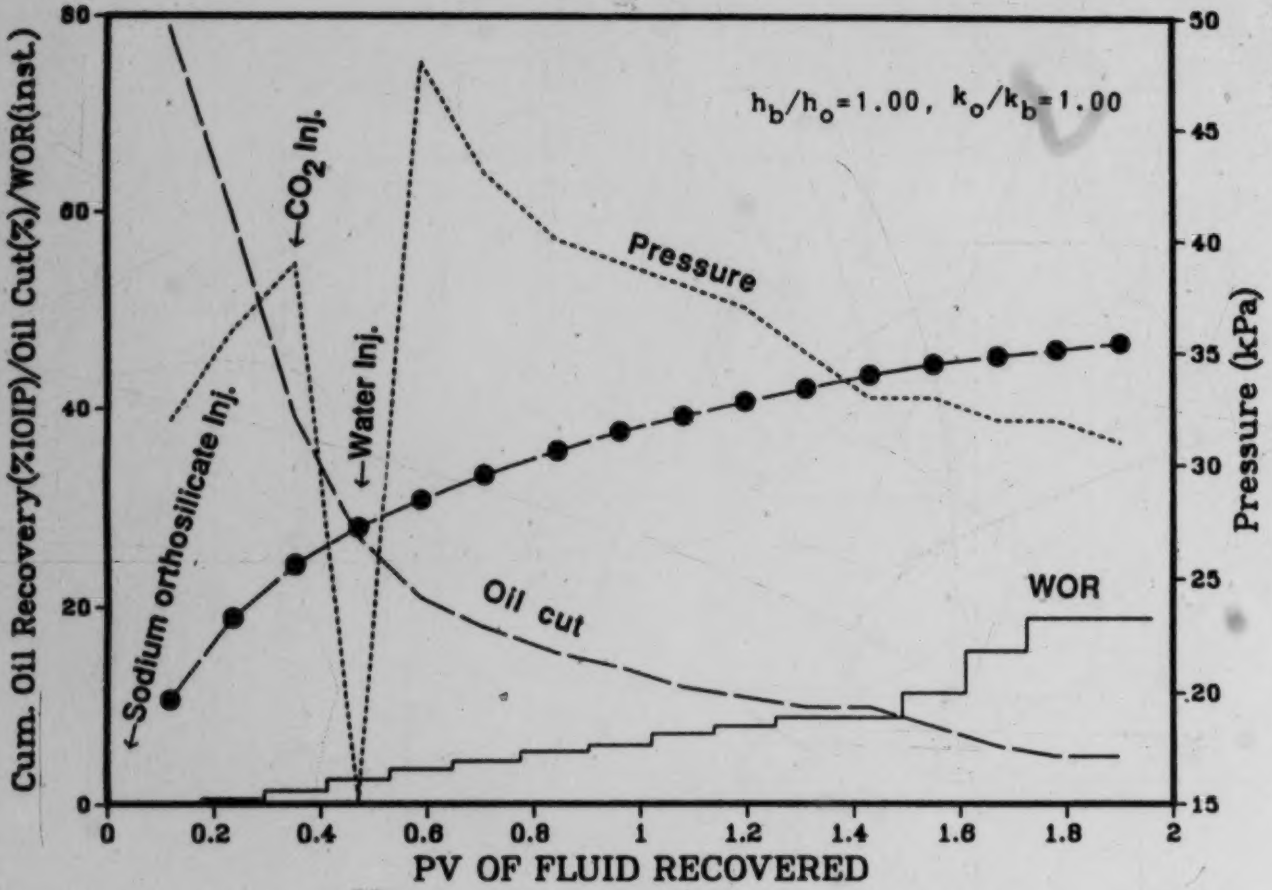

Fig. 72 CO_2 Activated Silica Gel Inj. and Waterflood Performance for Run 80

then followed by a waterflood at a flow rate of 400 ml/hr. For this run, gel breakthrough took place at 0.70 PV of liquid recovered. Following breakthrough, the injection pressure dropped sharply to a lower value at which it remained. During this period the oil cut decreased continuously. After gel breakthrough, however, the oil cut maintained a more stable value. Figure 73 depicts the WOR, pressure, oil cut and oil recovery performance for this run. At the end of the displacment test, a total of 58 percent of the IOIP was recovered. This value is less than two percent higher than that observed in Run 77 for which $k_o/k_b=1$ was used. However, this run gave about a two-fold improvement over a conventional waterflood.

Run 82: $h_b/h_o=1$, $k_o/k_b= 2.67$

In order to examine the effect of the oil-to-water zone thickness ratio for a tight bottom-water zone, Run 82 was conducted with a bottom-water zone as thick as the oil zone. For this run the acidified sodium orthosilicate solution was injected through the injection well. During this slug injection, the oil cut started with a very high value (85 percent). Such a high oil cut during the initial stages was not observed with any other mobility control agent. The initial sodium orthosilicate slug (0.40 PV) was followed by carbon dioxide through the injection well. The injection of carbon dioxide introduced an increase in injection pressure

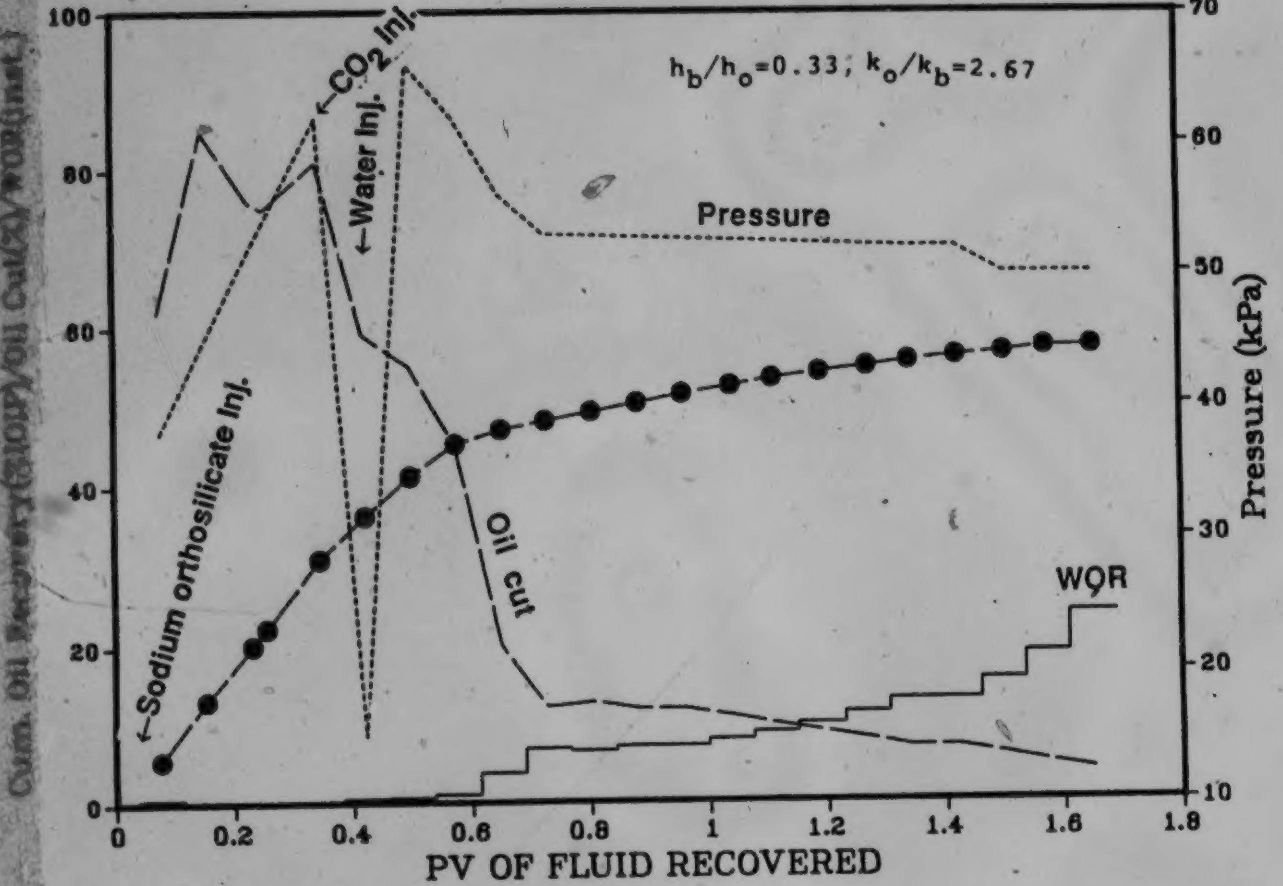

Fig. 73 CO$_2$ Activated Silica Gel Inj. and Waterflood Performance for Run 81

when a waterflood was initiated. However, the oil cut decreased continuously and the injection of carbon dioxide or water did not alter the shape of the oil-cut curve. Figure 74 depicts the WOR, pressure, oil cut and oil recovery performance for this run. At the end of the displacement test a total of 62 percent IOIP was recovered as the WOR reached a value of 20. This value is higher than that observed in Run 81 for which a thinner bottom-water zone was used. The reason for this anomalous behaviour will be discussed in the next chapter. A 62 percent of the IOIP recovery indicated about a 2.5-fold improvement over a conventional waterflood.

Run 83: $h_b/h_o = 0.20$, $k_o/k_b = 0.06$

Run 83 was conducted with a bottom-water zone 17 times more permeable than the oil zone in order to examine the effect of a very permeable bottom-water zone. However, a relatively thin ($h_b/h_o = 0.2$) bottom-water zone was used. For this run sodium orthosilicate solution was injected through the inlet end in order to have better access to the bottom-water zone. During this solution slug injection, the oil cut increased rapidly to reach a peak of 80 percent. A 15 percent sodium orthosilicate solution slug was injected. This was followed by carbon dioxide injection. During this whole period the oil cut increased. However, when the waterflood was started two hours after the carbon dioxide

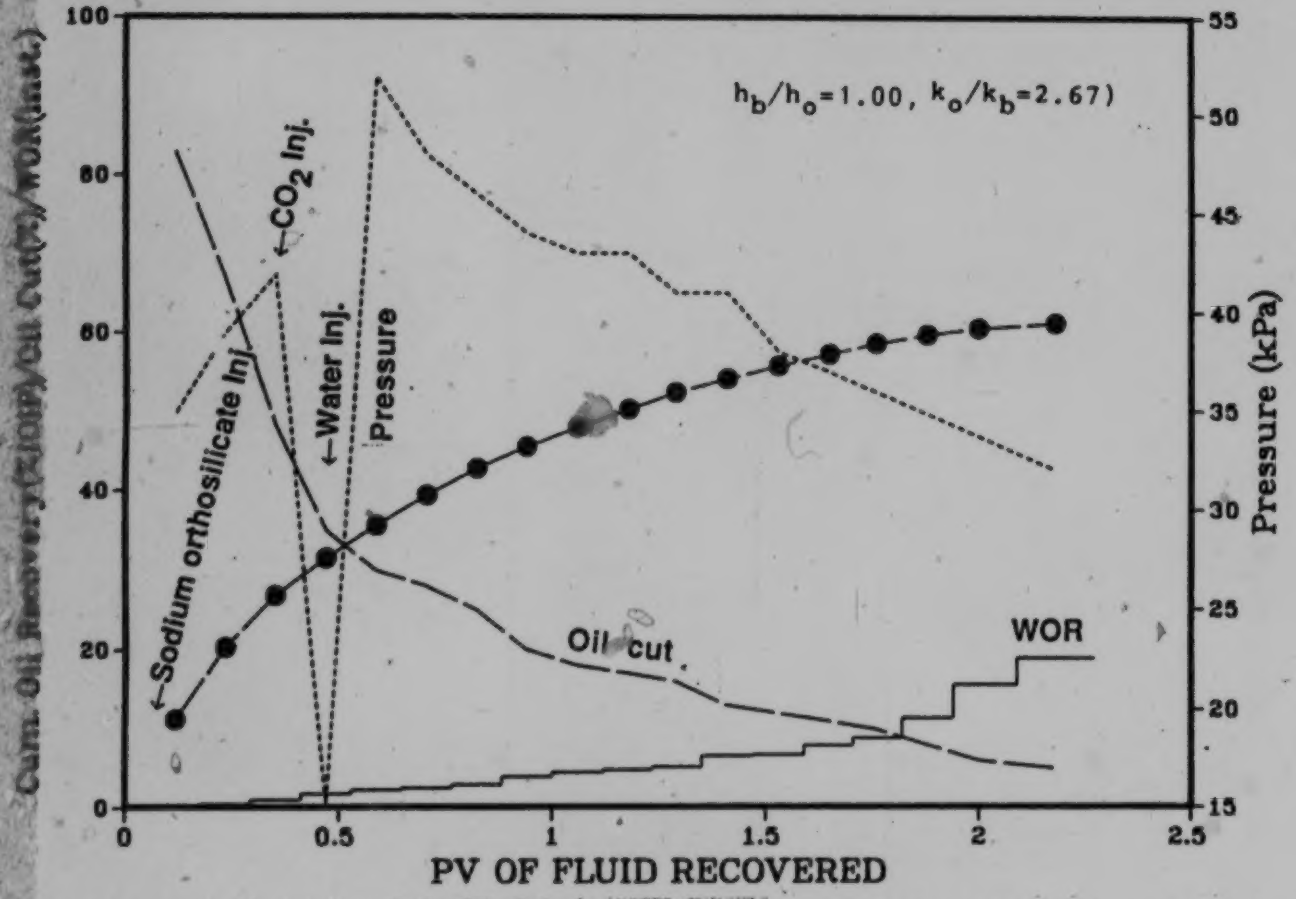

Fig. 74 CO_2 Activated Silica Gel Inj. and Waterflood Performance for Run 82

injection, the oil cut started decreasing. Figure 75 depicts the WOR, pressure, oil cut and oil recovery performance for this run. During the waterflood, gel breakthrough took place at 0.50 PV of fluid recovery. This value was somewhat lower than that observed with other runs with similarly thick but less permeable bottom-water zones. At the end of the displacement test a total of 48 percent of the IOIP was recovered. This indicated a seven-fold improvement over a conventional waterflood.

Run 84: $h_b/h_o = 0.33$, $k_o/k_b = 0.06$

In order to examine the effect of a thicker bottom-water zone for a very permeable bottom-water zone, Run 84 was conducted. For this run, a 0.20 PV slug of sodium orthosilicate solution was injected through the inlet end. As was the case in the previous run, the oil cut increased rapidly during the injection of sodium orthosilicate solution and also during the injection of the carbon dioxide that followed. Figure 76 depicts the WOR, pressure, oil cut and oil recovery performance for this run. A waterflood was carried out through the injection well. During the waterflood, the injection pressure increased slightly but the oil cut decreased continually. At 0.56 pore volume, gel breakthrough took place. This led to a decrease in injection pressure, but the oil cut decreased at the same rate as in the initial stage of the waterflood. At

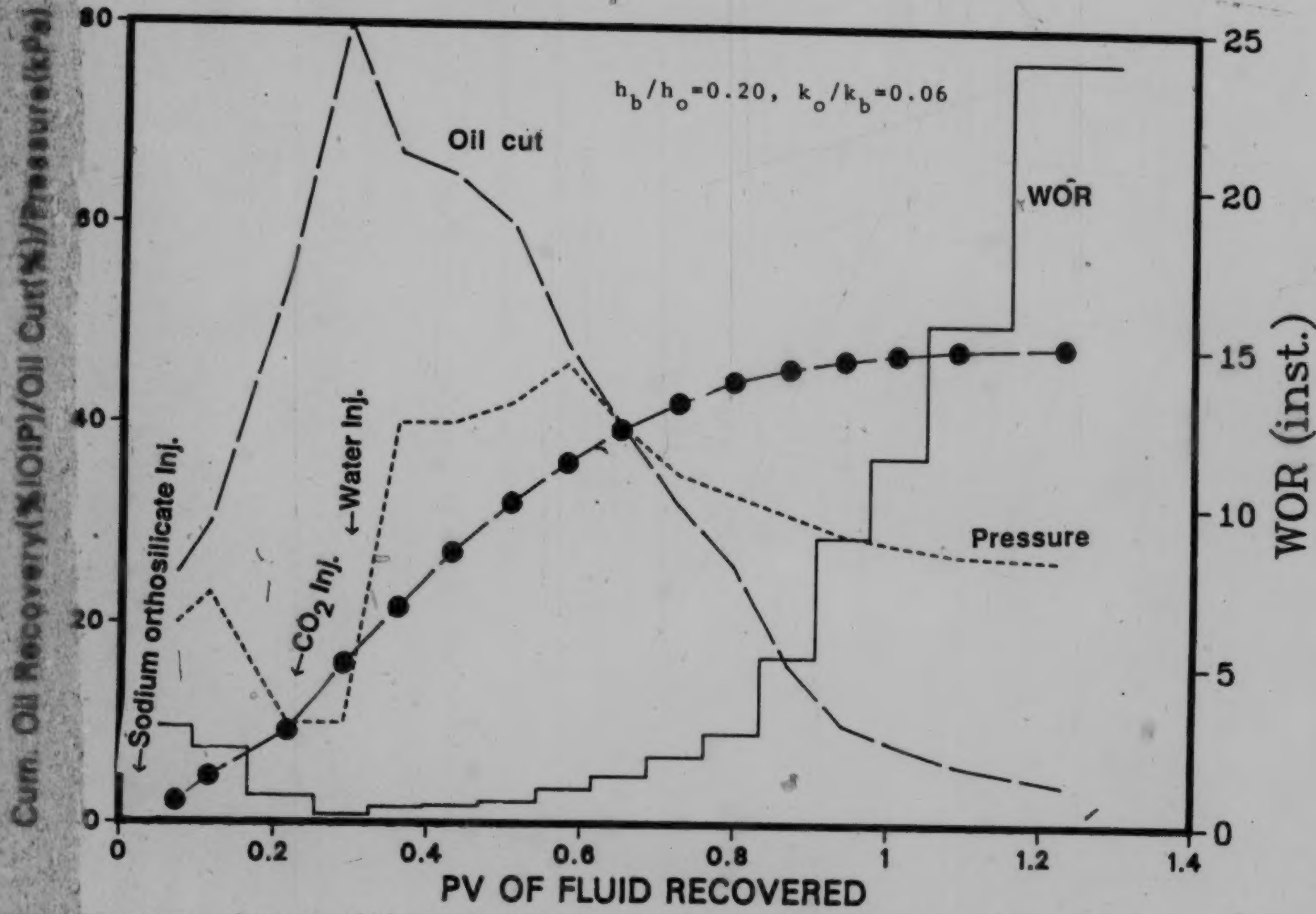

Fig. 75 CO_2 Activated Silica Gel Inj. and Waterflood Performance for Run 83

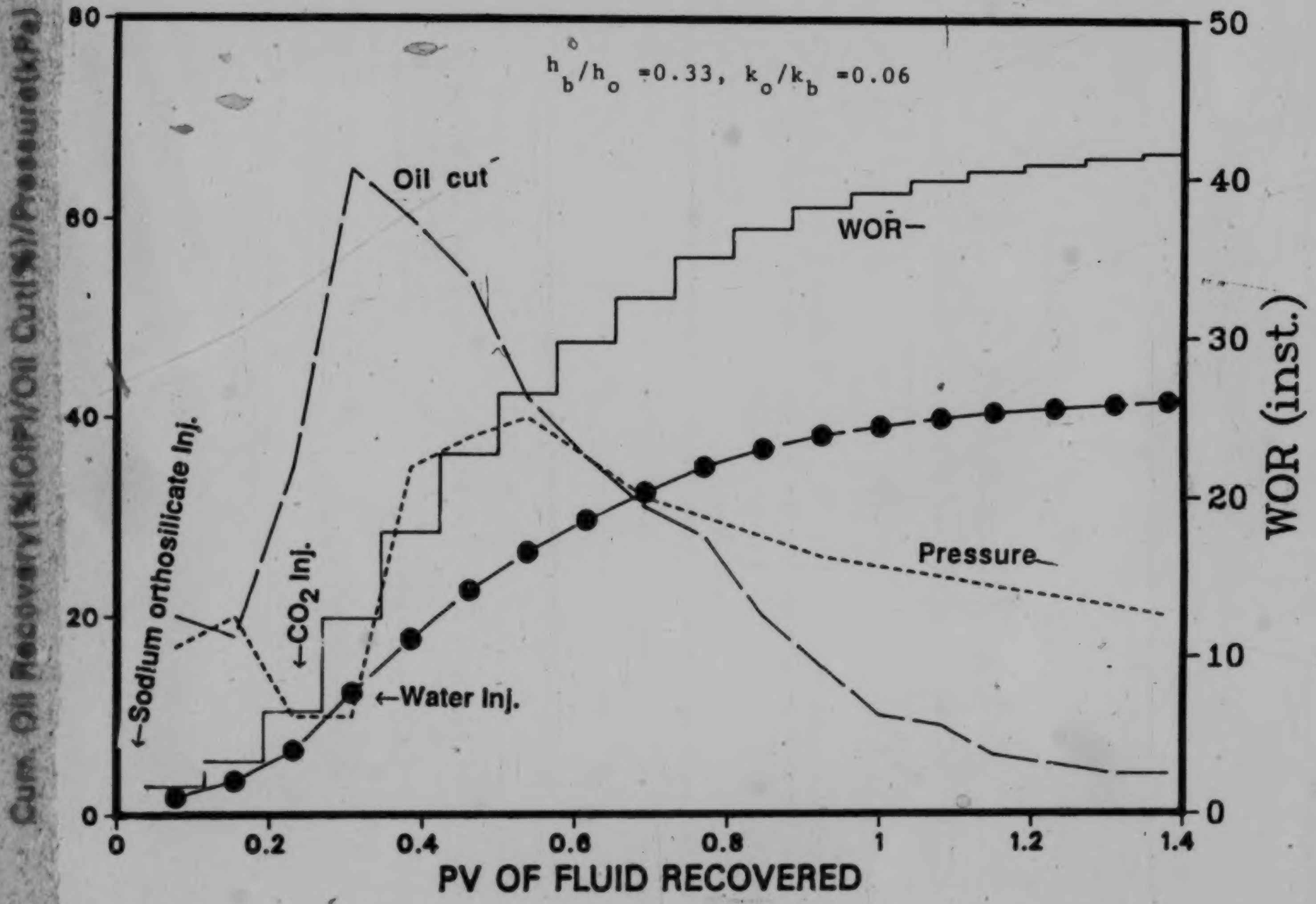

Fig. 76 CO_2 Activated Silica Gel Inj. and Waterflood Performance for Run 84

the end of the displacement test, a total of 41 percent of the IOIP was recovered. This indicated more than an eight-fold improvement over a conventional waterflood.

Run 85: h_b/h_o= 1.0, k_o/k_b= 0.06

In order to examine the effect of a thick and very permeable bottom-water zone Run 85 was conducted. This run had the most adverse conditions for a waterflood and a conventional waterflood gave only two percent of the IOIP for this run. Therefore, it was of particular interest to see the silica gel performance for this run. Initially, a 0.06 PV slug sodium orthosilicate solution was injected through the injection well. This injection point was chosen for the injection of mobility control agent for every run with an h_b/h_o of 1. Figure 77 depicts the WOR, oil cut, pressure and oil recovery performance for this run. At the end of the displacement test, a total of 38 percent of the IOIP was recovered. This indicated a 19-fold improvement over a conventional waterflood. Only polymer solution injection gave this high improvement.

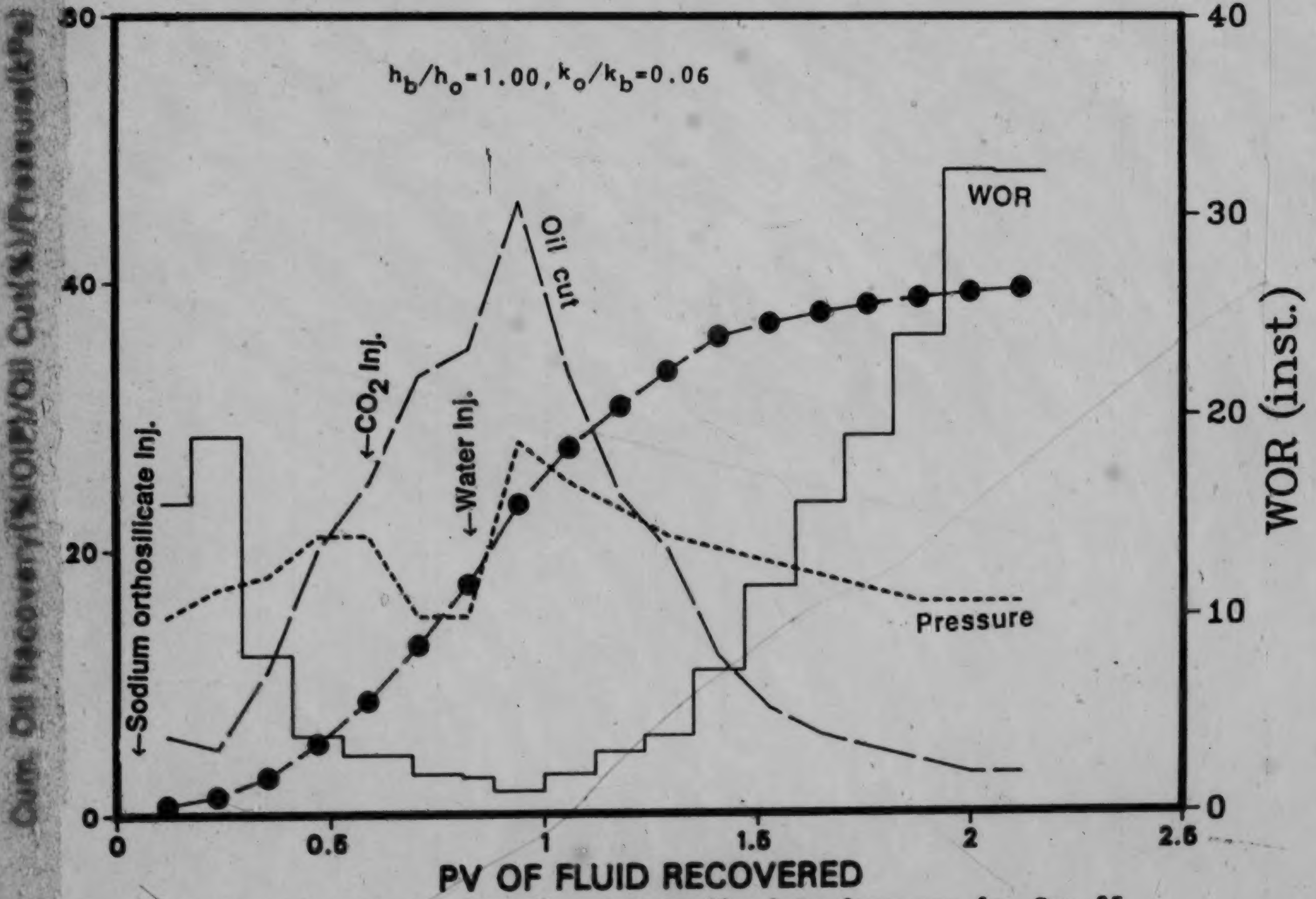

Fig. 77 CO_2 Activated Silica Gel Inj. and Waterflood Performance for Run 85

6. EXPERIMENTAL RESULTS AND DISCUSSION

Displacement tests were carried out with water and different mobility control agents, such as polymer, emulsion, air, gel, foam etc. A total of 85 different runs were conducted to test the effectiveness of each mobility control agent with permeability, relative oil-to-water layer thickness, oil viscosity, etc. as variables. These runs will be discussed under different sections according to the mobility control agent used.

6.1 Waterflood

Runs 1, 2 and 14 were conducted with a single-layer sandpack. As well, a waterflood was carried out in Runs 3 through 14 and 25 at the initial stage of the displacement in the presence of a bottom-water zone. These runs enabled examination of waterflood performance in a homogeneous sandpack as well as in the presence of a bottom-water zone.

6.1.1 Waterflood in a Homogeneous Pack

Runs 1, 2 and 14 were conducted with a single-layer sandpack. This provided the waterflood performance in the absence of a bottom-water layer. These runs were used to obtain the reservoir performance under base conditions enable comparison of the results with those with a bottom-water layer. Initially, waterfloods in homogeneous packs were conducted to determine the volumetric injection rate that would establish a pseudostable (Islam and Bentsen, 1987) regime. Runs 1 and 2 were conducted in a smaller core holder (2.54cm x 10.16cm x 30.5cm) at waterflooding rates of 400 ml/hr and 800 ml/hr, respectively. A flow rate of 500 ml/hr was used in Run 14 which was conducted in a larger core holder (7.26cm x 5.08cm x 122cm). The theoretical predictions of water breakthrough were made using a newly developed theory (Sarma and Bentsen, 1987). In order to calculate the instability number, the effective pseudointerfacial tension, σ_e has to be known. This value was taken from a recent publication (Islam and Bentsen, 1986) that reported the effective pseudointerfacial tension for a fluid/rock system similar to that of the present study. An estimation of k_{wr} and k_{or} was made in Run 1. These values were used to calculate the instabilitity numbers listed in Table 6.1. As can be seen from Table 6.1, all of these runs gave breakthrough recoveries very close to that which one would expect in the pseudostable flow regime. Even though some earlier researchers (Demetre et al., 1982) have pointed out that the pseudostable flow regime should start from an instability number of 900, recent studies have shown that, for a high mobility ratio (around 30), the breakthrough oil recovery becomes independent of the flow rate at a lower value of the instability number. Therefore, it is expected that theoretical (in the pseudostable flow regime) and experimental breakthrough points are similar for

TABLE 6.1 Breakthrough Recovery and Instability Numbers for Waterflood Runs

Run no.	Mobility Ratio	Actual Water bt(PV)	Theoretical Water bt (PV)	Instability No., I_{sr}
1	13.5	0.26	0.244	160
2	13.5	0.24	0.244	300
14	12.0	0.27	0.26	350

an instability number of around 300. The pseudostable flow regime is most likely to prevail in a field displacement and is marked by insensitivity to volumetric injection rate. Therefore, by using volumetric injection rates of around 400 ml/hr, a waterflood displacement in the field can be modelled. Consequently, a volumetric injection rate of 400 ml/hr was chosen for the waterflood runs. Note that there is no existing theory which is capable of predicting the stability boundary in a mixed system (e.g. polymer, water and oil), especially in the presence of a bottom-water zone. Moreover, pseudodilatancy of polymer flow had to be considered to determine the flow rate for polymer injection.

6.1.2 Waterflooding in the Presence of a Bottom-Water Zone

A waterflood was carried out during the initial stages of Runs 3 through 14 and 25 in the presence of a bottom-water zone. These runs had different h_b/h_o and k_o/k_b values. The detailed characterstics and results of these runs are listed in Table 6.2.

6.1.2.1 Effect of Water-to-Oil Zone Thickness and Permeability Ratio

Figure 78 compares oil recovery curves for different h_b/h_o values and for a k_o/k_b of 1. The effect of the oil-water zone thickness ratio is evident from this figure. For h_b/h_o values of 0.2 and 1.0, the WOR increased monotonically. However, for h_b/h_o values of 0.33, the WOR

TABLE 6.2: Waterflood Recovery Performance of Different Runs

Run no.	Water bt (%PV)	Rec. at WOR=5 (%IOIP)	μ_o/μ_w	h_b/h_o	Rec. at WOR=20 (%IOIP)
1	26	43	50.	0.00	64
2	24	31	"	0.00	N.Av.
3	0	0	"	1.00	3*
4	0	7.5	"	0.33	20
5	0	10	"	0.20	31
6	0	18	"	0.33	30
7	0	12	"	1.00	25
8	0	0	"	0.33	5
9	0	0	"	0.20	7
10	0	0	"	1.00	2*
11	7.5	56	1.0	0.33	61
12	6	35	7.5	0.33	41
13	0	0	200.	0.33	2*
14	27	40	50.	0.00	64
25	16.0	0	50.	0.25	4

* Initial WOR > 20

N.Av. abbreviation for Not Available

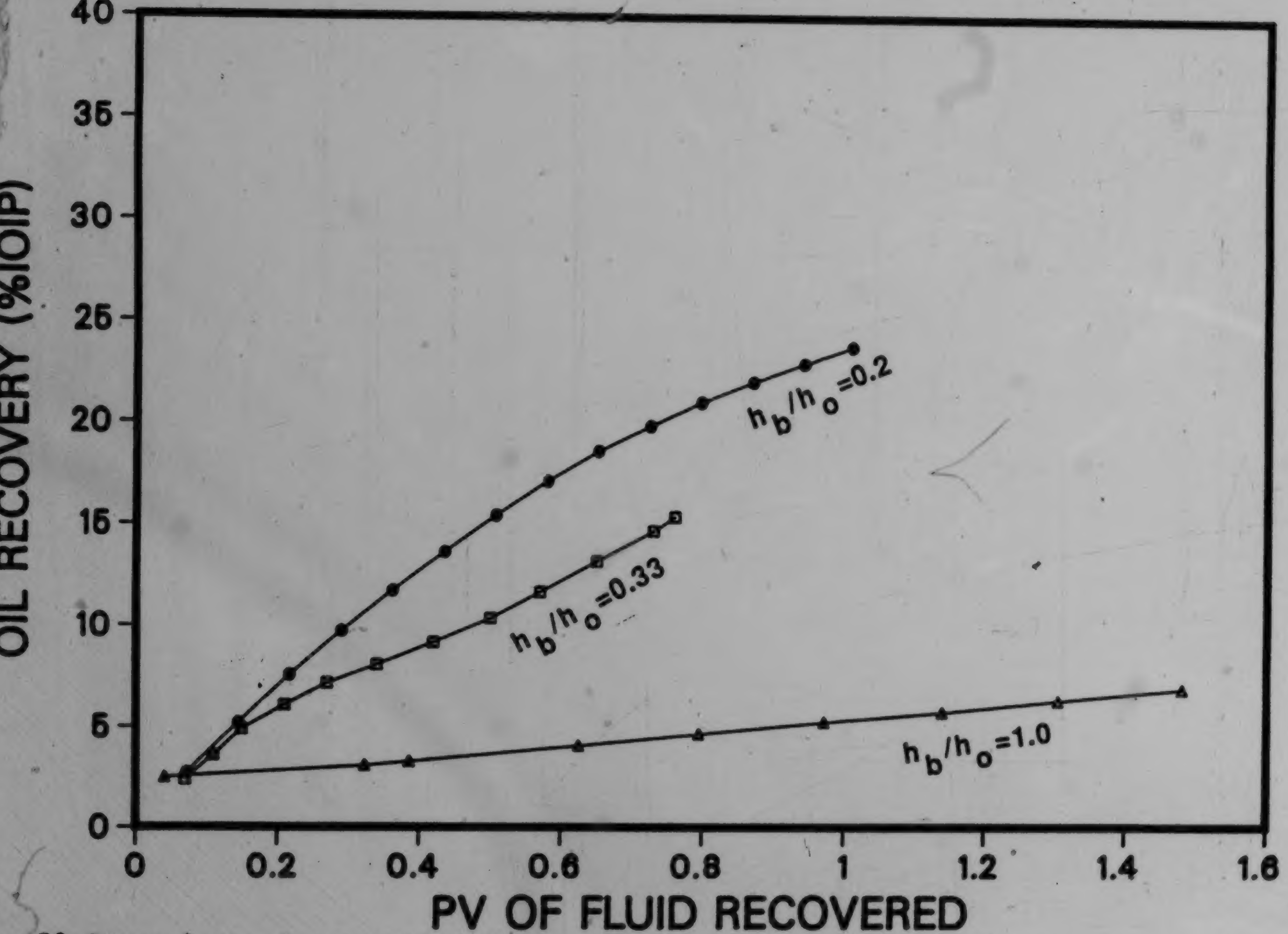

g. 78 Comparison of Waterflood Recovery for Different h_b/h_o and k_o/k_b=1 increased initially, then decreased slightly until a polymer flood was initiated. The increased slope at the later stage of the run with h_b/h_o= 0.33 is due to this anomalous WOR behaviour. The decrease in WOR takes place at around 0.30 PV of water injection. This value would correspond to water breakthrough in a homogeneous pack. As no tracer was used, no distinction was observable between injected and connate water (from the bottom-water zone) production. However, it is likely that the WOR continues to increase until the water front reaches the vicinity of the producing well. At this point the oil bank formed in front of the water front starts being produced and thereby decreases the WOR. A water-oil zone thickness ratio of 0.2 is too small to exhibit such a behaviour as the displacement is very close to that of a homogeneous pack for which the WOR increases monotonically. On the other hand, h_b/h_o=1.0 is so high that an oil bank is not formed ahead of the water front.

Figure 79 depicts oil recovery curves for different h_b/h_o values for k_o/k_b=0.06. These were the most unfavourable flooding conditions studied. The effect of h_b/h_o can be seen from this figure. However, a high bottom-water zone permeability led to so much channeling of the injected water that the ultimate recoveries for these runs did not reach beyond 10 percent of the IOIP. A further effect of the bottom-water zone permeability can be seen from Figure 80 which compares oil recovery for h_b/h_o values

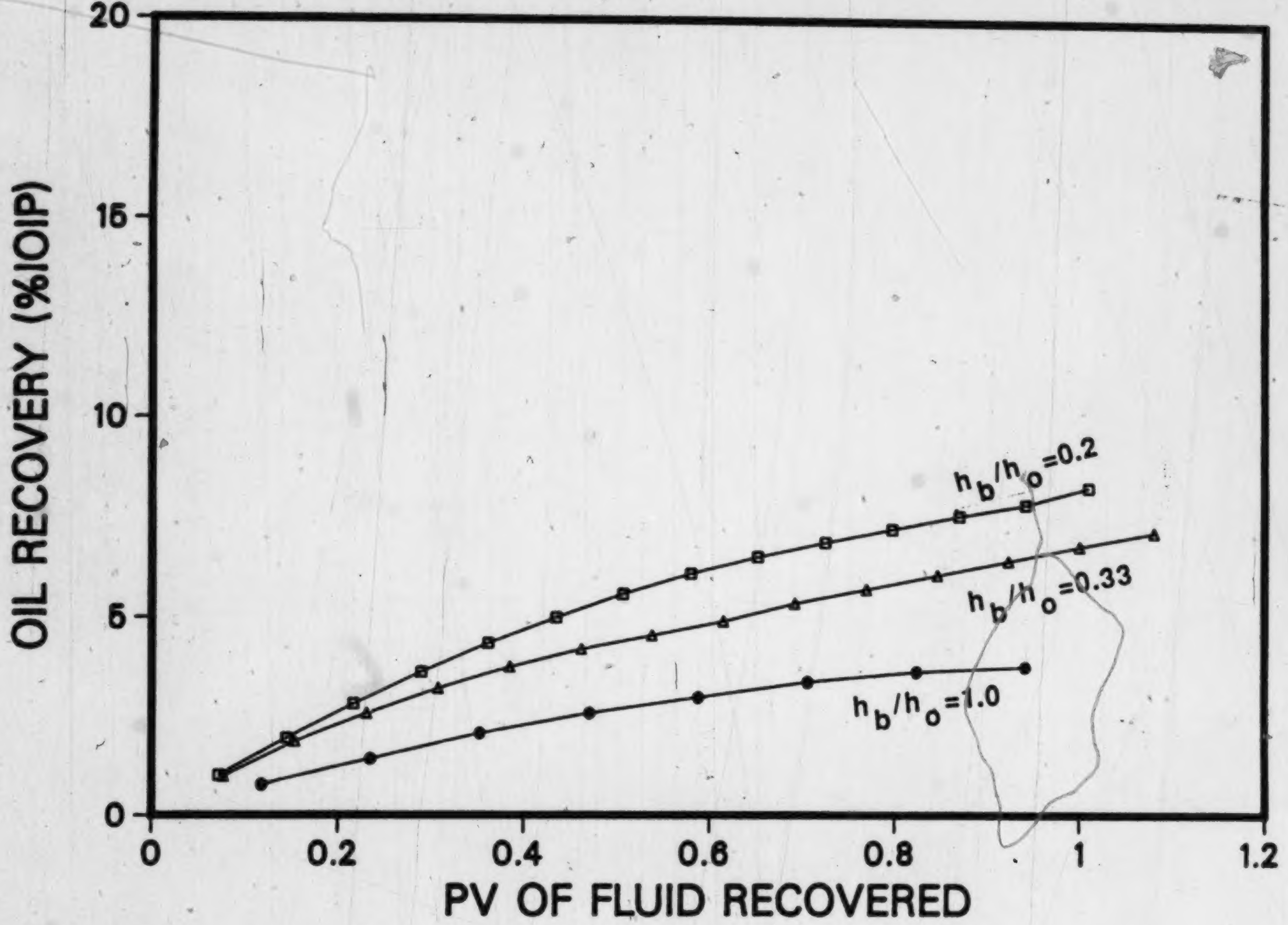

Fig. 79 Comparison of Waterflood Recovery for Different h_b/h_o and k_o/k_b=0.06

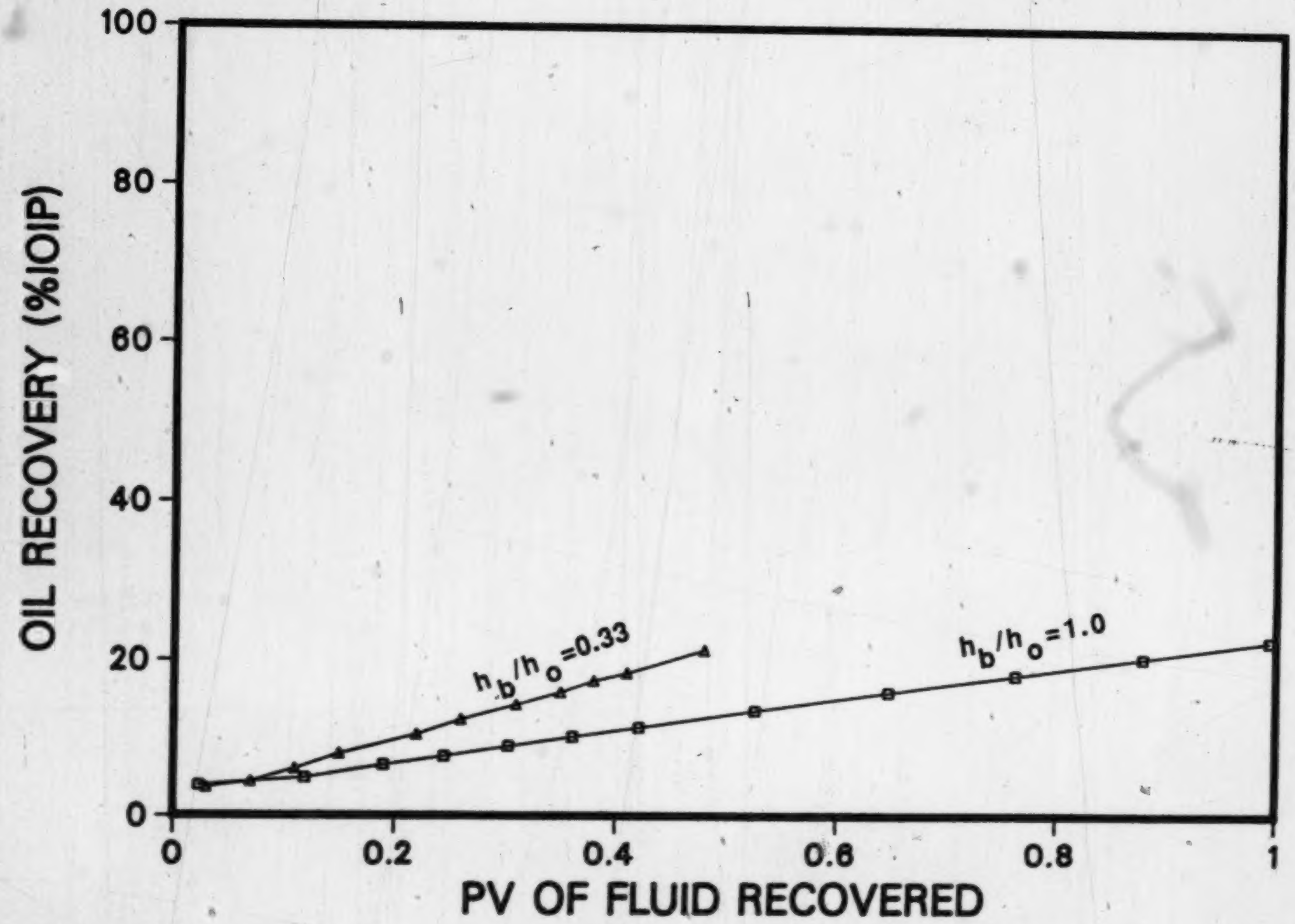

Fig. 80 Comparison of Waterflood Recovery for Different h_b/h_o and k_o/k_b=2.67

of 0.33 and 1 for a k_o/k_b of 2.67. For this set, WOR values did not increase monotonically. A tighter bottom-water zone led to much lower cross-flow between the layers, and the water front could not follow a particular saturation distribution pattern, and consequently, a monotonic increase in WOR was not observed.

Table 6.2 compares oil recoveries at a WOR of 5 and 20 for different waterflood runs. It can be seen in this table that water production started at the initiation of the waterflood for all the runs except for the homogeneous packs or the ones with lower oil viscosity (7.5 and 1.0 mPa.s). For unfavourable bottom-water conditions the oil recovery at a WOR of 5 was nil.

Ultimate oil recoveries for various waterflood runs are depicted in three-dimensional form in Figure 81. As can be seen from this figure, the oil-to-water zone permeability ratio has a significant impact on waterflood recoveries for $h_b/h_o=1$. For this case the ultimate recovery shows a many-fold improvement for $1.0 \leq k_o/k_b \geq 2.67$. The higher water-oil zone thickness ratios show a different trend. For $h_b/h_o \leq 1.0$ the oil recoveries increase rapidly with increasing values of k_o/k_b for $k_o/k_b \leq 1.5$. However, these oil recoveries are almost insensitive to k_o/k_b values which are greater than 1.5. For $h_b/h_o=1.0$ the oil recoveries show a different trend. They are less sensitive to k_o/k_b values at the lower range of these ratios, and increase very

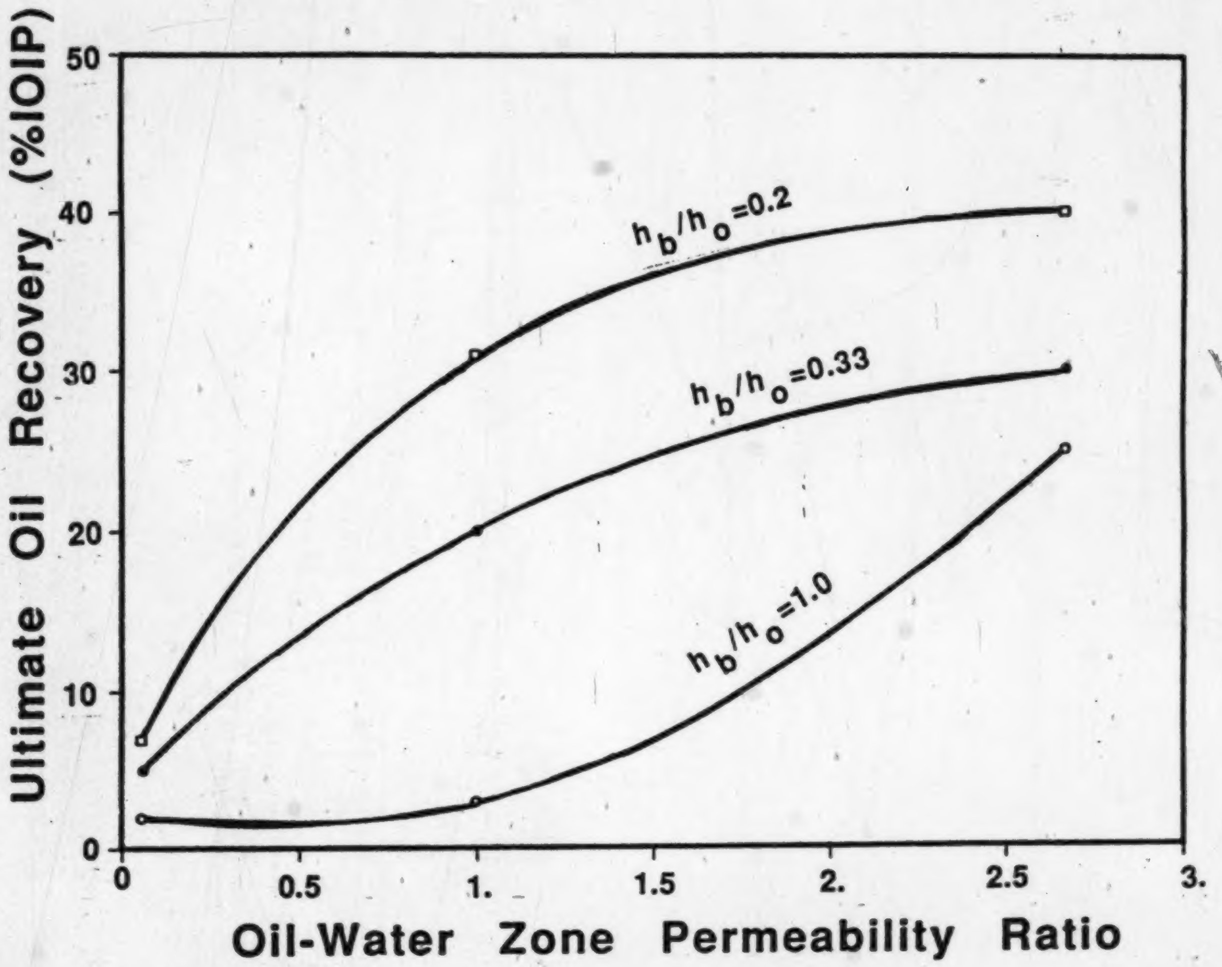

Fig. 81 Waterflood Performance as a Function of k_o/k_b and h_b/k_o

rapidly for increasing k_o/k_b values which are greater than 1.0. For this particular value of h_b/h_o, k_o/k_b has to be significantly higher to obtain a reasonable waterflood recovery.

Sensitivity to h_b/h_o for a particular value of k_o/k_b is depicted in Figure 82. The waterflood oil recovery is very poor for all displacements of k_o/k_b=0.06 even though some improvement takes place in the range of $0.2 \leq h_b/h_o \geq 0.33$. For k_o/k_b=1, a sharp decrease takes place for increasing h_b/h_o especially in the range of $0.2 \leq h_b/h_o \geq 0.33$. The ultimate recovery is much less sensitive to h_o/h_b values for k_o/k_b=2.67. This indicates that for k_o/k_b= 2.67, waterflood oil recovery would not depend so much on the thickness of the bottom-water zone, as the cross flow between layers is dictated by k_o/k_b.

The effect of k_o/k_b and h_b/h_o is also depicted in Figure 83. In this figure, the oil recovery for a homogeneous pack (h_b/h_o=0) is also included. This figure shows a comparison of oil recoveries for various k_o/k_b and h_b/h_o values.

6.1.2.2 Effect of Viscosity Ratio

Figure 84 compares waterflood oil recoveries for different oil-water viscosity ratios. All of these results were obtained for h_b/h_o=0.33 and k_o/k_b=1. As can be seen from this figure, the waterflood performs better for lower oil-water viscosity ratios. At the other extreme, the oil

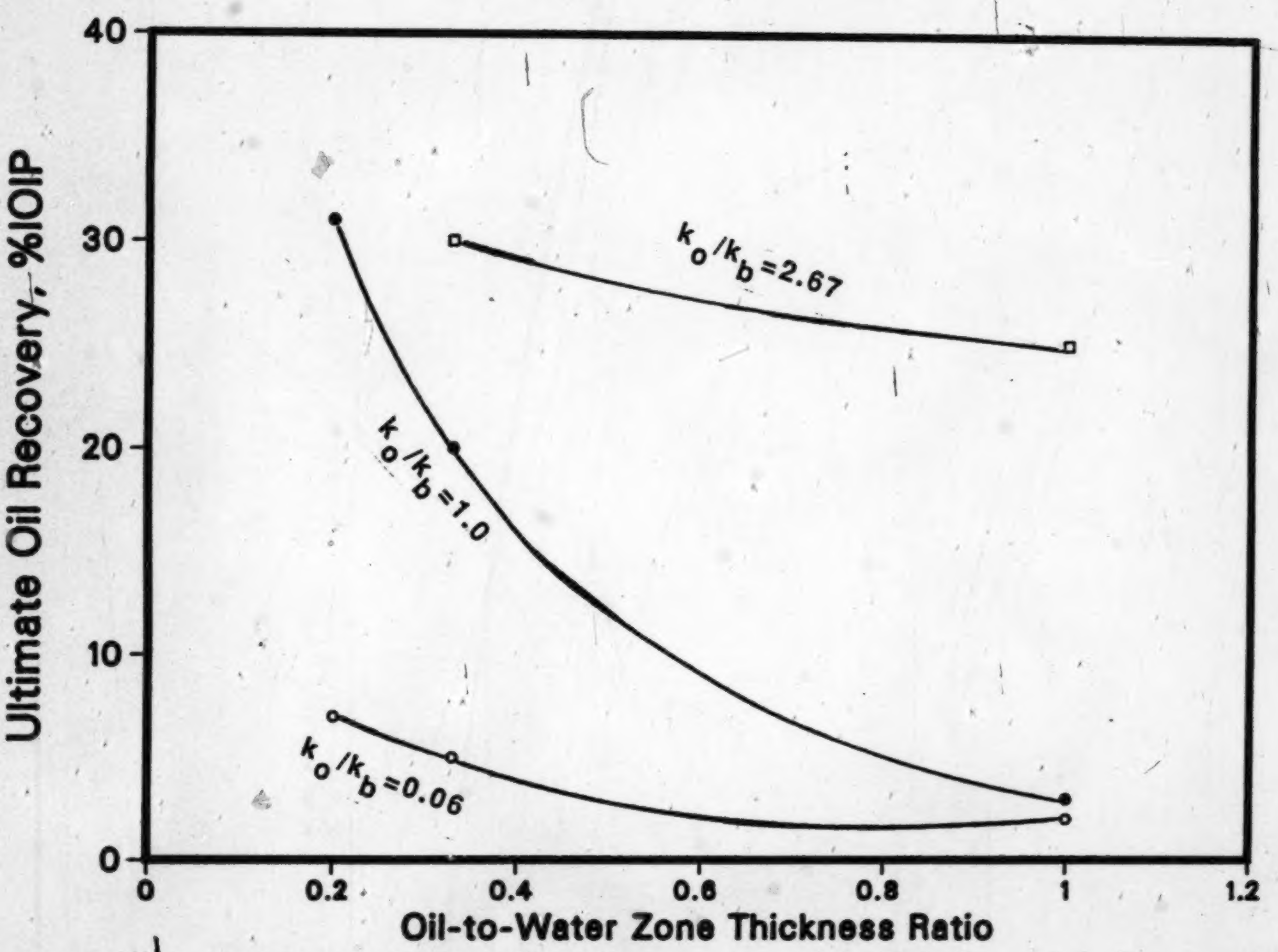

Fig. 82 Comparison of Waterflood Performance as a Function of h_b/h_o and k_o/k_b

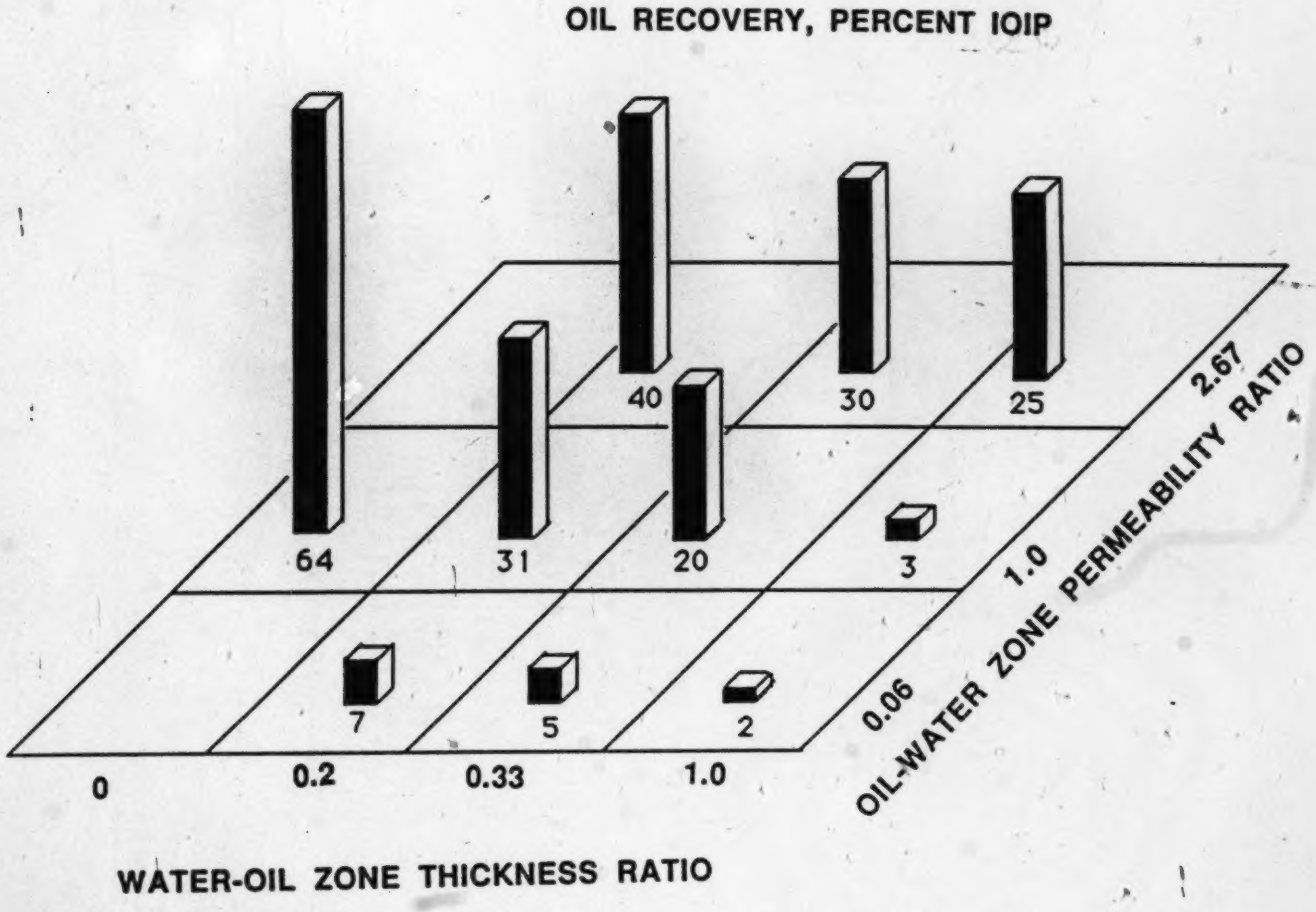

Fig. 83 Waterflood Recovery for Different h_b/h_o and k_o/k_b

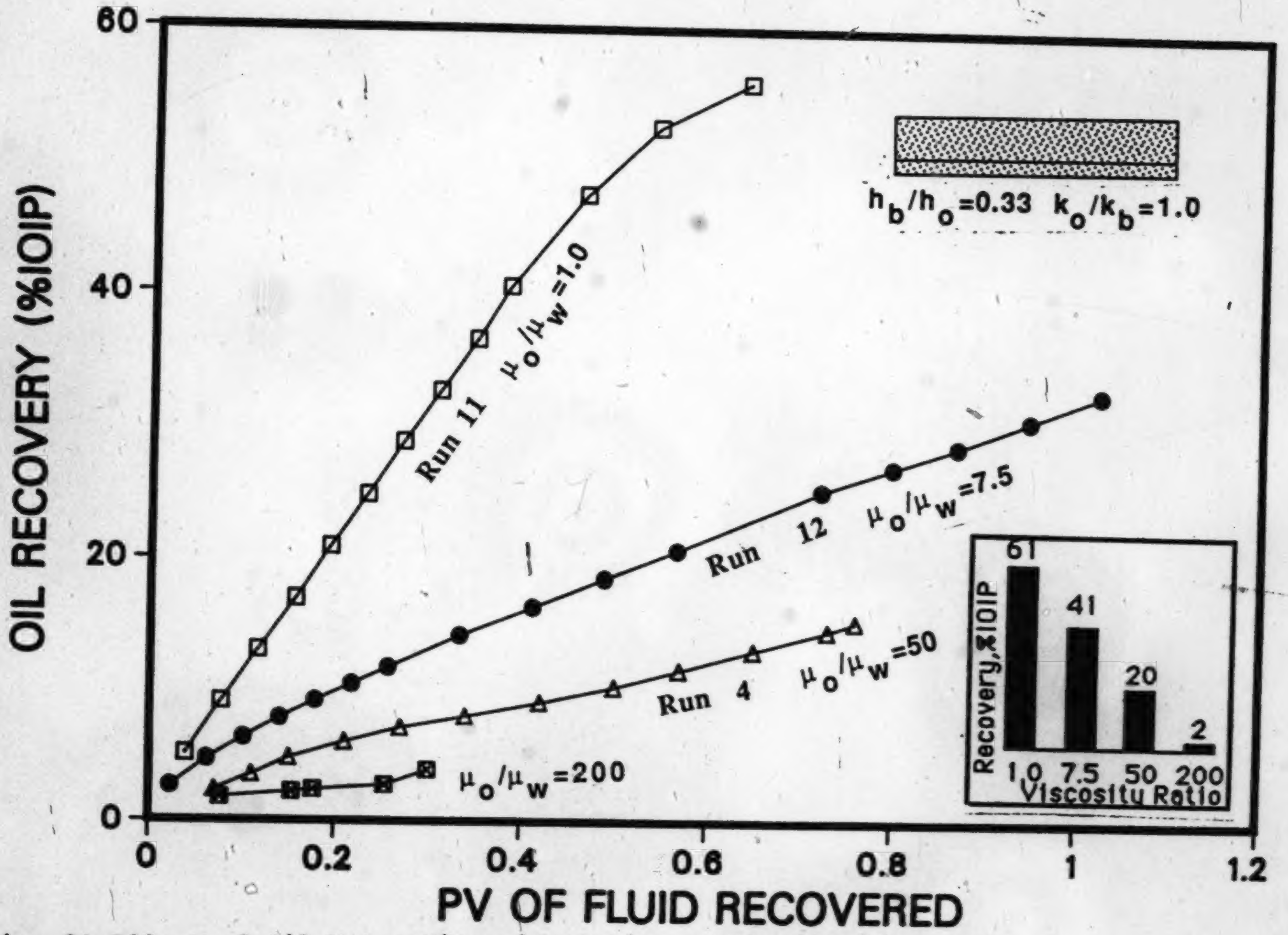

Fig. 84 Effect of Oil-Water Viscosity Ratio on Waterflood Recovery

recovery is extremely poor for a viscosity ratio of 200. As the viscosity ratio increases, the waterflood performance becomes poorer. Ultimate recoveries for these runs are depicted in the inset figure. As can be seen from the inset figure, only two percent of the IOIP was recovered for a viscosity ratio of 200. Also, the oil recovery drops quickly with increasing oil-water viscosity ratio showing the ineffectiveness of a waterflood in the presence of a bottom-water zone for higher oil-water viscosity ratios.

6.2 Waterflood with Polymer Slugs

Polymer slug runs were conducted in Runs 3 through 23 and 25. For Run 3 through 14 and 25, the polymer flood was initiated following an initial waterflood. The polymer injection points for these runs are listed in Table 5.2. For Runs 3 through 13, a polymer slug size of approximately 0.60 PV of the bottom-water zone was chosen. However, the effect of polymer slug sizes was investigated for $h_b/h_o=0.33$. Table 5.2 lists the polymer slug volumes for the different runs. In order to obtain better access to the bottom-water zone, polymer slugs were injected through the inlet end (rather than the injection well) for runs with $h_b/h_o<1$. For the thicker bottom-water zone ($h_b/h_o=1$), it was considered unnecessary to inject polymer through the inlet end as most of the injected fluid readily channeled through the bottom-water zone. For these runs the injection well was used for injecting polymer solution. The flood rate for polymer injection was chosen such that the polymer flow through the porous media remained higher than the lower limit of pseudodilatancy (Smith, 1970). This would prevent shear thinning of the polymer solution. However, thinning due to the presence of injected and connate water was expected. Several interesting phenomena were observed in different runs. They will be discussed in the following chapter.

6.2.1 Polymer Flood in a Homogeneous Pack

Run 15 was conducted to examine the effect of a continuous polymer flood in a homogeneous porous medium. A volumetric injection rate of 400 ml/hr was used for this run. This run was characterized by early water breakthrough. During the initial stages only water (not polymer) was produced. The initiation of the polymer flood led to a decrease in irreducible water saturation. This is a phenomenon that had to be taken into account while numerically simulating polymer floods. Actual polymer breakthrough took place at 0.3 pore volume of the oil zone. If polymer/oil and water/oil interfacial conditions are assumed to be the same, breakthrough of the displacing fluid at 0.3 pore volume is too early even if the displacement is pseudostable. In fact, in a homogeneous pack polymer does not improve oil recovery as much as it should from viscosity considerations alone. In a homogeneous pack the sweep with polymer flood is not as high as it would be if a different fluid with the same viscosity (a fluid that is not adsorbed by the solid surface) were used. This is due to the fact that the polymer solution is adsorbed in the porous medium and its viscosity decreases as it propagates along the length of the core. Besides, the existence of inaccessible pore volume leads to a part of the oil being trapped. However, these same qualities of polymers contribute to a remarkable improvement in performance as compared to a waterflood in the presence of a bottom-water zone.

6.2.2 Delay in Response

During injection of a polymer solution the injection pressure increased drastically as compared to that for a waterflood. Even though the pressure response was immediate, no improvement (over a waterflood) in oil cut was observed immediately. For every run, a delayed but sudden increase in oil cut was observed following the injection of the polymer slug. Table 5.2 lists the delay in response for polymer runs. The delays (in percent PV) are plotted against the oil-water zone thickness ratios for the different values of k_o/k_b in Figure 85. It is evident from this figure that a thicker bottom-water zone leads to a greater delay. Note that for all the runs a polymer slug of 0.60 PV of the bottom-water zone was injected. That is, the

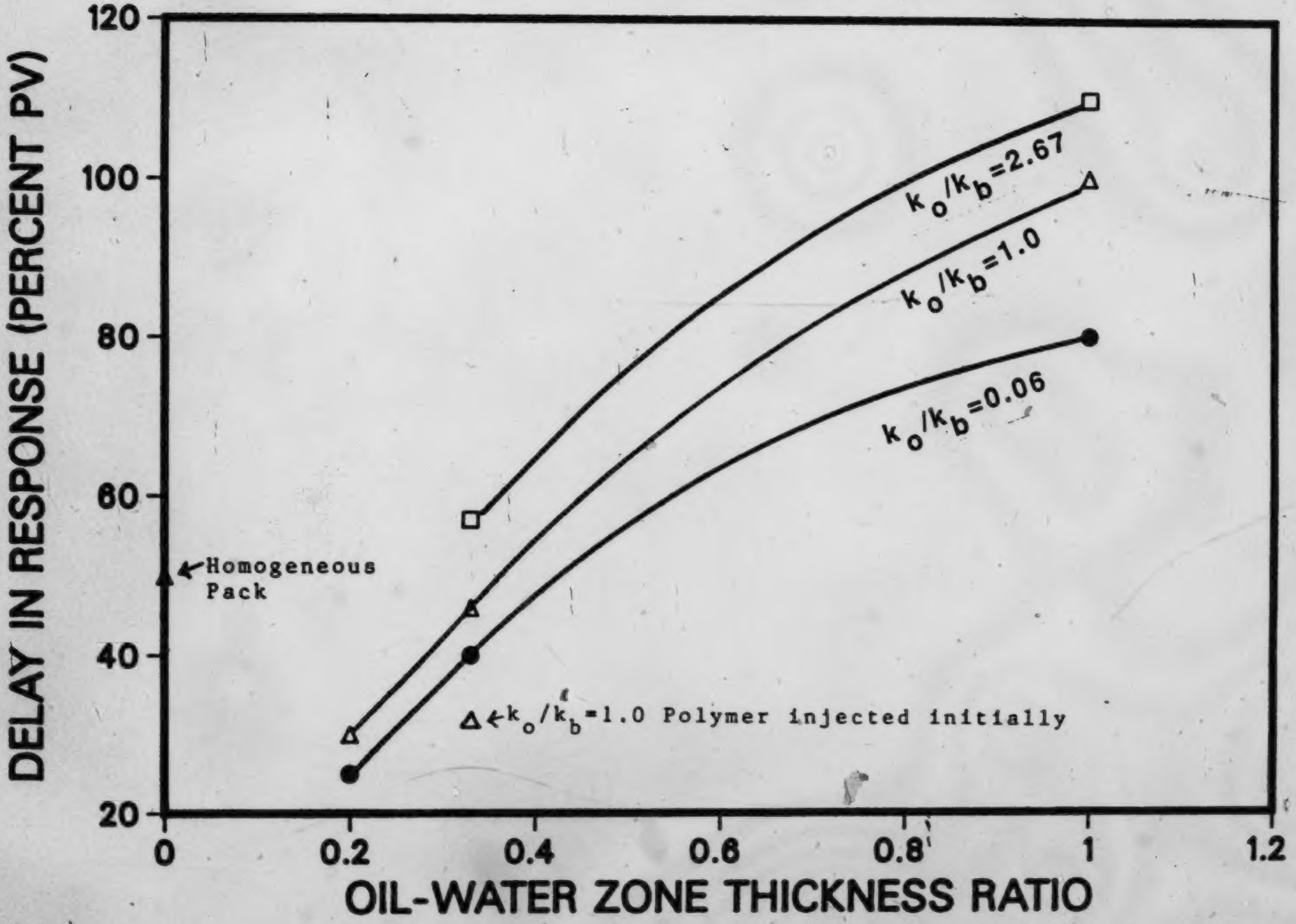

Fig. 85 Delay in Recovery Response (% PV) as a Function of h_b/h_o and k_o/k_b

polymer slug volume increased in proportion to the thickness of the bottom-water zone. In practical terms, even though a longer delay is expected for thicker bottom-water zones, the delays may be acceptable if considered in terms of the bottom-water zone pore volume, PV_b. This trend is evident when the same points are plotted as a fraction of PV_b as shown in Figure 86. This figure shows that a thicker bottom-water zone leads to a quicker response and only 0.80 PV_b of total fluid has to be injected before the oil cut starts showing an improvement. On the other hand, thinner bottom-water zones took as high as 1.7 PV_b before showing the same response. Note also that for all the cases the delay in response varies between 0.80 PV_b and 1.7 PV_b. This indicates that a large volume of the total fluid (not necessarily the polymer slug volume) has to be injected before any response in oil cut is observed at the producing well. A larger slug size does not have much of an impact on decreasing the delay in response time. In fact, a quicker response is observed for smaller slug sizes because the water following the polymer slug propagates more quickly to distribute polymer solution (in a thinned form) along the length of the core. A larger polymer slug contributes to decreasing the severity of fingering. Therefore, water fingers take longer time to breakthrough the polymer slug. Consequently, the polymer-rich water fingers take longer time to reach the producing end leading to a delayed

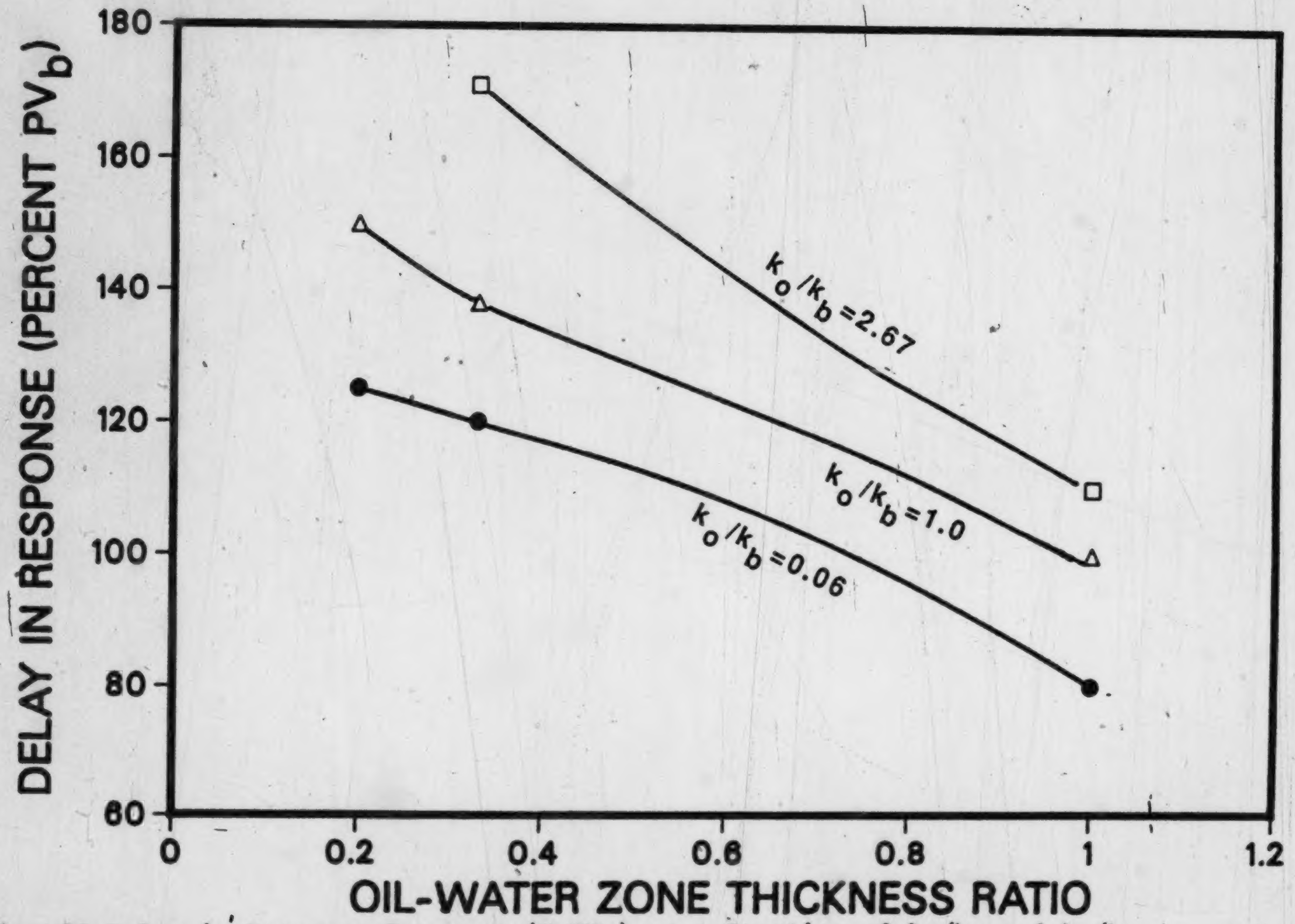

Fig. 86 Delay in Recovery Response (% PV_b) as a Function of h_b/h_o and k_o/k_b

response in oil cut. Figure 86 implies that only after the total fluid injection has reached a value of 1 PV_b, does the oil cut show a response. Indeed, recalling that the oil cut rises to more than 80 percent once the oil cut starts showing response and that such a high value may be obtained only in a homogeneous core, this is equivalent to blocking the whole bottom-water zone. Figures 85 and 86 also indicate that tighter bottom-water zones take a longer time to show a response in oil cut. A tighter bottom-water zone offers higher resistance to water flow and, therefore, delays the polymer solution distribution process during the waterflood that followed the polymer slug injection.

6.2.2.1 Mobility Control Mechanism with Polymer Flood

It has been shown by many researchers that polymer would be an excellent mobility control agent in view of the following properties:

- it reduces effective permeability to water without changing that to oil
- while injecting a polymer slug its high viscosity allows increased crossflow and the underrunning of the displacing fluid is diminished considerably.

As far as the second property is concerned, any viscous fluid would improve the recovery. This has been previously observed by Barnes (1962). However, the uniqueness of polymer lies in the first property, i.e., its ability to reduce the effective permeability to water without affecting the effective permeability to oil. In the literature, adsorption and mechanical entrapment have been mentioned as the basis for this particular property of polymers.

In order to examine the contribution of each of the above mentioned properties, Run 24 was conducted. In this run, a glycerine solution of 64 mPa.s viscosity was used as the mobility control agent. The packing characteristics were similar to those of Run 4. Also the slug size and injection point (after 0.76 PV of initial water injection) were the same for both runs. Figure 87 compares the oil recovery curves for Runs 4 and 24. As can be seen from this figure, the oil recoveries at the initial stage of the displacement are very similar. However, as the glycerine or polymer slugs were injected, polymer showed a quicker response in terms of increased oil cut. Also, as the waterflood continued after the injection of glycerine or polymer, the oil recovery with polymer was distinctly better than that with glycerine. This comparison showed clearly that polymer improves the oil recovery not only because it is more viscous than water but also because it has other properties that impede the flow of water to improve the oil recovery. At the end of the displacement test the injection of a polymer slug recovered about 20% more of the IOIP than that recovered with glycerine. Figure 88 depicts the relative contributions of the different mechanisms involved in polymer flooding.

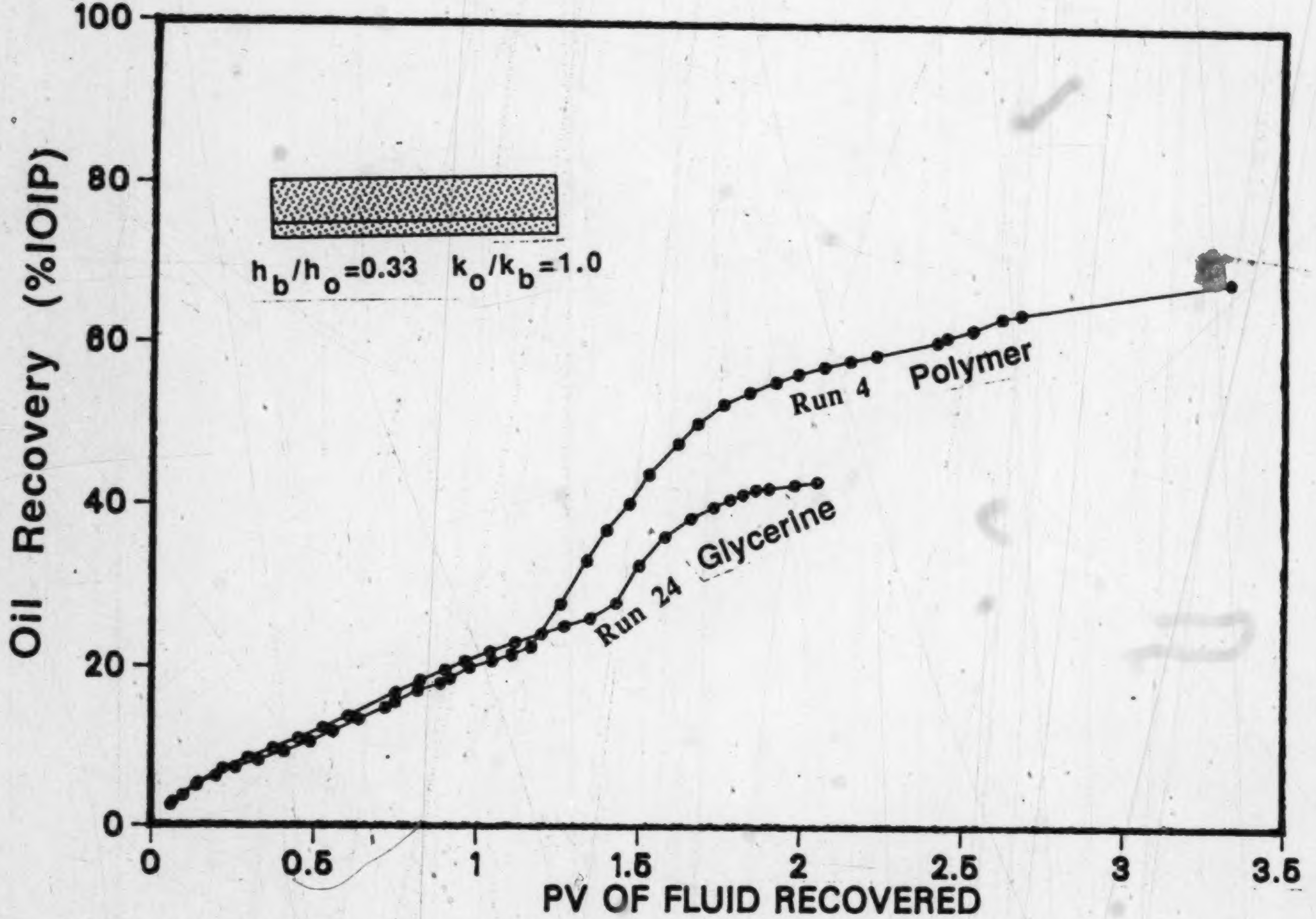

Fig. 87 Comparison of Oil Recovery by Polymer and Glycerine Injection

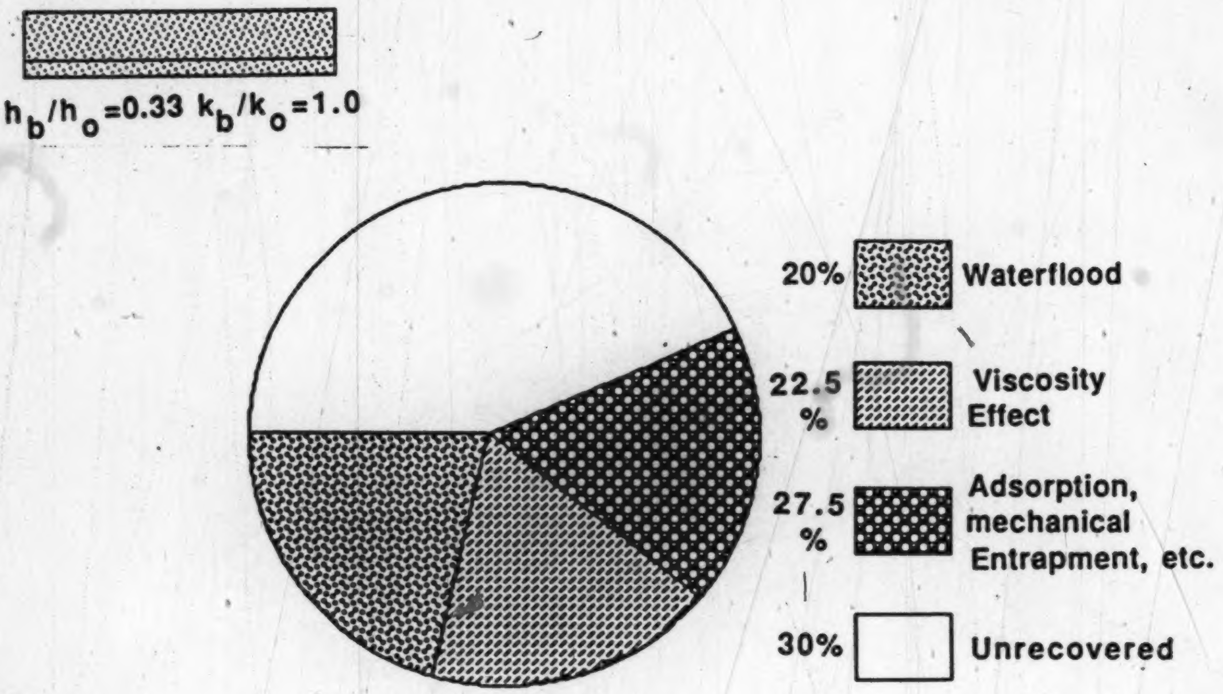

Fig. 88 Relative Contribution of Different Mechanisms Involved in Polymer Flooding

Polymer breakthrough points were monitored in Runs 14 to 23 and 25. It was observed that the peak in oil cut occurred just prior to polymer breakthrough. Following polymer breakthrough, the oil cut dropped quickly. However, a substantial amount of oil was produced for all runs before oil cut dropped considerably. This observation indicates that even though a polymer slug does not move as an entity, it does create blockage (in the bottom water zone) for the following waterflood, and as a consequence, water invades the oil zone to increase the oil cut by a significant amount. However, to see an improvement in the produced oil cut, a sufficient amount of water had to be injected so that the water front (presumably after fingering through the polymer slug) approached the production well. A sudden increase in oil cut at this point indicated that the bottom-water zone was completely inaccessible to the injected water. However, when the water containing polymer solution appeared at the production well, blockage of the bottom-water zone no longer occurred and watercut started to increase. Note that this phenomenon cannot be avoided by injecting a much larger polymer slug. This will be discussed in a later section where the effects of polymer slugs are discussed. Figure 89 shows polymer breakthrough as a function of polymer slug volume and polymer viscosity. All these points were obtained for Runs 16 through 23 for which h_b/h_o equalled 0.33 and k_o/k_b equalled 1. As can be

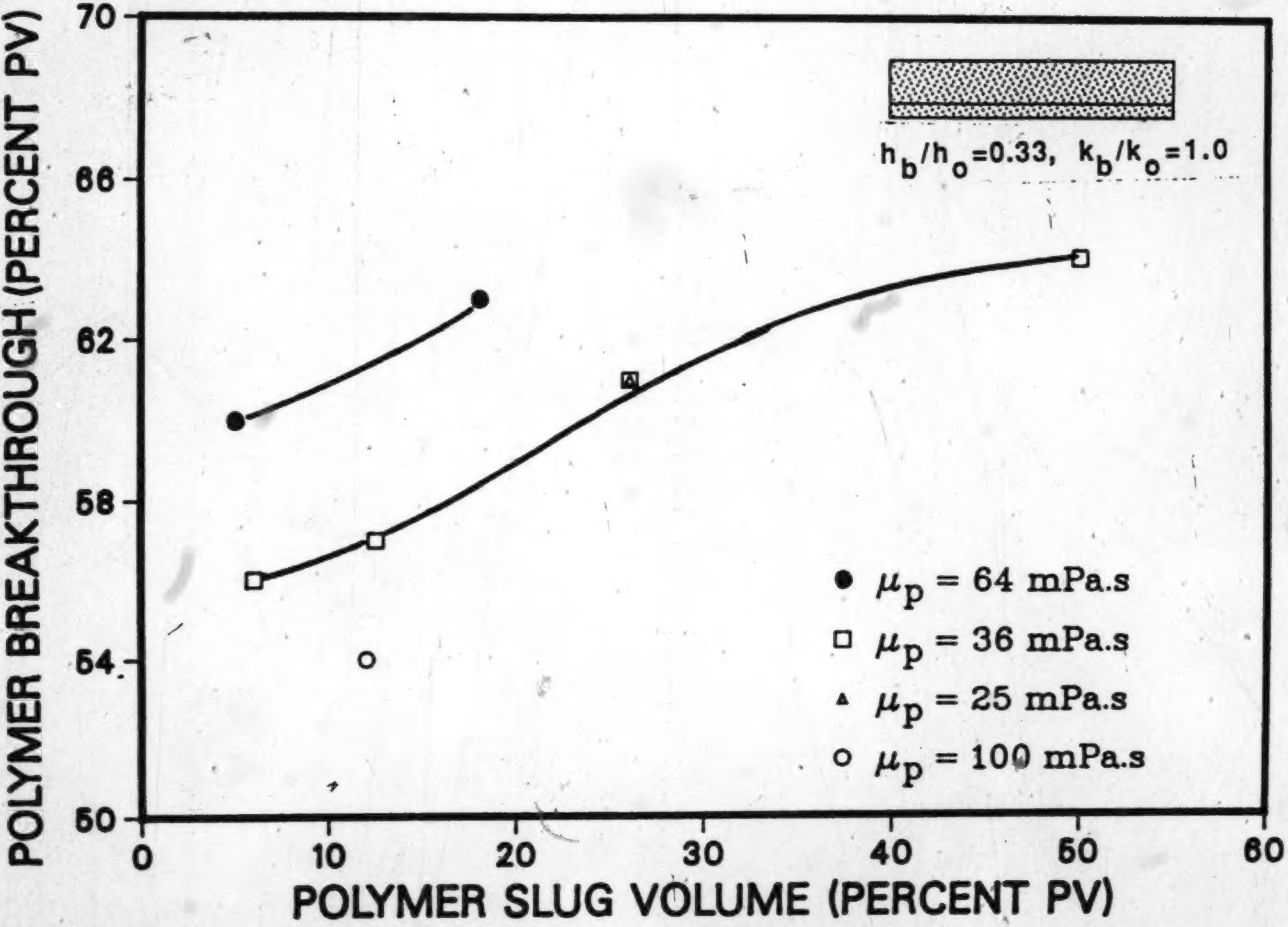

Fig. 89 Polymer Breakthrough as a Function of Slug Volume (h_b/h_o=0.33, k_o/k_b=1.0)

seen from Figure 89, the polymer breakthrough is delayed as the slug size increases. However, after increasing to a maximum at around 0.20 PV, the slope of the breakthrough vs. slug volume curve decreases gradually. Even though polymer breakthrough increased directly with polymer slug size, delay in response of the oil cut showed a different trend. The response was quickest (30% PV) for the six percent slug followed by a slug size of 26% PV (delay of 32% PV) and then for the 12.5% slug size (delay of 35% PV). Delayed polymer breakthrough was advantageous because, for most of the runs, a sharp decrease in oil cut was observed following the polymer breakthrough. This indicates that even though polymer slugs do not move as an entity, their presence in the porous medium is necessary to maintain blockage of the bottom-water zone. Moreover, polymer adsorption alone does not account for the decrease in effective permeability to water. However, even if polymer retention were much higher, the WOR would increase due to production of the injected water. Prior to polymer breakthrough, a sudden increase in oil cut took place indicating that the bottom-water zone was completely inaccessible to the injected water.

During water injection following polymer slug injection, the displacement was highly unstable. Due to the very high viscosity contrast, injected water fingered through the polymer slug (Coskuner and Bentsen, 1987). This was evident from the viscosity of the produced aqueous phase collected after polymer breakthrough occurred. A maximal viscosity of 7 mPa.s at six rpm for the produced aqueous solution was observed whereas the viscosity of the injected polymer was 64 mPa.s at six rpm. Figure 90 shows the variation in viscosity of the produced aqueous phase in Run 4 (after polymer breakthrough). An explanation as to why the producing aqueous phase viscosity vs. pore volume fluid recovered curve shows a maximum (Figure 90) follows. In the case of a continuous polymer inejection, the polymer adsorption rate is high during the initial stages of the displacement test. This increased adsorption rate leads to a lower polymer viscosity. However, as the displacement continues, the rock or sand surface becomes saturated with the polymer and the polymer adsorption rate decreases rapidly. Due to the above mentioned reason, the polymer concentration in the produced aqueous phase increases at the early stage of polymer breakthrough. Therefore, in the case of a continuous polymer injection the viscosity of the produced aqueous phase will assymptotically rise to the viscosity of the injected polymer. This phenomenon accounts for the initial increase in viscosity of the produced aqueous phase. In the case for which a certain amount of polymer slug is followed by a water slug, adsorption is not the only phenomenon that influences the viscosity of the produced aqueous phase. During water injection, the water fingers through the polymer slug due to a very high

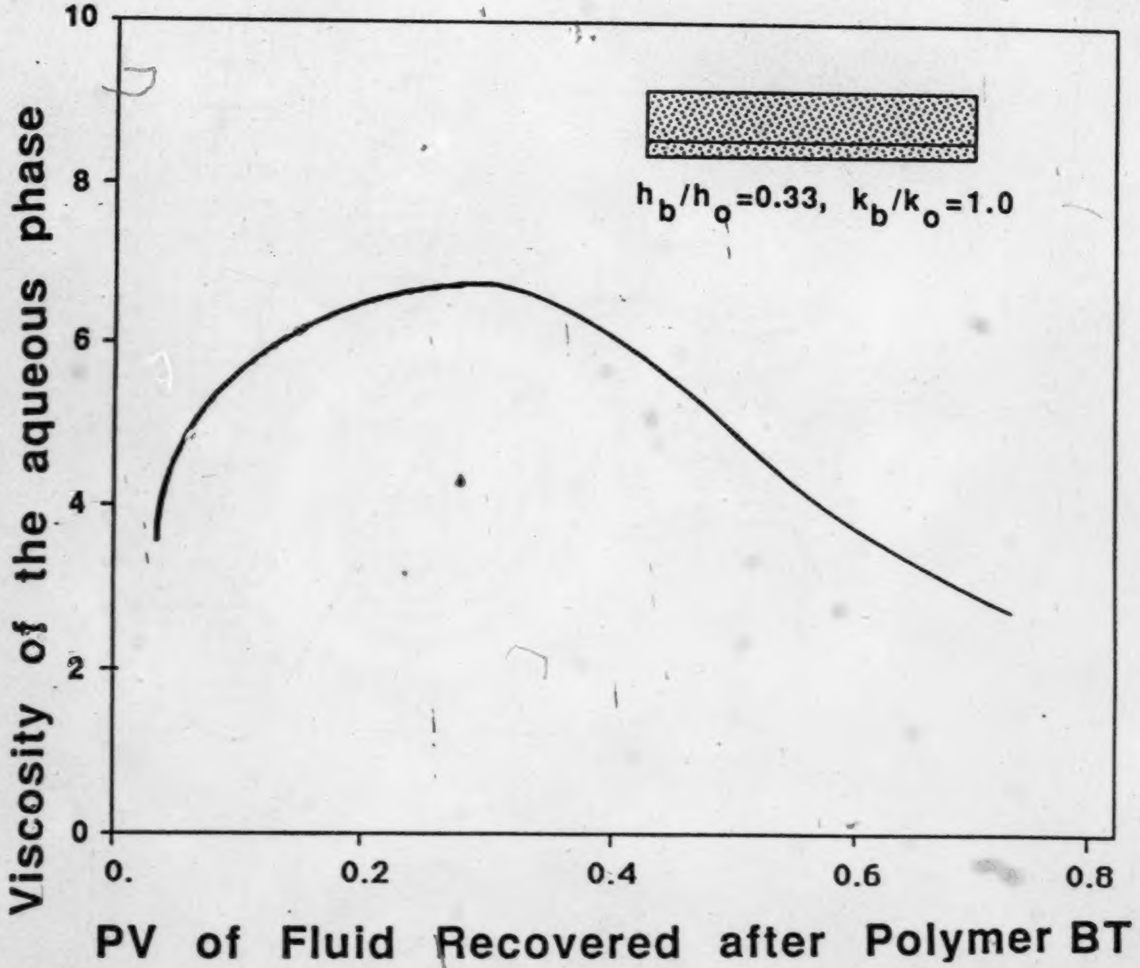

Fig. 90 Viscosity (in mPa.s) of the Effluent Aqueous Phase After Polymer Breakthrough

viscosity contrast between the polymer and the injected water. The severity of this fingering depends on the viscosity contrast between the polymer and water. As the water fingers propagate through the polymer slug, they are continously enriched with polymer due to dispersion. In this situation, however, the leading edge of water fingers is richer in polymer solution than is the trailing edge. Consequently, as the water fingers break through the producing end, the viscosity of the produced aqueous phase decreases asymptotically to the viscosity of water. This phenomenon accounts for the decreasing viscosity of the produced aqueous phase at the later stage of the displacement test. In this whole process, the polymer is also diluted by the bottom water. Consequently, the highest viscosity attained by the produced aqueous phase is only 7 mPa.s as compared to initial 64 mPa.s viscosity of the injected polymer.

6.2.3 Effect of Polymer Injection Point

To examine the effect of polymer injection points, Runs 14 and 15, and Runs 4 and 16 were compared. Runs 14 and 15 both were base runs without bottom water, whereas Runs 4 and 16 both had similar type and size of bottom-water zones. For Run 14, the displacement test was started with a waterflood and was continued until 1.2 PV of water had been injected. At this point a polymer slug of 0.45 PV was injected. This was again followed by a waterflood. For Run 15, polymer injection was started at the beginning of the displacement test and was continued until one PV of polymer had been injected. This was followed by a waterflood. Figure 91 compares Runs 14 and 15 along with Runs 4 and 16. As can be seen from this figure, the oil recovery was similar in Runs 14 and 15 during the initial stages (until 0.4 PV). However, due to a decreasing oil cut (during the waterflood), Run 14 showed poorer recovery performance as the displacement test continued. As shown in Table 3.2, the delays in response in terms of increasing oil cut after polymer injection were the same for these runs. However, polymer injection was initiated in Run 14 after a delay of 1.2 PV (as compared to immediate injection in Run 15). Consequently, there remains an initial period over which Run 15 showed better recovery than Run 14. But, as the displacement continued, the results of polymer injection started being felt and Run 14 showed better recovery. At the end of the displacement test, the ultimate oil recovery in Run 14 was 77 percent of the IOIP as compared to 74 percent of the IOIP in Run 15. This represents approximately four percent increase in oil recovery if injection of polymer is delayed.

Similarly, Runs 4 and 16 showed very similar oil recovery at the beginning of the test. Due to the quicker response to polymer injection (a delay of 0.3 PV only), Run

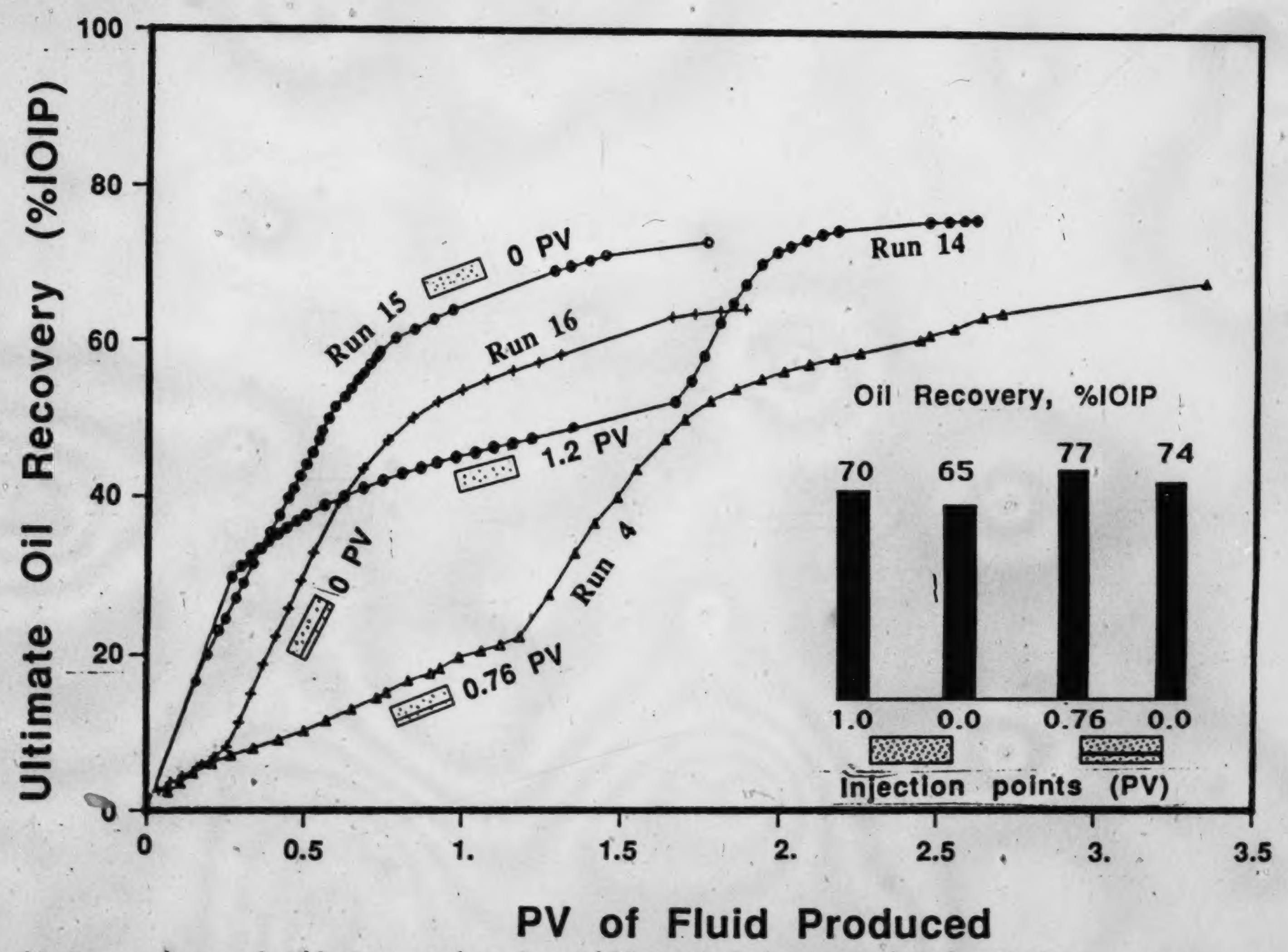

Fig. 91 Comparison of Oil Recoveries for Different Polymer Injection Points

16 showed better oil recovery performance. However, after injecting a polymer slug of 18 percent PV (same as that used in Run 16), a sharp increase in oil recovery in Run 4 started at 1.22 PV of total fluid injection. Following this, the oil recovery started improving in Run 4. Eventually, Run 4 showed an ultimate recovery of 70 percent of the IOIP as compared to 65 percent of the IOIP in Run 16.

Studying the results of both of these two sets of runs, it appears that delayed polymer injection led to a higher ultimate recovery for both reservoir models - with or without a bottom-water zone. However, the oil recovery performance by a waterflood for these runs is much better than that for runs with higher oil viscosity, or thicker bottom water, or higher bottom-water zone permeability. As a matter of fact, the WOR is so high for some of these latter cases that a waterflood cannot be continued and a polymer treatment should be started as soon as possible to bring the oil cut up to a reasonable value. For this reason, the effect of injection point was not studied for the cases for which the waterflood did not give any significant recovery.

Figure 85 shows the effect of polymer injection points on the delay in reponse for h_b/h_o=0.33. As can be seen from this figure, injecting polymer first and following it with a waterflood leads to a quicker response in oil cut. Apparently, injecting water prior to polymer creates a water channel at the producing end. Consequently, after polymer injection a larger volume of fluid has to be injected and the oil cut does not show any improvement until the aqueous solution containing thinned polymer reaches the producing well to prevent water channeling at that end. Such a phenomenon was not observed for a homogeneous pack (Runs 14 and 15) since no channeling from the bottom-water zone was involved.

6.2.3.1 Effect of Polymer Slug Size

Runs 17 through 21 were conducted with polymer of the same viscosity but different slug sizes. These runs had similar packing characteristics and bottom-water zone thicknesses. To be consistent in polymer injection point, polymer solution was injected at the beginning of each run. Injection of a polymer slug was followed by a waterflood. The polymer slug sizes were 12.5, 6.0, 26, and 50 percent PV in Runs 17, 18, 19, and 21, respectively. In Run 20, the size of the initial polymer slug was 5.0 percent PV. However, for this particular run a few more polymer slugs (six percent PV each) were each alternated with 0.5 PV slugs of water, injecting a total of 0.23 PV of polymer. Figure 92 compares the ultimate oil recoveries for all these runs. As can be seen from this figure, for smaller polymer slugs, the ultimate oil recovery increases linearly as the slug size increases. However, for higher values, the improvement is less pronounced. The shape of the ultimate oil recovery

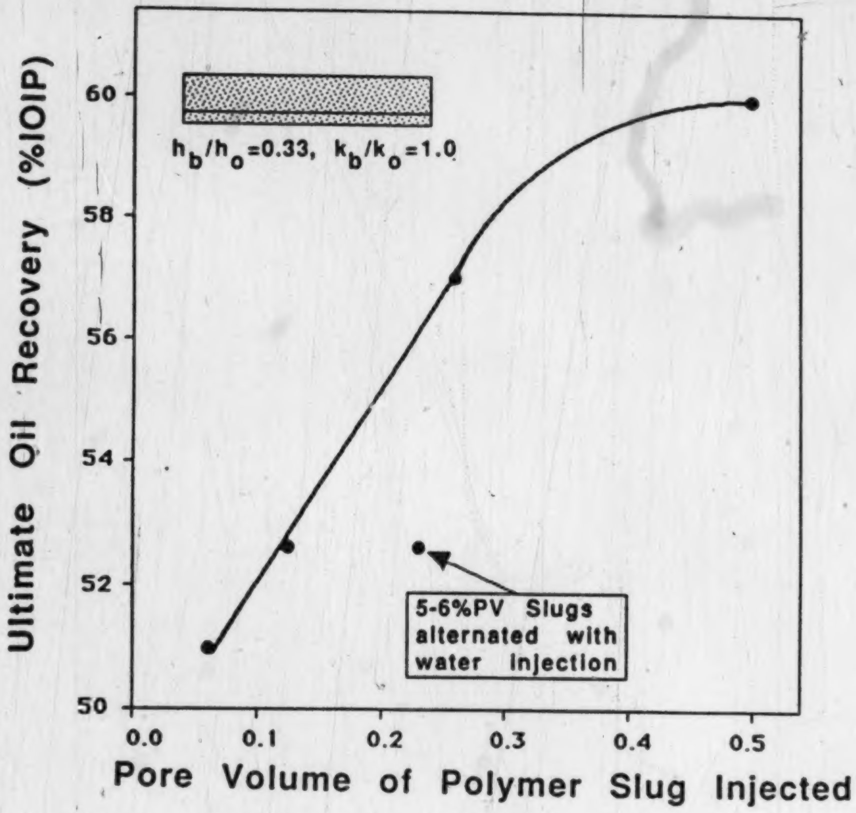

Fig. 92 Effect of Polymer Slug Size on Ultimate Oil Recovery (h_b/h_o=0.33, k_o/k_b=1.0)

vs. polymer slug size is explained in the following. The injection of a water slug following a polymer slug is dominated by viscous fingering. The severity of the fingering depends on the dC/dz value, where C is the concentration and z is the distance in the axial direction of flow. By taking an average concentration (across the fingers) for a given point, it may be concluded that the dC/dz value decreases for larger slug sizes. Consequently, the severity of viscous fingers decreases with increasing polymer slug sizes, leading to a higher displacement efficiency by water. This phenomenon explains the rapid increase in the ultimate oil recoveries for larger polymer slugs at the initial stages. However, as the slug size becomes larger, the dC/dz value asymptotically decreases to that of a continuous polymer injection (for which case dC/dz=0) and the oil recovery becomes insensitive to the slug size. At the extreme case of continuous polymer injection, the ultimate recovery is limited to the irreducible oil saturation, inaccessible pore volume (Duda et al., 1981), etc. In this context, it is prudent to choose an optimal polymer slug size for which the dC/dz value is substantially low and yet the slug volume is economical. Such a point will be located where the slope of the ultimate oil recovery vs. slug size curve starts decreasing rapidly. In this regard, a 0.25 PV (or 0.75 PV_b) of polymer slug may be considered optimal. The recovery performance is the lowest in Run 20 for which the polymer slugs were alternated with water. Even though a total of 0.23 PV of polymer was injected (at a total fluid injection of one PV), because the polymer solution was injected by alternating with waterflood, the oil recovery remained substantially poorer than that for all other runs. Polymer breakthrough occurred at 57, 56, 61, 60, and 64 percent PV in Runs 17 through 21, respectively. As can be seen from Table 5.2, at the time of breakthrough, much more oil was produced with a 0.125 PV slug as compared to that produced with six percent slug, whereas the increase obtained by more than a 100 percent increase in slug size did not have much of an impact. The breakthrough point becomes insensitive to the slug size for higher slug sizes. Run 20 showed that alternating polymer slugs with water slugs does not perform well as only 53 percent of the IOIP was recovered for a total polymer slug volume of 0.23 PV.

Figure 93 compares the oil recovery for the above runs as a function of the WOR. The WOR values are recorded once they started increasing monotonically. Figure 93 indicates that during initial stages of the flood oil recovery is not sensitive to the slug size. However, during the later stages of the displacement 6% and 12.5% slugs give very similar recoveries, as did the 26% and 50% slugs. Figure 93 shows clearly that for the larger slug sizes the recovery becomes independent of slug size.

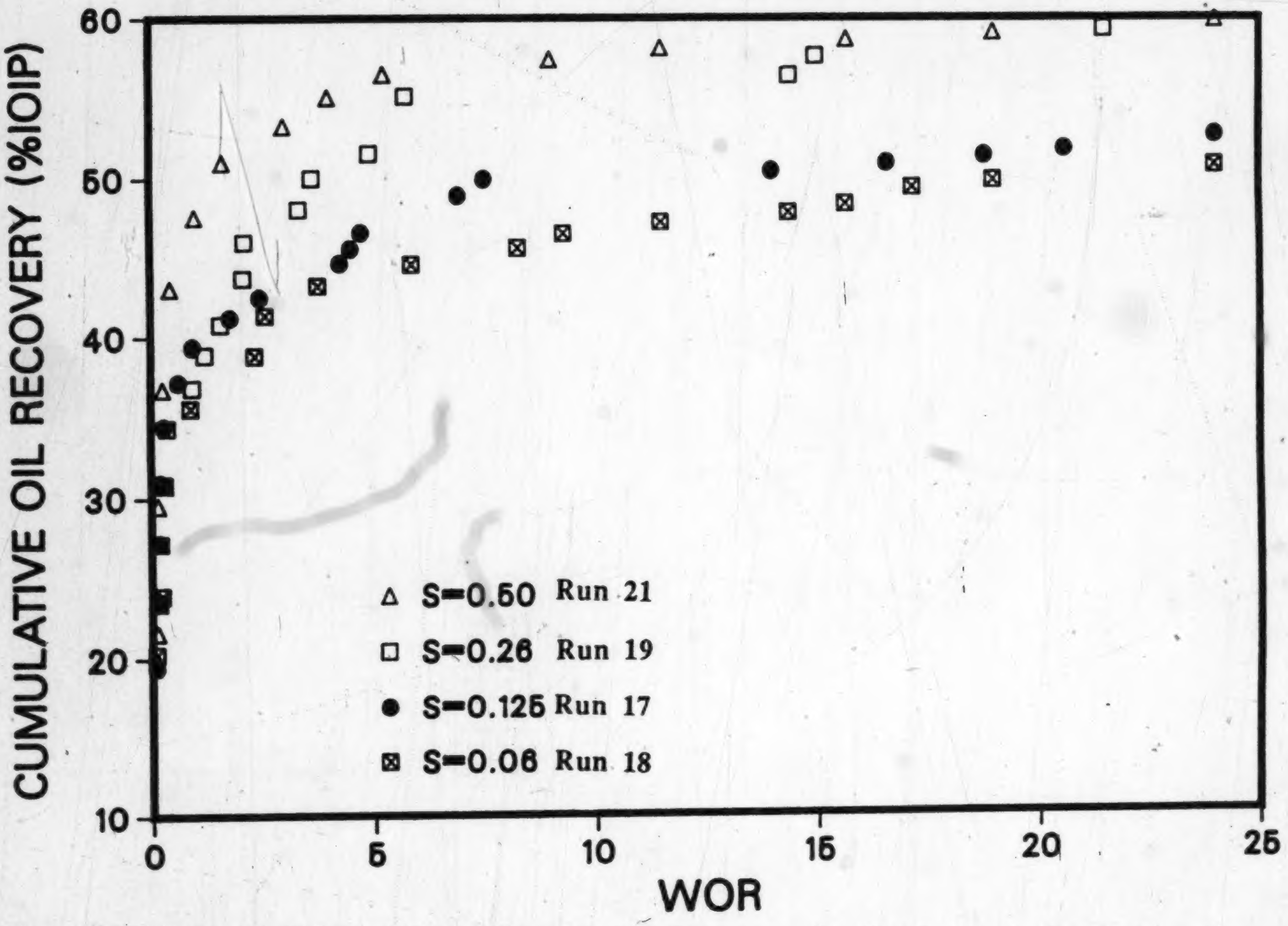

Fig. 93 Effect of Polymer Slug Size on Oil Recovery (h_b/h_o=0.33, k_o/k_b=1.0)

6.2.3.2 Effect of Polymer Viscosity

Runs 16, 19, 22, and 23 were conducted to examine the effect of polymer viscosity. The polymer used had viscosities of 25, 36, 64, and 100 mPa.s in Runs 22, 19, 16, and 23, respectively. Runs 19 and 22 both had a polymer slug size of 0.26 PV whereas Run 16 had a slug size of 0.18 PV. For all these runs, polymer solution was injected at the beginning of the displacement test. The comparison among recovery performances for the different runs is shown in Figure 94. The recovery performance was quite similar for Runs 19 and 16 until about one PV of fluid was injected. The recovery for Run 22, for which the lowest polymer viscosity was used, was lower than that of the other two runs. Note that the amount of polyacrylamide used for Runs 16, 19, and 23 was the same, yet the recovery was considerably better in Run 16. Of lesser significance, but still worthy of note, is the fact that, as can be seen from Table 5.2, polymer breakthrough occurred at 61, 61, 63, and 54 percent PV for Runs 22, 19, 16, and 23, respectively. Interestingly, even though the polymer breakthrough occurred at the same point for Runs 22 and 19, 38.5 percent of the IOIP was recovered in Run 19 whereas 34 percent of the IOIP was recovered in Run 22. Run 16 showed the highest oil recovery at the time of polymer breakthrough. As can be seen from Table 5.1, the maximal recovery at WOR=20 occurred in Run 16. This was followed by Runs 19 and 22. A large

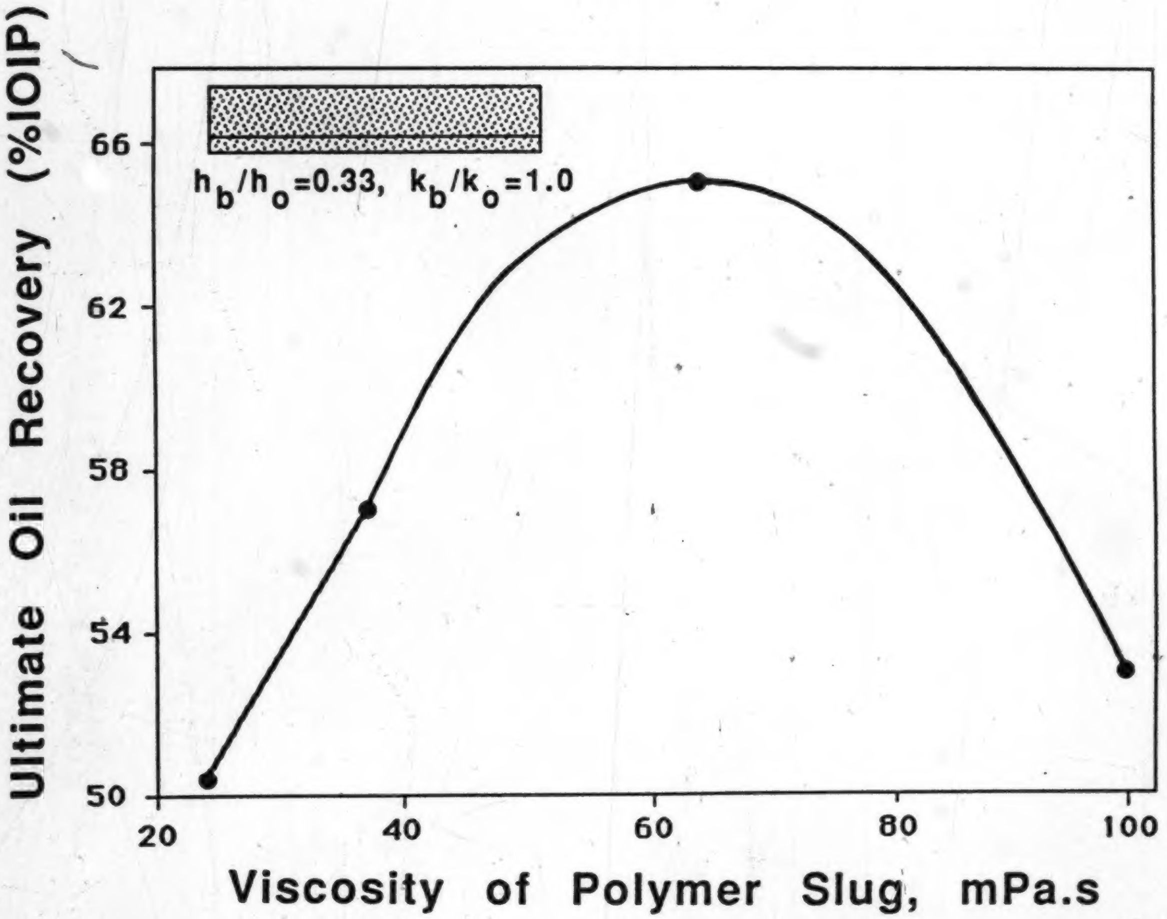

Fig. 94 Effect of Polymer Viscosity on Ultimate Oil Recovery (h_b/h_o=0.33, k_o/k_b=1.0)

decrease in ultimate oil recovery is observed for Run 23 for which a very high polymer viscosity contributed to an early improvement in polymer flood performance. From all these perspectives, the recovery performance appears to be best for Run 16 with a polymer viscosity of 64 mPa.s. An explanation as to why a 64 mPa.s viscosity polymer recovers the most oil follows. In a displacement the viscosity ratio of the displacing and displaced fluids plays an important role. In such a case, a high viscosity ratio of the displacing and displaced fluid is desired. In this regard Run 16 (μ_p/μ_o=1.28) should give better oil recovery than that for Run 19 (μ_p/μ_o=0.72). However, even though Run 23 (μ_p/μ_o=2) should give a higher recovery than that observed for the other runs, Run 23 gives the lowest oil recovery. This low recovery is due to an increased number of viscous fingers which grow while displacing the polymer slug with the water slug. Indeed, in a system where two displacement fronts are involved (one polymer and oil and another water and polymer), high viscosity of polymer gives rise to two competing phenomena. At the leading edge the high viscosity of the polymer enhances the recovery, while at the trailing edge the viscosity of the polymer results in viscous fingers which decrease the sweep efficiency. These competing phenomena give rise to an optimum for a polymer viscosity of 64 mPa.s. Since there is no existing theory that predicts the stability of such a complex system, the optimal value of the polymer viscosity cannot be determined theoretically. However, the existence of such an optimum has been shown experimentally.

6.2.3.3 Effect of Viscosity Ratio

Runs 4, 11, 12, and 13 were conducted to examine the effect of the oil-to-water viscosity ratio on oil recovery with polymer slug and water injection. All these runs had h_b/h_o equal to 0.33 and k_o/k_b equal to 1. However, oils of different viscosities were used for these runs. Figure 95 compares the oil recovery curves for all these runs. Also, the inset of this figure compares the ultimate oil recoveries. In all these runs, about 20 percent PV of polymer slug (which is also equivalent to 60 percent PV of the bottom water zone) was injected. All these runs showed a similar injection pressure and oil cut behaviour except Run 11, which did not show a peak in oil cut. Run 11, with the minimum oil-water viscosity ratio, showed no effect of polymer injection. However, this run showed very good oil recovery with waterflood (as compared to other runs). The oil recovery by waterflood was extremely low for Run 13 for which the most viscous oil was used. The injection of polymer gave a 17-fold improvement over a conventional waterflood for Run 13. This was by far the greatest improvement for all the runs conducted to examine the effect of oil-water viscosity ratio. These results suggest that the benefit of polymer slug injection increases as the

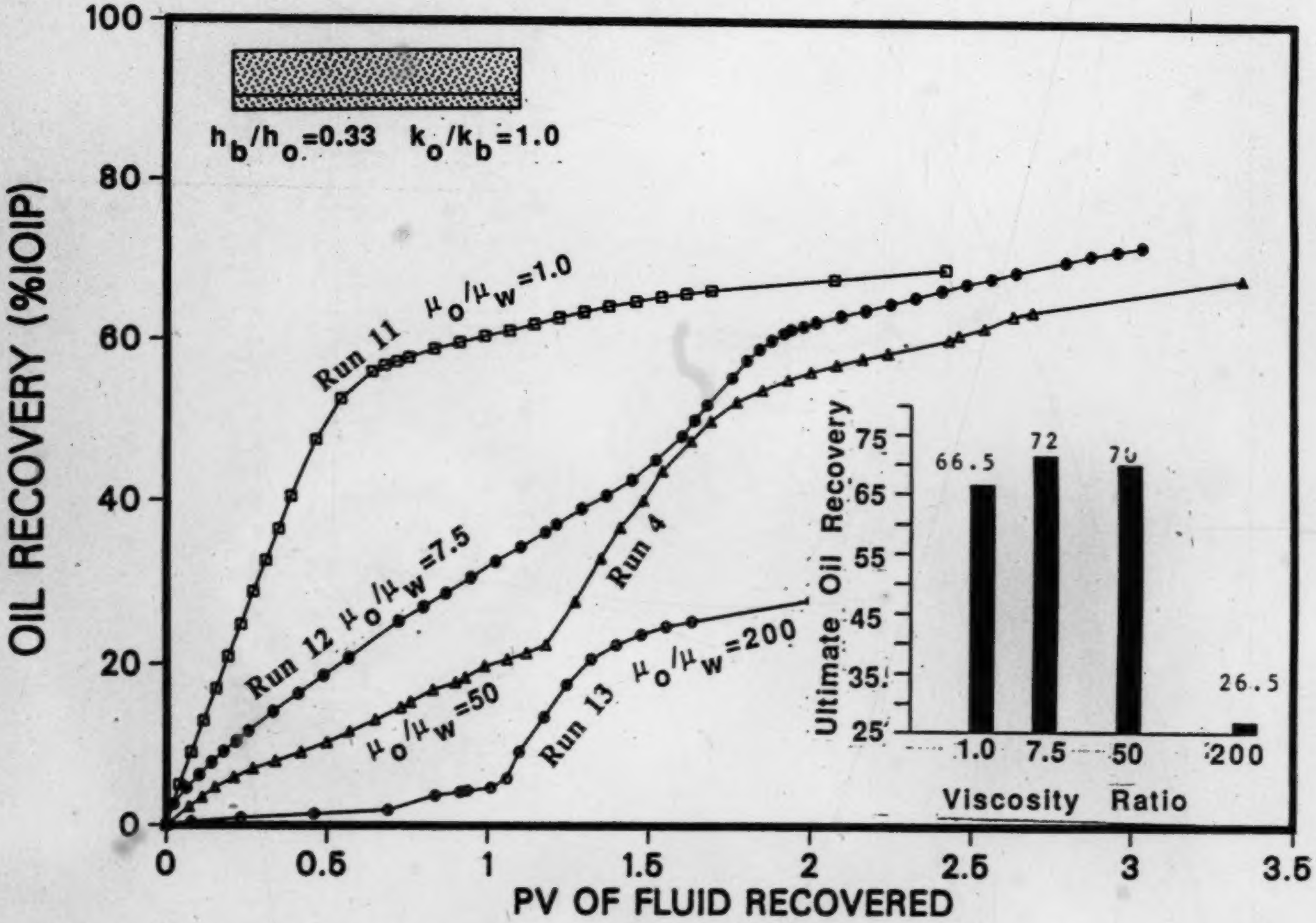

Fig. 95 Effect of Oil-Water Viscosity Ratio on Oil Recovery (h_b/h_o=0.33, k_o/k_b=1.0)

oil-water viscosity ratio increases. Run 13 showed the lowest ultimate recovery, indicating that for reservoirs with high oil viscosity a large portion of the oil in place would remain unrecovered even after polymer [illegible]atment. The highest oil recovery was obtained with 7.5 mPa.s viscosity even though recovery performance at the initial stage of the displacement was better for an oil viscosity of 1.0 mPa.s. For a homogeneous porous medium, low oil viscosity usually leads to a higher ultimate oil recovery provided other fluid characteristics (such as oil/water interfacial tension) are similar. However, the same performance cannot be expected for the case of a bottom-water zone. The reason for this behaviour may be explained in terms of different competing phenomena occurring during the use of a mobility control agent in the presence of a bottom-water zone. A high μ_o/μ_w ratio is unfavourable for a displacement of oil by water. However, for polymer injection in the presence of a bottom-water zone, a high oil-water viscosity ratio facilitates invasion of the bottom-water zone by the polymer solution. An increased amount of polymer in the bottom-water zone helps to reduce the mobility of the connate and injected water in the bottom-water zone. Therefore, μ_o/μ_w plays dual counteracting roles in recovering oil. Such an impact of the oil-water viscosity ratio suplies a possible explanation as to why there exists an optimal oil-water viscosity that is not necessarily the minimal.

6.2.3.4 Effect of Impermeable Barrier

Run 25 (k_o/k_b=1.0, h_b/h_o=1.0) was conducted to examine the effect of an impermeable barrier on polymer injection in the presence of a bottom-water zone. The barrier length was 25% of the total length of the model. The impact of an impermeable barrier is insignificant for this thick bottom water case. For instance, the presence of this barrier of 25% length improved the oil recovery with a waterflood from 3% to 7% of the IOIP. The ultimate recovery for this run (after polymer injection) was 67 percent as compared to 62 percent in Run 3 for which no barrier was used but the same packing characteristics were used.

6.2.3.5 Effect of Water-to-Oil Zone Thickness and Permeability Ratio

The oil-to-water zone thickness and permeability ratio had a large impact on oil recovery by waterfloods as well as polymer floods. Figures 96 through 98 compare the oil recovery curves for various k_o/k_b and h_b/h_o values. It can be seen from these figures that the oil recovery is not very sensitive to the oil-water thickness ratio for k_o/k_b=1, provided that $h_b/h_o \leq 0.33$. On the other hand, a much lower recovery is obtained for h_b/h_b=1. This distinction is diminished when the polymer solution is injected, which led to ultimate oil recoveries higher than 60 percent of the

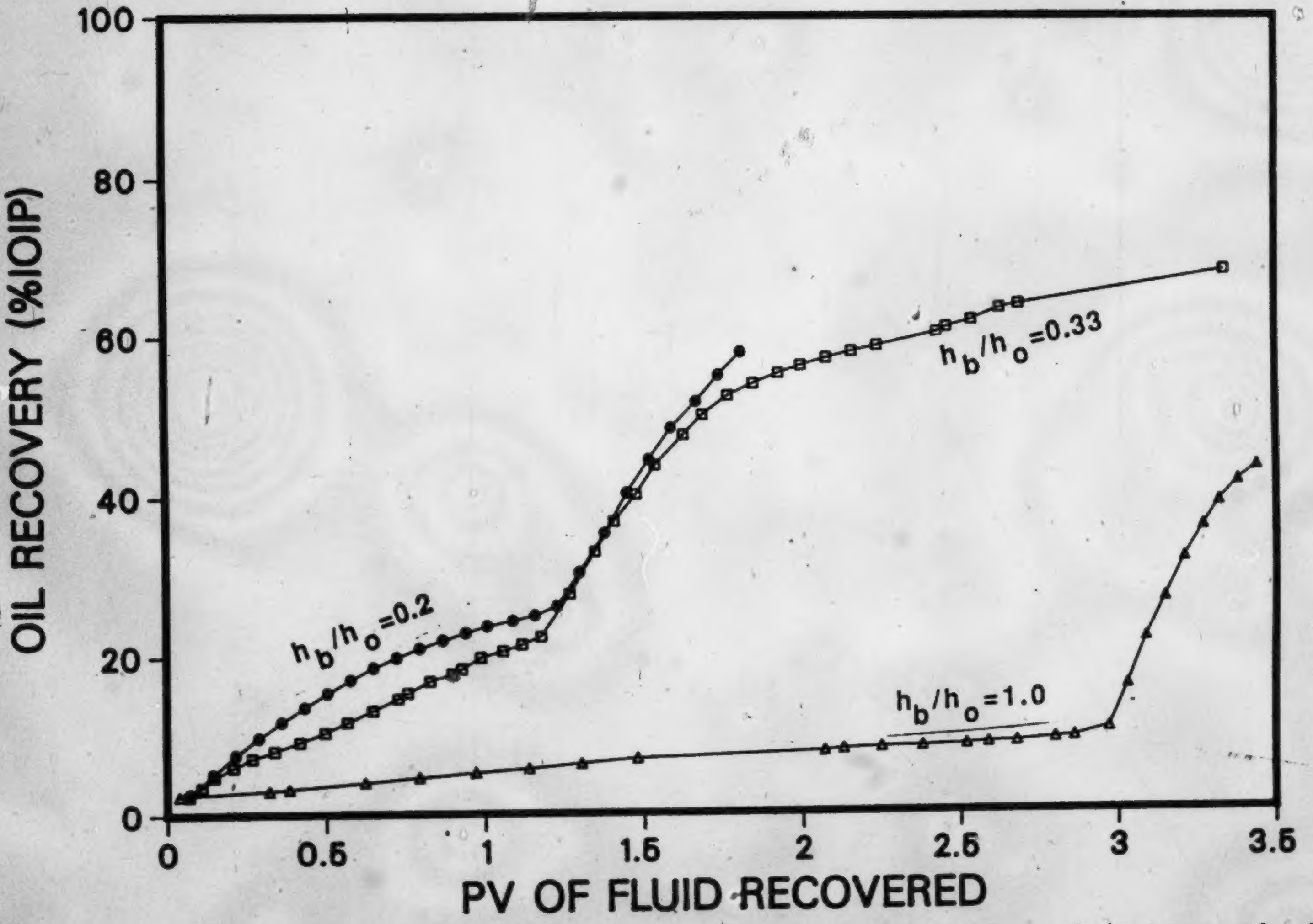

Fig. 96 Comparison of Oil Recoveries for different h_b/h_o and k_o/k_b=1.0 (Polymer Flood)

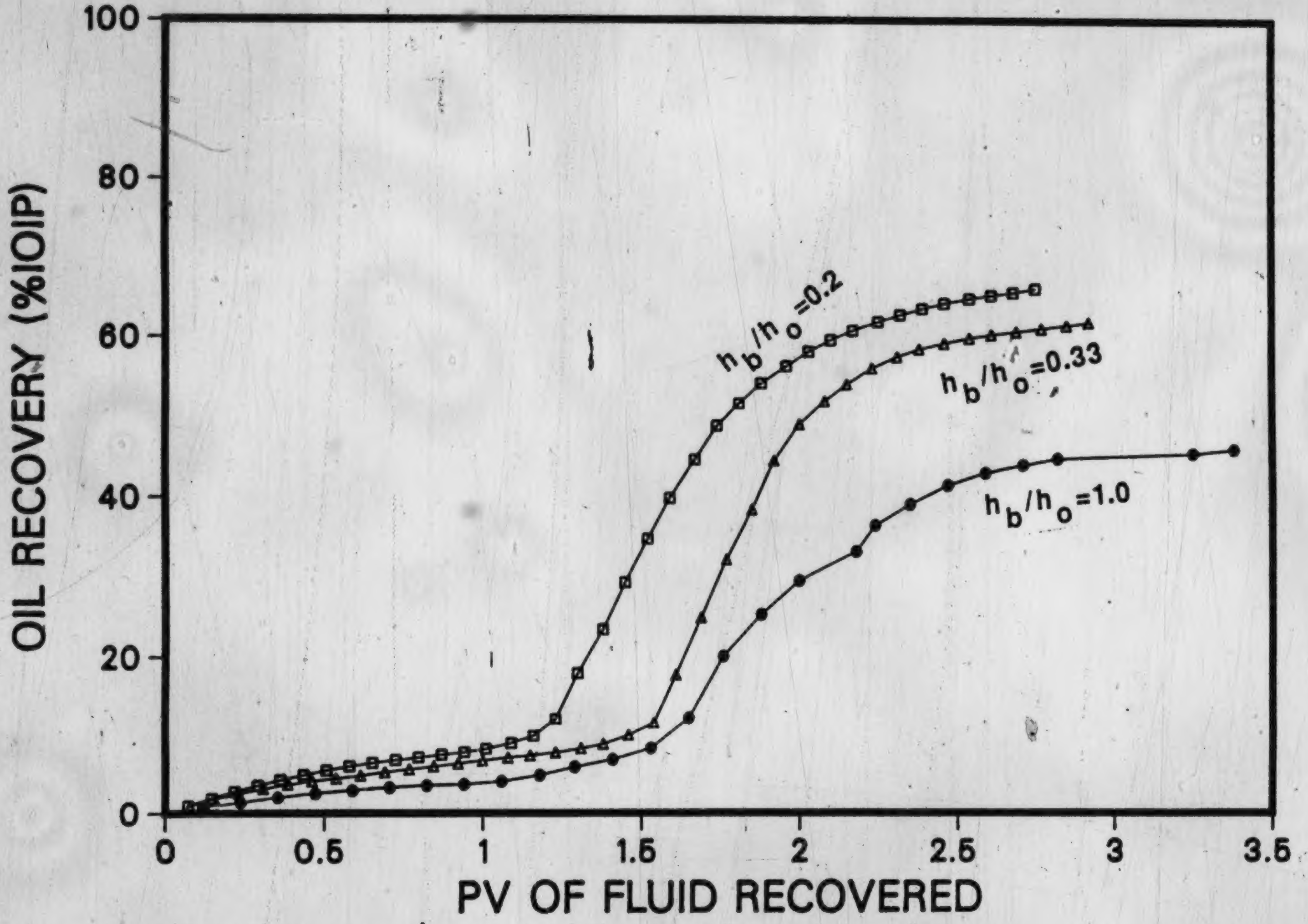

Fig. 97 Comparison of Oil Recoveries for h_b/h_o and $k_o/k_b=0.06$ (polymer Flood)

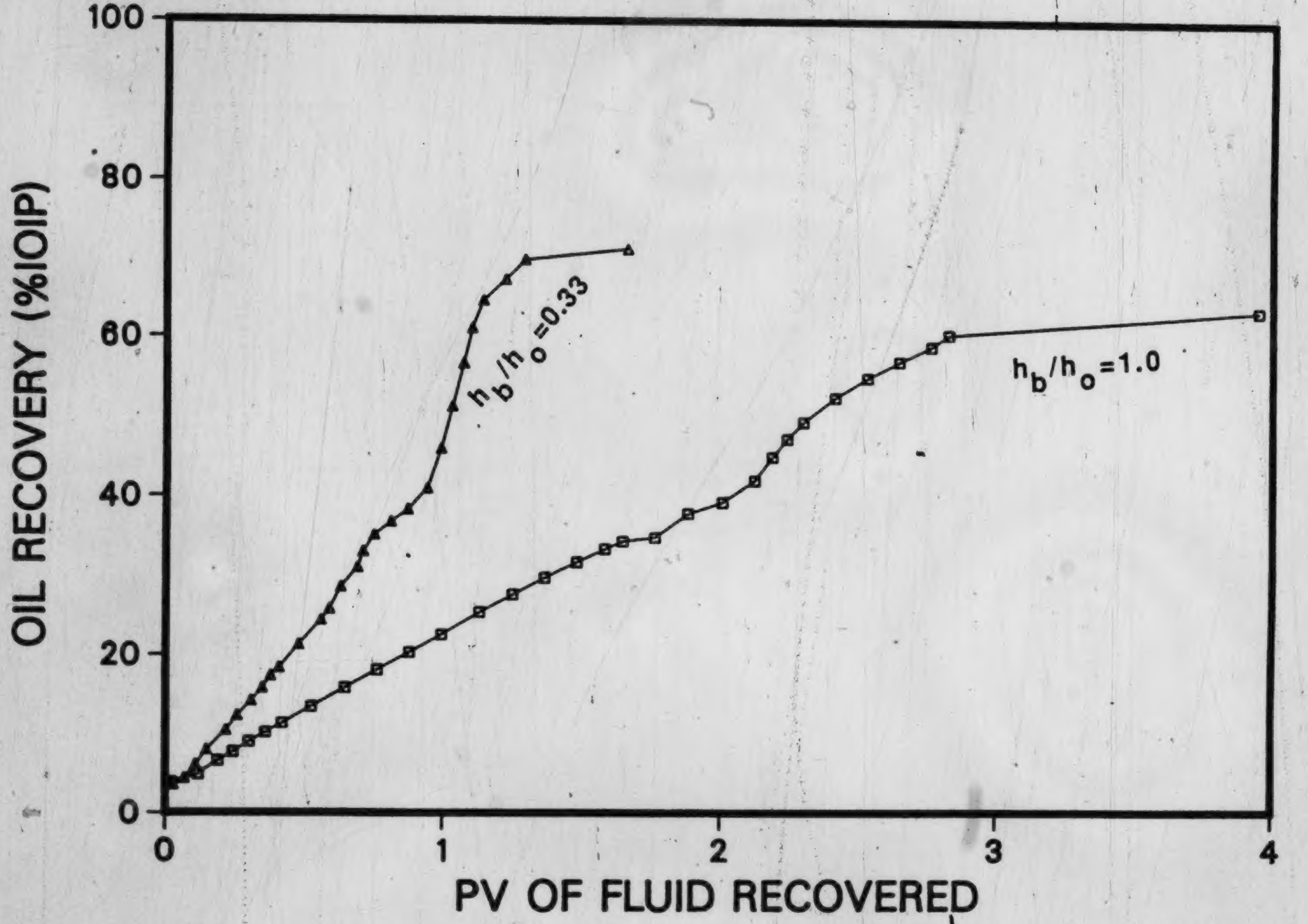

Fig. 98 Comparison of Oil Recoveries for h_b/h_o and k_o/k_b=2.67 (Polymer Flood)

IOIP. As can be seen from Figure 97, for k_o/k_b=0.06, the recovery was more sensitive to the thickness ratio. This is alleviated to some extent after polymer injection, yet the oil recovery remains considerably lower for h_b/h_o=1. As can be seen from Figure 98, for k_o/k_b=2.67, oil recovery is quite sensitive to the thickness ratio, but after polymer injection the ultimate recoveries are close. There were no data available for the case of h_o/h_b=0.2 and k_o/k_b=2.67.

Figure 99 depicts the ultimate oil recoveries (after polymer treatment) as a function of k_o/k_b and h_b/h_o. As was the case in a waterflood, k_o/k_b played the most important role for an h_b/h_o=1.0, especially in the for $0.06 \leq k_o/k_b \geq 1.0$. Even though h_b/h_o of 0.33 and 0.20 show a very similar trend, the dependence of ultimate recoveries on oil-to-water zone permeability ratio is less pronounced, especially as the ratio increases. At very low values of k_o/k_b, water-to-oil zone thickness ratio, h_b/h_o, plays a more prominent role and the ultimate oil recovery increases greatly with decreasing h_b/h_o values.

Figure 100 shows the sensitivity of ultimate recoveries on h_b/h_o values for a particular k_o/k_b value. As can be seen from this figure, ultimate recoveries become less sensitive to the value of h_b/h_o as k_o/k_b increases. Recall that during waterflooding, even the case of k_o/k_b=1 was very sensitive to h_b/h_o values.

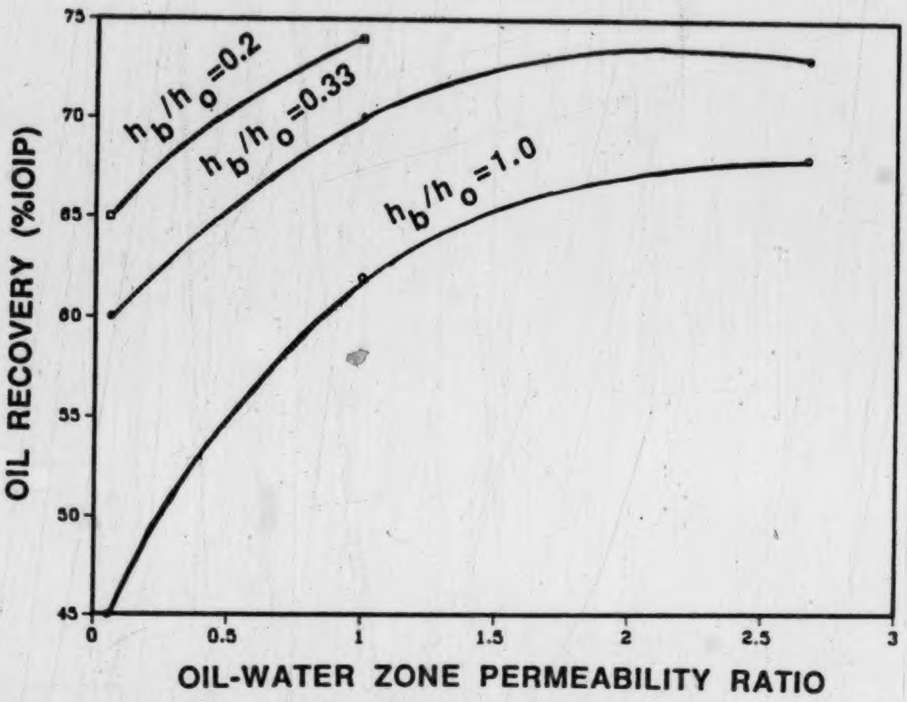

Fig. 99 Polymer Flood Performance as a Function of k_o/k_b and h_b/h_o

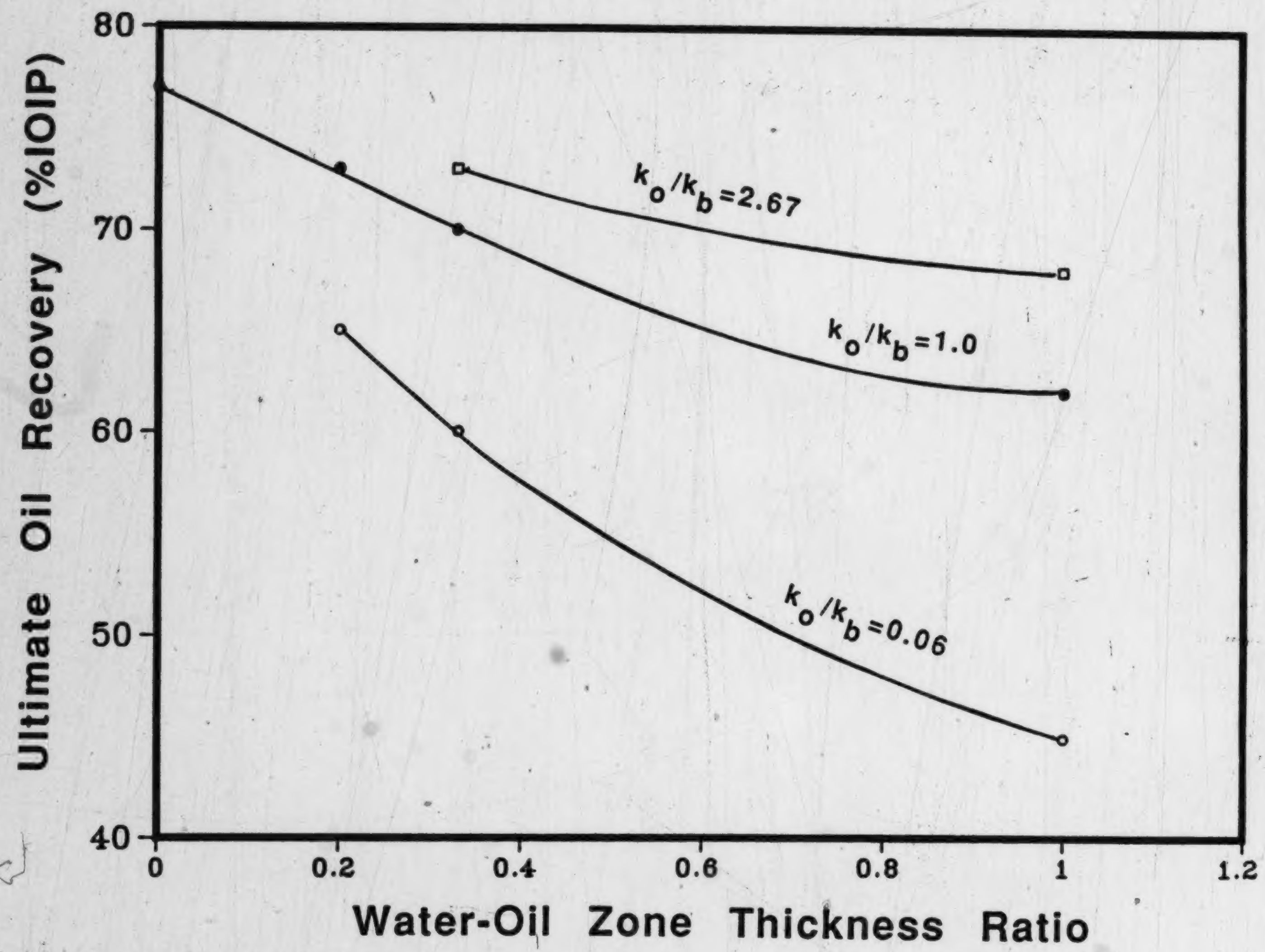

Fig. 100 Polymer Flood Performance as a Function of k_o/k_b and h_b/h_o

Figure 101 depicts oil recoveries with polymer as a function of k_o/k_b and h_b/h_o values and compares them with oil recoveries obtained with waterfloods. This figure shows that a polymer flood leads to oil recoveries with almost the same values, making a polymer flood more efficient in the cases for which oil recovery performance with waterfloods is poor. This effect is more pronounced when the percent improvement over a conventional waterflood is plotted as a function of h_b/h_o and k_o/k_b. This is done in Figure 102. Even though the highest oil recovery was obtained for base runs in the absence of bottom water, it can be seen that the relative improvement over waterflood is the highest for the cases in which the waterflood performance is very poor. For instance, for an extreme case of $k_o/k_b=0.06$ and $h_b/h_o=1$, the oil recovery with and without polymer slug differs by 22.5 times.

The shapes of these curves are dictated by the waterflood recovery curves. Recall that the curve for $k_o/k_b=1.0$ had the steepest slope for the waterflood. Polymer floods seem to result in ultimate oil recoveries that are quite similar regardless of the oil-to-water zone permeability or thickness ratios. This type of polymer flood behaviour may be observed from Figure 100 which does not show a steep slope for $k_o/k_b=1$. Consequently, when the percentage improvement over a waterflood is determined, the highest slope is observed for the curve of $k_o/k_b=1$. A

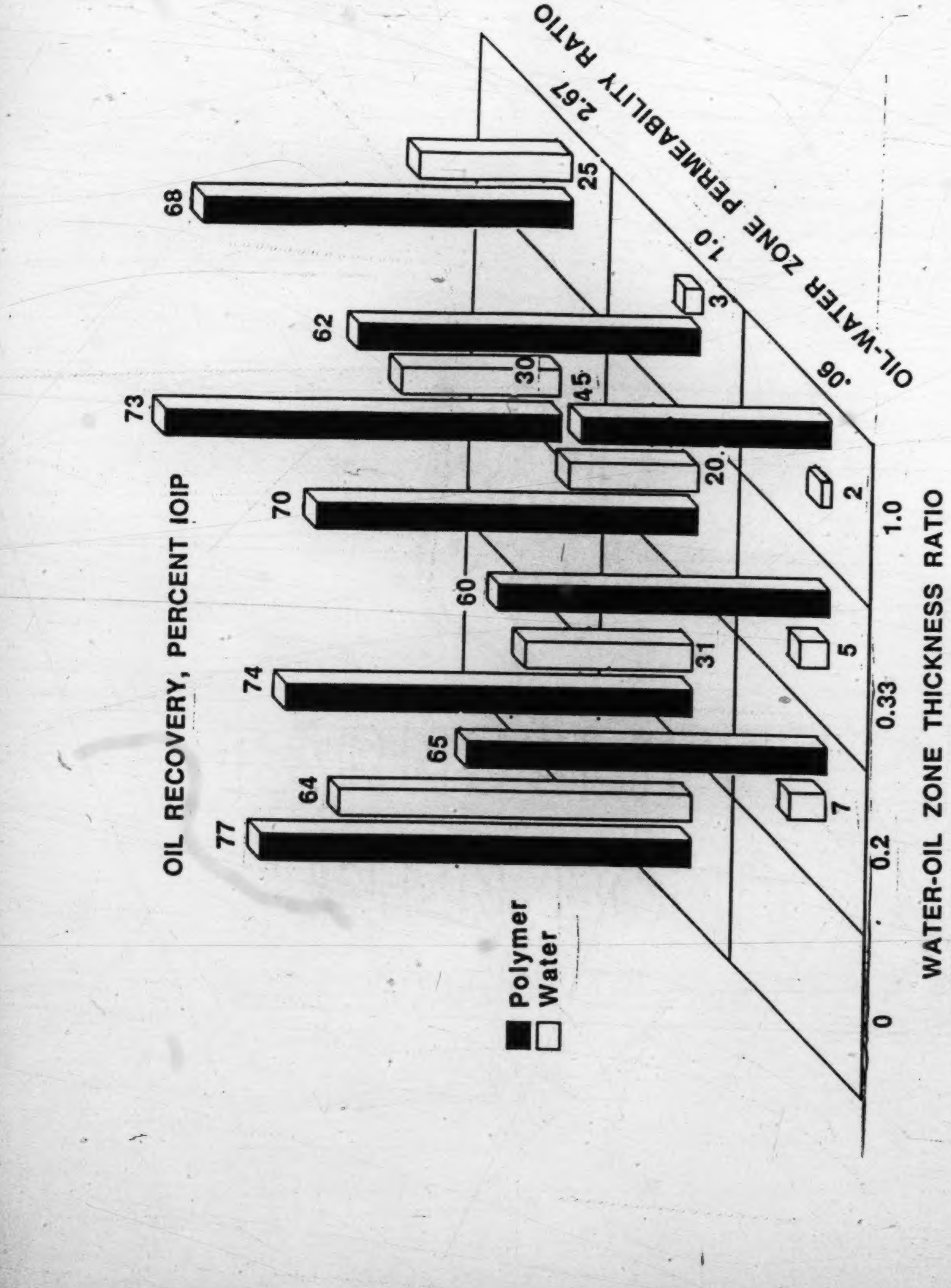

Fig. 101 Comparison of Polymer Flood with Waterflood

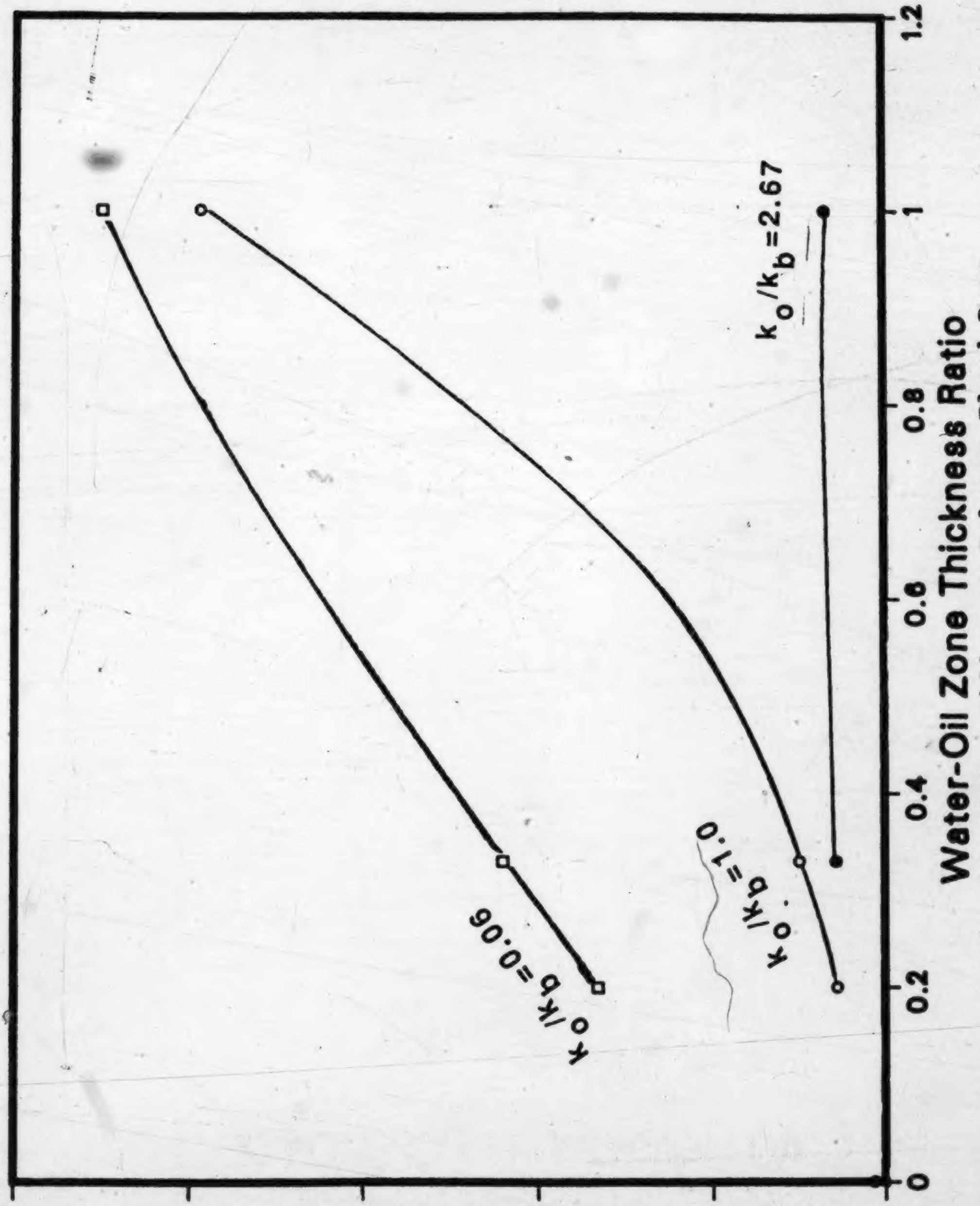

Fig. 102 Improvement Over a Waterflood for Different Polymer Flood Runs

similar explanation may be given for the shapes of the other curves of Figure 102.

6.3 Effect of Impermeable Barrier

Runs 24 to 27 were conducted to examine the effect of an impermeable barrier in the presence of a bottom-water zone. As can be seen in Table 5.1, the barrier lengths were 25% of the total length for Runs 24 and 25, and 50% of the total length for Runs 26 and 27. The impact of an impermeable barrier is much smaller for the thicker bottom water case. For instance, the presence of an impermeable barrier of 25% length improved the oil recovery with waterflood from 3% to 7% of the IOIP for $h_b/h_o=1$. A significant improvement was, however, observed for a greater length of the impermeable barrier. For a thinner bottom-water zone ($h_b/h_o=0.33$), on the other hand, a 25% length of impermeable barrier improved the waterflood recovery significantly. A much better performance was observed when the barrier length was 50% of the total length. From this comparison one can observe that the barrier length has to increase as the thickness of the bottom-water zone increases. This point is important for determining the volume of the mobility control agent.

6.4 Waterflood with Emulsion Slugs

Runs 29 to 45 were carried out with emulsion and water injection. A total of eighteen different runs were conducted to test the effectiveness of the emulsion as a blocking and diverting agent with oil-to-water zone thickness and permeability ratio, oil viscosity, emulsion slug size as variables. The results of these runs are compared with conventional waterfloods.

6.4.1 Emulsion Stability

In order to create effective blockage, a stable emulsion was sought. Both five and 10 percent O/W emulsions were produced at different surfactant concentrations and were left overnight to determine whether water-phase segregation occurred. Microscopic and visual observation of emulsion droplets and the emulsion pH behaviour at different surfactant concentrations were the criteria used to determine stability. Figure 103 depicts the dependence of the emulsion pH on the surfactant concentration for the five percent O/W emulsion. At very low surfactant concentrations, demulsification took place which is evident from the drop in pH values after a 24 hour delay as depicted in Figure 103. It was observed that the maintenance of the emulsion pH close to its original value is correlatable with the maintenance of emulsion stability observed in the microphotographs. An examination of the microphotographs of

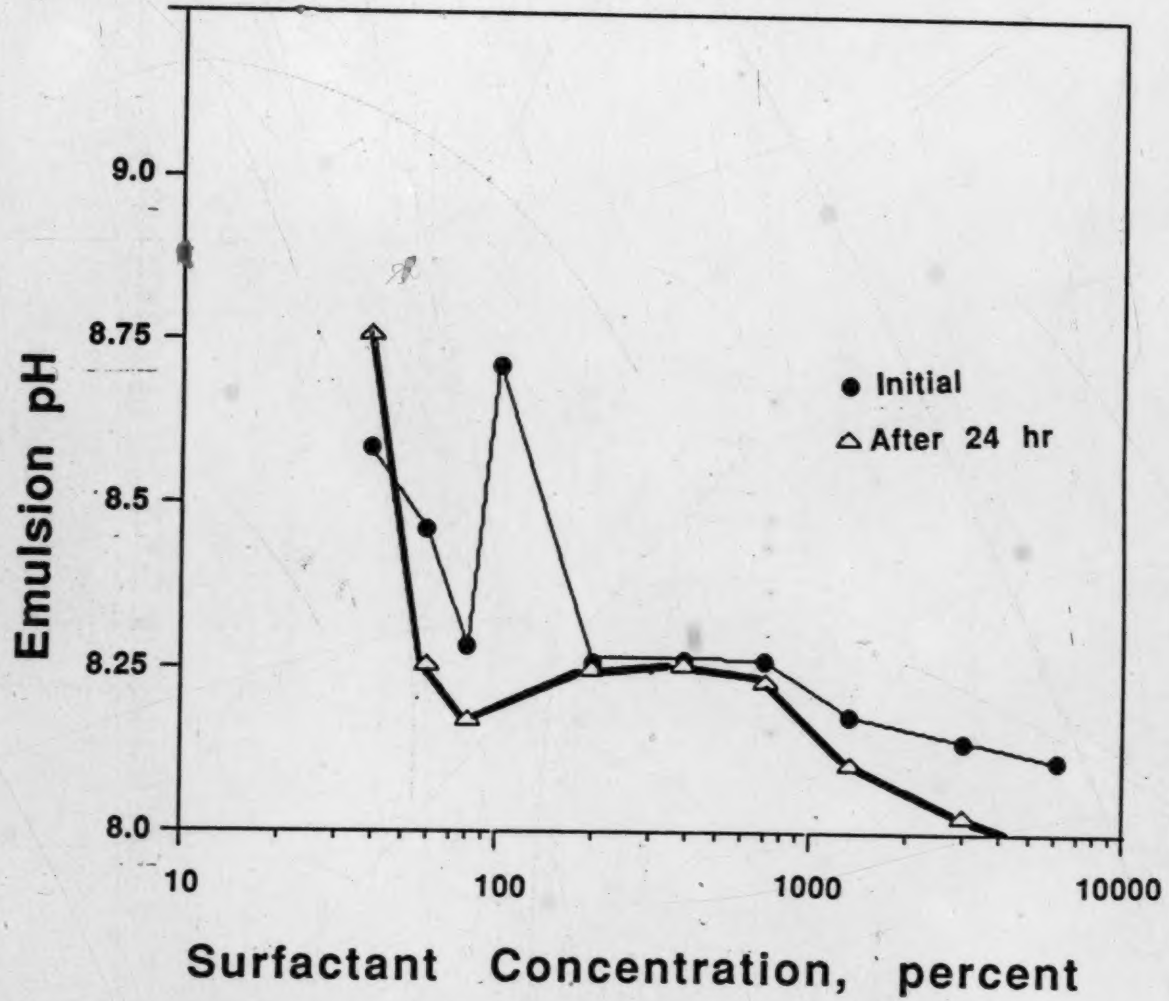

Fig. 103 Effect of Surfactant Concentration on Emulsion pH Stability

emulsions with very high surfactant concentration showed that these emulsions were not stable. This is due to surfactant dissociation that results in emulsion instability and a more acidic emulsion pH. On the other hand, a very low surfactant concentration did not form any stable emulsion. At 40 ppm, for instance, the emulsion formed broke down in a few minutes. From Figure 103 it is clear that a minimum of 200 to 300 ppm surfactant should be added to the aqueous phase in order to produce a stable emulsion. The pH vs. concentration curve for a 10 percent O/W emulsion followed a very similar trend to that for a five percent O/W emulsion. However, the choice of a five or 10 percent O/W emulsion could not be made from stability (outside the porous medium) considerations alone. Coreflood tests had to be conducted in order to decide the oil content of the emulsion.

6.4.2 Effect of Oil Content on Emulsion Blockage

Run 29 was conducted to examine the emulsion blockage with a five percent O/W emulsion. Initially the emulsion was injected through the inlet end. At the beginning of the run, the oil recovery was little better than that obtained with waterflooding. But emulsion breakthrough took place after 0.16 pore volume of emulsion injection. This early emulsion breakthrough meant a very small surface area was contacted by the emulsion. After injecting 0.21 PV of emulsion, the emulsion flood was followed by a waterflood at 400 ml/h. Water was injected through the injection well. As the waterflood continued, the oil cut was fairly stable at around 10 percent. The water slugs were then alternated with a few more emulsion slugs. At the beginning of each waterflood the oil cut increased slightly for a while but started decreasing as the waterflood continued. Even though the emulsion was stable when tested outside the core, a considerable amount of coalescence took place after the emulsion travelled along the core. This might have been responsible for the incomplete blockage. An analysis of the emulsion produced at the production well showed that coalesence took place and the quality of emulsion was degraded even though the emulsion persisted as an independent phase. Moreover, the emulsion itself showed considerable inhomogeneity in the distribution of oil droplets, as found by microscopic observation of the emulsion. A more homogeneous and stable form was obtained with 10 percent O/W emulsions. Run 30 was conducted to examine the effectiveness of a 10 percent O/W emulsion in blocking the bottom-water zone. This run was a repeat of Run 29 other than the fact that a 10 percent O/W emulsion was used. During emulsion injection, the oil cut decreased rapidly from 53 percent to 24 percent after an injection of 0.23 PV of emulsion. However, during the same period the injection pressure increased showing that considerable emulsion blockage was taking place. As the emulsion flood continued the oil cut increased rapidly to a maximum of 60 percent. At this point, emulsion breakthrough took place. This breakthrough time (0.47 PV) is much longer than that which was observed for Run 29 (0.16 PV). The oil cut decreased following emulsion breakthrough. As the emulsion slug was followed by a waterflood, both the injection pressure and oil cut decreased. However, these values were still significantly higher than those for a conventional waterflood.

Figure 104 compares the oil recovery curves for Runs 29 and 30. The benefit of the 10 percent O/W emulsion is clear because 54 percent of the IOIP was recovered for Run 30 as compared to only 32 percent of the IOIP for Run 29. For this reason a 10 percent O/W was used for all other runs. Also, for most of the runs (except those intended to study the effect of emulsion slug size) an emulsion slug of two pore volumes of the bottom-water zone was used. It was reported that most of the permeability reduction by emulsion flood took place after injecting two PV of emulsion (in the case of 100% water saturated cores) (Broz *et al.*, 1985). Consequently, an emulsion slug of two PV_b was used for most of the runs.

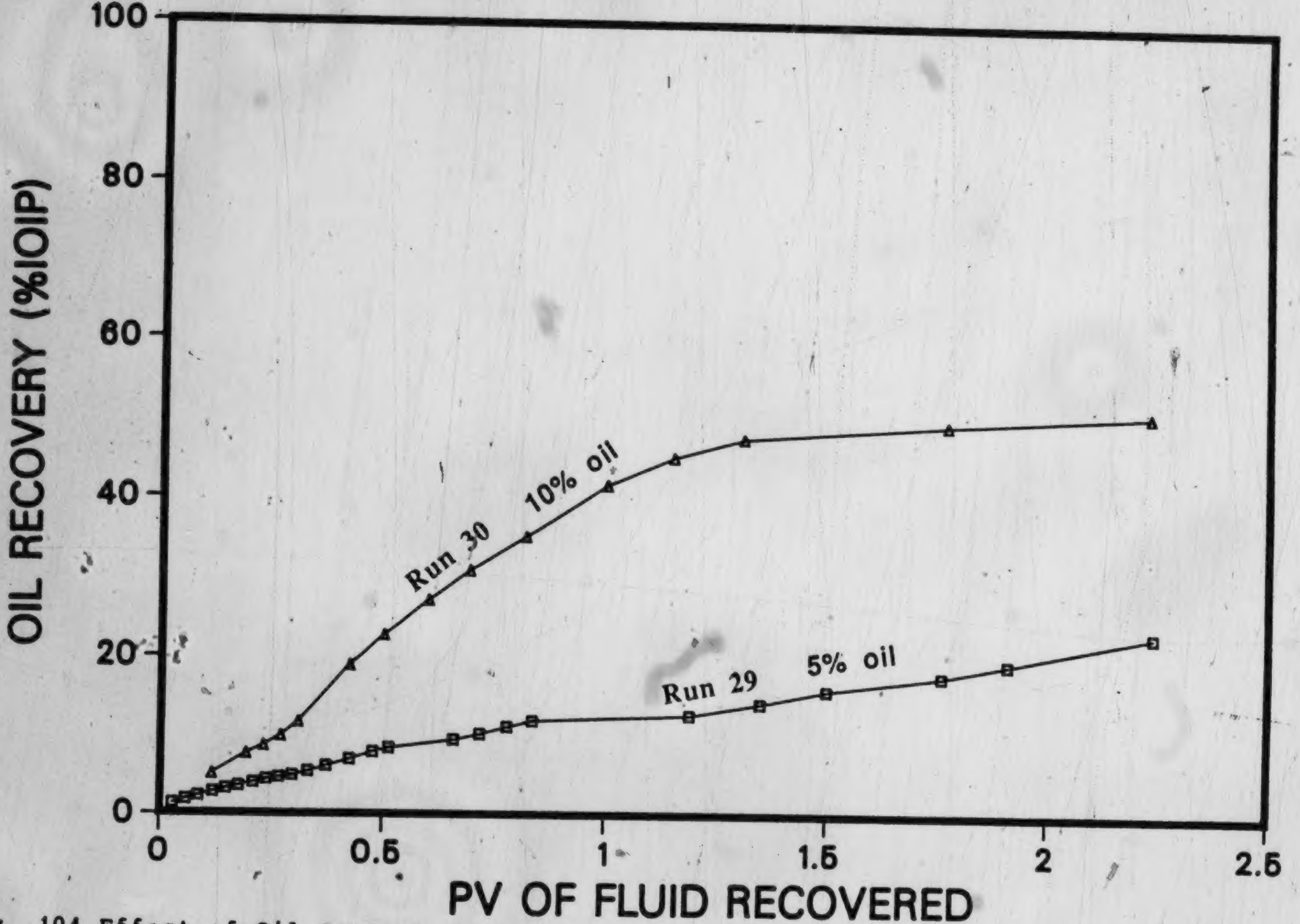

Fig. 104 Effect of Oil Content on Emulsion Blockage

6.4.3 Emulsion Flood in Homogeneous Oil Reservoirs

Run 31 was conducted to examine the effect of a continuous emulsion flood in a homogeneous porous medium. This run was characterized by a delayed breakthrough (as compared to waterflooding), which occurred at 36 percent PV. This compares with only 25 percent PV for a waterflood. The ultimate oil recovery for this run was 79 percent of the IOIP. This compares with 64 percent of the IOIP for a conventional waterflood. A more favourable mobility ratio is expected for an emulsion flood from viscosity considerations alone. However, this viscosity (1.8 mPa.s) will not account for a 23 percent increase in oil recovery. In fact, the texture of emulsions contributes to a better sweep efficiency whereas the decrease in interfacial tension contributes to decreasing the irreducible oil saturation. However, a quantitative analysis cannot be done with the limited data available. This performance is different from that of polymer injection that did not perform as well in a homogeneous pack as it was expected considering its high viscosity.

6.4.4 Emulsion Flood in the Presence of a Bottom-Water Zone

Typically, during the emulsion flood, the water breakthrough took place almost immediately (except for Runs with 1.0 and 7.5 mPa.s oil viscosity). Recall that a similar performance was observed in waterfloods as well.

Also, the oil cut decreased rapidly during the initial stages. During this period, however, the inlet pressure increased showing that a considerable emulsion blockage was taking place. As the emulsion flood continued, the oil cut increased rapidly to attain a maximum. Very often, this point of maximal oil cut corresponded to emulsion breakthrough. Following this, the oil cut decreased again and this was accompanied by a decrease in injection pressure. A relatively high value of the cumulative WOR at emulsion breakthrough indicated that a considerable amount of emulsion invaded the bottom-water zone, thus being able to create a blockage for the subsequent waterflood which was started immediately after the emulsion flood. Even though the injection pressure decreased following emulsion breakthrough, the injection pressure was much higher than that which one would expect from a waterflood.

6.4.4.1 Effect of Water-to-Oil Zone Thickness and Permeability Ratio

Different runs were conducted to investigate the effect of the h_b/h_o and k_o/k_b values. An injection rate of 400 ml/hr was chosen for both the emulsion and water injections. Typically, during the emulsion flood, the water breakthrough occurred instantly (except for cases with very low oil viscosity).

The emulsion slug size was determined depending on the size of the bottom-water zone. It has been reported (Broz et al., 1985) that most of the permeability reduction takes place after injecting two pore volumes of emulsion in the case of a 100 percent water-saturated core. Following this observation it was decided to inject two PV_b of emulsion for all the runs except for the ones that were conducted to study the effect of slug size.

Figures 105 through 107 compare oil recoveries for the k_o/k_b values of 1.0 and 2.67, respectively. During the emulsion flood the initial WOR was very close to that for a waterflood. However, as the emulsion flood continued, the WOR decreased and then increased again. Due to this WOR behaviour the oil recovery curves do not resemble those of waterfloods. As was the case with polymer flood runs, there was a delay in response before the WOR decreased and the oil cut started increasing to reach a peak. This delay could be directly correlated as a function of PV_b. Figure 108 depicts the delay in response time as a function of h_b/h_o and k_o/k_b. For all the runs with $h_b/h_o \geq 0.33$ the delay was approximately one pore volume of the bottom-water zone. The only exception was for $h_b/h_o=1$ and $k_o/k_b=0.06$. On the other hand, for $h_b/h_o=0.2$ the delay was higher than 1 PV_b. In fact, the recovery performance of this case of a thin bottom-water zone suggests that the emulsion flood recovery is quite high from the beginning of the displacement test and no drastic change in oil cut takes place, as the WOR does not fall as low as with other cases with a higher h_b/h_o

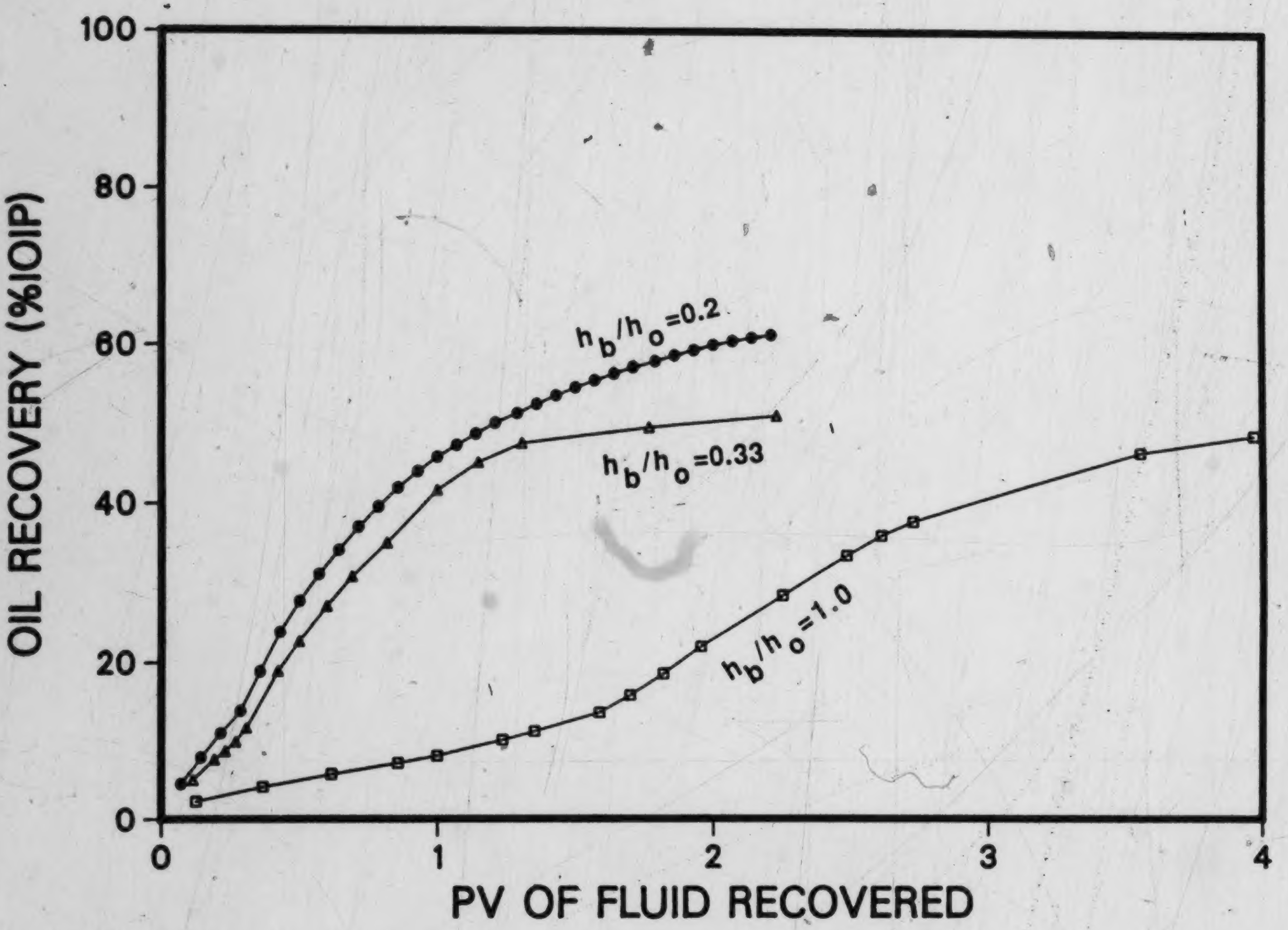

Fig. 105 Comparison of Oil Recoveries for different h_b/h_o and k_o/k_b=1.0 (Emulsion Flood)

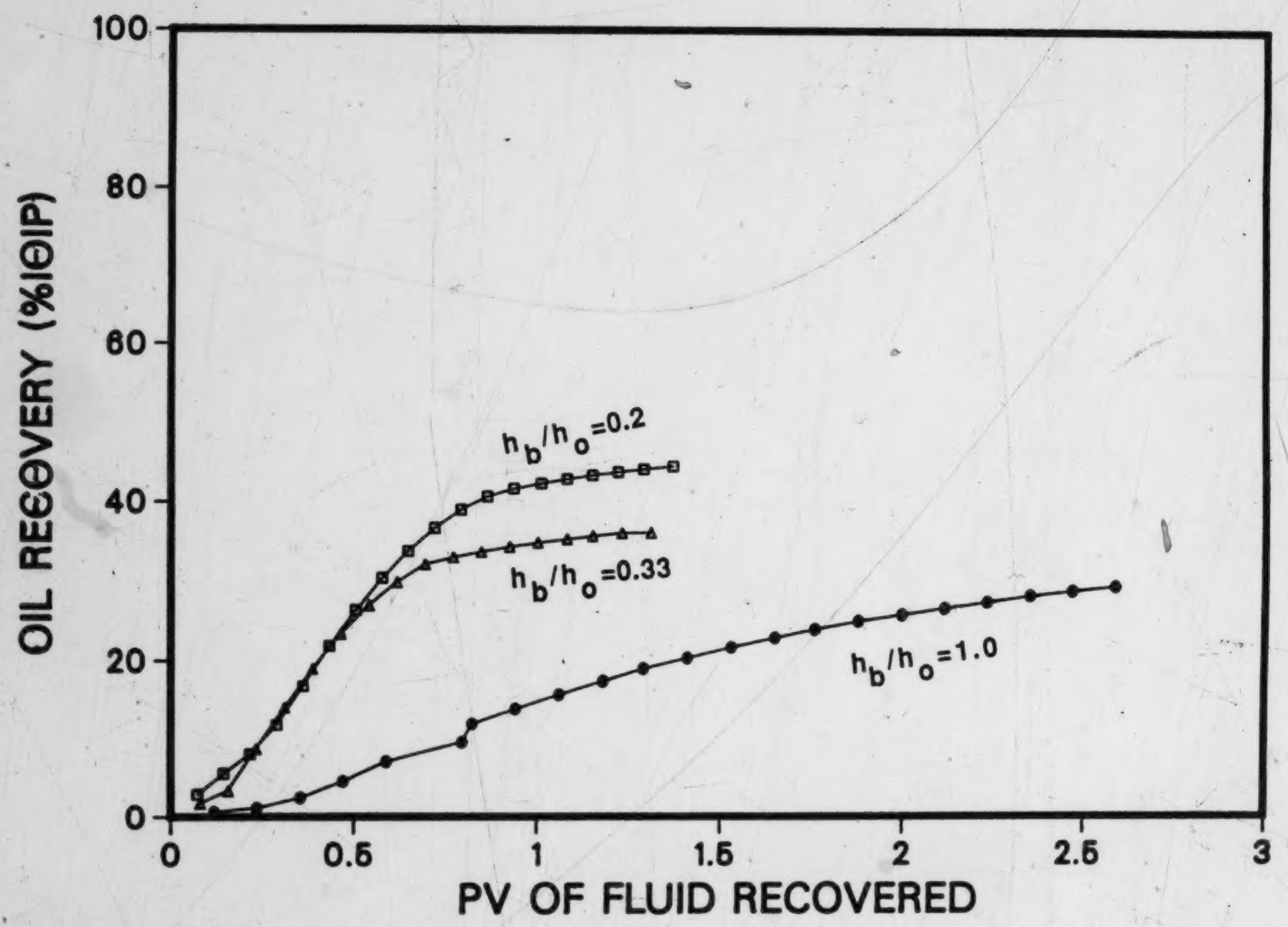

Fig. 106 Comparison of Oil Recoveries for h_b/h_o and $k_o/k_b=0.06$ (Emulsion Flood)

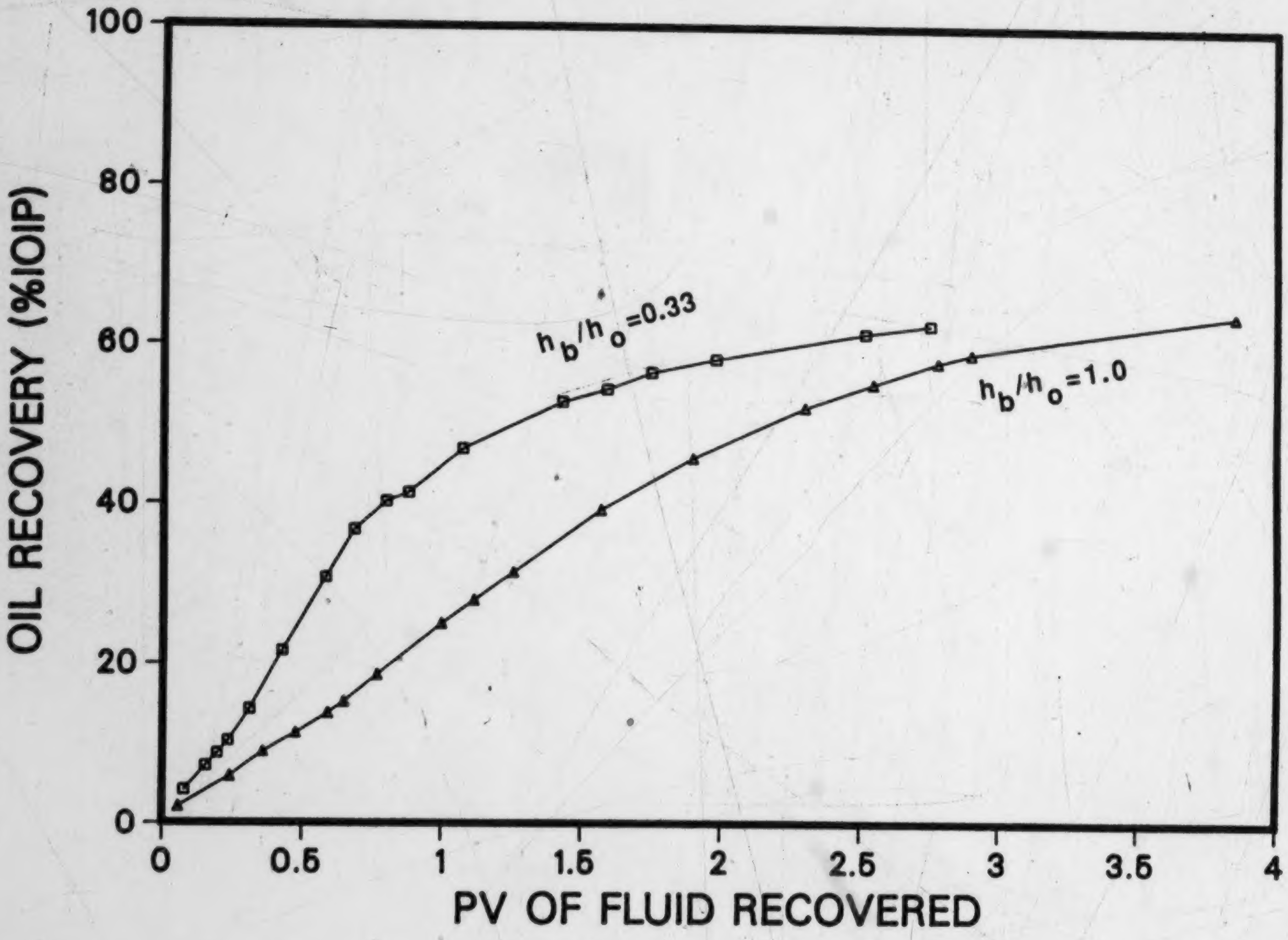

Fig. 107 Comparison of Oil Recoveries for h_b/h_o and k_o/k_b=2.67 (Emulsion Flood)

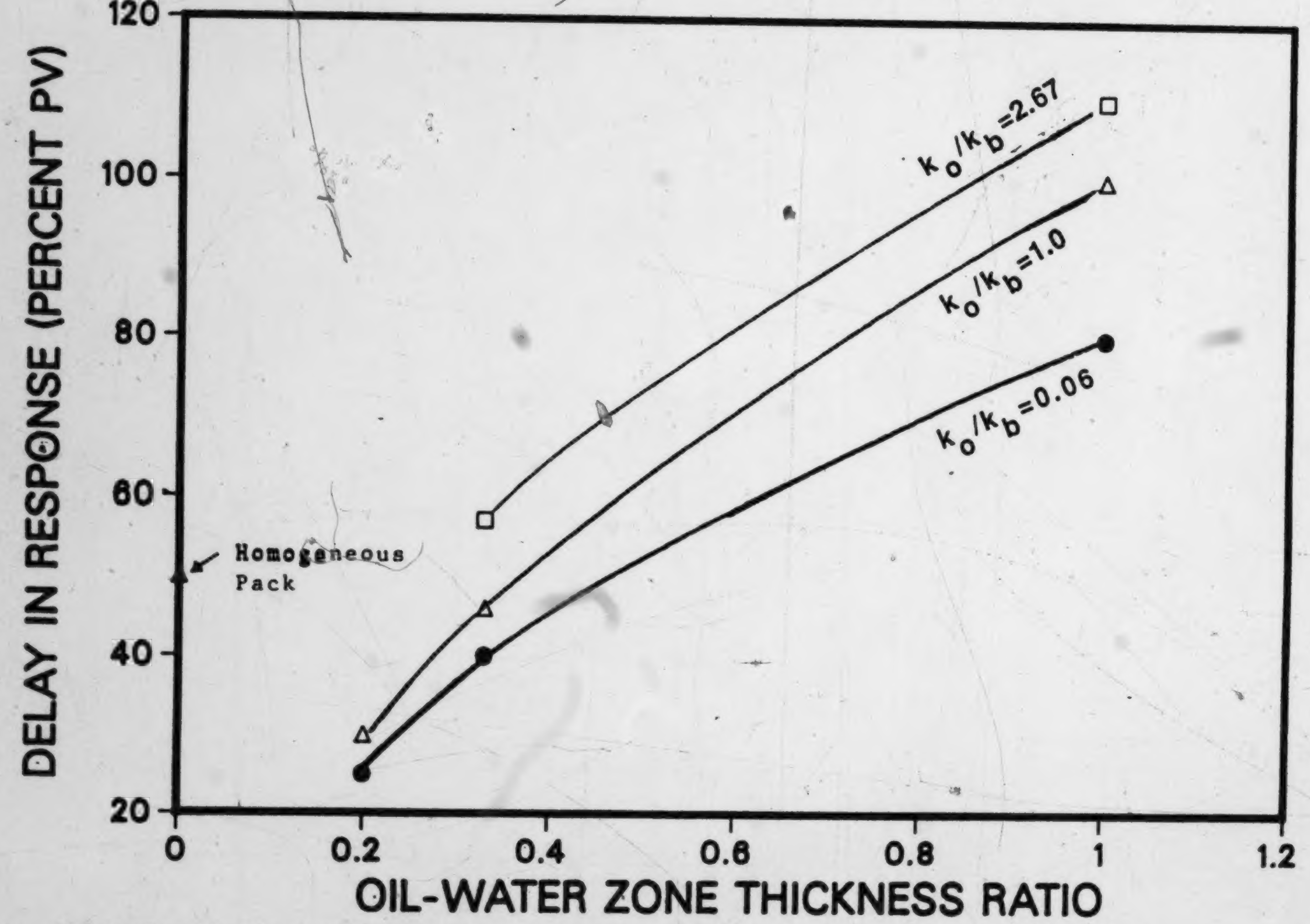

Fig. 108 Delay in Recovery Response for Emulsion Flood Runs

value. Also, it can be seen from the recovery performance reported in chapter V that at the extreme case of $h_b/h_o=0$, the WOR decreases monotonically as the emulsion flood continues. Therefore, such behaviour for $h_b/h_o=0.2$ is expected.

Figure 109 compares the ultimate oil recoveries for these runs. As can be seen from this figure, the ultimate oil recovery quickly decreases as the thickness of the bottom-water zone increases for oil-to-water zone permeability ratios of unity and 0.06. However, for a high k_o/k_b value only, the ultimate recovery increases slightly as the thickness of the bottom-water zone increases. A possible explanation for this phenomenon may be as follows. As the permeability of the bottom-water zone decreases, a smaller fraction of the injected emulsion invades the bottom-water zone. This effect of the bottom-water zone thickness is not important for lower k_o/k_b values as the high permeability of the bottom-water zone enhances high injectivity of the zone. Even though early invasion of the bottom-water zone with the emulsion enhances the oil recovery, when a waterflood follows the emulsion flood, the injected water does not encounter significant resistance from the bottom-water zone. Consequently, water channels through the bottom-water zone and the WOR increases rapidly leading to a poorer ultimate oil recovery with decreasing bottom-water zone thickness. However, if the effect of

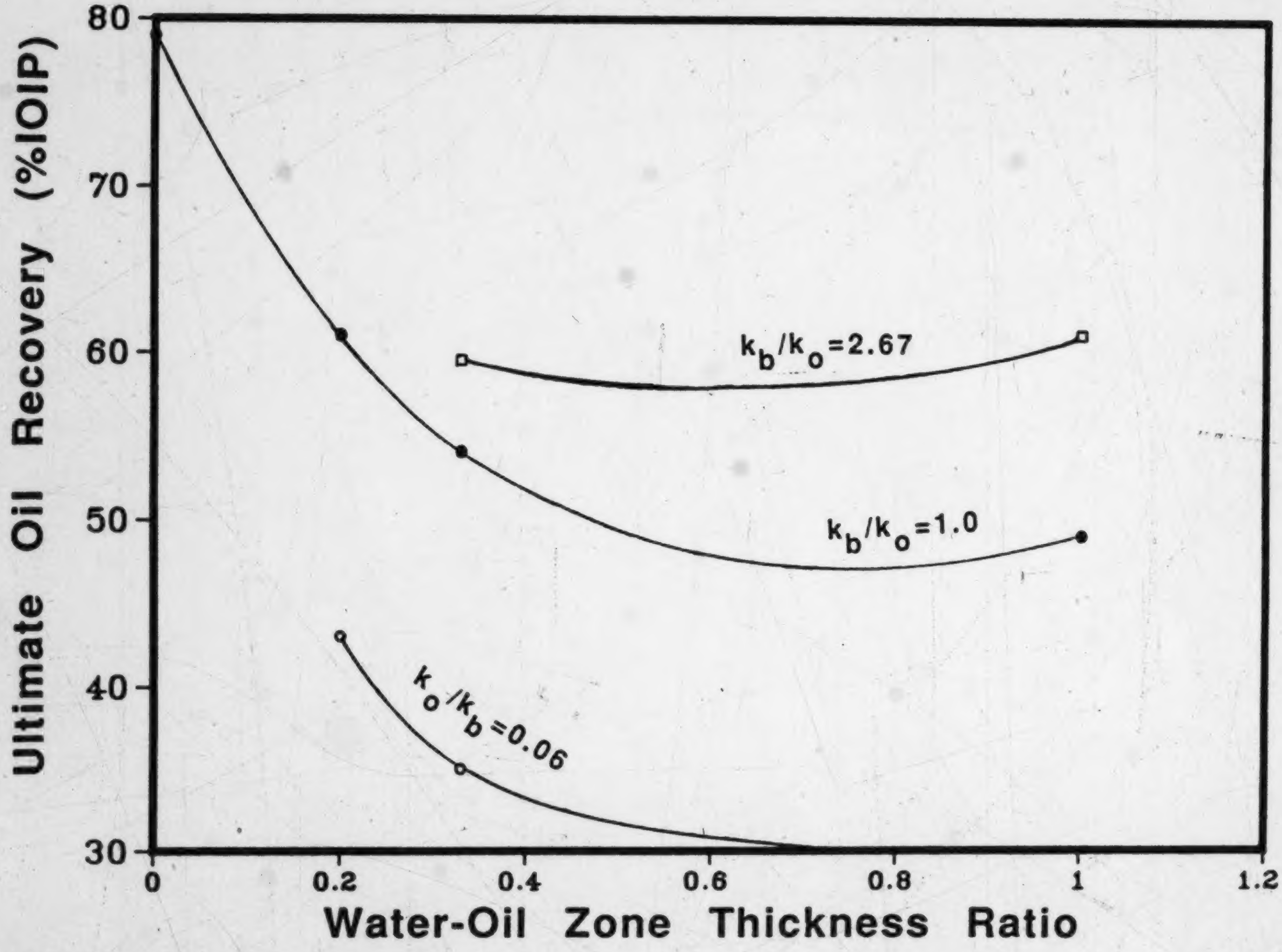

Fig. 109 Emulsion Flood Performance as a Function of k_o/k_b and h_b/h_o

permeability contrast is considered alone, a much higher ultimate oil recovery is obtained with a tighter bottom-water zone.

Figure 110 shows the dependence of oil recovery on the oil-to-water zone permeability ratio for a given h_b/h_o value. It can be seen from this figure that the case of $h_b/h_o=0.2$ is the most sensitive to k_o/k_b values. For $h_b/h_o=0.33$, the oil recovery is sensitive to k_o/k_b values at lower ranges of k_o/k_b (less than unity) and becomes less sensitive for higher values of k_o/k_b. On the other hand, the case of $h_b/h_o=1$ appears to be least sensitive to oil-water zone permeability ratio. For lower ranges of k_o/k_b values, the oil recovery increases rapidly with increasing k_o/k_b. But soon a plateau is reached and the oil recovery remains the same between $k_o/k_b=1$ and 2.67. For a thicker bottom-water zone, the thickness dominates emulsion blockage unless k_o/k_b is very low. It can be seen from Figure 110 that all three curves have very similar shapes provided $k_o/k_b \leq 1.0$. However, for higher values of k_o/k_b, the shapes differ for $h_b/h_o=0.33$ and $h_b/h_o=1$. For $h_b/h_o=0.33$, the ultimate oil recovery continues to increase, albeit with a continually decreasing slope, as the k_o/k_b value increases. An opposite trend is observed for $h_b/h_o=1$. No data were available for the intermediate range of k_o/k_b, but the shape of the curve for $h_b/h_o=1.0$ dictates that there is a maximum in the range $1<k_o/k_b<2.67$. For a particular

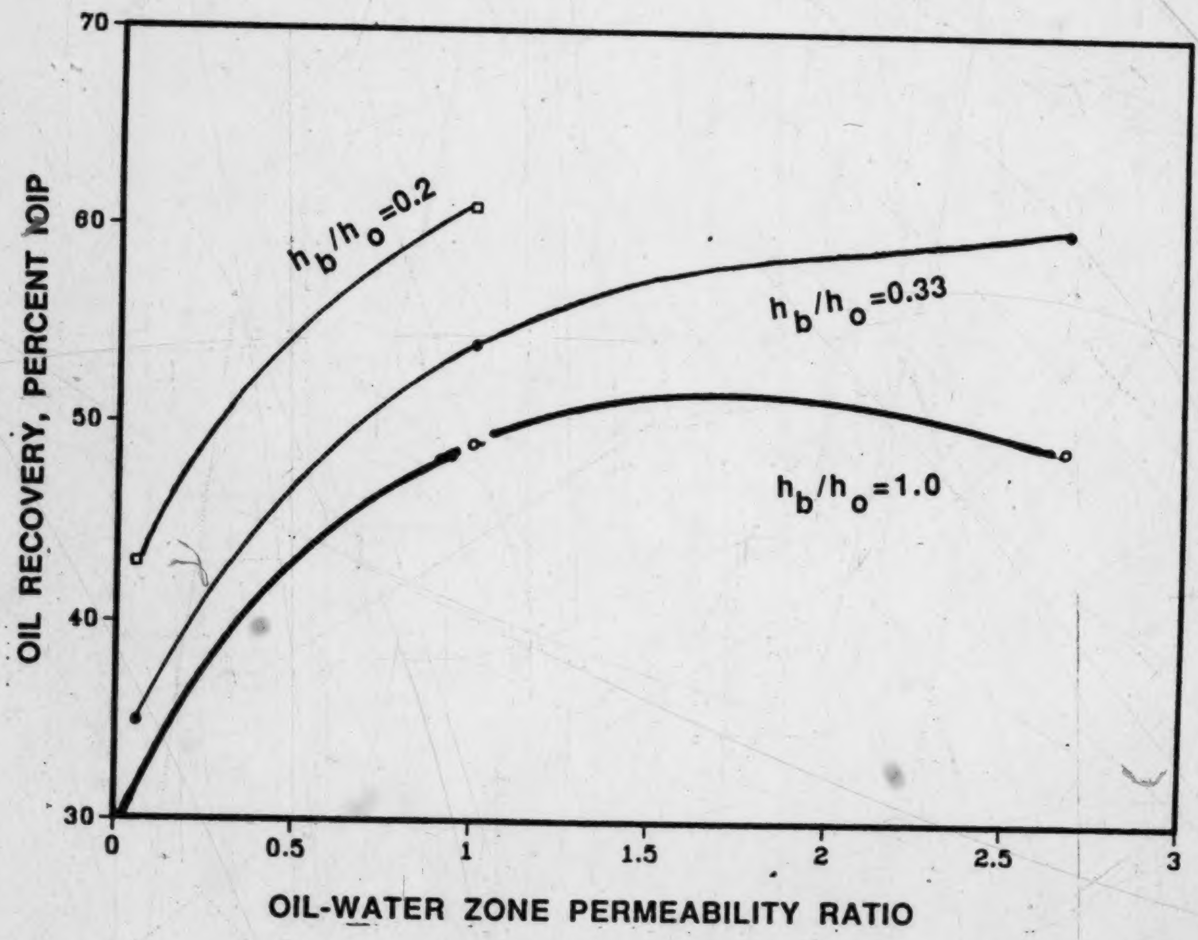

Fig. 110 Emulsion Flood Performance as a Function of k_o/[illegible]$_b$ and h_b/h_o

value of h_b/h_o, the oil-water zone permeability ratio plays dual roles. A high k_o/k_b value improves the waterflood recovery performance by impeding channeling through the bottom-water zone, but also decreases emulsion flux into that zone. A higher emulsion saturation in the bottom-water zone improves oil recovery by the waterflood because the injected water encounters more resistance from the bottom-water zone and is directed into the oil zone. This second phenomenon increases the oil recovery. Such competing effects within of the oil-water zone give rise to an optimal oil-water zone permeability ratio. However, it is very likely that the existence of an optimum is restricted to a particular oil-water zone thickness ratio, because a thicker or thinner bottom-water zone might diminish the sensitivity to the oil-water zone permeability ratio.

Figure 111 shows the wide range of oil recovery as a function of h_b/h_o and k_o/k_b values. As can be seen from this figure, emulsion improves oil recovery considerably over a waterflood even in the absence of a bottom-water zone. This figure shows the effects of k_o/k_b and h_b/h_o on the recovery performance with emulsion slugs. Figure 111 suggests that the oil recovery improves as the thickness and permeability of the bottom-water zone decrease. However, the wide difference in recovery shows that the permeability of the bottom-water zone plays a greater role in the case of

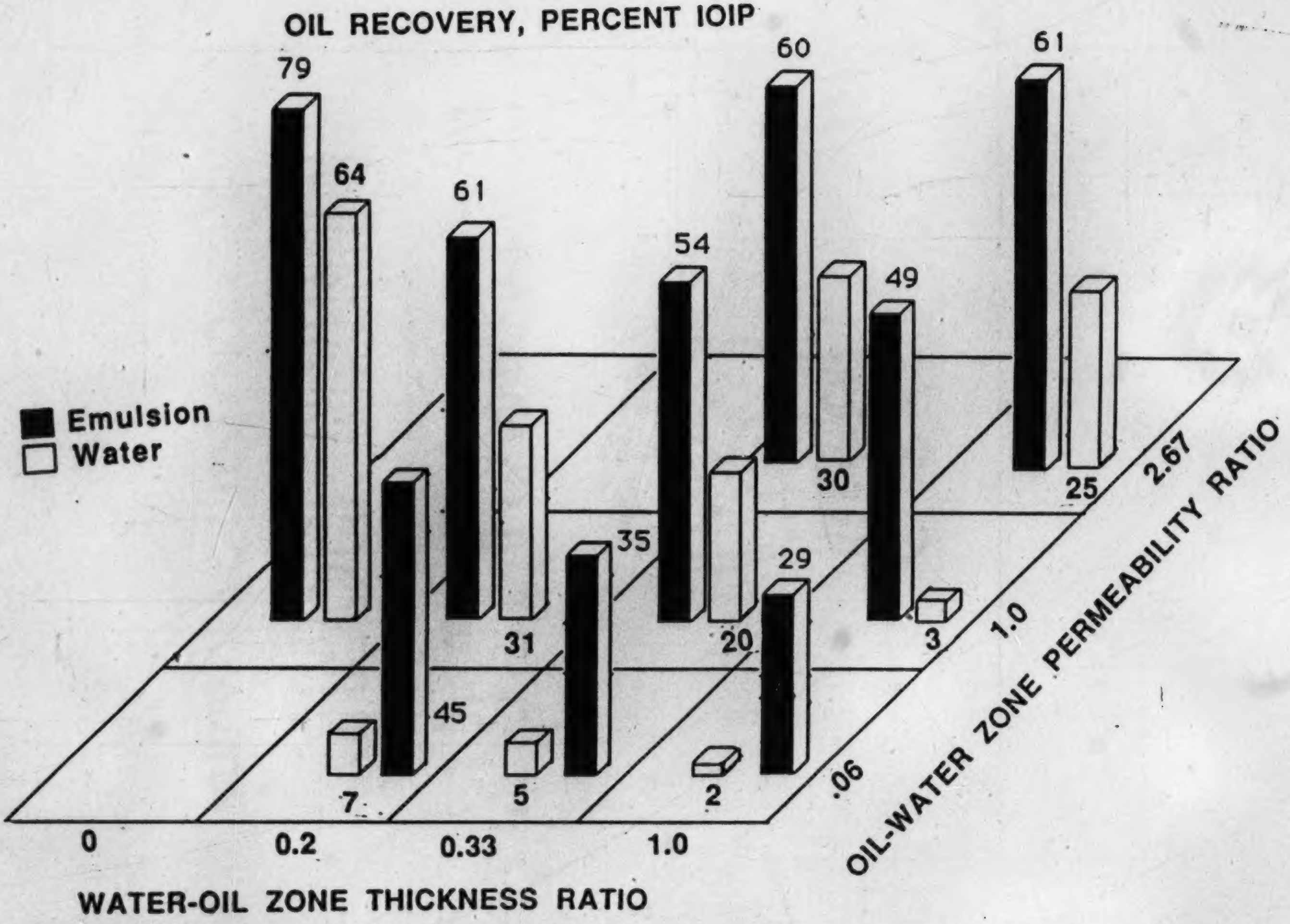

Fig. 111 Comparison of Emulsion Flood with Waterflood

a thicker bottom-water zone. For a very high bottom-water zone permeability (k_o/k_b=0.06) injection of the emulsion did not seem to be very effective. However, the same slug volume of emulsion was used for these runs (two pore volumes of the bottom-water-zone pore volume). A higher k_b/k_o value might warrant a larger slug size in order to create effective blockage. This aspect was not investigated in this study. Even though the absolute values of the ultimate oil recoveries favour high values of k_o/k_b and low values of h_b/h_o, as can be seen from Figure 112, the relative improvement of an emulsion flood over a waterflood is highest when the bottom-water zones exhibit the most unfavourable characteristics. From this consideration, emulsions appear to be most effective when the waterflood performance is the poorest.

6.4.4.2 Effect of Viscosity Ratio

Runs 30, 39, 40, and 41 were conducted to examine the effect of oil-water viscosity ratio on oil recovery with an emulsion slug and water injection. All these runs had h_b/h_o=0.33 and k_o/k_b=1. However, oils of different viscosities were used for these runs.

Runs 30 and 40 exhibited very similar injection pressure performance, i.e. the injection pressure initially increased until emulsion breakthrough took place. However, Run 39, for which kerosene was used as the oil phase, did not show any increase in pressure even though the oil cut

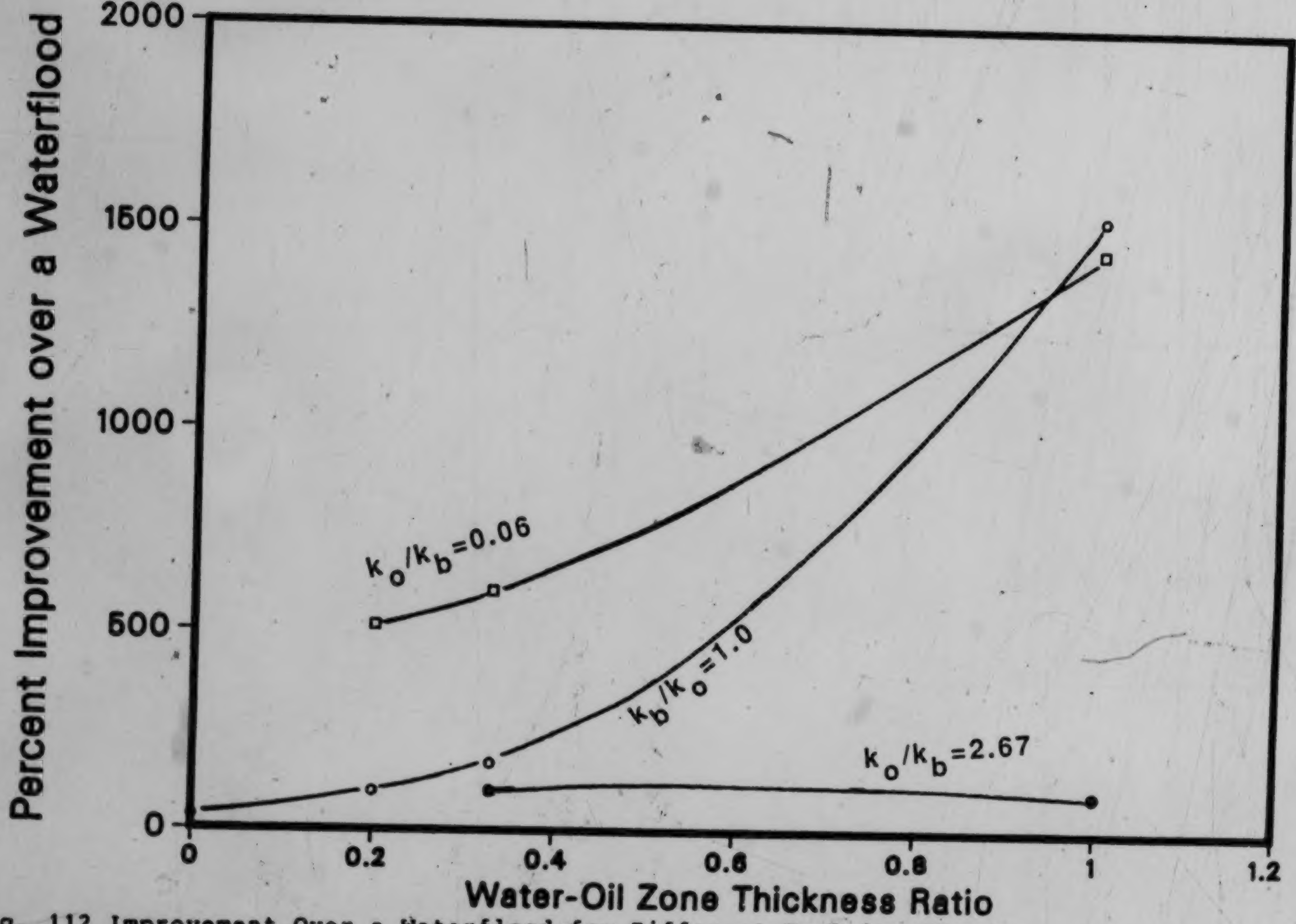

Fig. 112 Improvement Over a Waterflood for Different Emulsion Flood Runs

was quite high. This indicates that the emulsion was invading the oil and water zones uniformly. This idea is further supported by the fact that water breakthrough occurred at 0.079 PV as opposed to immediate breakthrough for the other runs. Figure 113 depicts the oil recoveries as a function of the oil-to-water viscosity ratio. During the initial stages the oil recoveries decreased as viscosity ratios increased. During the later stages, however, the best recovery performance was shown by Run 40. Also, there appears to be a tendency for delayed emulsion breakthrough as the oil viscosity decreases. Emulsion breakthrough occurred at 0.47, 0.68, 1.09 and 0.46 PV for Runs 30, 40, 39 and 41, respectively. This indicates that more emulsion invades the bottom-water zone as the oil viscosity increases. For the lower viscosity ratios, emulsion invaded both the oil and the water zones uniformly. However, emulsion invaded the bottom-water zone when the oil viscosity was high. Consequently, the oil recovery improved when emulsion was followed by a waterflood.

In terms of ultimate recovery, Run 40 (μ_o/μ_w=7.5) gave the highest oil recovery. Similar results were obtained for polymer flood runs as well. An explanation as to why there should be an optimal oil viscosity that would lead to a maximal ultimate recovery has been discussed in section 6.2.3.3 for polymer runs. A similar explanation is applicable for the case of emulsions as well. Even though

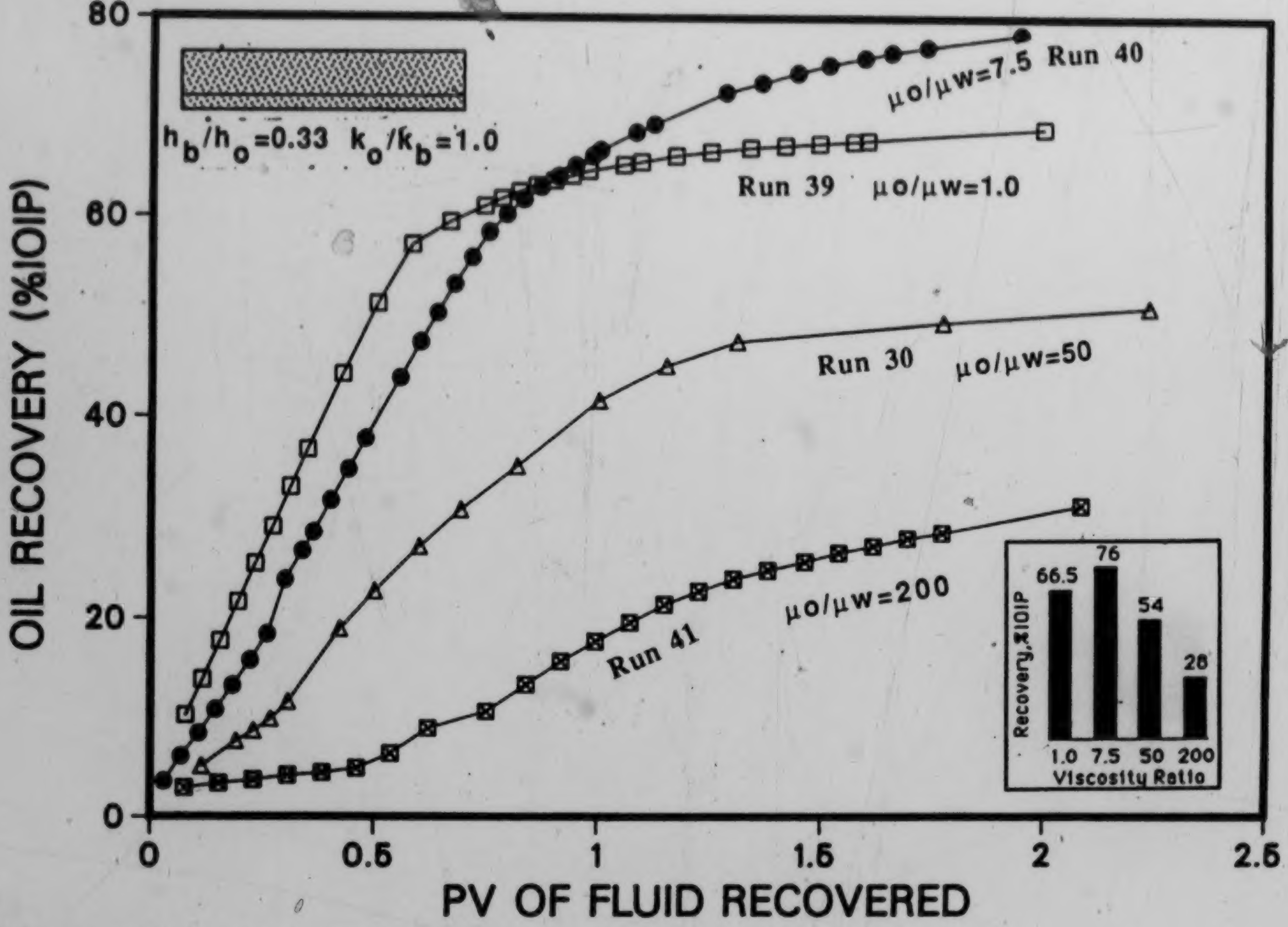

Fig. 113 Effect of Oil-Water Viscosity Ratio on Emulsion Flood Runs

the ultimate oil recovery for Run 30 was much lower than that for the other runs conducted to examine the effect of oil-water viscosity ratio, this value was still much higher than that which one would expect from a waterflood. Also, this value is comparable to the ultimate recovery obtained in base waterflood runs. Run 41, with a very high oil viscosity, gave the lowest ultimate oil recovery. However, this value is still very encouraging since a conventional waterflood for this case failed to produce anything more than two percent of the IOIP at an acceptable WOR(=20). On the other hand, a very good recovery was already obtained by a waterflood for the runs with lower oil viscosities and the improvement brought about by an emulsion flood is much more significant for runs with a higher oil viscosity.

6.4.4.3 Effect of Emulsion Slug Size

In order to examine the effect of emulsion slug size on the oil recovery performance, Runs 30, 42, 43, 44, and 45 were conducted. Figure 114 compares the oil recoveries for these runs. The emulsion slug volumes were 0.6, 0.32, 0.93, 0.16, and 1.2 PV for Runs 30, 42, 43, 44, and 45, respectively. In terms of pore volumes of the bottom-water zone, the slug sizes were two, one, three, one half, and four PV, respectively. All these runs (except Run 44) showed oil recoveries very close to one another up to a fluid injection of 0.80 PV. This indicates that blockage by emulsion is insensitive to slug size for the initial 0.8 PV

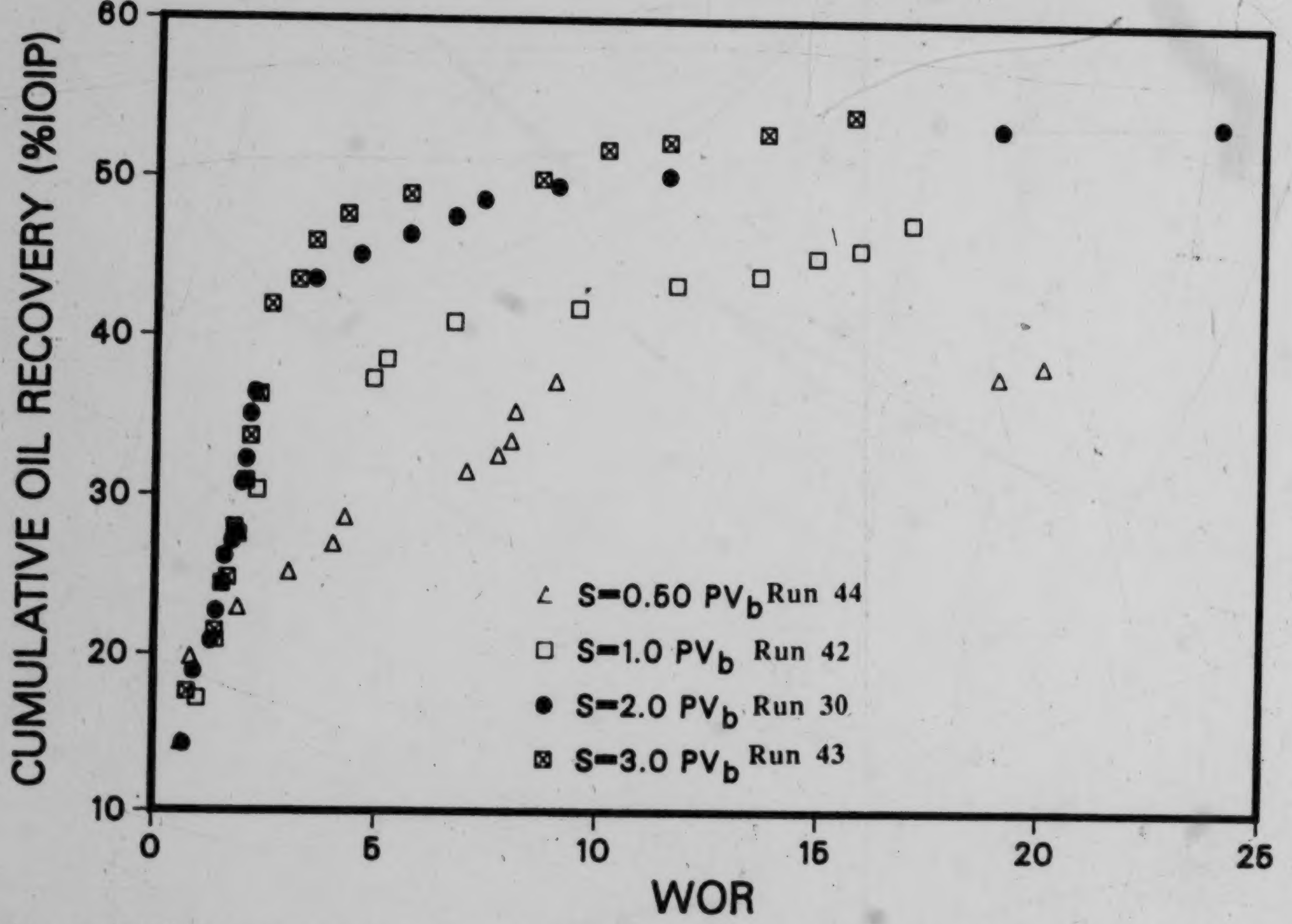

Fig. 114 Effect of Emulsion Slug Size on Emulsion Flood Performance

of fluid injection. Run 44, for which the smallest size of emulsion slug was used, showed the poorest recovery performance. For Run 43, emulsion breakthrough occurred slightly earlier than for Run 30, even though a larger emulsion slug was used for this run. This suggests that breakthrough points cannot be correlated with the size of the emulsion slug. As can be seen from Table 5.1, the recoveries at a WOR of 20 are 54, 49.5, 56.5, 38, and 57.5 percent of the IOIP for Runs 30, 42, 43, and 44, and 45, respectively. Even though an excess of one pore volume of the bottom-water zone of emulsion was injected in Run 45 (as compared to Run 44), only one percent more of the IOIP was recovered in Run 45. The ultimate recovery for Run 42 was lower than all the other runs (only 38 percent of the IOIP). It appears that, in order to create effective blockage with emulsion, at least one PV (of bottom water zone) of emulsion has to be injected. It can be seen from Figure 115 that for a larger emulsion slug the oil recovery does not increase by much. Moreover, a higher injection pressure is required throughout the displacement test with larger emulsion slugs. This would correspond to a low total production for a constant pressure case. This indicates an optimal slug volume of around 2.5 pore volumes of the bottom-water zone. The leveling off of the ultimate oil recovery vs. emulsion slug size may be explained by analogy to polymer flooding. This phenomenon of leveling off has been discussed in

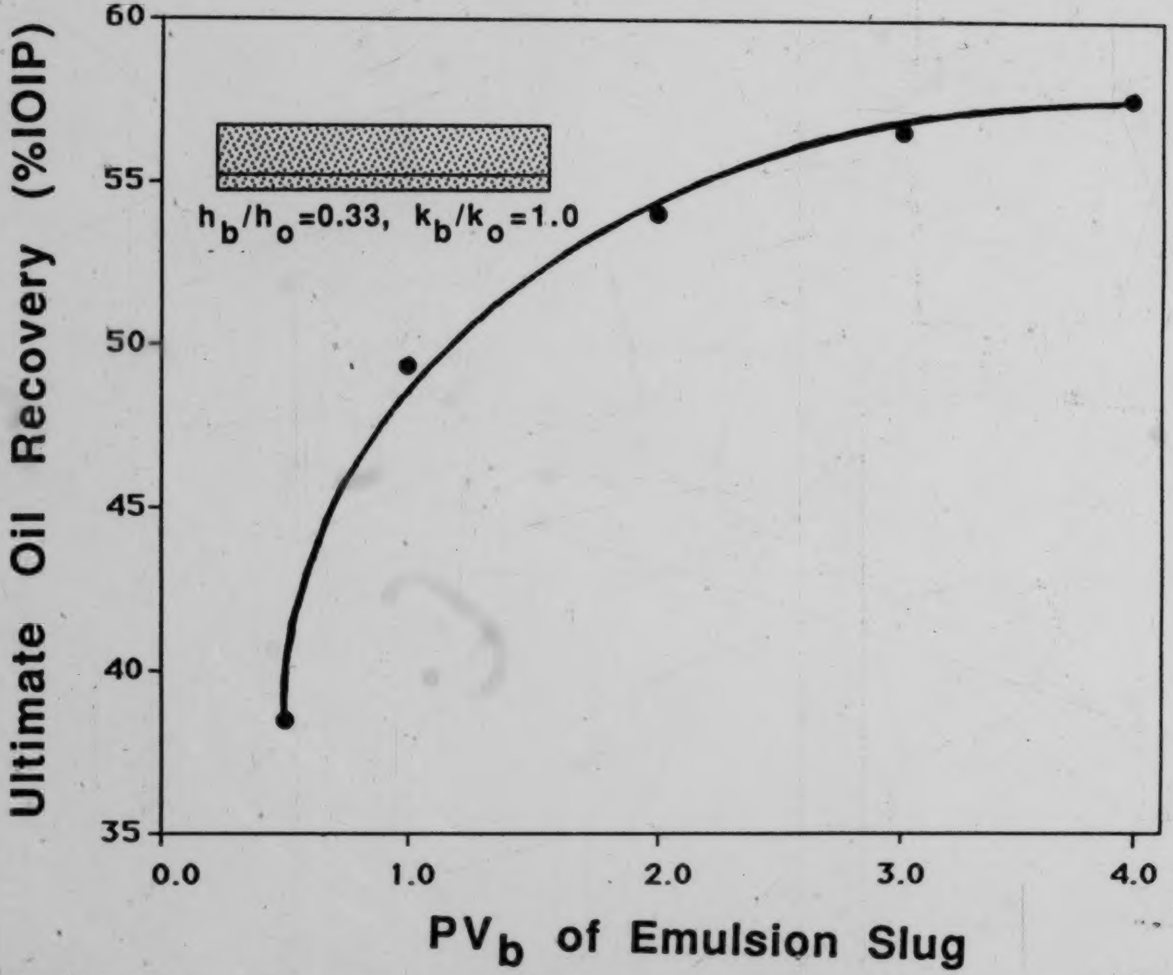

Fig. 115 Effect of Emulsion Slug Size on Ultimate Oil Recovery

section 6.2.3.1. The same reasoning is applicable for emulsions as well.

6.4.5 Mobility Control Mechanism with Emulsions

Run 46 was conducted to investigate the relative contributions of the different mechanisms involved in emulsion floods. For this run a 1.8 mPa.s viscosity glycerine solution was used as the blocking agent. The packing characteristics for this run were similar to those of Run 30. The ultimate recovery in this run was 28 percent of the IOIP as compared to 20 percent of the IOIP recovered by a waterflood. This improvement was due only to the viscosity effect of the glycerine solution. A contribution chart is presented in Figure 116. This indicates that 26% of the IOIP was recovered due to the unique blocking nature of the emulsion, whereas only eight percent was due to the viscosity effect. In fact, the use of an emulsion improves oil recovery performance much more than that which can be justified from viscosity considerations alone. The relatively lower viscosity of emulsion assures much better injectivity than that with polymer. This might be a key factor in field applications.

Table 5.3 contains a summary of the results obtained from emulsion flood runs. The emulsion breakthrough point was monitored for each of these runs. Monitoring breakthrough points was considered important as in most

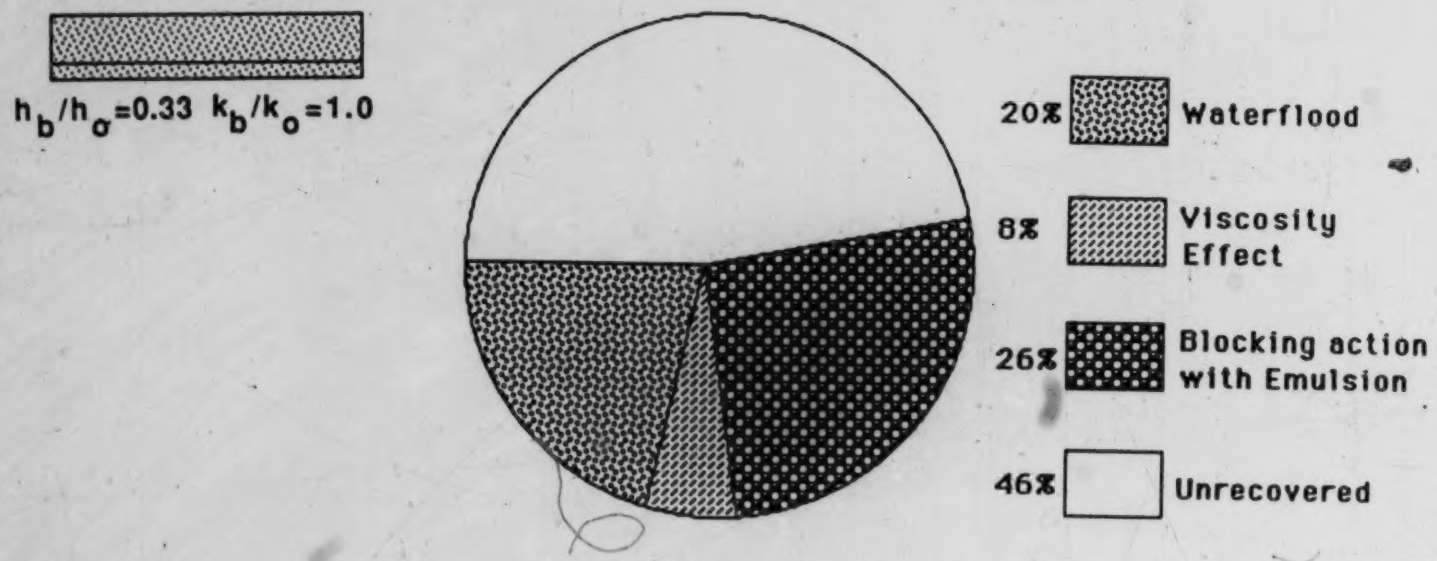

Fig. 116 Relative Contribution of Different Mechanisms in Emulsion Flooding

cases emulsion breakthrough was followed by a rapid decline in oil cut. For the runs with MCT-10, the longest breakthrough time was observed for $h_b/h_o=1$. Emulsion breakthrough is plotted as a function of k_o/k_b and h_b/h_o values in Figure 117. This figure indicates that the case of $h_b/h_o=1$ takes the longest time for emulsion breakthrough. Also, for this range emulsion breakthrough seems to be independent of the oil-to-water zone permeability ratio. The emulsion breakthrough points are much more sensitive to the oil-to-water zone permeability for lower values of h_b/h_o. The product of permeability and thickness of the bottom-water zone dictates the flux of emulsions into the bottom-water zone. However, the effects of high k_o/k_b and h_b/h_b compete with each other, i.e., a high k_o/k_b value decreases emulsion flux whereas a high h_b/h_o increases the flux. Consequently, a maximum in the breakthrough vs. oil-to-water zone permeability ratio curve is expected. However, the magnitude of these two competing effects dictates that the curves for h_o/h_b values of 0.33 and 0.20 do not show a maximum. Apart from this difference in these curves, as can be inferred from Figure 117, emulsion breakthough times are proportional to the pore volume of the bottom-water zone, PV_b. This observation implies that the emulsion propagates in a piston-like fashion, at least in the bottom-water zone. This behaviour could be concluded also from the form of the emulsion produced soon after the

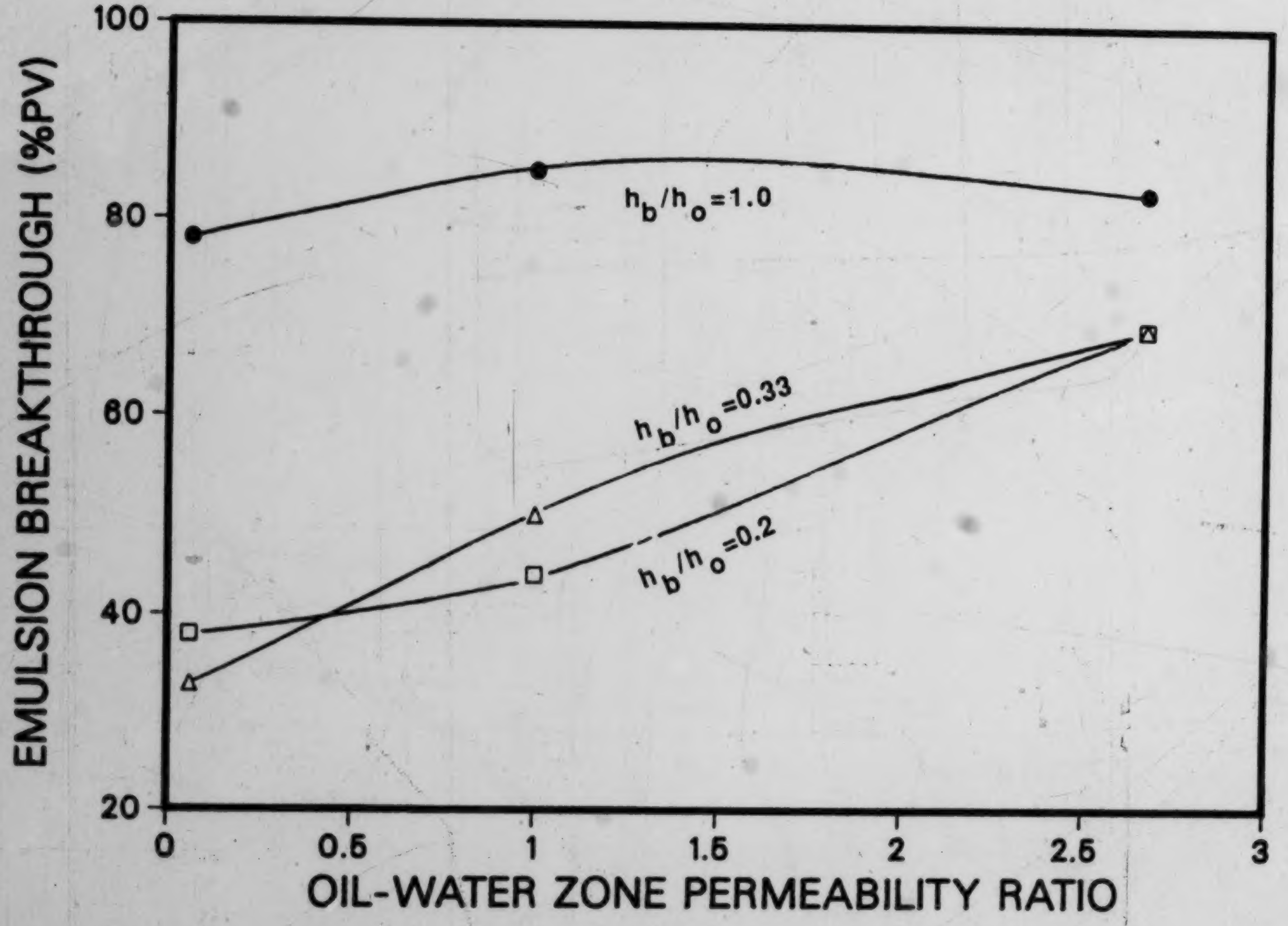

Fig. 117 Emulsion Breakthrough as a Function of k_o/k_b and h_b/h_o

breakthrough. It was observed with a microscope that the emulsion produced had a structure very similar to the structure of that injected. However, as the displacement test continued, the produced emulsion showed gradual thinning indicating that the emulsion was only partially displaced by water and a good part of it was left in the reservoir model, presumably in the bottom-water zone. However, when a water slug was injected following the emulsion slug, the water slug encountered resistance from the bottom-water zone due to the presence of emulsion in this zone. Consequently, water entered the oil zone and the oil recovery by the waterflood improved.

6.5 Waterflood with Air Injection

Runs 47 through 53 were conducted to examine the effectiveness of air as a mobility control agent. Air may decrease the effective permeability to water (injected after the air slug) by creating an extra phase in the bottom-water zone. Only the 50 mPa.s oil was used for these air injection runs. For these runs, the air was injected at constant pressure.

An increase in injection pressure was observed for waterfloods following air slug injection for runs of $k_o/k_b=1$. This indicated partial blockage of the bottom-water zone due to the presence of the air. For runs with a tighter bottom-water zone, there was no increase in pressure for water injection but the oil recovery was quite high. It was observed that as the displacement test continued the effect of the air slug was decreased. This indicates that, as the flood front propagates, the barrier created by the air ceases to be effective. Figures 118 and 119 compare oil recoveries for k_o/k_b values of 1.0 and 2.67, respectively. It can be seen from Figure 118 that the oil recovery performance is very poor for $h_o/h_b=1$. However, the oil recovery performance improves very quickly as the bottom-water zone thickness decreases. For $k_o/k_b=2.67$, the oil recovery is much less sensitive to the bottom-water zone thickness (see Figure 119). In fact, for a very low h_b/h_o (0.2) value, the recovery is poorer at the initial stage of the displacement test even though the ultimate recovery for this run was the highest. Figure 119 also compares the recovery performance between runs for which the same h_b/h_o value of 0.33 and k_o/k_b value of 2.67 were used, but for one of them the production well was used to inject air slugs. It can be seen that the recovery is better when air slugs are injected through the production well.

Figure 120 depicts ultimate recoveries as a function of h_b/h_o and k_o/k_b values. It can be seen from this figure that the cases of $h_b/h_o \geq 0.33$ are the most sensitive to the bottom-water zone permeability. For a very thin bottom-water zone ($h_b/h_o=0.20$), the ultimate recovery increases slightly from $k_o/k_b=1.0$ to $k_o/k_b=2.67$. The

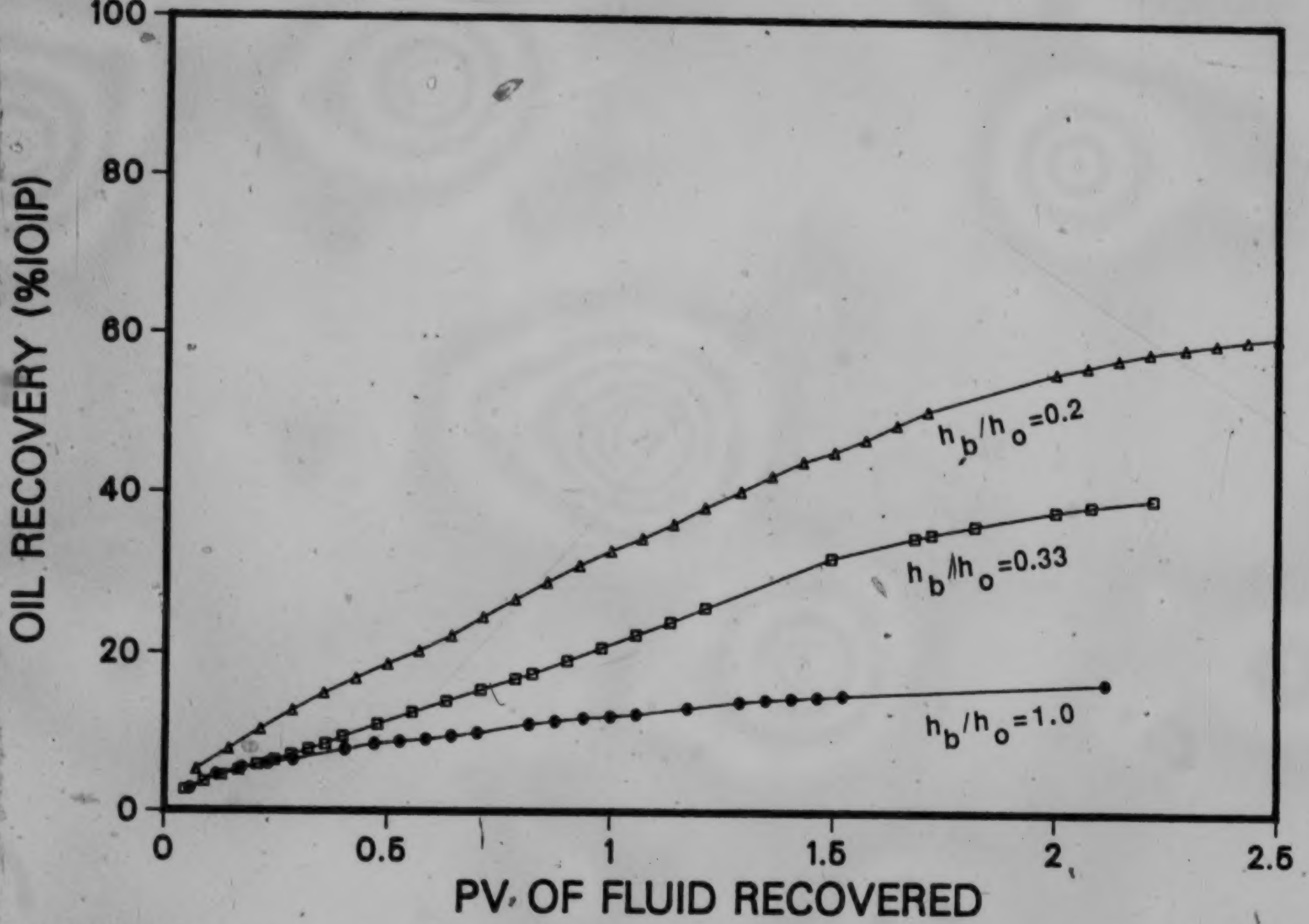

Fig. 118 Comparison of Oil Recoveries for different h_b/h_o and $k_o/k_b=1.0$ (Air Injection)

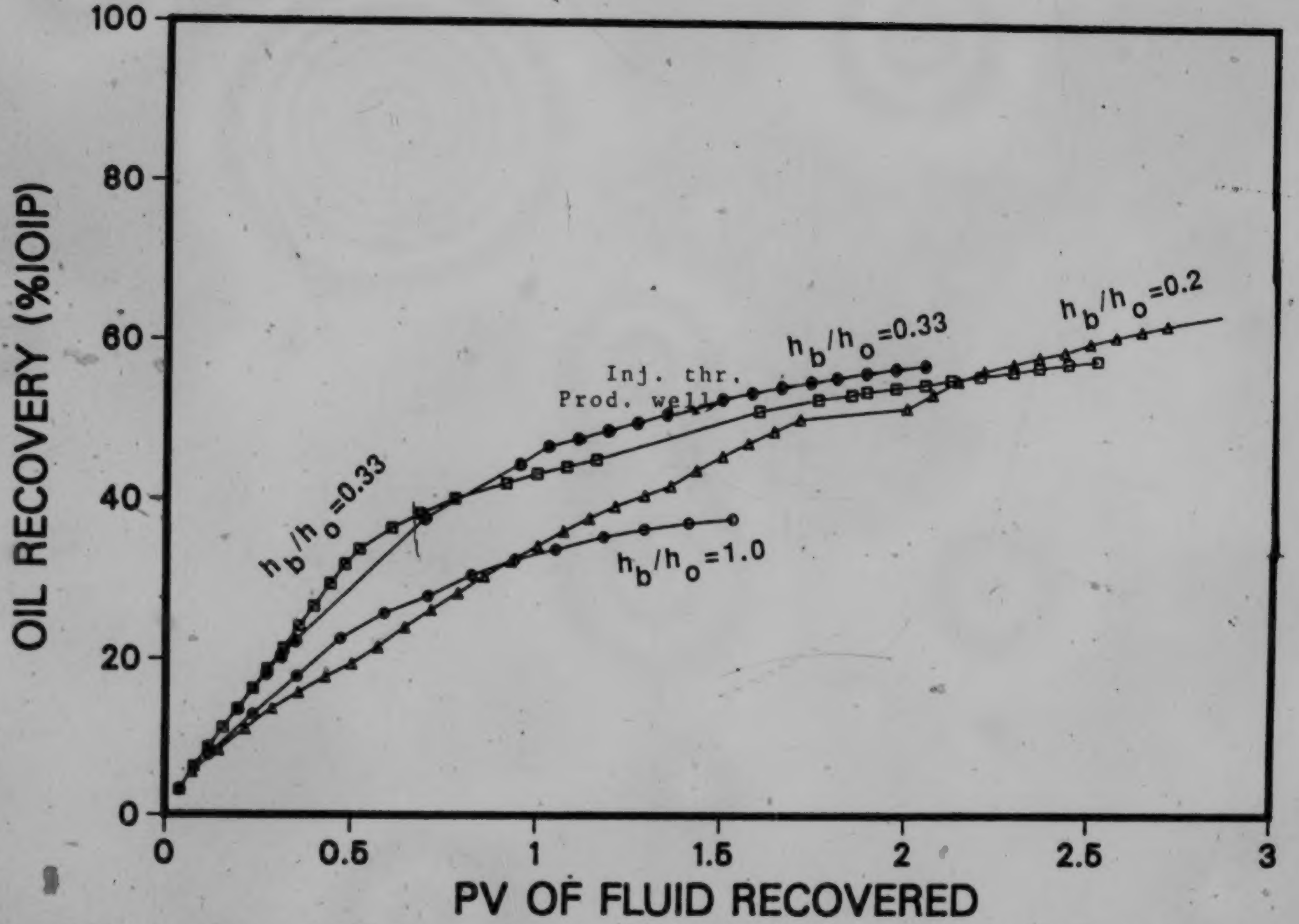

Fig. 119 Comparison of Oil Recoveries for h_b/h_o and k_o/k_b=2.67 (Air Injection)

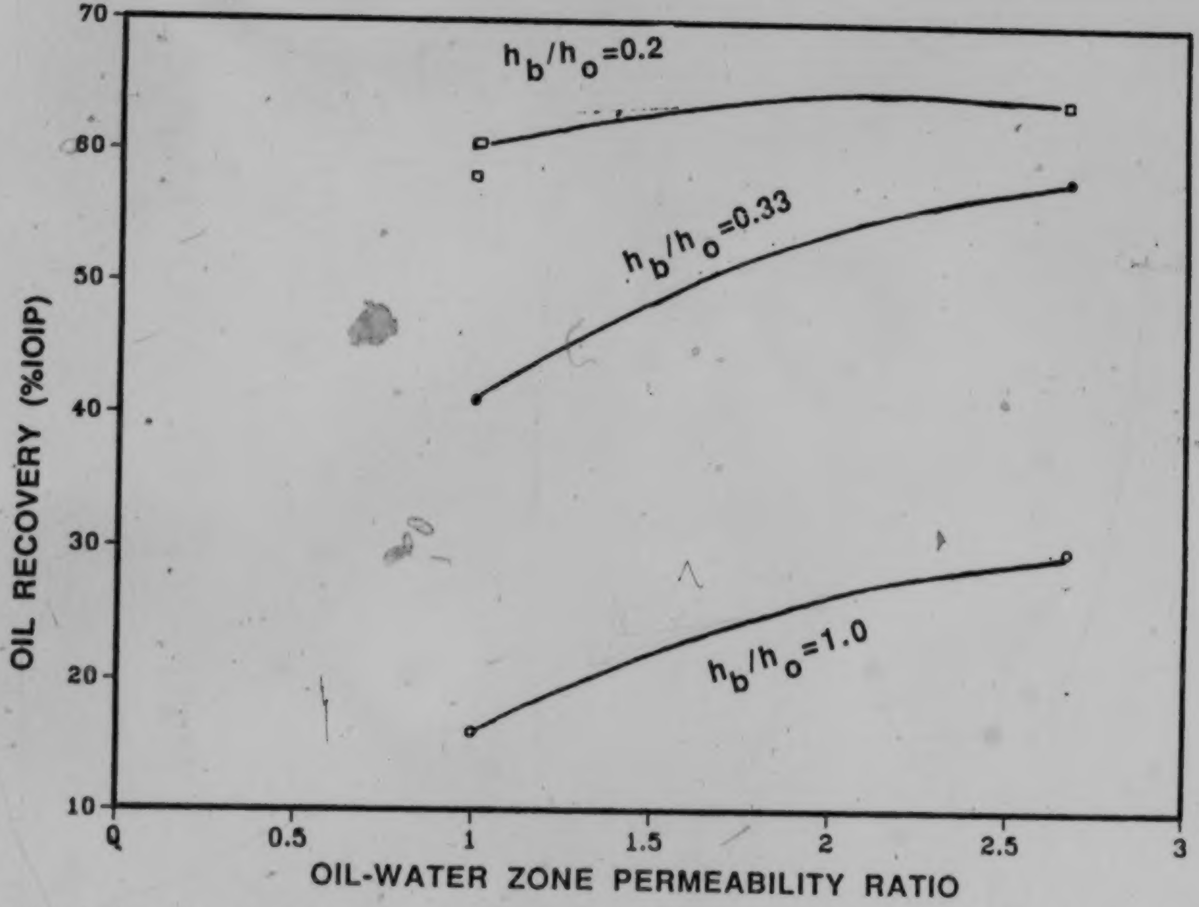

Fig. 120 Air Injection Performance as a Function of k_o/k_b and h_b/h_o

dependence of ultimate oil recoveries upon the values of k_o/k_b can be seen from Figure 121. Oil recoveries are very sensitive to the h_o/h_b values for lower values of h_b/h_o, especially for k_o/k_b=1.0.

Figure 122 depicts the oil recoveries in a three-dimensional form. As can be seen from this figure, the highest oil recovery is obtained for a tight, thin bottom-water zone. Run 52 is a repeat of Run 51 with the exception that the air slugs were injected through the production well for Run 52. It appears that the injection of air through the production well improves oil recovery. However, the improvement is not large. The ultimate recoveries for tight and thin bottom-water zones are comparable to those obtained with emulsion or polymer floods. Air injection seems to hold some promise for reservoirs with a tight bottom-water zones only.

Figure 123 depicts the percentage of improvement with air injection over a conventional waterflood. Even though the oil recoveries are higher for k_o/k_b=2.67, the biggest improvement takes place for k_o/k_b=1.0, especially for higher values of h_b/h_o. This is, however, due to the fact that the waterflood recovery is very low in this range of k_o/k_b and h_b/h_o. For k_o/k_b=2.67, the greatest improvement took place at around an h_b/h_o value of 0.5. For a homogeneous pack, air injection performed more poorly than a waterflood. Note, however, that continuous air injection was conducted

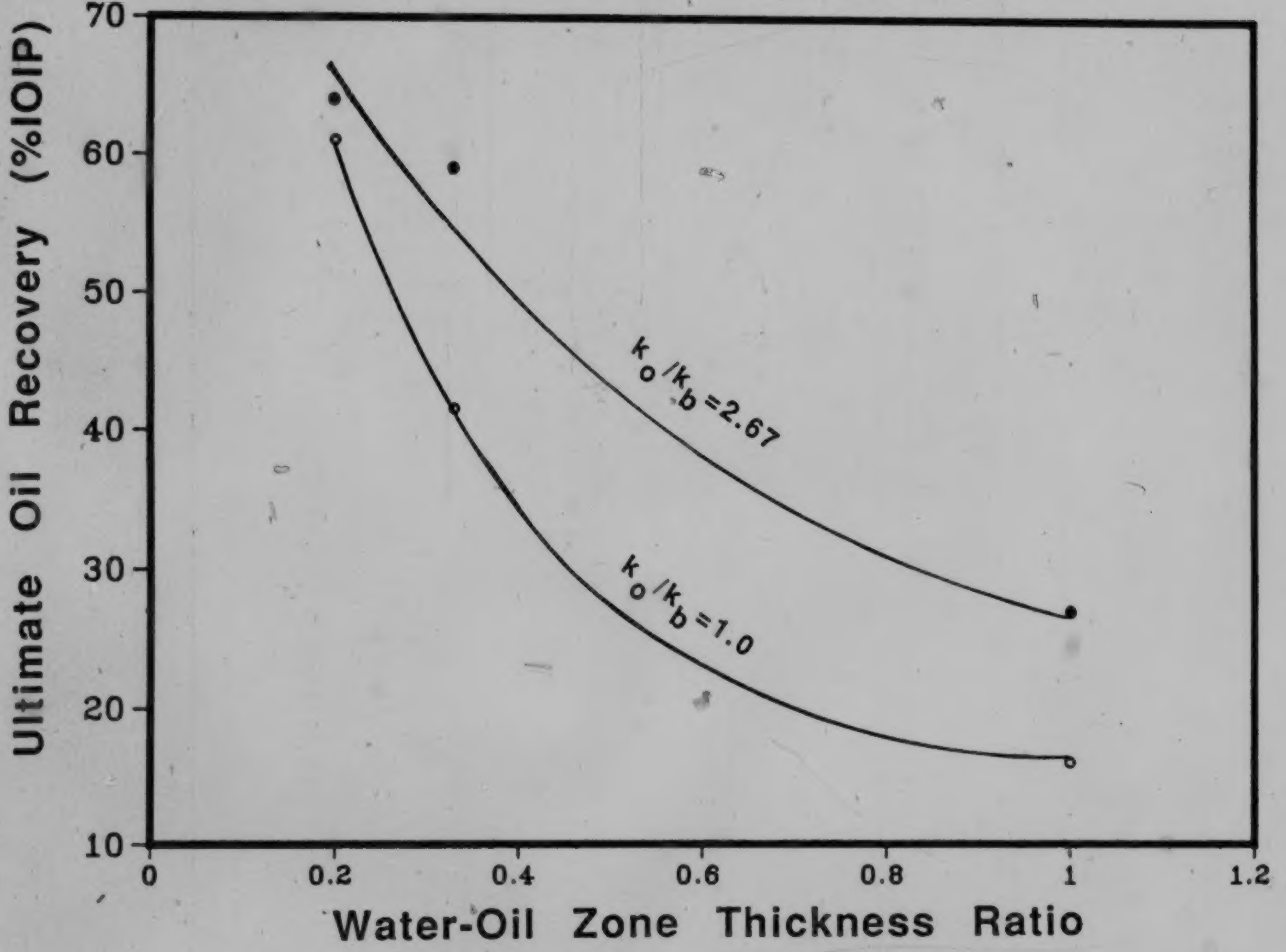

Fig. 121 Air Injection Performance as a Function of k_o/k_b and h_b/h_o

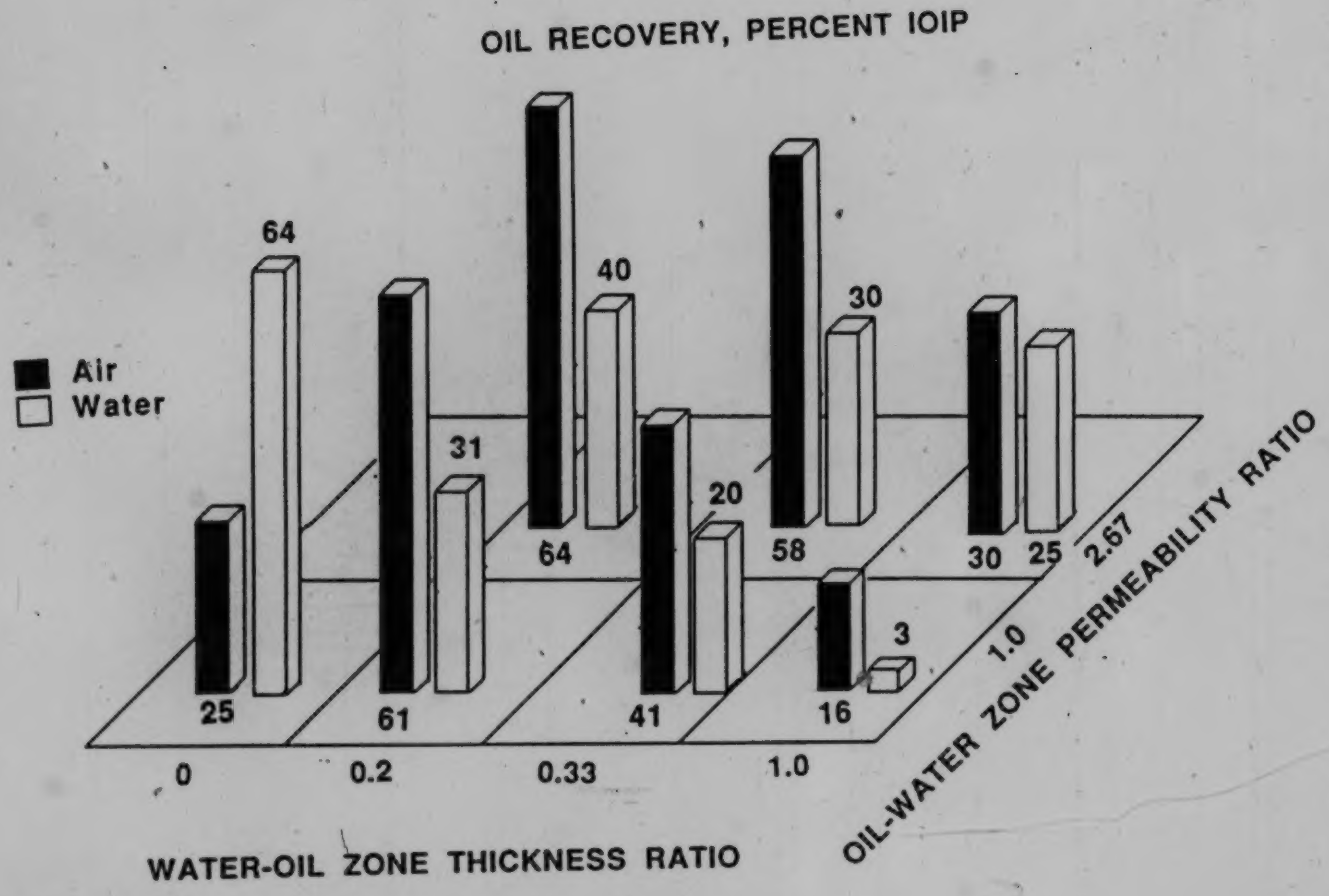

Fig. 122 Comparison of Air Injection with Waterflood

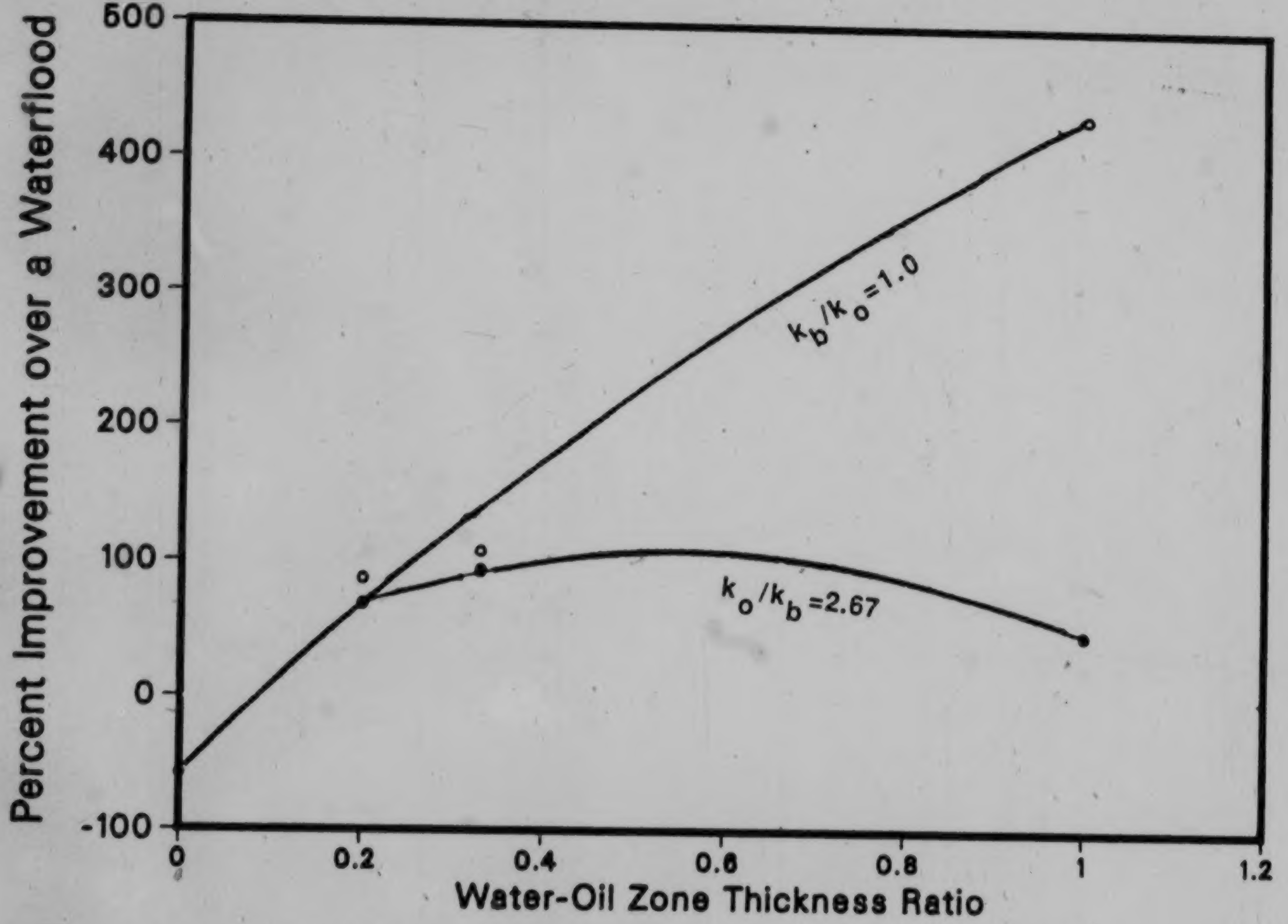

Fig. 123 Improvement Over a Waterflood for Different Air Injection Runs

in the homogeneous pack and the ultimate oil recovery was expected to be low due to a very unfavourable mobility ratio.

6.6 Injection of Biopolymer Gel

Runs 54 and 55 were conducted to investigate the effects of a biopolymer gel on oil recovery for reservoir models with both thin and thick bottom-water zones. The gel was prepared from 2000 ppm FLOCON 4800 cross-linked with Cr^{+3} at a proportion of 1:20. For Run 54, the gel was formed outside of the core. The gel was injected at a volumetric injection rate of 200 ml/hr. The oil cut for Run 54 was higher than that for a waterflood alone but the ultimate recovery was very poor (11.5 percent of the IOIP only). Injecting gel through the production well did not improve the recovery either. At the end of the displacement test, as the core was opened, it was found that the gel did not travel very far along the length of the core. Consequently, the water that followed the gel injection bypassed the gel-invaded bottom-water zone easily and the producing WOR remained very high. For Run 55, the gel was formed in situ with the expectation that it would travel far into the bottom-water zone. Even though the gel formed in situ gave better results than that formed externally, once the gel was formed the injection pressure for the water was quite high and the oil recovery was not comparable to those obtained by polymer or emulsion injection.

6.7 Foam Injection

Two different sets of displacement tests were conducted. One set was conducted to investigate the effects of various parameters in a homogeneous core and the other set was conducted to investigate the blocking action of foam in a core with a bottom-water layer. The experimental results are summarized in Tables 5.1 and 5.4.

6.7.1 Flow of Foam in a Homogeneous Porous Medium

Different displacement tests were performed to investigate the effect of surfactant concentration and volumetric injection rate on ultimate oil recovery, foam breakthrough and foam quality. Runs were also conducted to compare the performance of foam generated in situ.

6.7.1.1 Effect of Surfactant Concentration

Runs 56 to 61 were conducted to examine the effect of surfactant concentration on ultimate oil recovery. For all these runs, foam was generated in situ, i.e., surfactant water was alternated with nitrogen. For all these cases 0.2 PV of surfactant water was first injected. This surfactant-water slug was then followed by nitrogen. Nitrogen was then alternated with surfactant water again. As can be seen from Figure 124, at very low surfactant concentrations, the ultimate oil recovery approaches that

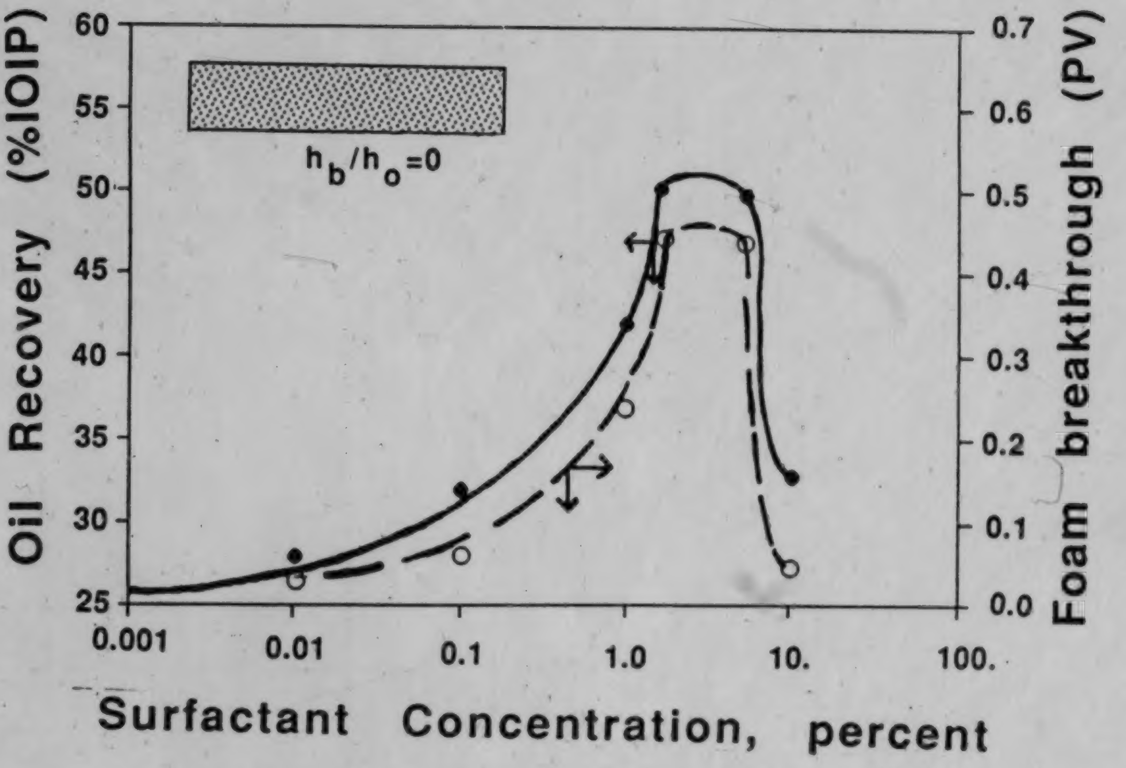

Fig. 124 Effect of Surfactant Concentration on Foam Injection Performance (h_b/h_o=0)

for nitrogen injection (Run 62 that gave 25 percent of the IOIP recovery). It should be mentioned here that ultimate recovery is considered to be the recovery at which point the gas-liquid ratio attained 7000. This value was arbitrarily fixed in order to be able to compare different runs. It should also be noted that none of these recoveries reach an ultimate recovery obtained with a conventional waterflood. It has been reported that, for such a system, a conventional waterflood will give an ultimate recovery of 64 percent of the IOIP. Figure 124 indicates that the optimal surfactant concentration would be in the range of one to eight percent. For this range of surfactant concentration the foam breakthrough is delayed considerably. During all the runs, a considerable amount of oil-in-water emulsion was produced as well. It was observed that the quantity of emulsion increased as the amount of effluent free gas increased. This leads to the conclusion that the emulsification was enhanced by the flow of free gas through the oil-rich part of the porous medium. After foam breakthrough occurred the gas-liquid ratio and the quality of the foam increased rapidly. Also, very little oil was recovered after foam breakthrough. As the foam quality increased, more surfactant-water slugs were injected. These were alternated with nitrogen. The new foam produced by this process increased the oil cut but the quantity of extra oil recovered was not significant. For these runs nitrogen was injected at a constant injection pressure of 69 kPa. Figure 125 depicts the contribution of nitrogen and foam in recovering oil from a homogeneous core.

6.7.1.2 Effect of Injection Pressure

Figure 126 compares the ultimate oil recovery for Runs 59, 63, and 64. For all these runs the surfactant concentration was two percent but the gas injection pressure was different. This figure shows a strong dependence of ultimate recoveries on the ΔP used. Similar dependence was observed in breakthrough recoveries as well. At high values of ΔP, a considerable amount of oil-in-water emulsion was produced. This might be one of the reasons for a poor oil recovery at high values of ΔP. This dependence of oil recovery on injection pressure is consistent with a previous observation by Huh and Handy(1986). It was observed also that the quality of foam decreased with increasing values of ΔP. This was previously observed by Marsden and Khan(1966) in the absence of oil. Whatever might be the reason, this dependence on injection pressure (or gas volumetric injection rate) poses a serious problem in using a single set of relative permeability curves in simulating foam flow in a porous medium.

It was also observed that during the later stages of the displacement test, four different phases were flowing at the outlet end: the aqueous phase, the oleic phase, foam and free gas. The presence of emulsion further complicated the

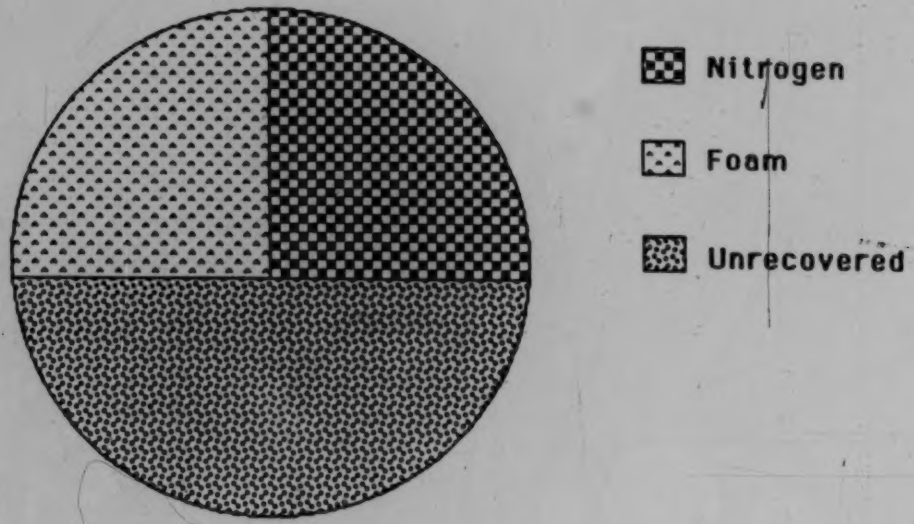

Fig. 125 Contribution of Air and Foam in Oil Recovery for $h_b/h_o=0$

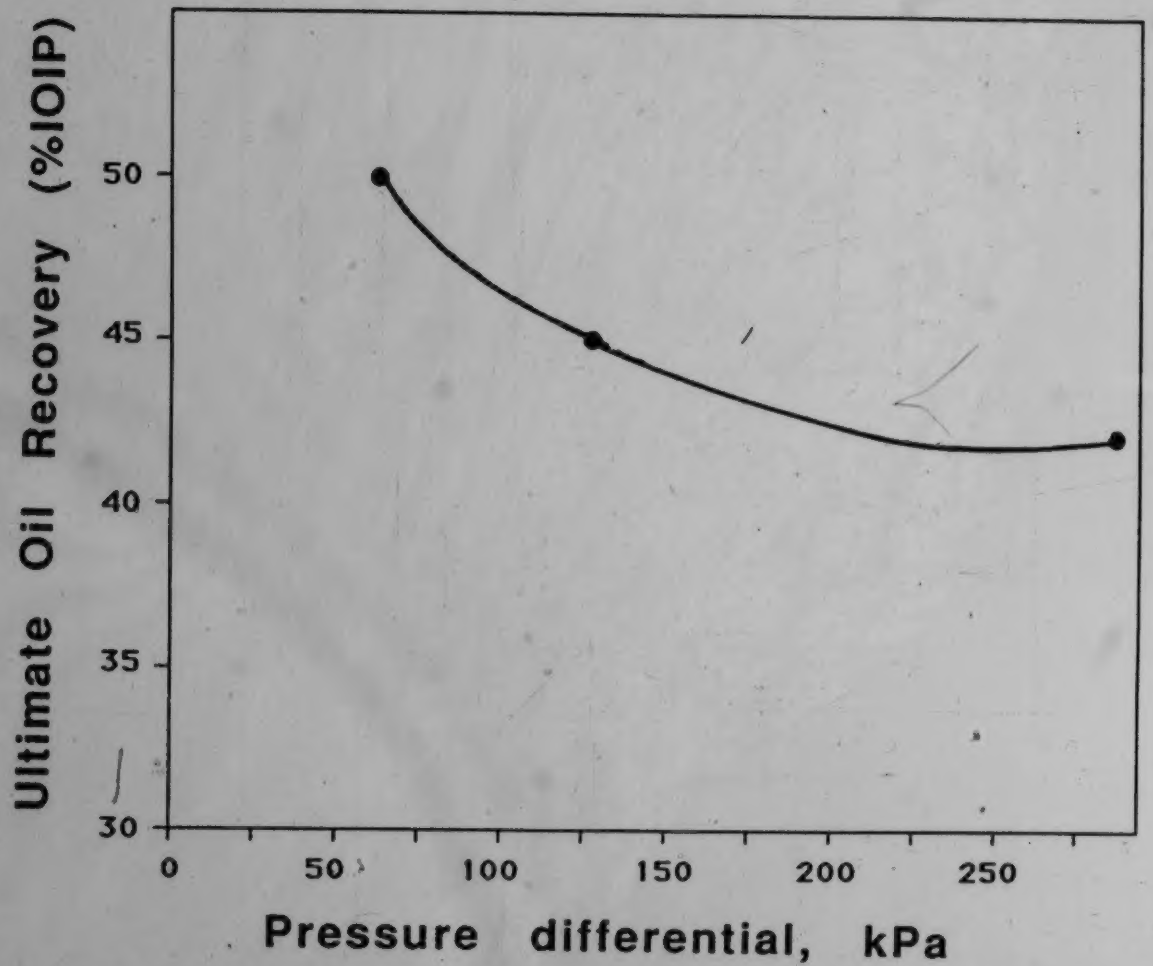

Fig. 126 Effect of Injection Pressure on Foam Injection Performance for $h_b/h_o=0$

process. This complex flow phenomenon might justify a more detailed study of flow mechanism in the presence of oil.

6.7.2 Foam Flow in the Presence of a Bottom Water Layer

Runs 65 to 75 were conducted to investigate the effects of surfactant concentration, oil-to-water-layer thickness ratio, oil-to-water viscosity ratio, and oil-to-water layer absolute permeability ratio.

6.7.2.1 Effect of Surfactant Concentration

Runs 65 to 67 were conducted to investigate the effect of surfactant concentration. Runs 65, 66 and 67 had surfactant concentrations of one percent, four percent, and 10 percent, respectively. For all these runs a thin bottom-water layer ($h_b/h_o=0.33$) was added to the oil zone. Also, the bottom-water layer had the same permeability as the oil zone. Figure 127 compares the oil recovery performance for these runs along with a previously reported run for which air was alternated with distilled water alone. As can be seen from this figure, the presence of surfactant improves the oil recovery for any amount of surfactant over the range studied in this work. However, unlike the results observed in a homogeneous core, the maximal oil recovery was obtained for a surfactant concentration of four percent. This was expected, since the injected surfactant water was diluted considerably due to its contact with the bottom water. However, since the exact nature of this mixing is

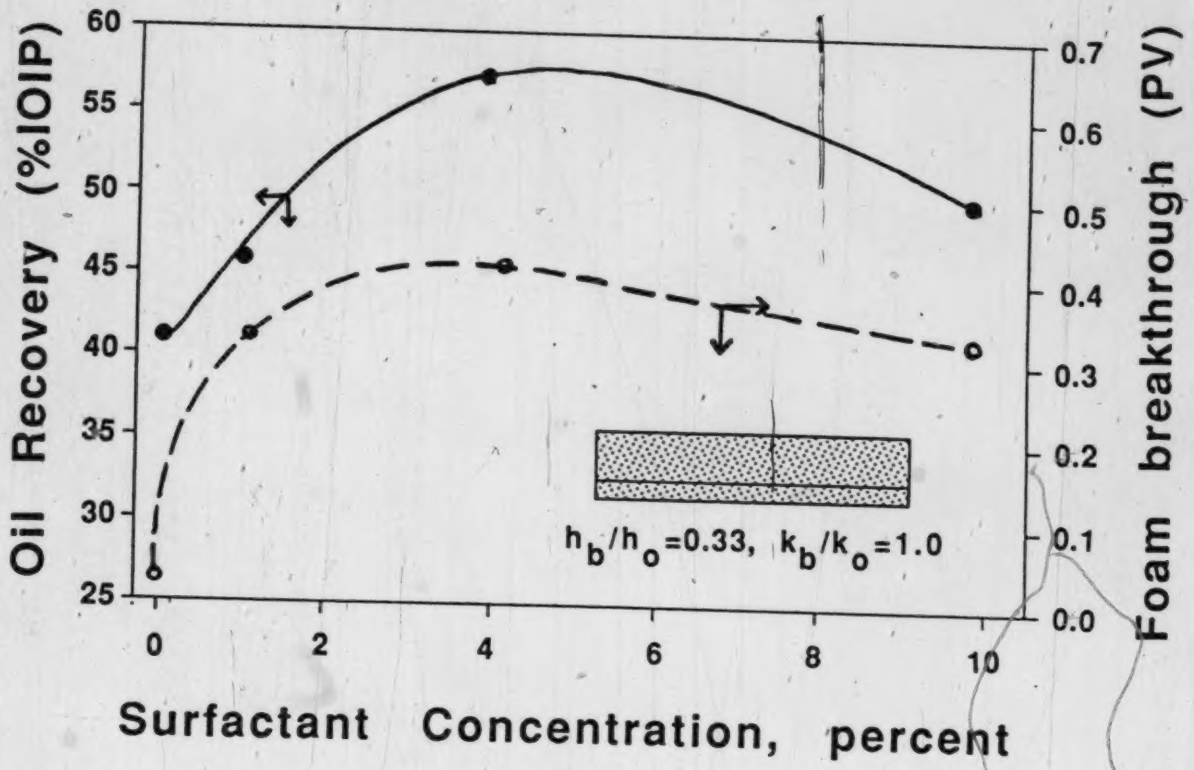

Fig. 127 Effect of Surfactant Concentration on Foam Injection Performance for h_b/h_o=0.33

unknown it is not possible to predetermine the optimal surfactant concentration from the data obtained in a homogeneous core. The comparison of Runs 65 to 67 led to the choice of a four-percent surfactant concentration for all other runs with a bottom-water layer.

6.7.2.2 Effect of Viscosity Ratio

Runs 66, 68, and 69 were conducted to investigate the effect of the oil-to-water viscosity ratio on the performance of foam in a core with a bottom-water layer. The oil-to-water viscosity ratios were 50, 7.5, and 200 for Runs 66, 68 and 69, respectively. Figure 128 compares the oil recovery curves for these runs. Also, the inset of this figure compares the ultimate oil recoveries for various oil-to-water viscosity ratios. As can be seen from this figure, Run 68 ($\mu_o/\mu_w=7.5$) gave the highest oil recovery. This is expected as the mobility ratio for this run is the most favourable. However, the oil recovery obtained in Run 66 ($\mu_o/\mu_w=50$) was very close to that for Run 68. This shows the effectiveness of foam in an adverse situation. In fact, for a conventional waterflood the runs with 7.5 mPa.s and 50 mPa.s viscosity oils showed a large difference in oil recoveries. The inset of Figure 128 shows the ultimate oil recoveries for these runs. Even though the ultimate recovery for Run 69 appears to be much less than that for Run 66, it should be remembered that, due to the very high oil viscosity, Run 69 would give an oil recovery of only a

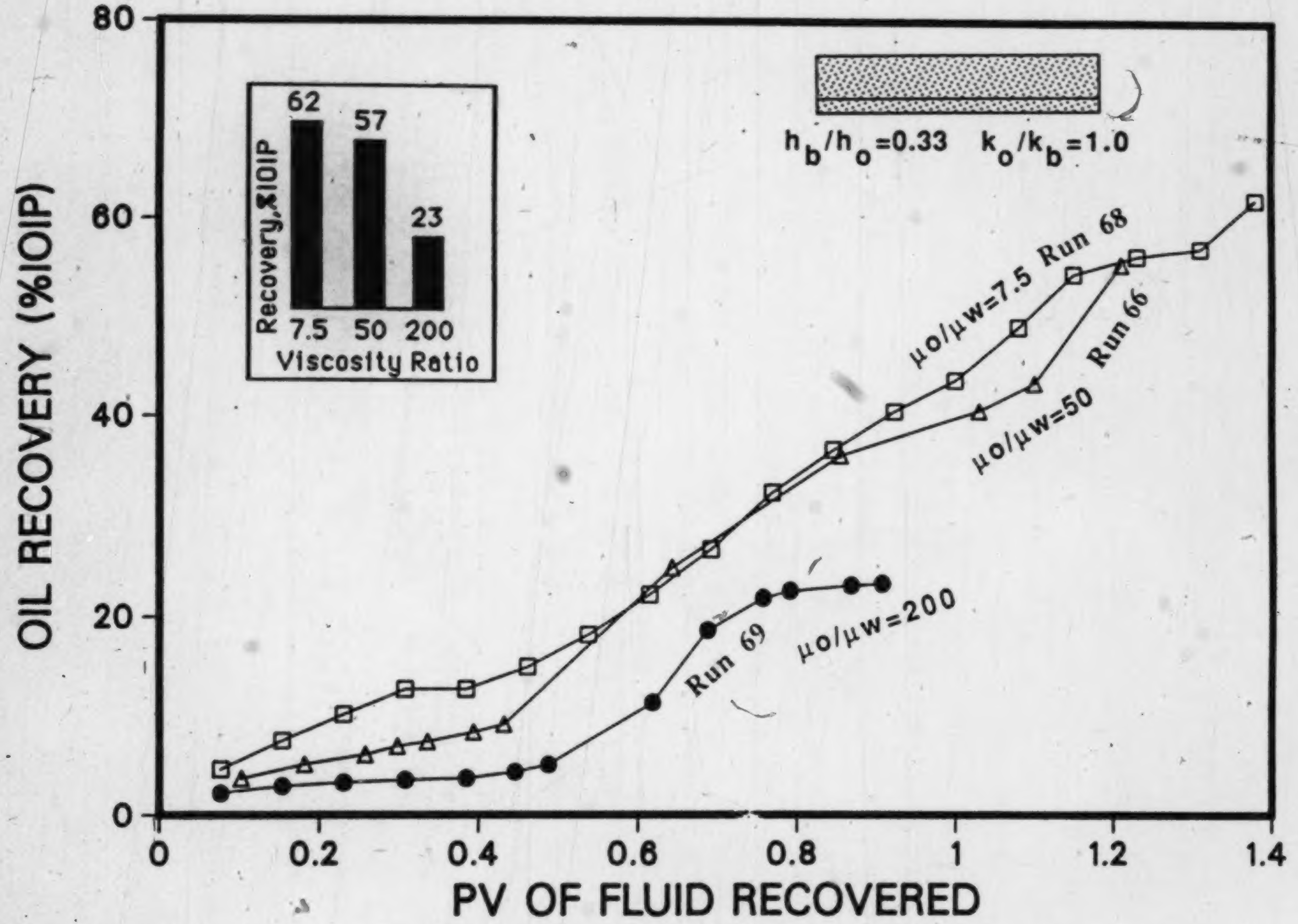

Fig. 128 Effect of Oil-Water Viscosity Ratio on Oil Recovery (Foam Injection)

small fraction of the initial oil in place and that the application of foam, instead of gas or waterflood, increased the oil recovery at least 10 times for this particular case of high oil viscosity. In fact, comparing the performance of foam for different oil viscosities in a core with a bottom-water zone, it appears that the enhancement (over waterflood or gas injection) accomplished with foam improved as the oil viscosity increased. It was observed that the volume of emulsion produced decreased as the viscosity of oil increased. This phenomenon might provide an explanation as to why a relatively better performance was observed with a higher oil viscosity. Also, the quality of foam was lower for the low-viscosity oil. Low-quality foam has a smaller bubble size as compared to high-quality foam. For the case of a bottom-water layer, a larger bubble of foam would cause more resistance to the flow of gas. Moreover, this resistance would be more pronounced in the bottom-water zone because most of the foam would have traveled into this zone due to least resistance to flow.

6.7.2.3 Effect of Bottom-water Zone Permeability

Runs 66, 70, and 71 were conducted to investigate the effect of bottom-water zone permeability on the performance with foam injection. These runs had bottom-water zone permeabilities of 16, 6, and 270 μm^2 respectively. All these runs had an oil-to-water zone thickness ratio of three. Figure 129 compares the oil recoveries for Runs 66,

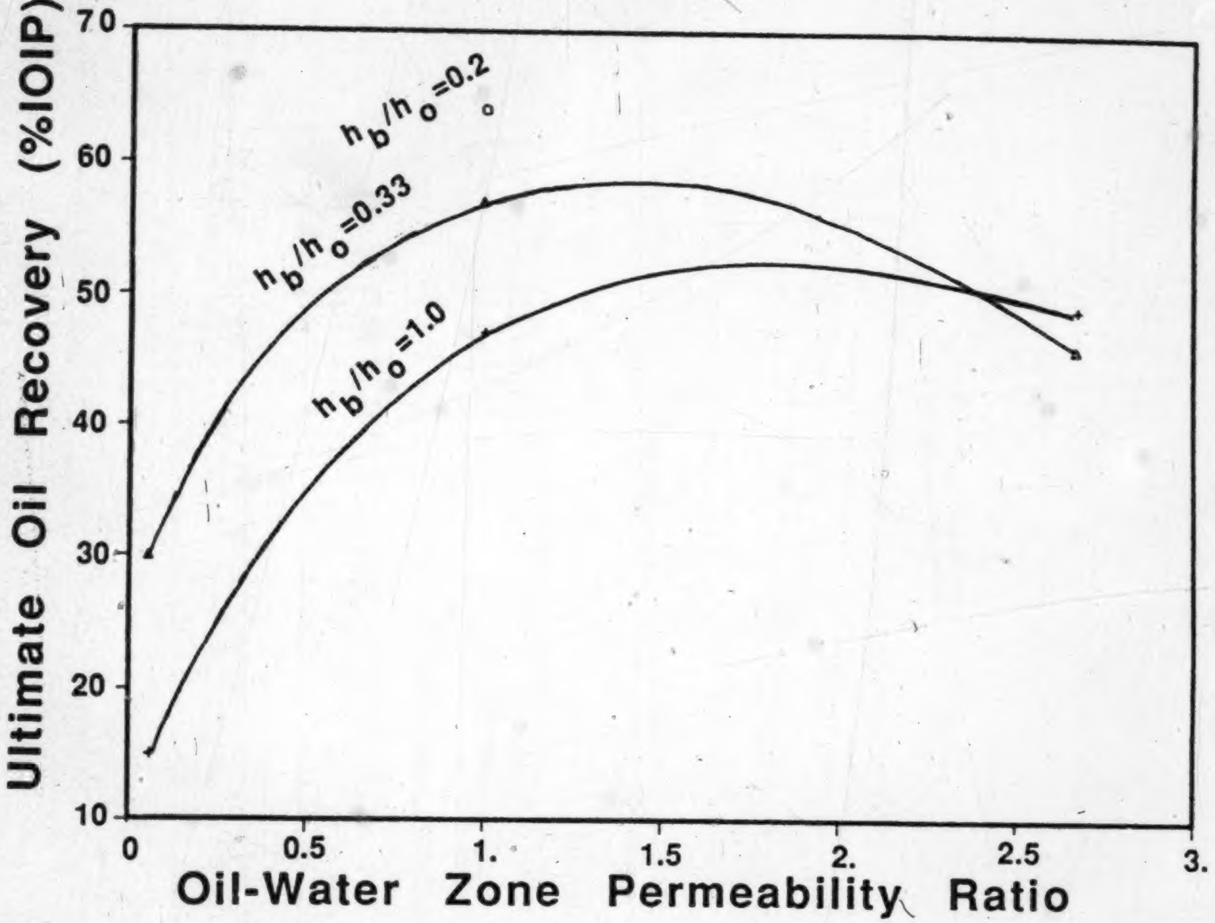

Fig. 129 Foam Injection Performance as a Function of k_o/k_b and h_b/h_o

70, and 71. As can be seen from this figure, there appears to be an optimum in terms of the oil-to-water zone permeability ratio. Of more importance is the observation that the ultimate oil recovery is not the best for the highest oil-to-water zone permeability ratio. In a system with a bottom-water zone, two different phenomena take place. As the bottom-water zone permeability increases the system is subjected to increased channeling into the bottom-water zone, and consequently the oil recovery declines. However, the absolute permeability has a different impact on the blocking action of foam. It has been reported earlier that the blocking action with foam improves ~~as~~ the absolute permeability increases (Raza, 1970; Best et al., 1985). Recently, it has been observed that (Khatib et al.,1986) there exists an optimal value (12 μm^2) at which the gas mobility is the lowest. A similar phenomenon is observed in this study. Some authors (Best et al., 1985) tried to explain this phenomenon in terms of the shear-thinning behaviour of foam. In this study, it has been observed for a homogeneous core that as the ΔP value increases the bubble size of the foam and the apparent foam viscosity decrease. This led to a decreasing ultimate oil recovery in the homogeneous pack. This was also observed by some of the previous researchers (Huh and Handy,1986, Fiedmann and Jensen,1986). A low permeability would be equivalent to a high ΔP for a constant injection rate, or to a low volumetric injection rate for a constant injection pressure. This study was done with constant injection pressure of nitrogen. Therefore, as the bottom-water zone permeability decreases, the volumetric injection rate into the bottom water zone decreases. If foam is indeed pseudoplastic in nature, this low shear stress should lead to a higher foam viscosity. As a consequence, in a core with a bottom-water zone, foam flux into the bottom-water zone decreases with decreasing permeability of the bottom-water zone. This leads to a better oil recovery for a low-permeability bottom-water case than for a high-permeability bottom-water case during the initial stages of nitrogen injection. However, as nitrogen injection continues, because only a small amount of foam penetrates the bottom-water zone, foam quality and bubble size increase and less resistance to flow of the gas is encountered in the bottom-water zone. Consequently, the injected nitrogen preferentially penetrates the bottom-water zone, and this leads to a poor ultimate oil recovery, which is lowest for a very high bottom-water zone permeability. For a highly permeable bottom-water zone, the bubble size of the foam might be too small to create any effective blockage. However, the clustering together of foam bubbles creates enough blockage for a many-fold improvement over a conventional waterflood. A conventional waterflood gave only 5% oil recovery in such a situation.

In general, the change of absolute permeability causes several effects and these are not easily explained in terms of apparent viscosity alone. For instance, by analogy with a tube, high permeability is equivalent to a larger tube radius. Therefore, high permeability should lead to a high apparent viscosity. However, this is in contradiction to the other observation which dictates that a low velocity, due to a low absolute permeability, would cause lower shear stress and, therefore, should lead to a higher apparent viscosity. It is more appropriate to interpret the blocking mechanism of foam in terms of mobility (ratio of effective gas permeability and apparent gas viscosity) rather than apparent viscosity alone. It should be mentioned here, however, that in some cases the effective gas permeability and apparent gas viscosity do not vary in the same direction and a balance of the two will dictate the effective mobility ratio.

6.7.2.4 Effect of Water-to-Oil Zone Thickness Ratio

Runs 72 through 74 were conducted with a water-to-oil zone thickness ratio of one. These runs could, therefore, be compared with Runs 66, 70 and 71 to examine the effects of the bottom-water zone thickness on three different k_o/k_b values: 1.0, 2.67, and 0.06. A comparison of the ultimate recoveries for these runs is depicted in Figure 130. For comparison, Run 59 (without bottom-water zone) has also been included. Figure 131 depicts the ultimate recoveries in a

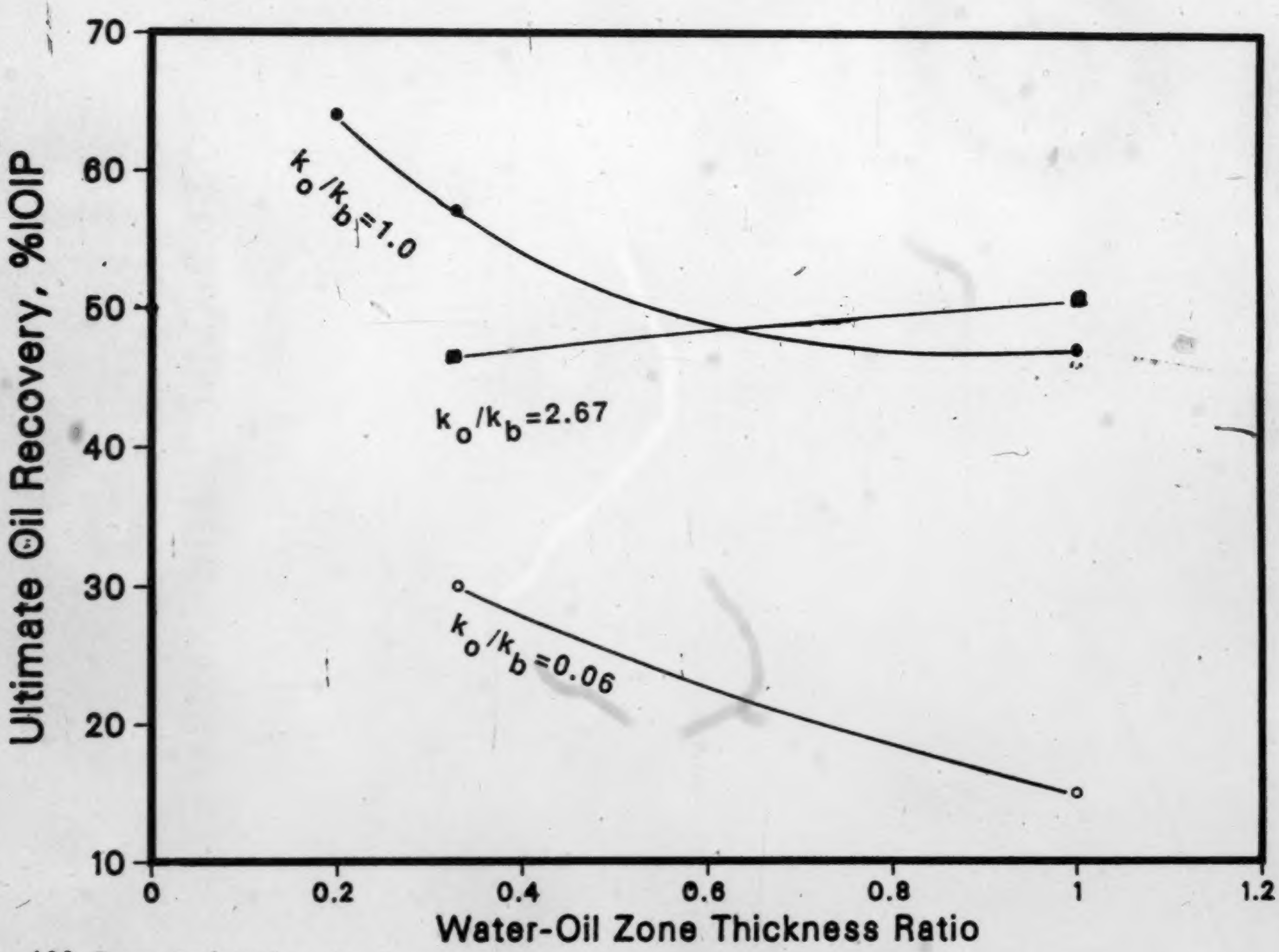

Fig. 130 Foam Injection Performance as a Function of k_o/k_b and h_b/h_o

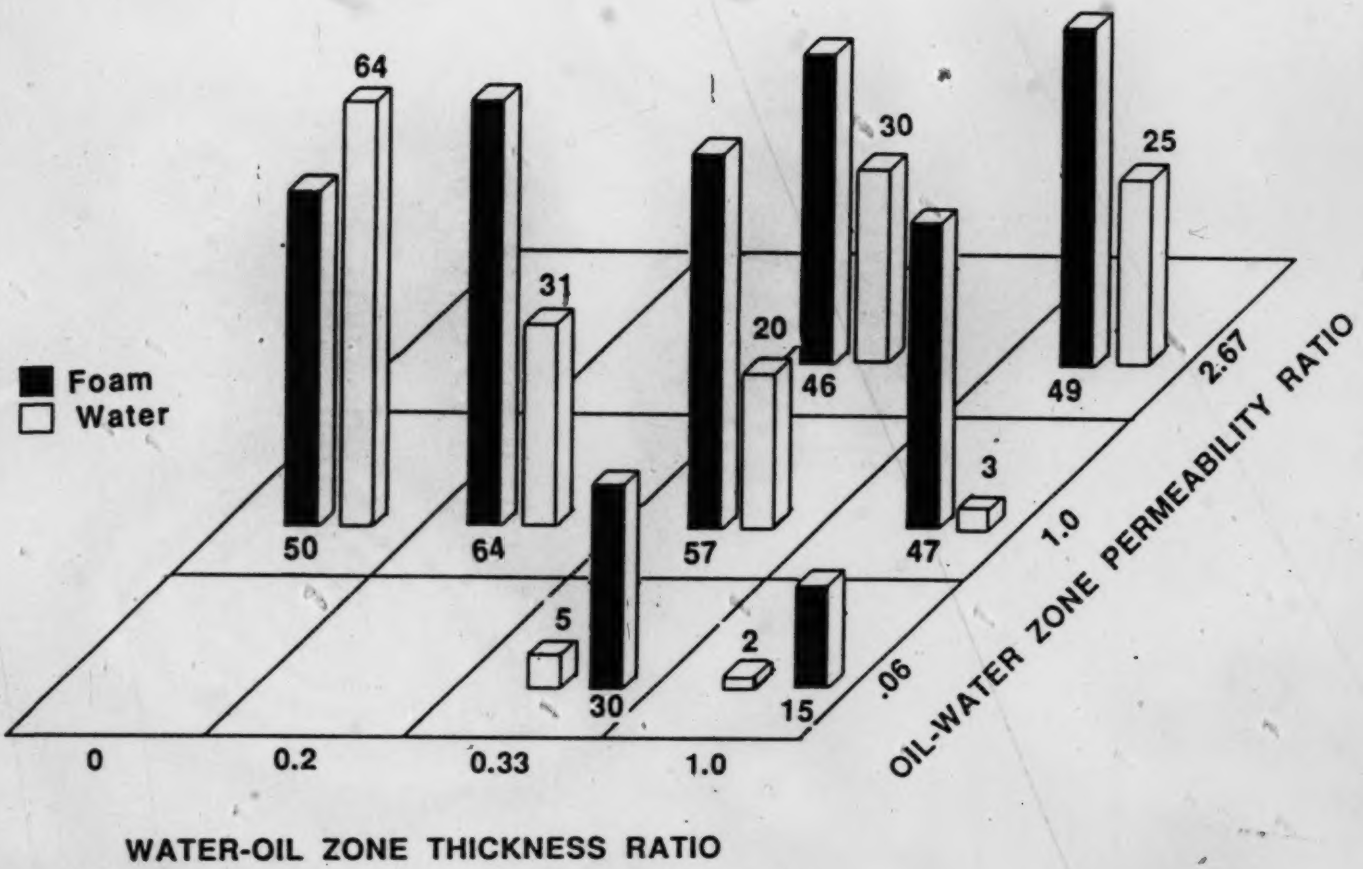

Fig. 131 Comparison of Foam Injection with Waterflood

three-dimensional form. The anomalous behaviour for a tighter bottom-water zone is evident from this figure. For $k_o/k_b=2.67$, the ultimate oil recoveries increase slightly with increasing bottom-water zone thickness. For $k_o/k_b=1.0$ the poorest recovery takes place for the homogeneous pack. In the presence of a bottom-water zone the optimal performance is shown at $h_b/h_o=0.2$. The recovery gradually decreases with increasing h_b/h_o values. Oil recovery is most sensitive to water-to-oil zone thickness ratio for $k_o/k_b=0.06$. An increase in bottom-water zone thickness is equivalent to an increase in permeability in terms of volumetric flux. This leads to a decrease in the apparent foam viscosity and consequently, the initial portion of the foam penetrates the bottom-water zone to create blockage of subsequent nitrogen flow into the bottom-water zone. As a result, the oil zone is swept by preference and the oil recovery increases. Figure 132 compares the percent improvement over a waterflood with foam injection. It can be seen from this figure that the ultimate oil recovery in a core with a bottom-water zone of an h_b/h_o value of 1.0 is higher than that in a homogeneous core. As discussed previously, foam injection in a homogeneous core is not the best recovery technique. However, blocking by foam in the presence of a bottom-water zone leads to a much improved performance because the bottom water acts as a carrier for the mobility control foam. Such a mechanism is nonexistent

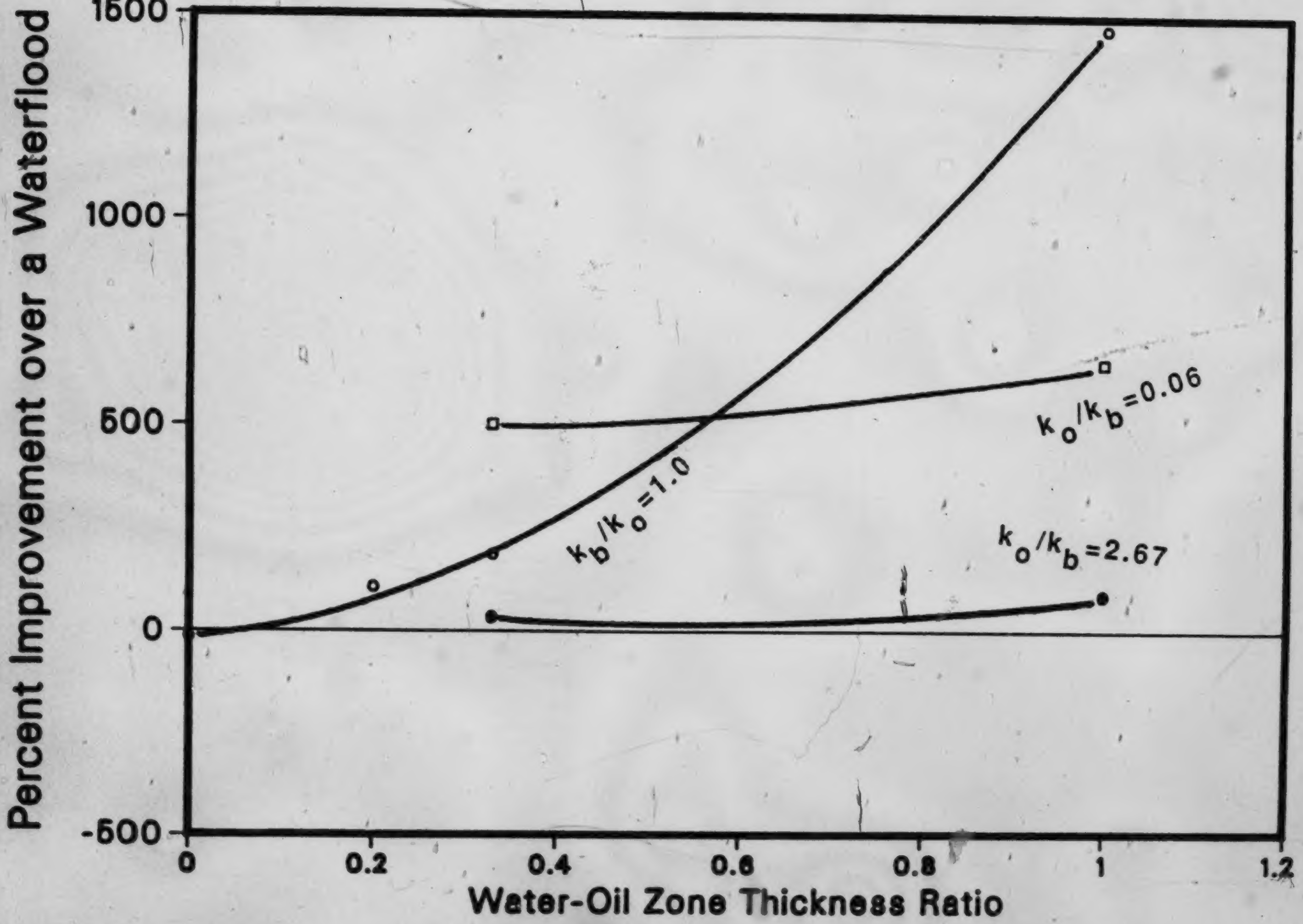

Fig. 132 Improvement Over a Waterflood for Different Foam Injection Runs

in a homogeneous core.

6.7.3 Effect of Waterflood on Foam

In order to examine the effect of waterflooding on the foam-blocking mechanism in the bottom-water zone, Run 75 was conducted. This run could be compared with Run 67 for which the same surfactant concentration was used, but no water slug (without surfactant) was alternated with foam injection. Both of these runs had the same k_o/k_b (=1) and h_b/h_o(=0.33) values. For Run 75 no foam was produced during the waterflood, indicating a possible 'wash away' effect by water. This effect was also reported by Holm (1970). Following this waterflood, nitrogen was again injected until a total of 1.16 PV of liquid was produced. During nitrogen injection, the WOR remained very high even though a considerable amount of foam was being produced (possibly due to the fact that sufficient surfactant had been added to water to generate foam even after dilution with connate and injected water). Following this nitrogen slug, surfactant water was injected again for 0.5 pore volume of the oil zone. This was followed by nitrogen injection, during which the WOR decreased considerably and the gas-liquid ratio started increasing rapidly. The displacement test was stopped when the gas-liquid ratio increased above 7000. A total of 43.8 percent of the IOIP was recovered at the end of the displacement test. Water injection after nitrogen injection does not seem to have any positive impact on recovery. At the end of this run (gas-liquid ratio=7000), 50 percent of the IOIP was recovered. This value is considerably higher than the 43.8 percent observed for the previous run. The only difference between these two runs is that nitrogen injection was followed by a waterflood for Run 75. This also indicates that foam creates blockage for nitrogen much more effectively than it does for a waterflood. A similar observation was previously reported by Holm (1968) who observed that the plugging action is greatest if gas, instead of water, is used.

6.7.3.1 Mobility Control Mechanism with Foam

Figure 133 depicts the relative contributions of waterflood, air injection without surfactant water, and air injection with surfactant water. This comparison is based on the runs conducted with a h_b/h_o value of 0.33 and a k_o/k_b value of 1. As can be seen from this chart a major portion the oil recovered by foam injection is actually recovered by the air itself. However, air fails to create a permanent blockage in the bottom-water zone and if the air injection were to have continued without alternating with waterflood the oil recovery would have been poorer. Surfactant water injection enhances the blocking mechanism of air by generating foam and creating blockage to subsequent gas flow in the zone. As a consequence, the ultimate oil recovery with gas injection becomes higher than that obtained with a

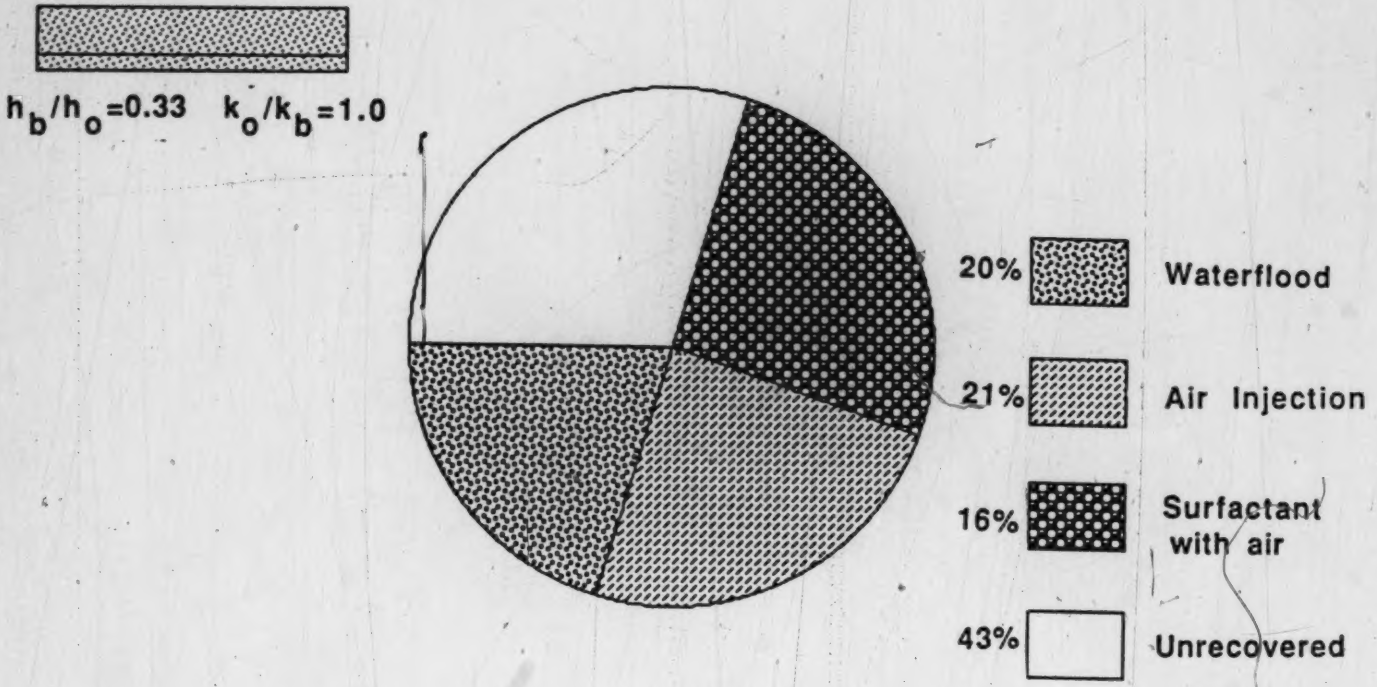

Fig. 133 Relative Contribution of Different Chemicals in Foam Injection

waterflood alone. Similar results are expected only in the presence of a high-permeability channel, such as a bottom-water zone.

6.8 Carbon Dioxide-Activated Silica Gel Injection

Runs 77 to 85 were conducted using an initial slug of silica gel followed by a water injection.

6.8.1 Effect of CO_2 Injection

Runs 77 and 78 were conducted under similar conditions except that no CO_2 was injected in Run 78. The ultimate recovery for Run 78 was 52 percent of the IOIP as compared to 57 percent of the IOIP for Run 77. This difference indicates that the injection of CO_2 enhances the gelation and helps in creating effective blockage of the bottom-water zone. As CO_2 travels through the bottom-water zone, increased gelation takes place preferentially in the bottom-water zone. Consequently, during a waterflood the water encounters higher resistance from the bottom-water zone leading to a better sweep of the oil zone. Besides, CO_2 helps by removing the gelling materials from the vicinity of the injection well, and leads to improved water injectivity in that zone. Because of these results, CO_2 was injected following the injection of sodium orthosilicate and HCl.

6.8.2 Effect of Water-to-Oil Zone Thickness and Permeability Ratio

Runs 77 and 79 to 85 were conducted to examine the effect of oil-to-water zone permeability and thickness ratios. Figures 134 through 136 compare oil recoveries for k_o/k_b values of 1.0, 0.06 and 2.67, respectively for different values of h_b/h_o. For k_o/k_b=1.0, even though the cases with h_b/h_o values of 0.33 and 0.20 show a considerable difference during the intermediate stages of the displacement, the ultimate recoveries with 0.2 and 0.33 are very close to each other. The case of k_o/k_b=0.06 appears to be very sensitive to h_b/h_o values. Interestingly, for this particular value of k_o/k_b, the ultimate oil recovery was higher for h_b/h_o=1 than that for h_b/h_o=0.33. An explanation of such a behaviour is given later.

Figure 137 compares the ultimate recoveries as a function of k_o/k_b and h_b/h_o values. As can be seen from this figure, the oil recovery increases almost linearly with k_b/k_o values for h_b/h_o=1.0. However, for h_b/h_o of 0.33, there appears to be maximum at a k_o/k_b value of 1.4. For this h_b/h_o, a very high k_o/k_b value decreases the flux of the sodium orthosilicate solution and CO_2 into the bottom-water zone. Consequently, the formation of gel in this zone is not complete. This leads to improper blockage of the bottom-water zone and, when water is injected following CO_2 injection, water channels through the

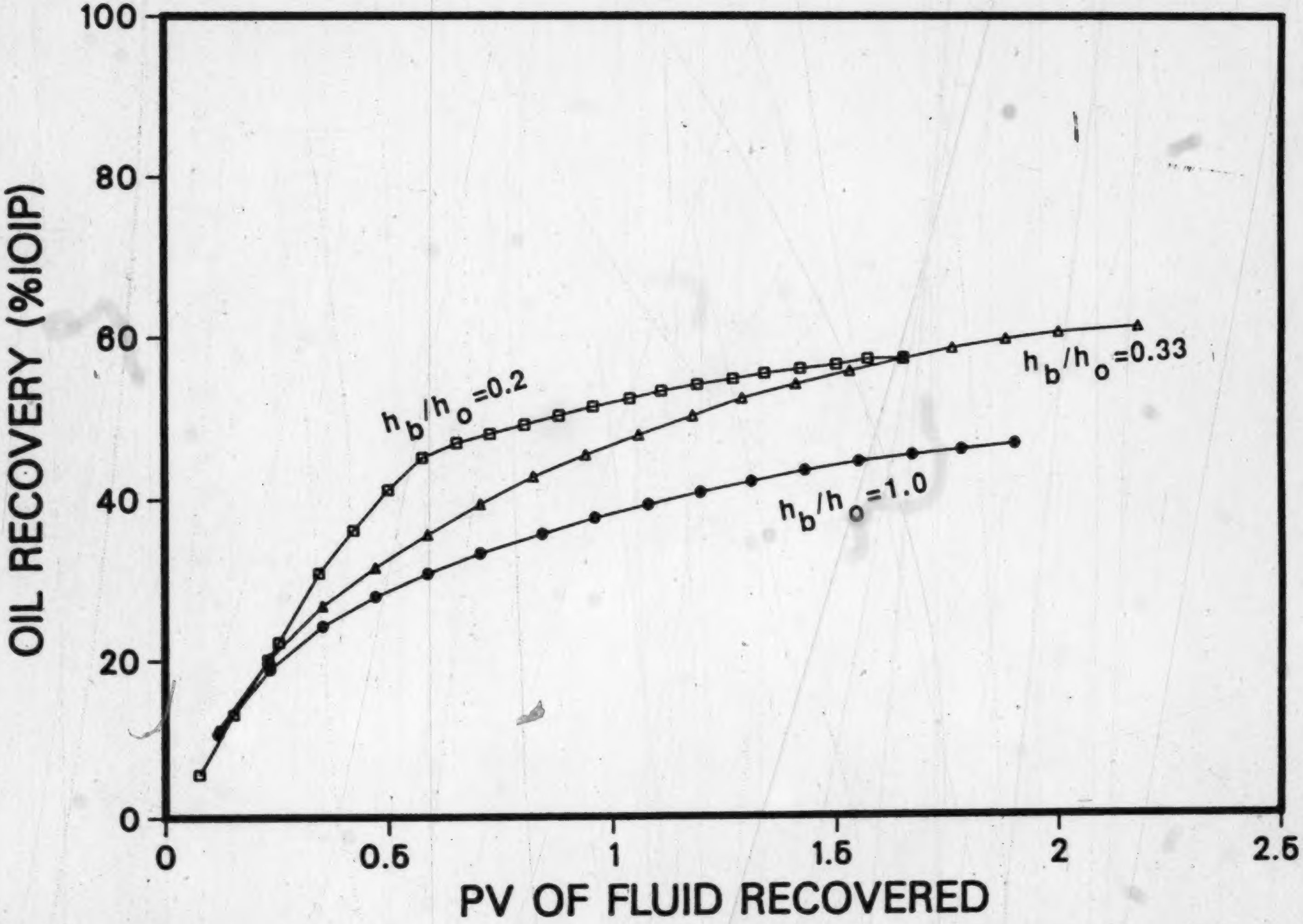

Fig. 134 Comparison of Oil Recoveries for different h_b/h_o and k_o/k_b=1.0 (Silica gel)

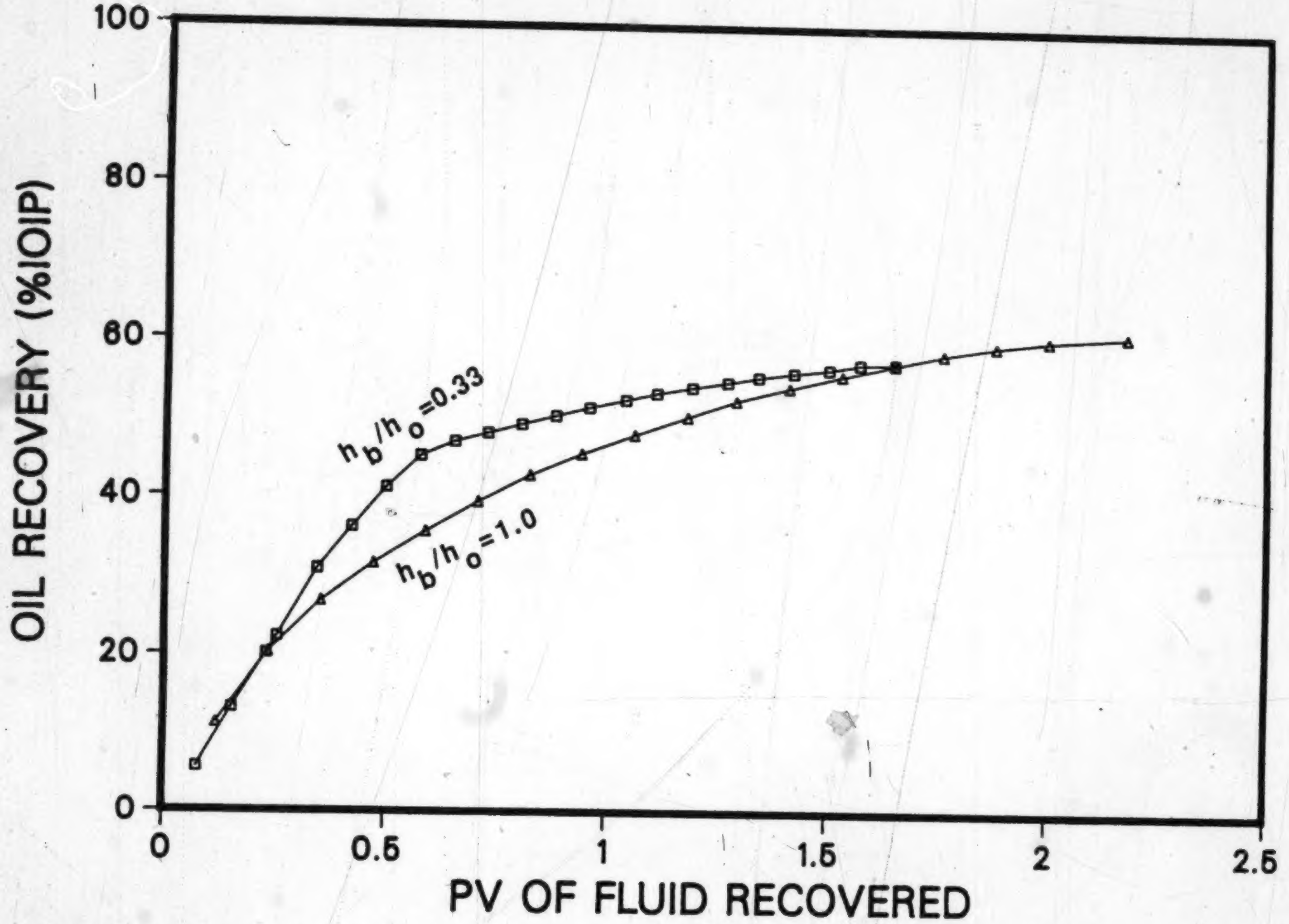

Fig. 135 Comparison of Oil Recoveries for h_b/h_o and k_o/k_b=0.06 (Silica gel)

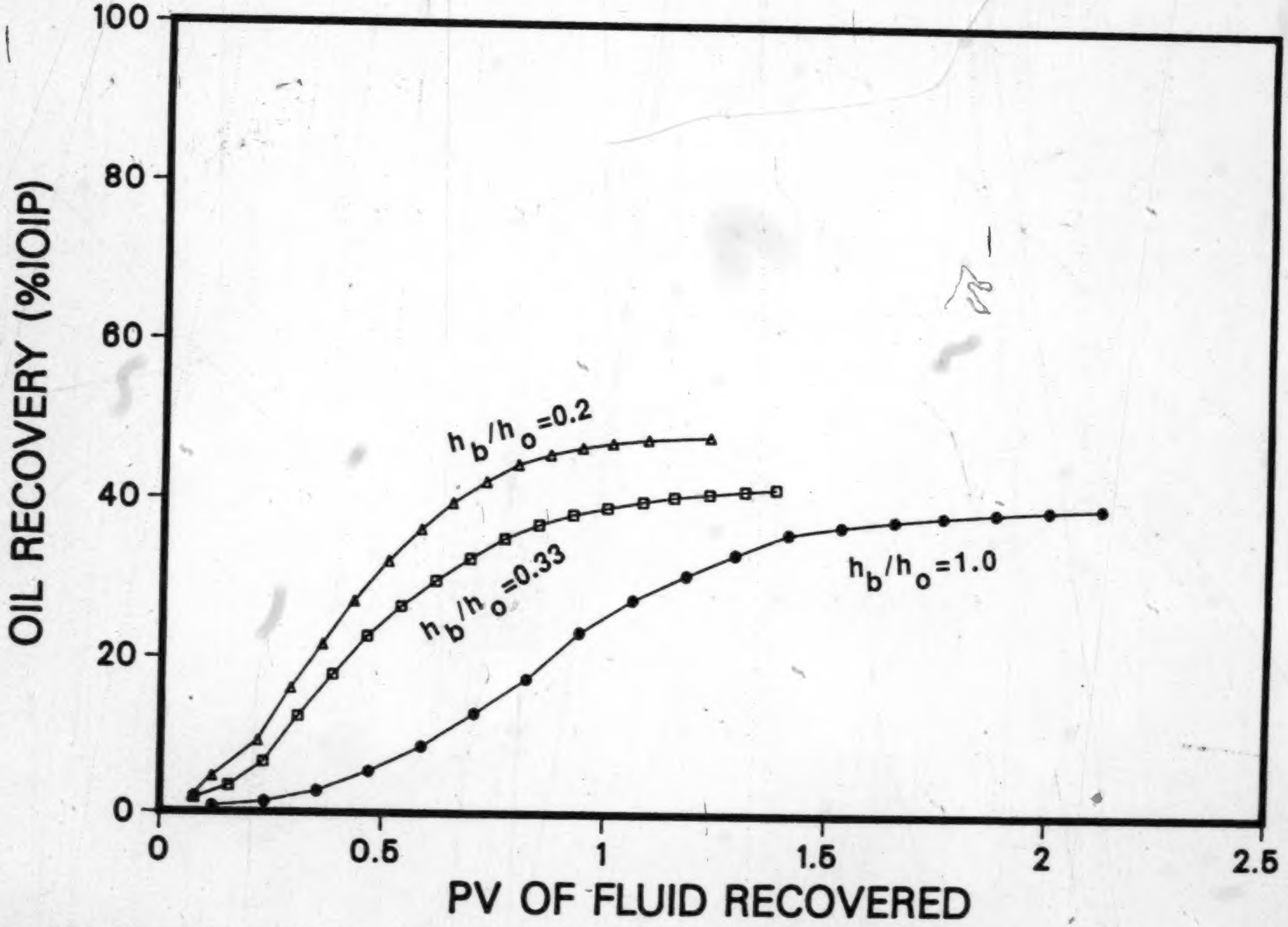

Fig. 136 Comparison of Oil Recoveries for h_b/h_o and k_o/k_b=2.67 (Silica gel)

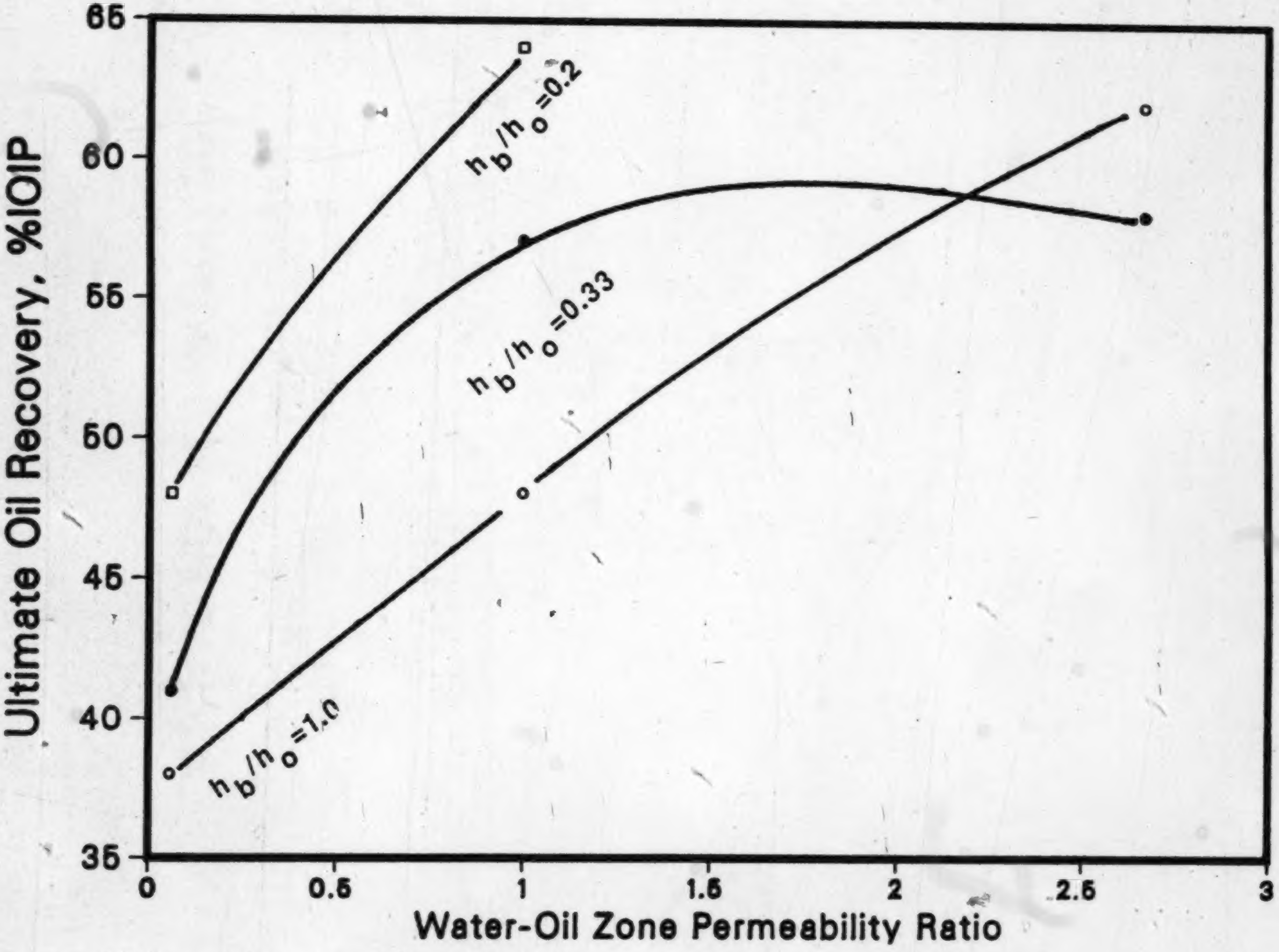

Fig. 137 Silica Gel Inj. Performance as a Function of k_o/k_b and h_b/h_o

bottom-water zone and the sweep of the oil zone is not very good. However, such a maximal ultimate recovery does not take place for the case of $h_b/h_o=1.0$ because of the fact that, for a thick bottom-water zone the capacity (product of permeability and thickness) is so high, due to thickness alone, that a decrease in permeability does not have an impact on the flux of gel into the bottom-water zone. For the case of a thick bottom-water zone, a decrease in bottom-water zone creates more resistance to flow into the zone and enhances the blockage by the gel. Figure 138 shows the sensitivity of the ultimate oil recoveries to the h_b/h_o values for a particular value k_o/k_b. For $k_o/k_b \leq 1$, a very sharp decrease in recovery takes place as the h_b/h_o value increases at low values of h_b/h_o. However, this decrease is less pronounced for $h_b/h_o \geq 0.5$. For higher k_o/k_b values, on the other hand, the dependence of the oil recovery on h_b/h_o values follows an opposite trend. For this regime, the oil recovery increased slightly as h_b/h_o value increased. A similar trend was observed for emulsion injection. In all cases, however, the improvement over a conventional waterflood is comparable to that resulting from polymer or emulsion injection. The only problem is that the silica gel does not block the bottom-water zone by preference, as does polymer or emulsion flooding, and the injectivity in the oil zone decreases considerably leading to high injection pressures for the waterflood that follows the gel injection.

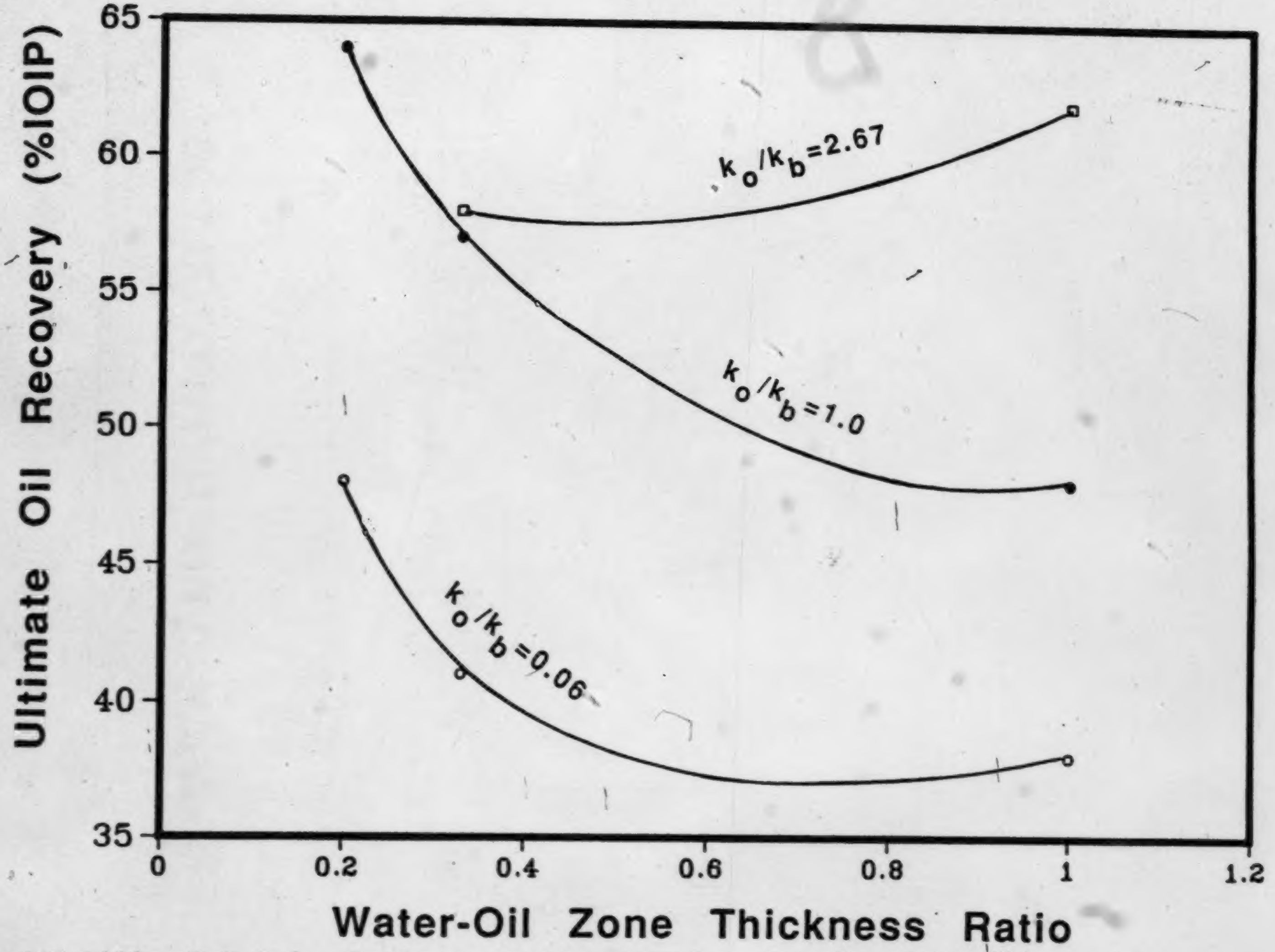

Fig. 138 Silica Gel Inj. Performance as a Function of k_o/k_b and h_b/h_o

However, this problem could be alleviated by injecting a larger slug of CO_2 immediately following the injection of sodium orthosilicate and HCl solution. CO_2 sweeps away the gel from the vicinity of the injection well and helps to form gel farther along in the bottom-water zone.

Figure 139 compares oil recoveries by silica gel with that by a waterflood. The effectiveness of silica gel in cases for which a waterflood is particularly poor is evident from this figure.

Figure 140 compares the relative improvement over a waterflood for different h_o/h_b and k_o/k_b values. This figure indicates that the largest improvement takes place for lower k_o/k_b values. Also, for a k_o/k_b value of 2.67 the improvement remains about the same for increasing values of h_b/h_o.

6.9 Comparison of Different Mobility Control Agents

Figures 141 through 143 depict the ultimate oil recoveries as a function of h_b/h_o and k_o/k_b values for runs with MCT-10 oil. This permits a comparison of the performance and relative merits of the different blocking agents. During the initial stages of the displacement, air injection showed a slight improvement over a waterflood. The gel injection performance was slightly better than that of air injection. During the initial stages, emulsion slug injection gave the highest oil recovery. As has already

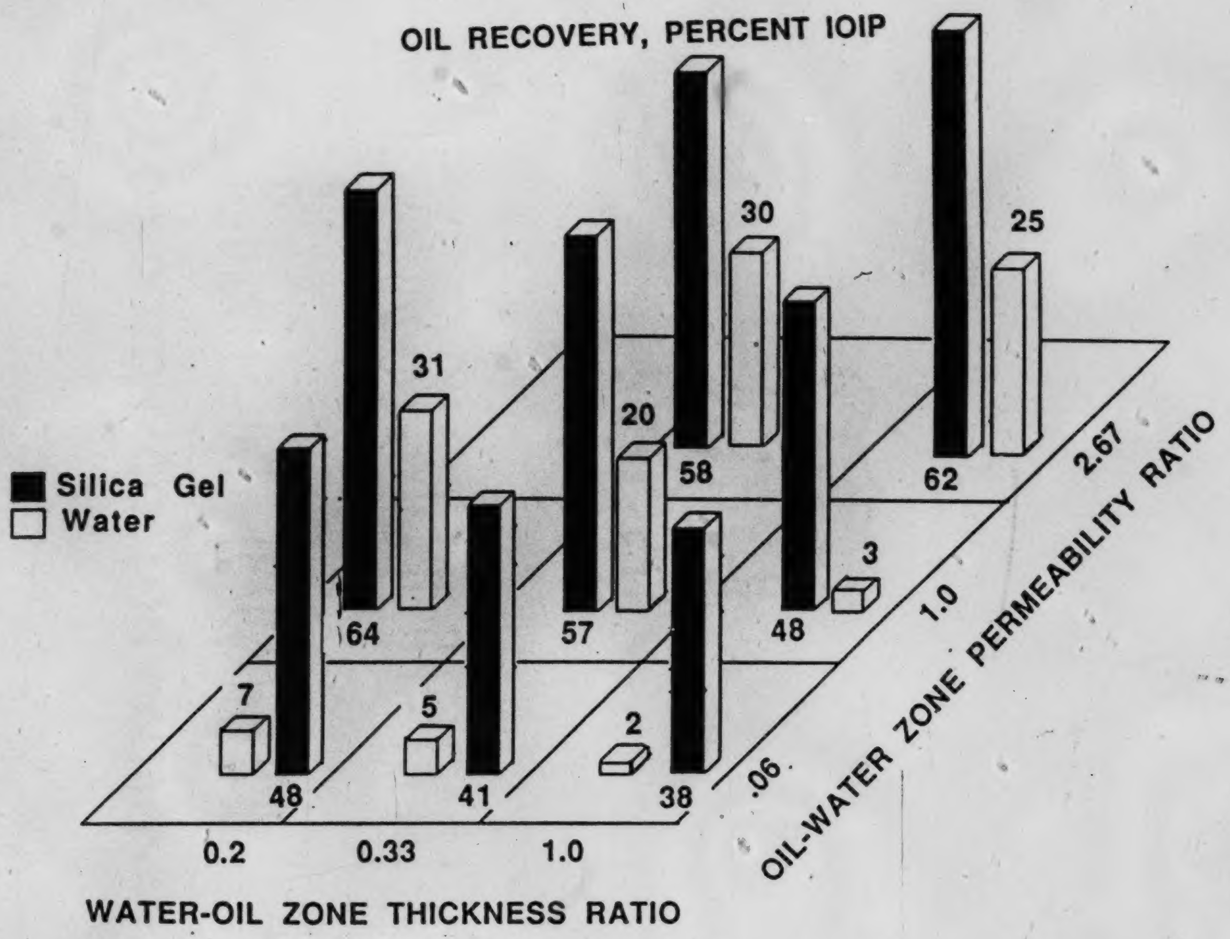

Fig. 139 Comparison of Silica Gel Inj. with Waterflood

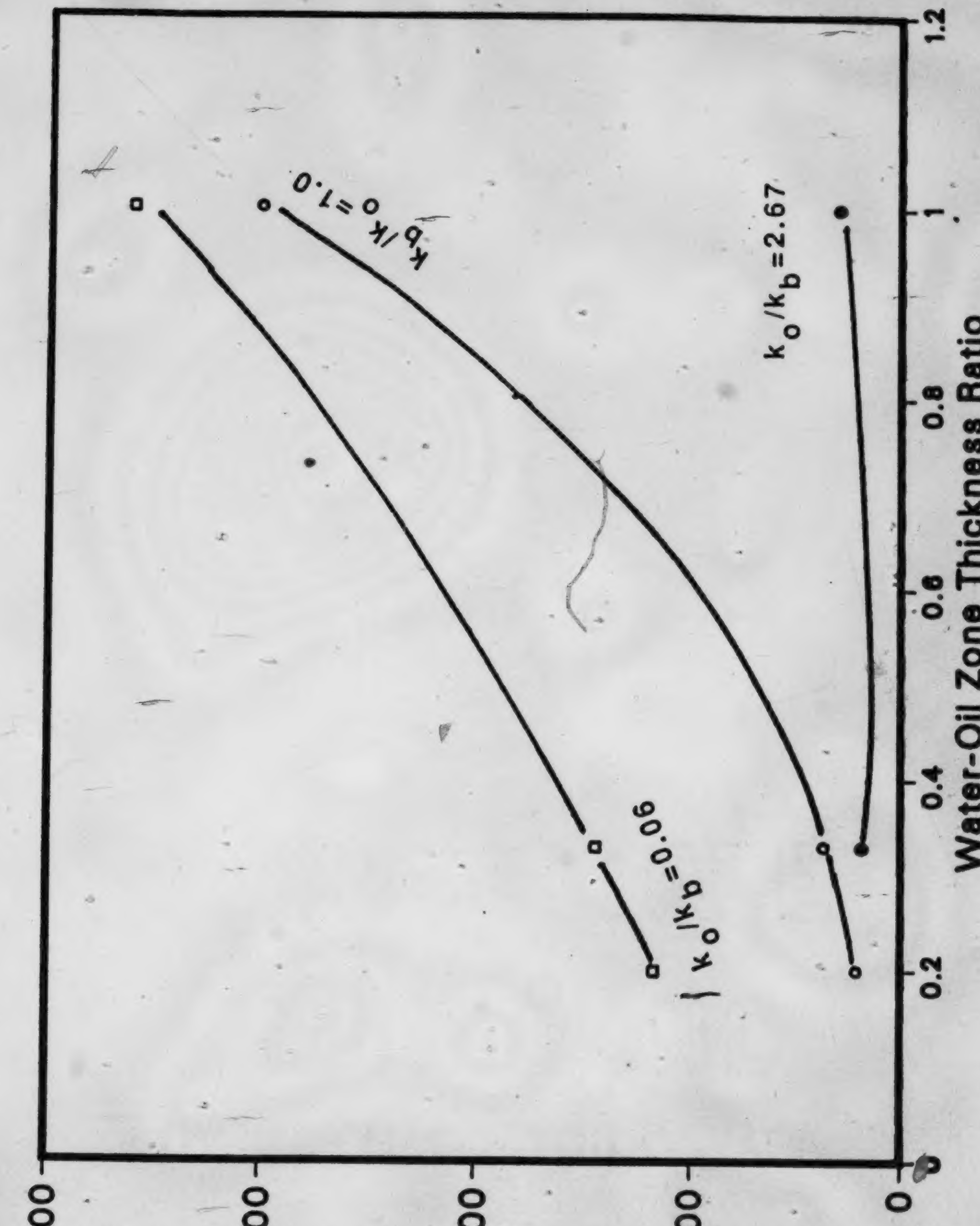

Fig. 140 Improvement Over a Waterflood for Different Silica Gel Inj. Runs

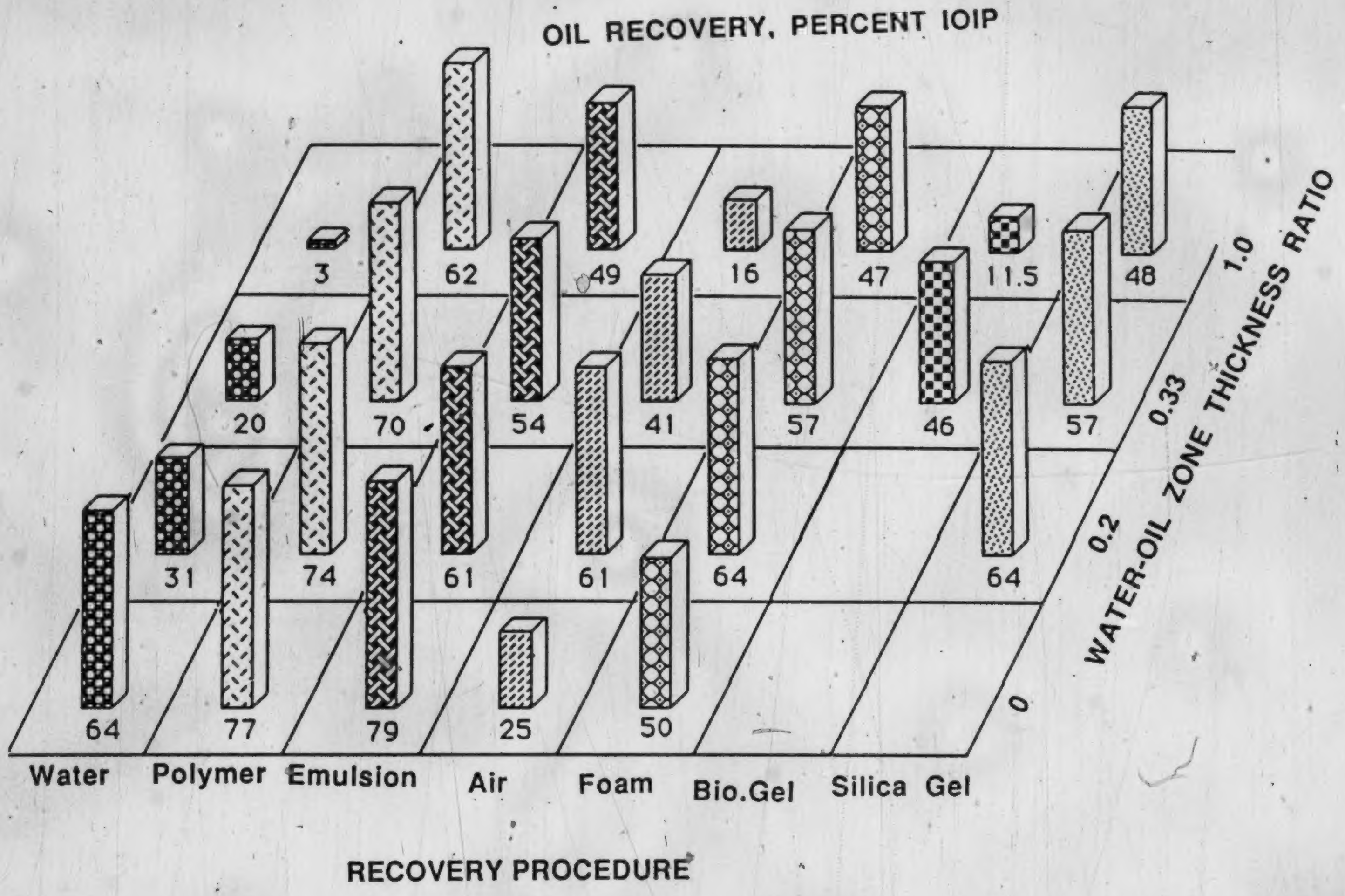

Fig. 141 Comparison of Oil Recoveries with Different Recovery Procedures for k_o/k_b of 1.0

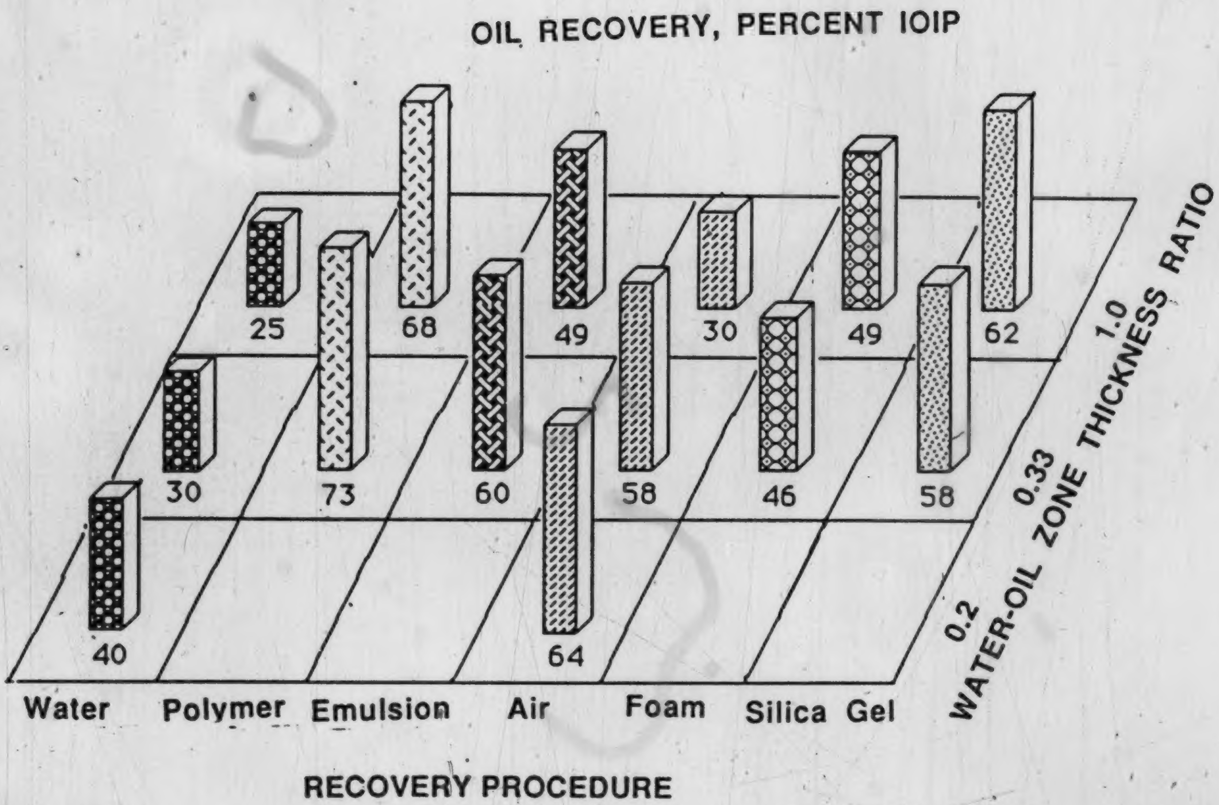

Fig. 142 Comparison of Oil Recoveries with Different Recovery Procedures for k_o/k_b of 2.67

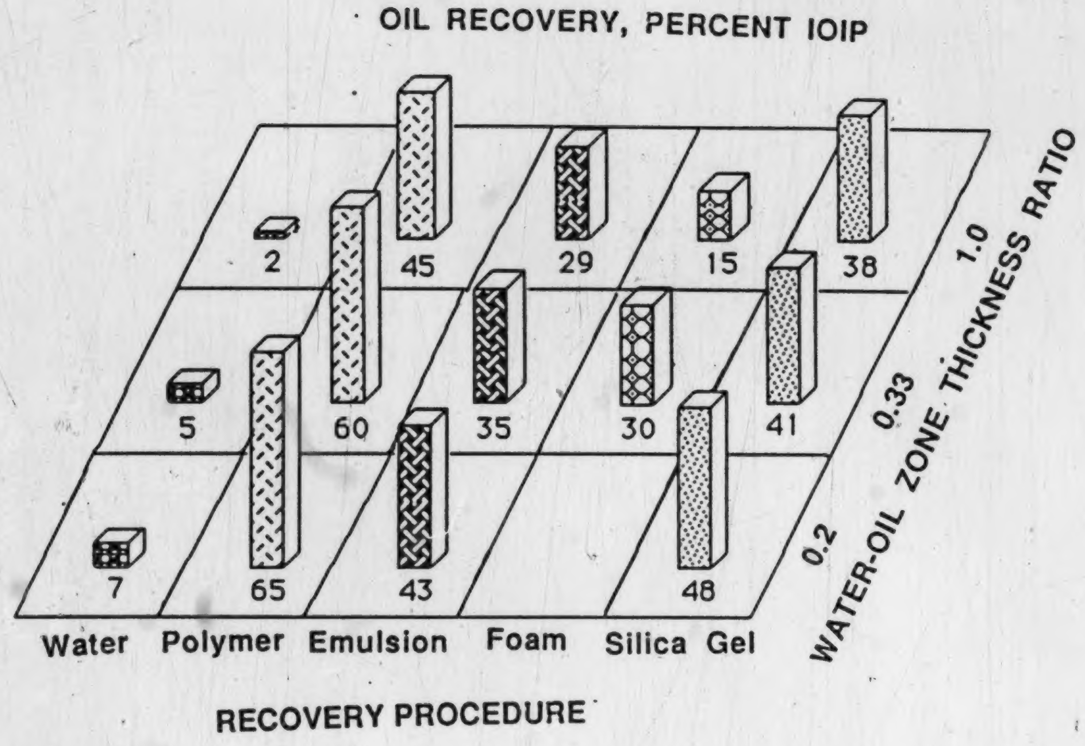

Fig. 143 Comparison of Oil Recoveries with Different Recovery Procedures for k_o/k_b of 0.06

been discussed, polymer injection showed a delay in response time in terms of increased oil cut, but such a delay was not seen during emulsion floods that resulted in an immediate improvement in oil cut. However, as the polymer slug started taking effect, the oil recovery increased rapidly. Also, during the late stages of the displacement tests, the polymer slug resulted in the highest oil recovery.

Air injection showed the maximal oil recovery up to about one PV of total fluid recovery for a tight and thin bottom-water zone. Even though the slug size during air injection was arbitrarily fixed, the oil recovery was better than that obtained with either waterfloods or emulsion floods. However, as the effect of polymer slug injection became apparent, the oil recovery by polymer slug injection showed the best performance. Besides, the recovery performances achieved by emulsion and air injection stayed very close to each other even at the later stages of the displacement test.

For $h_b/h_o=1$, the waterflood showed the poorest oil recovery among all the recovery procedures used. For this case even the emulsion flood showed a very low recovery during the initial stages whereas both the air and gel injection runs showed better recovery than that obtained by waterfloods or emulsion floods. However, as the displacement test continued, emulsion floods (followed by a waterflood) gave distinctly better recovery than that obtained by either gel or air injection. During the later stages, the polymer slug yielded the highest oil recovery. For a thick bottom-water zone, neither air nor gel injection approached the recoveries obtained by polymer or emulsion floods. However, foam injection gave a reasonable ultimate recovery of 46.6 percent of the IOIP. It appears that as long as the bottom-water zone has a permeability as high as that of the oil zone, foam injection considerably improves the oil recovery.

For a thick and tight bottom-water zone (h_b/h_o=1.0, k_o/k_b=2.67), polymer, emulsion and silica gel gave similar oil recoveries. However, foam did not perform well as compared to either polymer or emulsion. A similar failure was also observed for the run for which a tight and thin bottom-water zone was used. The foam used does not seem to be effective for tight bottom-water zones. As already mentioned earlier, this agrees with the observations made by Raza (1970) and Mast (1972). Similar behaviour was also observed for CO_2-activated silica gel.

The oil recovery performance achieved by polymer and emulsion injection for Mineralube and kerosene (7.5 mPa.s) is clear from Figure 144. During the initial stages of the displacement test emulsion slug injection showed much better recovery. However, the difference between the two became smaller after injecting two PV of total fluid. When the WOR reached a value of 20, 72 percent of the IOIP was recovered

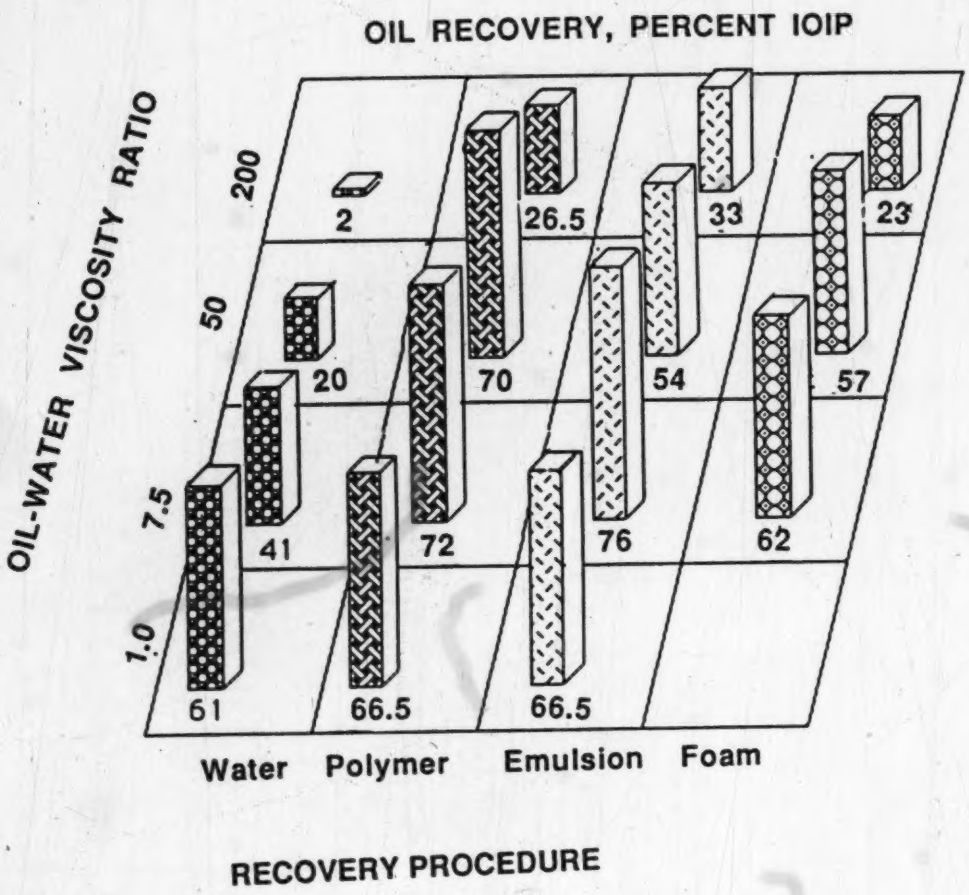

Fig. 144 Effect of Oil-Water Viscosity Ratio on Oil Recoveries with Different Procedures

by polymer injection as compared to 76 percent of the IOIP recovered by emulsion injection.

For a low viscosity oil (one mPa.s), a waterflood seemed to be just as efficient as a polymer or emulsion flood. Up to 0.6 PV of fluid injection, both waterflood and emulsion injection resulted in similar oil recoveries. At this point a polymer slug was injected and was subsequently followed by a waterflood. As the waterflood continued after polymer injection, oil recovery was substantially lower than that obtained by an emulsion flood. This improved performance by emulsion continued up to the later stages of the displacement test. As can be seen from Figure 144, when the WOR reached a value of 20, 66.5 percent of the IOIP was produced by both the runs.

The effect of high viscosity oil (200 mPa.s) on oil recovery is evident from Figure 144. Runs 12, 39 and 62 were performed with this oil. A polymer slug was injected for Run 12 and emulsion (made from 10% Faxam-100 in water) was injected for Run 39. For Run 62, surfactant water (4% surfactant) was alternated with nitrogen. As can be seen from Figure 144, the oil recovery was very low (≤33% of the IOIP) for all of these runs. It also appears that the waterflood performance is extremely poor for high oil viscosities even if the bottom water is thin. However, when the mobility control agent was injected at the beginning of the displacement test the recovery improved and the WOR decreased considerably. Ultimate recoveries in all these runs remained very small (26.5, 33, and 23 percent of the IOIP, respectively, for Runs 12, 39, and 62) and, even though the emulsion flood performed the best among all the runs, a substantial amount of oil remained unrecovered. For high viscosity oils, there is scope for further investigation as even a multifold improvement over a waterflood leaves a large portion of the oil unrecovered. Note, however, that due to very adverse mobility ratios with high viscosity oils, a waterflood would give a poor recovery even in the absence of a bottom-water zone.

Figures 145 through 147 compare percentage improvements over a waterflood by different mobility control agents as a function of the oil-to-water zone thickness and permeability ratios. Figure 145 indicates that the highest improvement for $k_o/k_b=1.0$ is given by a polymer flood over the entire range of h_b/h_o values studied. This is closely followed by emulsion, foam, and silica gel. For $k_o/k_b=1.0$, air does not perform as well as the other mobility control agents. Apparently, air is unable to create an effective blockage when the bottom-water zone is as permeable or more permeable than the oil zone. However, the biopolymer gave the poorest performance for all the cases. In order to be able to find the reason for such a failure, investigation in greater detail must be directed toward the rheology and flow behaviour of the biopolymer gel. In the present study, the

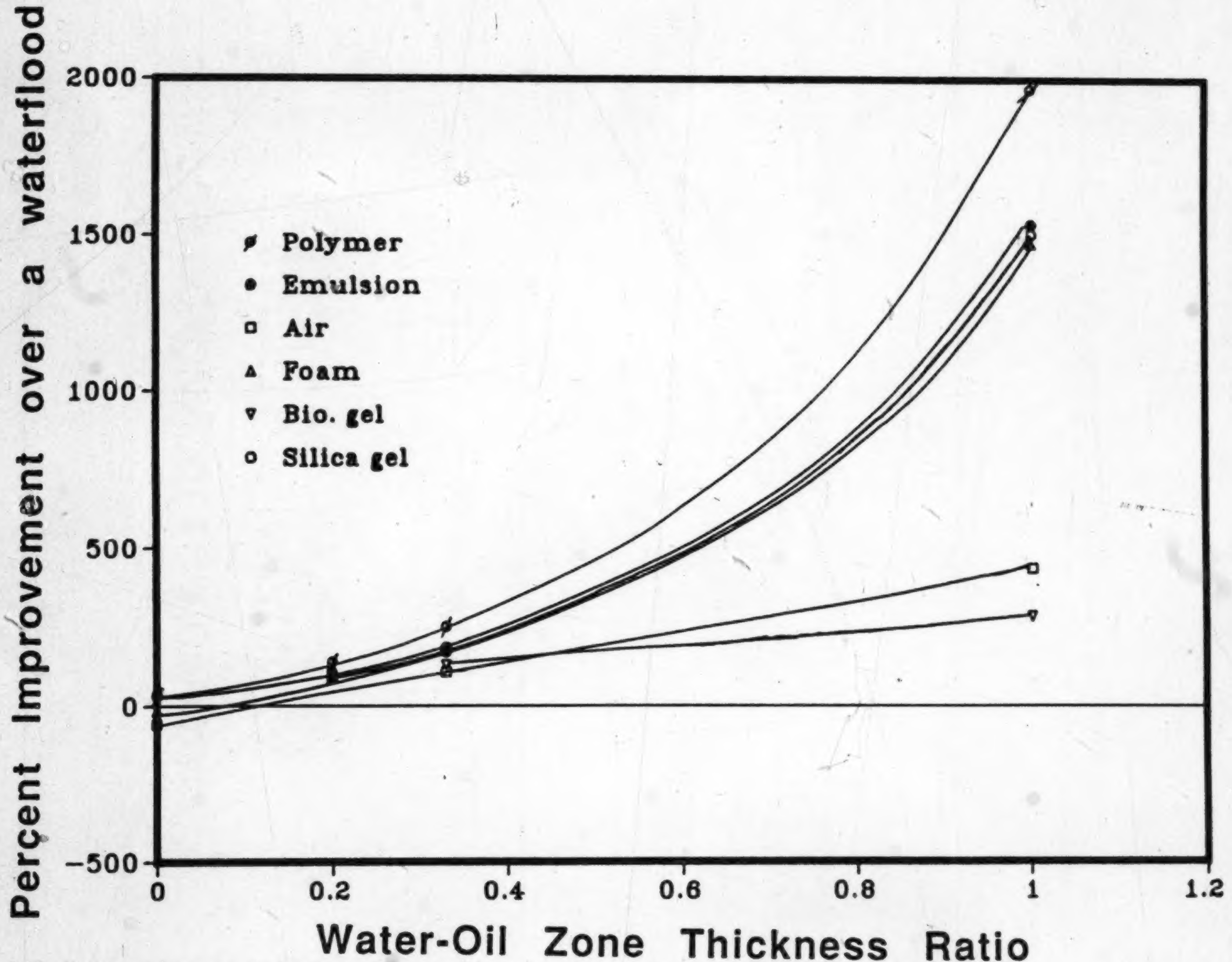

Fig. 145 Comparison of Different Mobility Control Agents for k_o/k_b of 1.0

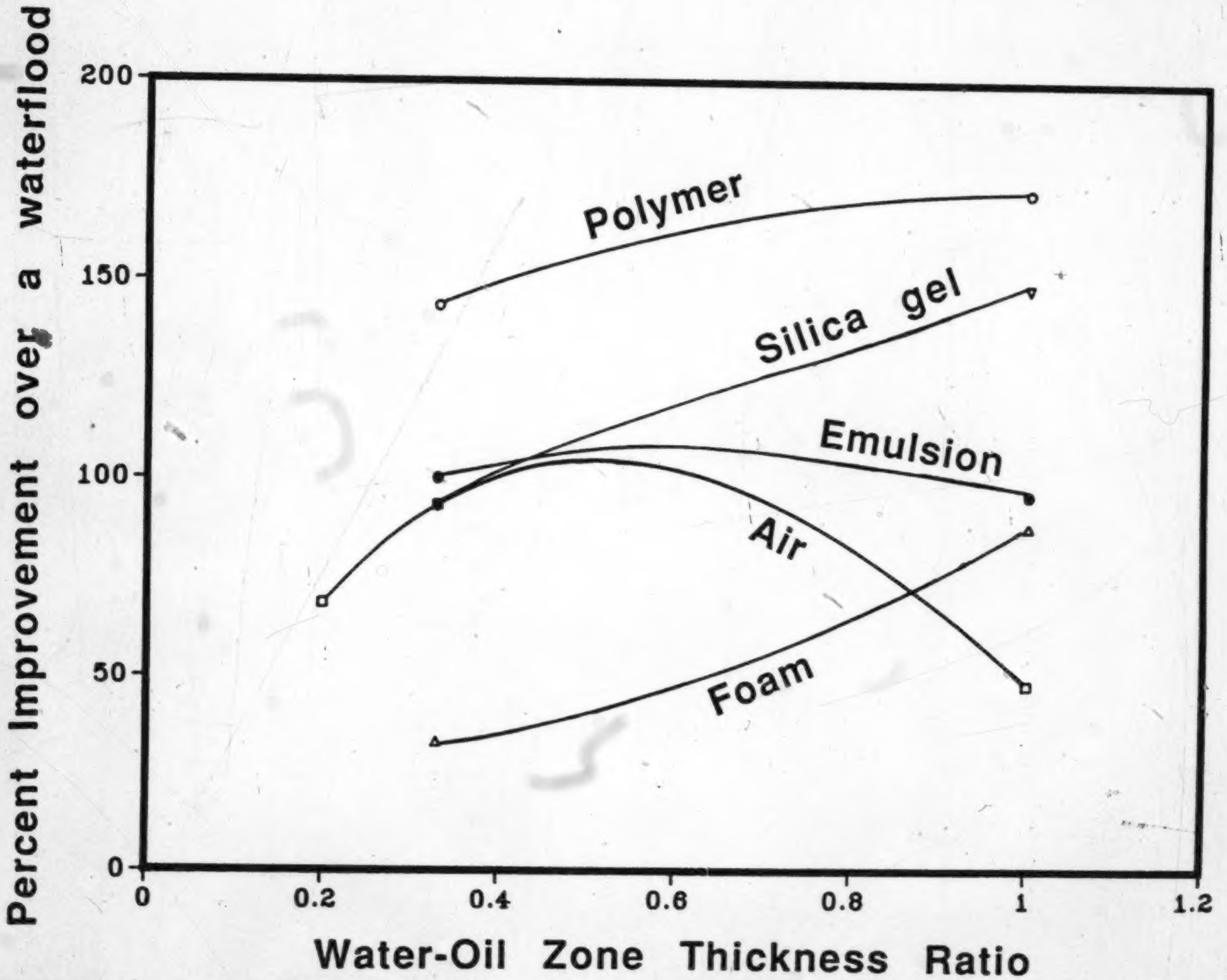

Fig. 146 Comparison of Different Mobility Control Agents for k_o/k_b of 2.67

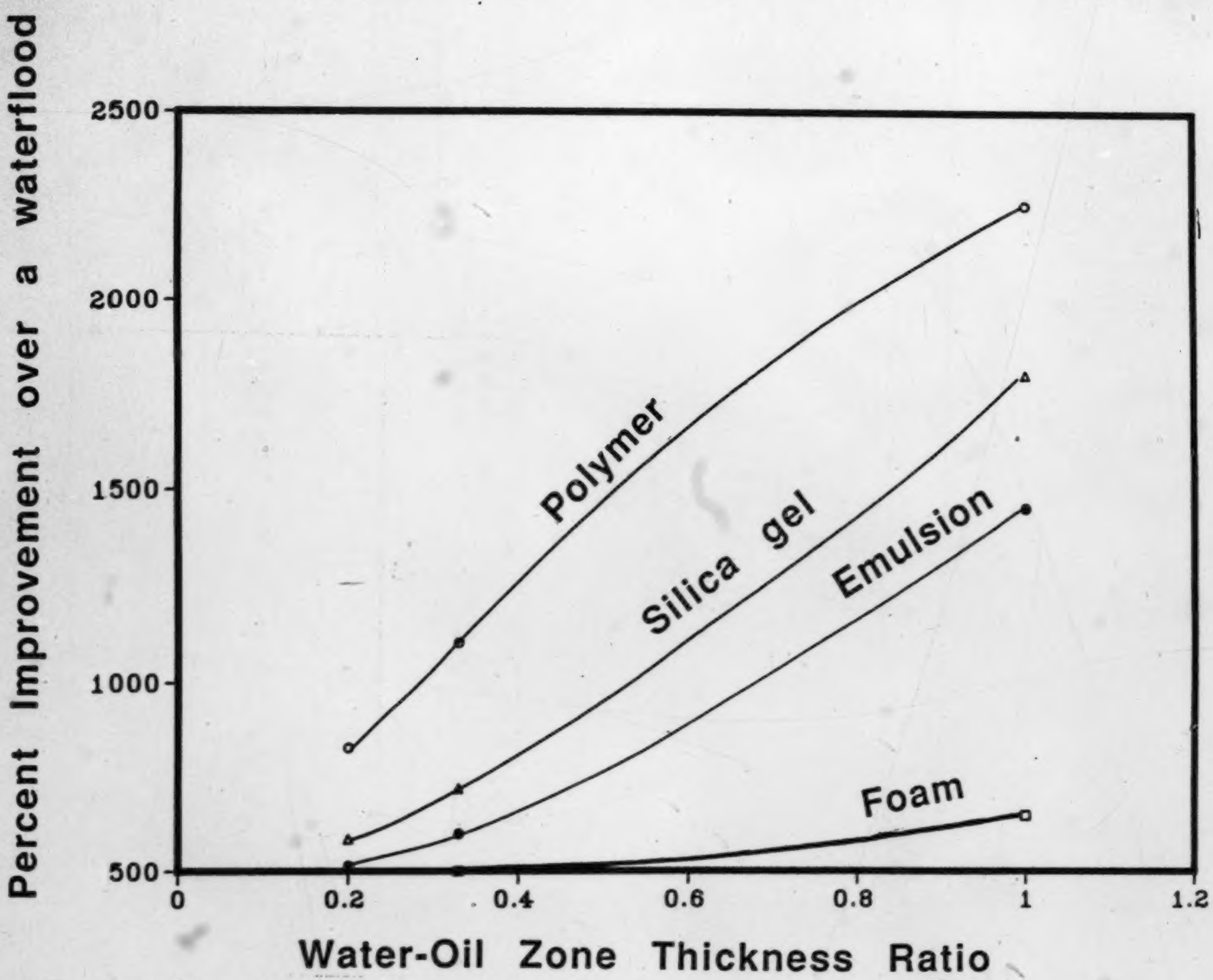

Fig. 147 Comparison of Different Mobility Control Agents for k_o/k_b of 0.06

very high injection pressure required for the gel to propagate in the sandpack appears to be the main reason for the gel's failure to create an effective blockage of the bottom-water zone.

Figure 146 indicates that polymer gives the highest improvement over a waterflood for $k_o/k_b=2.67$. For this case, silica gel performs better than emulsion, foam or air, especially at higher values of h_b/h_o. Foam injection performs the poorest at lower values of h_b/h_o. Only air injection shows an optimal performance as a function of h_b/h_o values at an h_b/h_o value of around 0.5.

For $k_o/k_b=0.06$, there is a large difference in improvement for the different mobility control agents. Polymer performs the best for the whole range of h_b/h_o values studied. This performance is followed by that of silica gel and then by emulsion. Foam injection gave the poorest performance for this value of k_o/k_b. It appears that foam is most effective only for $k_o/k_b=1.0$. The reason for this optimal performance for $k_o/k_b=1.0$ has been given earlier in this section.

7. NUMERICAL SIMULATION

One of the objectives of this study was to compare the experimental results obtained for the different mobility control agents with those obtained numerically with a model developed for the simulation of several mobility control mechanisms within the framework of three-dimensional, three-phase flow. Once the history match of an actual run was achieved, the model was used to simulate other hypothetical situations. It was thus possible to examine the sensitivity of model parameters and gain further insight into process mechanisms. Such numerical simulation studies were performed for polymer and emulsion floods. Two models were developed for this purpose. Each of these models will be discussed along with the conventional waterflooding model to highlight the differences.

7.1 MODEL ASSUMPTIONS AND FORMULATION

The model development is based on a material balance for each phase in the system considered. Three phases (either polymer solution/water/oil or emulsion/water/oil) flow simultaneously under equilibrium conditions in a porous medium. The rates of flow of the phases depend on injection rates and on the physical properties of each phase.

7.1.1 Assumptions

Two models were developed for numerical simulation studies. They were for polymer and emulsion flow in a porous medium in the presence of oil and a mobile water phase. The models were also valid in the absence of a bottom-water zone (homogeneous pack). The following assumptions were made in developing the models.

7.1.1.1 Polymer Flow

1. Isothermal flow exists in a porous medium.
2. Initial physical and chemical properties are uniform.
3. Water and oil are immiscible with each other.
4. Polymer solution maintains its viscosity at a constant value.
5. Polymer solution alters only the effective permeability to water.
6. Effective permeability to water is reduced after a porous medium is in contact with polymer solution. The amount of reduction in effective permeability to water is independent of the polymer slug size.
7. Polymer, oil and water are considered to form independent phases, with relative permeabilities a function of the saturations to each phase alone.
8. The absolute permeability is not changed as a result of polymer flooding.

7.1.1.2 Emulsion Flow

1. Isothermal flow exists in a porous medium.

2. Initial physical and chemical properties are uniform.

3. Water, oil and emulsion are immiscible with each other.

4. Emulsion viscosity is independent of pressure.

5. Emulsion reduces the absolute permeability; and the degree of reduction is a function of the initial permeability alone, and is independent of the emulsion slug size.

6. Emulsion, oil and water are considered to form indpendent phases with relative permeabilities a function of the saturations to each phase alone.

8. The relative permeabilities are not changed as a result of emulsion flooding.

7.1.2 Formulation

The mass balance of each phase flowing simultaneously in the formation is developed in Appendix-A. The flow equations are given as follows:

Oleic phase

$$- [\frac{\partial}{\partial x}(\frac{\rho_{lsc}}{B_l} v_{xl}) + \frac{\partial}{\partial y}(\frac{\rho_{lsc}}{B_l} v_{yl}) + \frac{\partial}{\partial z}(\frac{\rho_{lsc}}{B_l} v_{zl})] - q_l^* =$$

$$\frac{\partial}{\partial t}\left(\frac{\phi\rho_{lsc}S_l}{B_l}\right) \tag{7.1}$$

Aqueous phase

$$- \left[\frac{\partial}{\partial x}\left(\frac{\rho_{asc}}{B_a}v_{xa}\right) + \frac{\partial}{\partial y}\left(\frac{\rho_{asc}}{B_a}v_{ya}\right) + \frac{\partial}{\partial z}\left(\frac{\rho_{asc}}{B_a}v_{za}\right)\right] - q_a^* =$$

$$\frac{\partial}{\partial t}\left(\frac{\phi\rho_{asc}S_a}{B_a}\right) \tag{7.2}$$

Emulsion or polymer phase

$$- \left[\frac{\partial}{\partial x}\left(\frac{\rho_{msc}}{B_m}v_{xm} + \frac{R_{lm}\rho_{msc}}{B_l}v_{xl} + \frac{R_{am}\rho_{msc}}{B_a}v_{xa}\right)\right.$$

$$+ \frac{\partial}{\partial y}\left(\frac{\rho_{msc}}{B_m}v_{ym} + \frac{R_{lm}\rho_{msc}}{B_l}v_{yl} + + \frac{R_{am}\rho_{msc}}{B_a}v_{ya}\right) +$$

$$\frac{\partial}{\partial z}\left(\frac{\rho_{msc}}{B_m}v_{zm} + \frac{R_{lm}\rho_{msc}}{B_l}v_{xl} + \frac{R_{am}\rho_{msc}}{B_a}v_{xa}\right) - q_m^* =$$

$$\frac{\partial}{\partial t}\left(\phi\rho_{msc}\left(\frac{S_m}{B_m} + \frac{R_{lm}S_l}{B_l} + \frac{R_{am}S_a}{B_a}\right)\right)] \tag{7.3}$$

In the above equations, the densities (subscripted by 'sc') are at standard conditions.

a. Potential Relationship

The potential for oleic and aqueous phases are given by the following equations.

$$\Phi_l = p_l - \rho_l gz \tag{7.4}$$

$$\Phi_a = p_a - \rho_a gz \tag{7.5}$$

$$\Phi_i = p_i - \rho_l g z \tag{7.6}$$

where i is polymer or emulsion phase.

b. The phase saturations are related by

$$S_a + S_l + S_i = 1 \tag{7.7}$$

where i is emulsion or polymer phase.

c. Initial and Boundary Conditions

The reservoir is considered to be at irreducible water saturation. Further, the system is uniform in the lateral and axial direction. However, a bottom-water zone may be present in the reservoir. Then, the flow equations are subjected to the following initial conditions:

Oleic phase conditions:

$$S_l(X,Y,1,0) = 1 - S_{wi} \tag{7.8}$$

$$\Phi_l(X,Y,Z,0) = \Phi_o \tag{7.9}$$

$$S_l(X,Y,2,0) = 0 \tag{7.10}$$

Aqueous phase conditions:

$$S_a(X,Y,1,0) = S_{wi} \tag{7.11}$$

$$\Phi_a(X,Y,Z,0) = \Phi_o \tag{7.12}$$

$$S_a(X,Y,2,0) = 1 \tag{7.13}$$

Since the model is linear with no flow across the boundaries, the necessary boundary conditions are defined accordingly:

Boundary conditions for the oleic phase:

$$\frac{\partial \Phi_l}{\partial n} = 0 \qquad (7.14)$$

$$\frac{\partial S_l}{\partial n} = 0 \qquad (7.15)$$

for aqueous phase:

$$\frac{\partial \Phi_a}{\partial n} = 0 \qquad (7.16)$$

$$\frac{\partial S_a}{\partial n} = 0 \qquad (7.17)$$

and for emulsion or polymer phase:

$$\frac{\partial \Phi_i}{\partial n} = 0 \qquad (7.18)$$

$$\frac{\partial S_i}{\partial n} = 0 \qquad (7.19)$$

In this case, n is a normal unit vector to the domain of the porous medium, and points outward away from the surfaces.

Now the formulation is complete with specified initial and boundary conditions. The solution technique for this system of equations is described in detail in Appendix A.

7.1.3 Mechanisms and Evaluation of Properties

Even though the formulation is complete from a mathematical standpoint, many mechanisms and properties have to be defined before discussing the results of the numerical simulation.

7.1.3.1 Fluid and Rock Properties

The fluid properties are functions of pressure only. The temperature effect is neglected. However, due to a lack of adequate fluid rheology data in the porous medium, constant viscosities and densities for the polymer and the emulsion were assumed. The model allows these fluid properties to be dependent on pressure.

7.1.3.2 Relative Permeabilities

The relative permeabilities are the key to a successful experimental displacement. In fact, the present approach of simulating a polymer flood is based on choosing an adequate set of relative permeabilities before and after the polymer flood. Different sets of relative permeabilities were used for a waterflood, polymer flood and emulsion flood.

a. Waterflood

Numerical simulation was initiated using relative permeabilities obtained experimentally by the Johnson-Bossler-Naumann (JBN) method. However, in order to obtain a good match with the experimental results, relative permeabilites were adjusted. Relative permeabilities to oil were very close to those estimated by the JBN method. Model relative permeabilities to water had to be increased in order to obtain a good match with the experimental data, especially at the time of water breakthrough. Relative permeabilities to oil had to be adjusted in order to obtain a good match near the irreducible oil saturation. Further detail, are given in the next chapter.

b. Polymer Flood and Waterflood

Polymer is known for its unique ability to reduce the mobility of the aqueous phase only. The effect of polymer is almost negligible in an oil-saturated porous medium. In the present study, a three-phase flow model was used. It is assumed that the effective permeability to water in a porous medium swept with polymer solution is smaller than that in an unswept porous medium. A single set of relative permeabilities was used before the polymer reached a certain block of the porous medium. After the block was invaded by polymer, a different relative permeability to water was used. In this study, polymer adsorption and dispersion were not considered in the conventional manner. Instead, the major effect of a polymer flood, i.e., the reduction in the effective permeability to water, was taken into account by means of a different relative permeability curve.

c. Emulsion Flood

Oil-Water emulsions have been well known for their ability to reduce the absolute permeability of a porous medium. In a layered core, it has been reported that emulsions decrease the contrast in absolute permeabilities of different layers. However, unlike polymer flooding, the absolute permeability, rather than the effective permeability to water, is decreased. Besides this effect on absolute permeability, it has been reported in experimental studies that emulsions also improve the microscopic displacement efficiency leading to a better sweep even for a homogeneous porous medium. Relative permeabilities to each phase were estimated following the same procedure as in the case of a polymer flood. However, unlike polymer floods, only one set of relative permeabilities was used throughout the process of emulsion injection and waterflood. In order to take account of the reduction in absolute permeabilities, it was assumed that absolute permeabilities change as soon as a portion of the porous media was contacted by emulsions. The new value of the absolute permeability is then retained for the rest of the displacement test. The magnitude of the reduction in absolute permeabilities was determined by starting with the initial value and then reducing it successively until good agreement was obtained between the experimental and numerical results. Different experimental results were matched at the same time, since both relative permeabilities and absolute permeabilities were estimated by trial and error.

d. Capillary Pressure

The capillary pressure is a function of interfacial tension, and when the interfacial tension decreases, the capillary pressure decreases also. For such situations, the forces required to remove the oil from pore constrictions also decrease. It is apparent that there is a shift in capillary pressure curves similar to those observed in relative permeability curves. For the present study, there were no capillary pressure data available for the oils used. However, a recent study (Islam and Bentsen, 1986) reported capillary pressure data for an oil/water system that had an oil/water interfacial tension similar to that of the oil/water system used in this study. These data have been used in the simulator for the oil/water system. As both the polymer/water and emulsion/water interfacial tensions were thought to be small, they were neglected.

7.1.4 Computational Algorithm

The solution method has been discussed in detail in Appendix A. This was transformed into a computer code using FORTRAN IV language. The numerical code was run utilizing the Amdahl computer at the University of Alberta.

The simulation model consists of a main program and several subroutines and functions. A brief description of the important parts is presented here.

Main Program

Initial pressure, saturation, constant properties, such as thickness, grid size, formation depth, permeabilities, and porosities are read in the first section. The initial phase saturations and water initially in place are computed and printed out with the rest of the data.

The constant part of the transmissibilities is computed in the second section. It also controls the flow of computations and sets time step, cycle, and iteration parameters, and initializes all dependent variables for the first time step.

Transmissibility coefficients and mobilities in the production rates are computed at the beginning of each time step and also are continuously updated for every iteration.

In the third section, the pressure distribution is determined by using a band solver. Saturations are computed explicitly by back substitution. If convergence criteria are not met, properties are updated and calculations repeated. If no convergence is achieved after a given number of iterations, the cycle number is increased until it reaches the maximum cycle number. If there is still no convergence, then the time step is reduced and the properties are reset to the old values and computations repeated.

The last portion of the main program involves the computation of mass balances and printing out the final results. The most recent computed properties are stored and a new time step is initiated.

GRID

Grid block sizes are read and the node elevations are computed in this subroutine.

BANDI

A matrix of pressure equation coefficients is set up in this subroutine with standard ordering.

BAND

The pressure equation is solved by LU factorization in this subroutine.

PERM

Porosity and permeability arrays are read in this subroutine. For emulsion injection, permeability reduction factors are read as well, and a new set of absolute permeabilities for the bottom-water zone, after it has been invaded by emulsions, is stored.

RATE

Well rates are computed in this subroutine when the rate or explicit pressure constraint is activated.

FDATA

Fluid properties and relative permeability data are read in this subroutine. For a polymer flood, also a second set of relative permeabilities to water is read and this information is stored to use when a block is invaded by polymer.

The flow chart for the computational algorithm is presented in Figure 148.

7.1.5 Sensitivity Studies and Model Accuracy

Accurate simulation results are dependent on having high quality data for a large number of reservoir parameters. Much of these data may be of questionable accuracy, or even missing, for any given study. Also, it is generally not possible to predict a prioi which parameters will control model performance.

One technique that is frequently used to help guide the data gathering effort, and to allocate the data collection time to the critical parameters, is to use the simulation model to do sensitivity analyses on selected parameters. By varying each of several selected parameters over a reasonable range of uncertainty and observing the effect on simulator performance, the critical parameters controlling performance can be identified. Further efforts to gather better data should be concentrated on these critical parameters.

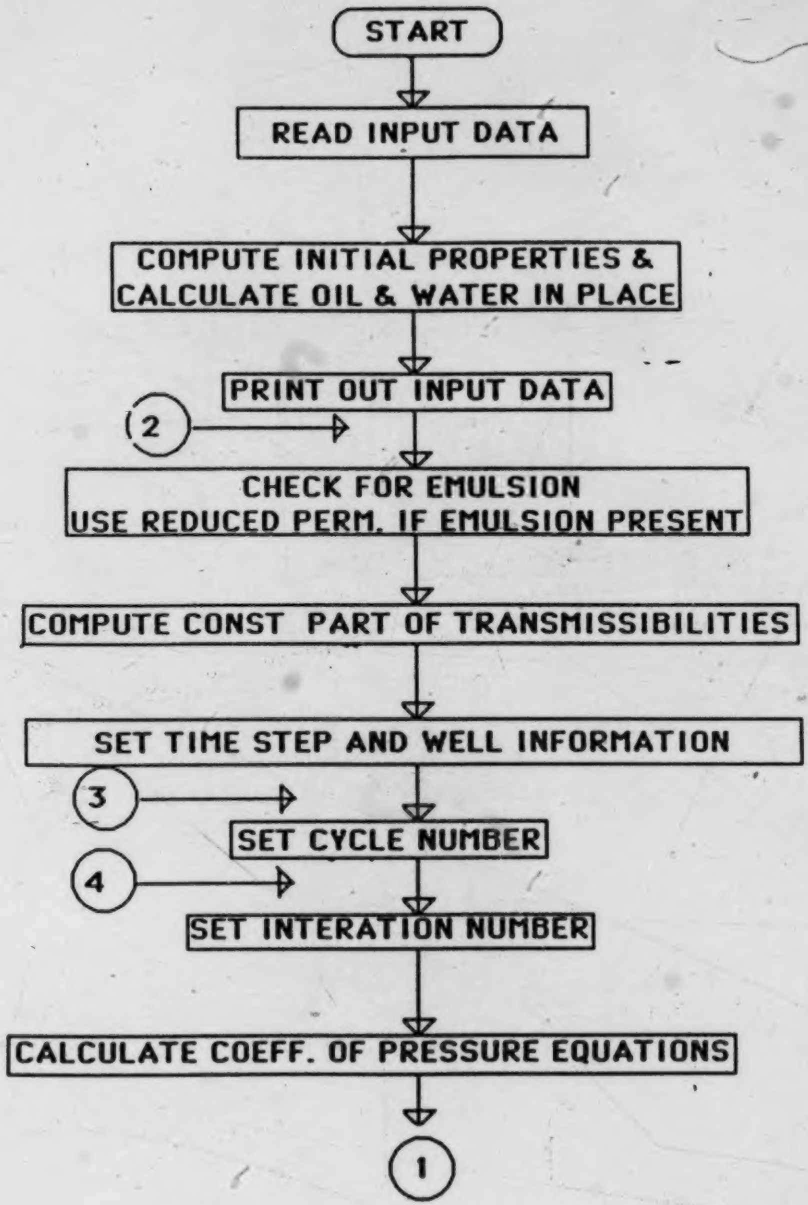
START
READ INPUT DATA
COMPUTE INITIAL PROPERTIES &
CALCULATE OIL & WATER IN PLACE
PRINT OUT INPUT DATA
2
CHECK FOR EMULSION
USE REDUCED PERM. IF EMULSION PRESENT
COMPUTE CONST PART OF TRANSMISSIBILITIES
SET TIME STEP AND WELL INFORMATION
3
SET CYCLE NUMBER
4
SET INTERATION NUMBER
CALCULATE COEFF. OF PRESSURE EQUATIONS
1

Fig. 148 Flow chart of the computational algorithme

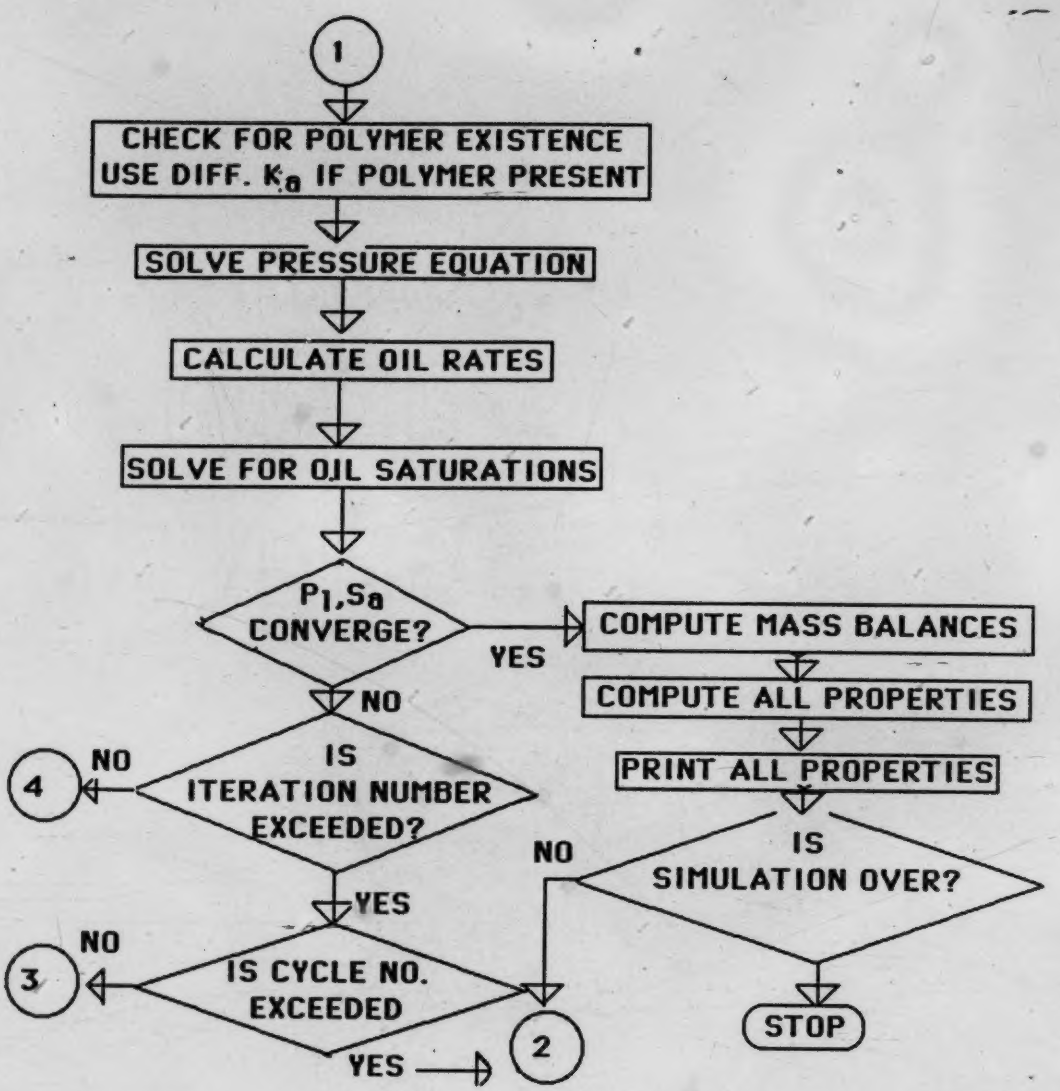
1
CHECK FOR POLYMER EXISTENCE
USE DIFF. K_a IF POLYMER PRESENT
SOLVE PRESSURE EQUATION
CALCULATE OIL RATES
SOLVE FOR OIL SATURATIONS
P_1, S_a CONVERGE?
YES
COMPUTE MASS BALANCES
COMPUTE ALL PROPERTIES
PRINT ALL PROPERTIES
NO
IS ITERATION NUMBER EXCEEDED?
NO
4
IS SIMULATION OVER?
NO
YES
IS CYCLE NO. EXCEEDED
NO
3
YES
2
STOP

Fig. 148 Contd.

7.2 Grid Sensitivity

Table 7.1 compares the time required for a waterflood, polymer flood and emulsion flood as a function of the grid size. It can be seen that by using a grid size of 10x1x2, it is possible to have very similar results as compared to a grid size of 10x2x4 whereas the computational time is much shorter. Note that the sensitivity study of the cumulative oil recovery automatically involves a check on the flow rate of oil which is considered to be a major parameter. Also, the greater computational time required for an emulsion or polymer flood is required, because in polymer or emulsion flooding every block is checked for the presence of polymer or emulsion at every time step. Based on this grid sensitivity study, a 10x1x2 grid size was chosen for further simulation studies.

7.3 History Matching

The objective of the history match is to reproduce with the simulator the actual reservoir performance. This is achieved by manipulating two fundamental processes which are controllable during history matching: the quantity and distribution of fluid within the system, and the movement of fluid within the system. These processes are manipulated by adjusting input data within reasonable limits of conditions existing in the field until a minimal difference remains between the historical data and the simulator calculations

TABLE 7.1 Grid Size Sensitivity for Waterflood, Emulsion flood and Polymer Flood Simulation Runs

Type	Time for 1 PV (ms)		Maximum Diff. in Recovery (%)
	10x1x2	10x2x4	
Waterflood	4.2	22.6	0.5
Emulsion flood	17.5	52.7	0.8
Polymer flood	12.0	43.2	0.7

at the same point in time.

Thus, history matching is the process of determining the values of inadequately known or unknown physical parameters which are needed as input to the mathematical reservoir model. The reliability of a history match depends, in large part, on knowledge of the process itself. In the present study, experimental results and interpretations were considered as a basis for history matching. The only parameter that was determined through history matching was the relative permeability to the different phases.

7.4 DISCUSSION OF RESULTS

Numerical simulations were performed for waterfloods, polymer floods and emulsion floods. A three-phase, three-dimensional model was used for polymer and emulsion flooding; and a two-phase, three-dimensional model was used for the waterfloods. Numerical results were compared with experimental results. For this purpose a series of runs was chosen. Table 7.2 lists these experimental runs with their major characterstics.

7.4.1 Waterflood

In order to validate the numerical simulator, a series of numerical runs was conducted to simulate experimental results of conventional waterfloods. Then the model was

TABLE 7.2: Characterstics of Experimental Runs Chosen for Simulation

Run no.	k_o (μm^2)	k_o/k_b	Blocking Agent	μ_o/μ_w	h_b/h_o	Simulation
4	16.0	1.00	Polymer	"	0.33	Waterflood
6	16.2	2.67	"	"	0.33	Waterflood
7	15.9	2.67	"	"	1.00	Waterflood
15	16.0	N.A.	"	"	0.00	Polymer Flood
16	16.0	1.00	"	"	0.33	Polymer Flood
17	16.0	1.00	"	"	0.33	Polymer Flood
18	16.2	1.00	"	"	0.33	Polymer Flood
19	16.0	1.00	"	"	0.33	Polymer Flood
22	15.9	1.00	"	"	0.33	Polymer Flood
30	16.1	1.00	Emulsion (10% oil)	"	0.33	Emulsion Flood
31	16.0	N.A.	"	"	0.00	Emulsion Flood
32	16.15	1.00	"	"	1.00	Emulsion Flood
34	16.0	2.67	"	"	0.33	Emulsion Flood
36	15.8	0.06	"	"	0.33	Emulsion Flood
42	16.0	1.00	"	"	0.33	Emulsion Flood
45	16.0	1.00	"	"	0.33	Emulsion Flood

used to predict ultimate oil recoveries (defined as the recovery at WOR=20) for the experimental runs which were terminated at a WOR lower than 20.

7.4.2 Waterflood in a Homogeneous Core

Oil/water capillary pressure data were obtained from a different study (Islam and Bentsen, 1986). Since the oil used in that study had an oil/water interfacial tension very close to that of the oil used in this study, similar capillary pressure behaviour was expected. Figure 149 shows the oil/water capillary pressure curve. Numerical simulation was initiated using relative permeabilities obtained experimentally by the Johnson-Bossler-Naumann (JBN) method. In order to obtain a match with the experimental data, only relative permeabilities were adjusted. Figure 150 shows relative permeabilities to oil and water. Relative permeabilities to oil were very close to those estimated by the JBN method. Model relative permeabilities to water had to be increased in order to obtain a good match with the experimental data, especially at the time of water breakthrough. Relative permeabilities to oil had to be adjusted in order to obtain a good match near the irreducible oil saturation. Figure 151 shows the comparison between experimental and numerical results for Run 14 for which a waterflood was conducted for one pore volume. As can be seen in this figure, an excellent match is obtained

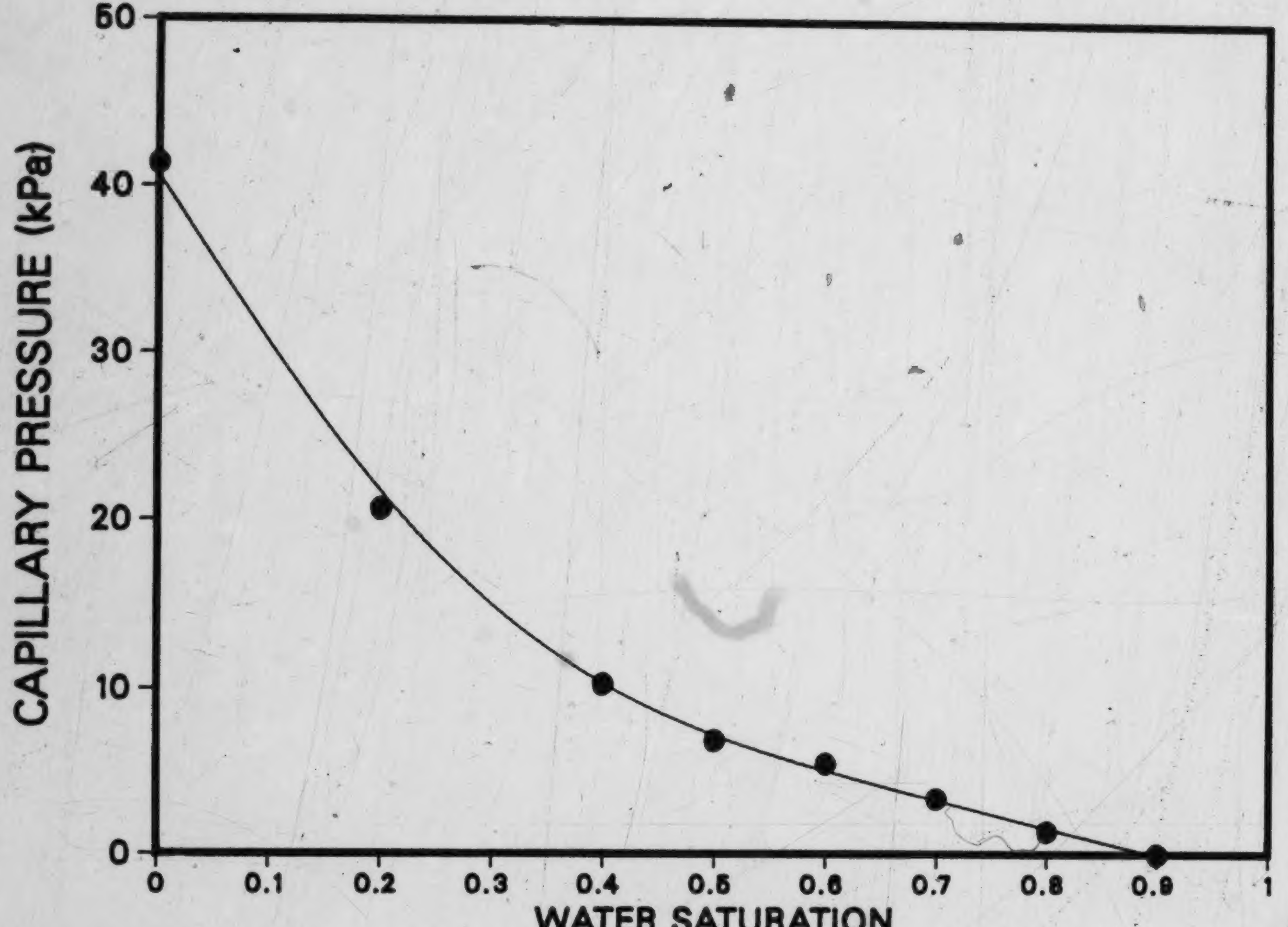

Fig. 149 Oil/Water Capillary Pressure Curve Used for Simulation

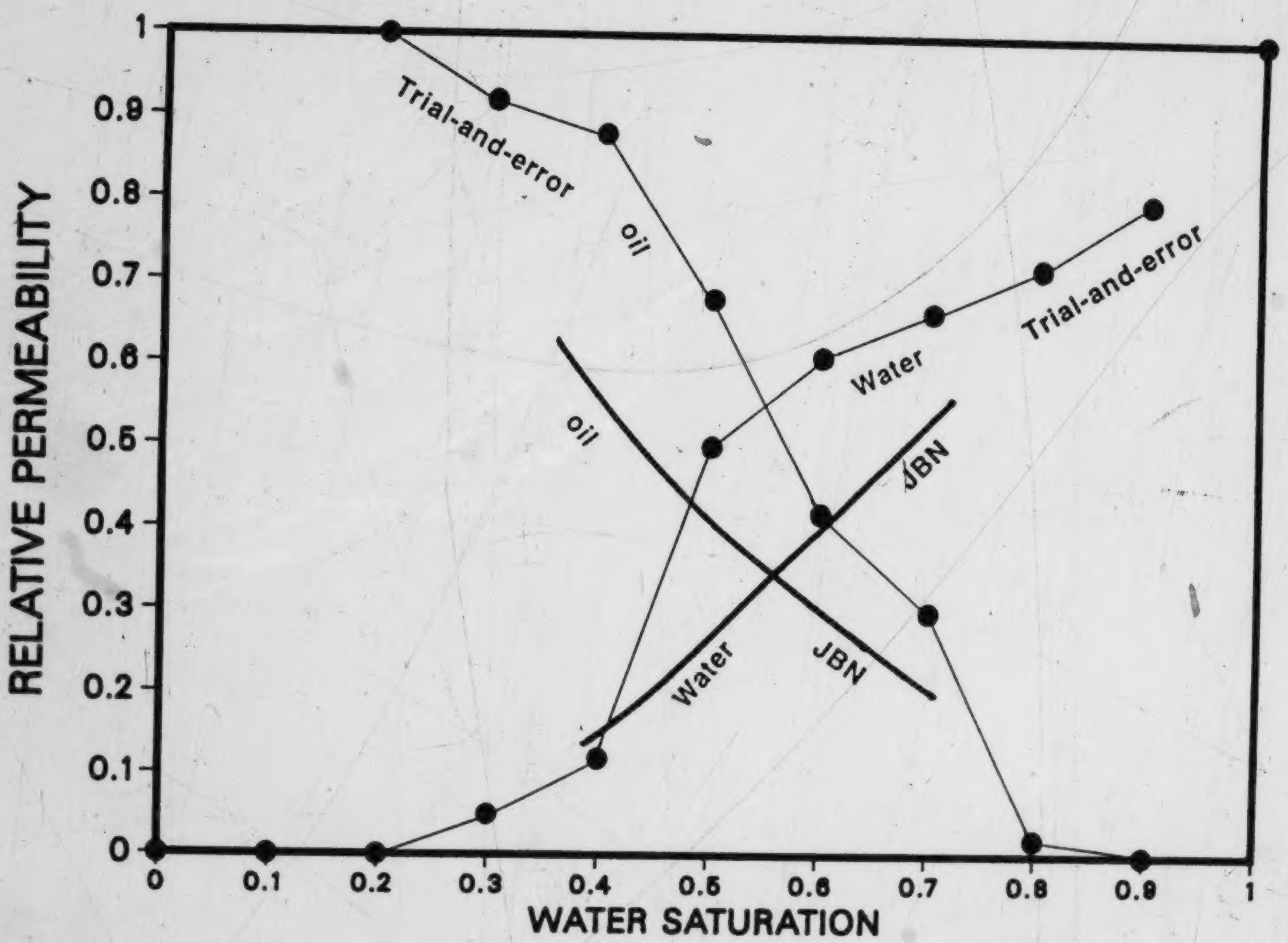

Fig. 150 Comparison of Oil/Water Relative Permeability Curves (JBN and Trial-and Error)

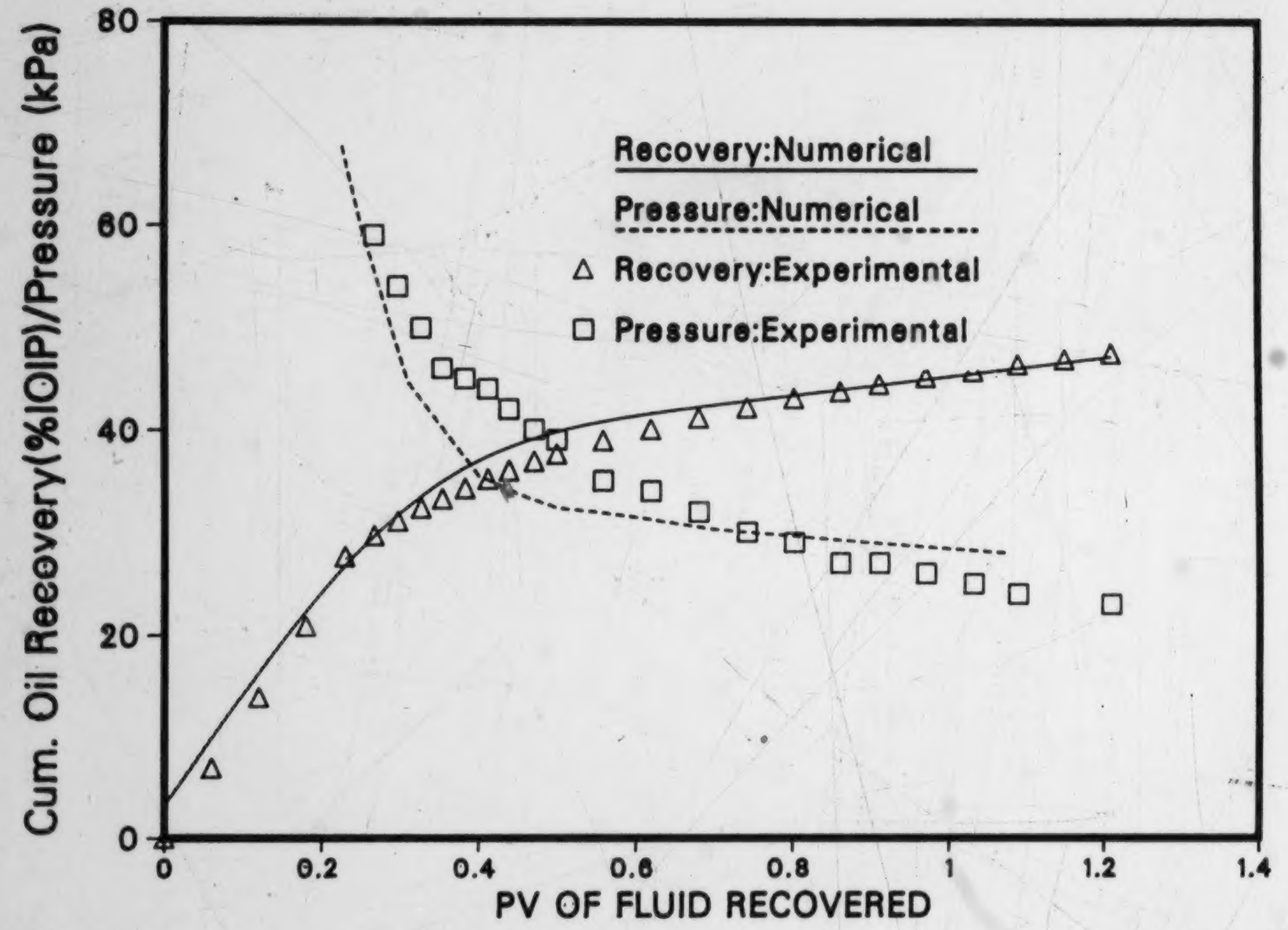

Fig. 151 Comparison of Experimental and Numerical Results with Waterflood for $h_b/h_o=0$

for oil recovery. A slight deviation is observed after water breakthrough, which might be because of experimental error in determining the breakthrough point. Numerical and experimetal pressures showed a similar deviation. Similar to oil recovery, the deviation between experimental and numerical values is observed soon after the water breakthrough point. The pressure curve appears to be shifted to the right near the breakthrough point. However, the maximal deviation in oil recovery was less than 10%. This small deviation represents a satisfactory simulation of the experimental data.

7.4.3 Waterflood in the Presence of a Bottom-Water Zone

Figure 152 compares the numerical results with the experimental results of Run 4 in which a waterflood was conducted at the initial stage of the displacement test. For this run the oil-water zone thickness and permeability ratios were 3 and 1, respectively. The same set of relative permeability curves as those in the homogeneous core was used for this run. Initially, k_z for the oil zone was assumed to be equal to the absolute permeability of the oil zone. This led to a lower numerical oil recovery than that observed experimentally. It was concluded that even though the oil- and water-saturated layers were in capillary contact, k_z was not the same as the horizontal permeability. Therefore, by assuming the same values for permeabilities

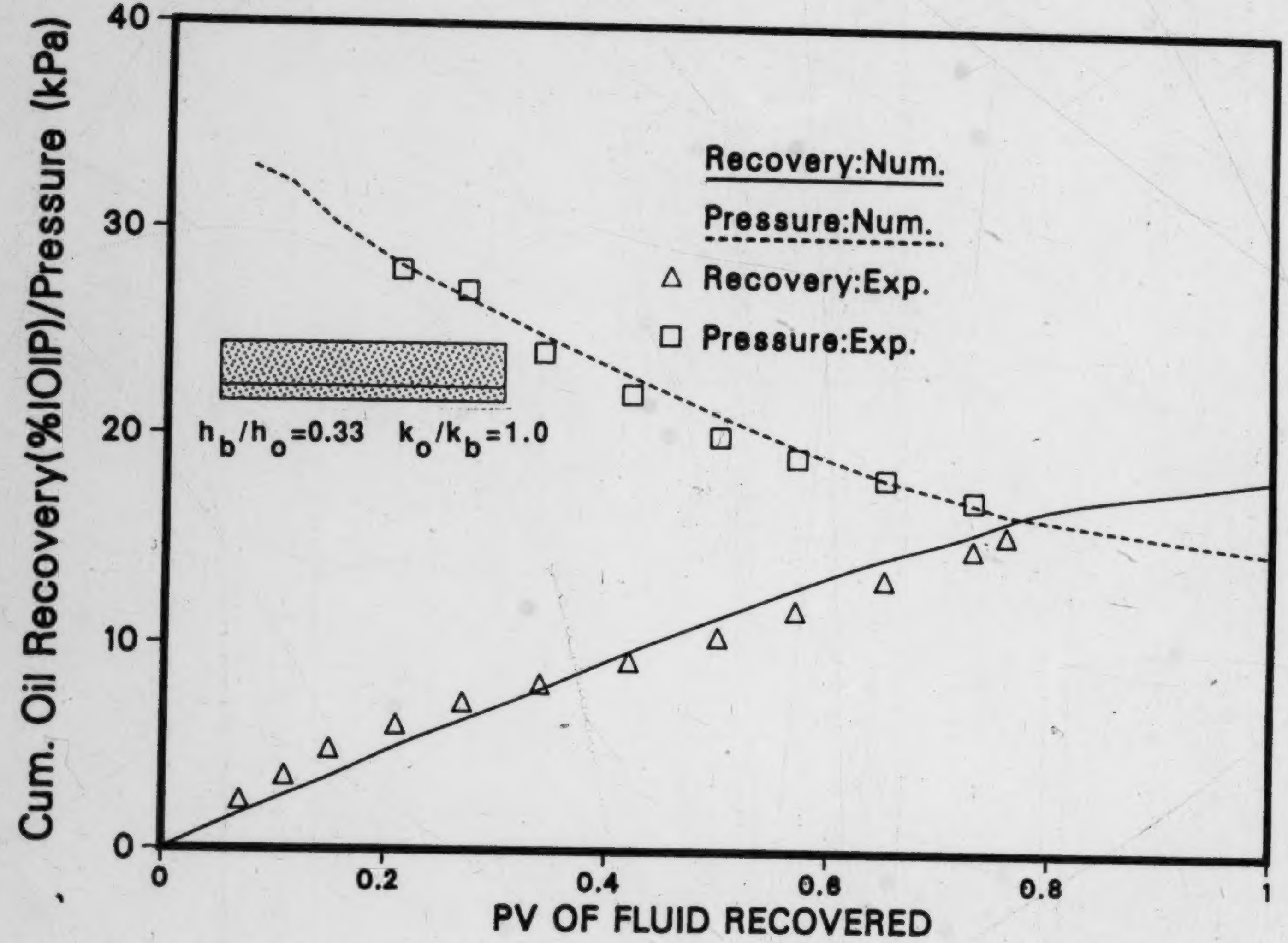

Fig. 152 Comparison of Experimental and Numerical Results with Waterflood for Run 4

for the vertical and axial directions, an error in the amount of crossflow was introduced. In order to remedy this error, k_z was reduced until a good agreement (see Figure 152) was observed between experimental and numerical results. The adjusted value of k_z was 70 percent of the horizontal permeability. This value was retained for the other runs as well.

Figures 153 and 154 compare the numerical results with the experimental results for Runs 6 and 7. In both cases, good agreement between experimental and numerical results is observed. However, for Run 6, the inlet pressures deviated considerably, especially at the initial stage of the displacement test. The match in pressures for Run 7 was less satisfactory. Run 7 had a bottom-water zone as thick as the oil zone.

7.4.4 Polymer Flood and Waterflood

Polymer is known for its unique ability to reduce only the mobility of the aqueous phase. Even though many researchers have reported that the decrease in water mobility is related to a reduction in absolute permeability, there has been increasing evidence that the effective permeability to water is the most affected. This evidence is supported by observations that only water-saturated zones are affected in cases of multi-layered porous media (Sparlin, 1976). In fact, the effect of polymer is almost

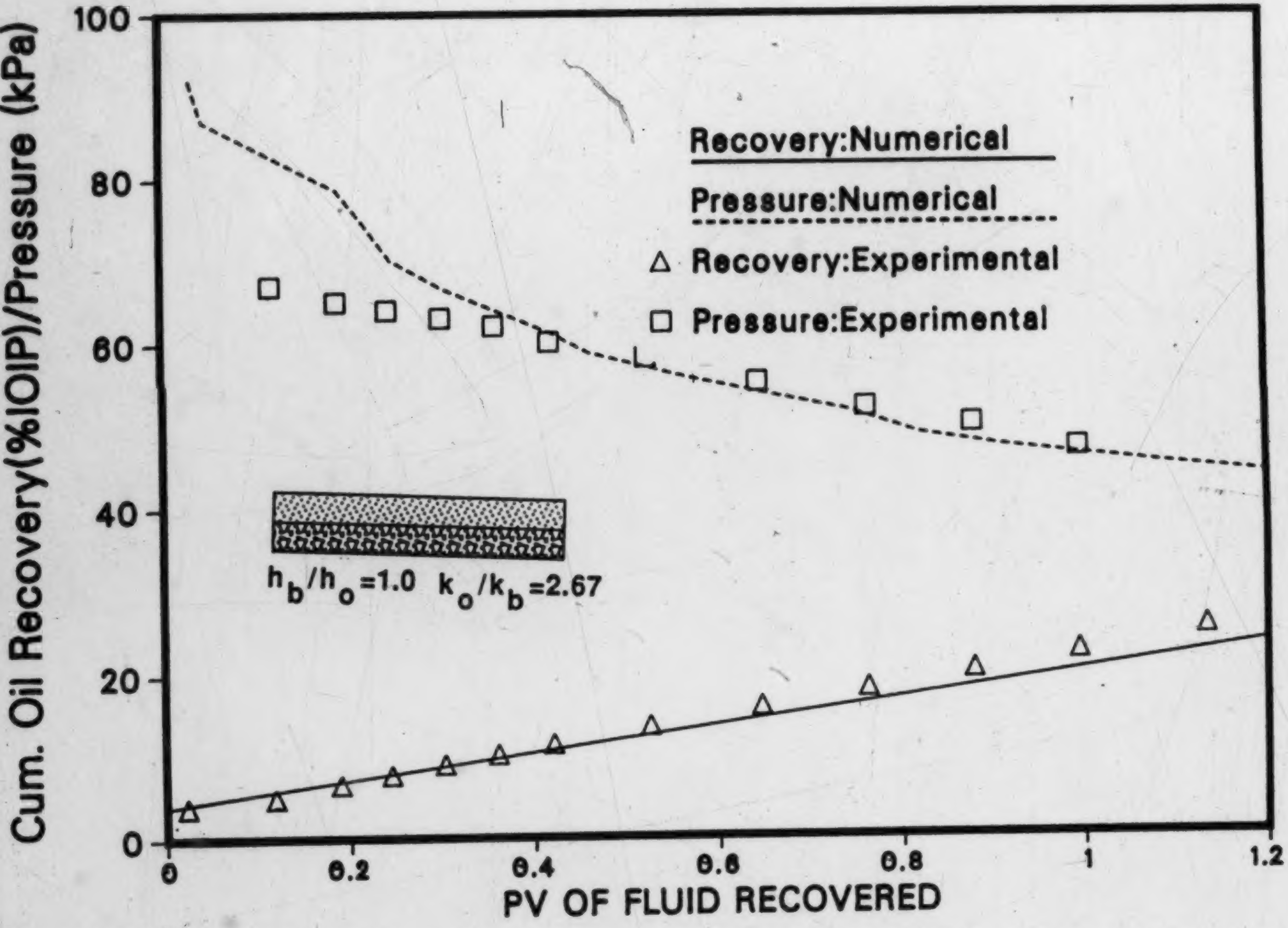

Fig. 153 Comparison of Experimental and Numerical Results with Waterflood for Run 7

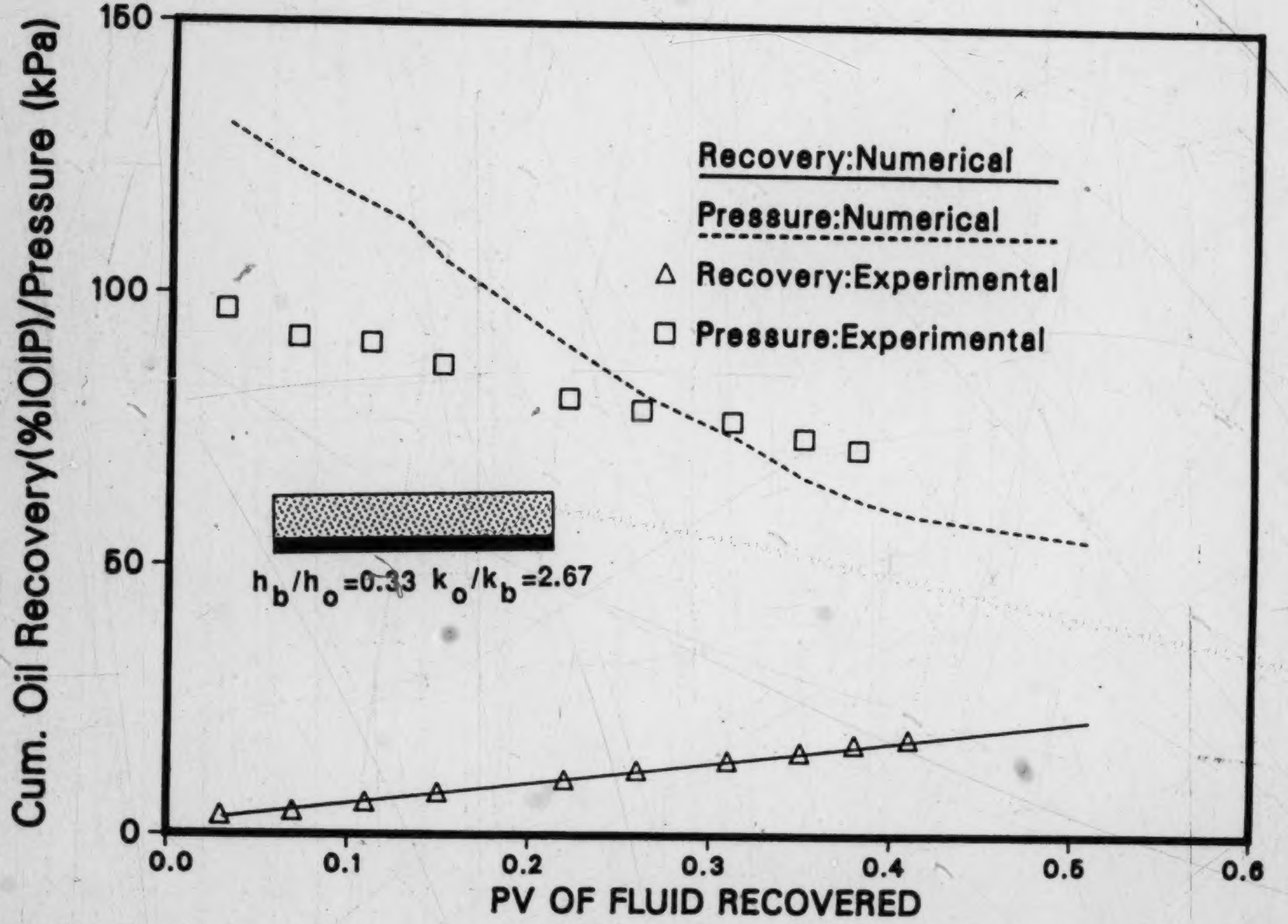

Fig. 154 Comparison of Experimental and Numerical Results with Waterflood for Run 6

negligible in the case of oil-saturated porous media. This property of polymer solutions is due to polymer adsorption (Harrington and Zimm, 1968) and mechanical entrapment. Adsorption affects directly the pore walls, thus altering the effective permeability to water in the case of water-wet porous media.

Whatever the mechanism involved, experimental evidence suggests that the effective permeability to water is the only parameter that is affected by a polymer flood. This is supported further by the present experimental study, which showed that improvement over a conventional waterflood was much better in the presence of mobile water than in the presence of irreducible water. Many authors have attempted to simulate polymer and water flow in a porous medium with limited success (Al-Seehati,1979). Their simulation took account of polymer dispersion in water and polymer adsorption by the solid rock surface. Even after introducing polymer dispersion and adsorption, a 'resistance factor' had to be introduced to account for the reduction in absolute permeability caused by the injected polymer solution. This procedure is redundant if polymer adsorption is considered to be the main cause of any reduction in absolute permeability. Also, the difficulty involved in this approach is that polymer is considered only as a component of the aqueous phase, and two-phase relative permeabilities are used. Besides, because only the absolute permeability is considered to be affected by polymer injection, this reasoning leads to an improper simulation of the relative permeabilities to water. On the whole, the current approach to simulation of polymer flooding cannot properly simulate the mobility control property of polymer which is most efficient in the presence of mobile water. Also, polymer solution is not readily miscible in water and considering two-phase flow would lead to a considerable error, especially during the initial stages of polymer injection. This error is magnified when the polymer slug volume is small as compared to the water slug volume.

In the present study, a three-phase flow model was used. It is assumed that the effective permeability to water in a porous medium swept with polymer solution is smaller than that in an unswept porous medium. A single set of relative permeabilities was used before polymer reached a given block of the porous medium. After the block was invaded by polymer, a different relative permeability to water was used. In this study, polymer adsorption and dispersion were not considered in the conventional manner. Instead, the major effect of polymer flood, i.e., reduction in the effective permeability to water, was taken into account by means of a different relative permeability curve.

7.4.5 Polymer Flood in a Homogeneous Core with Irreducible Water Saturation

Laboratory experiments performed in this study were chosen as the basis for numerical simulation. A polymer flood was conducted in Run 15 with a homogeneous core with irreducible water saturation, established by oil-flooding a water-saturated core. It has been discussed in the experimental study (Chapter VI) that polymer solution injection led to a higher oil recovery which was caused by a decrease in irreducible oil saturation. Therefore, the water relative permeability curve had to be shifted in order to simulate a mobile water phase during the initial stages of polymer injection. This shift enabled a proper match of the water breakthrough point. Figure 155 shows the relative permeabilities to water, oil and polymer. As can be seen in this figure, the water relative permeability curve differs considerably from a conventional water-oil two-phase relative permeability curve. This is because three-phase flow is considered for the polymer-water-oil system. Run 15 had a water saturation of only 11.5 percent. Consequently, relative permeabilities for higher water saturations had to be obtained by matching more experimental runs. Figure 156 compares the numerical results with the experimental results of Run 15. Breakthrough to water and to polymer were considered important, and relative permeabilities to polymer were adjusted in order to obtain a proper match of these

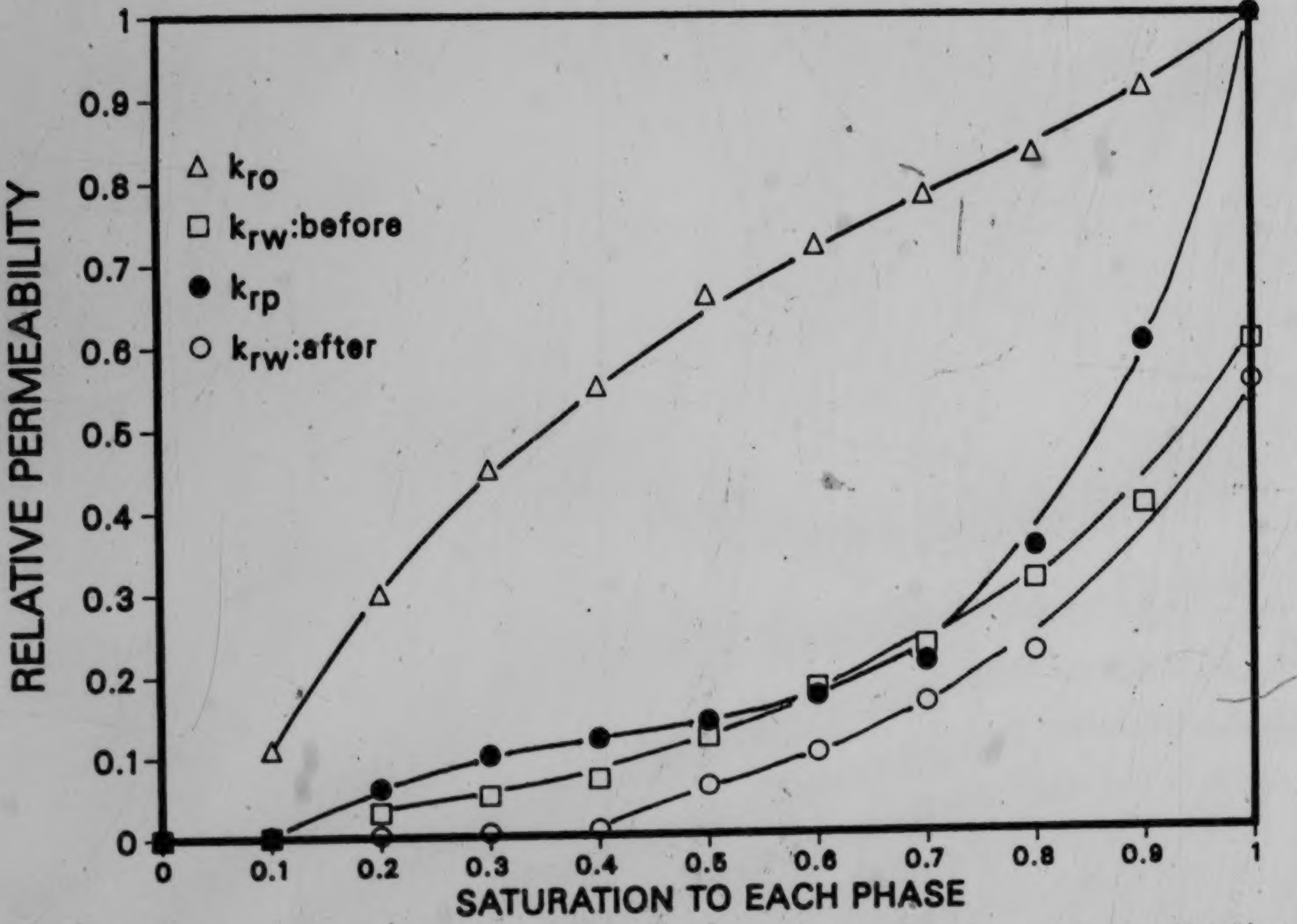

Fig. 155 Relative Permeability to Different Phases After and Before Polymer Flooding

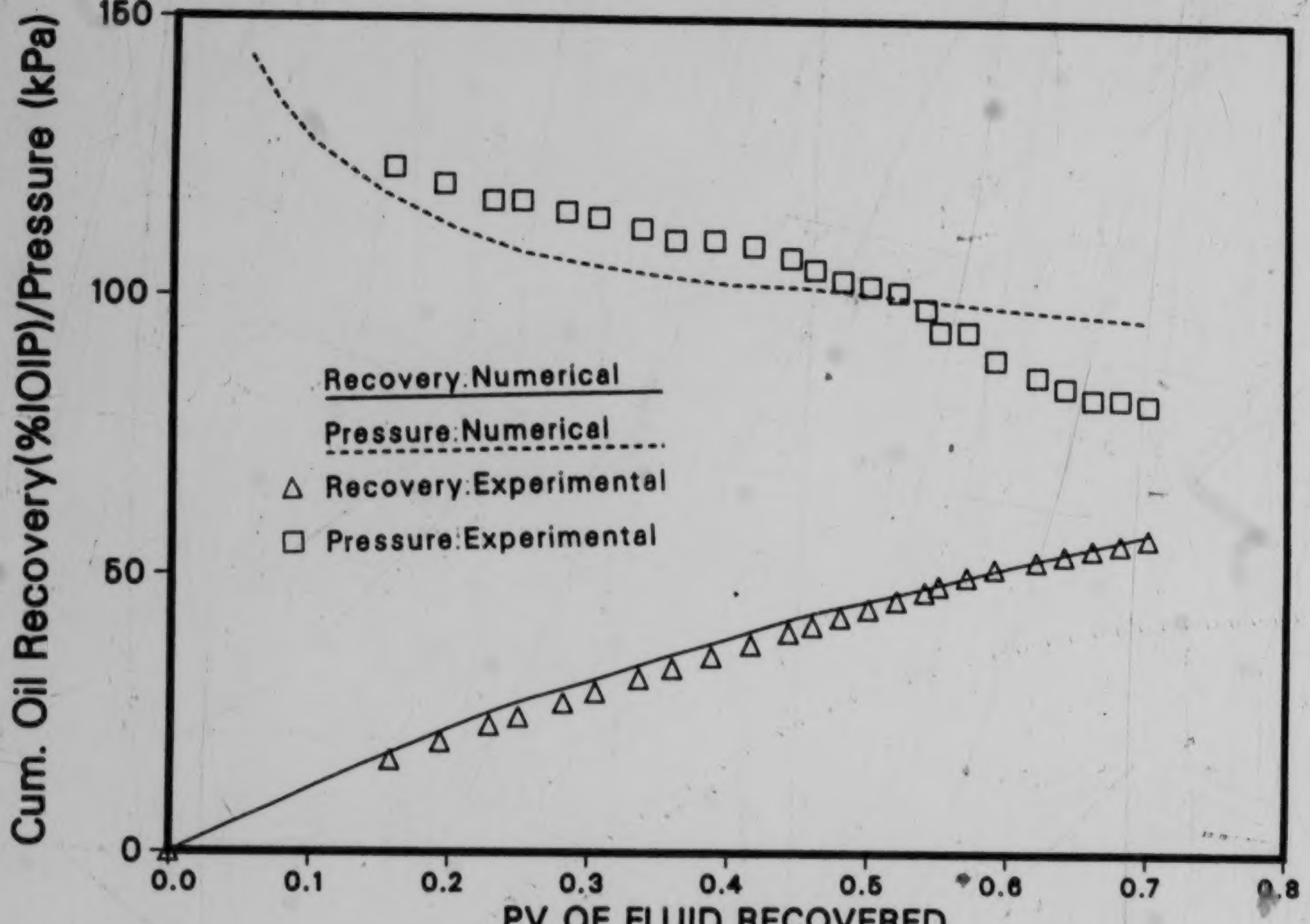

Fig. 156 Comparison of Experimental and Numerical Results for Run 15 (h_b/h_o=0.)

points. Figure 156 shows an excellent agreement in cumulative oil recoveries between numerical and experimental results. Also, the inlet pressures match closely until such time as 0.5 pore volume of polymer was injected. At this point (shortly after polymer breakthrough), the experimental inlet pressure declines rapidly and deviates from the predicted numerical points. This deviation may be due to adsorption and retention which decreased the polymer viscosity in the actual experiment, whereas the polymer viscosity was considered to be constant for the numerical simulation. However, the deviation between experimental and numerical pressures is less than 15 percent.

7.4.6 Polymer Flood in the Presence of a Bottom-Water Zone

A polymer flood in the presence of a bottom-water zone represents a difficult situation to simulate. Because polymer has the unique and not fully understood property of reducing water mobility, any simulation should also show increased recovery efficiency in the presence of a bottom-water zone. An effective simulation would also involve a good match in cases of different slug sizes and polymer viscosities. This was properly simulated in this study. The same set of relative permeabilities, as described in the previous section, was used. However, relative permeabilities to water were estimated by trial and error over the whole range of water saturations.

Run 19 (h_b/h_o=0.33, k_o/k_b=1, S=0.26, μ_p=36) was chosen as the basis for estimating relative permeabilities to water. Figure 157 shows the comparison between experimental and numerical results. An excellent agreement was obtained for cumulative oil recovery (maximum deviation of less than five percent). Also, both experimental and numerical inlet pressure curves followed essentially similar trends. The experimental points show a sharp decline after polymer injection had been terminated and a waterflood was begun. This decline was successfully simulated. However, the numerical inlet pressure reaches a higher peak. Because the polymer slug size is relatively large, adsorption and retention decrease polymer viscosity and, thus, the inlet pressures. As has already been discussed, a constant polymer viscosity was assumed for numerical simulation and, therefore, this deviation in pressure was expected. However, even with this deviation in pressure, the oil recovery data matched well, showing the validity of the simulation.

Figure 158 compares the numerical results of Run 18 (k_o/k_b=1, h_b/h_o=0.33, S=0.06, μ_p=36) with those obtained experimentally. Even though the same set of relative permeabilities as in previous cases was used, the agreement between experimental and numerical results is excellent. This shows that the effective permeability to water is independent of polymer viscosity and slug size. In other

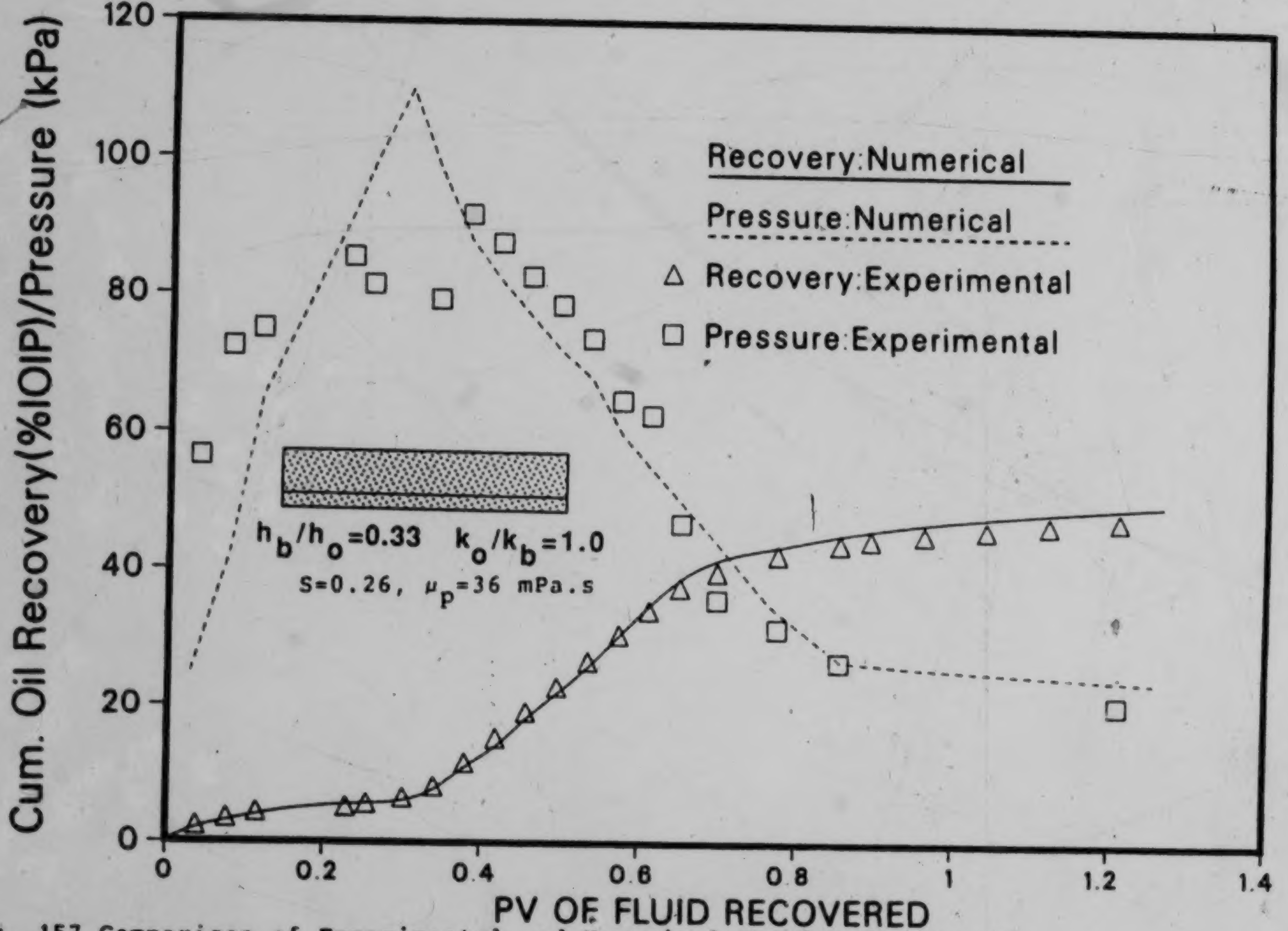

Fig. 157 Comparison of Experimental and Numerical Results for Run 19

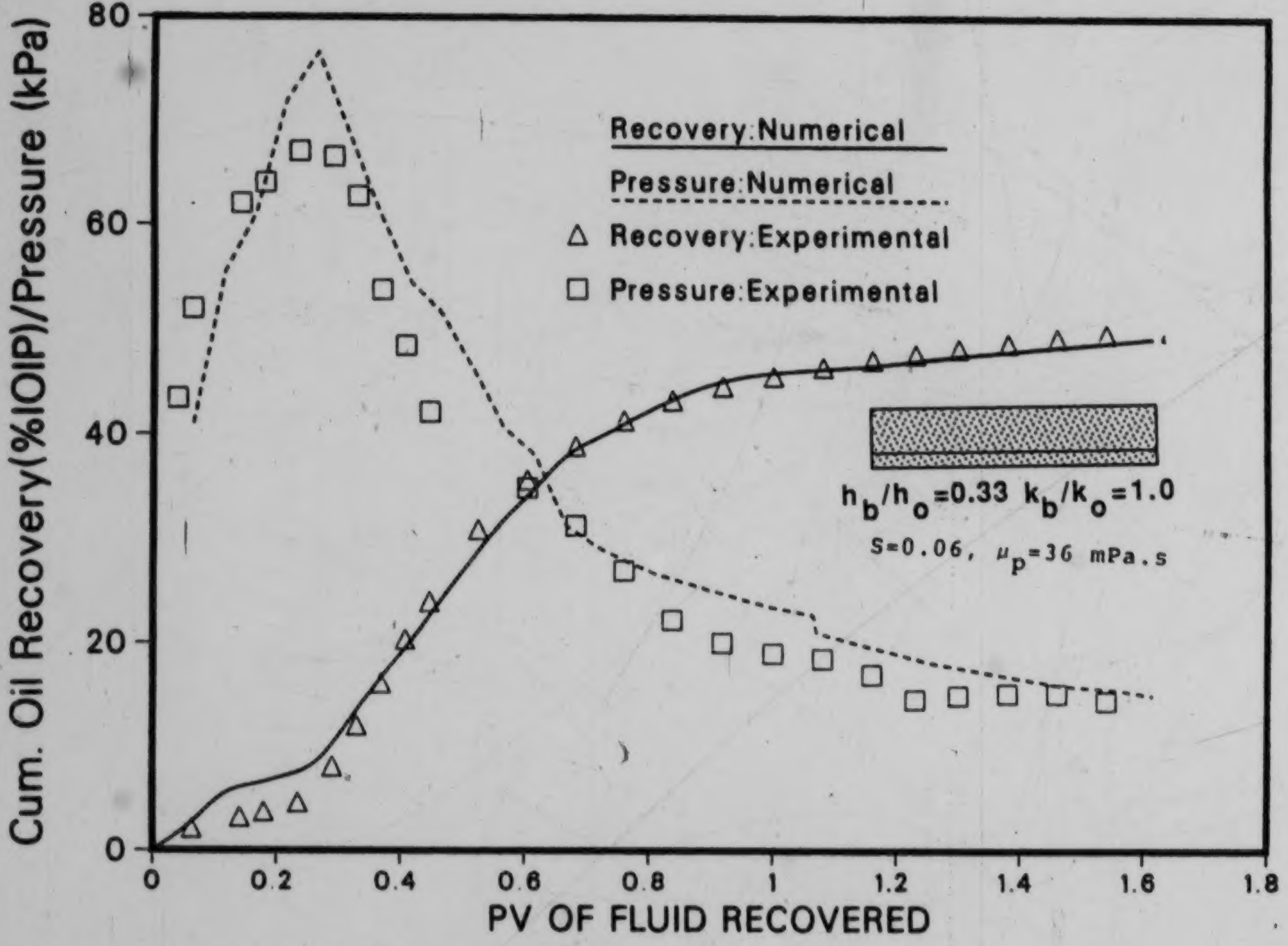

Fig. 158 Comparison of Experimental and Numerical Results for Run 18

words, a larger polymer slug results in a higher oil recovery during polymer injection itself, and even smaller polymer slugs contribute to the same extent by decreasing relative permeabilities to water. Also, a larger polymer slug leads to a higher polymer saturation in the bottom-water zone. Therefore, the bottom-water zone becomes less conductive to water during the waterflood that follows the polymer slug injection. For this particular run, the pressure curves are in better agreeement than in the previous cases. In fact, the smaller polymer slugs show relatively less degradation of polymer and the assumption of constant polymer viscosity is more justified for these cases.

The effectiveness of the numerical simulation is further verified by comparing numerical results with Runs 16 and 17 (Figures 159 and 160). For both of these runs, numerical and experimental pressures achieved the same peak, confirming the previous observation that pressures are simulated better for smaller slug volumes. Also, inlet pressures match better for Run 17 (Figure 160) for which a polymer solution of 36 mPa.s viscosity was used. Polymer degradation is higher for higher polymer viscosities. Therefore, a better match in pressure is expected for the lower range of polymer viscosity. In all cases, however, the agreement between experimental and numerical oil recoveries is excellent.

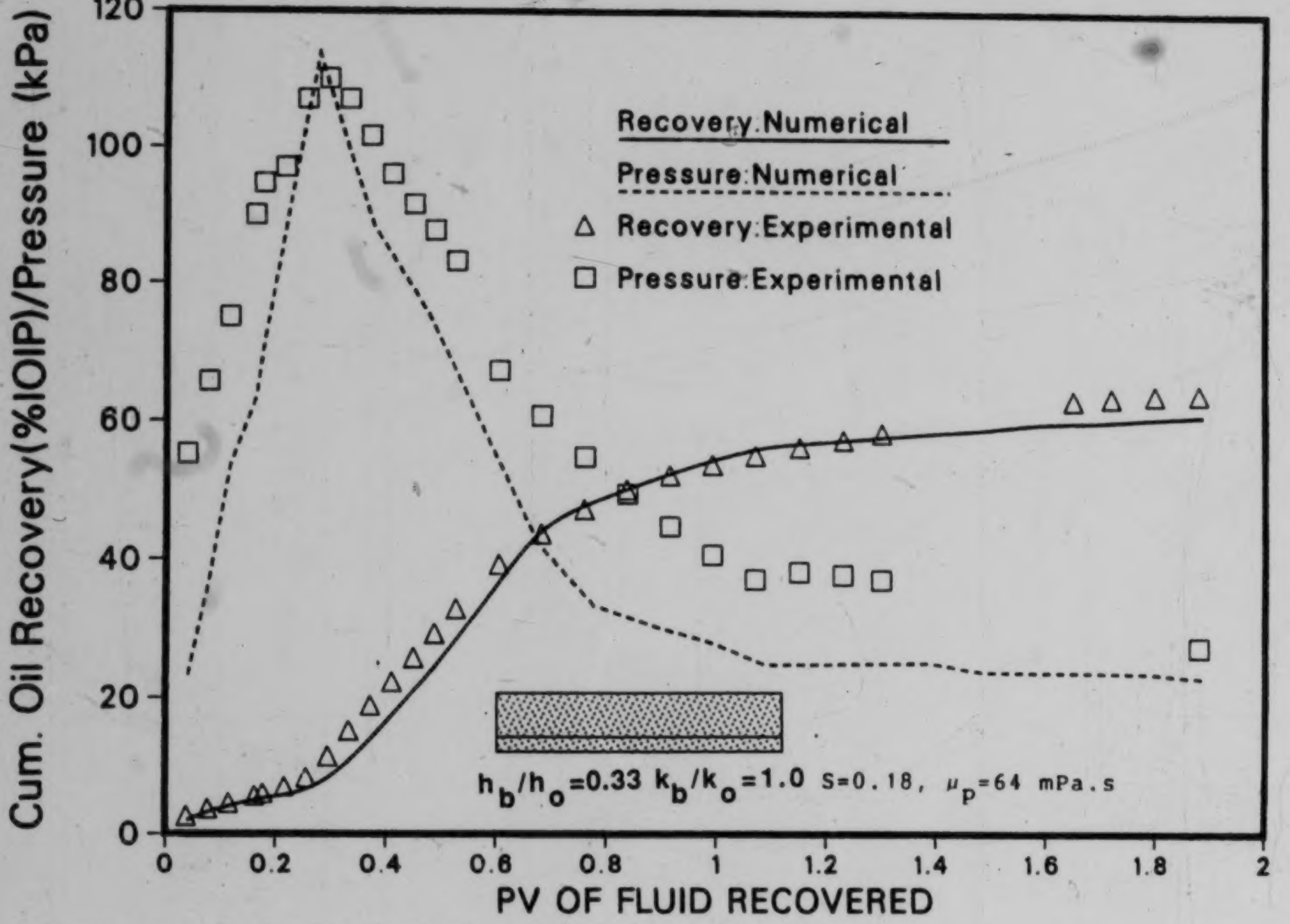

Fig. 159 Comparison of Experimental and Numerical Results for Run 16

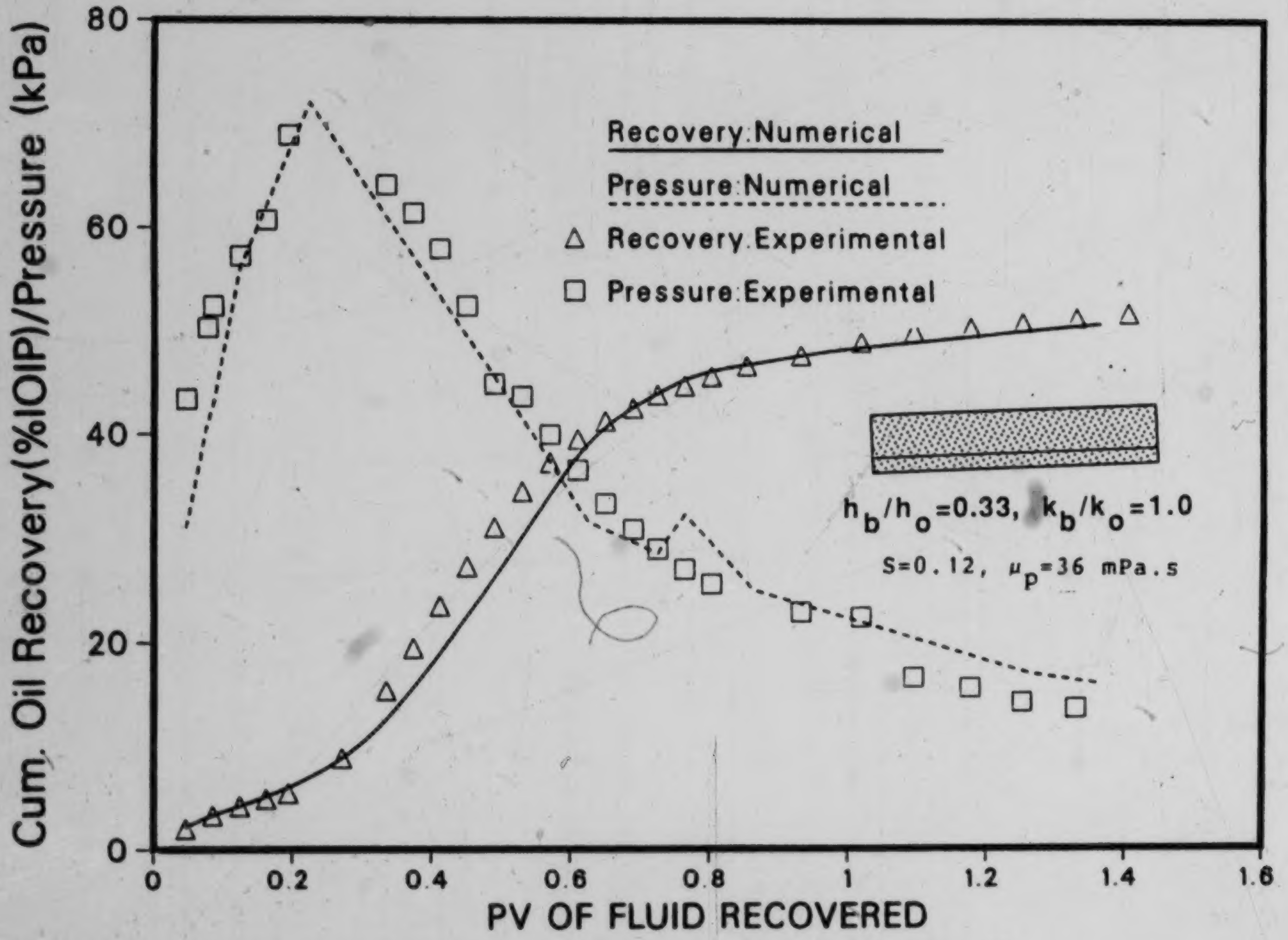

Fig. 160 Comparison of Experimental and Numerical Results for Run 17

A further comparison between experimental and numerical results is presented in Figure 161. This figure compares numerical results with the experimental results of Run 22. Cumulative oil recoveries show excellent agreement for this run. However, inlet pressures show a large deviation even though the trends are similar. This deviation may be partly because of the larger volume of polymer slug and mainly because of unusually large experimental pressures. This is evidenced by a comparison of these pressures with those of Run 19. Even though a higher polymer viscosity was used for Run 19, the injection pressure is lower for this run. This anomalous pressure behaviour may be explained in terms of local plugging (injection well). In the case of a normal operation, the agreement would have been much better for this run.

7.4.6.1 Effect of Oil-Water Viscosity Ratio

After obtaining good agreement between experimental and numerical results for different slug sizes and polymer viscosities, prediction runs were performed in order to examine the effect of the oil-water viscosity ratio. This effect was also investigated experimentally, but only for cases in which a polymer flood followed an initial waterflood. For numerical studies, the sequence of polymer and water slug injections was reversed and an initial polymer flood was followed by a waterflood.

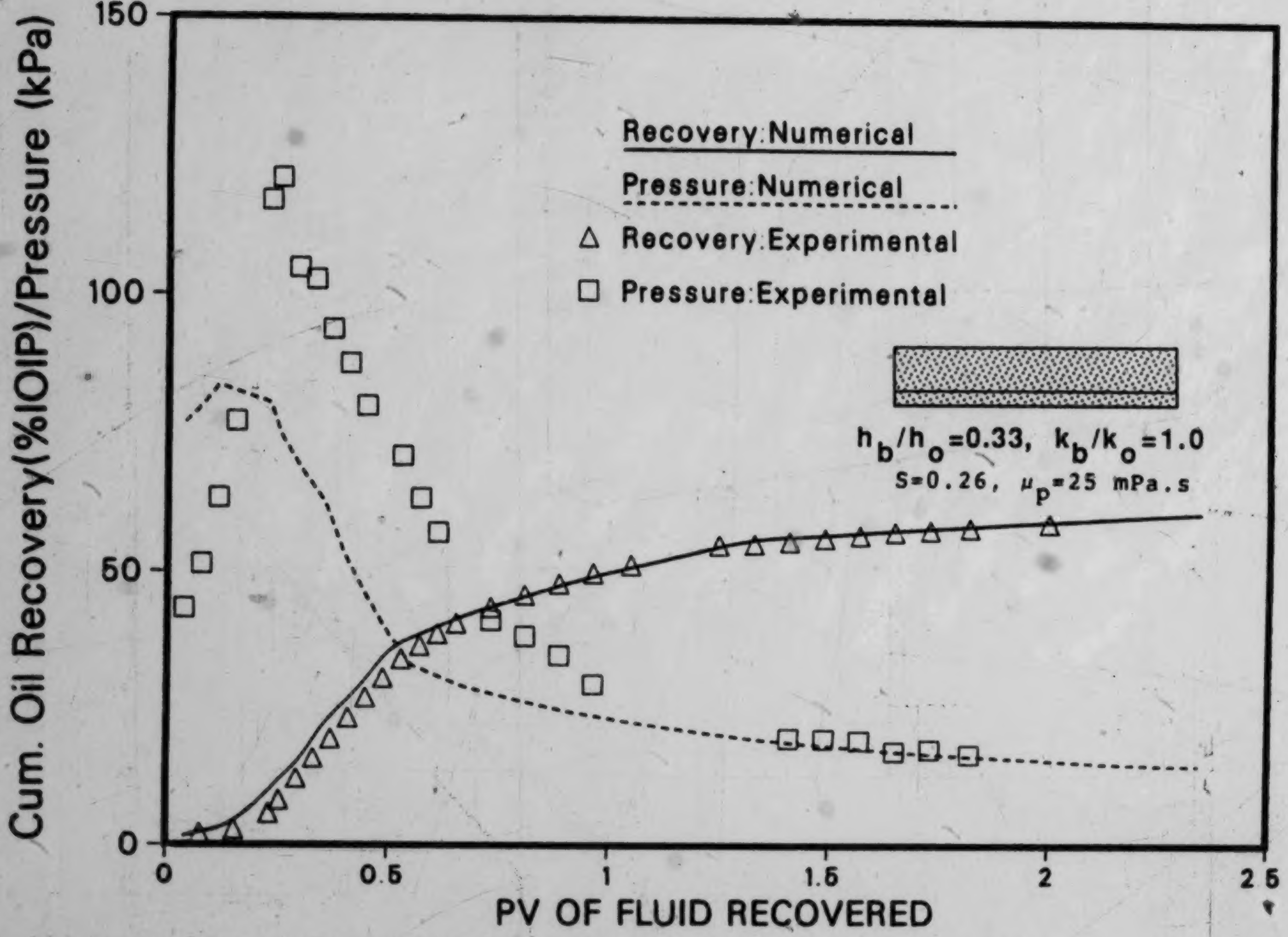

Fig. 161 Comparison of Experimental and Numerical Results for Run 22

Figure 162 compares cumulative oil recoveries for oil-water viscosity ratios of 1, 7.5, and 50 and an h_b/h_o value of 0.33. As expected from experimental observations, a lower oil viscosity leads to higher oil recovery during the initial stages of the displacement. One of the important observations in the experimental study was that the ultimate oil recovery was the highest for an oil-water viscosity ratio of 7.5. The numerical simulation showed the same trend. Also, ultimate recoveries were very close to those observed experimentally.

7.4.6.2 Effect of Polymer Slug Size for $h_b/h_o=1$

In the experimental study, the effect of polymer slug size was studied for $h_b/h_o=0.33$ only. Numerical simulation gave an opportunity to investigate this effect for $h_b/h_o=1$ as well. Figure 163 compares the cumulative oil recoveries for slug sizes of 0.2, 0.4, and 0.6 PV. As can be seen in this figure, the oil recovery increases rapidly between slug sizes of 0.4 to 0.6 PV. For a slug size of 0.2 pore volume, the oil recovery is very low as compared to that for higher slug sizes. However, even with a slug size of 0.2 pore volume, the oil recovery is much higher than that for a conventional waterflood.

7.4.6.3 Effect of Polymer Slug Size for $h_b/h_o=0.2$

The experimental study was conducted with only one slug size for $h_b/h_o=0.2$. Therefore, it was decided to

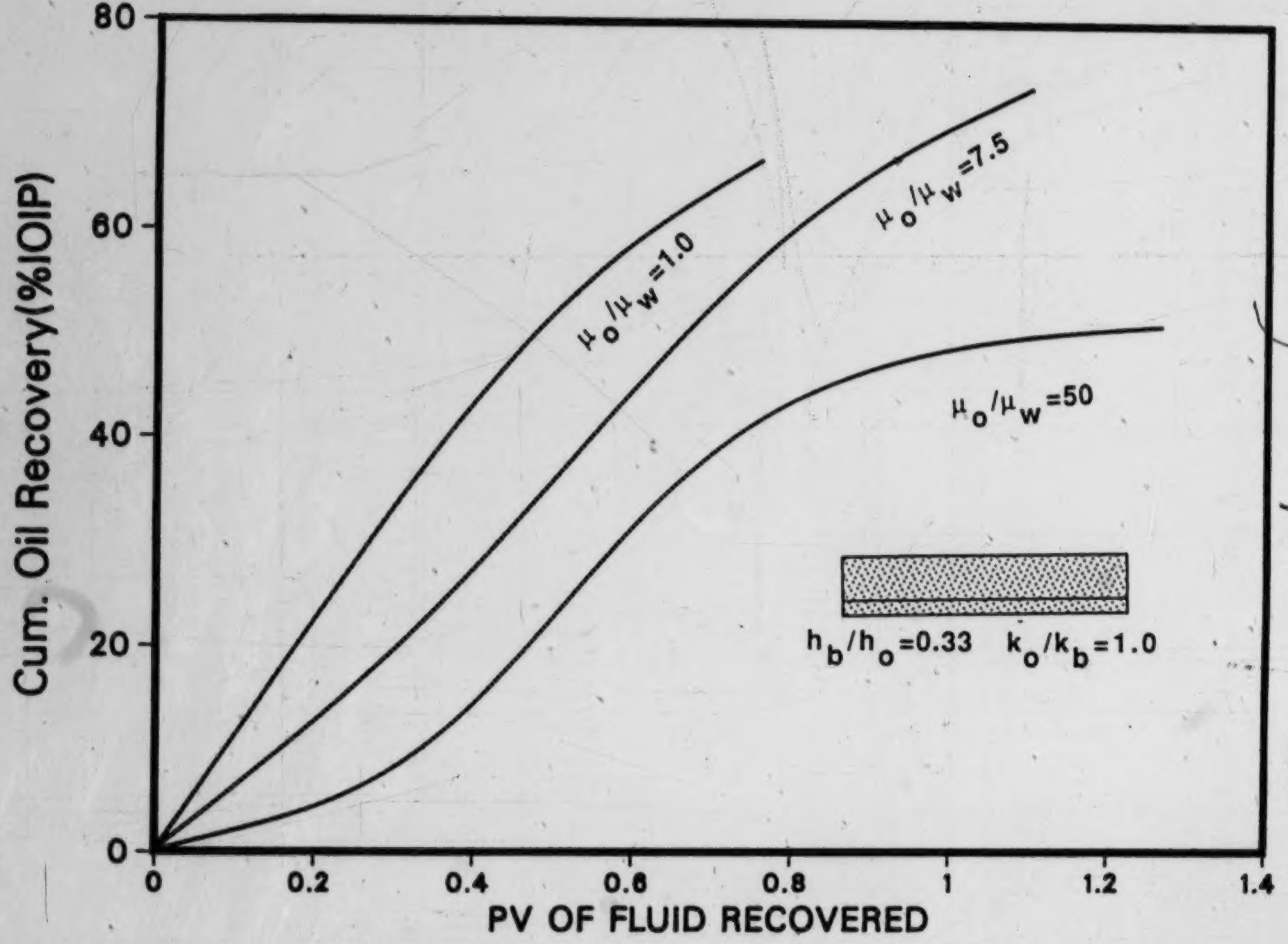

Fig. 162 Comparison of Polymer Floods for Different Oil-Water Viscosity Ratio

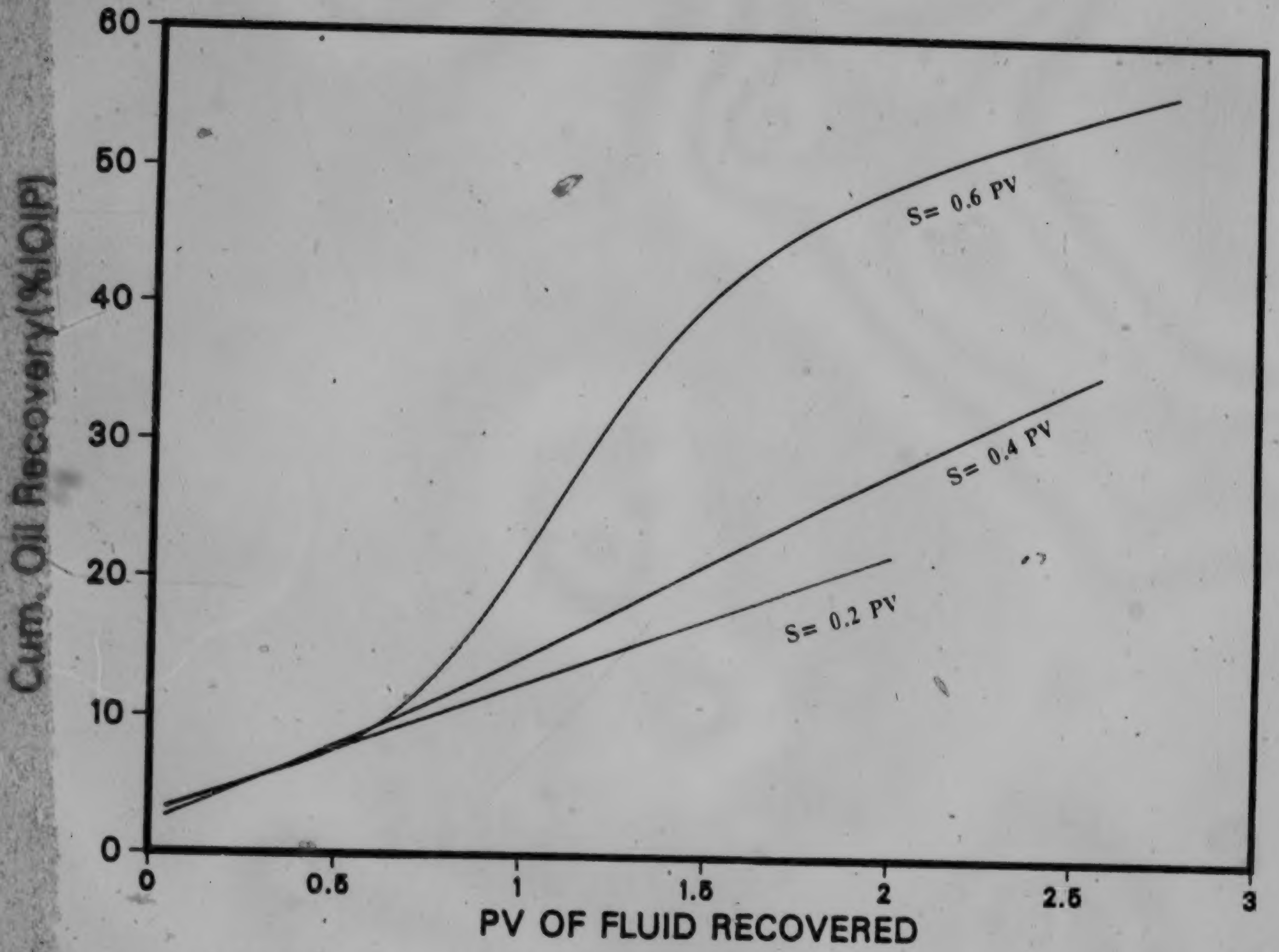

Fig. 163 Effect of Slug Size on Polymer Flood Recovery for $h_b/h_o=1.0$ and $k_o/k_b=1.0$

investigate the effect of slug size for this particular thickness of the bottom-water zone. Figure 164 compares the numerical results for slug sizes of 0.1, 0.2 and 0.3 PV. It can be seen from this figure that the oil recovery increases continually with increasing slug sizes and it is difficult to define an optimal slug size. A similar effect was observed for experimental investigations for $h_b/h_w=0.33$ as well. However, during the later stages of the displacement test a slug size of 0.20 PV appears to give the highest oil recovery. A larger polymer slug gives a higher oil recovery during the initial stages of the displacement, but continuous polymer injection does not give the highest oil recovery in the presence of a bottom-water zone. This is because, when a waterflood follows a polymer flood, increased resistance is offered by the water-saturated bottom-water zone and water is forced into the oil zone to increase the oil recovery. On the other hand, with continuous polymer injection, polymer encounters oil and polymer (in the bottom-water zone) and tends to go into the bottom-water zone due to the lower resistance offered by polymer as compared to the viscous oil.

7.4.6.4 Effect of Oil-Water Zone Permeability Ratio

In the experiments, three different oil-water zone permeability ratios were used: 1.0, 2.67 and 0.06. It was decided to examine numerically the effect of very high oil-water zone permeability ratios. Figure 165 compares the

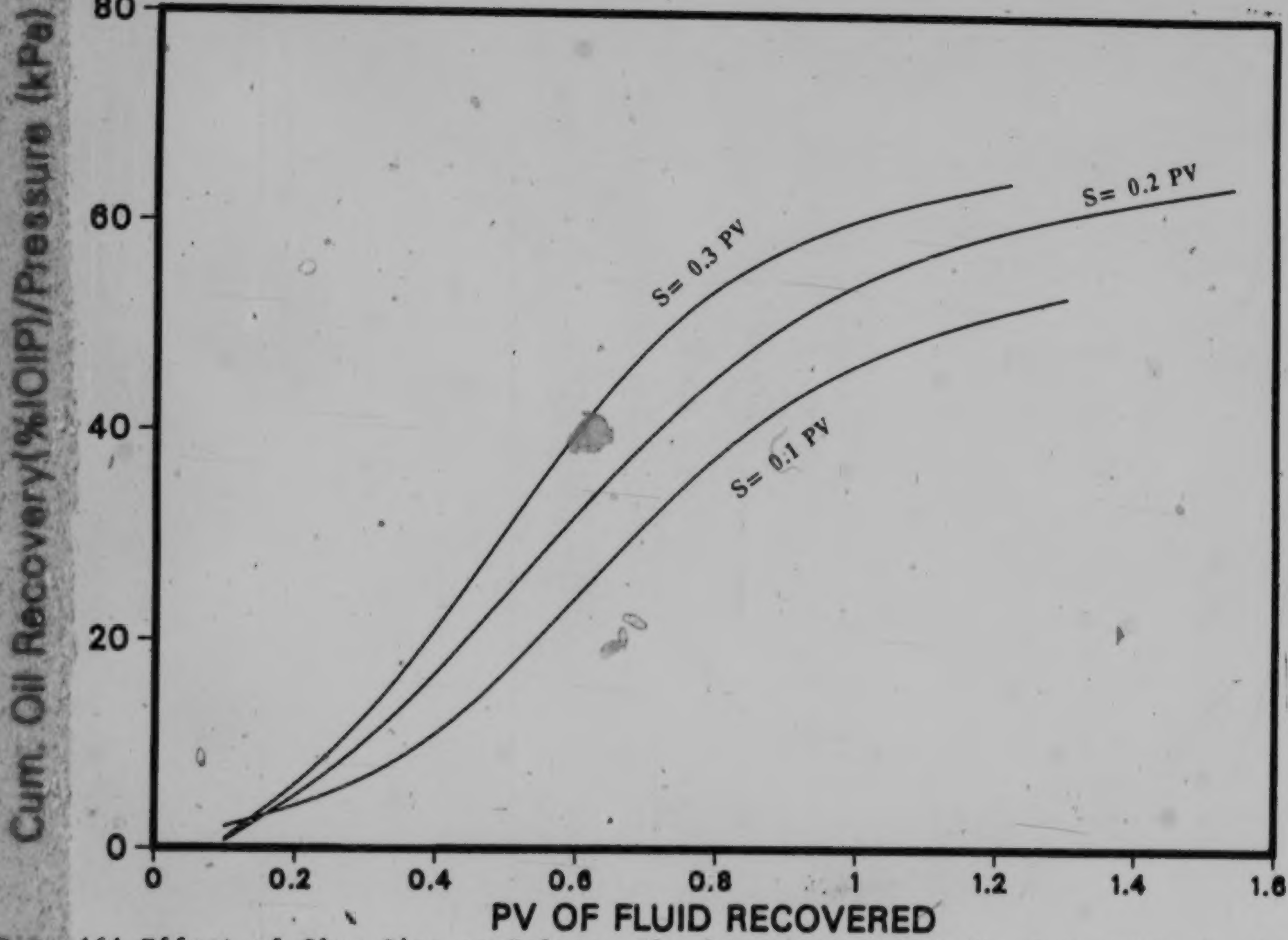

Fig. 164 Effect of Slug Size on Polymer Flood Recovery for $h_b/h_o=0.2$ and $k_o/k_b=1.0$

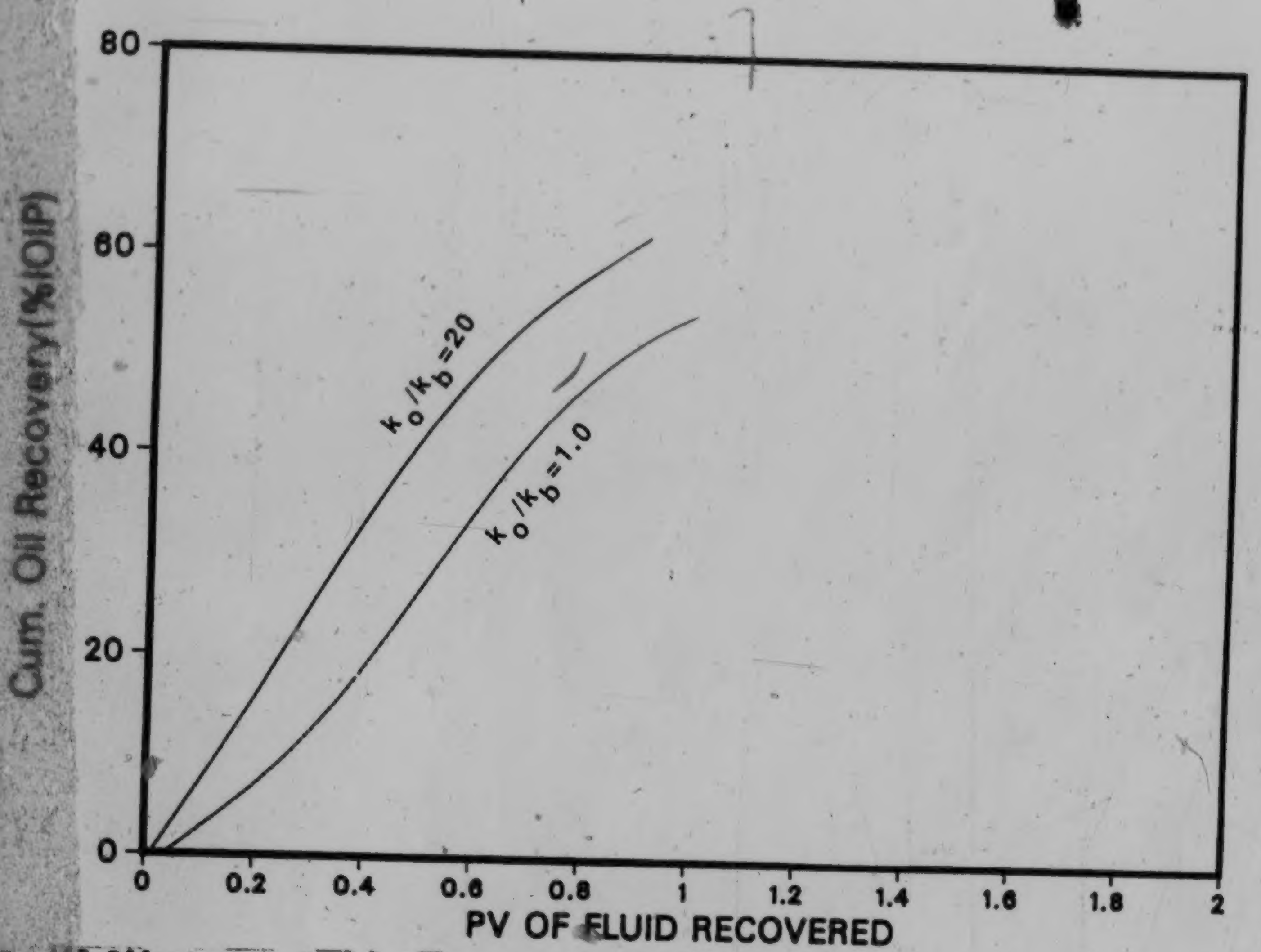

g. [illegible]5 Effect of k_o/k_b on Polymer Flood Recovery for h_b/h_o=0.33

oil recovery results for oil-water zone permeability ratios of 1 and 20. As can be seen from this figure, the oil recovery is the much better for a permeability ratio of 20. However, it should be mentioned here that even though the absolute values of oil recovery increase with increasing oil-water zone permeability ratio, the incremental oil recovery decreases relative to that for a conventional waterflood. This is because oil recovery decreases more rapidly with decreasing oil-water zone permeability ratio for a conventional waterflood. Even in terms of absolute values of oil recoveries, the ultimate recoveries are fairly close for permeability ratios of 20 and 1. The main difference is in the time necessary to achieve the ultimate oil recoveries.

7.4.7 Emulsion Flood

Oil-Water emulsions are well known for their ability to reduce the absolute permeability of a porous medium. Laboratory studies (Broz et al., 1985) indicate that emulsions decrease permanently the absolute permeability of a porous medium. In a layered core, it has been reported that emulsions decrease the absolute permeabilities of the more permeable layers with a greater rate, until a uniform in absolute permeability is reached in all the layers. This phenomenon is very helpful in preventing water channeling through the more permeable layers. However, unlike polymer flooding, the absolute permeability rather than the effective permeability to water is decreased. Besides this effect on absolute permeability, it has been reported in experimental studies that emulsions also improve microscopic displacement efficiency leading to a better sweep even for a homogeneous porous medium.

Numerical simulation of an emulsion flood has not been heretofore reported. Even though several emulsion rheology models have been proposed (Abou-Kassem and Farouq Ali, 1986a, 1986b) for emulsion flow in a porous medium, no attempt to describe emulsion flow in the presence of oil and water has been reported. In the experimental part of the present study (chapter VI), it was reported that oil-in-water emulsions retain their basic structure even after traveling along a porous medium. Even though emulsion thinning takes place with continuing contact with water (connate or injected), emulsions never lose their identity in an aqueous phase. Therefore, a compositional simulator capable of describing a micellar flood is not required, nor is it capable of simulating an emulsion flood. The type of emulsions studied (10 percent oil-in-water) may be treated as being immiscible with either oil or water. Because of this observation, a three-phase system was considered for emulsion injection in the presence of oil and water. Relative permeabilities to each phase were estimated following the same procedure used in the case of a polymer flood. However, unlike polymer floods, only one set of relative permeabilities was used throughout the emulsion injection and waterflood. Figure 166 shows the relative permeabilities of the water, oil and emulsion phases. In order to take account of the reduction in absolute permeabilities, it was assumed that the absolute permeabilities change as soon as the emulsion comes in contact with the porous medium. The new value of the absolute permeability is then retained for the rest of the displacement test. The magnitude of the reduction in absolute permeabilities was determined by starting with the initial value and by reducing it successively until good agreement was obtained between the experimental and numerical results. Different experimental results were matched while both relative permeabilities and absolute permeabilities were estimated by trial and error. The results will be discussed for each of the different runs.

7.4.8 Continuous Emulsion Injection in a Homogeneous Porous Medium

Run 31 was conducted with continuous emulsion injection for a homogeneous sandpack containing an irreducible water saturation. However, it was observed experimentally that an emulsion flood displaced a part of the irreducible water saturation. Consequently, water production started shortly after the emulsion injection started. In order to simulate

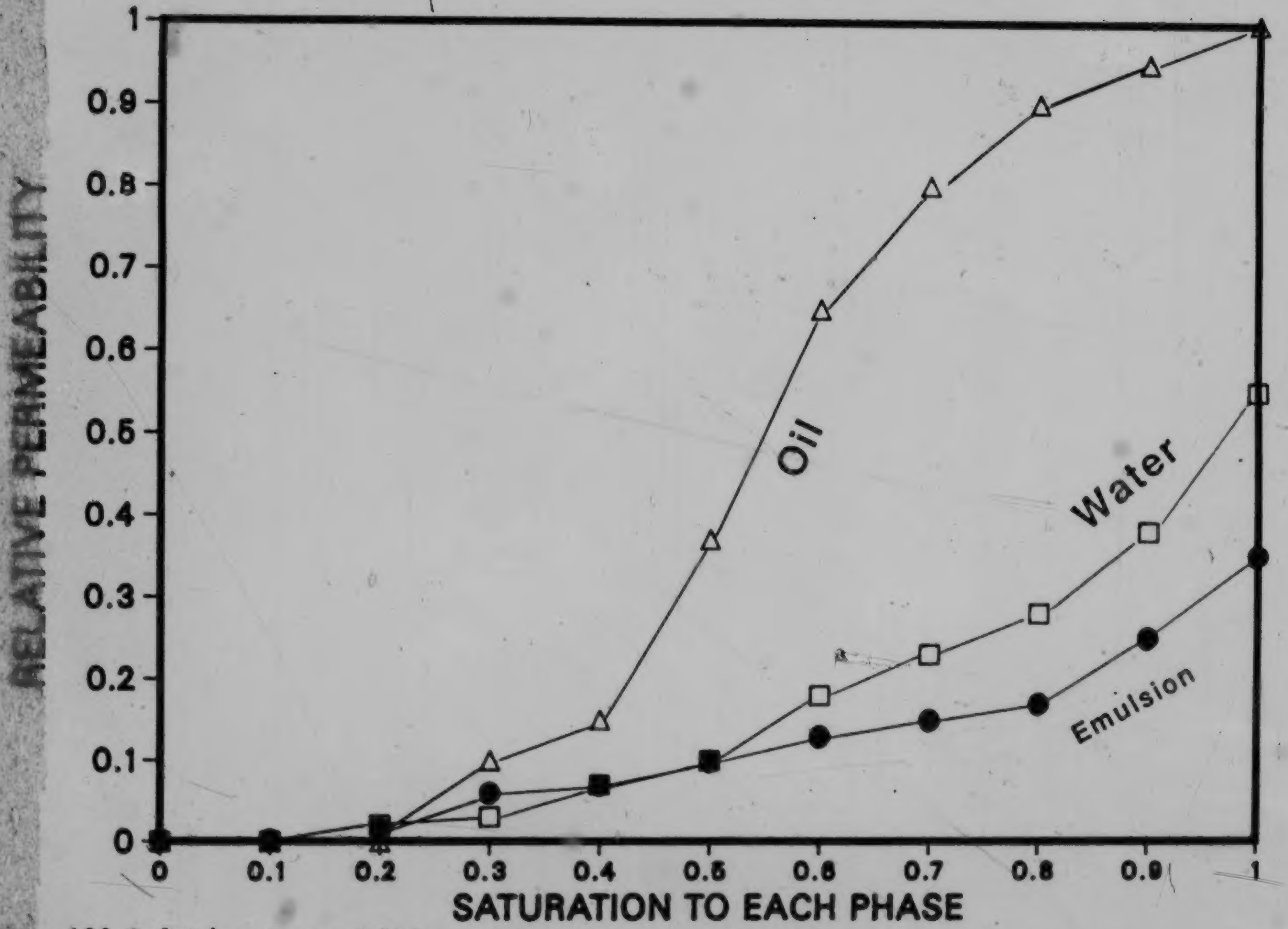

Fig. 166 Relative Permeability to Each Phase in Oil/Water/Emulsion System

this phenomenon, relative permeabilities to water had to be adjusted. The total range of relative permeabilities to water was estimated from the data acquired in several different runs. Also, a reduction in absolute permeability was introduced following the emulsion flood. After many numerical runs with successively decreasing absolute permeabilities, the optimal values for permeability reduction were determined. It was found that a straight line was obtained when these values were plotted on a semilog graph against the absolute permeabilities. This is shown in Figure 167. By using this correlation, excellent agreement was obtained both for cumulative oil recovery and pressure data. The straight line was then extended to obtain extrapolated values for different permeabilities. Figure 168 shows the comparison between numerical and experimental results for Run 31. As can be seen from this figure, both pressure and oil recovery data show excellent agreement between numerical and experimental results. Also, the emulsion breakthrough points were matched. The adjustment in absolute permeability was found to be crucial in matching the peak and subsequent decline in pressure data.

7.4.9 Emulsion Flood in the Presence of a Bottom-Water Zone

In order to compare numerical results with experimental results, Runs 30, 32, 34, 42, and 43 (all with various types

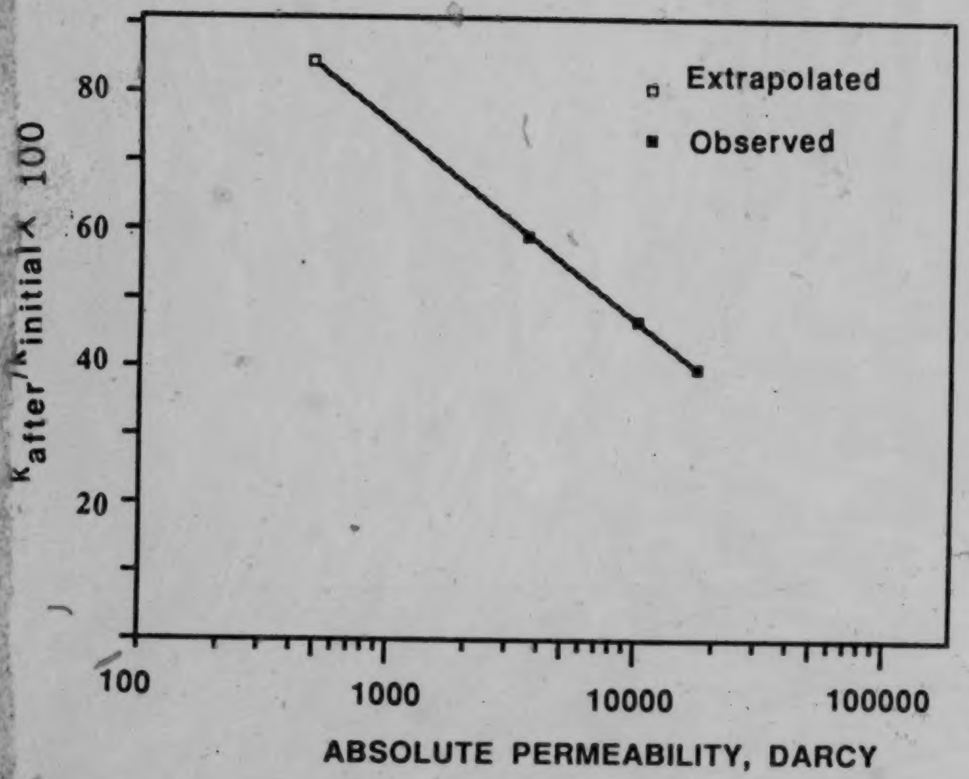

. 167 Correlation of Permeability Reduction with Emulsion

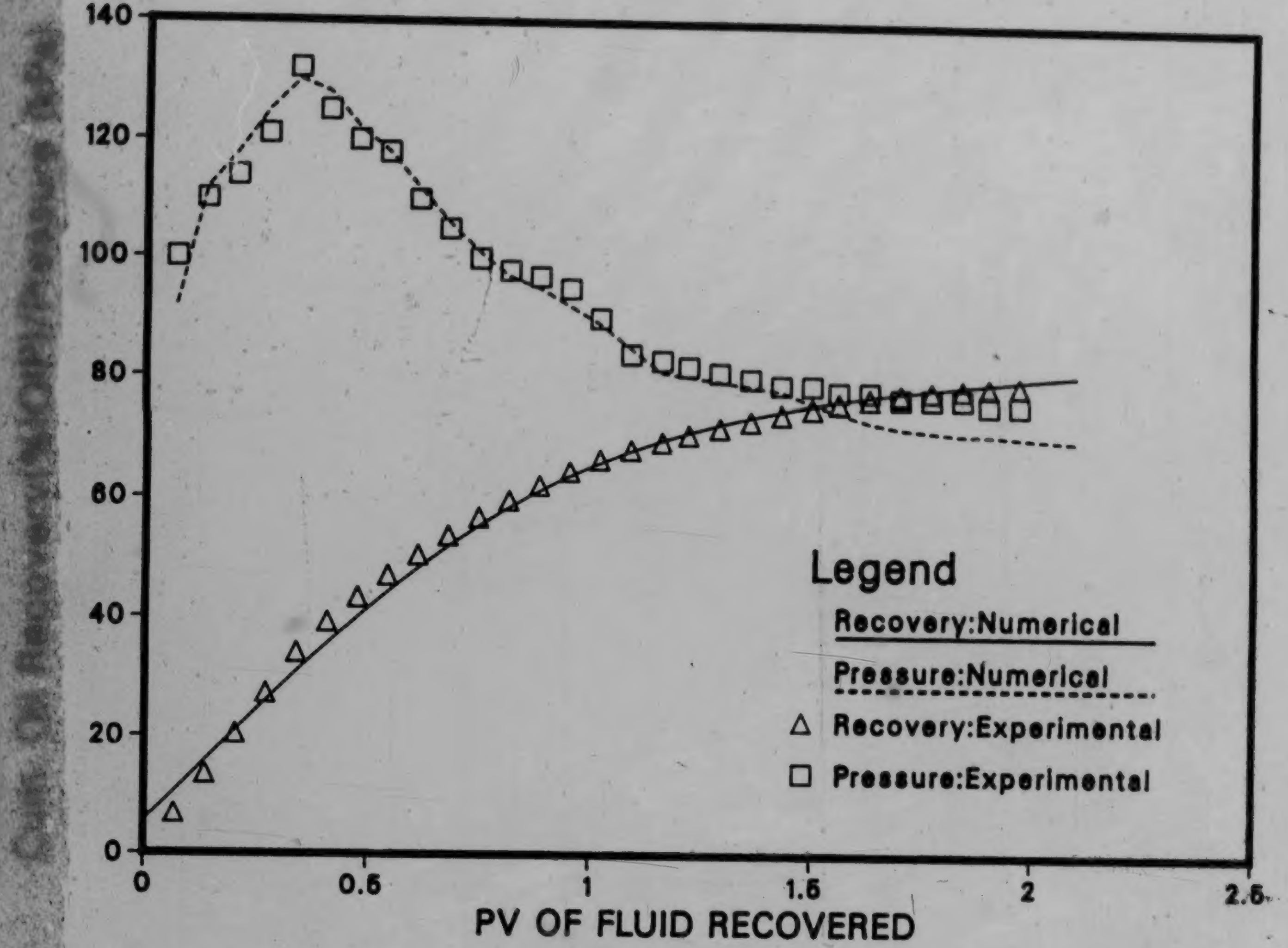

168 Comparison of Experimental and Numerical Results for Run 31 ($h_b/h_o=0$)

of bottom-water zones) were chosen. Because some of these runs were conducted with different permeabilities of the bottom-water zones, these runs helped to determine the reduction factor for the absolute permeability as depicted in Figure 167. Also, Runs 30, 42 and 43 were conducted with various emulsion slug sizes for the same type of bottom-water zone. Therefore, by matching these experimental results with numerical results the validity of the simulator was confirmed. Following this initial data matching, several prediction runs were also performed.

Figure 169 depicts a comparison of the numerical results with experimental results for Run 30. By choosing a reduction factor of 0.65 for the absolute permeability, an excellent agreement was obtained for this run which used 16 μm^2 as the permeability of both the oil and the water layers. This run was performed for an emulsion slug size of 0.6 PV (or 2 PV_b).

Figure 170 depicts a comparison of the numerical and experimental results for Run 42. This run was similar to Run 30 but a smaller slug size (1 PV_b) was used. It can be seen from Figure 170 that the agreement between experimental and numerical data is good but not as close as in the previous run. The slug size was not introduced as an independent parameter in reducing the absolute permeability and it was assumed that both relative and absolute permeabilities were independent of the slug size. This

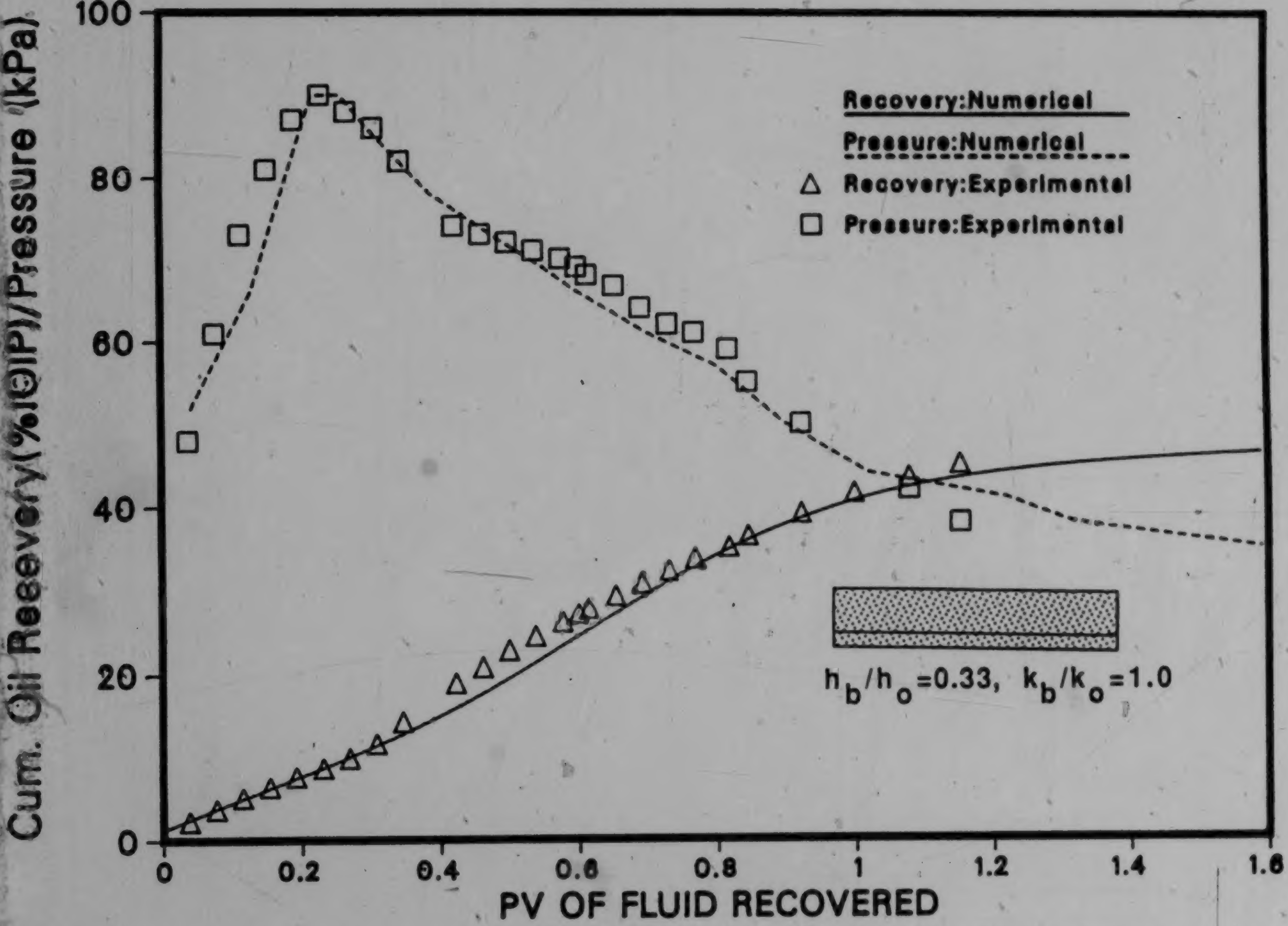

169 Comparison of Experimental and Numerical Results for Run 30 ($S=2\ PV_b$)

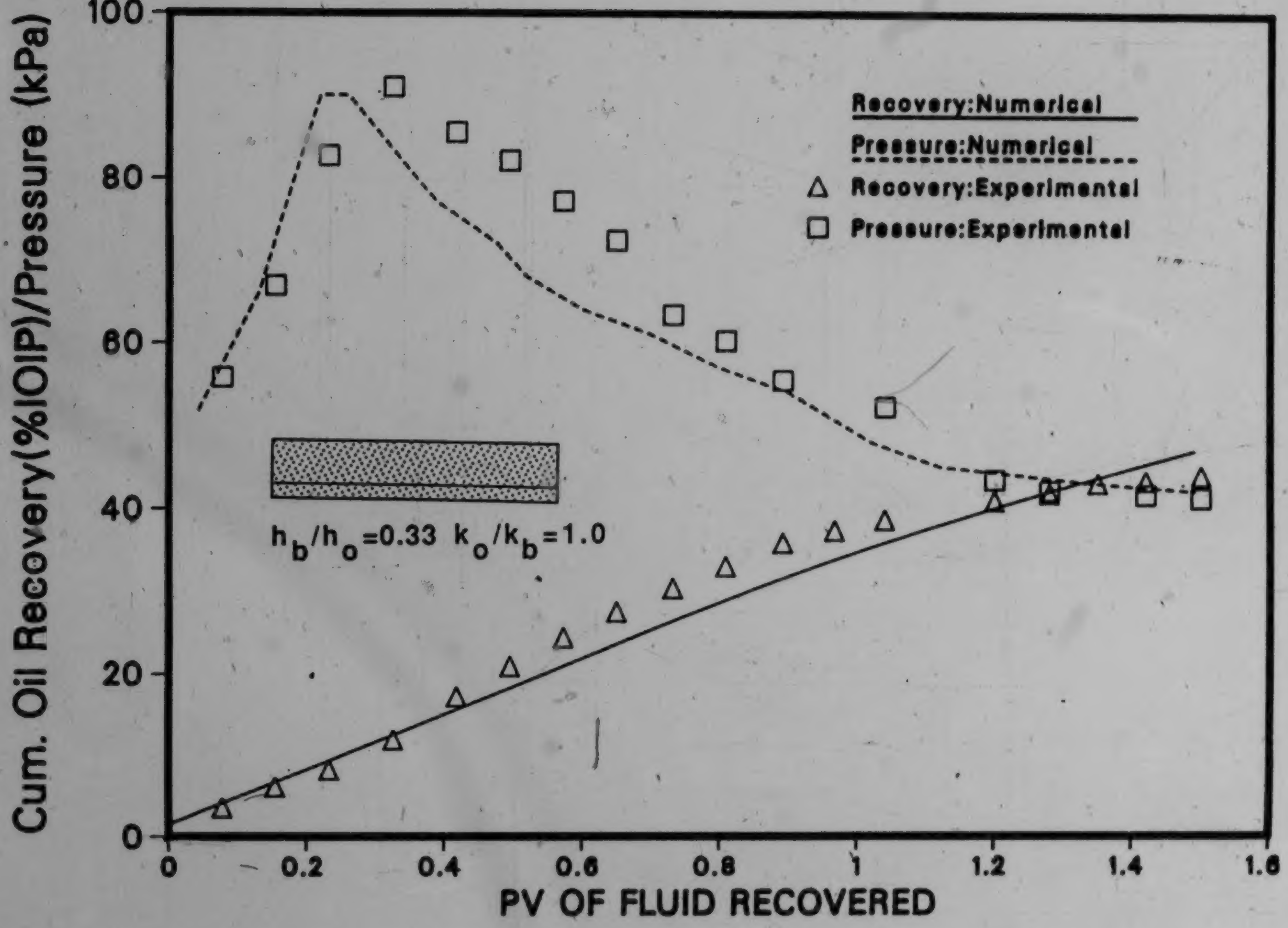

g. 170 Comparison of Experimental and Numerical Results for Run 42 (S=1 PV_b)

assumption leads to the expectation that the reduction in absolute permeability is independent of emulsion slug size. Consequently, there has to be a compromise in matching experimental results for different slug sizes. In this respect, more importance was given to matching Run 30 (which used an emulsion slug of 2 PV_b) since most of the other runs used the same emulsion slug size. However, the numerical results for oil production in all the runs followed experimental results very closely, showing the validity of the assumption in the range of the emulsion slug sizes studied.

Figure 171 depicts a comparison of the numerical results with the experimental results for Run 43 (h_b/h_o=0.33 and emulsion slug size= 3 PV_b). This run shows a poor match of the pressure data, indicating that because of the very large emulsion slug size, the inlet pressure during the water injection that followed the emulsion injection maintained a very large value. However, after emulsion breakthrough the injection pressure should decrease. Moreover, a further decrease should take place after initiation of water injection (μ_w is 1.0 mPa.s as compared to μ_m of 1.18 mPa.s). Therefore, the apparent stability in pressure at a high value is more likely to be due to plugging, etc. However, the oil recovery data showed excellent agreement.

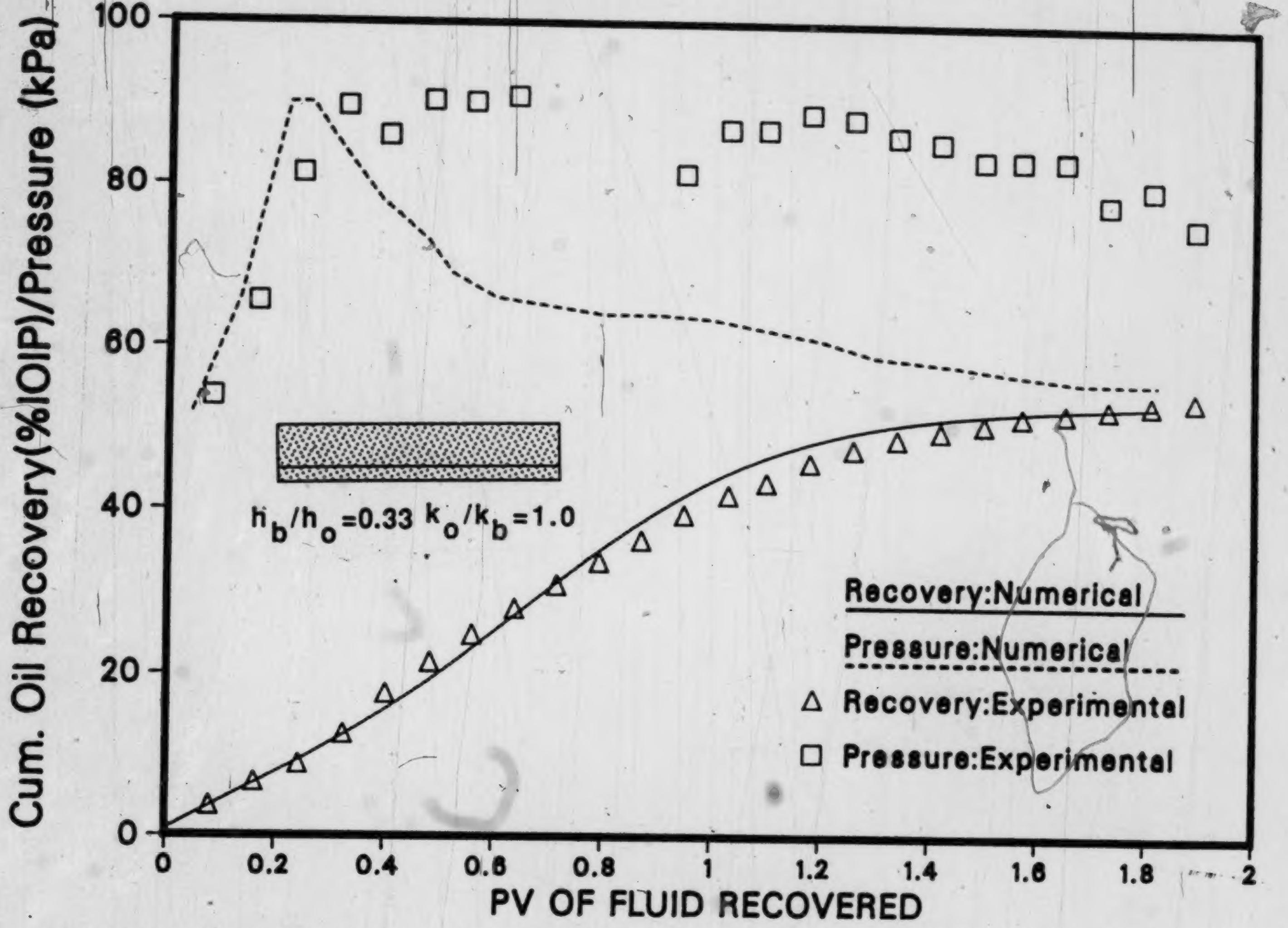

Fig. 171 Comparison of Experimental and Numerical Results for Run 45 (S=3 PV_b)

Figure 172 compares the numerical results with experimental results for Run 34 ($h_b/h_o=0.33$, $k_o/k_b=2.67$). This numerical run enabled examination of the validity of the numerical approach for the tighter bottom-water zone cases. As can be seen from Figure 172, both the oil recovery and the pressure data match very well. However, this was possible only after an absolute permeability of 3.9 darcies was assigned to the bottom-water zone. This value was determined after many trial-and-error runs. Figure 173 depicts the experimental results of Run 36 ($h_b/h_o=0.33$, $k_o/k_b=0.06$) along with the numerical results. In order to obtain a good match between the experimental and the numerical results, a permeability reduction factor of 0.4 was used for the bottom-water zone. Again, the factor was obtained by trial-and-error. This value of permeability reduction was plotted in Figure 167 along with the other values obtained for different k_o/k_b values as a function of the initial absolute permeability. These data gave a straight line on a semilog plot. This straight line was used in order to predict the emulsion flood performance for higher k_o/k_b values.

The effect of the oil-water zone thickness ratio on emulsion flooding was tested by simulating Run 32 ($h_b/h_o=1.0$, $k_o/k_b=1.0$). Figure 174 compares the numerical results with the experimental results of this run. The agreement between experimental and numerical results is very

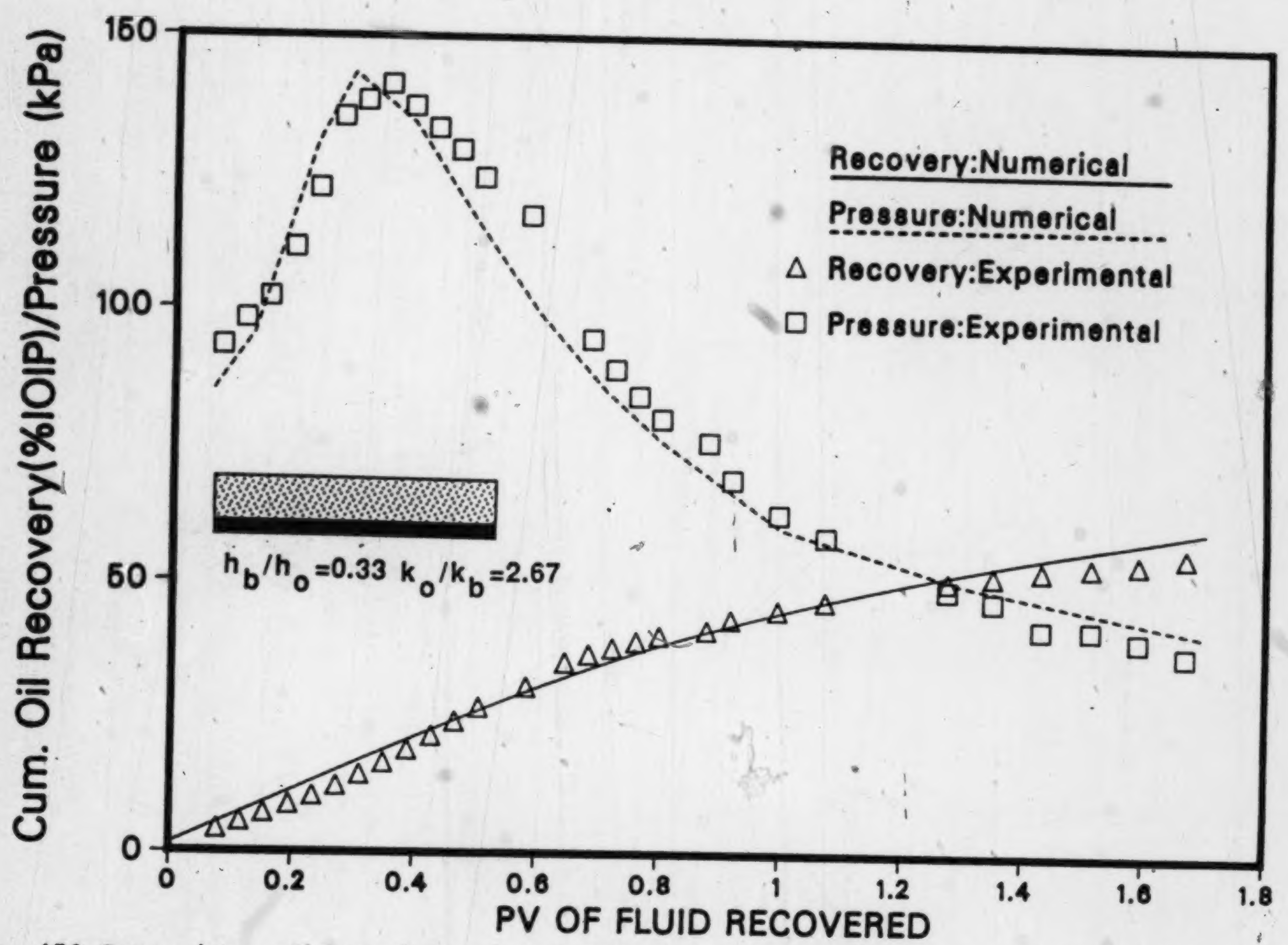

Fig. 172 Comparison of Experimental and Numerical Results for Run 34 (S=2 PV_b)

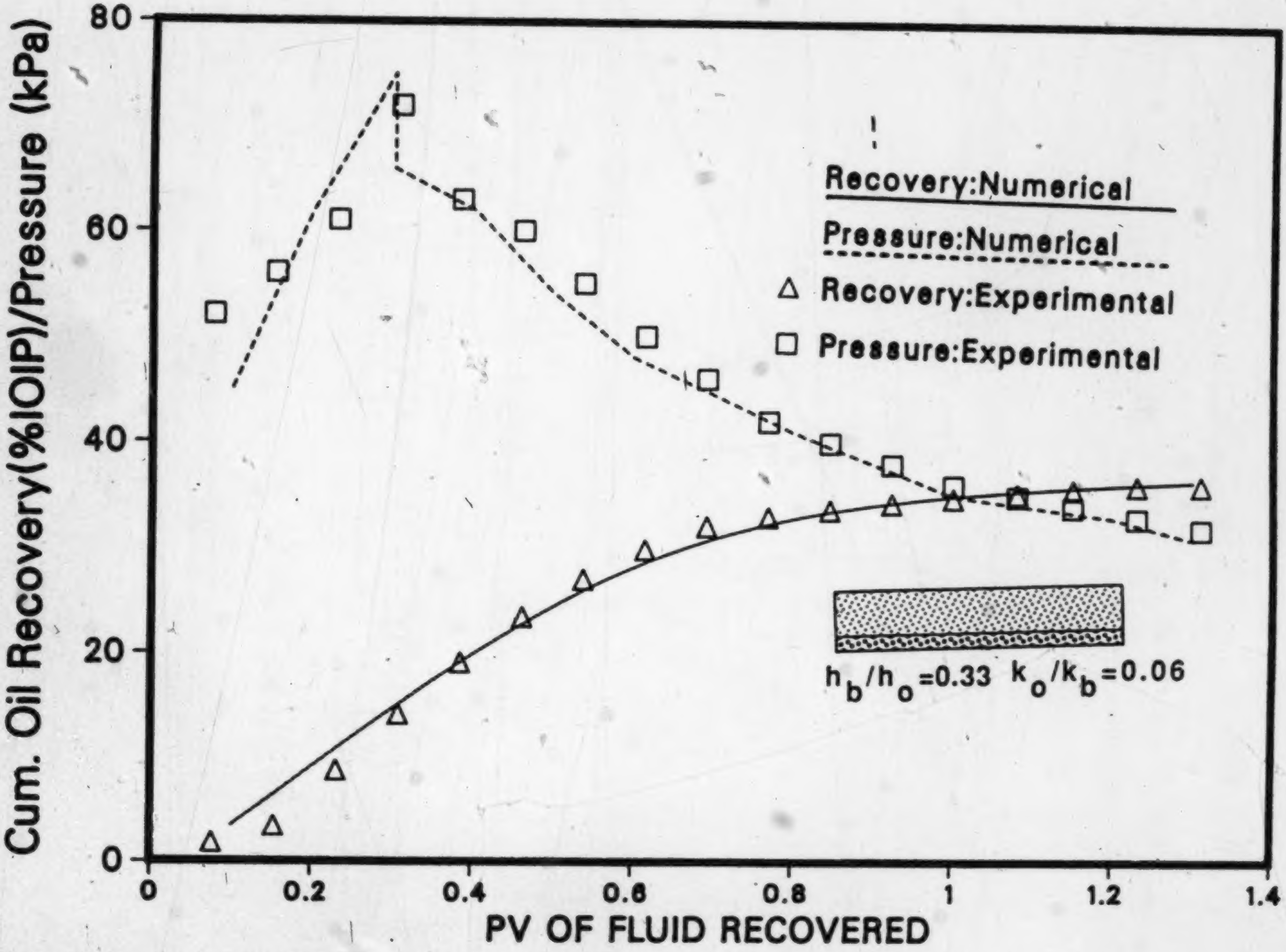

Fig. 173 Comparison of Experimental and Numerical Results for Run 36 (S=2 PV_b)

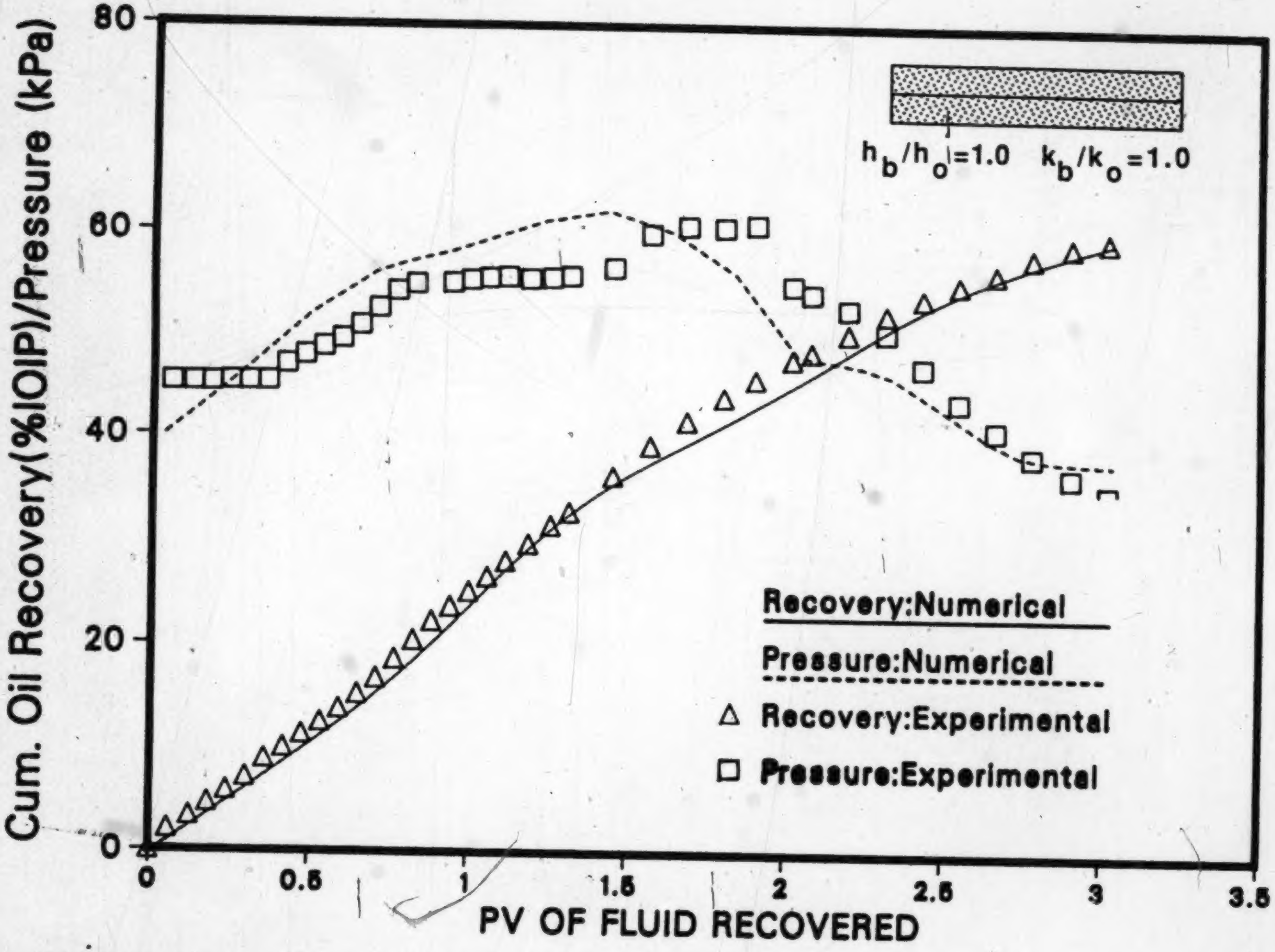

Fig. 174 Comparison of Experimental and Numerical Results for Run 32

good. This run showed the effectiveness of the simulation approach as no input data was adjusted for the history match.

7.4.9.1 Effect of Emulsion Slug Size for k_o/k_b=2.67 and h_b/h_o=0.33

In the experimental study, the effect of emulsion slug size was studied for k_o/k_b=1.0 and h_b/h_o=1.0 only. Numerical simulation gave an opportunity to investigate this effect for k_o/k_b=2.67 as well. For this purpose, the effect of emulsion slug size was studied for h_b/h_o=0.33. Figure 175 compares the cumulative oil recoveries for slug sizes of 1.0 and 2.0 PV_b. As can be seen in this figure, the difference between the two increases as soon as the emulsion flood is terminated for the slug size of 1.0 PV_b. At one pore volume of fluid injection 30 percent excess oil was produced with the larger slug. Even with a slug size of 1.0 PV_b, the oil recovery is much higher than that for a conventional waterflood. However, to have an effective blockage with emulsion slugs, 2 PV_b of emulsion was adequate. The results with k_o/k_b=2.67 were similar to that for k_o/k_b=1.0. The effect of slug size seems to be independent of k_o/k_b.

7.4.9.2 Effect of Oil-Water Zone Permeability Ratio

In the experiments, three different oil-water zone permeability ratios were used: 1.0, 2.67 and 0.06. It was

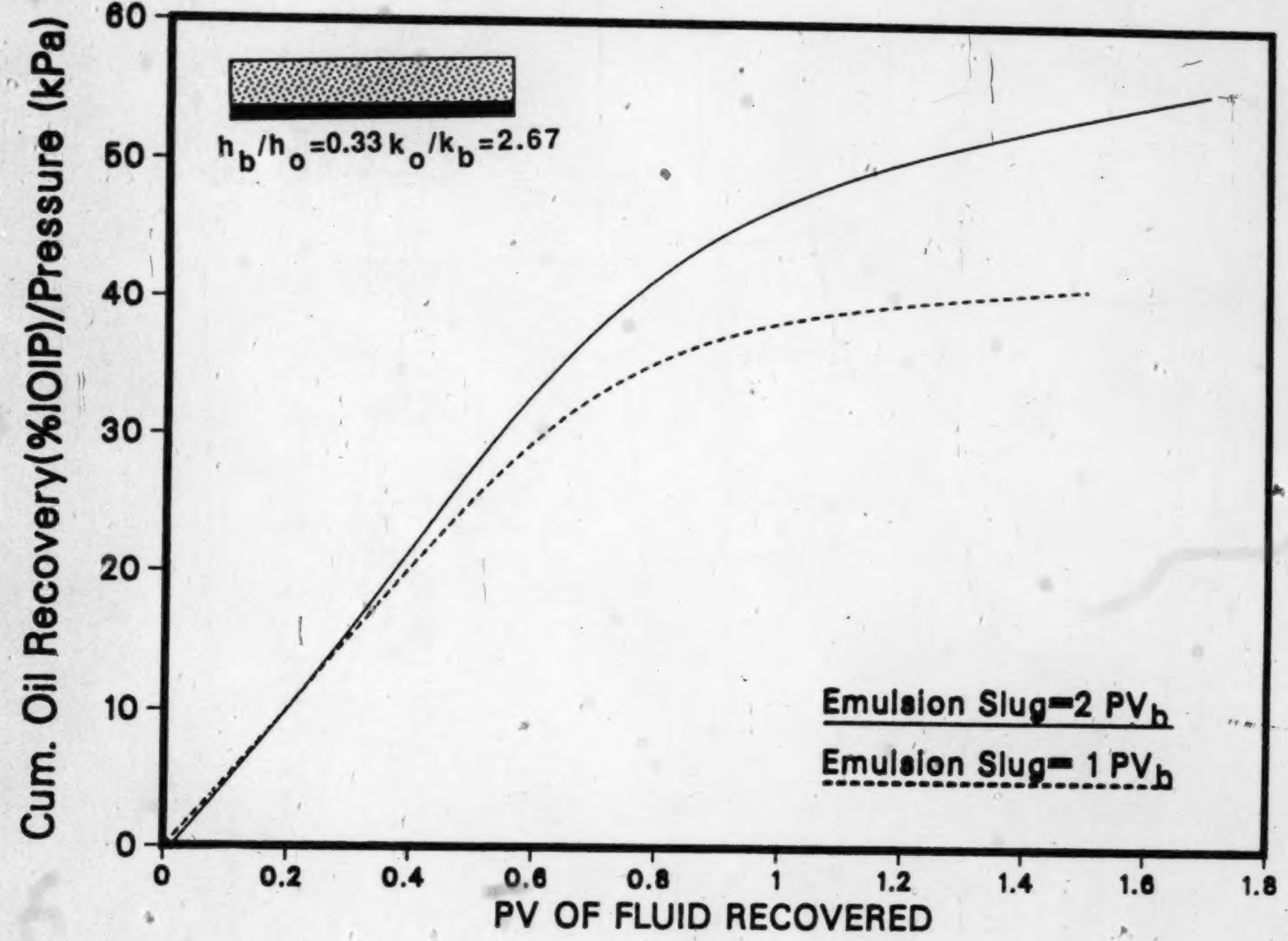

Fig. 175 Comparison of Oil Recoveries for Different Slug Sizes (h_b/h_o=0.33, k_o/k_b=2.67)

decided to examine numerically the effect of very high oil-water zone permeability ratios. Figure 176 compares the oil recovery results for oil-water zone permeability ratios of 0.06, 1.0, 2.67, and 20. As can be seen from this figure, the oil recovery is the highest for a permeability ratio of 20. However, it should be mentioned here that even though the absolute values of oil recovery increase with increasing oil-water zone permeability ratio, the incremental oil recovery decreases relative to a conventional waterflood. This is because oil recovery decreases more rapidly with decreasing oil-water zone permeability ratio for a conventional waterflood. Even in terms of absolute values of oil recoveries, the ultimate recoveries are fairly close for permeability ratios of 20 and 1. The main difference is in the amount of time needed to achieve the ultimate oil recovery, which is much longer for higher oil-water zone permeability ratios.

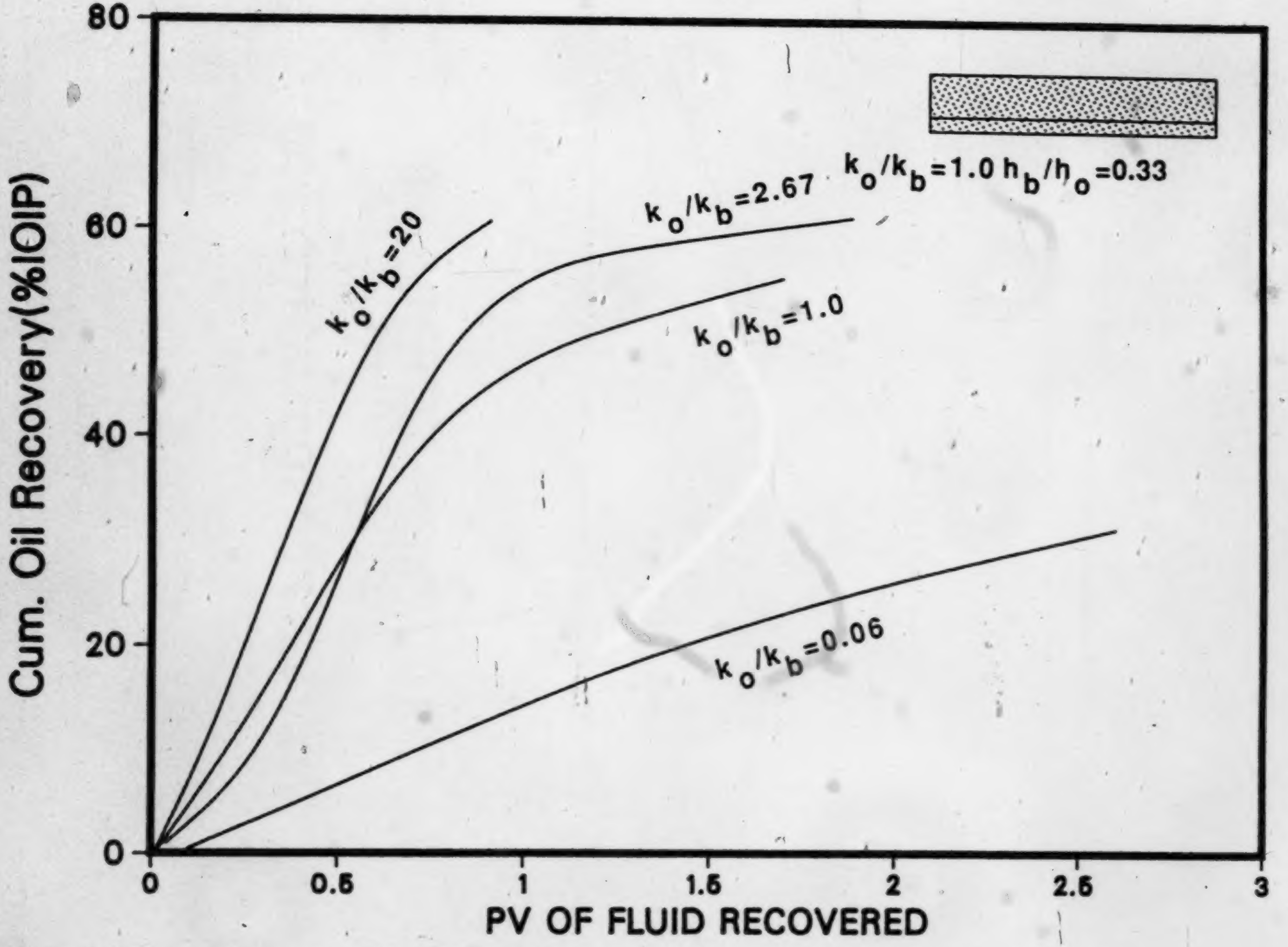

Fig. 176 Comparison of Oil Recoveries for Different k_o/k_b for h_b/h_o=0.33

8. SCALING CRITERIA FOR POLYMER, EMULSION AND FOAM INJECTION

A set of scaling criteria for polymer, emulsion and foam flooding experiments was derived using inspectional and dimensional analyses. In order to derive the similarity groups by inspectional analysis, the differential equations governing the process were developed for polymer, emulsion and foam. Several options were investigated for emulsion and foam as the exact nature of the flow might be different, depending on the quality of the foam and emulsion. Initial and boundary conditions, constitutive relationships and constraints were also defined for each of the cases studied. The problem formulated and described by these equations was reduced to dimensionless form. This was done by writing each variable as a function of its dimensionless form and its reference quantity. All the reference quantities constitute coefficients which multiply the original equation in its dimensionless form. To make the equations dimensionless, the entire equation is divided throughout by one of the coefficients. The resulting coefficients in the dimensionless equations are the similarity groups.

The inspectional analysis is important because if all the dimensionless properties are the same functions of the dimensionless variables in the model and the prototype, and all the similarity groups are the same in the model and the prototype, the equations governing the process in the model are exactly the same equations governing the process in the prototype. Therefore, the results of the prototype can be directly extrapolated to the field.

8.1 DEVELOPMENT OF THE SCALING CRITERIA

8.1.1 Polymer Flood

The process of a polymer flood is actually the flow of two phases, the oleic phase and the aqueous phase. The oleic phase contains only oil and the aqueous phase contains water and polymer. Therefore, the mass transfer between water and oil or polymer and oil is neglected. In addition to this, the following assumptions are made:

1. Isothermal flow occurs in a homogeneous and isotropic medium;
2. Connate water, make-up water for polymer solution, and drive water have the same physical properties;
3. The polymer resides in the aqueous phase due to its hydrophilic property which makes it dissolve and hydrolyze in water;
4. Darcy's and Fick's laws are valid;
5. Dispersion can be described by a relationship similar in form to Fick's equation;
6. Adsorption, desorption, and retention of polymer occur instantaneously, and the amount adsorbed is

controlled by the adsorptive capacity of the rock.

With the above assumptions the mass balance equations for different components may be written as described below.

The equation for the mass balance of oil is

$$\frac{\partial}{\partial t}(\phi S_1 \rho_1) = \nabla.(\frac{\rho_1}{\mu_1} K_1 \ (\nabla P_1+\rho_1 g \nabla z))$$

The equation for the mass balance of polymer is

$$\frac{\partial}{\partial t}(\phi S_a C_{ap} \rho_a) + \frac{\rho_r (1-\phi) A_p}{(1+BC_p)^2} \frac{\partial}{\partial t} (\rho_a C_{ap}) =$$

$$\nabla.((D_a+D^*_{ap})\phi S_a.\nabla(C_{ap}\rho_a))+\nabla.(C_{ap}\rho_a \frac{K_a}{\mu_a} (\nabla P_a + \rho_a g \nabla z))$$

The equation for the mass balance of water is

$$\frac{\partial}{\partial t}(\phi S_a C_{aw} \rho_a) = \nabla.(C_{aw}\frac{\rho_a}{\mu_a} K_a \ (\nabla P_a+\rho_a g \nabla z)) +$$

$$\nabla.(\phi S_a (D_a+D^*_{aw}).\ \nabla(C_{aw}\rho_a))$$

8.1.1.1 Boundary and Initial Conditions

Boundary conditions:

$$\rho_1 v_{1n} = - \frac{\rho_1 K_1}{\mu_1} (\nabla_n P_1 + \rho_1 g \nabla_n z) = 0$$

$$\rho_a v_{an} = - \frac{\rho_a K_a}{\mu_a} (\nabla_n P_a + \rho_a g \nabla_n z) = 0$$

Injection well:

$$\int_{A_{inj}} \rho_a \frac{K_a}{\mu_a} (\nabla P_a + \rho_a g \nabla z)\, dA = W_{aw} + W_{ap}$$

Production well:

$$P_l = P_{lprod}$$

$$P_a = P_{lprod} + P_{cla}$$

Initial conditions:

$$S_a(0,x_1,x_2,x_3) = S_{ai}(0,x_1,x_2,x_3)$$

$$S_l(0,x_1,x_2,x_3) = S_{li}(0,x_1,x_2,x_3)$$

$$P_a(0,x_1,x_2,x_3) = P_{ai}(0,x_1,x_2,x_3)$$

8.1.1.2 Constitutive Relationships and Constraints

1) $S_a + S_l = 1$

2) $C_{ap} + C_{aw} = 1$

3) $\rho_l = \rho_l(P_l)$

4) $\rho_a = \rho_a(P_a, C_{ap})$

5) $\mu_l = \mu_l(P_l)$

6) $\mu_a = \mu_a(P_a, C_{ap})$

7) $P_a = P_l - P_{lca}\ (S_a)$

8) ϕ = constant

9) g = constant

10) $K_l = K_l(S_a, R^1)$

11) $K_a = K_a(S_a, R)$

12) $D_a + D^*_{aw} = D_{aw}(D_{Law}, D_{Taw})$

13) $D_a + D^*_{ap} = D_{ap}(D_{Lap}, D_{Tap})$

14) $z = z(x_1, x_2, x_3)$

15) ρ_r = constant

8.1.2 Emulsion Flood

Three different sets of assumptions are used for this process. The governing equations have been set up according to the assumptions made.

---

[1] The effective permeabilities are considered to be modified after polymer injection. The modified permeabilities are related to the initial permeabilities through the so-called 'resistance factor', R. The oleic- and aqueous-phase effective permeabilities after adsorption are given by Al-Seehati (1979):

$K_{lmod} = K_{li}\sqrt{R}$

$K_{amod} = K_{ai}\sqrt{R}$

where $R = 1+(R_{rf}-1)C_{rp}/C^*_{rp}$,

$$\text{with Rrf} = \frac{K(\text{before polymer flood})}{K(\text{after polymer flood})}$$

8.1.3 Emulsion Flood: Two-Phase Flow

This process is considered to be two-phase flow. These phases are an aqueous phase and an oleic phase. The two phases flow simultaneously in a porous medium under equilibrium conditions. The components present in the oleic phase are oil and emulsion, and the components present in the aqueous phase are water and emulsion. However, this is only one way of describing the process. In fact, the emulsion may be treated also as an independent phase which interacts with both the aqueous and the oleic phases. In this case a three-phase relative permeability curve has to be used. It is difficult to rule out any one of these approaches due to the lack of both adequate experimental evidence and a mechanistic description. If two-phase flow is assumed, along with the relevant assumptions made under polymer flood conditions, one obtains the following set of equations are obtained:

The equation for the mass balance of oil is

$$\frac{\partial}{\partial t}(\phi S_l C_{lo} \rho_l) = \nabla . (\frac{\rho_l C_{lo}}{\mu_l} K_l \ (\nabla P_l + \rho_l g \nabla z) +$$

$$\phi S_l (D_l + D^*_{lo}) . \nabla (C_{lo} \rho_l))$$

The equation for the mass balance of emulsion is

$$\frac{\partial}{\partial t}(\phi S_l C_{lm} \rho_l + \phi S_a C_{am} \rho_a) = \nabla . (\frac{C_{lm} \rho_l K_l}{\mu_l} \ (\nabla P_l + \rho_l g \nabla z) +$$

$$\frac{C_{am}\rho_a K_a}{\mu_a} (\nabla P_a+\rho_a g\nabla z)) + \nabla(\phi S_l (D_l+D_{lm}^*).\nabla(C_{lm}\rho_l) +$$

$$\phi S_a (D_a+D_{am}^*).\nabla(C_{am}\rho_a))$$

The equation for the mass balance of water is

$$\frac{\partial}{\partial t}(\phi S_a C_{aw}\rho_a) = \nabla.(C_{aw}\frac{\rho_a}{\mu_a}K_a (\nabla P_a+\rho_a g\nabla z)) +$$

$$\nabla.(\phi S_a (D_a+D_{aw}^*).\nabla(C_{aw}\rho_a))$$

8.1.3.1 Boundary and Initial Conditions

Boundary conditions:

$$\rho_l v_{ln} = -\frac{\rho_l K_l}{\mu_l} (\nabla_n P_l + \rho_l g\nabla_n z) = 0$$

$$\rho_a \overline{v_{an}} = -\frac{\rho_a K_a}{\mu_a} (\nabla_n P_a + \rho_a g\nabla_n z) = 0$$

Injection well:

$$\int_{A_{inj}} \rho_a \frac{K_a}{\mu_a} (\nabla P_a + \rho_a g\nabla z)\, dA = W_{aw} + W_{am}$$

$$\int_{A_{inj}} \rho_l \frac{K_l}{\mu_l} (\nabla P_l + \rho_l g\nabla z)\, dA = W_{lm}$$

Production well:

$$P_l = P_{prod}$$

$P_a = P_{prod} + P_{cla}$

Initial conditions:

$S_a(0,x_1,x_2,x_3) =$ [illegible]$_{ai}(0,x_1,x_2,x_3)$

$S_l(0,x_1,x_2,x_3) = S_{li}(0,x_1,x_2,x_3)$

$P_a(0,x_1,x_2,x_3) = P_{ai}(0,x_1,x_2,x_3)$

8.1.3.2 Constitutive Relationships and Constraints

1) $S_a + S_l = 1$

2) $C_{lo} + C_{lm} = 1$

3) $C_{am} + C_{aw} = 1$

4) $\rho_l = \rho_l(P_l, C_{lo})$

5) $\rho_a = \rho_a(P_a, C_{aw})$

6) $\mu_l = \mu_l(P_l, C_{lo})$

7) $\mu_a = \mu_a(P_a, C_{aw})$

8) $P_a = P_l - P_{cla}(S_a)$

9) ϕ =constant

10) g =constant

11) $K_l = K_l(S_a, K)$

12) $K_a = K_a(S_a, K)$

13) $D_l + D^*_{lo} = D_{lo}(D_{Llo}, D_{Tlo})$

14) $D_a + D^*_{am} = D_{am}(D_{Lam}, D_{Tam})$

15) $D_a + D^*_{aw} = D_{aw}(D_{Law}, D_{Taw})$

16) $z = z(x_1,x_2,x_3)$

17) ρ_r = constant

8.1.4 Emulsion Flood: Emulsion Miscible in Aqueous Phase Only

In this process the water-rich emulsion solution is assumed to mix with the aqueous phase only. For this case, the equation for the mass balance of oil becomes:

$$\frac{\partial}{\partial t}(\phi S_l C_{lo} \rho_l) = \nabla.(\frac{\rho_l C_{lo}}{\mu_l} K_l(\nabla P_l + \rho_l g \nabla z))$$

The equation for the mass balance of emulsion becomes:

$$\frac{\partial}{\partial t}(\phi S_a C_{am} \rho_a) = \nabla.(\frac{C_{am} \rho_a K_a}{\mu_a} (\nabla P_a + \rho_a g \nabla z) +$$

$$\nabla(\phi S_a (D_a + D^*_{am}).\nabla(C_{am} \rho_a))$$

The equation for the mass balance of water is

$$\frac{\partial}{\partial t}(\phi S_a C_{aw} \rho_a) = \nabla.(C_{aw} \frac{\rho_a}{\mu_a} K_a (\nabla P_a + \rho_a g \nabla z)) +$$

$$\nabla.(\phi S_a (D_a + D^*_{aw}).\nabla(C_{aw} \rho_a))$$

8.1.4.1 Boundary and Initial Conditions

Boundary conditions:

$$\rho_l v_{ln} = -\frac{\rho_l K_l}{\mu_l} (\nabla_n P_l + \rho_l g \nabla_n z) = 0$$

$$\rho_a v_{an} = -\frac{\rho_a K_a}{\mu_a} (\nabla_n P_a + \rho_a g \nabla_n z) = 0$$

Injection well:

$$\int_{A_{inj}} \rho_a \frac{K_a}{\mu_a} (\nabla P_a + \rho_a g \nabla z)\, dA = W_{aw} + W_{am}$$

Production well:

$$P_l = P_{prod}$$

$$P_a = P_{prod} + P_{cla}$$

Initial conditions:

$$S_a(0,x_1,x_2,x_3) = S_{ai}(0,x_1,x_2,x_3)$$

$$S_l(0,x_1,x_2,x_3) = S_{li}(0,x_1,x_2,x_3)$$

$$P_a(0,x_1,x_2,x_3) = P_{ai}(0,x_1,x_2,x_3)$$

8.1.4.2 Constitutive Relationships and Constraints

1) $S_a + S_l = 1$

2) $C_{am} + C_{aw} = 1$

3) $\rho_l = \rho_l(P_l)$

4) $\rho_a = \rho_a(P_a, C_{aw})$

5) $\mu_l = \mu_l(P_l)$

6) $\mu_a = \mu_a(P_a, C_{aw})$

7) $P_a = P_l - P_{cla}(S_a)$

8) ϕ =constant

9) g =constant

10) $K_l = K_l(S_a, K)$

11) $K_a = K_a(S_a, K)$

12) $D_a + D^*_{am} = D_{am}(D_{Lam}, D_{Tam})$

13) $D_a + D^*_{aw} = D_{aw}(D_{Law}, D_{Taw})$

14) $z = z(x_1, x_2, x_3)$

15) ρ_r = constant

8.1.5 Emulsion Flood: Three-Phase Flow

In this process three-phase flow is considered. These phases are aqueous phase, oleic phase and emulsion phase. All of these phases flow simultaneously under equilibrium conditions in a porous medium. This treatment of the process requires three-phase relative permeability data for a water, oil and emulsion system. For this process one obtains the following set of governing equations. The equation for mass balance of oil is

$$\frac{\partial}{\partial t}(\phi S_l C_{lo} \rho_l) = \nabla.(\frac{\rho_l C_{lo}}{\mu_l} K_l (\nabla P_l + \rho_l g \nabla z))$$

The equation for the mass balance of emulsion is

$$\frac{\partial}{\partial t}(\phi S_m C_{mm} \rho_m + \phi S_a C_{am} \rho_a) = \nabla.(\frac{C_{mm} \rho_m K_m}{\mu_m} (\nabla P_m + \rho_m g \nabla z) +$$

$$\frac{C_{am} \rho_a K_a}{\mu_a} (\nabla P_a + \rho_a g \nabla z)) + \nabla(\phi S_m (D_m + D^*_{mm}).\nabla(C_{mm} \rho_m) +$$

$$\phi S_a (D_a + D^*_{am}).\nabla(C_{am} \rho_a))$$

The equation for the mass balance of water is

$$\frac{\partial}{\partial t}(\phi S_m C_{mw} \rho_m + \phi S_a C_{aw} \rho_a) = \nabla.(\frac{C_{mw} \rho_m K_m}{\mu_m} (\nabla P_m + \rho_m g \nabla z) +$$

$$\frac{C_{aw}\rho_a K_a}{\mu_a} (\nabla P_a+\rho_a g\nabla z)) + \nabla(\phi S_m(D_m+D^*_{mw}).\nabla(C_{mw}\rho_m) +$$

$$\phi S_a(D_a+D^*_{aw}).\nabla(C_{aw}\rho_a))$$

8.1.5.1 Boundary and Initial Conditions

Boundary conditions:

$$\rho_1 v_{1n} = - \frac{\rho_1 K_1}{\mu_1} (\nabla_n P_1 + \rho_1 g \nabla_n z) = 0$$

$$\rho_a v_{an} = - \frac{\rho_a K_a}{\mu_a} (\nabla_n P_a + \rho_a g \nabla_n z) = 0$$

$$\rho_m v_{mn} = - \frac{\rho_m K_m}{\mu_m} (\nabla_n P_m + \rho_m g \nabla_n z) = 0$$

Injection well:

$$\int_{A_{inj}} \rho_a \frac{K_a}{\mu_a} (\nabla P_a + \rho_a g \nabla z)\, dA = W_{aw} + W_{am}$$

Production well:

$$P_1 = P_{prod}$$

$$P_a = P_{prod} + P_{cla}$$

$$P_m = P_{prod} + P_{clm}$$

Initial conditions:

$$S_a(0,x_1,x_2,x_3) = S_{ai}(0,x_1,x_2,x_3)$$

$$S_1(0,x_1,x_2,x_3) = S_{1i}(0,x_1,x_2,x_3)$$

$S_m(0,x_1,x_2,x_3) = S_{mi}(0,x_1,x_2,x_3)$

$P_a(0,x_1,x_2,x_3) = P_{ai}(0,x_1,x_2,x_3)$

$P_m(0,x_1,x_2,x_3) = P_{mi}(0,x_1,x_2,x_3)$

8.1.5.2 Constitutive Relationships and Constraints

1) $S_a + S_l + S_m = 1$

2) $C_{am} + C_{aw} = 1$

3) $C_{mm} + C_{mw} = 1$

4) $\rho_l = \rho_l(P_l)$

5) $\rho_a = \rho_a(P_a,C_{aw})$

6) $\rho_m = \rho_m(P_m,C_{mm})$

7) $\mu_l = \mu_l(P_l)$

8) $\mu_a = \mu_a(P_a,C_{aw})$

9) $\mu_m = \mu_m(P_m,C_{mm})$

10) $P_a = P_l - P_{cla}(S_a,S_l)$

11) $P_m = P_l - P_{clm}(S_a,S_m)$

12) ϕ =constant

13) g =constant

14) $K_l = K_l(S_a,S_l,K)$

15) $K_a = K_a(S_a,S_l,K)$

16) $K_m = K_m(S_m,S_a,K)$

17) $D_a + D^*_{am} = D_{am}(D_{Lam},D_{Tam})$

18) $D_a + D^*_{aw} = D_{aw}(D_{Law},D_{Taw})$

19) $D_m + D^*_{mm} = D_{mm}(D_{Lmm},D_{Tmm})$

20) $D_m + D^*_{mw} = D_{mw}(D_{Lmw},D_{Tmw})$

21) $z = z(x_1,x_2,x_3)$

22) ρ_r = constant

8.1.6 Foam Injection

The foam-flooding process is the most debatable one because the exact nature of the flow is unknown. In this study, two different scenarios have been considered. The governing equations for such a process would depend on the assumptions made.

8.1.7 Foam Injection: Four-Phase Flow

This process is considered to be four-phase flow. The phases are the aqueous phase, foam phase, oleic phase and gaseous phase. Such a description of the process is based on the observation that whenever a gas (nitrogen) is injected, only a fraction of the injected gas actually produces foam and the rest of it flows as an independent phase. Although there is some controversy concerning the extent to which foam flows as an entity, it is assumed for the present case that foam and all other phases flow simultaneously. For this process four-phase relative permeability data are required. Along with other assumptions, it is assumed that N_2 is the gas that is being injected, and that it is immiscible with the oleic or aqueous phase. The components present in the foam phase are water, N_2 and surfactant; the components present in the gaseous phase are nitrogen and surfactant; and the components present in the aqueous phase are surfactant and water. For this particular case the governing equations may be written as follows, the equation for the mass balance of oil becoming

$$\frac{\partial}{\partial t}(\phi S_1 C_{1o} \rho_1) = \nabla . (\frac{\rho_1 C_{1o}}{\mu_1} K_1 (\nabla P_1 + \rho_1 g \nabla z))$$

The equation for the mass balance of surfactant is

$$\frac{\partial}{\partial t}(\phi S_1 C_{1s} \rho_1 + \phi S_g C_{gs} \rho_g + \phi S_a C_{as} \rho_a + \phi S_f C_{fs} \rho_f)$$

$$= \nabla . (\frac{C_{1s} \rho_1 K_1}{\mu_1}(\nabla P_1 + \rho_1 g \nabla z) +$$

$$\nabla . (\frac{C_{gs} \rho_g K_g}{\mu_g}(\nabla P_g + \rho_g g \nabla z) +$$

$$\nabla . (\frac{C_{as} \rho_a K_a}{\mu_a}(\nabla P_a + \rho_a g \nabla z) +$$

$$\nabla . (\frac{C_{fs} \rho_f K_f}{\mu_f}(\nabla P_f + \rho_f g \nabla z) +$$

$$\nabla . (\phi S_1 (D_1 + D^*_{1s}) . \nabla (C_{1s} \rho_1) +$$

$$\nabla . (\phi S_g (D_g + D^*_{gs}) . \nabla (C_{gs} \rho_g) +$$

$$\nabla . (\phi S_a (D_a + D^*_{as}) . \nabla (C_{as} \rho_a) +$$

$$\nabla . (\phi S_f (D_f + D^*_{fs}) . \nabla (C_{fs} \rho_f))$$

The equation for the mass balance of nitrogen is

$$\frac{\partial}{\partial t}(\phi S_g C_{gN} \rho_g + \phi S_f C_{fN} \rho_f) = \nabla . (\frac{C_{gN} \rho_g K_g}{\mu_g}(\nabla P_g + \rho_g g \nabla z) +$$

$$\nabla.(\frac{C_{fN}\rho_f K_f}{\mu_f}(\nabla P_f+\rho_f g\nabla z) +$$

$$\nabla.(\phi S_g(D_g+D^*_{gN}).\nabla(C_{gN}\rho_g) +$$

$$\nabla.(\phi S_f(D_f+D^*_{fN}).\nabla(C_{fN}\rho_f))$$

The mass balance equation for water is

$$\frac{\partial}{\partial t}(\phi S_a C_{aw}\rho_a+\phi S_f C_{fw}\rho_f)$$

$$= \nabla.(\frac{C_{aw}\rho_a K_a}{\mu_a}(\nabla P_a+\rho_a g\nabla z) +$$

$$\nabla.(\frac{C_{fw}\rho_f K_f}{\mu_f}(\nabla P_f+\rho_f g\nabla z) +$$

$$\nabla.(\phi S_a(D_a+D^*_{aw}).\nabla(C_{aw}\rho_a) +$$

$$\nabla.(\phi S_f(D_f+D^*_{fw}).\nabla(C_{fw}\rho_f))$$

8.1.7.1 Boundary and Initial Conditions

Boundary conditions:

$$\rho_1 v_{1n} = - \frac{\rho_1 K_1}{\mu_1} (\nabla_n P_1 + \rho_1 g\nabla_n z) = 0$$

$$\rho_a v_{an} = - \frac{\rho_a K_a}{\mu_a} (\nabla_n P_a + \rho_a g\nabla_n z) = 0$$

$$\rho_f v_{fn} = - \frac{\rho_f K_f}{\mu_f} (\nabla_n P_f + \rho_f g\nabla_n z) = 0$$

$$\rho_g v_{gn} = - \frac{\rho_g K_g}{\mu_g} (\nabla_n P_g + \rho_g g \nabla_n z) = 0$$

Injection well:

$$\int_{A_{inj}} \rho_a \frac{K_a}{\mu_a} (\nabla P_a + \rho_a g \nabla z) \, dA = W_{aw} + W_{as}$$

$$\int_{A_{inj}} \rho_l \frac{K_l}{\mu_l} (\nabla P_l + \rho_l g \nabla z) \, dA = W_{ls}$$

$$\int_{A_{inj}} \rho_f \frac{K_f}{\mu_f} (\nabla P_f + \rho_f g \nabla z) \, dA = W_{fw} + W_{fs} + W_{fN}$$

$$\int_{A_{inj}} \rho_g \frac{K_g}{\mu_g} (\nabla P_g + \rho_g g \nabla z) \, dA = W_{gs} + W_{gN}$$

Production well:

$$P_l = P_{prod}$$

$$P_a = P_{prod} + P_{cla}$$

$$P_g = P_{prod} + P_{clg}$$

Initial conditions:

$$S_a(0,x_1,x_2,x_3) = S_{ai}(0,x_1,x_2,x_3)$$

$$S_l(0,x_1,x_2,x_3) = S_{li}(0,x_1,x_2,x_3)$$

$$S_g(0,x_1,x_2,x_3) = S_{gi}(0,x_1,x_2,x_3)$$

$$P_a(0,x_1,x_2,x_3) = P_{ai}(0,x_1,x_2,x_3)$$

$$P_g(0,x_1,x_2,x_3) = P_{gi}(0,x_1,x_2,x_3)$$

8.1.7.2 Constitutive Relationships and Constraints

1) $S_a + S_l + S_f + S_g = 1$

2) $C_{lo} + C_{ls} = 1$

3) $C_{fw} + C_{fN} + C_{fs} = 1$

4) $C_{aw} + C_{as} = 1$

5) $C_{gN} + C_{gs} = 1$

6) $\rho_l = \rho_l(P_l, C_{lo})$

7) $\rho_a = \rho_a(P_a, C_{aw})$

8) $\rho_f = \rho_f(P_f, C_{fN}, C_{fs})$

9) $\rho_g = \rho_g(P_g, C_{gN})$

10) $\mu_l = \mu_l(P_l, C_{lo})$

11) $\mu_a = \mu_a(P_a, C_{aw})$

12) $\mu_f = \mu_f(P_f, C_{fg}, C_{fs})$

13) $\mu_g = \mu_g(P_g, C_{gN}, C_{gs})$

14) $P_a = P_l - P_{cla}(S_a, S_l)$

15) $P_f = P_l - P_{clf}(S_f, S_l, S_a)$

16) $P_g = P_l - P_{clg}(S_g, S_l)$

17) ϕ = constant

18) g = constant

19) $K_l = K_l(S_a, S_l, S_f, K)$

20) $K_a = K_a(S_a, S_l, S_f, K)$

21) $K_f = K_f(S_a, S_l, S_f, K)$

22) $K_g = K_g(S_a, S_l, S_f, K)$

23) $D_a + D^*_{as} = D_{as}(D_{Las}, D_{Tas})$

24) $D_a + D^*_{aw} = D_{aw}(D_{Law}, D_{Taw})$

25) $D_f + D^*_{fw} = D_{fw}(D_{Lfw}, D_{Tfw})$

26) $D_f + D^*_{fN} = D_{fN}(D_{Lfg}, D_{Tfg})$

27) $D_f + D^*_{fs} = D_{fs}(D_{Lfs}, D_{Tfs})$

28) $D_g + D^*_{gN} = D_{gN}(D_{LgN}, D_{TgN})$

29) $D_g + D^*_{gs} = D_{gs}(D_{Lgs}, D_{Tgs})$

30) $z = z(x_1, x_2, x_3)$

31) ρ_r = constant

8.1.8 Foam Injection: Three-Phase Flow

The process of foam injection is considered to be three-phase flow. These phases are the aqueous, foam, and oleic phases. Therefore, the amount of gas (nitrogen) injected is considered to be just enough to create a foam which leaves no free gaseous phase in the system. For this process three-phase relative permeability data are required. As was the case for four-phase flow, it is assumed that N_2 is the gas that is being injected and that it is immiscible with the oleic or the aqueous phase. The components present in the foam phase are water, N_2 and surfactant; the components present in oleic phase are oil and surfactant; and the components present in the aqueous phase are surfactant and water. For this particular description the governing equations may be written as follows.

The equation for the mass balance of oil becomes

$$\frac{\partial}{\partial t}(\phi S_1 C_{1o} \rho_1) = \nabla.(\frac{\rho_1 C_{1o}}{\mu_1} K_1(\nabla P_1 + \rho_1 g \nabla z))$$

The equation for the mass balance of surfactant is

$$\frac{\partial}{\partial t}(\phi S_l C_{ls}\rho_l + \phi S_a C_{as}\rho_a + \phi S_f C_{fs}\rho_f)$$

$$= \nabla.(\frac{C_{ls}\rho_l K_l}{\mu_l}(\nabla P_l + \rho_l g \nabla z) +$$

$$\nabla.(\frac{C_{fs}\rho_f K_f}{\mu_f}(\nabla P_f + \rho_f g \nabla z) +$$

$$\nabla.(\phi S_l (D_l + D^*_{ls}).\nabla(C_{ls}\rho_l) +$$

$$\nabla.(\phi S_g (D_g + D^*_{gs}).\nabla(C_{gs}\rho_g) +$$

$$\nabla.(\phi S_a (D_a + D^*_{as}).\nabla(C_{as}\rho_a) +$$

$$\nabla.(\phi S_f (D_f + D^*_{fs}).\nabla(C_{fs}\rho_f))$$

The equation for the mass balance of nitrogen is

$$\frac{\partial}{\partial t}(\phi S_f C_{fN}\rho_f)$$

$$= \nabla.(\frac{C_{fN}\rho_f K_f}{\mu_f}(\nabla P_f + \rho_f g \nabla z) +$$

$$\nabla.(\phi S_f (D_f + D^*_{fN}).\nabla(C_{fN}\rho_f))$$

The mass balance equation for water is

$$\frac{\partial}{\partial t}(\phi S_a C_{aw}\rho_a + \phi S_f C_{fw}\rho_f)$$

$$= \nabla.(\frac{C_{aw}\rho_a K_a}{\mu_a}(\nabla P_a + \rho_a g \nabla z) +$$

$$\nabla.(\frac{C_{fw}\rho_f K_f}{\mu_f}(\nabla P_f + \rho_f g \nabla z) +$$

$$\nabla.(\phi S_a (D_a + D^*_{aw}).\nabla(C_{aw}\rho_a) +$$

$$\nabla.(\phi S_f(D_f+D^*_{fw}).\nabla(C_{fw}\rho_f))$$

8.1.8.1 Boundary and Initial Conditions

Boundary conditions:

$$\rho_l v_{ln} = -\frac{\rho_l K_l}{\mu_l}(\nabla_n P_l + \rho_l g \nabla_n z) = 0$$

$$\rho_a v_{an} = -\frac{\rho_a K_a}{\mu_a}(\nabla_n P_a + \rho_a g \nabla_n z) = 0$$

$$\rho_f v_{fn} = -\frac{\rho_f K_f}{\mu_f}(\nabla_n P_f + \rho_f g \nabla_n z) = 0$$

Injection well:

$$\int_{A_{inj}} \rho_a \frac{K_a}{\mu_a}(\nabla P_a + \rho_a g \nabla z)\, dA = W_{aw} + W_{as}$$

$$\int_{A_{inj}} \rho_l \frac{K_l}{\mu_l}(\nabla P_l + \rho_l g \nabla z)\, dA = W_{ls}$$

$$\int_{A_{inj}} \rho_f \frac{K_f}{\mu_f}(\nabla P_f + \rho_f g \nabla z)\, dA = W_{fw} + W_{fs} + W_{fN}$$

Production well:

$$P_l = P_{prod}$$

$$P_a = P_{prod} + P_{cla}$$

Initial conditions:

$$S_a(0,x_1,x_2,x_3) = S_{ai}(0,x_1,x_2,x_3)$$

$S_l(0,x_1,x_2,x_3) = S_{li}(0,x_1,x_2,x_3)$

$P_a(0,x_1,x_2,x_3) = P_{ai}(0,x_1,x_2,x_3)$

$P_f(0,x_1,x_2,x_3) = P_{fi}(0,x_1,x_2,x_3)$

8.1.8.2 Constitutive Relationships and Constraints

1) $S_a + S_l + S_f = 1$
2) $C_{lo} + C_{ls} = 1$
3) $C_{fw} + C_{fN} + C_{fs} = 1$
4) $C_{aw} + C_{as} = 1$
5) $\rho_l = \rho_l(P_l, C_{lo})$
6) $\rho_a = \rho_a(P_a, C_{aw})$
7) $\rho_f = \rho_f(P_f, C_{fN}, C_{fs})$
8) $\rho_g = \rho_g(P_g, C_{gN})$
9) $\mu_l = \mu_l(P_l, C_{lo})$
10) $\mu_a = \mu_a(P_a, C_{aw})$
11) $\mu_f = \mu_f(P_f, C_{fN}, C_{fs})$
12) $P_a = P_l - P_{cla}(S_a, S_l)$
13) $P_f = P_l - P_{clf}(S_f, S_l)$
14) ϕ =constant
15) g =constant
16) $K_l = K_l(S_a, S_l, S_f, K)$
17) $K_a = K_a(S_a, S_l, S_f, K)$
18) $K_f = K_f(S_a, S_l, S_f, K)$
19) $D_a + D^*_{as} = D_{as}(D_{Las}, D_{Tas})$

20) $D_a + D_{aw}^* = D_{aw}(D_{Law}, D_{Taw})$

21) $D_f + D_{fw}^* = D_{fw}(D_{Lfw}, D_{Tfw})$

22) $D_f + D_{fg}^* = D_{fN}(D_{Lfg}, D_{Tfg})$

23) $D_f + D_{fs}^* = D_{fs}(D_{Lfs}, D_{Tfs})$

24) $z = z(x_1, x_2, x_3)$

25) ρ_r = constant

8.2 DIMENSIONLESS PROPERTIES AND CONDITIONS

One of the major requirements for all of the scaling criteria is that the dimensionless properties be the same functions of the dimensionless parameters for the model and the prototype. The dimensionless properties and conditions for each case are listed in this section.

8.2.1 Polymer Flood

$\rho_{aD}(P_D, C_{awD}, C_{apD})$

$\rho_{lD}(P_D)$

$K_{iD}(S_{lD}, S_{aD})$ i=a,l

$\mu_{aD}(P_D, C_{awD}, C_{apD})$

$\mu_{lD}(P_D)$

$P_{claD}(S_{aD}, \sigma_{al}, K)$

$z_D(x_{1D}, x_{2D}, x_{3D})$

$D_{LiD}(D_i^*, F, \phi, v, \sigma, d_p)$ i=ap,aw

$D_{TiD}(D_i^*, F, \phi, v, \sigma, d_p)$ i=ap,aw

8.2.2 Emulsion Flood: Two-Phase Flow

$\rho_{aD}(P_D, C_{awD}, C_{amD})$
$\rho_{lD}(P_D, C_{lwD}, C_{lmD})$
$K_{iD}(S_{lD}, S_{aD})$ $i=a,l$
$\mu_{aD}(P_D, C_{awD}, C_{amD})$
$\mu_{lD}(P_D, C_{lwD}, C_{lmD})$
$P_{claD}(S_{aD}, \sigma_{al}, K)$
$z_D(x_{1D}, x_{2D}, x_{3D})$
$D_{LiD}(D_i^*, F, \phi, v, \sigma, d_p)$ $i=aw,am,lo,lm$
$D_{TiD}(D_i^*, F, \phi, v, \sigma, d_p)$ $i=aw,am,lo,lm$

8.2.3 Emulsion Flood: Emulsion Miscible in Aqueous Phase Only

$\rho_{aD}(P_D, C_{awD}, C_{amD})$
$\rho_{lD}(P_D)$
$K_{iD}(S_{lD}, S_{aD})$ $i=a,l$
$\mu_{aD}(P_D, C_{awD}, C_{amD})$
$\mu_{lD}(P_D)$
$P_{claD}(S_{aD}, \sigma_{al}, K)$
$z_D(x_{1D}, x_{2D}, x_{3D})$
$D_{LiD}(D_i^*, F, \phi, v, \sigma, d_p)$ $i=aw,am$
$D_{TiD}(D_i^*, F, \phi, v, \sigma, d_p)$ $i=aw,am$

8.2.4 Emulsion Flood: Three-Phase Flow

$\rho_{aD}(P_D, C_{awD}, C_{amD})$
$\rho_{lD}(P_D)$

$\rho_{mD}(P_D, C_{mwD}, C_{mmD})$

$\mu_{aD}(P_D, C_{awD}, C_{amD})$

$\mu_{1D}(P_D)$

$\mu_{mD}(P_D, C_{mwD}, C_{mmD})$

$P_{claD}(S_{aD}, \sigma_{a1}, K)$

$P_{clmD}(S_{1D}, \sigma_{1m}, K)$

$z_D(x_{1D}, x_{2D}, x_{3D})$

$D_{LiD}(D_i^*, F, \phi, v, \sigma, d_p)$ i=aw,am,mw,mm

$D_{TiD}(D_i^*, F, \phi, v, \sigma, d_p)$ i=aw,am,mw,mm

8.2.5 Foam Injection: Four-Phase Flow

$\rho_{aD}(P_D, C_{awD}, C_{asD})$

$\rho_{1D}(P_D, C_{1oD}, C_{1sD})$

$\rho_{fD}(P_D, C_{fwD}, C_{fgD}, C_{fsD})$

$\rho_{gD}(P_D, C_{gND}, C_{gsD})$

$\mu_{aD}(P_D, C_{awD}, C_{asD})$

$\mu_{1D}(P_D, C_{1oD}, C_{1sD})$

$\mu_{fD}(P_D, C_{fwD}, C_{fgD}, C_{fsD})$

$\mu_{gD}(P_D, C_{gND}, C_{gsD})$

$P_{claD}(S_{aD}, S_{1D}, \sigma_{a1}, K)$

$P_{clfD}(S_{1D}, S_{fD}, \sigma_{1f}, K)$

$P_{clgD}(S_{gD}, S_{1D}, \sigma_{1g}, K)$

$z_D(x_{1D}, x_{2D}, x_{3D})$

$D_{LiD}(D_i^*, F, \phi, v, \sigma, d_p)$ i=aw,as,fw,fg,fs,lo,ls

$D_{TiD}(D_i^*, F, \phi, v, \sigma, d_p)$ i=fw,fg,fs,lo,ls

8.2.6 Foam Injectiion: Three-Phase Flow

$\rho_{aD}(P_D, C_{awD}, C_{asD})$

$\rho_{lD}(P_D, C_{loD}, C_{lsD})$

$\rho_{fD}(P_D, C_{fwD}, C_{fsD})$

$\mu_{aD}(P_D, C_{awD}, C_{asD})$

$\mu_{lD}(P_D, C_{loD}, C_{lsD})$

$\mu_{fD}(P_D, C_{fwD}, C_{fsD})$

$P_{claD}(S_{aD}, S_{lD}, \sigma_{al}, K)$

$P_{clfD}(S_{lD}, S_{fD}, \sigma_{lf}, K)$

$P_{clgD}(S_{lD}, \sigma_{lg}, K)$

$z_D(x_{1D}, x_{2D}, x_{3D})$

$D_{LiD}(D_i^*, F, \phi, v, \sigma, d_p)$ $\quad i = aw, as, fw, fs, lo, ls$

$D_{TiD}(D_i^*, F, \phi, v, \sigma, d_p)$ $\quad i = aw, as, fw, fs, lo, ls$

8.3 DIFFERENT APPROACHES TO SATISFY THE SCALING CRITERIA

A sample derivation of a complete set of scaling criteria for the cases described above is presented in Appendix B. In order to scale these processes all of the scaling criteria have to be satisfied. However, all of the scaling criteria are very difficult to satisfy and, depending on the major phenomena occurring in the process, it may be necessary to relax a few of these criteria. In this section, a number of subsets of scaling criteria for the different approaches taken is presented. The method used by Kimber et al. (1986) has been used for the development of the scaling criteria.

8.3.1 Polymer Flood

8.3.1.1 Approach #1 - Same Fluids, Different Porous Media, Different Pressure Drop, Geometric Similarity

The scaling groups which are satisfied in this approach are

$$\frac{W}{L},\ \frac{\mu_{1R}K_{aR}}{\mu_{aR}K_{1R}},\ \frac{\rho_{1R}}{\rho_{aR}},\ \frac{W_{apR}}{W_{awR}},\ \phi_R,\ \frac{S_{aiR}}{S_{aR}},$$

$$\frac{P_{1iR}}{P_{1R}},\ \frac{\rho_{rR}A_{pR}}{S_{aR}},\ \frac{P_{prod}}{P_{1R}},\ \frac{A_{injR}}{L^2},\ R,$$

$$\frac{H}{L},\ \frac{\rho_{aR}g_R L}{P_{aR}},\ BC_{apR},\ \frac{W_{awR}\mu_{aR}}{K_{aR}P_{aR}\rho_{aR}L},\ \frac{S_{aR}D^*_{apR}\mu_{aR}}{K_{aR}P_{aR}F_R},$$

$$\frac{D^*_{awR}}{D^*_{apR}},\ \frac{C_{apR}}{C_{awR}}$$

As can be seen above, the dimensionless groups scaling geometry, viscous, and gravitational forces are satisfied. As a consequence, the pressure drop across the model and the prototype is different. Such a requirement leads to a different porous medium for the model. This approach cannot scale the effects of dispersion and capillary forces. Also, because of the varying properties of the different porous media, the scaling of irreducible saturations, resistance factor, adsorption, and relative permeabilities is questionable.

In order for R to be the same for the model and the prototype, the polymer slug size has to be the same.

However, a reference slug size has to be matched for specific cases, such as heterogeneous porous media.

In addition to the aforementioned requirements, all of the dimensionless properties must be the same function of their dimensionless variables for the prototype and the model. The implications of these scaling criteria for a model reduced in length by a scaling factor of 'a' are:

1) ϕ, S_{ai}, F, C_{ap}, R must remain the same.
2) H, W, ΔP_{max}, $(P_i - P_{prod})$, W_{ap}, W_{aw} must be reduced by 'a'.
3) K must be increased by 'a'.
4) t will be reduced by 'a^2'.

8.3.1.2 Approach #2 - Same Fluids, Same Porous Medium, Same Pressure Drop, Geometric Similarity

The scaling groups that are satisfied in this approach are:

$$\frac{W}{L},\ \frac{\mu_{1R}K_{aR}}{\mu_{aR}K_{1R}},\ \frac{\rho_{1R}}{\rho_{aR}},\ \frac{W_{apR}}{W_{awR}},\ \phi_R,\ \frac{S_{aiR}}{S_{aR}},$$

$$\frac{P_{1iR}}{P_{1R}},\ \frac{\rho_{rR}A_{pR}}{S_{aR}},\ \frac{P_{prod}}{P_{1R}},\ \frac{A_{injR}}{L^2},\ \frac{H}{L},\ R,$$

$$BC_{apR},\ \frac{W_{awR}\mu_{aR}}{K_{aR}P_{aR}\rho_{aR}L},\ \frac{S_{aR}D^*_{apR}\mu_{aR}}{K_{aR}P_{aR}F_R},\ \frac{D^*_{awR}}{D^*_{apR}},$$

$$\frac{C_{apR}}{C_{awR}},\ \frac{P_{aR}}{P_{claR}}$$

This approach allows the same pressure in the model as in the prototype. The identity of pressure enables the properties which depend on pressure to be properly scaled. Also, irreducible saturations, relative permeabilities and adsorption may be scaled more precisely by using the same porous medium. However, this approach may not scale gravitational forces properly. Also, the effect of dispersion at high flow rate is not scaled under the conditions.

In addition to the above requirements, all of the dimensionless properties must be the same function of their dimensionless variables for the prototype and the model. The implications of these scaling criteria for a model reduced in length by a scaling factor of 'a' and employing the same fluids as the prototype are:

1) ΔP_{max}, P_i, P_{prod}, K, ϕ, S_{ai}, F, C_{ap}, R must be same.
2) H, W, W_{aw}, W_{ap} must be reduced by 'a'.
3) t will be reduced by 'a^2'.

8.3.1.3 Approach #3 - Same Fluids, Same Porous Medium, Same Pressure Drop, Geometric Scaling Relaxed

The scaling groups that are satisfied in this approach are:

$$\frac{W}{L},\ \frac{\mu_{1R}K_{aR}}{\mu_{aR}K_{1R}},\ \frac{\rho_{1R}}{\rho_{aR}},\ \frac{W_{apR}}{W_{awR}},\ \phi_R,\ \frac{S_{aiR}}{S_{aR}},$$

$$\frac{P_{1iR}}{P_{1R}},\ \frac{\rho_{rR}A_{pR}}{S_{aR}},\ \frac{P_{prod}}{P_{1R}},\ \frac{A_{injR}P_{aR}}{L^3\rho_{aR}g_R},\ R,$$

$$\frac{HP_{aR}}{\rho_{aR} g_R L^2},\ BC_{apR},\ \frac{W_{awR}\mu_{aR}}{K_{aR}\rho_{aR}^2 g_R L^2},\ \frac{S_{aR} D^*_{apR}\mu_{aR}}{K_{aR}P_{aR}F_R},$$

$$\frac{D^*_{awR}}{D^*_{apR}},\ \frac{C_{apR}}{C_{awR}}$$

In order to scale gravitational effects by using the same fluids, and the same porous medium at similar pressure conditions, geometric similarity has to be relaxed. Also, the capillary forces and the effect of dispersion are not scaled properly. The most significant difference in this approach is the choice of the reference quantity for the vertical coordinate, x_2. It becomes

$$x_{2R} = \rho_{aR} g_R L^2 / P_{aR}$$

In addition to the above requirements, all of the dimensionless properties must be the same function of their dimensionless variables for the prototype and the model. The implications of these scaling criteria for a model reduced in length by a scaling factor of 'a' and employing the same fluids as the prototype are:

1) ΔP_{max}, P_i, P_{prod}, K, ϕ, S_{ai}, F, C_{ap}, R must remain the same.

2) W must be reduced by a.

3) H, W_{aw}, W_{ap} must be reduced by 'a^2'.

4) The reservoir must be horizontal.

5) t will be reduced by 'a^2'.

8.3.1.4 Approach #4 - Same Fluids, Same Porous Medium, Same Pressure Drop, Geometric Scaling Relaxed, Dispersion at High Flow Rate

The scaling groups that are satisfied in this approach are:

$$\frac{W}{L},\ \frac{\mu_{1R}K_{aR}}{\mu_{aR}K_{1R}},\ \frac{\rho_{1R}}{\rho_{aR}},\ \frac{W_{apR}}{W_{awR}},\ \phi_R,\ \frac{S_{aiR}}{S_{aR}},\ R,$$

$$\frac{P_{1iR}}{P_{1R}},\ \frac{\rho_{rR}A_{pR}}{S_{aR}},\ \frac{P_{prod}}{P_{1R}},\ \frac{A_{injR}}{L(\phi_R S_{aR} x_R d_{pR} L)^{1/2}},$$

$$\frac{H}{(\phi_R S_{aR} x_R d_{pR} L)^{1/2}},\ BC_{apR},\ \frac{W_{awR}\mu_{aR}}{\rho_{aR}K_{aR}P_{aR}(\phi_R S_{aR} x_R d_{pR} L)^{1/2}},$$

$$\frac{S_{aR}D^*_{apR}\mu_{aR}}{K_{aR}P_{aR}F_R},\ \frac{D^*_{awR}}{D^*_{apR}},\ \frac{C_{apR}}{C_{awR}}$$

This approach is aimed at scaling processes that are dominated by transverse dispersion. However, in order to accommodate transverse dispersion, scaling of gravitational and capillary effects must be relaxed. In order to scale dispersion, the reference quantity must be chosen for the vertical coordinate as

$$x_{2R} = (\phi_R S_{aR} x_R d_{pR} L)^{1/2}$$

In addition to the above requirements, all of the dimensionless properties must be the same function of their dimensionless variables for the prototype and the model. The implications of these scaling criteria for a model reduced in length by a scaling factor of 'a' and employing the same fluids as the prototype are:

1) ΔP_{max}, P_i, P_{prod}, K, ϕ, S_{ai}, F, C_{ap}, R must remain the same.

2) W must be reduced by a.

3) H, W_{aw}, W_{ap} must be reduced by '$a^{1/2}$'

4) t will be reduced by 'a^2'.

8.3.1.5 Approach #5 - Same Fluids, Different Porous Media, Different Pressure Drop, Geometric Scaling Relaxed, Dispersion at High Flow Rate

The scaling groups that are satisfied in this approach are:

$$\frac{W}{L},\ \frac{\mu_{lR}K_{aR}}{\mu_{aR}K_{lR}},\ \frac{\rho_{lR}}{\rho_{aR}},\ \frac{W_{apR}}{W_{awR}},\ \phi_R,\ \frac{S_{aiR}}{S_{aR}},\ R,$$

$$\frac{P_{liR}}{P_{lR}},\ \frac{\rho_{rR}A_{pR}}{S_{aR}},\ \frac{P_{prod}}{P_{lR}},\ \frac{A_{injR}P_{aR}}{L^3\rho_{aR}g_R},$$

$$\frac{HP_{aR}}{\rho_{aR}g_R L^2},\ BC_{apR},\ \frac{W_{awR}\mu_{aR}}{\rho_{aR}^{\ 2}g_R K_{aR}L^2},$$

$$\frac{P_{aR}S_{aR}D^*_{apR}\mu_{aR}}{K_{aR}\rho_{aR}^{\ 2}g_R^{\ 2}F_R L^2},\ \frac{D^*_{awR}}{D^*_{apR}},\ \frac{C_{apR}}{C_{awR}},$$

$$\frac{\phi_R S_{aR}x_R P_{aR}^{\ 2}(K_{aR})^{1/2}}{\rho_{aR}^{\ 2}g_R^{\ 2}L^3}$$

In this approach an attempt is made to balance the viscous and gravitational forces while scaling transverse dispersion. However, the effects of capillary forces cannot be scaled by this method. Also, relative permeabilities and irreducible saturations may not be scaled properly because of the use of different porous media. Moreover, time is scaled down by only four fifths power of the scaling factor, rather than by its square. This leads to a rather lengthy experiment. In developing the set of scaling criteria for this approach the reference quantity for x_2 is chosen such that

$$x_{2R} = \rho_{aR} g_R L^2 / P_{aR}$$

In addition to the above requirements, all of the dimensionless properties have to be the same function of their dimensionless variables for the prototype and the model. The implications for a model reduced in length by a scaling factor of 'a' and employing the same fluids as the prototype are:

1) ϕ, S_{ai}, F, C_{ap}, R must be the same.
2) L, W must be reduced by 'a'.
3) K must be increased by '$a^{2/5}$'.
4) ΔP_{max}, W_{aw}, W_{ap} must be reduced by '$a^{8/5}$'.
5) H must be reduced by '$a^{2/5}$'.
6) t will be reduced by '$a^{4/5}$'.

8.3.2 Emulsion Flood: Two-Phase Flow

8.3.2.1 Approach #1 - Same Fluids, Different Porous Media, Different Pressure Drop, Geometric Similarity

The scaling groups that may be satisfied with this approach are:

$$\frac{W}{L}, \frac{\mu_{lR}K_{aR}}{\mu_{aR}K_{lR}}, \frac{\rho_{lR}}{\rho_{aR}}, \frac{W_{amR}}{W_{awR}}, \frac{W_{lmR}}{W_{lwR}}, \phi_R,$$

$$\frac{S_{aiR}}{S_{aR}}, \frac{P_{liR}}{P_{lR}}, \frac{P_{prod}}{P_{lR}}, \frac{A_{injR}}{L^2},$$

$$\frac{H}{L}, \frac{\rho_{aR}g_R L}{P_{aR}}, \frac{W_{awR}\mu_{aR}}{K_{aR}P_{aR}\rho_{aR}L},$$

$$\frac{S_{aR}D^*_{awR}\mu_{aR}}{K_{aR}P_{aR}F_R}, \frac{D^*_{loR}}{D^*_{lmR}}, \frac{D^*_{awR}}{D^*_{amR}},$$

$$\frac{C_{loR}}{C_{lmR}}, \frac{C_{amR}}{C_{awR}}$$

In addition to the aforementioned requirements, all of the dimensionless properties must be the same function of their dimensionless variables for the prototype and the model. The implications of these scaling criteria for a model reduced in length by a scaling factor of 'a' are:

1) ϕ, S_{ai}, F, C_{amR}, C_{lmR} must remain the same.

2) H, W, ΔP_{max}, $(P_i - P_{prod})$, W_{aw}, W_{am}, W_{lm} must be reduced by 'a'.

3) K must be increased by 'a'.

4) t will be reduced by 'a^2'.

8.3.2.2 Approach #2 - Same Fluids, Same Porous Medium, Same Pressure Drop, Geometric Similarity

The scaling groups that may be satisfied with this approach are:

$$\frac{W}{L},\ \frac{\mu_{lR}K_{aR}}{\mu_{aR}K_{lR}},\ \frac{\rho_{lR}}{\rho_{aR}},\ \frac{W_{amR}}{W_{awR}},\ \frac{W_{lmR}}{W_{lwR}},\ \phi_R,\ \frac{S_{aiR}}{S_{aR}},$$

$$\frac{P_{liR}}{P_{lR}},\ \frac{P_{prod}}{P_{lR}},\ \frac{A_{injR}}{L^2},$$

$$\frac{H}{L},\ \frac{W_{awR}\mu_{aR}}{K_{aR}P_{aR}\rho_{aR}L},\ \frac{S_{aR}D^*_{awR}\mu_{aR}}{K_{aR}P_{aR}F_R},\ \frac{D^*_{loR}}{D^*_{lmR}},$$

$$\frac{D^*_{awR}}{D^*_{amR}},\ \frac{C_{loR}}{C_{lmR}},\ \frac{C_{amR}}{C_{awR}},\ \frac{P_{aR}}{P_{claR}}$$

In addition to the above requirements, all of the dimensionless properties must be the same function of their dimensionless variables for the prototype and the model. The implications of these scaling criteria for a model reduced in length by a scaling factor of 'a' and employing the same fluids as the prototype are:

1) ΔP_{max}, P_i, P_{prod}, K, ϕ, S_{ai}, F, C_{amR}, C_{lmR} must remain the same.

2) H, W, W_{aw}, W_{am}, W_{lm} must be reduced by 'a'.

3) t will be reduced by 'a^2'.

8.3.2.3 Approach #3 - Same Fluids, Same Porous Medium, Same Pressure Drop, Geometric Scaling Relaxed

The scaling groups that are satisfied in this approach are:

$$\frac{W}{L},\ \frac{\mu_{lR}K_{aR}}{\mu_{aR}K_{lR}},\ \frac{\rho_{lR}}{\rho_{aR}},\ \frac{W_{amR}}{W_{awR}},\ \frac{W_{lmR}}{W_{lwR}},\ \phi_R,\ \frac{S_{aiR}}{S_{aR}},$$

$$\frac{P_{liR}}{P_{lR}},\ \frac{S_{liR}}{S_{lR}},\ \frac{P_{prod}}{P_{lR}},$$

$$\frac{HP_{aR}}{\rho_{aR}g_RL^2},\ \frac{W_{awR}\mu_{aR}}{K_{aR}\rho_{aR}^{2}g_RL^2},\ \frac{S_{aR}D^*_{amR}\mu_{aR}}{K_{aR}P_{aR}F_R},\ \frac{A_{injR}P_{aR}}{L^3\rho_{aR}g_R},$$

$$\frac{D^*_{loR}}{D^*_{lmR}},\ \frac{D^*_{awR}}{D^*_{amR}},\ \frac{C_{loR}}{C_{lmR}},\ \frac{C_{amR}}{C_{awR}}$$

In addition to the above requirements, all of the dimensionless properties must be the same function of their dimensionless variables for the prototype and the model. The implications of these scaling criteria for a model reduced in length by a scaling factor of 'a' and employing the same fluids as the prototype are:

1) ΔP_{max}, P_i, P_{prod}, K, ϕ, S_{ai}, F, C_{amR}, C_{lmR} must remain the same.

2) W must be reduced by a.

3) H, W_{aw}, W_{am}, W_{lm} must be reduced by 'a^2'.

4) The reservoir must be horizontal.

5) t will be reduced by 'a^2'.

8.3.2.4 Approach #4 - Same Fluids, Same Porous Medium, Same Pressure Drop, Geometric Scaling Relaxed, Dispersion at High Flow Rate

The scaling groups that are satisfied in this approach are:

$$\frac{W}{L},\ \frac{\mu_{lR}K_{aR}}{\mu_{aR}K_{lR}},\ \frac{\rho_{lR}}{\rho_{aR}},\ \frac{W_{amR}}{W_{awR}},\ \frac{W_{lmR}}{W_{lwR}},\ \phi_R,\ \frac{S_{aiR}}{S_{aR}},$$

$$\frac{A_{injR}}{L(\phi_R S_{aR} x_R d_{pR} L)^{1/2}},\ \frac{P_{liR}}{P_{lR}},\ \frac{P_{prod}}{P_{lR}},$$

$$\frac{H}{(\phi_R S_{aR} x_R d_{pR} L)^{1/2}},\ \frac{W_{awR}\mu_{aR}}{\rho_{aR}K_{aR}P_{aR}(\phi_R S_{aR} x_R d_{pR} L)^{1/2}},$$

$$\frac{S_{aR}D^*_{amR}\mu_{aR}}{K_{aR}P_{aR}F_R},\ \frac{D^*_{loR}}{D^*_{lmR}},\ \frac{D^*_{awR}}{D^*_{amR}},\ \frac{C_{amR}}{C_{awR}},\ \frac{C_{loR}}{C_{lmR}}$$

In addition to the above requirements, all of the dimensionless properties must be the same function of their dimensionless variables for the prototype and the model. The implications of these scaling criteria for a model reduced in length by a scaling factor of 'a' and employing the same fluids as the prototype are:

1) ΔP_{max}, P_i, P_{prod}, K, ϕ, S_{ai}, F, C_{amR}, C_{lmR} must remain the same.

2) W must be reduced by a.

3) H, W_{aw}, W_{am}, W_{lm} must be reduced by '$a^{1/2}$'

4) t will be reduced by 'a^2'.

8.3.2.5 Approach #5 - Same Fluids, Different Porous Media, Different Pressure Drop, Geometric Scaling Relaxed, Dispersion at High Flow Rate

The scaling groups that are satisfied in this approach are:

$$\frac{W}{L},\ \frac{\mu_{1R}K_{aR}}{\mu_{aR}K_{1R}},\ \frac{\rho_{1R}}{\rho_{aR}},\ \frac{W_{amR}}{W_{awR}},\ \frac{W_{1mR}}{W_{1wR}},\ \phi_R,\ \frac{S_{aiR}}{S_{aR}},$$

$$\frac{A_{injR}P_{aR}}{L^3\rho_{aR}g_R},\ \frac{P_{1iR}}{P_{1R}},\ \frac{P_{prod}}{P_{1R}},$$

$$\frac{HP_{aR}}{\rho_{aR}g_RL^2},\ \frac{W_{awR}\mu_{aR}}{\rho_{aR}^2g_RK_{aR}L^2},\ \frac{D^*_{1oR}}{D^*_{1mR}},$$

$$\frac{D^*_{awR}}{D^*_{amR}},\ \frac{P_{aR}S_{aR}D^*_{apR}\mu_{aR}}{K_{aR}\rho_{aR}^2g_R^2F_RL^2},\ \frac{C_{amR}}{C_{awR}},\ \frac{C_{1oR}}{C_{1mR}},$$

$$\frac{\phi_RS_{aR}x_RP_{aR}^2(K_{aR})^{1/2}}{\rho_{aR}^2g_R^2L^3}$$

In addition to the above requirements, all of the dimensionless properties have to be the same function of their dimensionless variables for the prototype and the model. The implications for a model reduced in length by a scaling factor of 'a' and employing the same fluids as the prototype are:

1) ϕ, S_{ai}, F, C_{amR}, C_{1mR} must be the same
2) L, W must be reduced by 'a'
3) K must be increased by '$a^{2/5}$'
4) ΔP_{max}, W_{aw}, W_{am}, W_{1m} must be reduced by '$a^{8/5}$'

5) H must be reduced by '$a^{2/5}$', and

6) t will be reduced by '$a^{4/5}$'

8.3.3 Emulsion Flood: Emulsion Miscible in Aqueous Phase Only

8.3.3.1 Approach #1 - Same Fluids, Different Porous Media, Different Pressure Drop, Geometric Similarity

The scaling groups that may be satisfied with this approach are:

$$\frac{W}{L},\ \frac{\mu_{lR}K_{aR}}{\mu_{aR}K_{lR}},\ \frac{\rho_{lR}}{\rho_{aR}},\ \frac{W_{amR}}{W_{awR}},\ \phi_R,\ \frac{S_{aiR}}{S_{aR}},$$

$$\frac{P_{liR}}{P_{lR}},\ \frac{P_{prod}}{P_{lR}},\ \frac{H}{L},\ \frac{A_{injR}}{L^2},$$

$$\frac{\rho_{aR}g_R L}{P_{aR}},\ \frac{W_{awR}\mu_{aR}}{K_{aR}P_{aR}\rho_{aR}L},\ \frac{S_{aR}D^*_{awR}\mu_{aR}}{K_{aR}P_{aR}F_R},$$

$$\frac{D^*_{awR}}{D^*_{amR}},\ \frac{C_{amR}}{C_{awR}}$$

In addition to the aforementioned requirements, all of the dimensionless properties must be the same function of their dimensionless variables for the prototype and the model. The implications of these scaling criteria for a model reduced in length by a scaling factor of 'a' are:

1) ϕ, S_{ai}, F, C_{amR} must remain the same.

2) H, W, ΔP_{max}, $(P_i - P_{prod})$, W_{aw}, W_{aw} must be reduced by 'a'.

3) K must be increased by 'a'.

4) t will be reduced by 'a^2'.

8.3.3.2 Approach #2 - Same Fluids, Same Porous Medium, Same Pressure Drop, Geometric Similarity

The scaling groups that may be satisfied with this approach are:

$$\frac{W}{L},\ \frac{\mu_{lR}K_{aR}}{\mu_{aR}K_{lR}},\ \frac{\rho_{lR}}{\rho_{aR}},\ \frac{W_{amR}}{W_{awR}},\ \phi_R,\ \frac{S_{aiR}}{S_{aR}},$$

$$\frac{P_{liR}}{P_{lR}},\ \frac{P_{prod}}{P_{lR}},\ \frac{H}{L},\ \frac{A_{injR}}{L^2},$$

$$\frac{W_{awR}\mu_{aR}}{K_{aR}P_{aR}\rho_{aR}L},\ \frac{S_{aR}D^*_{awR}\mu_{aR}}{K_{aR}P_{aR}F_R},\ \frac{D^*_{awR}}{D^*_{amR}},$$

$$\frac{C_{amR}}{C_{awR}},\ \frac{P_{aR}}{P_{claR}}$$

In addition to the above requirements, all of the dimensionless properties must be the same function of their dimensionless variables for the prototype and the model. The implications of these scaling criteria for a model reduced in length by a scaling factor of 'a' and employing the same fluids as the prototype are:

1) ΔP_{max}, P_i, P_{prod}, K, ϕ, S_{ai}, F, C_{amR} must be same.

2) H, W, W_{aw}, W_{am} must be reduced by 'a'.

3) t will be reduced by 'a^2'.

8.3.3.3 Approach #3 - Same Fluids, Same Porous Medium, Same Pressure Drop, Geometric Scaling Relaxed

The scaling groups that are satisfied in this approach are:

$$\frac{W}{L},\ \frac{\mu_{lR}K_{aR}}{\mu_{aR}K_{lR}},\ \frac{\rho_{lR}}{\rho_{aR}},\ \frac{W_{amR}}{W_{awR}},\ \phi_R,\ \frac{S_{aiR}}{S_{aR}},$$

$$\frac{P_{liR}}{P_{lR}},\ \frac{P_{prod}}{P_{lR}},$$

$$\frac{A_{injR}P_{aR}}{L^3\rho_{aR}g_R},\ \frac{HP_{aR}}{\rho_{aR}g_RL^2},\ \frac{W_{awR}\mu_{aR}}{K_{aR}\rho_{aR}^2g_RL^2},\frac{S_{aR}D^*_{amR}\mu_{aR}}{K_{aR}P_{aR}F_R},$$

$$\frac{D^*_{awR}}{D^*_{amR}},\ \frac{C_{amR}}{C_{awR}}$$

In addition to the above requirements, all of the dimensionless properties must be the same function of their dimensionless variables for the prototype and the model. The implications of these scaling criteria for a model reduced in length by a scaling factor of 'a' and employing the same fluids as the prototype are:

1) ΔP_{max}, P_i, P_{prod}, K, ϕ, S_{ai}, F, C_{am} must remain the same.

2) W must be reduced by a.

3) H, W_{aw}, W_{am} must be reduced by 'a^2'.

4) The reservoir must be horizontal.

5) t will be reduced by 'a^2'.

8.3.3.4 Approach #4 - Same Fluids, Same Porous Medium, Same Pressure Drop, Geometric Scaling Relaxed, Dispersion at High Flow Rate

The scaling groups that are satisfied in this approach are:

$$\frac{W}{L}, \frac{\mu_{lR}K_{aR}}{\mu_{aR}K_{lR}}, \frac{\rho_{lR}}{\rho_{aR}}, \frac{W_{amR}}{W_{awR}}, \phi_R, \frac{S_{aiR}}{S_{aR}},$$

$$\frac{P_{liR}}{P_{lR}}, \frac{P_{prod}}{P_{lR}}, \frac{A_{injR}}{L(\phi_R S_{aR} x_R d_{pR} L)^{1/2}},$$

$$\frac{H}{(\phi_R S_{aR} x_R d_{pR} L)^{1/2}}, \frac{W_{awR}\mu_{aR}}{\rho_{aR}K_{aR}P_{aR}(\phi_R S_{aR} x_R d_{pR} L)^{1/2}},$$

$$\frac{S_{aR}D^*_{amR}\mu_{aR}}{K_{aR}P_{aR}F_R}, \frac{D^*_{awR}}{D^*_{amR}}, \frac{C_{amR}}{C_{awR}}$$

In addition to the above requirements, all of the dimensionless properties must be the same function of their dimensionless variables for the prototype and the model. The implications of these scaling criteria for a model reduced in length by a scaling factor of 'a' and employing the same fluids as the prototype are:

1) ΔP_{max}, P_i, P_{prod}, K, ϕ, S_{ai}, F, C_{amR} must remain the same.

2) W must be reduced by a.

3) H, W_{aw}, W_{am} must be reduced by '$a^{1/2}$'

4) t will be reduced by 'a^2'.

8.3.3.5 Approach #5 - Same Fluids, Different Porous Media, Different Pressure Drop, Geometric Scaling Relaxed, Dispersion at High Flow Rate

The scaling groups that are satisfied in this approach are:

$$\frac{W}{L},\ \frac{\mu_{1R}K_{aR}}{\mu_{aR}K_{1R}},\ \frac{\rho_{1R}}{\rho_{aR}},\ \frac{W_{amR}}{W_{awR}},\ \phi_R,\ \frac{S_{aiR}}{S_{aR}},$$

$$\frac{P_{1iR}}{P_{1R}},\ \frac{P_{prod}}{P_{1R}},\ \frac{A_{injR}P_{aR}}{L^3\rho_{aR}g_R},$$

$$\frac{HP_{aR}}{\rho_{aR}g_R L^2},\ \frac{W_{awR}\mu_{aR}}{\rho_{aR}^2 g_R K_{aR} L^2},\ \frac{P_{aR}S_{aR}D^*_{apR}\mu_{aR}}{K_{aR}\rho_{aR}^2 g_R^2 F_R L^2},$$

$$\frac{D^*_{awR}}{D^*_{amR}},\ \frac{C_{amR}}{C_{awR}},\ \frac{\phi_R S_{aR} X_R P_{aR}^2 (K_{aR})^{1/2}}{\rho_{aR}^2 g_R^2 L^3}$$

In addition to the above requirements, all of the dimensionless properties have to be the same function of their dimensionless variables for the prototype and the model. The implications for a model reduced in length by a scaling factor of 'a' and employing the same fluids as the prototype are:

1) ϕ, S_{ai}, F, C_{am} must be the same
2) L, W must be reduced by 'a'
3) K must be increased by '$a^{2/5}$'
4) ΔP_{max}, W_{aw}, W_{am} must be reduced by '$a^{8/5}$'
5) H must be reduced by '$a^{2/5}$', and
6) t will be reduced by '$a^{4/5}$'

8.3.4 Emulsion Flood: Three-Phase Flow

8.3.4.1 Approach #1 - Same Fluids, Different Porous Media, Different Pressure Drop, Geometric Similarity

The scaling groups that may be satisfied with this approach are:

$$\frac{W}{L},\ \frac{\mu_{lR}K_{aR}}{\mu_{aR}K_{lR}},\ \frac{\mu_{mR}K_{aR}}{\mu_{aR}K_{mR}},\ \frac{\rho_{lR}}{\rho_{aR}},\ \frac{\rho_{mR}}{\rho_{aR}},$$

$$\frac{W_{amR}}{W_{awR}},\ \frac{W_{mmR}}{W_{mwR}},\ \phi_R,\ \frac{S_{aiR}}{S_{aR}},\ \frac{S_{liR}}{S_{lR}},$$

$$\frac{P_{liR}}{P_{lR}},\ \frac{P_{miR}}{P_{mR}},\ \frac{P_{prod}}{P_{lR}},\ \frac{A_{injR}}{L^2},\ \frac{H}{L},$$

$$\frac{\rho_{aR}g_R L}{P_{aR}},\ \frac{W_{awR}\mu_{aR}}{K_{aR}P_{aR}\rho_{aR}L},\ \frac{S_{aR}D^*_{awR}\mu_{aR}}{K_{aR}P_{aR}F_R},$$

$$\frac{D^*_{awR}}{D^*_{amR}},\ \frac{D^*_{mmR}}{D^*_{mwR}},\ \frac{C_{amR}}{C_{awR}},\ \frac{C_{mwR}}{C_{mmR}}\ .$$

In addition to the aforementioned requirements, all of the dimensionless properties must be the same function of their dimensionless variables for the prototype and the model. The implications of these scaling criteria for a model reduced in length by a scaling factor of 'a' are:

1) ϕ, S_{ai}, F, C_{amR}, C_{mmR} must remain the same.

2) H, W, ΔP_{max}, (P_i-P_{prod}), W_{aw}, W_{mw}, W_{aw} must be reduced by 'a'.

3) K must be increased by 'a'.

4) t will be reduced by 'a^2'.

8.3.4.2 Approach #2 - Same Fluids, Same Porous Medium, Same Pressure Drop, Geometric Similarity

The scaling groups that may be satisfied with this approach are:

$$\frac{W}{L},\ \frac{\mu_{lR}K_{aR}}{\mu_{aR}K_{lR}},\ \frac{\mu_{mR}K_{aR}}{\mu_{aR}K_{mR}},\ \frac{\rho_{lR}}{\rho_{aR}},\ \frac{\rho_{mR}}{\rho_{aR}}\ \frac{W_{amR}}{W_{awR}},\ \frac{W_{mmR}}{W_{mwR}},\ \phi_R,$$

$$\frac{S_{aiR}}{S_{aR}},\ \frac{S_{liR}}{S_{lR}},\ \frac{A_{injR}}{L^2},\ \frac{P_{liR}}{P_{lR}},\ \frac{P_{miR}}{P_{mR}},\ \frac{P_{prod}}{P_{lR}},\ \frac{H}{L},$$

$$\frac{W_{awR}\mu_{aR}}{K_{aR}P_{aR}\rho_{aR}L},\ \frac{S_{aR}D^*_{awR}\mu_{aR}}{K_{aR}P_{aR}F_R},\ \frac{D^*_{awR}}{D^*_{amR}},\ \frac{D^*_{mmR}}{D^*_{mwR}},$$

$$\frac{C_{amR}}{C_{awR}},\ \frac{C_{mwR}}{C_{mmR}},\ \frac{P_{aR}}{P_{claR}},\ \frac{P_{lR}}{P_{clmR}}$$

In addition to the above requirements, all of the dimensionless properties must be the same function of their dimensionless variables for the prototype and the model. The implications of these scaling criteria for a model reduced in length by a scaling factor of 'a' and employing the same fluids as the prototype are:

1) ΔP_{max}, P_i, P_{prod}, K, ϕ, S_{ai}, F must be same.
2) H, W, W_{aw}, W_{ap} must be reduced by 'a'.
3) t will be reduced by 'a^2'.

8.3.4.3 Approach #3 - Same Fluids, Same Porous Medium, Same Pressure Drop, Geometric Scaling Relaxed

The scaling groups that are satisfied in this approach are:

$$\frac{W}{L}, \frac{\mu_{lR}K_{aR}}{\mu_{aR}K_{lR}}, \frac{\mu_{mR}K_{aR}}{\mu_{aR}K_{mR}}, \frac{\rho_{lR}}{\rho_{aR}}, \frac{\rho_{mR}}{\rho_{aR}}, \frac{W_{amR}}{W_{awR}}, \phi_R,$$

$$\frac{S_{aiR}}{S_{aR}}, \frac{W_{mmR}}{W_{mwR}}, \phi_R, \frac{A_{injR}P_{aR}}{L^3\rho_{aR}g_R},$$

$$\frac{P_{liR}}{P_{lR}}, \frac{P_{miR}}{P_{mR}}, \frac{S_{liR}}{S_{lR}}, \frac{P_{prod}}{P_{lR}},$$

$$\frac{HP_{aR}}{\rho_{aR}g_RL^2}, \frac{W_{awR}\mu_{aR}}{K_{aR}\rho_{aR}{}^2g_RL^2}, \frac{S_{aR}D^*_{amR}\mu_{aR}}{K_{aR}P_{aR}F_R},$$

$$\frac{D^*_{awR}}{D^*_{amR}}, \frac{D^*_{mmR}}{D^*_{mwR}}, \frac{C_{amR}}{C_{awR}}, \frac{C_{mwR}}{C_{mmR}}$$

In addition to the above requirements, all of the dimensionless properties must be the same function of their dimensionless variables for the prototype and the model. The implications of these scaling criteria for a model reduced in length by a scaling factor of 'a' and employing the same fluids as the prototype are:

1) ΔP_{max}, P_i, P_{prod}, K, ϕ, S_{ai}, F, C_{amR}, C_{mmR} must remain the same.

2) W must be reduced by a.

3) H, W_{aw}, W_{am}, W_{mw}, W_{mm} must be reduced by 'a^2'.

4) The reservoir must be horizontal.

5) t will be reduced by 'a^2'.

8.3.4.4 Approach #4 - Same Fluids, Same Porous Medium, Same Pressure Drop, Geometric Scaling Relaxed, Dispersion at High Flow Rate

The scaling groups that are satisfied in this approach are:

$$\frac{W}{L}, \frac{\mu_{lR}K_{aR}}{\mu_{aR}K_{lR}}, \frac{\mu_{mR}K_{aR}}{\mu_{aR}K_{mR}}, \frac{\rho_{lR}}{\rho_{aR}}, \frac{\rho_{mR}}{\rho_{aR}},$$

$$\frac{W_{amR}}{W_{awR}}, \frac{W_{mmR}}{W_{mwR}}, \phi_R, \frac{S_{aiR}}{S_{aR}}, \frac{S_{liR}}{S_{lR}},$$

$$\frac{A_{injR}}{L(\phi_R S_{aR} x_R d_{pR} L)^{1/2}}, \frac{P_{liR}}{P_{lR}}, \frac{P_{miR}}{P_{mR}}, \frac{P_{prod}}{P_{lR}},$$

$$\frac{H}{(\phi_R S_{aR} x_R d_{pR} L)^{1/2}}, \frac{W_{awR}\mu_{aR}}{\rho_{aR} K_{aR} P_{aR} (\phi_R S_{aR} x_R d_{pR} L)^{1/2}},$$

$$\frac{S_{aR} D^*_{amR} \mu_{aR}}{K_{aR} P_{aR} F_R}, \frac{D^*_{awR}}{D^*_{amR}}, \frac{D^*_{mmR}}{D^*_{mwR}}, \frac{C_{amR}}{C_{awR}}, \frac{C_{mwR}}{C_{mmR}},$$

In addition to the above requirements, all of the dimensionless properties must be the same function of their dimensionless variables for the prototype and the model. The implications of these scaling criteria for a model reduced in length by a scaling factor of 'a' and employing the same fluids as the prototype are:

1) ΔP_{max}, P_i, P_{prod}, K, ϕ, S_{ai}, F, C_{amR}, C_{mmR} must remain the same.

2) W must be reduced by a.

3) H, W_{aw}, W_{am}, W_{mw}, W_{mm} must be reduced by '$a^{1/2}$'

4) t will be reduced by 'a^2'.

8.3.4.5 Approach #5 - Same Fluids, Different Porous Media, Different Pressure Drop, Geometric Scaling Relaxed, Dispersion at High Flow Rate

The scaling groups that are satisfied in this approach are:

$$\frac{W}{L},\ \frac{\mu_{lR}K_{aR}}{\mu_{aR}K_{lR}},\ \frac{\mu_{mR}K_{aR}}{\mu_{aR}K_{mR}},\ \frac{\rho_{lR}}{\rho_{aR}},\ \frac{\rho_{mR}}{\rho_{aR}},$$

$$\frac{W_{amR}}{W_{awR}},\ \frac{W_{mmR}}{W_{mwR}},\ \phi_R,\ \frac{S_{aiR}}{S_{aR}},\ \frac{S_{liR}}{S_{lR}},$$

$$\frac{P_{liR}}{P_{lR}},\ \frac{P_{miR}}{P_{mR}},\ \frac{P_{prod}}{P_{lR}},\ \frac{A_{injR}P_{aR}}{L^3\rho_{aR}g_R},$$

$$\frac{HP_{aR}}{\rho_{aR}g_RL^2},\ \frac{W_{awR}\mu_{aR}}{\rho_{aR}^2g_RK_{aR}L^2}\ \frac{P_{aR}S_{aR}D^*_{apR}\mu_{aR}}{K_{aR}\rho_{aR}^2g_R^2F_RL^2},$$

$$\frac{D^*_{awR}}{D^*_{amR}},\ \frac{D^*_{mmR}}{D^*_{mwR}},\ \frac{C_{amR}}{C_{awR}},\ \frac{C_{mwR}}{C_{mmR}},$$

$$\frac{\phi_RS_{aR}x_RP_{aR}^2(K_{aR})^{1/2}}{\rho_{aR}^2g_R^2L^3}$$

In addition to the above requirements, all of the dimensionless properties have to be the same function of their dimensionless variables for the prototype and the model. The implications for a model reduced in length by a scaling factor of 'a' and employing the same fluids as the prototype are:

1) ϕ, S_{ai}, F, C_{amR}, C_{mmR} must be the same

2) L, W must be reduced by 'a',

3) K must be increased by '$a^{2/5}$'

4) ΔP_{max}, W_{aw}, W_{am}, W_{mm}, W_{mw} must be reduced by '$a^{8/5}$'

5) H must be reduced by '$a^{2/5}$', and

6) t will be reduced by '$a^{4/5}$'

8.3.5 Foam Injection - Four-Phase Flow

8.3.5.1 Approach #1 - Same Fluids, Different Porous Media, Different Pressure Drop, Geometric Similarity

The scaling groups that may be satisfied with this approach are:

$$\frac{W}{L},\ \frac{\mu_{lR}K_{aR}}{\mu_{aR}K_{lR}},\ \frac{\mu_{lR}K_{fR}}{\mu_{fR}K_{lR}},\ \frac{\mu_{qR}K_{aR}}{\mu_{aR}K_{gR}},$$

$$\frac{\rho_{lR}}{\rho_{aR}},\ \frac{\rho_{fR}}{\rho_{aR}},\ \frac{\rho_{qR}}{\rho_{aR}},\ \frac{A_{injR}}{L^2},$$

$$\frac{W_{asR}}{W_{awR}},\ \frac{W_{fsR}}{W_{fgR}},\ \frac{W_{lsR}}{W_{loR}},\ \frac{W_{fqR}}{W_{fwR}},\ \phi_R,$$

$$\frac{S_{liR}}{S_{lR}},\ \frac{S_{aiR}}{S_{aR}},\ \frac{S_{qiR}}{S_{gR}},$$

$$\frac{P_{liR}}{P_{lR}},\ \frac{P_{fiR}}{P_{fR}},\ \frac{P_{qiR}}{P_{gR}},\ \frac{P_{prod}}{P_{lR}},\ \frac{H}{L},$$

$$\frac{\rho_{aR}g_RL}{P_{aR}},\ \frac{W_{awR}\mu_{aR}}{K_{aR}P_{aR}\rho_{aR}L},\ \frac{S_{aR}D^*_{awR}\mu_{aR}}{K_{aR}P_{aR}F_R},$$

$$\frac{D^*_{loR}}{D^*_{lsR}},\ \frac{D^*_{awR}}{D^*_{asR}},\ \frac{D^*_{fwR}}{D^*_{fsR}},\ \frac{D^*_{fqR}}{D^*_{fsR}},$$

$$\frac{C_{loR}}{C_{lsR}}, \frac{C_{asR}}{C_{awR}}, \frac{C_{fsR}}{C_{fgR}}, \frac{C_{fwR}}{C_{fgR}}$$

In addition to the aforementioned requirements, all of the dimensionless properties must be the same function of their dimensionless variables for the prototype and the model. The implications of these scaling criteria for a model reduced in length by a scaling factor of 'a' are:

1) ϕ, S_{ai}, F, C_{asR}, C_{fsR}, C_{fwR}, C_{lsR} must remain the same.

2) H, W, ΔP_{max}, $(P_i - P_{prod})$, W_{aw}, W_{as}, W_{fs}, W_{ls}, W_{fg} must be reduced by 'a'.

3) K must be increased by 'a'.

4) t will be reduced by 'a^2'.

8.3.5.2 Approach #2 - Same Fluids, Same Porous Medium, Same Pressure Drop, Geometric Similarity

The scaling groups that may be satisfied with this approach are:

$$\frac{W}{L}, \frac{\mu_{lR}K_{aR}}{\mu_{aR}K_{lR}}, \frac{\mu_{lR}K_{fR}}{\mu_{fR}K_{lR}}, \frac{\mu_{gR}K_{aR}}{\mu_{aR}K_{gR}},$$

$$\frac{\rho_{lR}}{\rho_{aR}}, \frac{\rho_{fR}}{\rho_{aR}}, \frac{\rho_{gR}}{\rho_{aR}}, \frac{A_{injR}}{L^2},$$

$$\frac{W_{asR}}{W_{awR}}, \frac{W_{fsR}}{W_{fgR}}, \frac{W_{lsR}}{W_{loR}}, \frac{W_{fgR}}{W_{fwR}},$$

$$\phi_R, \frac{S_{aiR}}{S_{aR}}, \frac{S_{liR}}{S_{lR}}, \frac{S_{giR}}{S_{gR}},$$

$$\frac{P_{liR}}{P_{lR}},\ \frac{P_{fiR}}{P_{fR}},\ \frac{P_{giR}}{P_{gR}},\ \frac{P_{prod}}{P_{lR}},\ \frac{H}{L},$$

$$\frac{W_{awR}\mu_{aR}}{K_{aR}P_{aR}\rho_{aR}L},\ \frac{S_{aR}D^{*}_{awR}\mu_{aR}}{K_{aR}P_{aR}F_{R}},\ \frac{D^{*}_{fwR}}{D^{*}_{fsR}},\ \frac{D^{*}_{fgR}}{D^{*}_{fsR}},$$

$$\frac{D^{*}_{loR}}{D^{*}_{lsR}},\ \frac{D^{*}_{awR}}{D^{*}_{asR}},\ \frac{P_{aR}}{P_{claR}},\ \frac{P_{fR}}{P_{clfR}},\ \frac{P_{aR}}{P_{cafR}},$$

$$\frac{C_{loR}}{C_{lsR}},\ \frac{C_{asR}}{C_{awR}},\ \frac{C_{fsR}}{C_{fgR}},\ \frac{C_{fwR}}{C_{fgR}}$$

In addition to the above requirements, all of the dimensionless properties must be the same function of their dimensionless variables for the prototype and the model. The implications of these scaling criteria for a model reduced in length by a scaling factor of 'a' and employing the same fluids as the prototype are:

1) ΔP_{max}, P_i, P_{prod}, K, ϕ, S_{ai}, F, C_{asR}, C_{fsR}, C_{fwR}, C_{lsR} must be same.

2) H, W, W_{aw}, W_{as}, W_{fs}, W_{ls}, W_{fg} must be reduced by 'a'.

3) t will be reduced by 'a^2'.

8.3.5.3 Approach #3 - Same Fluids, Same Porous Medium, Same Pressure Drop, Geometric Scaling Relaxed

The scaling groups that are satisfied in this approach are:

$$\frac{W}{L},\ \frac{\mu_{lR}K_{aR}}{\mu_{aR}K_{lR}},\ \frac{\mu_{lR}K_{fR}}{\mu_{fR}K_{lR}},\ \frac{\mu_{gR}K_{aR}}{\mu_{aR}K_{gR}},\ \frac{\rho_{lR}}{\rho_{aR}},$$

$$\frac{A_{injR}}{L(\phi_R S_{aR} \chi_R d_{pR} L)^{1/2}}, \frac{\rho_{gR}}{\rho_{aR}}, \frac{\rho_{fR}}{\rho_{aR}},$$

$$\frac{W_{asR}}{W_{awR}}, \frac{W_{fsR}}{W_{fgR}}, \frac{W_{lsR}}{W_{loR}}, \frac{W_{fgR}}{W_{fwR}},$$

$$\phi_R, \frac{P_{liR}}{P_{lR}}, \frac{P_{fiR}}{P_{fR}}, \frac{P_{giR}}{P_{gR}},$$

$$\frac{S_{aiR}}{S_{aR}}, \frac{S_{liR}}{S_{lR}}, \frac{S_{giR}}{S_{gR}}, \frac{P_{prod}}{P_{lR}},$$

$$\frac{HP_{aR}}{\rho_{aR} g_R L^2}, \frac{W_{awR} \mu_{aR}}{K_{aR} \rho_{aR}^{2} g_R L^2}, \frac{S_{aR} D^*_{awR} \mu_{aR}}{K_{aR} P_{aR} F_R},$$

$$\frac{D^*_{loR}}{D^*_{lsR}}, \frac{D^*_{fwR}}{D^*_{fsR}}, \frac{D^*_{fgR}}{D^*_{fsR}}, \frac{D^*_{awR}}{D^*_{asR}},$$

$$\frac{C_{loR}}{C_{lsR}}, \frac{C_{asR}}{C_{awR}}, \frac{C_{fsR}}{C_{fgR}}, \frac{C_{fwR}}{C_{fgR}}$$

In addition to the above requirements, all of the dimensionless properties must be the same function of their dimensionless variables for the prototype and the model. The implications of these scaling criteria for a model reduced in length by a scaling factor of 'a' and employing the same fluids as the prototype are:

1) ΔP_{max}, P_i, P_{prod}, K, ϕ, S_{ai}, F, C_{asR}, C_{fsR}, C_{fwR}, C_{lsR} must remain the same.

2) W must be reduced by a.

3) H, W_{aw}, W_{as}, W_{fs}, W_{ls}, W_{fg} must be reduced by 'a^2'.

4) The reservoir must be horizontal.

5) t will be reduced by 'a^2'.

8.3.5.4 Approach #4 - Same Fluids, Same Porous Medium, Same Pressure Drop, Geometric Scaling Relaxed, Dispersion at High Flow Rate

The scaling groups that are satisfied in this approach are:

$$\frac{W}{L},\ \frac{\mu_{lR}K_{aR}}{\mu_{aR}K_{lR}},\ \frac{\mu_{lR}K_{fR}}{\mu_{fR}K_{lR}},\ \frac{\mu_{gR}K_{aR}}{\mu_{aR}K_{gR}},\ \frac{\rho_{lR}}{\rho_{aR}},\ \frac{\rho_{fR}}{\rho_{aR}},$$

$$\frac{W_{asR}}{W_{awR}},\ \frac{W_{fsR}}{W_{fgR}},\ \frac{W_{lsR}}{W_{loR}},\ \frac{W_{fgR}}{W_{fwR}},\ \phi_R,$$

$$\frac{P_{liR}}{P_{lR}},\ \frac{P_{fiR}}{P_{fR}},\ \frac{P_{giR}}{P_{gR}},\ \frac{S_{aiR}}{S_{aR}},$$

$$\frac{S_{giR}}{S_{gR}},\ \frac{S_{liR}}{S_{lR}},\ \frac{P_{prod}}{P_{lR}},\ \frac{H}{(\phi_R S_{aR} x_R d_{pR} L)^{1/2}},$$

$$\frac{A_{injR}}{L(\phi_R S_{aR} x_R d_{pR} L)^{1/2}},\ \frac{W_{awR}\mu_{aR}}{\rho_{aR} K_{aR} P_{aR}(\phi_R S_{aR} x_R d_{pR} L)^{1/2}},$$

$$\frac{S_{aR} D^*_{awR}\mu_{aR}}{K_{aR} P_{aR} F_R},\ \frac{D^*_{fwR}}{D^*_{fsR}},\ \frac{D^*_{fgR}}{D^*_{fsR}},$$

$$\frac{D^*_{loR}}{D^*_{lsR}},\ \frac{C_{asR}}{C_{awR}},\ \frac{C_{loR}}{C_{lsR}},\ \frac{C_{fwR}}{C_{fgR}},\ \frac{P_{prod}}{P_{lR}}$$

In addition to the above requirements, all of the dimensionless properties must be the same function of their dimensionless variables for the prototype and the model. The implications of these scaling criteria for a model reduced in length by a scaling factor of 'a' and employing the same fluids as the prototype are:

1) ΔP_{max}, P_i, P_{prod}, K, ϕ, S_{ai}, F, C_{asR}, C_{fsR}, C_{fwR}, C_{lsR} must remain the same.

2) W must be reduced by a.

3) H, W_{aw}, W_{as}, W_{fs}, W_{ls}, W_{fg} must be reduced by '$a^{1/2}$'.

4) t will be reduced by 'a^2'.

8.3.5.5 Approach #5 - Same Fluids, Different Porous Media, Different Pressure Drop, Geometric Scaling Relaxed, Dispersion at High Flow Rate

The scaling groups that are satisfied in this approach are:

$$\frac{W}{L}, \frac{\mu_{lR}K_{aR}}{\mu_{aR}K_{lR}}, \frac{\mu_{lR}K_{fR}}{\mu_{fR}K_{lR}}, \frac{\mu_{gR}K_{aR}}{\mu_{aR}K_{gR}}, \frac{\rho_{lR}}{\rho_{aR}},$$

$$\frac{\rho_{fR}}{\rho_{aR}}, \frac{A_{injR}P_{aR}}{L^3\rho_{aR}g_R},$$

$$\frac{W_{asR}}{W_{awR}}, \frac{W_{fsR}}{W_{fgR}}, \frac{W_{lsR}}{W_{loR}}, \frac{W_{fgR}}{W_{fwR}},$$

$$\phi_R, \frac{P_{liR}}{P_{lR}}, \frac{P_{fiR}}{P_{fR}}, \frac{P_{giR}}{P_{gR}},$$

$$\frac{S_{aiR}}{S_{aR}}, \frac{S_{giR}}{S_{gR}}, \frac{S_{liR}}{S_{lR}},$$

$$\frac{P_{prod}}{P_{lR}}, \frac{HP_{aR}}{\rho_{aR}g_RL^2}, \frac{W_{awR}\mu_{aR}}{\rho_{aR}{}^2g_RK_{aR}L^2}$$

$$\frac{P_{aR}S_{aR}D^*_{apR}\mu_{aR}}{K_{aR}\rho_{aR}{}^2g_R{}^2F_RL^2}, \frac{D^*_{fwR}}{D^*_{fsR}},$$

$$\frac{D^*_{fgR}}{D^*_{fsR}}, \frac{D^*_{loR}}{D^*_{lsR}}, \frac{C_{asR}}{C_{awR}}, \frac{C_{loR}}{C_{lsR}},$$

$$\frac{C_{fwR}}{C_{fgR}}, \frac{P_{prod}}{P_{lR}}$$

In addition to the above requirements, all of the dimensionless properties have to be the same function of their dimensionless variables for the prototype and the model. The implications for a model reduced in length by a scaling factor of 'a' and employing the same fluids as the prototype are:

1) ϕ, S_{ai}, F, C_{asR}, C_{fsR}, C_{fwR}, C_{lsR} must be the same

2) L, W must be reduced by 'a'

3) K must be increased by '$a^{2/5}$'

4) ΔP_{max}, W_{aw}, W_{as}, W_{fs}, W_{ls}, W_{fg} must be reduced by '$a^{8/5}$'

5) H must be reduced by '$a^{2/5}$', and

6) t will be reduced by '$a^{4/5}$'

8.3.6 Foam Injection: Three-Phase Flow

8.3.6.1 Approach #1 - Same Fluids, Different Porous Media, Different Pressure Drop, Geometric Similarity

The scaling groups that may be satisfied with this approach are:

$$\frac{W}{L}, \frac{\mu_{lR}K_{aR}}{\mu_{aR}K_{lR}}, \frac{\mu_{lR}K_{fR}}{\mu_{fR}K_{lR}}, \frac{\rho_{lR}}{\rho_{aR}}, \phi_R, \frac{\rho_{fR}}{\rho_{aR}},$$

$$\frac{A_{injR}}{L^2}, \frac{W_{asR}}{W_{awR}}, \frac{W_{lsR}}{W_{loR}}, \frac{S_{liR}}{S_{lR}},$$

$$\frac{S_{aiR}}{S_{aR}}, \frac{P_{liR}}{P_{lR}}, \frac{P_{fiR}}{P_{fR}}, \frac{P_{prod}}{P_{lR}},$$

$$\frac{H}{L}, \frac{\rho_{aR} g_R L}{P_{aR}}, \frac{W_{awR} \mu_{aR}}{K_{aR} P_{aR} \rho_{aR} L},$$

$$\frac{S_{aR} D^*_{awR} \mu_{aR}}{K_{aR} P_{aR} F_R}, \frac{D^*_{loR}}{D^*_{lsR}}, \frac{D^*_{awR}}{D^*_{asR}},$$

$$\frac{D^*_{fwR}}{D^*_{fsR}}, \frac{C_{loR}}{C_{lsR}}, \frac{C_{asR}}{C_{awR}}$$

In addition to the aforementioned requirements, all of the dimensionless properties must be the same function of their dimensionless variables for the prototype and the model. The implications of these scaling criteria for a model reduced in length by a scaling factor of 'a' are:

1) ϕ, S_{ai}, F, C_{asR}, C_{fsR}, C_{fwR}, C_{lsR} must remain the same.

2) H, W, ΔP_{max}, $(P_i - P_{prod})$, W_{aw}, W_{as}, W_{fs}, W_{ls} must be reduced by 'a'.

3) K must be increased by 'a'.

4) t will be reduced by 'a^2'.

8.3.6.2 Approach #2 - Same Fluids, Same Porous Medium, Same Pressure Drop, Geometric Similarity

The scaling groups that may be satisfied with this approach are:

$$\frac{W}{L},\ \frac{\mu_{lR}K_{aR}}{\mu_{aR}K_{lR}},\ \frac{\mu_{lR}K_{fR}}{\mu_{fR}K_{lR}},\ \frac{\rho_{lR}}{\rho_{aR}},\ \frac{\rho_{fR}}{\rho_{aR}},\ \phi_R,$$

$$\frac{W_{asR}}{W_{awR}},\ \frac{W_{lsR}}{W_{loR}},\ \frac{S_{aiR}}{S_{aR}},\ \frac{S_{liR}}{S_{lR}},\ \frac{A_{injR}}{L^2},$$

$$\frac{P_{liR}}{P_{lR}},\ \frac{P_{fiR}}{P_{fR}},\ \frac{P_{prod}}{P_{lR}},\ \frac{H}{L},$$

$$\frac{W_{awR}\mu_{aR}}{K_{aR}P_{aR}\rho_{aR}L},\ \frac{S_{aR}D^*_{awR}\mu_{aR}}{K_{aR}P_{aR}F_R},\ \frac{D^*_{fwR}}{D^*_{fsR}},$$

$$\frac{D^*_{loR}}{D^*_{lsR}},\ \frac{D^*_{awR}}{D^*_{asR}},\ \frac{P_{aR}}{P_{claR}},\ \frac{P_{fR}}{P_{clfR}},\ \frac{C_{loR}}{C_{lsR}},$$

$$\frac{C_{asR}}{C_{awR}}$$

In addition to the above requirements, all of the dimensionless properties must be the same function of their dimensionless variables for the prototype and the model. The implications of these scaling criteria for a model reduced in length by a scaling factor of 'a' and employing the same fluids as the prototype are:

1) ΔP_{max}, P_i, P_{prod}, K, ϕ, S_{ai}, F, C_{asR}, C_{fsR}, C_{fwR}, C_{lsR} must be same.

2) H, W, W_{aw}, W_{as}, W_{fs}, W_{ls} must be reduced by 'a'.

3) t will be reduced by 'a^2'.

8.3.6.3 Approach #3 - Same Fluids, Same Porous Medium, Same Pressure Drop, Geometric Scaling Relaxed

The scaling groups that are satisfied in this approach are:

$$\frac{W}{L}, \frac{\mu_{lR}K_{aR}}{\mu_{aR}K_{lR}}, \frac{\mu_{lR}K_{fR}}{\mu_{fR}K_{lR}}, \frac{\rho_{lR}}{\rho_{aR}}, \frac{\rho_{fR}}{\rho_{aR}},$$

$$\frac{W_{asR}}{W_{awR}}, \frac{W_{lsR}}{W_{loR}}, \frac{A_{injR}P_{aR}}{L^3\rho_{aR}g_R}, \phi_R,$$

$$\frac{P_{liR}}{P_{lR}}, \frac{P_{fiR}}{P_{fR}}, \frac{S_{aiR}}{S_{aR}}, \frac{S_{liR}}{S_{lR}}, \frac{P_{prod}}{P_{lR}},$$

$$\frac{HP_{aR}}{\rho_{aR}g_RL^2}, \frac{W_{awR}\mu_{aR}}{K_{aR}\rho_{aR}^2g_RL^2}, \frac{S_{aR}D^*_{awR}\mu_{aR}}{K_{aR}P_{aR}F_R},$$

$$\frac{D^*_{loR}}{D^*_{lsR}}, \frac{D^*_{fwR}}{D^*_{fsR}}, \frac{D^*_{awR}}{D^*_{asR}}, \frac{C_{loR}}{C_{lsR}}, \frac{C_{asR}}{C_{awR}}$$

In addition to the above requirements, all of the dimensionless properties must be the same function of their dimensionless variables for the prototype and the model. The implications of these scaling criteria for a model reduced in length by a scaling factor of 'a' and employing the same fluids as the prototype are:

1) ΔP_{max}, P_i, P_{prod}, K, ϕ, S_{ai}, F, C_{asR}, C_{fsR}, C_{fwR}, C_{lsR} must remain the same.

2) W must be reduced by a.

3) H, W_{aw}, W_{as}, W_{fs}, W_{ls} must be reduced by 'a^2'.

4) The reservoir must be horizontal.

5) t will be reduced by 'a^2'.

8.3.6.4 Approach #4 - Same Fluids, Same Porous Medium, Same Pressure Drop, Geometric Scaling Relaxed, Dispersion at High Flow Rate

The scaling groups that are satisfied in this approach are:

$$\frac{W}{L}, \frac{\mu_{lR}K_{aR}}{\mu_{aR}K_{lR}}, \frac{\mu_{lR}K_{fR}}{\mu_{fR}K_{lR}}, \frac{\rho_{lR}}{\rho_{aR}}, \frac{\rho_{fR}}{\rho_{aR}}, \phi_R,$$

$$\frac{A_{injR}}{L(\phi_R S_{aR} x_R d_{pR} L)^{1/2}}, \frac{W_{asR}}{W_{awR}}, \frac{W_{lsR}}{W_{loR}},$$

$$\frac{P_{liR}}{P_{lR}}, \frac{P_{fiR}}{P_{fR}}, \frac{S_{aiR}}{S_{aR}}, \frac{S_{liR}}{S_{lR}},$$

$$\frac{P_{prod}}{P_{lR}}, \frac{H}{(\phi_R S_{aR} x_R d_{pR} L)^{1/2}},$$

$$\frac{W_{awR}\mu_{aR}}{\rho_{aR}K_{aR}P_{aR}(\phi_R S_{aR} x_R d_{pR} L)^{1/2}}, \frac{S_{aR}D^{*}_{awR}\mu_{aR}}{K_{aR}P_{aR}F_R},$$

$$\frac{D^{*}_{fwR}}{D^{*}_{fsR}}, \frac{D^{*}_{loR}}{D^{*}_{lsR}}, \frac{C_{asR}}{C_{awR}}, \frac{C_{loR}}{C_{lsR}},$$

$$\frac{P_{prod}}{P_{lR}}$$

In addition to the above requirements, all of the dimensionless properties must be the same function of their dimensionless variables for the prototype and the model. The implications of these scaling criteria for a model reduced in length by a scaling factor of 'a' and employing the same fluids as the prototype are:

1) ΔP_{max}, P_i, P_{prod}, K, ϕ, S_{ai}, F, C_{asR}, C_{fsR}, C_{fwR}, C_{lsR} must remain the same.

2) W must be reduced by a.

3) H, W_{aw}, W_{as}, W_{fs}, W_{ls} must be reduced by '$a^{1/2}$'

4) t will be reduced by 'a^2'.

8.3.6.5 Approach #5 - Same Fluids, Different Porous Media, Different Pressure Drop, Geometric Scaling Relaxed, Dispersion at High Flow Rate

The scaling groups that are satisfied in this approach are:

$$\frac{W}{L},\ \frac{\mu_{lR}K_{aR}}{\mu_{aR}K_{lR}},\ \frac{\mu_{lR}K_{fR}}{\mu_{fR}K_{lR}},\ \frac{\rho_{lR}}{\rho_{aR}},\ \frac{\rho_{fR}}{\rho_{aR}},\ \phi_R,$$

$$\frac{A_{injR}P_{aR}}{L^3\rho_{aR}g_R},\ \frac{W_{asR}}{W_{awR}},\ \frac{W_{lsR}}{W_{loR}},$$

$$\frac{P_{liR}}{P_{lR}},\ \frac{P_{fiR}}{P_{fR}},\ \frac{S_{aiR}}{S_{aR}},\ \frac{S_{liR}}{S_{lR}},$$

$$\frac{P_{prod}}{P_{lR}},\ \frac{HP_{aR}}{\rho_{aR}g_RL^2},\ \frac{W_{awR}\mu_{aR}}{\rho_{aR}^2g_RK_{aR}L^2}$$

$$\frac{P_{aR}S_{aR}D^*_{apR}\mu_{aR}}{K_{aR}\rho_{aR}^2g_R^2F_RL^2},\ \frac{D^*_{fwR}}{D^*_{fsR}},\ \frac{D^*_{loR}}{D^*_{lsR}},$$

$$\frac{C_{asR}}{C_{awR}},\ \frac{C_{loR}}{C_{lsR}},\ \frac{P_{prod}}{P_{lR}}$$

In addition to the above requirements, all of the dimensionless properties have to be the same function of their dimensionless variables for the prototype and the model. The implications for a model reduced in length by a scaling factor of 'a' and employing the same fluids as the prototype are:

1) ϕ, S_{ai}, F, C_{asR}, C_{fsR}, C_{fwR}, C_{lsR} must be the same.
2) L, W must be reduced by 'a'.
3) K must be increased by '$a^{2/5}$'.
4) ΔP_{max}, W_{aw}, W_{as}, W_{fs}, W_{ls} must be reduced by '$a^{8/5}$'.
5) H must be reduced by '$a^{2/5}$'.
6) t will be reduced by '$a^{4/5}$'.

8.4 Dimensional Analysis

The similarity groups can also be derived by dimensional analysis. This method consists of selecting the relevant variables for the process. Similarity groups can be obtained by using the Buckingham π-theorem (Johnstone and Thring, 1957). Table 8.1 lists the symbols, dimensions and a description of the variables selected. There are only two new groups which did not appear when using inspectional analysis. They are the Reynolds number ($\rho v k^{1/2}/\mu$) and the ratio k/l^2. Geertsma et al.(1956) pointed out that the group k/L^2 may be relaxed if the average diameter of the pores is much smaller than the smallest dimension of the reservoir. In addition, when the flow is slow (creeping flow) in both the model and the prototype, the influence of the inertial forces is not significant, so that the Reynolds number can also be relaxed. Also, another scaling group ($\sigma/P_c^{1/2}$), which was obtained by dimensional analysis, did not arise explicitly in the inspectional analysis; but, as was pointed out by Kimber et al.(1986), the requirement that

Table 8.1 List of Variables Considered for Dimensional Analysis

Symbol	Dimensions	Description
l,L	L	Well spacing
H	L	Thickness of the oil zone
ρ_i	M/L^3	Density '
g	L/t^2	Acceleration due to gravity
P_i	M/Lt^2	Pressure
k_i	L^2	Effective permeability
μ_i	M/Lt	Viscosity
ϕ	___	Porosity
D_{Lij}	L^2/t	Logitudinal dispersion
D_{Tij}	L^2/t	Transverse disperssion
P_{cij}	M/Lt^2	Capillary pressure
W_{ai}	M/t	Injection rate of water
σ_{ij}	M/t^2	Interfacial tension between phases
v	L/t	superficial velocity

'i=water, oil, emulsion, foam, polymer
j=different phases, such as aqueous, oleic, etc.

the dimensionless capillary pressures be the same function of their dimensionless variables implies that this or a similar group must be satisfied. In order to avoid redundancy, the similarity groups derived by dimensional analysis are not listed here.

8.5 COMPARISON OF DIFFERENT SCALING APPROACHES

8.5.1 Polymer Flood

Since gravitational effects are not important in this system, Approach #2 gives rise to the most suitable set. As this approach uses the same porous medium for the model and the prototype, the effect of adsorption and retention (the most important phenomena in polymer flooding) may be properly scaled. Moreover, this approach does not risk altering the irreducible saturation or relative permeabilities as is the case with Approach #1. Approach #3, which uses the same fluids and porous medium, scales gravitational effects properly at the expense of relaxing geometric similarity. However, the effect of dispersion is accounted for in this approach. This might be a point of concern as dispersion is not negligible in a waterflood following polymer injection. Approaches #1 and #2 scale the effect of diffusion properly. However, for the case of polymer injection, dispersion is a more important phenomenon. Pozzi and Blackwell (1963) determined conditions for miscible processes where scaling of viscous and dispersive forces can be achieved by relaxing the geometric and gravitational scaling requirements. Approach #4 properly scales dispersion at the cost of poorly scaling gravitational and capillary forces. However, as it uses the same porous medium, it scales relative permeability and irreducible saturations properly. Approach #5 properly scales gravitational forces and dispersion but suffers from the same shortcomings as Approach #1.

If polymer is considered to be a mobility control agent for a heterogeneous reservoir (such as a reservoir containing a bottom-water zone), the resistance factor plays an important role. In order to obtain a similar resistance factor, adsorption and mechanical entrapment should be similar in the model and the prototype. This shows the need of using the same porous media for the model and the prototype. Dispersion plays an important role in polymer flooding but a more dominant mechanism is the viscous instability which arises when a waterflood follows a polymer flood. The contribution of the dispersion factor may be revealed by comparing the results from Approaches #2 and #4.

As has been mentioned, in order to have the same reference concentration in the model and the prototype, a similar polymer concentration and type should be used. This would ensure the scaling of the pressure-dependent properties, adsorption, and the blocking action of the polymer.

8.5.2 Emulsion Flood

Three different cases of emulsion flooding were studied. However, each of these cases is applicable, depending on the quality of the emulsions used. It is possible to obtain an emulsion that is miscible in both the aqueous and the oleic phases. On the other hand, a low-quality emulsion would be practically immiscible in the oleic phase. In either case, the effect of dispersion is important in the aqueous phase. Unlike a polymer flood, no resistance factor is involved in the governing equations for emulsion displacements. However, the blocking action may be incorporated by modifying the relative permeability of the phases considered. The fact that the emulsion does improve the oil recovery by more than what would have been recovered, by just improving the mobility ratio, makes the scaling more complicated. When emulsion is being considered as a blocking agent, matching the relative permeability curves is more important. This emphasizes the need of having the same porous media for the model and the prototype. Approach #4, because the use of the same porous medium results in proper scaling of the dispersion terms, needs to be considered for best scaling results.

In order to have the same reference concentration in the model and prototype, the same type and quality of emulsion must be used. The emulsion quality will also dictate similar dispersion and diffusion. Viscous instability is not a major factor to be considered in an emulsion flood and therefore scaling dispersion and diffusion should lead to adequate results.

8.5.3 Foam Injection

Foam injection is the only system for which gravity plays an important role. This leads to the choice of Approach #3 in which gravity effects are scaled properly. However, scaling foam injection would need a most careful treatment because the recovery depends largely on factors, such as type and concentration of surfactant, absolute permeability, and even injection pressure. The same concentration and quality of foam is needed in order to ensure a similar blocking action with respect to nitrogen. This will also ensure similar foam stability and bubble size, factors that play an important role in the blocking action of the foam. Also, the type of porous medium plays an important role unless the permeability-sensitive region is avoided.

As has been pointed out, if four different phases are flowing simultaneously, a more detailed study is necessary in order to match the relative permeability data. This problem may be avoided only when the amount of surfactant is such that only three-phase flow takes place in the system.

In this situation, a foam flood may be treated as a three-phase problem, if a single set of relative permeability data is capable of representing the process adequately.

A puzzling factor is that the behaviour of all three mobility control agents is different in homogeneous and heterogeneous porous media. It was observed in the experimental part of this study that the improvement for foam is better in the presence of a bottom water zone. For polymer floods, this is a well-known fact. These observations suggest that the existence of a bottom-water zone should be considered as a global phenomenon and the scaling groups have to be reconsidered. It is postulated that when a bottom-water zone is present its existence does not show only in terms of the oil-to-water zone thickness ratio and that the resistance factor or blocking mechanism have to be considered.

9. SUMMARY AND CONCLUSIONS

Based on the experimental results presented here, the following observations and conclusions can be made.

(1) The presence of a bottom-water layer adversely affects the waterflood performance of a reservoir model, the permeability (k_o/k_b), thickness (h_b/h_o), and viscosity ratios (μ_o/μ_w) being the controlling parameters. For very high value of any of these parameters the waterflood recovery is very small (k_o and k_b are the absolute permeabilities and h_o and h_b are the thicknesses of the oil and water zones, respectively).

(2) For $k_o/k_b=1$, polymer flood gives the highest oil recovery improvement over a waterflood, with increasing improvement as the h_b/h_o value increases. This trend is followed by emulsion, silica gel and foam floods. Air and biopolymer gel give improvements comparable to the others only for smaller values of h_b/h_o.

For a permeability ratio of 2.67, the relative improvement over a waterflood is the highest with a polymer flood even though air injection gives the highest oil recovery during the initial stages of the displacement test. Silica gel injection also shows good performance. However, the maximal improvement over a waterflood is less than two-fold, mainly due to the good waterflood performance for this range of permeability ratios. Only emulsion and air show decreasing improvement as the thickness ratio increases. Foam flood performance is the poorest over most of the thickness ratio. For a value of $k_o/k_b=0.06$, the best improvement is shown by polymer and silica gel.

For a high oil viscosity (200 mPa.s), emulsion, polymer, and foam floods improve oil recovery significantly as compared to a waterflood (around 15-fold improvement over waterflood). The emulsion floods perform better than either polymer or foam floods.

For very low values of the viscosity ratio, μ_o/μ_w (e.g., 1.0 and 7.5), and for an h_b/h_o value of 0.33 and a k_o/k_b value of 1, a waterflood outperforms any mobility control agent.

(3) For polymer injection, a slug of 0.75 PV_b and of viscosity of around 60 mPa.s is optimal for $h_b/h_o=0.33$. Injection of a polymer slug at the beginning of a displacement test is more advantageous than the injection after an initial waterflood, unless the waterflood performance is extremely poor. Injecting polymer slugs alternating with water does not perform as well as continuous polymer injection. It is preferable to inject polymer closer to the bottom-water zone only for thickness ratios smaller than one.

(4) A 10% O/W emulsion (200 ppm surfactant in the water phase) is most effective in blocking the bottom-water zone. The minimal volume of emulsion slug required to produce any blockage is one pore volume of the bottom-water zone.

However, an emulsion slug of 2.5 PV_b is optimal and reduces the bottom-water zone permeability permanently.

(5) An impermeable barrier length of around 50% of total flow path is required before any significant oil recovery occurs for a thickness ratio of 0.33. However, a considerable improvement over a waterflood is observed with smaller barriers for a thickness ratio of 0.33.

(6) Air injection improves the efficiency of a waterflood in all cases studied. This is mainly due to the presence of an extra (gas) phase in the bottom-water zone. Injecting air through a production well is more beneficial than injecting through the injection well.

(7) Injection of gel produced from biopolymer with Cr^{+3} cross-linking is not effective in blocking the bottom-water zone.

(8) Foam generated in situ performs the best when the bottom water permeability is the same as the oil zone permeability. Alternating surfactant water with nitrogen gives good results, whereas alternating with slugs of water 'washes away' the foam.

(9) The new approach developed can numerically simulate polymer blockage in the presence of a bottom-water zone. The agreement between experimental and numerical results was found to be excellent.

(10) Emulsion flow in an oil reservoir zone can be effectively simulated by employing a three-phase,

three-dimensional model, which incorporates a novel approach for absolute permeability reduction. The amount of reduction in permeability depends on the initial value of the permeability and the emulsion throughput.

(11) Different possible theoretical representations of polymer, emulsion, and foam flow are investigated to obtain, for the first time, a complete set of scaling groups for these processes. Five different approaches are considered in order to scale the different mechanisms properly. It is shown that, in order to scale a certain phenomenon properly, certain scaling requirements must be relaxed. The sets of scaling groups depend on the nature of the flow occurring.

(12) The scaling of a heterogeneous (e.g. an oil reservoir with a bottom-water zone) porous medium needs careful consideration because heterogeneity does not appear as a single scaling group. Polymer, emulsion, and foam are all very effective mobility control agents in hetergeneous porous media due to their ability to reduce the effects of heterogeneity. Consequently, while scaling heterogeneous porous media, the specific mechanisms that make these agents effective in mobility control must be scaled properly.

10. REFERENCES

Abou-Kassem, J.H, and Farouq Ali, S.M., 1986,"Evaluation of Emulsion Flow in Porous Media", Submitted for publication to Soc. Pet. Eng. J.

Abou-Kassem, J.H., and Farouq Ali, S.M., 1986a, "Mathematical Representation of Single-Phase Emulsion Flow in Porous Media", Submitted for publication to Soc. Pet. Eng. J.

Al-Khafaji, A.H., Wang, P.F., Castanier, L.M., 1982 and Brigham, W.E., "Steam Surfactant Systems at Reservoir Conditions", Paper SPE 10777, 52nd California Regional Meeting held in San Francisco, CA.

Al-Seehati, S.A., 1979,"Numerical Simulation of the Micellar-Polymer Slug Process for a One-Dimensional, Two-Phase, and Four-Component System with Interphase Mass Transfer", Ph.D. Dissertation, Pennsylvania State University.

Alvarado, D.A., 1975, "The Flow of Macroemulsions Through Porous Media", Ph.D. Dissertation, Dept. of Pet. Eng., Stanford University,

Barnes, A.L., 1962, " The Use of a Viscous Slug to Improve Waterflood Efficiency In a Reservoir Partially Invaded by Bottom Water", J. Pet. Tech., Oct., pp. 1147-1153.

Bear, J. and Bachmat, Y., 1982, "Transport Phenomena in Porous Media - Basic Equations", Presented at the NATO Advanced Study Institute on Mechanics of Fluids in Porous Media", Newark, Delaware.

Becher, P., 1965, Emulsion: Theory and Practice, Reinhold Publishing Corporation, N.Y., pp. 2, 59-85.

Bentsen, R.G., 1978, "Conditions Under Which the Capillary Term May Be Neglected", J. Can. Pet. Tech., 17(4), p. 25.

Bentsen, R.G., 1985, "A New Approach to Instability Theory in Porous Media", Soc. Pet. Eng. J., 15, Oct., p.765-779.

Bernard, G.G., 1963, "Effect of Foam on Recovery of Oil by Gas-Drive", Producers Monthly, Jan., pp. 18-21.

Bernard, G.G., Holm, L.W., and Jacobs, W.A., 1965, "Effect of Foam on Trapped Gas Saturation and on Permeability of Porous Media to Water", Soc. Pet. Eng. J., 5, pp. 295-300.

Bernard, G.G., and Holm, L.W., 1964, "Effect of Foam on Permeability of Porous Media to Gas", Soc. Pet. Eng. J., 4(4), pp. 267-274.

Best, D.A., Tam, E.S., and Isaacs, E., 1985, "A Discussion on the Mechanism of Foam Flow Through Porous Media", Paper presented at the 3rd International Conference on Heavy Crude and Tar Sands, UNITAR, held in Longbeach, CA.

Bond, D.G., and Bernard, G.G., 1966, "Rheology of Foams in Porous Media", Paper presented at the SPE-AIChE Joint Symposium, Dallas, TX.

Bondor, P.L., Hirasaki, G.J., and Tham, M.J., 1972, "Mathematical Simulation of Polymer Flooding in Complex Reservoirs", Soc. Pet. Eng. J., 12(4), pp. 369-382.

Borchardt, J.K., Bright, D.B., Dickson, M.K., and Wellington, S.L., 1985, "Surfactant for CO_2 Foam Flooding", Paper SPE 14394, presented at the 60th Annual Technical Conference and Exhibition held in Las Vegas, NV.

Broz, J.S., French, T.R., and Caroll, H.B., 1985, "Blocking of High Permeability Zones in Steamflooding by Emulsions", Paper presented at the 3rd International Conference on Heavy Crude and Tar Sands, UNITAR, California.

Burcik, E.J., 1967, "Pseudo-Dilatant Flow of Polyacrylamide Solutions in Porous Media", Producers Monthly, 32(3), pp. 27-31.

Burcik, E.J., and Ferrer, J., 1968, "The Mechanism of Pseudo Dilatant Flow", Producers Monthly, 32(3), pp. 7-10.

Chatenever, A., and Calhoun, J.C., 1952, "Visual Examination of Fluid Behavior in Porous Media", Trans. AIME, 195, pp. 149-155.

Coskuner, G., and Bentsen, R.G., 1987, "Prediction of Instability for Miscible Displacements in a Hele-Shaw Cell, Rev. de l'IFP, 42(2), pp. 151-162.

Cooke, C.E., Williams, R.E., and Kolodzie, P.A., 1974, "Oil Recovery by Alkaline Waterflooding", J. Pet. Tech., Dec., pp. 1365-1374.

Dabbous, M.K., 1977, "Displacement of Polyacrylamide in Waterflooded Porous Media and Its Effects on a Subsequent Micellar Flood", Soc. Pet. Eng. J., 17, Oct., pp. 358-368.

Dauben, D.L., and Menzie, D.E., 1967, "Flow of Polymer Solutions Through Porous Media", J. Pet. Tech., Aug., pp. 1065-1072.

Duerksen, J.H., 1984, "Laboratory Study of Foaming Surfactants as Steam-Diverting Additives", Paper SPE 12785, presented at the 54th California Regional Meeting held in Longbeach, CA.

Dawson, R., and Lantz, R.B., 1972, "Inaccessible Pore Volume in Polymer Flooding", Soc. Pet. Eng. J., 12, Oct., pp. 448-452.

Demetre, G.P, Bentsen, R.G., and Flock, D.L., 1982, "A Multi-Dimensional Approach to Scaled Immiscible Fluid Displacement", J. Can. Pet. Tech., 21(4), pp. 49-61.

Desremaux, L., Chauveteau, G., and Martin, M., 1971, "Comportement des Solutions de Polymers en Milieu Poreux", Rev. de l'IFP, 26(6), pp. 495-519.

Dominguez, J.G., and Willhite, G.P., 1977, "Retention and Flow Characteristics of Polymer Solutions in Porous Media", Soc. Pet. Eng. J., 17, April, pp. 111-121.

Duda, J.L., Klaus, E.E., and Fan, S.K., 1981, "Influence of Polymer-Molecule/Wall Interactions on Mobility Control", Soc. Pet. Eng. J., 21, pp. 613-622.

Eson, R.L., Fitch, J.P., and Shannon, A.M., 1981, "North Kern Front Field Steam Drive with Ancillary Materials", Paper SPE/DOE 9778, presented at the Second Joint Symposium on Enhanced Oil Recovery held in Tulsa, Okla.

Eson, R.L. and O'Nesky, S.K., 1982 "Evaluation of a Conventional Steam Drive with Ancillary Materials: North Kern Front Field", Paper SPE 10775, presented at the 52nd California Regional Meeting held in San Francisco, CA.

Eson, R.L. and O'Nesky, S.K., 1983a "The Application of In-Situ Steam Foams to Improve Recovery In Mature Steam Drives", Paper SPE 11704, presented at the 53rd California Regional Meeting held in Ventura, CA.

Eson, R.L., 1983b, "Improvement in Sweep Efficiencies in Thermal Oil-Recovery Projects Through the Application of In-Situ Foams", Paper SPE 11806, International Symposium on Oilfield and Geothermal Chemistry held in Denver, CO.

Eson, R.L, Cooke, R.W., 1985, "Field Results of Steam Diversion Agents in Cyclic Steam Applications", Paper presented at the 3rd International Conference on Heavy Crude and Tar Sands, UNITAR, held in Longbeach, CA.

Falls, A.H., Lawson, J.B., and Hirasaki, G.J., 1986, "The Role of Noncondensible Gas in Steam Foams", Paper SPE 15053, Paper presented at the 56th California Regional Meeting held in Oakland, CA.

Farouq Ali, S.M., and Selby, R.J., 1986, "Function, Characteristics of EOR Foam Behavior Covered in Laboratory Investigations", *Oil and Gas J.*, Feb. 3, pp. 57-63.

Farouq Ali, S.M., Thomas, S., and Baharu, R., 1986, "Tertiary Recovery of Two Alberta Oils by Micellar Flooding", Paper presented at the 38th ATM of the PS of CIM, Calgary.

Fiedmann, F. and Jensen, J.A., 1986, "Some Parameters Influencing the Formation and Propagation of Foams in Porous Media", Paper SPE 15087, presented at the 56th California Regional Meeting held in Oakland, CA.

Fitch, R.A., and Griffith, J.D., 1964, "Experimental and Calculated Performance of Miscible Floods in Stratified Reservoirs", *J. Pet. Tech.*, Nov., pp. 1289-1298.

Flemming, P.D., Thomas, C.P., and Winter, W.K., 1981, "Formulation of a General Multiphase, Multicomponent Chemical Flood Model", *Soc. Pet. Eng. J.*, 21(1), pp. 63-76.

Fried, A.N., 1961, "The Foam Drive Process for Increased Recovery of Oil", U.S. Bureau of Mines Report #5866.

Geertsma, J., Croes, G.A., and Schwarz, N., 1956, "Theory of Dimensionally Scaled Models of Petroleum Reservoirs", *Trans. AIME*, 207, pp. 118-127.

Gogarty, W.B., 1967, "Mobility Control with Polymer Solutions", *Soc. Pet. Eng. J.*, 7, June, pp. 161-170.

Greaser, G.R. and Shore, R.A., 1981, "Steamflood Performance in the Kern River Field", Paper SPE 8834, Second Joint Paper SPE/DOE Symposium of Enhanced Oil Recovery of the SPE, Tulsa, OK.

Harrington, R.E., and Zimm, B.H., 1968, "Anomalous Plugging of Sintered Glass Filters by High Molecular Weight Polymers", J. Polymer Science, part A.2 , 6, p. 294.

Heller, J.P., Lien, C.L., and Kuntamukkula, M.S., 1982, "Foam-Like Dispersions for Mobility Control in CO_2 Floods", Paper SPE 11233, presented at the 57th Annual Fall Technical Conference and Exhibition held in New Orleans, LA.

Henley, D.H., Owens, W.W., and Craig, F.F., Jr., 1961, "A Scale-Model Study of Bottom Water Drives", J. Pet. Tech., pp. 90-98.

Holm, L.W., 1968, "The Mechanism of Gas and Liquid Flow Through Porous Media in the Presence of Foam", Soc. Pet. Eng. J. , 8, pp. 359-369.

Holm, L.W., 1970, "Foam Injection Test in the Siggins Field, Illinois", J. Pet. Tech., Dec., pp. 1499-1506.

Huh, D.G., and Handy, L.L., 1986, "Comparison of Steady and Unsteady-State Flow of Gas and Foaming Solution in Porous Media", Paper presented at the 56th California Regional Meeting, Oakland, CA.

Isaacs, E.E., McCarthy, F.C., and Maunder, J.D., 1986, "Investigation of Foam Stability in Porous Media at Elevated Temperatures", Paper SPE 15647, presented at the 61st Annual Technical Conference and Exhibition held in New Orleans, LA.

Islam, M.R., and Bentsen, R.G., 1987, "Effect of Different Parameters or Two-Phase Relative Permeability", AOSTRA J. Res., 3, pp. 69-90.

Islam, M.R., and Bentsen, R.G., 1986, "A Dynamic Method For Measuring Relative Permeability", J. Can. Pet. Tech., 25(1), pp. 39-50.

Jennings, R.R., Rogers, J.H., and West, T.J., 1971, "Factors Influencing Mobility Control By Polymer Solutions", J. Pet. Tech., March, pp. 391-401.

Jennings, H.Y.,Jr., Williams, R.E., and Kolodzie, P.A., 1974, "Oil Recovery by Alkaline Waterflooding", J. Pet. Tech., pp. 1344-1374.

Johnson, C.E., 1976, "Status of Caustic and Emulsion Rheology and Flow Through Unconsolidated Synthetic Porous Media", Paper SPE 3004, presented at SPE-AIME 45th Annual Fall Meeting, Houston, January.

Johnstone, R.E. and Thring, N.W., 1957, Pilot Plants, Models and Scale-Up Methods in Chemical Engineering, McGraw-Hill Book Co., New York.

Khan, A.R., 1970, "A Scaled Model Study of Water Coning", J. Pet. Tech., June, 1970, pp. 771-776.

Khan, A.R., and Caudle, B.H., 1969, " Scaled Model Studies of Thin Oil Columns Produced by Natural Water Drive", Soc. Pet. Eng. J., 9, Sept., pp. 317-322.

Khatib, Z.I., Hirasaki, G.J., and Falls, A.H., 1986, "Effects of Capillary Pressure on Coalescence and Phase Mobilities in Foams Flowing Through Porous Media", Paper SPE 15442, presented at the 61st Annual Technical Conference and Exhibition held in New Orleans, LA.

Kimber, K.D., Puttagunta, V.R., and Farouq Ali, S.M., 1986, "New Scaling Criteria and Their Relative Merits for Steam Recovery Experiments", Paper presented at the 37th ATM of the PS of CIM, Calgary.

Knight, B.L., 1973, "Reservoir Stability of Polymer Solutions", J. Pet. Tech., Nov., pp. 618-626.

Keizer, P.P.M., Muiijs, H.M., Rosuoelen, J.R., Teeuw, D., Pino, H., Avila, J., and Rondon, L., 1986, "Application of Steam Foam in the Tia Juana Field, Venezuela: Laboratory Tests and Field Results", Paper SPE/DOE 14905, presented at the 5th Symposium on EOR of the SPE and the DOE, Tulsa, OK.

Kolb, G.E., 1964, "Several Parameters Affecting the Foam-Drive Process for the Removal of Water from Consolidated Porous Media", M.S. Thesis, Pennsylvania State University.

Lee, W.D. and Kamilos, G.N., 1985, "Chevron Field Tests Its Foam Diverter in Steam Floods with Encouraging Results", Pet. Eng. Int., Nov., 36-44.

Maerker, J.M., 1973, "Dependence of Polymer Retention on Flow Rate", J. Pet. Tech., Nov., pp. 1307-1308.

Maini, B.B. and Ma, V., 1984, "Relationship Between Foam Stability Measured in Static Tests and Flow Behavior of Foams in Porous Media", Paper SPE 13073, presented at the 59th Annual Technical Conference and Exhibition held in Houston, TX.

Maini, B.B., 1986, "Laboratory Evaluation of Foaming Agents for High Temperature Applications-III. Effect of Residual Oil on Mobility Reduction Performance", Paper CIM 86-37-01, presented at the 37th Annual Technical Meeting of the PS of CIM, Calgary.

Maini, B.B., 1985, "Laboratory Evaluation of Foaming Agents for High Temperature Applications - II. Measurements of Thermal Stability and Foam Mobility in Porous Media", Paper CIM 85-36-30, presented at the 36th Annual Technical Meeting of the PS of CIM, Edmonton.

Marsden, S.S., and Khan, S.A., 1966, "The Flow of Foam Through Short Porous Media and Apparent Viscosity Measurements", Soc. Pet. Eng. J., 6, pp. 17-25.

Mast, R.F., 1972, "Microscopic Behavior of Foam in Porous Media", Paper SPE 3997 presented for the 47th Annual Fall Meeting held in San Antonio, Tex.

McAuliffe, C.D., 1973a, "Oil-in-Water Emulsions and Their Flow Properties in Porous Media", J. Pet. Tech., June, pp. 727-733.

McAuliffe, C.D., 1973b, "Crude-Oil-in-Water Emulsions To Improve Fluid Flow in An Oil Reservoir",J. Pet. Tech., June, pp. 721-726.

Minssieux, L., 1974, "Oil Displacement by Foams in Relation to Their Physical Properties in Porous Media", J. Pet. Tech., January, pp. 100-108.

Mohammadi, S.S. and McCollum, T.J., 1986, "Steam-Foam Pilot Project in Guadalupe Field, California", Paper SPE 15054, presented at the 56th California Regional Meeting held in Oakland, CA.

Mungan, N., 1969, "Rheology and Adsorption of Aqueous Polymer Solutions", J. Can. Pet. Tech., 8, p.45.

Mungan, N., 1969, "Le Controle de la Mobilite dans les Injections de Polymers", Revue de l'IFP, 14(2), pp. 232-246.

Mungan, N., 1979, "Laboratory Study of Water Coning in a Layered Model", J. Can. Pet. Tech., 19(3), pp. 66-70.

Mungan, N., Smith, F.W., and Thompson, J.L., 1966, "Some Aspects of Polymer Floods", J. Pet. Tech., Sept., pp. 1143-1150.

Nicolov, A.D., Wasan, D.T., Huang, D.W., and Edwards, D.A., 1986, "The Effect of Oil on Foam Stability: Mechanisms and Implications for Oil Displacement by Foam in Porous Media", Paper SPE 15443, presented at the 61st Annual Technical Conference and Exhibition held in New Orleans, LA.

Novosad, J., Maini, B.B., and Huang, A., 1985, "Retention of Foam Forming Surfactants at Elevated Temperatures", Paper CIM 85-36-29, 36th Annual Technical Meeting of the PS of CIM, held in Edmonton.

Owette, O.S, Castiner, L.M., and Brigham, W.E., 1983 "Flow Behavior of Foam in Porous Media", Stanford University Petroleum Recovery Institute Report.

Pasini, J., 1966, "Initial Results of Oil Recovery Tests on Cow Run Sandstone Cores Using Polymer Solutions", Producers' Monthly, 30(1), pp. 2-3.

Perkins, T.K., and Johnston, O.C., 1962, "A Review of Diffusion and Dispersion in Porous Media", Soc. Pet. Eng. J., 3, pp. 70-80.

Pope, G.A., Wang, B., and Tsaur, K., 1979, "A Sensitivity Study of Micellar/Polymer Flooding", Soc. Pet. Eng. J., 19(5), pp. 357-368.

Pozzi, A.L., and Blackwell, R.J., 1963, "Design of Laboratory Models for Study of Miscible Displacement", Soc. Pet. Eng. J., 4, pp. 28-40.

Pye, D.J., 1964, "Improved Secondary Recovery by Control of Water Mobility", J. Pet. Tech., Aug., pp. 911-916.

Raza, S.H., 1970, "Foam in Porous Media: Characteristics and Potential Applications", Soc. Pet. Eng. J., 10(4), pp. 328-336.

Robertson, J.O, Jr., and Oefelein, F.H., 1967, "Plugging Thief Zones in Water Injection Wells", J. Pet. Tech., August, pp. 999-1004.

Rojas, G.A., 1985, "Scaled Model Studies of Immiscible Carbon Dioxide Displacements of Heavy Oil", Ph.D. Dissertation, University of Alberta.

Sarma, H.K., and Bentsen, R.G., 1987, "An Experimental Verification of a Modified Instability Theory for Immiscible Displacements in Porous Media", J. Can. Pet. Tech., 26(4), pp. 88-99.

Satter, A., Shum, Y.M., Adams, W.T. and Davis, L.A., 1977, "Chemical Transport in Porous Media", Paper presented at the 52nd Annual Fall Technical Conference, Denver, CO.

Sandiford, B.B., 1964, "Laboratory and Field Studies of Waterfloods Using Polymer Solutions to Increase Oil Recoveries", J. Pet. Tech., Aug., pp. 917-922.

Sandiford, B.B., Knight, R.K., Sarem, A.M., and Amott, E., 1967, "Discussion", Soc. Pet. Eng. J., 7, pp. 170-171.

Sherborne, J.E., Sarem, A.M., and Sandiford, B.B., 1967, "Flooding Oil-Containing Formations with Solutions of Polymer in Water", 7th World Pet. Congr., Mexico City.

Sigmund, P.M., Sarma, H.K., Sheldon, D., and Aziz, K.,1985, "Flow Instability in Porous Media; Rate Dependence of Unstable Waterfloods", 35th Annual Technical Meeting of the Canadian Society of Chemical Engineers, Calgary.

Smith, F.W., 1970, "The Behavior of Partially Hydrolyzed Polyacrylamide Solutions in Porous Media", J. Pet. Tech., Feb., pp. 148-156.

Smith, L.R., Fast, C.R., and Wagner, O.R., 1969, "Development and Field Testing of Large Volume Remedial Treatments for Gross Water Channeling", J. Pet. Tech., Aug., pp. 1015-1025.

Soo, H., and Radke, C.J., 1984, "The Flow of Dilute, Stable Emulsions in Porous Media", Ind. Eng. Chem. Fund., 23(3), pp. 342-347.

Sparlin, D.D., 1976, "An Evaluation of Polyacrylamides for Reducing Water Production", J. Pet. Tech., Aug., pp. 906-914.

Sparlin, D.D., 1977, "Polyacrylamide Can Restrict Water, Oil and Gas Production - It's Your Choice", SPE-6473, Paper presented at Oklahoma City Regional Meeting, Oklahoma City.

Szabo, M.T., 1975a, "Some Aspects of Polymer Retention in Porous Media Using a C^{14}-Tagged Hydrolyzed Polyacrylamide", Soc. Pet. Eng. J., 15, Aug., pp. 323-337.

Szabo, M.T., 1975b, "Laboratory Investigations of Factors Influencing Polymer Flood Performance", Soc. Pet. Eng. J., 15, Aug., pp. 338-346.

Thomas, C.P., 1976, "The Mechanism of Reduction of Water Mobility by Polymers in Glass Capillary Arrays", Soc. Pet. Eng. J., 16, June, pp. 130-136.

Uzoigwe, A.C., and Marsden, S.S., Jr., 1970, "Emulsion Rheology and Flow Through Unconsolidated Synthetic Porous Media", Paper SPE 3004, presented at SPE-AIME 45th Annual Fall Meeting, Houston.

11. APPENDIX - A

11.1 DERIVATION OF THE FLOW EQUATION

11.1.1 Mass Balance

A mass balance will be considered about a small control volume as shown in Figure A-1 with length Δx, width Δy, and height Δz. For all phases a mass balance can be written as follows:

Mass entering the block - Mass leaving the block + net change over time in the control volume = 0

If q is the fluid flux (rate of flow of mass per unit cross-sectional area normal to the direction of flow), the mass entering the block in a time interval of Δt may be written as

$$[(q_x)_x \Delta y \Delta z + (q_y)_y \Delta x \Delta z + (q_z)_z \Delta x \Delta y]\Delta t = \text{Mass in} \qquad (A.1)$$

where $(q_i)_i$ denotes the i-direction flux at location i, for i=x, y, or z.

On the other hand, mass leaving the control volume is given by,

$$[(q_x)_{x+\Delta x} \Delta y \Delta z + (q_y)_{y+\Delta y} \Delta x \Delta z + (q_z)_{z+\Delta z} \Delta x \Delta y]\Delta t + q^* \Delta x \Delta y \Delta z \Delta t = \text{Mass out} \qquad (A.2)$$

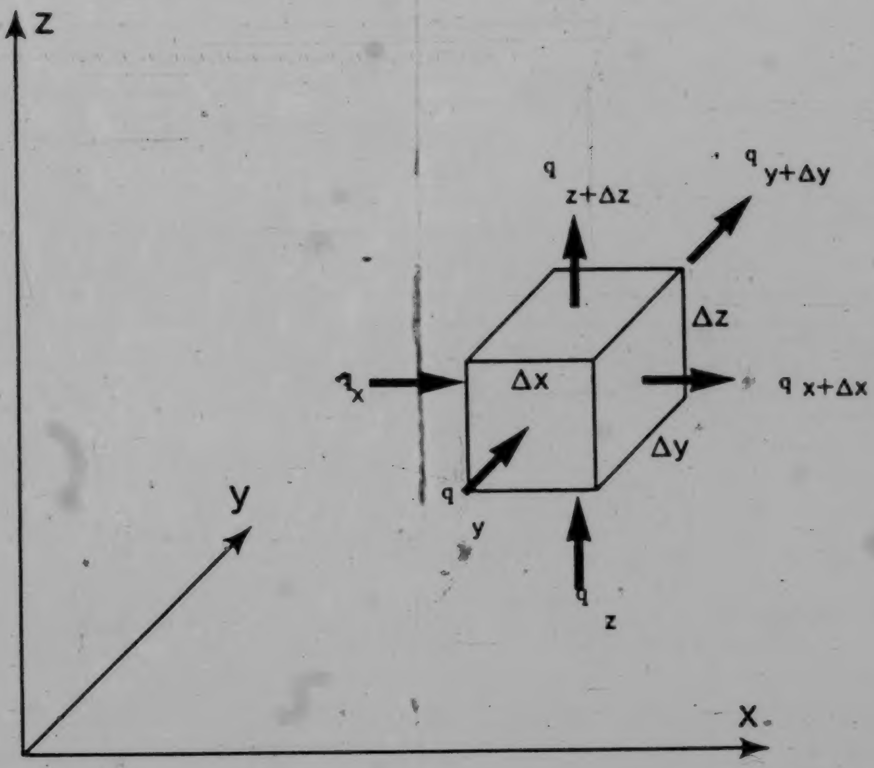
Z
y
X
q z+Δz
q y+Δy
Δz
q x
Δx
q x+Δx
Δy
q y
q z

Fig. A-1 Control Volume for Mass Balance where q^* represents the mass flow into or out of a well. A producer is represented by $q>0$, and an injector is represented by $q<0$.

Accumulation of mass in the block is the change in concentration of phase i (C_i in the block over the time interval Δt). If the saturation C_i is defined as the total mass of phase i (oil, water, or emulsion or polymer) in the block divided by the block volume, then the accumulation term becomes:

$$[(C_i)_{t+\Delta t} - (C_i)_t]\Delta x\Delta y\Delta z \tag{A.3}$$

Using Equations A.1 through A.3 in the mass conservation equality, one obtains

$$\begin{aligned}&[(q_x)_x\Delta y\Delta z + (q_y)_y\Delta x\Delta z + (q_z)_z\Delta x\Delta y]\Delta t - \\ &[(q_x)_{x+\Delta x}\Delta y\Delta z + (q_y)_{y+\Delta y}\Delta x\Delta z + (q_z)_{z+\Delta z}\Delta x\Delta y]\Delta t - \\ &q^*\Delta x\Delta y\Delta z\Delta t = [(C_i)_{t+\Delta t} - (C_i)_t]\Delta x\Delta y\Delta z\end{aligned} \tag{A.4}$$

Dividing Equation (A.4) by $\Delta x\Delta y\Delta z\Delta t$ and rearranging gives

$$\begin{aligned}&- \frac{(q_x)_{x+\Delta x} - (q_x)_x}{\Delta x} - \frac{(q_y)_{y+\Delta y} - (q_y)_y}{\Delta y} \\ &- \frac{(q_z)_{z+\Delta z} - (q_z)_z}{\Delta z} - q^* = (\frac{C_i)_{t+\Delta t} - (C_i)_t}{\Delta t}\end{aligned} \tag{A.5}$$

In the limit as Δx, Δy, Δz and Δt go to zero Equation A.5 becomes the continuity equation given as:

$$-\frac{\partial q_x}{\partial x} - \frac{\partial q_y}{\partial y} - \frac{\partial q_z}{\partial z} - q^* = \frac{\partial C_i}{\partial t} \qquad (A.6)$$

Each phase satisfies a mass conservation equation having the form of Equation (A.6).

In the present system it has been assumed that oil, water and emulsion or polymer form a three-phase system very similar to oil, water and gas. The flow equations for each phase will be determined by specifying the fluxes and concentrations of the conservation equations corresponding to each phase. A flux in a given direction can be written as the density of the fluid times its velocity in the given direction. Letting a, l and m denote aqueous, oleic and emulsion (or polymer), respectively; then the fluxes become:

$$(q)_l = \frac{\rho_{lsc}}{B_l} v_l \qquad (A.7)$$

$$(q)_a = \frac{\rho_{asc}}{B_a} v_a \qquad (A.8)$$

$$(q)_m = \frac{\rho_{msc}}{B_m} v_m + \frac{R_{sl}\rho_{msc}}{B_l} v_l + \frac{R_{sa}\rho_{msc}}{B_a} v_a \qquad (A.9)$$

where R_{sl} and R_{sa} are emulsion (or polymer) solubilities, and B_l, B_a, B_m are formation volume factors in reservoir volume/standard volume. The densities considered above are measured at standard condtions. The velocities v are assumed to be Darcy velocities and their x-components are given by

$$v_{xl} = - k_x \frac{k_{rl}}{\mu_l} \frac{\partial}{\partial x} [p_l - \rho_l gz] \qquad (A.10)$$

$$v_{xa} = - k_x \frac{k_{ra}}{\mu_a} \frac{\partial}{\partial x} [p_a - \rho_a gz] \qquad (A.11)$$

$$v_{xm} = - k_x \frac{k_{rm}}{\mu_m} \frac{\partial}{\partial x} [p_m - \rho_m gz] \qquad (A.12)$$

Similar expressions may be written for the y and z directions as well.

On the other hand, concentrations are given by

$$C_l = \phi \rho_l S_l / B_l \qquad (A.13)$$

$$C_a = \phi \rho_a S_a / B_a \qquad (A.14)$$

$$C_m = \phi \rho_m \left[\frac{S_m}{B_m} + \frac{R_{sl} S_l}{B_l} + \frac{R_{sa} S_a}{B_a}\right] \qquad (A.15)$$

where ϕ is the porosity and S_i is the saturation for the phase i (i=oil, water, emulsion or polymer). The saturations satisfy the constraint

$$S_l + S_a + S_m = 1 \qquad (A.16)$$

Combining Equations (A.6), (A.7) through (A.9) and (A.13) through (A.15) gives a mass conservation equation for each phase:

Oleic phase

$$- [\frac{\partial}{\partial x}(\frac{\rho_{1sc}}{B_1}v_{x1}) + \frac{\partial}{\partial y}(\frac{\rho_{1sc}}{B_1}v_{y1}) + \frac{\partial}{\partial z}(\frac{\rho_{1sc}}{B_1}v_{z1})] - q_1^* =$$

$$\frac{\partial}{\partial t} (\frac{\phi\rho_{1sc}S_1}{B_1}) \qquad (A.17)$$

Aqueous phase

$$- [\frac{\partial}{\partial x}(\frac{\rho_{asc}}{B_a}v_{xa}) + \frac{\partial}{\partial y}(\frac{\rho_{asc}}{B_a}v_{ya}) + \frac{\partial}{\partial z}(\frac{\rho_{asc}}{B_a}v_{za})] - q_a^* =$$

$$\frac{\partial}{\partial t} (\frac{\phi\rho_{asc}S_a}{B_a}) \qquad (A.18)$$

Aqueous phase

$$- [\frac{\partial}{\partial x}(\frac{\rho_{msc}}{B_m}v_{xm} + \frac{R_{s1}\rho_{msc}}{B_1}v_{x1} + \frac{R_{sa}\rho_{msc}}{B_a}v_{xa})$$

$$+ \frac{\partial}{\partial y}(\frac{\rho_{msc}}{B_m}v_{ym} + \frac{R_{s1}\rho_{msc}}{B_1}v_{y1} + + \frac{R_{sa}\rho_{msc}}{B_a}v_{ya}) +$$

$$\frac{\partial}{\partial z}(\frac{\rho_{msc}}{B_m}v_{zm} + \frac{R_{s1}\rho_{msc}}{B_1}v_{x1} + \frac{R_{sa}\rho_{msc}}{B_a}v_{xa}) - q_m^* =$$

$$\frac{\partial}{\partial t}(\phi\rho_{msc}(\frac{S_m}{B_m} + \frac{R_{s1}S_1}{B_1} + \frac{R_{sa}S_a}{B_a})] \qquad (A.19)$$

In the above equations, the densities (subscripted by 'sc') are at standard conditions. A much simpler appearing form of the above equations is:

$$- \nabla\cdot\frac{v_1}{B_1} - \frac{q_1}{\rho_{1sc}} = \frac{\partial}{\partial t}(\frac{\phi S_1}{B_1}) \qquad (A.20)$$

$$-\nabla\cdot\frac{v_a}{B_a} - \frac{q_a}{\rho_{asc}} = \frac{\partial}{\partial t}\left(\frac{\phi S_a}{B_a}\right) \qquad (A.21)$$

and

$$-\nabla\cdot\left(\frac{v_m}{B_m} + \frac{R_{sl}}{B_l}v_l + \frac{R_{sa}}{B_a}v_a\right) - \frac{q_m}{\rho_{msc}} = \frac{\partial}{\partial t}\left[\frac{\phi S_m}{B_m} + \frac{R_{sl}S_l}{B_l} + \frac{R_{sa}S_a}{B_a}\ )\right] \qquad (A.22)$$

where the symbol $\nabla\cdot v$ is defined by:

$$\nabla\cdot v = \frac{\partial}{\partial x}v_x + \frac{\partial}{\partial y}v_y + \frac{\partial}{\partial z}v_z \qquad (A.23)$$

Also the Darcy velocities may be simplified by defining the potential of phase i as

$$\Phi_i = p_i - \rho_i g z \qquad (A.24)$$

By using this definition, one obtains:

$$\frac{\nabla k\lambda_l\nabla\Phi_l}{B_l} - \frac{q_l}{\rho_{lsc}} = \frac{\partial}{\partial t}\left(\phi\frac{S_l}{B_l}\right) \qquad (A.25)$$

$$\frac{\nabla k\lambda_a\nabla\Phi_a}{B_a} - \frac{q_a}{\rho_{asc}} = \frac{\partial}{\partial t}\left(\phi\frac{S_a}{B_a}\right) \qquad (A.26)$$

and

$$\nabla\cdot k\left[\frac{\lambda_m\nabla\Phi_m}{B_m} + \frac{R_{sl}\lambda_l\nabla\Phi_l}{B_l} + \frac{R_{sa}\lambda_a\nabla\Phi_a}{B_a}\right] - \frac{q_m}{\rho_{msc}} =$$

$$\frac{\partial}{\partial t}[\phi(\frac{S_m}{B_m} + \frac{R_{sl}S_l}{B_l} + \frac{R_{sa}S_a}{B_a})] \qquad (A.27)$$

Using capillary pressures defined as

$$p_{cla} = p_l - p_a \qquad (A.28)$$

and

$$p_{cml} = p_m - p_l \qquad (A.29)$$

the phase potentials become:

$$\Phi_a = p_l - p_{cla} - \rho_a gz \qquad (A.30)$$

and

$$\Phi_m = p_l + p_{cml} - \rho_m gz \qquad (A.31)$$

Therefore, the flow equations become:

Oleic phase

$$\nabla \cdot k \cdot (\frac{\lambda_l}{B_l}) \nabla p_l + CG_l - \frac{q_l}{\rho_{lsc}} = \frac{\partial}{\partial t}(\phi \frac{S_l}{B_l}) \qquad (A.32)$$

Aqueous phase

$$\nabla \cdot k \cdot (\frac{\lambda_a}{B_a}) \nabla p_a + CG_a - \frac{q_a}{\rho_{asc}} = \frac{\partial}{\partial t}(\phi \frac{S_a}{B_a}) \qquad (A.32)$$

Emulsion or polymer phase

$$\nabla\cdot[k\cdot(\frac{\lambda_m}{B_m} + \frac{R_{sl}\lambda_l}{B_l} + \frac{R_{sa}\lambda_a}{B_l})]\nabla p_l + CG_m - \frac{q_m}{\rho_{msa}} =$$

$$\frac{\partial}{\partial t}[\phi(\frac{S_m}{B_m} + \frac{R_{sl}S_l}{B_l} + \frac{R_{sa}S_a}{B_a})] \qquad (A.33)$$

In the above equations the gravity and capillary contributions to the phase pressures have been collected in the terms CG_l, CG_a, and CG_m:

$$CG_l = -\nabla\cdot k\cdot(\frac{\lambda_l}{B_l})\ \nabla(\rho_l gz) \qquad (A.34)$$

$$CG_a = -\nabla\cdot k\cdot(\frac{\lambda_a}{B_a})\ \nabla(\rho_a gz + p_{cla}) \qquad (A.35)$$

and

$$CG_m = \nabla\cdot\{k\cdot[\frac{\lambda_m}{B_m})\nabla(p_{cml} - \rho_m gz) - \frac{R_{sl}\lambda_l}{B_l}\ \nabla(\rho_l gz)$$

$$- \frac{R_{sa}\lambda_a}{B_a}\ \nabla(p_{cla} + \rho_a gz)]\} \qquad (A.36)$$

The task involved is to solve equations (A.31) through (A.33) and (A.35) for the four unknowns p_l, S_l, S_a, and S_m. All other physical properties in the equations are known, in principle, as functions of the four unknowns, or from laboratory data.

Recognizing that the formation volume factors, solubilities, and porosity are functions of pressure, one can use the chain rule to expand the accumulation terms (time derivatives) of the flow equations:

Oleic phase accumulation term

$$L_l = \frac{\phi\ \partial S_l}{B_l \partial t} + [\frac{S_l}{B_l}\frac{\partial \phi}{\partial p_l} - \frac{S_l \phi}{B_l{}^2}\frac{\partial B_l}{\partial p_l}]\ \frac{\partial p_o}{\partial t} \tag{A.37}$$

Aqueous phase accumulation term

$$L_a = \frac{\phi}{B_a}\frac{\partial S_a}{\partial t} + [\ \frac{S_a \partial \phi}{B_a \partial p_a} - \frac{S_a \phi}{B_a}\frac{\partial \phi}{\partial p_a} - \frac{S_a \phi}{B_a{}^2}\frac{\partial B_a}{\partial p_a}]\ \frac{\partial p_o}{\partial t} \tag{A.38}$$

Polymer or emulsion phase accumulation term

$$\begin{aligned} L_m = {} & \frac{\phi}{B_m}\frac{\partial S_m}{\partial t} + [\ \frac{S_m}{B_m}\frac{\partial \phi}{\partial p_m} - \frac{S_m \phi}{B_m{}^2}\frac{\partial B_m}{\partial p_m}]\ \frac{\partial p_o}{\partial t} + \frac{\phi R_{sl}}{B_l{}^2}\frac{\partial S_l}{\partial t} + \\ & [\ \frac{S_l R_{sl}}{B_l}\frac{\partial \phi}{\partial p_l} + \frac{\phi S_l}{B_l}\frac{\partial R_{sl}}{\partial p_l} - \frac{\phi S_l R_{sl} \partial B_l}{B_l{}^2\ \ \partial p_l}]\frac{\partial p_l}{\partial t} + [\ \frac{S_a R_{sa}}{B_a}\frac{\partial \phi}{\partial p_a} \\ & + \frac{\phi S_a}{B_a}\frac{\partial R_{sa}}{\partial p_a} - \frac{\phi S_a R_{sa} \partial B_a}{B_a{}^2\ \ \partial p_a}]\frac{\partial p_a}{\partial t} \end{aligned} \tag{A.39}$$

The equality

$$S_l + S_a + S_m = 1 \tag{A.40}$$

is now used to remove $\partial S_m/\partial t$ from Equation (A.38). Differentiating Equation (A.40) w.r.t. t and rearranging, one obtains

$$\frac{S_m}{\partial t} = - \frac{S_l}{\partial t} - \frac{\partial S_a}{\partial t} \tag{A.41}$$

This expression permits further simplification of Equation (A.39); that is:

$$(\frac{\phi R_{sl}}{B_l} - \frac{\phi}{B_m})\frac{\partial S_l}{\partial t} + (\frac{\phi R_{sa}}{B_a} - \frac{\phi}{B_m})\frac{\partial S_a}{\partial t} + \{\ \frac{S_m \partial \phi}{B_m \partial p_l}$$

$$- \frac{S_m \phi \partial \phi}{{B_m}^2 \partial p_1} + \frac{S_1 R_{s1} \partial \phi}{B_1 \ \partial p_1} + \frac{\phi S_1 \partial \phi}{B_1 \ \partial p_1} \tag{A.42}$$

$$- \frac{\phi S_1 R_{s1} \partial B_1}{{B_1}^2 \ \partial p_1} + \frac{S_a R_{sa} \partial \phi}{B_a \ \partial p_1} + - \frac{\phi S_a R_{sa} \partial B_a}{{B_a}^2 \ \partial p_a} + \frac{S_a R_{sa} \partial \phi}{B_a \ \partial p_a} \} \frac{\partial p_1}{\partial t}$$

Now, multiplying the oil equation by $(B_1 - R_{s1}B_m)$, the water equation by $(B_a - R_{sa}B_m)$, and the emulsion or polymer equation by B_m and adding the results, one obtains after simplification:

$$(B_1 - R_{s1}B_m)L_1 + (B_a - R_{sa}B_m)L_a + B_m L_m =$$

$$[(S_m + S_a + S_1)\frac{\partial \phi}{\partial p_1} - \frac{\phi S_m}{B_m} + \phi S_1 (\frac{B_m \partial R_{s1}}{B_1 \partial p_1} - \frac{1 \ 1 \ \partial B_1}{B_1 B_1 \partial p_1} + \tag{A.43}$$

$$+ \phi S_1 (\frac{B_m \partial R_{sa}}{B_a \partial p_1} - \frac{1 \ 1 \ \partial B_a}{B_a B_a \partial p_1}] \frac{\partial p_1}{\partial t}$$

Different fluid and rock compressibilities are identified as:

$$c_1 = - \frac{1 \ \partial B_1}{B_1 \partial p_1} + \frac{B_m \partial R_{s1}}{B_1 \partial p_1} \tag{A.44}$$

$$c_a = - \frac{1 \ \partial B_a}{B_a \partial p_1} + \frac{B_m \partial R_{sa}}{B_a \partial p_1} \tag{A.45}$$

$$c_m = - \frac{1 \ \partial B_m}{B_m \partial p_1} \tag{A.46}$$

$$c_r = - \frac{1 \partial \phi}{\phi \partial p_1} \tag{A.47}$$

and

$$c_t = c_r + c_l S_l + c_a S_a + c_m S_m \tag{A.48}$$

Employing these definitions, the pressure equation becomes:

$$\begin{aligned} &(B_l - R_{sl}B_m)\ [\ \nabla\cdot k\cdot\frac{\lambda_l}{B_l}\nabla p_l + CG_l - \frac{q_l}{\rho_{lsc}}] + \\ &(B_a - R_{sa}B_m)\ [\ \nabla\cdot k\cdot\frac{\lambda_a}{B_a}\nabla p_a + CG_a - \frac{q_a}{\rho_{asc}}] + \\ &B_m[\nabla\cdot k\cdot(\frac{\lambda_m}{B_m} + \frac{R_{sl}\lambda_l}{B_l} + \frac{R_{sa}\lambda_a}{B_a})\nabla p_l + CG_m - \frac{q_m}{\rho_{msc}}] = \frac{\phi c_t \partial p_l}{\partial t} \end{aligned} \tag{A.49}$$

This three-phase, three-dimensional flow equation is solved numerically for p_l. Then, using this result the phase saturations are determined.

11.2 Finite Difference Equations

Using finite difference approximations the above mentioned partial differential equations are converted into algebraic equations. The equations to be solved are the pressure equation (A.49), and the water equation. These equations are first multiplied through by the bulk volume element $V_{b\ i,j,k}$. Next, a linear difference operator is defined as follows:

$$\Delta A \Delta p = \Delta_x A_x \Delta p_x + \Delta_y A_y \Delta p_y + \Delta_z A_z \Delta p_z \tag{A.50}$$

where

$$\nabla_x A_x \nabla p_x = A_{i-\frac{1}{2},j,k} \left(p_{i-1,j,k} - p_{i,j,k}\right) + A_{i+\frac{1}{2},j,k} \left(p_{i+1,j,k} - p_{i,j,k}\right) \tag{A.51}$$

Using the above notation, the resulting difference equations become:

Pressure

$$\left(B_l^n - B_m^n R_{sl}^n\right)_{ijk} \left(\Delta A_l^n \Delta p^{n+1} + GLAT - \frac{q_l V_b}{\rho_{bsc}}_{ijk}\right.$$

$$+ \left(B_a^n - B_m^n R_{sa}^n\right)_{ijk} \left(\Delta A_a^n \Delta p^{n+1} + GLAT\right. \tag{A.52}$$

$$- \frac{q_a V_b}{\rho_{bsc}}_{ijk} + \left(B_m^n\right)_{ijk} \left(\Delta A_m^n \Delta p^{n+1} + \Delta R_{sl}^n A_l^n \Delta p^{n+1} + \right.$$

$$\left.\Delta p^{n+1} + \Delta R_{sa}^n A_a^n \Delta p^{n+1} + GGAT - \frac{q_m V_b}{\rho_{msc}}\right)_{ijk} =$$

$$\left(\frac{\overline{V}_p^n c_t^n}{\Delta t}_{ijk} \left(p^{n+1} - p^n\right)_{ijk}\right.$$

Oil

$$\left(\Delta A_l^n \Delta p^{n+1} + GLAT - \frac{q_l V_b}{\rho_{lsc}}\right)_{ijk} = \tag{A.53}$$

$$\frac{1}{\Delta t}\left[\left(\frac{V_p S_l}{B_l}\right)^{n+1} - \left(\frac{V_p S_l}{B_l}\right)^{n}\right]_{ijk}$$

Water

$$\left(\Delta A_a^n \Delta p^{n+1} + GAAT - \frac{q_a V_b}{\rho_{asc}}_{ijk} = \right. \tag{A.54}$$

$$\frac{1}{\Delta t}\left[\left(\frac{V_pS_a}{B_a}\right)^{n+1} - \left(\frac{V_pS_a}{B_a}\right)\right]_{ijk}$$

where V_p is the grid block pore volume:

$$V_p = V_b\phi \tag{A.55}$$

Note that a forward difference approximation has been used for representing the time derivatives. The superscripts n and n+1 denote the present and next future time level respectively. Quantities with superscript n can be computed using existing data, whereas quantities with superscript n+1 are unknown variables to be determined.

Gravity and capillary pressure effects are contained in GLAT, GAAT and GGAT:

$$GLAT = -\Delta A_l^n \Delta(\rho_l gz)^n \tag{A.56}$$

$$GAAT = -\Delta A_a^n \Delta(\rho_a gz + p_{cla})^n \tag{A.57}$$

$$GGAT = \Delta[A_m^n \Delta(p_{cml} - \rho_m gz)^n - R_{sl}^n A_l^n \Delta(\rho_l gz)^n$$

$$- R_{sa} A_a^n \Delta(p_{cla} + \rho_a gz)^n] \tag{A.58}$$

We now have all of the basic elements necessary for writing down the algebraic system of equations corresponding to the nonlinear, partial differential flow equations.

11.3 Solution Methods

The finite difference form of the pressure equation leads to a system of linear equations for the I·J·K unknowns $p_{i,j,k}$; $1 \le i \le I$, $1 \le j \le J$, $1 \le k \le K$. Here $p_{i,j,k}$ denotes the pressure at grid block (i,j,k) at the new (n+1) time level. Such a system of equations may be written as

$$\left(\begin{array}{l} a_{1,1}p_1 + a_{1,2}p_2 + \ldots + a_{1,N}p_N = q_1 \\ \\ a_{2,1}p_1 + a_{2,2}p_2 + \ldots + a_{2,N}p_N = q_1 \\ \\ \cdot \\ \cdot \\ \cdot \\ \\ a_{N,1}p_1 + a_{N,2}p_2 + \ldots + a_{N,N}p_N = q_1 \end{array}\right) \qquad \text{(A.59)}$$

where N = I·J·K, and the new (n+1) time level superscripts have been supressed.

Alternatively, the same set of equations may be expressed in a more compact form using matrix notation as follows:

$$\underline{\underline{A}}\,\underline{p} = \underline{q} \qquad \text{(A.60)}$$

where $\underline{\underline{A}}$ is the coefficient matrix, and $\underline{p}$, $\underline{q}$ are column vectors as given below.

$$\underline{\underline{A}} = \begin{pmatrix} a_{1,1} & a_{1,2} & \cdots & a_{1,N} \\ a_{2,1} & a_{2,2} & \cdots & a_{2,N} \\ \vdots & & & \\ a_{N,1} & a_{N,2} & \cdots & a_{N,N} \end{pmatrix} \qquad \underline{p} = \begin{pmatrix} p_1 \\ p_2 \\ \vdots \\ p_N \end{pmatrix} \qquad \underline{q} = \begin{pmatrix} q_1 \\ q_2 \\ \vdots \\ q_N \end{pmatrix} \tag{A.61}$$

This system of linear equations is solved by the direct method (Peaceman, 1977). The details of the direct method are readily available in the literature and, therefore, are not repeated here.

11.4 Well Representation

There are essentially two methods for representing a well in a simulator: by rate constraint, or by pressure constraint.

11.4.1 Oil Production Rate Specified

In this representation, rates may be specified for injectors or producers. If the well of interest is a producer, its specified rate may be either the oil rate Q_1 or the total fluid rate Q_t. Assuming the well may be completed in K layers, the production rates of layer k for a specified oil rate are:

Oil

$$Q_{1k} = Q_1 \frac{[(PI)\lambda_1/B_1]_k}{\sum_{i=1}^{n}[(PI)\lambda_1/B_1]_k} \qquad \text{(A.62)}$$

Water

$$Q_{ak} = Q_{1k}\left(\frac{\lambda_a/B_a}{\lambda_1/B_1}\right)_k \qquad \text{(A.63)}$$

polymer or emulsion

$$Q_{mk} = \left(\frac{\lambda_m/B_m}{\lambda_1/B_1}\right)_k Q_{1k} + (R_{s1})_k Q_{1k} + (R_{sa})_k Q_{ak} \qquad \text{(A.64)}$$

The above formulation allows PI's to be specified by layers. Therefore, permeability contrast may be taken into account.

11.4.2 Injection Rate Specified

If the well is a water or gas injector, the total water or emulsion (or polymer) injection rates must be specified along with injectivity indices for each layer. The injection rate for each layer is then allocated as follows:

Water Injection Rate

$$Q_{ak} = Q_a \frac{[WI(\lambda_1 + \lambda_a + \lambda_m)]_k}{\sum_{i=1}^{n}[\ WI(\lambda_1 + \lambda_a + \lambda_m)\ ]_k} \qquad \text{(A.65)}$$

Emulsion or Polymer Injection Rate

$$Q_{mk} = Q_m \frac{[WI(\lambda_l + \lambda_a + \lambda_m)]_k}{\sum_{i=1}^{n} [\, WI(\lambda_l + \lambda_a + \lambda_m)\,]_k} \qquad (A.66)$$

11.4.3 Implicit Pressure Constraint Representation

The source/sink terms may be written as

$$\frac{q_p V_b}{\rho_{isc}} = [\ PID\ (\frac{\lambda_i}{B_i}]_k^n\ (p^{n+1} - PWF) \qquad (A.67)$$

where the subscript i signifies the appropriate oil, water, or emulsion (or polymer) phase. If the well is a producer, PID=PI and $p^{n+1} > PWF$ where PWF is the well flowing pressure. If the well is an injector, PID=WI and $p^{n+1} < PWF$.

Equation (A.67) may be used to to solve for pressure implicitly. The computed pressure p^{n+1} is then replaced in Equation (A.67) to yield rates. This procedure is accomplished simply by redefining the coefficients of the pressure equation such that

$$E_{ijk}^{new} = E_{ijk}^{old} - CPI \qquad (A.68)$$

and

$$B_{ijk}^{new} = B_{ijk}^{old} - CPI*PWF \qquad (A.69)$$

where

$$CPI = PID_k[(B_l - B_m R_{sl})\ (\frac{\lambda_l}{B_l} + (B_a - B_m R_{sl})\ (\frac{\lambda_a}{B_a})$$

$$+ \left(B_m - B_m(\frac{\lambda_m}{B_m}\right) \tag{A.70}$$

The new E and B terms are defined immediately before solving the linear system of pressure equations and after the E and B matrices are first computed.

12. APPENDIX-B

12.1 Governing Equations in Terms of Their Dimensionless Variables

Each variable or property can be written in dimensionless form by dividing it by some characteristic reference quantity. For example, for the property P, $P_D = P/P_R$, where P_D is the dimensionless form of the property P, and P_R is some constant, characterstic reference quantity. By substituting $P_R P_D$ for P in the partial difference equations, the set of equations take the following form:

12.1.1 Polymer Flood

The equation for the mass balance of oil in terms of the dimensionless variables and their reference quantities is:

$$\left[\frac{\phi_R S_{1R}\rho_{1R}}{t_R}\right]\frac{\partial}{\partial t_D}(\phi_D S_{1D}\rho_{1D}) = \left[\frac{\rho_{1R}K_{1R}P_{1R}}{x_{1R}^{2}\mu_{1R}}\right]\frac{\partial}{\partial x_{1D}}\left(\frac{\rho_{1D}K_{1D}}{\mu_{1D}}\frac{\partial P_{1D}}{\partial x_{1D}}\right) +$$

$$\left[\frac{\rho_{1R}^{2}K_{1R}g_R z_R}{\mu_{1R}x_{1R}^{2}}\right]\frac{\partial}{\partial x_{1D}}\left(\frac{\rho_{1D}^{2}K_{1D}g_D}{\mu_{1D}}\frac{\partial z_D}{\partial x_{1D}}\right)$$

$$+\left[\frac{\rho_{1R}K_{1R}P_{1R}}{x_{2R}^{2}\mu_{1R}}\right]\frac{\partial}{\partial x_{2D}}\left(\frac{\rho_{1D}K_{1D}}{\mu_{1D}}\frac{\partial P_{1D}}{\partial x_{2D}}\right)$$

$$+\left[\frac{\rho_{1R}^{2}K_{1R}g_R z_R}{\mu_{1R}\,x_{2R}^{2}}\right]\frac{\partial}{\partial x_{2D}}\left(\frac{\rho_{1D}^{2}K_{1D}g_D}{\mu_{1D}}\frac{\partial z_D}{\partial x_{2D}}\right)$$

$$+\left[\frac{\rho_{1R}K_{1R}P_{1R}}{x_{3R}^{2}\mu_{1R}}\right]\frac{\partial}{\partial x_{3D}}\left(\frac{\rho_{1D}K_{1D}}{\mu_{1D}}\frac{\partial P_{1D}}{\partial x_{3D}}\right)$$

$$+ \left[\frac{\rho_{1R}^{2} K_{1R} g_R z_R}{\mu_{1R}\, x_{3R}^{2}}\right] \frac{\partial}{\partial x_{3D}} \left(\frac{\rho_{1D} g_D}{\mu_{1D}} \frac{\partial z_D}{\partial x_{3D}}\right)$$

$$+ \left[\frac{\phi_R S_{1R} D_{L1oR} \rho_{1R}}{x_{1R}^{2}}\right] \frac{\partial}{\partial x_{1D}} \left(\phi_D S_{1D} D_{L1oD} \frac{\partial}{\partial x_{1D}} (\rho_{1D})\right)$$

$$+ \left[\frac{\phi_R S_{1R} D_{T1oR} \rho_{1R}}{x_{2R}^{2}}\right] \frac{\partial}{\partial x_{2D}} \left(\phi_D S_{1D} D_{T1oD} \frac{\partial}{\partial x_{2D}} (\rho_{1D})\right)$$

$$+ \left[\frac{\phi_R S_{1R} D_{T1oR} \rho_{1R}}{x_{3R}^{2}}\right] \frac{\partial}{\partial x_{3D}} \left(\phi_D S_{1D} D_{T1oD} \frac{\partial}{\partial x_{3D}} (\rho_{1D})\right)$$

The equation for the mass balance of polymer in terms of the dimensionless variables and their reference quantities is:

$$\left[\frac{\phi_R S_{aR} C_{apR} \rho_{aR}}{t_R}\right] \frac{\partial}{\partial t_D} (\phi_D S_{aD} C_{apD} \rho_{aD}) \; +$$

$$\left[\frac{\rho_{rD} \rho_{rR} (1-\phi_R \phi_D) A_{pR} A_{pD} \rho_{aR} C_{apR}}{(1+BM_p C_{apR} C_{apD})^2 t_R}\right] \frac{\partial}{\partial t_D} (\rho_{aD} C_{apD}) \; =$$

$$\left[\frac{C_{apR} \phi_R S_{aR} D_{LapR} \rho_{aR}}{x_{1R}^{2}}\right] \frac{\partial}{\partial x_{1D}} \left(\phi_D S_{aD} D_{LapD} \frac{\partial}{\partial x_{1D}} (C_{aD} \rho_{aD})\right) \; +$$

$$\left[\frac{C_{apR} \phi_R S_{aR} D_{TapR} \rho_{aR}}{x_{2R}^{2}}\right] \frac{\partial}{\partial x_{2D}} \left(\phi_D S_{aD} D_{TapD} \frac{\partial}{\partial x_{2D}} (C_{aD} \rho_{aD})\right) \; +$$

$$\left[\frac{C_{apR} \phi_R S_{aR} D_{TapR} \rho_{aR}}{x_{3R}^{2}}\right] \frac{\partial}{\partial x_{3D}} \left(\phi_D S_{aD} D_{TapD} \frac{\partial}{\partial x_{3D}} (C_{aD} \rho_{aD})\right) \; +$$

$$\left[\frac{C_{apR} \rho_{aR} K_{aR} P_{aR}}{\mu_{aR} x_{1R}^{2}}\right] \frac{\partial}{\partial x_{1D}} \left(\frac{C_{apD} \rho_{aD} K_{aD}}{\mu_{aD}} \frac{\partial P_{aD}}{\partial x_{1D}}\right) \; +$$

$$\left[\frac{C_{apR} \rho_{aR}^{2} K_{aR} g_R z_R}{\mu_{aR} x_{1R}^{2}}\right] \frac{\partial}{\partial x_{1D}} \left(\frac{C_{apD} \rho_{aD}^{2} K_{aD} g_D}{\mu_{aD}} \frac{\partial z_D}{\partial x_{1D}}\right) \; +$$

$$[\frac{C_{apR}\rho_{aR}K_{aR}P_{aR}}{\mu_{aR}x_{1R}^{2}}]\frac{\partial}{\partial x_{1D}}(\frac{C_{apD}\rho_{aD}K_{aD}}{\mu_{aD}}\frac{\partial P_{aD}}{\partial x_{1D}}) +$$

$$[\frac{C_{apR}\rho_{aR}^{2}K_{aR}g_{R}z_{R}}{\mu_{aR}x_{2R}^{2}}]\frac{\partial}{\partial x_{2D}}(\frac{C_{apD}\rho_{aD}^{2}K_{aD}g_{D}}{\mu_{aD}}\frac{\partial z_{D}}{\partial x_{2D}}) +$$

$$[\frac{C_{apR}\rho_{aR}K_{aR}P_{aR}}{\mu_{aR}x_{2R}^{2}}]\frac{\partial}{\partial x_{2D}}(\frac{C_{apD}\rho_{aD}K_{aD}}{\mu_{aD}}\frac{\partial P_{aD}}{\partial x_{2D}}) +$$

$$[\frac{C_{apR}\rho_{aR}^{2}K_{aR}g_{R}z_{R}}{\mu_{aR}x_{3R}^{2}}]\frac{\partial}{\partial x_{3D}}(\frac{C_{apD}\rho_{aD}^{2}K_{aD}g_{D}}{\mu_{aD}}\frac{\partial z_{D}}{\partial x_{3D}}) +$$

$$[\frac{C_{apR}\rho_{aR}K_{aR}P_{aR}}{\mu_{aR}x_{3R}^{2}}]\frac{\partial}{\partial x_{3D}}(\frac{C_{apD}\rho_{aD}K_{aD}}{\mu_{aD}}\frac{\partial P_{aD}}{\partial x_{3D}})$$

The equation for the mass balance of water in terms of the dimensionless variables and their reference quantities is:

$$[\frac{\phi_{R}S_{aR}C_{awR}\rho_{aR}}{t_{R}}]\frac{\partial}{\partial t_{D}}(\phi_{D}S_{aD}\rho_{aD}) =$$

$$[\frac{C_{awR}\rho_{aR}K_{aR}P_{aR}}{x_{1R}^{2}\mu_{aR}}]\frac{\partial}{\partial x_{1D}}(\frac{C_{awD}\rho_{aD}K_{aD}}{\mu_{aD}}\frac{\partial P_{aD}}{\partial x_{1D}}) +$$

$$[\frac{\rho_{aR}^{2}C_{awR}K_{aR}g_{R}z_{R}}{\mu_{aR}x_{1R}^{2}}]\frac{\partial}{\partial x_{1D}}(\frac{\rho_{aD}^{2}K_{aD}g_{D}C_{awD}}{\mu_{aD}}\frac{\partial z_{D}}{\partial x_{1D}}) +$$

$$[\frac{C_{awR}\rho_{aR}K_{aR}P_{aR}}{x_{2R}^{2}\mu_{aR}}]\frac{\partial}{\partial x_{2D}}(\frac{C_{awD}\rho_{aD}K_{aD}}{\mu_{aD}}\frac{\partial P_{aD}}{\partial x_{2D}}) +$$

$$[\frac{\rho_{aR}^{2}C_{awR}K_{aR}g_{R}z_{R}}{\mu_{aR}x_{2R}^{2}}]\frac{\partial}{\partial x_{2D}}(\frac{\rho_{aD}^{2}K_{aD}g_{D}C_{awD}}{\mu_{aD}}\frac{\partial z_{D}}{\partial x_{2D}}) +$$

$$[\frac{C_{awR}\rho_{aR}K_{aR}P_{aR}}{x_{3R}^{2}\mu_{aR}}]\frac{\partial}{\partial x_{3D}}(\frac{C_{awD}\rho_{aD}K_{aD}}{\mu_{aD}}\frac{\partial P_{aD}}{\partial x_{3D}}) +$$

$$\left[\frac{\rho_{aR}^{2} C_{awR} K_{aR} g_{R} z_{R}}{\mu_{aR} x_{3R}^{2}}\right] \frac{\partial}{\partial x_{3D}} \left(\frac{\rho_{aD}^{2} K_{aD} g_{D} C_{awD}}{\mu_{aD}} \frac{\partial z_{D}}{\partial x_{3D}} \right) +$$

$$\left[\frac{\phi_{R} S_{aR} C_{awR} D_{LawR} \rho_{aR}}{x_{1R}^{2}}\right] \frac{\partial}{\partial x_{1D}} \left(\phi_{D} S_{aD} D_{LawD} \frac{\partial}{\partial x_{1D}} (C_{awD} \rho_{aD}) \right) +$$

$$\left[\frac{\phi_{R} S_{aR} C_{awR} D_{LawR} \rho_{aR}}{x_{2R}^{2}}\right] \frac{\partial}{\partial x_{2D}} \left(\phi_{D} S_{aD} D_{LawD} \frac{\partial}{\partial x_{2D}} (C_{awD} \rho_{aD}) \right) +$$

$$\left[\frac{\phi_{R} S_{aR} C_{awR} D_{LawR} \rho_{aR}}{x_{3R}^{2}}\right] \frac{\partial}{\partial x_{3D}} \left(\phi_{D} S_{aD} D_{LawD} \frac{\partial}{\partial x_{3D}} (C_{awD} \rho_{aD}) \right)$$

The reference quantities in the square brackets represent the coefficient for that term in the equation. All coefficients have the same dimensions. Consequently, similarity groups may be determined by dividing the entire equation by one of these coefficients. This yields the dimensionless form of the equation and the similarity groups or dimensionless coefficients. Once the dimensionless groups are obtained, the set may be replaced by any other set obtained from the products of the groups with any other group raised to any power.

Dividing both sides of the oil equation by $\frac{\rho_{1R} K_{1R} P_{1R}}{x_{1R}^{2} \mu_{1R}}$, one obtains the following dimensionless groups:

$$\left[\frac{\phi_{R} S_{1R} x_{1R}^{2} \mu_{1R}}{t_{R} K_{1R} P_{1R}}\right], \quad \left[\frac{\rho_{1R} g_{R} z_{R}}{P_{1R}}\right], \quad \left[\frac{x_{1R}^{2}}{x_{2R}^{2}}\right], \quad \left[\frac{x_{1R}^{2}}{x_{3R}^{2}}\right]$$

Dividing both sides of the polymer equation by

$\frac{C_{apR}\bar{\rho}_{aR}K_{aR}P_{aR}}{\mu_{aR}x_{1R}^2}$, one obtains the following dimensionless

groups:

$$[\frac{\phi_R S_{aR}\mu_{aR}x_{1R}^2}{t_R K_{aR}P_{aR}}],\ [\frac{\rho_{rR}A_{pR}}{\phi_R S_{aR}}],$$

$$[\frac{\phi_R S_{aR}D_{LapR}\mu_{aR}}{K_{aR}P_{aR}}],\ [\frac{\phi_R S_{aR}D_{TapR}\mu_{aR}}{K_{aR}P_{aR}}],$$

$$[\frac{\rho_{aR}g_R z_R}{P_{aR}}],\ [\frac{x_{1R}^2}{x_{1R}^2}],\ [\frac{x_{1R}^2}{x_{1R}^2}],\ [BC_{apR}]$$

Dividing both sides of the water equation by

$\frac{C_{awR}\bar{\rho}_{aR}K_{aR}P_{aR}}{x_{1R}^2\ \mu_{aR}}$, one obtains the following

dimensionless groups:

$$[\frac{\phi_R S_{aR}\mu_{aR}x_{1R}^2}{t_R K_{aR}P_{aR}}],\ [\frac{\rho_{aR}g_R z_R}{P_{aR}}],\ [\frac{x_{1R}^2}{x_{2R}^2}],\ [\frac{x_{1R}^2}{x_{3R}^2}]$$

$$[\frac{\phi_R S_{aR}D_{LawR}\mu_{aR}}{K_{aR}P_{aR}}],\ [\frac{\phi_R S_{aR}D_{TawR}\mu_{aR}}{K_{aR}P_{aR}}],\ [\frac{\phi_R S_{aR}D_{TawR}\mu_{aR}}{K_{aR}P_{aR}}]$$

The dimensionless groups that arise from the boundary and initial conditions are:

$$[\frac{C_{apR}}{C_{awR}}\frac{W_{apR}}{W_{awR}}],\ [\frac{L}{x_{1R}}],\ [\frac{W}{x_{2R}}],\ [\frac{H}{x_{3R}}],$$

$$[\frac{S_{ai}}{S_{ai}}],\ [\frac{S_{1i}}{S_{1R}}],\ [\frac{S_{aR}}{S_{1R}}],\ [\frac{P_{prod}}{P_{1R}}],\ [\frac{P_{aR}}{P_{claR}}],$$

$$[\frac{W_{awR}C_{awR}\mu_{aR}}{P_{aR}A_{inj}}],\ [\frac{P_{1iR}}{P_{1R}}]$$

The dimensionless groups obtained from constraints and constitutive relationships are:

$$[\frac{C_{apR}}{C_{awR}}],\ [\frac{C_{apR}}{C_{awR}}],\ [\frac{\rho_{1R}}{\rho_{1R}}],\ [\frac{P_{aR}}{P_{1R}}],\ [\phi_R],\ [\frac{D^*_{awR}}{D^*_{apR}}],\ [R]$$

12.1.2 Emulsion Flood

12.1.2.1 Emulsion Flood: Two-Phase Flow

The equation for the mass balance of oil in terms of the dimensionless variables and their reference quantity is:

$$[\frac{\phi_R S_{1R}\rho_{1R}C_{1oR}}{t_R}]\ \frac{\partial}{\partial t_D}\ (\phi_D S_{1D}C_{1oD}\rho_{1D}) =$$

$$[\frac{\rho_{1R}C_{1oR}K_{1R}P_{1R}}{x_{1R}^2\mu_{1R}}]\ \frac{\partial}{\partial x_{1D}}\ (\frac{\rho_{1D}C_{1oD}K_{1D}}{\mu_{1D}}\ \frac{\partial P_{1D}}{\partial x_{1D}}) +$$

$$[\frac{\rho_{1R}^2C_{1oR}K_{1R}g_R z_R}{x_{1R}^2\mu_{1R}}]\ \frac{\partial}{\partial x_{1D}}\ (\frac{\rho_{1D}^2C_{1oD}K_{1D}g_D}{\mu_{1D}}\ \frac{\partial z_D}{\partial x_{1D}}) +$$

$$[\frac{\rho_{1R}C_{1oR}K_{1R}P_{1R}}{x_{2R}^2\mu_{1R}}]\ \frac{\partial}{\partial x_{2D}}\ (\frac{\rho_{1D}C_{1oD}K_{1D}}{\mu_{1D}}\ \frac{\partial P_{1D}}{\partial x_{2D}}) +$$

$$[\frac{\rho_{1R}^2C_{1oR}K_{1R}g_R z_R}{x_{2R}^2\mu_{1R}}]\ \frac{\partial}{\partial x_{2D}}\ (\frac{\rho_{1D}^2C_{1oD}K_{1D}g_D}{\mu_{1D}}\ \frac{\partial z_D}{\partial x_{2D}}) +$$

$$[\frac{\rho_{1R}C_{1oR}K_{1R}P_{1R}}{x_{3R}^2\mu_{1R}}]\ \frac{\partial}{\partial x_{3D}}\ (\frac{\rho_{1D}C_{1oD}K_{1D}}{\mu_{1D}}\ \frac{\partial P_{1D}}{\partial x_{3D}}) +$$

$$\left[\frac{\rho_{1R}{}^{2}C_{1oR}K_{1R}g_{R}z_{R}}{x_{3R}{}^{2}\mu_{1R}}\right]\frac{\partial}{\partial x_{3D}}\left(\frac{\rho_{1D}{}^{2}C_{1oD}K_{1D}g_{D}}{\mu_{1D}}\frac{\partial z_{D}}{\partial x_{3D}}\right) +$$

$$\left[\frac{\phi_{R}C_{1oR}S_{1r}D_{L1oR}\rho_{1R}}{x_{1R}{}^{2}}\right]\frac{\partial}{\partial x_{1D}}\left(\phi_{D}C_{1oD}S_{1D}D_{LoD}\frac{\partial}{\partial x_{1D}}\left(C_{1oD}\rho_{1D}\right)\right)$$

$$\left[\frac{\phi_{R}C_{1oR}S_{1r}D_{T1oR}\rho_{1R}}{x_{2R}{}^{2}}\right]\frac{\partial}{\partial x_{2D}}\left(\phi_{D}C_{1oD}S_{1D}D_{ToD}\frac{\partial}{\partial x_{2D}}\left(C_{1oD}\rho_{1D}\right)\right)$$

$$\left[\frac{\phi_{R}C_{1oR}S_{1r}D_{T1oR}\rho_{1R}}{x_{3R}{}^{2}}\right]\frac{\partial}{\partial x_{3D}}\left(\phi_{D}C_{1oD}S_{1D}D_{ToD}\frac{\partial}{\partial x_{3D}}\left(C_{1oD}\rho_{1D}\right)\right)$$

The equation for the mass balance of emulsion in terms of the dimensionless variables and their reference quantity is:

$$\left[\frac{\phi_{R}S_{1R}C_{1mR}\rho_{1R}}{t_{R}}\right]\frac{\partial}{\partial t_{D}}\left(\phi_{D}S_{1D}C_{1mD}\rho_{1D}\right) +$$

$$\left[\frac{\phi_{R}S_{aR}C_{amR}\rho_{aR}}{t_{R}}\right]\frac{\partial}{\partial t_{D}}\left(\phi_{D}S_{aD}C_{amD}\rho_{aD}\right) =$$

$$\left[\frac{\rho_{1R}C_{1mR}K_{1R}P_{1R}}{x_{1R}{}^{2}\mu_{1R}}\right]\frac{\partial}{\partial x_{1D}}\left(\frac{\rho_{1D}C_{1mD}K_{1D}}{\mu_{1D}}\frac{\partial P_{1D}}{\partial x_{1D}}\right) +$$

$$\left[\frac{\rho_{1R}{}^{2}C_{1mR}K_{1R}g_{R}z_{R}}{x_{1R}{}^{2}\mu_{1R}}\right]\frac{\partial}{\partial x_{1D}}\left(\frac{\rho_{1D}{}^{2}C_{1mD}K_{1D}g_{D}}{\mu_{1D}}\frac{\partial z_{D}}{\partial x_{1D}}\right) +$$

$$\left[\frac{\rho_{1R}C_{1mR}K_{1R}P_{1R}}{x_{2R}{}^{2}\mu_{1R}}\right]\frac{\partial}{\partial x_{2D}}\left(\frac{\rho_{1D}C_{1mD}K_{1D}}{\mu_{1D}}\frac{\partial P_{1D}}{\partial x_{2D}}\right) +$$

$$\left[\frac{\rho_{1R}{}^{2}C_{1mR}K_{1R}g_{R}z_{R}}{x_{2R}{}^{2}\mu_{1R}}\right]\frac{\partial}{\partial x_{2D}}\left(\frac{\rho_{1D}{}^{2}C_{1mD}K_{1D}g_{D}}{\mu_{1D}}\frac{\partial z_{D}}{\partial x_{2D}}\right) +$$

$$\left[\frac{\rho_{1R}C_{1mR}K_{1R}P_{1R}}{x_{3R}{}^{2}\mu_{1R}}\right]\frac{\partial}{\partial x_{3D}}\left(\frac{\rho_{1D}C_{1mD}K_{1D}}{\mu_{1D}}\frac{\partial P_{1D}}{\partial x_{3D}}\right) +$$

$$\left[\frac{\rho_{1R}^{2}C_{1mR}K_{1R}g_{R}z_{R}}{x_{3R}^{2}\mu_{1R}}\right]\frac{\partial}{\partial x_{3D}}\left(\frac{\rho_{1D}^{2}C_{1mD}K_{1D}g_{D}}{\mu_{1D}}\frac{\partial z_{D}}{\partial x_{3D}}\right)+$$

$$\left[\frac{\rho_{aR}C_{amR}K_{aR}P_{aR}}{x_{1R}^{2}\mu_{aR}}\right]\frac{\partial}{\partial x_{1D}}\left(\frac{\rho_{aD}C_{amD}K_{aD}}{\mu_{aD}}\frac{\partial P_{aD}}{\partial x_{1D}}\right)+$$

$$\left[\frac{\rho_{aR}^{2}C_{amR}K_{aR}g_{R}z_{R}}{x_{1R}^{2}\mu_{aR}}\right]\frac{\partial}{\partial x_{1D}}\left(\frac{\rho_{aD}^{2}C_{amD}K_{aD}g_{D}}{\mu_{aD}}\frac{\partial z_{D}}{\partial x_{1D}}\right)+$$

$$\left[\frac{\rho_{aR}C_{amR}K_{aR}P_{aR}}{x_{2R}^{2}\mu_{aR}}\right]\frac{\partial}{\partial x_{2D}}\left(\frac{\rho_{aD}C_{amD}K_{aD}}{\mu_{aD}}\frac{\partial P_{aD}}{\partial x_{2D}}\right)+$$

$$\left[\frac{\rho_{aR}^{2}C_{amR}K_{aR}g_{R}z_{R}}{x_{2R}^{2}\mu_{aR}}\right]\frac{\partial}{\partial x_{2D}}\left(\frac{\rho_{aD}^{2}C_{amD}K_{aD}g_{D}}{\mu_{aD}}\frac{\partial z_{D}}{\partial x_{2D}}\right)+$$

$$\left[\frac{\rho_{aR}C_{amR}K_{aR}P_{aR}}{x_{3R}^{2}\mu_{aR}}\right]\frac{\partial}{\partial x_{3D}}\left(\frac{\rho_{aD}C_{amD}K_{aD}}{\mu_{aD}}\frac{\partial P_{aD}}{\partial x_{3D}}\right)+$$

$$\left[\frac{\rho_{aR}^{2}C_{amR}K_{aR}g_{R}z_{R}}{x_{3R}^{2}\mu_{aR}}\right]\frac{\partial}{\partial x_{3D}}\left(\frac{\rho_{aD}^{2}C_{amD}K_{aD}g_{D}}{\mu_{aD}}\frac{\partial z_{D}}{\partial x_{3D}}\right)+$$

$$\left[\frac{\phi_{R}C_{1mR}S_{1R}D_{L1mR}\rho_{1R}}{x_{1R}^{2}}\right]\frac{\partial}{\partial x_{1D}}\left(\phi_{D}C_{1mD}S_{1D}D_{L1mD}\frac{\partial}{\partial x_{1D}}(C_{1mD}\rho_{1D})\right)+$$

$$\left[\frac{\phi_{R}C_{1mR}S_{1R}D_{T1mR}\rho_{1R}}{x_{2R}^{2}}\right]\frac{\partial}{\partial x_{2D}}\left(\phi_{D}C_{1mD}S_{1D}D_{T1mD}\frac{\partial}{\partial x_{2D}}(C_{1mD}\rho_{1D})\right)+$$

$$\left[\frac{\phi_{R}C_{1mR}S_{1R}D_{T1mR}\rho_{1R}}{x_{3R}^{2}}\right]\frac{\partial}{\partial x_{3D}}\left(\phi_{D}C_{1mD}S_{1D}D_{T1mD}\frac{\partial}{\partial x_{3D}}(C_{1mD}\rho_{1D})\right)+$$

$$\left[\frac{\phi_{R}C_{amR}S_{aR}D_{LamR}\rho_{aR}}{x_{1R}^{2}}\right]\frac{\partial}{\partial x_{1D}}\left(\phi_{D}C_{amD}S_{aD}D_{LamD}\frac{\partial}{\partial x_{1D}}(C_{amD}\rho_{aD})\right)+$$

$$\left[\frac{\phi_{R}C_{amR}S_{aR}D_{TamR}\rho_{aR}}{x_{2R}^{2}}\right]\frac{\partial}{\partial x_{2D}}\left(\phi_{D}C_{amD}S_{aD}D_{TamD}\frac{\partial}{\partial x_{2D}}(C_{amD}\rho_{aD})\right)+$$

$$\left[\frac{\phi_{R}C_{amR}S_{aR}D_{TamR}\rho_{aR}}{x_{3R}^{2}}\right]\frac{\partial}{\partial x_{3D}}\left(\phi_{D}C_{amD}S_{aD}D_{TamD}\frac{\partial}{\partial x_{3D}}(C_{amD}\rho_{aD})\right)$$

The equation for the mass balance of water in terms of the dimensionless variables and their reference quantities is:

$$
\begin{aligned}
&\left[\frac{\phi_R S_{aR} \rho_{aR} C_{awR}}{t_R}\right] \frac{\partial}{\partial t_D} (\phi_D S_{aD} C_{awD} \rho_{aD}) = \\
&\left[\frac{\rho_{aR} C_{awR} K_{aR} P_{aR}}{x_{1R}^{2} \mu_{aR}}\right] \frac{\partial}{\partial x_{1D}} \left(\frac{\rho_{aD} C_{awD} K_{aD}}{\mu_{aD}} \frac{\partial P_{aD}}{\partial x_{1D}}\right) + \\
&\left[\frac{\rho_{aR}^{2} C_{awR} K_{aR} g_R z_R}{x_{1R}^{2} \mu_{aR}}\right] \frac{\partial}{\partial x_{1D}} \left(\frac{\rho_{aD}^{2} C_{awD} K_{aD} g_D}{\mu_{aD}} \frac{\partial z_D}{\partial x_{1D}}\right) + \\
&\left[\frac{\rho_{aR} C_{awR} K_{aR} P_{aR}}{x_{2R}^{2} \mu_{aR}}\right] \frac{\partial}{\partial x_{2D}} \left(\frac{\rho_{aD} C_{awD} K_{aD}}{\mu_{aD}} \frac{\partial P_{aD}}{\partial x_{2D}}\right) + \\
&\left[\frac{\rho_{aR}^{2} C_{awR} K_{aR} g_R z_R}{x_{2R}^{2} \mu_{aR}}\right] \frac{\partial}{\partial x_{2D}} \left(\frac{\rho_{aD}^{2} C_{awD} K_{aD} g_D}{\mu_{aD}} \frac{\partial z_D}{\partial x_{2D}}\right) + \\
&\left[\frac{\rho_{aR} C_{awR} K_{aR} P_{aR}}{x_{3R}^{2} \mu_{aR}}\right] \frac{\partial}{\partial x_{3D}} \left(\frac{\rho_{aD} C_{awD} K_{aD}}{\mu_{aD}} \frac{\partial P_{aD}}{\partial x_{3D}}\right) + \\
&\left[\frac{\rho_{aR}^{2} C_{awR} K_{aR} g_R z_R}{x_{3R}^{2} \mu_{aR}}\right] \frac{\partial}{\partial x_{3D}} \left(\frac{\rho_{aD}^{2} C_{awD} K_{aD} g_D}{\mu_{aD}} \frac{\partial z_D}{\partial x_{3D}}\right) + \\
&\left[\frac{\phi_R C_{awR} S_{aR} D_{LawR} \rho_{aR}}{x_{1R}^{2}}\right] \frac{\partial}{\partial x_{1D}} \left(\phi_D C_{awD} S_{aD} D_{LawD} \frac{\partial}{\partial x_{1D}} (C_{awD} \rho_{aD})\right) + \\
&\left[\frac{\phi_R C_{awR} S_{aR} D_{TawR} \rho_{aR}}{x_{2R}^{2}}\right] \frac{\partial}{\partial x_{2D}} \left(\phi_D C_{awD} S_{aD} D_{TawD} \frac{\partial}{\partial x_{2D}} (C_{awD} \rho_{aD})\right) + \\
&\left[\frac{\phi_R C_{awR} S_{aR} D_{TawR} \rho_{aR}}{x_{3R}^{2}}\right] \frac{\partial}{\partial x_{3D}} \left(\phi_D C_{awD} S_{aD} D_{TawD} \frac{\partial}{\partial x_{3D}} (C_{awD} \rho_{aD})\right)
\end{aligned}
$$

Dividing both sides of the mass balance equation for oil by $\frac{\rho_{1R}C_{1oR}K_{1R}P_{1R}}{x_{1R}^2\mu_{1R}}$, one obtains the following dimensionless groups:

$$[\frac{\phi_R S_{1R}\mu_{1R}x_{1R}^2}{t_R K_{1R}P_{1R}}],\ [\frac{g_R z_R \rho_{1R}}{P_{1R}}],\ [\frac{x_{1R}^2}{x_{2R}^2}],\ [\frac{x_{1R}^2}{x_{3R}^2}],$$

$$[\frac{\phi_R S_{1R}D_{L1oR}\mu_{1R}}{K_{1R}P_{1R}}],\ [\frac{\phi_R S_{1R}D_{T1oR}\mu_{1R}}{K_{1R}P_{1R}}]$$

Dividing both sides of the mass balance equation for emulsion by $\frac{\rho_{1R}C_{1mR}K_{1R}P_{1R}}{x_{1R}^2\mu_{1R}}$, one obtains the following dimensionless groups:

$$[\frac{\phi_R S_{1R}\mu_{1R}x_{1R}^2}{t_R K_{1R}P_{1R}}],\ [\frac{\rho_{1R}g_R z_R}{P_{1R}}],\ [\frac{x_{1R}^2}{x_{2R}^2}],\ [\frac{x_{1R}^2}{x_{3R}^2}],$$

$$[\frac{\rho_{aR}C_{amR}K_{aR}P_{aR}\mu_{1R}}{\rho_{1R}C_{1mR}K_{1R}P_{1R}\mu_{aR}}],\ [\frac{\rho_{aR}^2C_{amR}K_{aR}g_R z_R\mu_{1R}}{\rho_{1R}C_{1mR}K_{1R}P_{1R}\mu_{aR}}],$$

$$[\frac{\phi_R S_{1R}D_{L1mR}\mu_{1R}}{K_{1R}P_{1R}}],\ [\frac{\phi_R S_{1R}D_{T1mR}\mu_R x_{1R}^2\mu_{1R}}{x_{2R}^2K_{1R}P_{1R}}],\ [\frac{S_{aR}}{S_{1R}}],$$

$$[\frac{\phi_R C_{amR}S_{aR}D_{LamR}\rho_{aR}\mu_{1R}}{\rho_{1R}C_{1mR}K_{1R}P_{1R}}],\ [\frac{\phi_R C_{amR}S_{aR}D_{TamR}\rho_{aR}\mu_{1R}}{\rho_{1R}C_{1mR}K_{1R}P_{1R}}]$$

Dividing both sides of the mass balance equation for water by $\frac{\rho_{aR}C_{awR}K_{aR}P_{aR}}{x_{1R}^2\mu_{aR}}$, one obtains the following dimensionless groups:

$$[\frac{\phi_R S_{aR} \mu_{aR} x_{1R}^2}{t_R K_{aR} P_{aR}}], \ [\frac{g_R z_R \rho_{aR}}{P_{aR}}], \ [\frac{x_{1R}^2}{x_{2R}^2}], \ [\frac{x_{1R}^2}{x_{3R}^2}],$$

$$[\frac{\phi_R S_{aR} D_{LawR} \mu_{aR}}{K_{aR} P_{aR}}], \ [\frac{\phi_R S_{aR} D_{TawR} \mu_{aR}}{K_{aR} P_{aR}}]$$

From the initial and boundary conditions, constitutive relationships and constraints, one obtains the following dimensionless groups:

$$[\frac{S_{aR}}{S_{1R}}], \ [\frac{C_{1oR}}{C_{1mR}}], \ [\frac{C_{amR}}{C_{awR}}], \ [\frac{\rho_{1R}}{\rho_{aR}}], \ [\frac{P_{1R}}{P_{aR}}],$$

$$[\phi_R], \ [\frac{P_{1R}}{P_{cla}}], \ [\frac{D^*_{1oR}}{D^*_{1mR}}], \ [\frac{D^*_{awR}}{D^*_{amR}}], \ [\frac{W_{amR}}{W_{awR}}],$$

$$[\frac{W_{awR} C_{awR} \mu_{aR} x_{1R}}{K_{aR} P_{aR} A_{injR}}], \ [\frac{P_{prod}}{P_{1R}}], \ [\frac{P_{aR}}{P_{claR}}], \ [\frac{S_{ai}}{S_{aR}}], \ [\frac{S_{1i}}{S_{1R}}], \ [\frac{P_{1i}}{P_{1R}}],$$

$$[\frac{W}{x_{1R}}], \ [\frac{H}{x_{3R}}], \ [\frac{L}{x_{1R}}]$$

12.1.2.2 Emulsion Flood: Emulsion Miscible in Aqueous Phase Only

In a similar way one may write down the governing equations for this case in dimensionless form. The mass balance equation for oil gives rise to the following dimensionless groups:

$$[\frac{\phi_R S_{1R} \mu_{1R} x_{1R}^2}{t_R K_{1R} P_{1R}}], \ [\frac{g_R z_R \rho_{1R}}{P_{1R}}], \ [\frac{x_{1R}^2}{x_{2R}^2}], \ [\frac{x_{1R}^2}{x_{3R}^2}]$$

The mass balance equation for emulsion gives rise to the following dimensionless groups:

$$\left[\frac{\phi_R S_{aR} \mu_{aR} x_{1R}^2}{t_R K_{aR} P_{aR}}\right], \left[\frac{\rho_{aR} g_R z_R}{P_{aR}}\right], \left[\frac{x_{1R}^2}{x_{2R}^2}\right], \left[\frac{x_{1R}^2}{x_{3R}^2}\right],$$

$$\left[\frac{\phi_R C_{amR} S_{aR} D_{LamR} \rho_{aR} \mu_{aR}}{\rho_{aR} C_{amR} K_{aR} P_{aR}}\right], \left[\frac{\phi_R C_{amR} S_{aR} D_{TamR} \rho_{aR} \mu_{aR}}{\rho_{aR} C_{amR} K_{aR} P_{aR}}\right]$$

The mass balance equation for water gives rise to the following dimensionless groups:

$$\left[\frac{\phi_R S_{aR} \mu_{aR} x_{1R}^2}{t_R K_{aR} P_{aR}}\right], \left[\frac{g_R z_R \rho_{aR}}{P_{aR}}\right], \left[\frac{x_{1R}^2}{x_{2R}^2}\right], \left[\frac{x_{1R}^2}{x_{3R}^2}\right],$$

$$\left[\frac{\phi_R S_{aR} D_{LawR} \mu_{aR}}{K_{aR} P_{aR}}\right], \left[\frac{\phi_R S_{aR} D_{TawR} \mu_{aR}}{K_{aR} P_{aR}}\right]$$

From the initial and boundary conditions, constitutive relationships and constraints, one obtains the following dimensionless groups:

$$\left[\frac{S_{aR}}{S_{1R}}\right], \left[\frac{C_{amR}}{C_{awR}}\right], \left[\frac{\rho_{1R}}{\rho_{aR}}\right], \left[\frac{P_{1R}}{P_{aR}}\right],$$

$$[\phi_R], \left[\frac{P_{1R}}{P_{claR}}\right], \left[\frac{D^*_{awR}}{D^*_{amR}}\right], \left[\frac{W_{amR}}{W_{amR}}\right],$$

$$\left[\frac{W_{awR} C_{awR} \mu_{aR} x_{1R}}{K_{aR} P_{aR} A_{injR}}\right], \left[\frac{P_{prod}}{P_{1R}}\right], \left[\frac{P_{aR}}{P_{claR}}\right], \left[\frac{S_{ai}}{S_{aR}}\right], \left[\frac{S_{li}}{S_{1R}}\right], \left[\frac{P_{li}}{P_{1R}}\right],$$

$$\left[\frac{W}{x_{1R}}\right], \left[\frac{H}{x_{3R}}\right], \left[\frac{L}{x_{1R}}\right]$$

12.1.2.3 Emulsion Flood: Three-Phase Flow

In a similar way one may write down the governing equations for the case of three-phase flow. The mass balance equation for oil gives rise to the following dimensionless groups:

$$\left[\frac{\phi_R S_{1R} \mu_{1R} x_{1R}^2}{t_R K_{1R} P_{1R}}\right], \quad \left[\frac{g_R z_R \rho_{1R}}{P_{1R}}\right], \quad \left[\frac{x_{1R}^2}{x_{2R}^2}\right], \quad \left[\frac{x_{1R}^2}{x_{3R}^2}\right]$$

The mass balance equation for emulsion gives rise to the following dimensionless groups:

$$\left[\frac{\phi_R S_{aR} \mu_{aR} x_{1R}^2}{t_R K_{aR} P_{aR}}\right], \quad \left[\frac{\rho_{aR} g_R z_R}{P_{aR}}\right], \quad \left[\frac{x_{1R}^2}{x_{2R}^2}\right], \quad \left[\frac{x_{1R}^2}{x_{3R}^2}\right],$$

$$\left[\frac{\rho_{aR} C_{amR} K_{aR} P_{aR} \mu_{mR}}{\rho_{mR} C_{mmR} K_{mR} P_{mR} \mu_{aR}}\right], \quad \left[\frac{\rho_{aR}^2 C_{amR} K_{aR} g_R z_R \mu_{mR}}{\rho_{mR} C_{mmR} K_{mR} P_{mR} \mu_{aR}}\right],$$

$$\left[\frac{\phi_R S_{mR} D_{LmmR} \mu_{mR}}{K_{mR} P_{mR}}\right], \quad \left[\frac{\phi_R S_{mR} D_{TmmR} \mu_R x_{1R}^2 \mu_{mR}}{x_{2R}^2 K_{mR} P_{mR}}\right],$$

$$\left[\frac{\phi_R C_{amR} S_{aR} D_{LamR} \rho_{aR} \mu_{mR}}{\rho_{mR} C_{mmR} K_{mR} P_{mR}}\right], \quad \left[\frac{\phi_R C_{amR} S_{aR} D_{TamR} \rho_{aR} \mu_{mR}}{\rho_{mR} C_{mmR} K_{mR} P_{mR}}\right]$$

$$\left[\frac{\phi_R S_{aR} D_{LawR} \mu_{aR}}{K_{aR} P_{aR}}\right], \quad \left[\frac{\phi_R S_{aR} D_{TawR} \mu_{aR}}{K_{aR} P_{aR}}\right],$$

$$\left[\frac{C_{mwR}}{C_{mmR}}\right]$$

From the initial and boundary conditions, constitutive relationships and constraints, one obtains the following dimensionless groups:

$$[\frac{S_{aR}}{S_{lR}}],\ [\frac{C_{loR}}{C_{lmR}}],\ [\frac{C_{amR}}{C_{awR}}],\ [\frac{\rho_{lR}}{\rho_{aR}}],\ [\frac{P_{lR}}{P_{aR}}],\ [\frac{P_{mR}}{P_{aR}}],\ [\frac{\rho_{mR}}{\rho_{aR}}],$$

$$[\frac{S_{aR}}{S_{mR}}],\ [\frac{P_{mR}}{P_{cmaR}}],\ [\frac{W_{awR}}{W_{mmR}}],\ [\frac{S_{mi}}{S_{mR}}],$$

$$[\phi_R],\ [\frac{P_{lR}}{P_{claR}}],\ [\frac{D^*_{amR}}{D^*_{awR}}],\ [\frac{D^*_{awR}}{D^*_{amR}}],\ [\frac{D^*_{mwR}}{D^*_{mmR}}],\ [\frac{W_{amR}}{W_{awR}}],$$

$$[\frac{W_{awR}C_{awR}\mu_{aR}x_{1R}}{K_{aR}P_{aR}A_{injR}}],\ [\frac{P_{prod}}{P_{lR}}],\ [\frac{P_{aR}}{P_{claR}}],\ [\frac{S_{ai}}{S_{aR}}],\ [\frac{S_{li}}{S_{lR}}],\ [\frac{P_{li}}{P_{lR}}],$$

$$[\frac{W}{x_{1R}}],\ [\frac{H}{x_{3R}}],\ [\frac{L}{x_{1R}}],\ [\frac{P_{lR}}{P_{clmR}}],\ [\frac{P_{mi}}{P_{lR}}],$$

12.1.3 Foam Injection

Two different possibilities were investigated for the foam injection. They are described in the following.

12.1.3.1 Foam Injection: Four-Phase Flow

The equation for the mass balance of oil in terms of the dimensionless variables and their reference quantity is:

$$[\frac{\phi_R S_{lR}\rho_{lR}C_{loR}}{t_R}]\ \frac{\partial}{\partial t_D}\ (\phi_D S_{lD}C_{loD}\rho_{lD}) =$$

$$[\frac{\rho_{lR}C_{loR}K_{lR}P_{lR}}{x_{1R}^2\mu_{lR}}]\ \frac{\partial}{\partial x_{1D}}\ (\frac{\rho_{lD}C_{loD}K_{lD}}{\mu_{lD}}\ \frac{\partial P_{lD}}{\partial x_{1D}})\ +$$

$$[\frac{\rho_{lR}^2C_{loR}K_{lR}g_R z_R}{x_{1R}^2\mu_{lR}}]\ \frac{\partial}{\partial x_{1D}}\ (\frac{\rho_{lD}^2C_{loD}K_{lD}g_D}{\mu_{lD}}\ \frac{\partial z_D}{\partial x_{1D}})\ +$$

$$[\frac{\rho_{lR}C_{loR}K_{lR}P_{lR}}{x_{2R}^2\mu_{lR}}]\ \frac{\partial}{\partial x_{2D}}\ (\frac{\rho_{lD}C_{loD}K_{lD}}{\mu_{lD}}\ \frac{\partial P_{lD}}{\partial x_{2D}})\ +$$

$$\left[\frac{\rho_{1R}^{2} C_{1oR} K_{1R} g_R z_R}{x_{2R}^{2} \mu_{1R}}\right] \frac{\partial}{\partial x_{2D}} \left(\frac{\rho_{1D}^{2} C_{1oD} K_{1D} g_D}{\mu_{1D}} \frac{\partial z_D}{\partial x_{2D}}\right) +$$

$$\left[\frac{\rho_{1R} C_{1oR} K_{1R} P_{1R}}{x_{3R}^{2} \mu_{1R}}\right] \frac{\partial}{\partial x_{3D}} \left(\frac{\rho_{1D} C_{1oD} K_{1D}}{\mu_{1D}} \frac{\partial P_{1D}}{\partial x_{3D}}\right) +$$

$$\left[\frac{\rho_{1R}^{2} C_{1oR} K_{1R} g_R z_R}{x_{3R}^{2} \mu_{1R}}\right] \frac{\partial}{\partial x_{3D}} \left(\frac{\rho_{1D}^{2} C_{1oD} K_{1D} g_D}{\mu_{1D}} \frac{\partial z_D}{\partial x_{3D}}\right) +$$

The equation for the mass balance of surfactant in terms of the dimensionless variables and their reference quantity is:

$$\left[\frac{\phi_R S_{1R} C_{1sR} \rho_{1R}}{t_R}\right] \frac{\partial}{\partial t_D} (\phi_D S_{1D} C_{1sD} \rho_{1D}) +$$

$$\left[\frac{\phi_R S_{aR} C_{asR} \rho_{aR}}{t_R}\right] \frac{\partial}{\partial t_D} (\phi_D S_{aD} C_{asD} \rho_{aD}) +$$

$$\left[\frac{\phi_R S_{fR} C_{fsR} \rho_{fR}}{t_R}\right] \frac{\partial}{\partial t_D} (\phi_D S_{fD} C_{fsD} \rho_{fD}) +$$

$$\left[\frac{\phi_R S_{gR} C_{gsR} \rho_{gR}}{t_R}\right] \frac{\partial}{\partial t_D} (\phi_D S_{gD} C_{gsD} \rho_{gD}) =$$

$$\left[\frac{\rho_{1R} C_{1sR} K_{1R} P_{1R}}{x_{1R}^{2} \mu_{1R}}\right] \frac{\partial}{\partial x_{1D}} \left(\frac{\rho_{1D} C_{1sD} K_{1D}}{\mu_{1D}} \frac{\partial P_{1D}}{\partial x_{1D}}\right) +$$

$$\left[\frac{\rho_{1R}^{2} C_{1sR} K_{1R} g_R z_R}{x_{1R}^{2} \mu_{1R}}\right] \frac{\partial}{\partial x_{1D}} \left(\frac{\rho_{1D}^{2} C_{1sD} K_{1D} g_D}{\mu_{1D}} \frac{\partial z_D}{\partial x_{1D}}\right) +$$

$$\left[\frac{\rho_{1R} C_{1sR} K_{1R} P_{1R}}{x_{2R}^{2} \mu_{1R}}\right] \frac{\partial}{\partial x_{2D}} \left(\frac{\rho_{1D} C_{1sD} K_{1D}}{\mu_{1D}} \frac{\partial P_{1D}}{\partial x_{2D}}\right) +$$

$$\left[\frac{\rho_{1R}^{2} C_{1sR} K_{1R} g_R z_R}{x_{2R}^{2} \mu_{1R}}\right] \frac{\partial}{\partial x_{2D}} \left(\frac{\rho_{1D}^{2} C_{1sD} K_{1D} g_D}{\mu_{1D}} \frac{\partial z_D}{\partial x_{2D}}\right) +$$

$$\left[\frac{\rho_{1R}C_{1sR}K_{1R}P_{1R}}{x_{3R}^{2}\mu_{1R}}\right]\frac{\partial}{\partial x_{3D}}\left(\frac{\rho_{1D}C_{1sD}K_{1D}}{\mu_{1D}}\frac{\partial P_{1D}}{\partial x_{3D}}\right)+$$

$$\left[\frac{\rho_{1R}^{2}C_{1sR}K_{1R}g_{R}z_{R}}{x_{3R}^{2}\mu_{1R}}\right]\frac{\partial}{\partial x_{3D}}\left(\frac{\rho_{1D}^{2}C_{1sD}K_{1D}g_{D}}{\mu_{1D}}\frac{\partial z_{D}}{\partial x_{3D}}\right)+$$

$$\left[\frac{\rho_{aR}C_{asR}K_{aR}P_{aR}}{x_{1R}^{2}\mu_{aR}}\right]\frac{\partial}{\partial x_{1D}}\left(\frac{\rho_{aD}C_{asD}K_{aD}}{\mu_{aD}}\frac{\partial P_{aD}}{\partial x_{1D}}\right)+$$

$$\left[\frac{\rho_{aR}^{2}C_{asR}K_{aR}g_{R}z_{R}}{x_{1R}^{2}\mu_{aR}}\right]\frac{\partial}{\partial x_{1D}}\left(\frac{\rho_{aD}^{2}C_{asD}K_{aD}g_{D}}{\mu_{aD}}\frac{\partial z_{D}}{\partial x_{1D}}\right)+$$

$$\left[\frac{\rho_{aR}C_{asR}K_{aR}P_{aR}}{x_{2R}^{2}\mu_{aR}}\right]\frac{\partial}{\partial x_{2D}}\left(\frac{\rho_{aD}C_{asD}K_{aD}}{\mu_{aD}}\frac{\partial P_{aD}}{\partial x_{2D}}\right)+$$

$$\left[\frac{\rho_{aR}^{2}C_{asR}K_{aR}g_{R}z_{R}}{x_{2R}^{2}\mu_{aR}}\right]\frac{\partial}{\partial x_{2D}}\left(\frac{\rho_{aD}^{2}C_{asD}K_{aD}g_{D}}{\mu_{aD}}\frac{\partial z_{D}}{\partial x_{2D}}\right)+$$

$$\left[\frac{\rho_{aR}C_{asR}K_{aR}P_{aR}}{x_{3R}^{2}\mu_{aR}}\right]\frac{\partial}{\partial x_{3D}}\left(\frac{\rho_{aD}C_{asD}K_{aD}}{\mu_{aD}}\frac{\partial P_{aD}}{\partial x_{3D}}\right)+$$

$$\left[\frac{\rho_{aR}^{2}C_{asR}K_{aR}g_{R}z_{R}}{x_{3R}^{2}\mu_{aR}}\right]\frac{\partial}{\partial x_{3D}}\left(\frac{\rho_{aD}^{2}C_{asD}K_{aD}g_{D}}{\mu_{aD}}\frac{\partial z_{D}}{\partial x_{3D}}\right)+$$

$$\left[\frac{\rho_{gR}C_{gsR}K_{gR}P_{gR}}{x_{1R}^{2}\mu_{gR}}\right]\frac{\partial}{\partial x_{1D}}\left(\frac{\rho_{gD}C_{gsD}K_{gD}}{\mu_{gD}}\frac{\partial P_{gD}}{\partial x_{1D}}\right)+$$

$$\left[\frac{\rho_{gR}^{2}C_{gsR}K_{gR}g_{R}z_{R}}{x_{1R}^{2}\mu_{gR}}\right]\frac{\partial}{\partial x_{1D}}\left(\frac{\rho_{gD}^{2}C_{gsD}K_{gD}g_{D}}{\mu_{gD}}\frac{\partial z_{D}}{\partial x_{1D}}\right)+$$

$$\left[\frac{\rho_{gR}C_{gsR}K_{gR}P_{gR}}{x_{2R}^{2}\mu_{gR}}\right]\frac{\partial}{\partial x_{2D}}\left(\frac{\rho_{gD}C_{gsD}K_{gD}}{\mu_{gD}}\frac{\partial P_{gD}}{\partial x_{2D}}\right)+$$

$$\left[\frac{\rho_{gR}^{2}C_{gsR}K_{gR}g_{R}z_{R}}{x_{2R}^{2}\mu_{gR}}\right]\frac{\partial}{\partial x_{2D}}\left(\frac{\rho_{gD}^{2}C_{gsD}K_{gD}g_{D}}{\mu_{gD}}\frac{\partial z_{D}}{\partial x_{2D}}\right)+$$

$$\left[\frac{\rho_{gR}C_{gsR}K_{gR}P_{gR}}{x_{3R}^{2}\mu_{gR}}\right]\frac{\partial}{\partial x_{3D}}\left(\frac{\rho_{gD}C_{gsD}K_{gD}}{\mu_{gD}}\frac{\partial P_{gD}}{\partial x_{3D}}\right)+$$

$$\left[\frac{\rho_{gR}^{2}C_{gsR}K_{gR}g_{R}z_{R}}{x_{3R}^{2}\mu_{gR}}\right]\frac{\partial}{\partial x_{3D}}\left(\frac{\rho_{gD}^{2}C_{gsD}K_{gD}g_{D}}{\mu_{gD}}\frac{\partial z_{D}}{\partial x_{3D}}\right)+$$

$$\left[\frac{\rho_{fR}C_{fsR}K_{fR}P_{fR}}{x_{1R}^{2}\mu_{fR}}\right]\frac{\partial}{\partial x_{1D}}\left(\frac{\rho_{fD}C_{fsD}K_{fD}}{\mu_{fD}}\frac{\partial P_{fD}}{\partial x_{1D}}\right)+$$

$$\left[\frac{\rho_{fR}^{2}C_{fsR}K_{fR}g_{R}z_{R}}{x_{1R}^{2}\mu_{fR}}\right]\frac{\partial}{\partial x_{1D}}\left(\frac{\rho_{fD}^{2}C_{fsD}K_{fD}g_{D}}{\mu_{fD}}\frac{\partial z_{D}}{\partial x_{1D}}\right)+$$

$$\left[\frac{\rho_{fR}C_{fsR}K_{fR}P_{fR}}{x_{2R}^{2}\mu_{fR}}\right]\frac{\partial}{\partial x_{2D}}\left(\frac{\rho_{fD}C_{fsD}K_{fD}}{\mu_{fD}}\frac{\partial P_{fD}}{\partial x_{2D}}\right)+$$

$$\left[\frac{\rho_{fR}^{2}C_{fsR}K_{fR}g_{R}z_{R}}{x_{2R}^{2}\mu_{fR}}\right]\frac{\partial}{\partial x_{2D}}\left(\frac{\rho_{fD}^{2}C_{fsD}K_{fD}g_{D}}{\mu_{fD}}\frac{\partial z_{D}}{\partial x_{2D}}\right)+$$

$$\left[\frac{\rho_{fR}C_{fsR}K_{fR}P_{fR}}{x_{3R}^{2}\mu_{fR}}\right]\frac{\partial}{\partial x_{3D}}\left(\frac{\rho_{fD}C_{fsD}K_{fD}}{\mu_{fD}}\frac{\partial P_{fD}}{\partial x_{3D}}\right)+$$

$$\left[\frac{\rho_{fR}^{2}C_{fsR}K_{fR}g_{R}z_{R}}{x_{3R}^{2}\mu_{fR}}\right]\frac{\partial}{\partial x_{3D}}\left(\frac{\rho_{fD}^{2}C_{fsD}K_{fD}g_{D}}{\mu_{fD}}\frac{\partial z_{D}}{\partial x_{3D}}\right)+$$

$$\left[\frac{\phi_{R}C_{lsR}S_{lR}D_{LlsR}\rho_{lR}}{x_{1R}^{2}}\right]\frac{\partial}{\partial x_{1D}}\left(\phi_{D}C_{lsD}S_{lD}D_{LlsD}\frac{\partial}{\partial x_{1D}}(C_{lsD}\rho_{lD})\right)+$$

$$\left[\frac{\phi_{R}C_{lsR}S_{lR}D_{TlsR}\rho_{lR}}{x_{2R}^{2}}\right]\frac{\partial}{\partial x_{2D}}\left(\phi_{D}C_{lsD}S_{lD}D_{TlsD}\frac{\partial}{\partial x_{2D}}(C_{lsD}\rho_{lD})\right)+$$

$$\left[\frac{\phi_{R}C_{lsR}S_{lR}D_{TlsR}\rho_{lR}}{x_{3R}^{2}}\right]\frac{\partial}{\partial x_{3D}}\left(\phi_{D}C_{lsD}S_{lD}D_{TlsD}\frac{\partial}{\partial x_{3D}}(C_{lsD}\rho_{lD})\right)+$$

$$\left[\frac{\phi_{R}C_{asR}S_{aR}D_{LasR}\rho_{aR}}{x_{1R}^{2}}\right]\frac{\partial}{\partial x_{1D}}\left(\phi_{D}C_{asD}S_{aD}D_{LasD}\frac{\partial}{\partial x_{1D}}(C_{asD}\rho_{aD})\right)+$$

$$\left[\frac{\phi_{R}C_{asR}S_{aR}D_{TasR}\rho_{aR}}{x_{2R}^{2}}\right]\frac{\partial}{\partial x_{2D}}\left(\phi_{D}C_{asD}S_{aD}D_{TasD}\frac{\partial}{\partial x_{2D}}(C_{asD}\rho_{aD})\right)+$$

$$\left[\frac{\phi_{R}C_{asR}S_{aR}D_{TasR}\rho_{aR}}{x_{3R}^{2}}\right]\frac{\partial}{\partial x_{3D}}\left(\phi_{D}C_{asD}S_{aD}D_{TasD}\frac{\partial}{\partial x_{3D}}(C_{asD}\rho_{aD})\right)$$

$$\left[\frac{\phi_R C_{gsR} S_{gR} D_{LgsR} \rho_{gR}}{x_{1R}^2}\right] \frac{\partial}{\partial x_{1D}} \left(\phi_D C_{gsD} S_{gD} D_{LgsD} \frac{\partial}{\partial x_{1D}} (C_{gsD} \rho_{gD})\right) +$$

$$\left[\frac{\phi_R C_{gsR} S_{gR} D_{TgsR} \rho_{gR}}{x_{2R}^2}\right] \frac{\partial}{\partial x_{2D}} \left(\phi_D C_{gsD} S_{gD} D_{TgsD} \frac{\partial}{\partial x_{2D}} (C_{gsD} \rho_{gD})\right) +$$

$$\left[\frac{\phi_R C_{gsR} S_{gR} D_{TgsR} \rho_{gR}}{x_{3R}^2}\right] \frac{\partial}{\partial x_{3D}} \left(\phi_D C_{gsD} S_{gD} D_{TgsD} \frac{\partial}{\partial x_{3D}} (C_{gsD} \rho_{gD})\right) +$$

$$\left[\frac{\phi_R C_{fsR} S_{fR} D_{LfsR} \rho_{fR}}{x_{1R}^2}\right] \frac{\partial}{\partial x_{1D}} \left(\phi_D C_{fsD} S_{fD} D_{LfsD} \frac{\partial}{\partial x_{1D}} (C_{fsD} \rho_{fD})\right) +$$

$$\left[\frac{\phi_R C_{fsR} S_{fR} D_{TfsR} \rho_{fR}}{x_{2R}^2}\right] \frac{\partial}{\partial x_{2D}} \left(\phi_D C_{fsD} S_{fD} D_{TfsD} \frac{\partial}{\partial x_{2D}} (C_{fsD} \rho_{fD})\right) +$$

$$\left[\frac{\phi_R C_{fsR} S_{fR} D_{TfsR} \rho_{fR}}{x_{3R}^2}\right] \frac{\partial}{\partial x_{3D}} \left(\phi_D C_{fsD} S_{fD} D_{TfsD} \frac{\partial}{\partial x_{3D}} (C_{fsD} \rho_{fD})\right)$$

The equation for the mass balance of water in terms of the dimensionless variables and their reference quantities is:

$$\left[\frac{\phi_R S_{aR} \rho_{aR} C_{awR}}{t_R}\right] \frac{\partial}{\partial t_D} (\phi_D S_{aD} C_{aoD} \rho_{aD}) +$$

$$\left[\frac{\phi_R S_{fR} \rho_{fR} C_{fwR}}{t_R}\right] \frac{\partial}{\partial t_D} (\phi_D S_{fD} C_{fwD} \rho_{fD}) =$$

$$\left[\frac{\rho_{aR} C_{awR} K_{aR} P_{aR}}{x_{1R}^2 \mu_{aR}}\right] \frac{\partial}{\partial x_{1D}} \left(\frac{\rho_{aD} C_{awD} K_{aD}}{\mu_{aD}} \frac{\partial P_{aD}}{\partial x_{1D}}\right) +$$

$$\left[\frac{\rho_{aR}^2 C_{awR} K_{aR} g_R z_R}{x_{1R}^2 \mu_{aR}}\right] \frac{\partial}{\partial x_{1D}} \left(\frac{\rho_{aD}^2 C_{awD} K_{aD} g_D}{\mu_{aD}} \frac{\partial z_D}{\partial x_{1D}}\right) +$$

$$\left[\frac{\rho_{aR} C_{awR} K_{aR} P_{aR}}{x_{2R}^2 \mu_{aR}}\right] \frac{\partial}{\partial x_{2D}} \left(\frac{\rho_{aD} C_{awD} K_{aD}}{\mu_{aD}} \frac{\partial P_{aD}}{\partial x_{2D}}\right) +$$

$$\left[\frac{\rho_{aR}^2 C_{awR} K_{aR} g_R z_R}{x_{2R}^2 \mu_{aR}}\right] \frac{\partial}{\partial x_{2D}} \left(\frac{\rho_{aD}^2 C_{awD} K_{aD} g_D}{\mu_{aD}} \frac{\partial z_D}{\partial x_{2D}}\right) +$$

$$[\frac{\rho_{aR}C_{awR}K_{aR}P_{aR}}{x_{3R}^{2}\mu_{aR}}]\ \frac{\partial}{\partial x_{3D}}\ (\frac{\rho_{aD}C_{awD}K_{aD}}{\mu_{aD}}\ \frac{\partial P_{aD}}{\partial x_{3D}})\ +$$

$$[\frac{\rho_{aR}^{2}C_{awR}K_{aR}g_{R}z_{R}}{x_{3R}^{2}\mu_{aR}}]\ \frac{\partial}{\partial x_{3D}}\ (\frac{\rho_{aD}^{2}C_{awD}K_{aD}g_{D}}{\mu_{aD}}\ \frac{\partial z_{D}}{\partial x_{3D}})\ +$$

$$[\frac{\rho_{fR}C_{fwR}K_{fR}P_{fR}}{x_{1R}^{2}\mu_{fR}}]\ \frac{\partial}{\partial x_{1D}}\ (\frac{\rho_{fD}C_{fwD}K_{fD}}{\mu_{fD}}\ \frac{\partial P_{fD}}{\partial x_{1D}})\ +$$

$$[\frac{\rho_{fR}^{2}C_{fwR}K_{fR}g_{R}z_{R}}{x_{1R}^{2}\mu_{fR}}]\ \frac{\partial}{\partial x_{1D}}\ (\frac{\rho_{fD}^{2}C_{fwD}K_{fD}g_{D}}{\mu_{fD}}\ \frac{\partial z_{D}}{\partial x_{1D}})\ +$$

$$[\frac{\rho_{fR}C_{fwR}K_{fR}P_{fR}}{x_{2R}^{2}\mu_{fR}}]\ \frac{\partial}{\partial x_{2D}}\ (\frac{\rho_{fD}C_{fwD}K_{fD}}{\mu_{fD}}\ \frac{\partial P_{fD}}{\partial x_{2D}})\ +$$

$$[\frac{\rho_{fR}^{2}C_{fwR}K_{fR}g_{R}z_{R}}{x_{2R}^{2}\mu_{fR}}]\ \frac{\partial}{\partial x_{2D}}\ (\frac{\rho_{fD}^{2}C_{fwD}K_{fD}g_{D}}{\mu_{fD}}\ \frac{\partial z_{D}}{\partial x_{2D}})\ +$$

$$[\frac{\rho_{fR}C_{fwR}K_{fR}P_{fR}}{x_{3R}^{2}\mu_{fR}}]\ \frac{\partial}{\partial x_{3D}}\ (\frac{\rho_{fD}C_{fwD}K_{fD}}{\mu_{fD}}\ \frac{\partial P_{fD}}{\partial x_{3D}})\ +$$

$$[\frac{\rho_{fR}^{2}C_{fwR}K_{fR}g_{R}z_{R}}{x_{3R}^{2}\mu_{fR}}]\ \frac{\partial}{\partial x_{3D}}\ (\frac{\rho_{fD}^{2}C_{fwD}K_{fD}g_{D}}{\mu_{fD}}\ \frac{\partial z_{D}}{\partial x_{3D}})\ +$$

$$[\frac{\phi_{R}C_{awR}S_{aR}D_{LawR}\rho_{aR}}{x_{1R}^{2}}]\ \frac{\partial}{\partial x_{1D}}\ (\phi_{D}C_{awD}S_{aD}D_{LawD}\frac{\partial}{\partial x_{1D}}(C_{awD}\rho_{aD}))\ +$$

$$[\frac{\phi_{R}C_{awR}S_{aR}D_{TawR}\rho_{aR}}{x_{2R}^{2}}]\ \frac{\partial}{\partial x_{2D}}\ (\phi_{D}C_{awD}S_{aD}D_{TawD}\frac{\partial}{\partial x_{2D}}(C_{awD}\rho_{aD}))\ +$$

$$[\frac{\phi_{R}C_{awR}S_{aR}D_{TawR}\rho_{aR}}{x_{3R}^{2}}]\ \frac{\partial}{\partial x_{3D}}\ (\phi_{D}C_{awD}S_{aD}D_{TawD}\frac{\partial}{\partial x_{3D}}(C_{awD}\rho_{aD}))$$

$$[\frac{\phi_{R}C_{fwR}S_{fR}D_{LfwR}\rho_{fR}}{x_{1R}^{2}}]\ \frac{\partial}{\partial x_{1D}}\ (\phi_{D}C_{fwD}S_{fD}D_{LfwD}\frac{\partial}{\partial x_{1D}}(C_{fwD}\rho_{fD}))\ +$$

$$[\frac{\phi_{R}C_{fwR}S_{fR}D_{TfwR}\rho_{fR}}{x_{2R}^{2}}]\ \frac{\partial}{\partial x_{2D}}\ (\phi_{D}C_{fwD}S_{fD}D_{TfwD}\frac{\partial}{\partial x_{2D}}(C_{fwD}\rho_{fD}))\ +$$

$$\left[\frac{\phi_R C_{fwR} S_{fR} D_{TfwR} \rho_{fR}}{x_{3R}^2}\right] \frac{\partial}{\partial x_{3D}} \left(\phi_D C_{fwD} S_{fD} D_{TfwD} \frac{\partial}{\partial x_{3D}} (C_{fwD} \rho_{fD})\right)$$

The equation for the mass balance of N_2 in terms of the dimensionless variables and their reference quantities is:

$$\left[\frac{\phi_R S_{gR} \rho_{gR} C_{gNR}}{t_R}\right] \frac{\partial}{\partial t_D} (\phi_D S_{gD} C_{goD} \rho_{gD}) +$$

$$\left[\frac{\phi_R S_{fR} \rho_{fR} C_{foR}}{t_R}\right] \frac{\partial}{\partial t_D} (\phi_D S_{fD} C_{foD} \rho_{fD}) =$$

$$\left[\frac{\rho_{gR} C_{gNR} K_{gR} P_{gR}}{x_{1R}^2 \mu_{gR}}\right] \frac{\partial}{\partial x_{1D}} \left(\frac{\rho_{gD} C_{gND} K_{gD}}{\mu_{gD}} \frac{\partial P_{gD}}{\partial x_{1D}}\right) +$$

$$\left[\frac{\rho_{gR}^2 C_{gNR} K_{gR} g_R z_R}{x_{1R}^2 \mu_{gR}}\right] \frac{\partial}{\partial x_{1D}} \left(\frac{\rho_{gD}^2 C_{gND} K_{gD} g_D}{\mu_{gD}} \frac{\partial z_D}{\partial x_{1D}}\right) +$$

$$\left[\frac{\rho_{gR} C_{gNR} K_{gR} P_{gR}}{x_{2R}^2 \mu_{gR}}\right] \frac{\partial}{\partial x_{2D}} \left(\frac{\rho_{gD} C_{gND} K_{gD}}{\mu_{gD}} \frac{\partial P_{gD}}{\partial x_{2D}}\right) +$$

$$\left[\frac{\rho_{gR}^2 C_{gNR} K_{gR} g_R z_R}{x_{2R}^2 \mu_{gR}}\right] \frac{\partial}{\partial x_{2D}} \left(\frac{\rho_{gD}^2 C_{gND} K_{gD} g_D}{\mu_{gD}} \frac{\partial z_D}{\partial x_{2D}}\right) +$$

$$\left[\frac{\rho_{gR} C_{gNR} K_{gR} P_{gR}}{x_{3R}^2 \mu_{gR}}\right] \frac{\partial}{\partial x_{3D}} \left(\frac{\rho_{gD} C_{gND} K_{gD}}{\mu_{gD}} \frac{\partial P_{gD}}{\partial x_{3D}}\right) +$$

$$\left[\frac{\rho_{gR}^2 C_{gNR} K_{gR} g_R z_R}{x_{3R}^2 \mu_{gR}}\right] \frac{\partial}{\partial x_{3D}} \left(\frac{\rho_{gD}^2 C_{gND} K_{gD} g_D}{\mu_{gD}} \frac{\partial z_D}{\partial x_{3D}}\right) +$$

$$\left[\frac{\rho_{fR} C_{fNR} K_{fR} P_{fR}}{x_{1R}^2 \mu_{fR}}\right] \frac{\partial}{\partial x_{1D}} \left(\frac{\rho_{fD} C_{fND} K_{fD}}{\mu_{fD}} \frac{\partial P_{fD}}{\partial x_{1D}}\right) +$$

$$\left[\frac{\rho_{fR}^2 C_{fNR} K_{fR} g_R z_R}{x_{1R}^2 \mu_{fR}}\right] \frac{\partial}{\partial x_{1D}} \left(\frac{\rho_{fD}^2 C_{fND} K_{fD} g_D}{\mu_{fD}} \frac{\partial z_D}{\partial x_{1D}}\right) +$$

$$\left[\frac{\rho_{fR} C_{fNR} K_{fR} P_{fR}}{x_{2R}^2 \mu_{fR}}\right] \frac{\partial}{\partial x_{2D}} \left(\frac{\rho_{fD} C_{fND} K_{fD}}{\mu_{fD}} \frac{\partial P_{fD}}{\partial x_{2D}}\right) +$$

$$[\frac{\rho_{fR}{}^{2}C_{fNR}K_{fR}g_{R}z_{R}}{x_{2R}{}^{2}\mu_{fR}}] \frac{\partial}{\partial x_{2D}} (\frac{\rho_{fD}{}^{2}C_{fND}K_{fD}g_{D}}{\mu_{fD}} \frac{\partial z_{D}}{\partial x_{2D}}) +$$

$$[\frac{\rho_{fR}C_{fNR}K_{fR}P_{fR}}{x_{3R}{}^{2}\mu_{fR}}] \frac{\partial}{\partial x_{3D}} (\frac{\rho_{fD}C_{fND}K_{fD}}{\mu_{fD}} \frac{\partial P_{fD}}{\partial x_{3D}}) +$$

$$[\frac{\rho_{fR}{}^{2}C_{fNR}K_{fR}g_{R}z_{R}}{x_{3R}{}^{2}\mu_{fR}}] \frac{\partial}{\partial x_{3D}} (\frac{\rho_{fD}{}^{2}C_{fND}K_{fD}g_{D}}{\mu_{fD}} \frac{\partial z_{D}}{\partial x_{3D}}) +$$

$$[\frac{\phi_{R}C_{gNR}S_{gR}D_{LgNR}\rho_{gR}}{x_{1R}{}^{2}}] \frac{\partial}{\partial x_{1D}} (\phi_{D}C_{gND}S_{gD}D_{LgND}\frac{\partial}{\partial x_{1D}}(C_{gND}\rho_{gD})) +$$

$$[\frac{\phi_{R}C_{gNR}S_{gR}D_{TgNR}\rho_{gR}}{x_{2R}{}^{2}}] \frac{\partial}{\partial x_{2D}} (\phi_{D}C_{gND}S_{gD}D_{TgND}\frac{\partial}{\partial x_{2D}}(C_{gND}\rho_{gD})) +$$

$$[\frac{\phi_{R}C_{gNR}S_{gR}D_{TgNR}\rho_{gR}}{x_{3R}{}^{2}}] \frac{\partial}{\partial x_{3D}} (\phi_{D}C_{gND}S_{gD}D_{TgND}\frac{\partial}{\partial x_{3D}}(C_{gND}\rho_{gD}))$$

$$[\frac{\phi_{R}C_{fNR}S_{fR}D_{LfNR}\rho_{fR}}{x_{1R}{}^{2}}] \frac{\partial}{\partial x_{1D}} (\phi_{D}C_{fND}S_{fD}D_{LfND}\frac{\partial}{\partial x_{1D}}(C_{fND}\rho_{fD})) +$$

$$[\frac{\phi_{R}C_{fNR}S_{fR}D_{TfNR}\rho_{fR}}{x_{2R}{}^{2}}] \frac{\partial}{\partial x_{2D}} (\phi_{D}C_{fND}S_{fD}D_{TfND}\frac{\partial}{\partial x_{2D}}(C_{fND}\rho_{fD})) +$$

$$[\frac{\phi_{R}C_{fNR}S_{fR}D_{TfNR}\rho_{fR}}{x_{3R}{}^{2}}] \frac{\partial}{\partial x_{3D}} (\phi_{D}C_{fND}S_{fD}D_{TfND}\frac{\partial}{\partial x_{3D}}(C_{fND}\rho_{fD}))$$

Dividing both sides of the mass balance equation by for oil by $\frac{\rho_{1R}C_{1oR}K_{1R}P_{1R}}{x_{1R}{}^{2}\mu_{1R}}$, one obtains the following dimensionless groups:

$$[\frac{\phi_{R}S_{1R}\mu_{1R}x_{1R}{}^{2}}{t_{R}K_{1R}P_{1R}}],\ [\frac{g_{R}z_{R}\rho_{1R}}{P_{1R}}],\ [\frac{x_{1R}{}^{2}}{x_{2R}{}^{2}}],\ [\frac{x_{1R}{}^{2}}{x_{3R}{}^{2}}]$$

Dividing both sides of the mass balance equation for surfactant by $\frac{\rho_{1R}C_{1sR}K_{1R}P_{1R}}{x_{1R}^2\mu_{1R}}$, one obtains the following dimensionless groups:

$$[\frac{\phi_R S_{1R}\mu_{1R}x_{1R}^2}{t_R K_{1R}P_{1R}}],\ [\frac{\rho_{1R}g_R z_R}{P_{1R}}],\ [\frac{x_{1R}^2}{x_{2R}^2}],\ [\frac{x_{1R}^2}{x_{3R}^2}],$$

$$[\frac{\rho_{aR}C_{asR}K_{aR}P_{aR}\mu_{1R}}{\rho_{1R}C_{1sR}K_{1R}P_{1R}\mu_{aR}}],\ [\frac{\rho_{aR}^2C_{asR}K_{aR}g_R z_R\mu_{1R}}{\rho_{1R}C_{1sR}K_{1R}P_{1R}\mu_{aR}}],$$

$$[\frac{\rho_{fR}C_{fsR}K_{fR}P_{fR}\mu_{1R}}{\rho_{1R}C_{1sR}K_{1R}P_{1R}\mu_{fR}}],\ [\frac{\rho_{fR}^2C_{fsR}K_{fR}g_R z_R\mu_{1R}}{\rho_{1R}C_{1sR}K_{1R}P_{1R}\mu_{fR}}],$$

$$[\frac{\rho_{gR}C_{gsR}K_{gR}P_{gR}\mu_{1R}}{\rho_{1R}C_{1sR}K_{1R}P_{1R}\mu_{gR}}],\ [\frac{\rho_{gR}^2C_{gsR}K_{gR}g_R z_R\mu_{1R}}{\rho_{1R}C_{1sR}K_{1R}P_{1R}\mu_{gR}}],$$

$$[\frac{\phi_R S_{1R}D_{L1sR}\mu_{1R}}{K_{1R}P_{1R}}],\ [\frac{\phi_R S_{1R}D_{T1sR}\mu_R x_{1R}^2\mu_{1R}}{x_{2R}^2K_{1R}P_{1R}}],$$

$$[\frac{\phi_R C_{asR}S_{aR}D_{LasR}\rho_{aR}\mu_{1R}}{\rho_{1R}C_{1sR}K_{1R}P_{1R}}],\ [\frac{\phi_R C_{asR}S_{aR}D_{TasR}\rho_{aR}\mu_{1R}}{\rho_{1R}C_{1sR}K_{1R}P_{1R}}],$$

$$[\frac{\phi_R C_{fsR}S_{fR}D_{LfsR}\rho_{fR}\mu_{1R}}{\rho_{1R}C_{1sR}K_{1R}P_{1R}}],\ [\frac{\phi_R C_{fsR}S_{fR}D_{TfsR}\rho_{fR}\mu_{1R}}{\rho_{1R}C_{1sR}K_{1R}P_{1R}}],$$

$$[\frac{\phi_R C_{gsR}S_{gR}D_{LgsR}\rho_{gR}\mu_{1R}}{\rho_{1R}C_{1sR}K_{1R}P_{1R}}],\ [\frac{\phi_R C_{gsR}S_{gR}D_{TgsR}\rho_{gR}\mu_{1R}}{\rho_{1R}C_{1sR}K_{1R}P_{1R}}]$$

Dividing both sides of the mass balance equation for water by $\frac{\rho_{aR}C_{awR}K_{aR}P_{aR}}{x_{1R}^2\mu_{aR}}$, one obtains the following dimensionless groups:

$$[\frac{\phi_R S_{aR}\mu_{aR}x_{1R}^2}{t_R K_{aR}P_{aR}}],\ [\frac{g_R z_R\rho_{aR}}{P_{aR}}],\ [\frac{x_{1R}^2}{x_{2R}^2}],\ [\frac{x_{1R}^2}{x_{3R}^2}],$$

$$\left[\frac{\phi_R S_{fR} \mu_{fR} x_{1R}^2}{t_R K_{fR} P_{fR}}\right], \left[\frac{g_R z_R \rho_{fR}}{P_{fR}}\right],$$

$$\left[\frac{\phi_R S_{aR} D_{LawR} \mu_{aR}}{K_{aR} P_{aR}}\right], \left[\frac{\phi_R S_{aR} D_{TawR} \mu_{aR}}{K_{aR} P_{aR}}\right],$$

$$\left[\frac{\phi_R S_{fR} D_{LfwR} \mu_{fR}}{K_{fR} P_{fR}}\right], \left[\frac{\phi_R S_{fR} D_{TfwR} \mu_{fR}}{K_{fR} P_{fR}}\right]$$

Dividing both sides of the mass balance equation for nitrogen by $\frac{\rho_{gR} C_{gNR} K_{gR} P_{gR}}{x_{1R}^2 \mu_{gR}}$, one obtains the following dimensionless groups:

$$\left[\frac{\phi_R S_{gR} \mu_{gR} x_{1R}^2}{t_R K_{gR} P_{gR}}\right], \left[\frac{g_R z_R \rho_{gR}}{P_{gR}}\right], \left[\frac{x_{1R}^2}{x_{2R}^2}\right], \left[\frac{x_{1R}^2}{x_{3R}^2}\right],$$

$$\left[\frac{\phi_R S_{fR} \mu_{fR} x_{1R}^2}{t_R K_{fR} P_{fR}}\right], \left[\frac{g_R z_R \rho_{fR}}{P_{fR}}\right],$$

$$\left[\frac{\phi_R S_{gR} D_{LgNR} \mu_{gR}}{K_{gR} P_{gR}}\right], \left[\frac{\phi_R S_{gR} D_{TgNR} \mu_{gR}}{K_{gR} P_{gR}}\right],$$

$$\left[\frac{\phi_R S_{fR} D_{LfNR} \mu_{fR}}{K_{fR} P_{fR}}\right], \left[\frac{\phi_R S_{fR} D_{TfNR} \mu_{fR}}{K_{fR} P_{fR}}\right]$$

From the initial and boundary conditions, constitutive relationships and constraints, one obtains the following dimensionless groups:

$$\left[\frac{S_{aR}}{S_{lR}}\right], \left[\frac{C_{loR}}{C_{lsR}}\right], \left[\frac{C_{asR}}{C_{awR}}\right], \left[\frac{\rho_{lR}}{\rho_{aR}}\right], \left[\frac{P_{lR}}{P_{aR}}\right], \left[\frac{P_{fR}}{P_{aR}}\right],$$

$$\left[\frac{S_{fR}}{S_{lR}}\right], \left[\frac{S_{gR}}{S_{lR}}\right], \left[\frac{C_{gNR}}{C_{awR}}\right], \left[\frac{\rho_{fR}}{\rho_{lR}}\right], \left[\frac{\rho_{gR}}{\rho_{gR}}\right],$$

$$[\frac{D^*_{asR}}{D^*_{awR}}],\ [\frac{D^*_{asR}}{D^*_{fwR}}],\ [\frac{D^*_{asR}}{D^*_{gNR}}],\ [\frac{S_{gi}}{S_{gR}}],\ [\frac{P_{gi}}{P_{gR}}],$$

$$[\phi_R],\ [\frac{P_{lR}}{P_{claR}}],\ [\frac{D^*_{loR}}{D^*_{lsR}}],\ [\frac{D^*_{awR}}{D^*_{asR}}],\ [\frac{W_{asR}}{W_{awR}}],$$

$$[\frac{W_{awR}C_{awR}\mu_{aR}x_{1R}}{K_{aR}P_{aR}A_{injR}}],\ [\frac{P_{prod}}{P_{lR}}],\ [\frac{P_{aR}}{P_{claR}}],\ [\frac{S_{ai}}{S_{aR}}],\ [\frac{S_{li}}{S_{lR}}],\ [\frac{P_{li}}{P_{lR}}],$$

$$[\frac{W}{x_{1R}}],\ [\frac{H}{x_{3R}}],\ [\frac{L}{x_{1R}}],\ [\frac{P_{fi}}{P_{fR}}],\ [\frac{P\eta_i}{P_{gR}}]$$

12.1.3.2 Foam Injection: Three-Phase Flow

In a similar way one may write the governing equations for this case in terms of the reference quantities. The mass balance equation gives rise to the following dimensionless groups:

$$[\frac{\phi_R S_{lR}\mu_{lR}x_{1R}^2}{t_R K_{lR}P_{lR}}],\ [\frac{g_R z_R \rho_{lR}}{P_{lR}}],\ [\frac{x_{1R}^2}{x_{2R}^2}],\ [\frac{x_{1R}^2}{x_{3R}^2}]$$

The mass balance equation for surfactant gives rise to the following dimensionless groups:

$$[\frac{\phi_R S_{lR}\mu_{lR}x_{1R}^2}{t_R K_{lR}P_{lR}}],\ [\frac{\rho_{lR}g_R z_R}{P_{lR}}],\ [\frac{x_{1R}^2}{x_{2R}^2}],\ [\frac{x_{1R}^2}{x_{3R}^2}],$$

$$[\frac{\rho_{aR}C_{asR}K_{aR}P_{aR}\mu_{lR}}{\rho_{lR}C_{lsR}K_{lR}P_{lR}\mu_{aR}}],\ [\frac{\rho_{aR}^2 C_{asR}K_{aR}g_R z_R\mu_{lR}}{\rho_{lR}C_{lsR}K_{lR}P_{lR}\mu_{aR}}],$$

$$[\frac{\rho_{fR}C_{fsR}K_{fR}P_{fR}\mu_{lR}}{\rho_{lR}C_{lsR}K_{lR}P_{lR}\mu_{fR}}],\ [\frac{\rho_{fR}^2 C_{fsR}K_{fR}g_R z_R\mu_{lR}}{\rho_{lR}C_{lsR}K_{lR}P_{lR}\mu_{fR}}],$$

$$[\frac{\phi_R S_{lR}D_{LlsR}\mu_{lR}}{K_{lR}P_{lR}}],\ [\frac{\phi_R S_{lR}D_{TlsR}\mu_R x_{1R}^2\mu_{lR}}{x_{2R}^2 K_{lR}P_{lR}}],$$

$$[\frac{\phi_R C_{asR} S_{aR} D_{LasR} \rho_{aR} \mu_{1R}}{\rho_{1R} C_{1sR} K_{1R} P_{1R}}],\ [\frac{\phi_R C_{asR} S_{aR} D_{TasR} \rho_{aR} \mu_{1R}}{\rho_{1R} C_{1sR} K_{1R} P_{1R}}],$$

$$[\frac{\phi_R C_{fsR} S_{fR} D_{LfsR} \rho_{fR} \mu_{1R}}{\rho_{1R} C_{1sR} K_{1R} P_{1R}}],\ [\frac{\phi_R C_{fsR} S_{fR} D_{TfsR} \rho_{fR} \mu_{1R}}{\rho_{1R} C_{1sR} K_{1R} P_{1R}}],$$

The mass balance equation for water gives rise to the following dimensionless groups:

$$[\frac{\phi_R S_{aR} \mu_{aR} x_{1R}^2}{t_R K_{aR} P_{aR}}],\ [\frac{g_R z_R \rho_{aR}}{P_{aR}}],\ [\frac{x_{1R}^2}{x_{2R}^2}],\ [\frac{x_{1R}^2}{x_{3R}^2}],$$

$$[\frac{\phi_R S_{fR} \mu_{fR} x_{1R}^2}{t_R K_{fR} P_{fR}}],\ [\frac{g_R z_R \rho_{fR}}{P_{fR}}],$$

$$[\frac{\phi_R S_{aR} D_{LawR} \mu_{aR}}{K_{aR} P_{aR}}],\ [\frac{\phi_R S_{aR} D_{TawR} \mu_{aR}}{K_{aR} P_{aR}}],$$

$$[\frac{\phi_R S_{fR} D_{LfwR} \mu_{fR}}{K_{fR} P_{fR}}],\ [\frac{\phi_R S_{fR} D_{TfwR} \mu_{fR}}{K_{fR} P_{fR}}]$$

The mass balance equation for N_2 gives rise to the following dimensionless groups

$$[\frac{\phi_R S_{fR} \mu_{fR} x_{1R}^2}{t_R K_{fR} P_{fR}}],\ [\frac{g_R z_R \rho_{fR}}{P_{fR}}],\ [\frac{x_{1R}^2}{x_{2R}^2}],\ [\frac{x_{1R}^2}{x_{3R}^2}],$$

$$[\frac{\phi_R S_{fR} \mu_{fR} x_{1R}^2}{t_R K_{fR} P_{fR}}],$$

$$[\frac{\phi_R S_{fR} D_{LfNR} \mu_{fR}}{K_{fR} P_{fR}}],\ [\frac{\phi_R S_{fR} D_{TfNR} \mu_{fR}}{K_{fR} P_{fR}}],$$

From the initial and boundary conditions, constitutive relationships and constraints, one obtains the following dimensionless groups:

$[\frac{S_{aR}}{S_{lR}}]$, $[\frac{C_{loR}}{C_{lsR}}]$, $[\frac{C_{asR}}{C_{awR}}]$, $[\frac{\rho_{lR}}{\rho_{aR}}]$, $[\frac{P_{lR}}{P_{aR}}]$,

$[\frac{S_{fR}}{S_{lR}}]$, $[\frac{C_{gNR}}{C_{awR}}]$, $[\frac{\rho_{fR}}{\rho_{lR}}]$,

$[\frac{D^*_{asR}}{D^*_{awR}}]$, $[\frac{D^*_{asR}}{D^*_{fwR}}]$, $[\frac{D^*_{asR}}{D^*_{fNR}}]$, $[\frac{S_{li}}{S_{lR}}]$, $[\frac{P_{fi}}{P_{fR}}]$, $\genfrac{}{}{0pt}{}{P_{ai}}{P_{aR}}$

$[\phi_R]$, $[\frac{P_{lR}}{P_{claR}}]$, $[\frac{D^*_{loR}}{D^*_{lsR}}]$, $[\frac{D^*_{awR}}{D^*_{asR}}]$, $[\frac{W_{asR}}{W_{awR}}]$,

$[\frac{W_{awR}C_{awR}\mu_{aR}x_{1R}}{K_{aR}P_{aR}A_{injR}}]$, $[\frac{P_{prod}}{P_{lR}}]$, $[\frac{P_{aR}}{P_{claR}}]$, $[\frac{S_{ai}}{S_{aR}}]$, $[\frac{S_{li}}{S_{lR}}]$, $[\frac{P_{li}}{P_{lR}}]$,

$[\frac{W}{x_{1R}}]$, $[\frac{H}{x_{3R}}]$, $[\frac{L}{x_{1R}}]$